**European Joint Programme
on Radioactive Waste Management**

Deliverable 3.6: CORI-Final report on results generated in Task 2 of CORI

Deliverable 3.7: CORI-Final report on organic retention in cementitious systems

Deliverable 3.8: CORI-Final report on radionuclide mobility in cementitious materials in the presence of organics

Work Package 3, CORI

http://www.ejp-eurad.eu/

Document information

Project Acronym	**EURAD**
Project Title	**European Joint Programme on Radioactive Waste Management**
Project Type	**European Joint Programme (EJP)**
EC grant agreement No.	**847593**
Project starting / end date	**1st June 2019 – 30 May 2024**
Work Package No.	**3**
Work Package Title	**Cement Organic Radionuclide Interaction**
Work Package Acronym	**CORI**
Deliverable No.	**3.6; 3.7 and 3.8**
Deliverable Title	**Final reports**
Lead Beneficiary	**KIT**
Contractual Delivery Date	**M56**
Actual Delivery Date	**05/07/2024**
Type	**Report**
Dissemination level	**PU**
Authors	**CORI WP Board:**
	Marcus Altmaier [**KIT**]; Denise Ricard [**Andra**]; Johan Vandenborre [**CNRS-SUBATECH**], David García [**KIT (Amphos21)**]; Pierre Henocq [**Andra**], Nathalie Macé [**CEA**]; Tiziana Missana [**CIEMAT**]

To be cited as:

Altmaier M., Ricard D., Vandenborre J., Garcia D., Henocq P., Macé N., Missana T. (2024): Final report o results generated in CORI. Final version of deliverables D3.6, D3.7 and D.8 of the HORIZON 2020 project EURAD. EC Grant agreement no: 847593.

Disclaimer

All information in this document is provided "as is" and no guarantee or warranty is given that the information is fit for any particular purpose. The user, therefore, uses the information at its sole risk and liability. For the avoidance of all doubts, the European Commission or the individual Colleges of EURAD (and their participating members) has no liability in respect of this document, which is merely representing the authors' view.

Acknowledgement

EURAD (Deliverables n° 3.6, 3.7 and 3.8) - Final Report of results generated in CORI
Dissemination level: PU
Date of issue of this report: **05/07/2024**

Page 2

Status of deliverable		
	By	Date
Delivered (Lead Beneficiary)	KIT	10/04/2024
Verified (WP Leader)	KIT	26/06/2024
Reviewed (Reviewers)	S. Saslow (PNNL, USA)	14/05/2024
Approved (PMO)	B. Grambow	05/07/2024
Submitted to EC	Andra (Coordinator)	05/07/2024

EURAD (Deliverables n° 3.6, 3.7 and 3.8) - Final Report of results generated in CORI
Dissemination level: PU
Date of issue of this report: **05/07/2024**

Page 3

Executive Summary

To meet its objectives the WP3 CORI is divided in three R&D oriented tasks:

- Task 2: Organic degradation
- Task 3: Organic-Cement-Interactions
- Task 4: radionuclides-Organic-Cement-Interactions

CORI Task 1 is dedicated to the coordination of the three other tasks.

The aim of Task 2 was to improve knowledge of degradation of organic wastes in conditions representative of disposal facilities. The degradation of organic materials was studied regarding the effect of the irradiation (radiolysis) and effect of presence of alkaline pore water (hydrolysis). The focus is the characterization of degradation products such as gas production and release of soluble organic species. As some results were already available for the gas production originated by radiolytical degradation of organic compounds, the main efforts of these studies were related to the characterization of soluble species in solution that have been used as input for Task 3 and Task 4. The organic materials studied in the Task 2 are the following: polyvinyl chloride PVC, cellulose, ion exchange resins (IER) and superplasticizers (cementitious additives).

The specific objective of CORI Task 3 was to investigate the sorption and diffusion processes of different organic molecules onto cement-based materials. The investigated organic molecules were defined to include (i) main degradation products such as ISA or phthalates (ii) C14-bearing molecules identified in the European project CAST and (iii) real degradation products resulting from Task 2. EDTA is also studied as strong complexing molecule as well as low molecular weight molecules (*e.g.* acetate). Regarding the investigated cementitious materials, CEM I and CEM V are used at various degradation stages (including altered/carbonated stages) according to the requirements by WMOs, as well as pure solid phases such as portlandite, C-(A)-S-H, AFt and AFm-phases to allow for improved process understanding.

CORI Task 4 was dedicated to study the competition or synergetic effect in ternary systems (*i.e.* organic/ radionuclide/ cement) and intends to give some new insights for a better mechanistic understanding of radionuclide (RN) interactions and diffusion data in cementitious environments. The RNs of interest in Task 4 were: ^{3}H (as tritiated water, HTO in diffusion experiments), ^{14}C (for radiolabelled organic species), ^{134}Cs, ^{36}Cl, Pb(stable), ^{63}Ni, ^{152}Eu, ^{241}Am, ^{248}Cm, ^{232,234}Th, ^{238,239}Pu and ^{233,238}U.

This final report constitutes the WP3 CORI deliverables 3.6, 3.7 and 3.8 and provides the final results obtained in each of these R&D tasks.

Keywords

Cement – Organic – Radiolysis – Hydrolysis – Degradation - Radionuclide – Speciation - Retention - Diffusion

EURAD (Deliverables n° 3.6, 3.7 and 3.8) - Final Report of results generated in CORI
Dissemination level: PU
Date of issue of this report: **05/07/2024**

Page 4

Table of content

EURAD (Deliverables n° 3.6, 3.7 and 3.8) - Final Report of results generated in CORI
Dissemination level: PU
Date of issue of this report: **05/07/2024**

Page 5

List of Figures

EURAD (Deliverables n° 3.6, 3.7 and 3.8) - Final Report of results generated in CORI   Page 8
Dissemination level: PU
Date of issue of this report: **05/07/2024**

EURAD (Deliverables n° 3.6, 3.7 and 3.8) - Final Report of results generated in CORI
Dissemination level: PU
Date of issue of this report: **05/07/2024**

Page 9

EURAD (Deliverables n° 3.6, 3.7 and 3.8) - Final Report of results generated in CORI
Dissemination level: PU
Date of issue of this report: **05/07/2024**

Page 10

EURAD (Deliverables n° 3.6, 3.7 and 3.8) - Final Report of results generated in CORI
Dissemination level: PU
Date of issue of this report: **05/07/2024**

Page 11

EURAD (Deliverables n° 3.6, 3.7 and 3.8) - Final Report of results generated in CORI
Dissemination level: PU
Date of issue of this report: **05/07/2024**

Page 12

EURAD (Deliverables n° 3.6, 3.7 and 3.8) - Final Report of results generated in CORI
Dissemination level: PU
Date of issue of this report: **05/07/2024**

Page 13

EURAD (Deliverables n° 3.6, 3.7 and 3.8) - Final Report of results generated in CORI
Dissemination level: PU
Date of issue of this report: **05/07/2024**

Page 14

EURAD (Deliverables n° 3.6, 3.7 and 3.8) - Final Report of results generated in CORI
Dissemination level: PU
Date of issue of this report: **05/07/2024**

Page 15

EURAD (Deliverables n° 3.6, 3.7 and 3.8) - Final Report of results generated in CORI   Page 16
Dissemination level: PU
Date of issue of this report: **05/07/2024**

EURAD (Deliverables n° 3.6, 3.7 and 3.8) - Final Report of results generated in CORI   Page 17
Dissemination level: PU
Date of issue of this report: **05/07/2024**

EURAD (Deliverables n° 3.6, 3.7 and 3.8) - Final Report of results generated in CORI
Dissemination level: PU
Date of issue of this report: **05/07/2024**

Page 18

EURAD (Deliverables n° 3.6, 3.7 and 3.8) - Final Report of results generated in CORI
Dissemination level: PU
Date of issue of this report: **05/07/2024**

Page 19

EURAD (Deliverables n° 3.6, 3.7 and 3.8) - Final Report of results generated in CORI
Dissemination level: PU
Date of issue of this report: **05/07/2024**

Page 20

EURAD (Deliverables n° 3.6, 3.7 and 3.8) - Final Report of results generated in CORI
Dissemination level: PU
Date of issue of this report: **05/07/2024**

Page 21

the presence of HIBA, HBA, GTA. All data correspond to Stage II, with pH = (12.4 ± 0.1). Solid line and grey-shaded area indicate the average R_d values and corresponding uncertainty reported in Tasi et al. (2021) for the uptake of Pu(IV) by HCP under analogous experimental conditions in the absence of organic ligands. Crossed circles shown sorption data from the same experimental study but in the presence of ISA.. 241

EURAD (Deliverables n° 3.6, 3.7 and 3.8) - Final Report of results generated in CORI
Dissemination level: PU
Date of issue of this report: **05/07/2024**

Page 22

List of Tables

EURAD (Deliverables n° 3.6, 3.7 and 3.8) - Final Report of results generated in CORI
Dissemination level: PU
Date of issue of this report: **05/07/2024**

Page 23

EURAD (Deliverables n° 3.6, 3.7 and 3.8) - Final Report of results generated in CORI
Dissemination level: PU
Date of issue of this report: **05/07/2024**

Page 24

EURAD (Deliverables n° 3.6, 3.7 and 3.8) - Final Report of results generated in CORI
Dissemination level: PU
Date of issue of this report: **05/07/2024**

Page 26

Glossary

AA: acetic acid

ACW: Artificial Cement pore Water

ADI: Adipate

AFm: monosulfoaluminate

AFt: Trisulfoaluminate

C-A-S-H or C-A-S-H: Calcium Aluminate Silicate Hydrates

CIT: Citric acid

C-S-H: Calcium Silicate Hydrates

DA: Digital autoradiography

DGR: Deep Geological Repositories

DOC: Dissolved Organic Carbon

EDTA: Ethylenediamine tetra-acetic acid

ETT: Ettringite

FOR or FA: Formic acid

GA: Glycolic acid

GLU: Glutaric acid

GTA: glutaric acid

HBA: 3-hydroxybutyric acid

HCP: Hardened Cement Paste

HIBA: α-hydroxyisobutyric acid

IER: Ion Exchange resin

ISA: Isosaccharinic acid

L: ligand

LA: Lactic acid

LS: LignoSulfonate

NPOC : Non-Purgeable Organic Carbon

NTA: Nitrilotriacetic acid

OL: Organic ligand

ORGA: organic species

OXA or OA: Oxalic acid

PAN: Polyacrylonitrile

PE: polyethylene

PBTC: 2-phosphonobutane-1,2,4,-tricarboxylate

PHT: Phthalic acid

EURAD (Deliverables n° 3.6, 3.7 and 3.8) - Final Report of results generated in CORI
Dissemination level: PU
Date of issue of this report: **05/07/2024**

Page 27

POR: Portlandite

RCM: Reference Cement Material, HCP based on CEM I, provided by the Czeck team

RDP: Real Degradation products (From Task 2)

RN: Radionuclide

SP: Superplasticizer

TRLFS: Time-Resolved Laser Fluorescence Spectroscopy

PAE: PolyAryl Ether

PCE: PolyCarboxylate Ether

PMS: PolyMelamine Sulfonate

TMA: Tri-methyl-amine

WAXS: Wide-Angle X-ray Scattering

EURAD (Deliverables n° 3.6, 3.7 and 3.8) - Final Report of results generated in CORI
Dissemination level: PU
Date of issue of this report: **05/07/2024**

Page 28

1. Introduction

WP3 CORI aims to improve the knowledge on the organic release issues that can accelerate the radionuclide migration in the context of the post closure phase of geological repositories for ILW and LLW/VLLW, including surface/shallow disposal. Cement-based materials are widely used as waste matrices, backfill materials and structural components in current and planned repositories for low, intermediate and high level radioactive waste. Depending on their origins, waste matrices incorporate diverse types of materials such as organic components (cellulose materials, exchange resins, plastic waste, superplaticizers …) which may affect radionuclides (RN) behavior. This potential effect is related to the formation of complexes in solution with some RN of interest, which can (i) increase the radionuclide solubility and (ii) decrease the radionuclide sorption. Although radionuclides sorption on hardened cement paste (HCP) is well described in literature, data on binary (Organic-Cement) and ternary (RN-Organic-Cement) systems are very scarce.

The aim of Task 2 was to improve knowledge of degradation of organic wastes in conditions representative of disposal facilities. The degradation of organic materials was studied regarding the effect of the irradiation (radiolysis) and effect of presence of alkaline pore water (hydrolysis). The focus is the characterization of degradation products such as gas production and release of soluble organic species. As some results was already available for the gas production originated by radiolytical degradation of organic compounds, the main efforts of these studies was related to the characterization of soluble species in solution that have been used as input for Task 3 and Task 4. The organic materials studied in the Task 2 are the following: polyvinyl chloride PVC, cellulose, ion exchange resins (IER) and superplasticizers (cementitious additives).

The specific objective of CORI Task 3 is to investigate the sorption and diffusion processes of different organic molecules onto cement-based materials. The investigated organic molecules were defined to include (i) main degradation products such as ISA or phthalates (ii) C14-bearing molecules identified in the European project CAST and (iii) degradation products resulting from Task 2. EDTA is also studied as strong complexing molecule as well as low molecular weight molecules (*e.g.* acetate). Regarding the investigated cementitious materials, CORI partners investigated selected systems of high interest. CEM I and CEM V are used at various degradation stages (including altered/carbonated stages) according to the requirements by WMOs, as well as pure solid phases such as portlandite, , C-A-S-H, AFt and AFm-phases to allow for improved process understanding.

CORI Task 4 was dedicated to study the competition or synergetic effect in ternary systems (*i.e.* organic/ radionuclide/ cement) and intends to give some new insights for a better mechanistic understanding of radionuclide (RN) interactions and diffusion data in cementitious environments. The RNs of interest in Task 4 were: ^{3}H (as tritiated water, HTO in diffusion experiments), ^{14}C (for radiolabelled organic species), ^{134}Cs, ^{36}Cl, Pb(stable), ^{63}Ni, ^{152}Eu, ^{241}Am, ^{248}Cm, ^{232,234}Th, ^{238,239}Pu and ^{233,238}U.

The present document is divided in four main sections to present: i) results obtained in Task 2; ii) materials and methods dedicated to Task 3 and Task 4; iii) results obtained in Task 3 and iv) results obtained in Task4.

This final report constitutes the WP3 CORI deliverables 3.6, 3.7 and 3.8.

eurad
European Joint Programme
on Radioactive Waste Management

EURAD (Deliverables n° 3.6, 3.7 and 3.8) - Final Report of results generated in CORI
Dissemination level: PU
Date of issue of this report: **05/07/2024**

Page 29

2. Results obtained in Task 2

The following organic materials were studied in Task 2: polyvinyl chloride (PVC), cellulose, ion exchange resins (IER) and superplasticizers (SP). The selection of these materials was based on abundance in the WMO's inventories and/or in the lack of knowledge regarding the degradation aspects.

Degradation process and soluble degradation species were studied regarding the effect of the irradiation and the presence of alkaline pore water. These degradation processes might occur in disposal; the first one associated to the self-irradiation related to the presence of radionuclides (several MGy of total absorbed dose for intermediate-level radioactive waste) and the second one associated to presence of pore water after saturation of disposal cells.

The main results obtained are presented in the following sections by type of organic material studied.

2.1 Degradation of cellulose

2.1.1 Introduction

In many countries, low- and intermediate-level radioactive waste (L/ILW) is planned to be stored in deep geological repositories (DGR). Prior to storage, this type of waste is typically solidified in a cement matrix and, after waste emplacement, caverns and access tunnels will be backfilled with cementitious materials, thus establishing highly alkaline conditions in the near-field of the repository.

Lignocellulosic materials can be found in a significant fraction of the current low- and intermediate-level radioactive waste. During storage and final disposal, these materials will undergo radiolytic and/or hydrolytic degradation. Radiolytic degradation may lead to a significant gas production and changes to the physico-chemical properties of the lignocellulosic materials. In the highly alkaline cementitious environment of a disposal system, hydrolytic degradation is known to lead to the production of radionuclide-complexing agents, such as the α and β isomers of isosaccharinic acid (α- and β-ISA). Especially α-ISA has been shown to form complexes with radionuclides present in the waste, which could reduce their sorption on cement phases and thus enhance their migration.

Cellulose slowly degrades into water soluble organic compounds under alkaline conditions, according to a combination of peeling, stopping and alkaline hydrolysis reactions, as shown in Fig 2.1. In general, alkaline degradation of polysaccharides begins at the reducing end of the molecule and proceeds in a stepwise manner along the polymer chain. Each of these peeling reactions removes an individual glucose unit from the reducing end of the cellulose chain and generates a new reducing end, allowing the reaction to continue.

EURAD (Deliverables n° 3.6, 3.7 and 3.8) - Final Report of results generated in CORI
Dissemination level: PU
Date of issue of this report: **05/07/2024**

Page 30
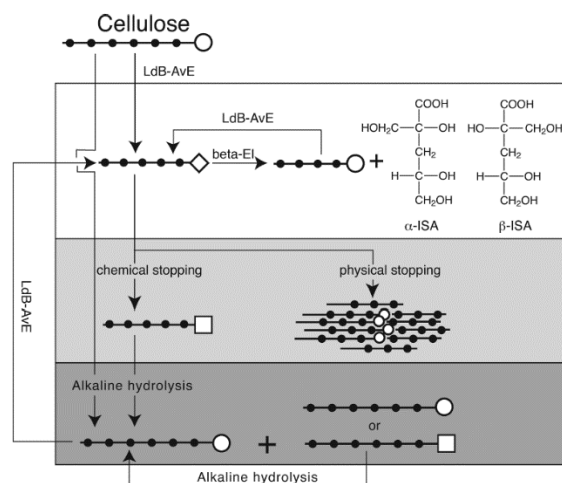
Figure 2-1: Simplified reaction scheme for the processes involved in the alkaline degradation of cellulose (Glaus and Van Loon, 2008).

As radiolytic degradation may change the physico-chemical properties of cellulose, it may affect its hydrolytic degradation and thus the production of ISA during disposal.

Hence, both the radiolytic and subsequent hydrolytic degradation (at pH ~13) of lignocellulosic materials (paper tissues) was investigated by **[SCK CEN]** under various storage and disposal conditions. Gas production yields were determined for cellulosic tissues irradiated with gamma rays under either oxic or anoxic conditions and at a broad range of absorbed doses. Physico-chemical changes of the cellulose due to irradiation were evaluated and indicate that chain scission is the main radiolytic degradation process under anoxic conditions, while under oxic conditions additional radio-oxidation of the polymer backbone occurs. When these (irradiated) tissues were submersed in artificial cement water (pH > 13), a clear increase of the release of DOC (dissolved organic carbon) and ISA can be observed with an increasing absorbed dose during pre-irradiation and even more so for tissues irradiated under oxic conditions (at least for tissues pre-irradiated from 0.05 MGy).

The effects of the presence of portlandite and zero-valent metallic iron powder on the cellulose degradation process as well as on the stability of one of its main degradation products, α-ISA, have been investigated by PSI under alkaline, reducing conditions at a temperature of 90°C to accelerate potential degradation reactions. According to literature, metallic iron can potentially catalyze the degradation of organic compounds (Bell et al. (1994); McCollom and Seewald (2003a, b); Seewald (2001). This material is abundantly present in a cementitious near-field of a DGR (rebars, drum walls,…).

The long-term prediction for the abiotic cellulose degradation under anoxic alkaline conditions at ambient temperatures is also studied by [**PSI**]. Experiments with different cellulose materials carried out at [**PSI**] under such conditions have been running since ~1995.

2.1.2 Studied Materials

Two kinds of cellulose materials are studied, cellulose tissues and cellulose powder as indicated in *Table 1*. Besides cellulose materials, α-ISA, the main degradation product of cellulose by hydrolysis, is also studied by **[PSI]**.

EURAD (Deliverables n° 3.6, 3.7 and 3.8) - Final Report of results generated in CORI
Dissemination level: PU
Date of issue of this report: **05/07/2024**

Page 31

Table 1: Cellulose materials studied in TASK 2 "Organic Degradation". *DP_w: degree of polymerization based on weight average molecular weight M_w; CI: crystallinity index; D: polydispersivity = M_w/M_n with M_n the number average molecular weight; G_r: molar fraction of reducing end groups*

Type	Origin	Partner	Degradation process	Physical properties
Cellulosic tissues	Tork Facial Tissues	**[SCK CEN]**	Radiolysis (dry conditions) and hydrolysis of pre-irradiated systems	$DP_w = 1719$ $CI = 0.55$ $D = 4.2$ $G_r = 6.5 \cdot 10^{-4}$
Cellulose power	Aldrich	**[PSI]**	Hydrolysis	$18 - 22\ \mu m$ spheres $DP_w = \sim120^*$
α-ISA lactone	Synthetised as in Glaus *et al.* (1999a)	**[PSI]**	Hydrolysis	

*Glaus and Van Loon (2004)

The composition of the cellulosic tissues (Extra Soft Tork Facial Tissues) studied by **[SCK CEN]** was determined by PTS (Papiertechnische Stiftung, Germany) reported in *Table 2*.

Table 2: Overview of the composition of the cellulosic tissues and the procedures used. The average content is derived from two measurements. The indicated uncertainty has been calculated using the Student's test for 95% confidence.

Component	Average content (wt%)	Procedure
Dry content	95.6 ± 1.9	Using an infrared moisture analysis balance
α-cellulose	88.1 ± 0.6[a]	Adapted from TAPPI standard T203 cm-99 (TAPPI, 2009)
hemicellulose	11.4 ± 0.4[a]	Based on alkaline solubility S_5 (DIN standard 54356) (DIN, 1977)
lignin	0.5 ± 0[a]	TAPPI standard T222 om-21 (TAPPI, 2021)
inorganic additives	0.54 ± 0[a]	ISO standard 1762 (ISO, 2019)

[a] expressed in g per 100 g dry material

Table 3 gives an overview of the sample types used by **[PSI]** for studying the long-term behavior of cellulose under alkaline conditions at room temperature. **[PSI]** also performed experiments of degradation of cellulose in presence of Fe(0). For these experiments, Merck-Aldrich purified microcrystalline cellulose powder, 20 µm spheres (Merck Product-Nr. 310697 was used.

EURAD (Deliverables n° 3.6, 3.7 and 3.8) - Final Report of results generated in CORI
Dissemination level: PU
Date of issue of this report: **05/07/2024**

Page 32

Table 3: Overview of the sample types used for studying the long-term behavior of cellulose under alkaline conditions at room temperature. The samples were mixed at a solid:liquid ratio of 100 g cellulose per L of an artificial cement pore water (ACW-I) containing 0.114 M NaOH, 0.180 M KOH. An excess (10 g/L) of $Ca(OH)_2$ was added to provide the maximum concentration of Ca^{2+} with respect to solubility of portlandite (~2.3 mM) at the pH of ACW-I (13.3).

Series label	Label of last batch	Type of cellulose	DP_v[a]	DP_r[b]
Series A	A15	Aldrich cellulose	117	128 (116, 143)
Series C1	C1.5	Tela tissues	1110	417 (286, 769)
Series C2	C2.5	Cotton	1800	3125 (1613, 49000)
Series C3	C3.5	Recycling paper	290	83 (63, 125)
Series D	D5	Aldrich cellulose[c]	117	128 (116, 143)
Blank	B	None[d]	—	—

[a] Degree of polymerisation determined by viscosimetry as determined from the Cuen method using evaluation parameters from Sihtola *et al.* (1963).

[b] Determined from measurements of the number of reducing end groups, which is the reciprocal value of *DP* (provided that each of cellulose chain contains one reducing end group). The first value in parenthesis gives the lower limit, the second value the upper limit calculated from the overall measurement uncertainties.

[c] Identical composition as series A, with the exception that Fe(II) was added

[d] Containing all components except for cellulose for the determination of background values

2.1.3 Degradation of cellulose and identification of degradation products

2.1.3.1 Gas production

Cellulosic tissues (Tork Facial Tissues) were irradiated to gamma irradiation by **[SCK CEN]** with a total absorbed dose ranging from 10 kGy to ~1.4 MGy. For the systems irradiated with a total absorbed dose of about 50 kGy and 800 kGy, the effect of the dose rate (0.3 vs 0.6 kGy/h) and of the presence of O_2 while irradiating, was studied as well. Gamma irradiation was performed in a gas tight container at the Geuse II facility of SCK CEN (Belgium). More details are provided by Bleyen *et al.* (2023).

After irradiation, the headspace in the container was sampled and analyzed by µGC-TCD (micro gas chromatography with thermal conductivity detector) to determine the radiolytically produced gases. The results of the radiolytic gas production show that H_2, CO and CO_2 are the most important gaseous degradation products after gamma irradiation of cellulosic tissues, although traces of CH_4 were found as well (*Table 4*).

Table 4: Radiolytic gas yield values (including 95% confidence intervals) for gamma irradiation of cellulosic tissues. The indicated uncertainties on the G values represent the 95% confidence interval and take into account the uncertainties on the pressure, gas concentration, weight of tissues and volumetric measurements.

Sample code	Absorbed dose (kGy)	Dose rate (kGy/h)	Irradiation atmosphere	G values (x 10^{-7} moles/J)			
				H_2	CO_2	CO	CH_4
C0	-	-	-	<DL	<DL	<DL	<DL
C1	10 ± 2	0.63 ± 0.14	Ar	2.8 ± 0.7	1.3 ± 0.3	0.3 ± 0.1	<DL
C2	47 ± 11	0.63 ± 0.14	Ar	2.5 ± 0.6	1.1 ± 0.3	0.3 ± 0.1	<DL
C3	47 ± 11	0.63 ± 0.14	Air	2.3 ± 0.6	6.0 ± 1.4	1.4 ± 0.3	0.03 ± 0.02
C4	48 ± 7	0.34 ± 0.05	Ar	2.3 ± 0.4	1.1 ± 0.2	0.22 ± 0.04	<DL

EURAD (Deliverables n° 3.6, 3.7 and 3.8) - Final Report of results generated in CORI
Dissemination level: PU
Date of issue of this report: **05/07/2024**

Page 33

C5	48 ± 7	0.34 ± 0.05	Air	2.3 ± 0.4	6.4 ± 1.0	1.5 ± 0.2	0.03 ± 0.02
C6	180 ± 40	0.69 ± 0.16	Ar	2.0 ± 0.5	1.1 ± 0.2	0.23 ± 0.05	0.007 ± 0.006
C7	352 ± 56	0.67 ± 0.11	Ar	1.8 ± 0.3	1.0 ± 0.2	0.21 ± 0.03	0.004 ± 0.003
C8	760 ± 92	0.62 ± 0.08	Ar	1.6 ± 0.4	1.1 ± 0.4	0.24 ± 0.09	0.003 ± 0.001
C9	760 ± 92	0.62 ± 0.08	Air	1.4 ± 0.2	11.1 ± 3.2	1.9 ± 0.6	0.04 ± 0.01
C10	764 ± 91	0.31 ± 0.04	Ar	1.4 ± 0.2	0.7 ± 0.2	0.15 ± 0.05	0.003 ± 0.001
C11	764 ± 91	0.31 ± 0.04	Air	1.2 ± 0.2	10.6 ± 3.2	1.7 ± 0.5	0.024 ± 0.010
C12	1368 ± 160	0.55 ± 0.06	Ar	1.1 ± 0.2	1.1 ± 0.3	0.10 ± 0.03	0.007 ± 0.002

< DL: below detection limit of the equipment (H_2: 20 ppm, CO_2: 3 ppm, CO: 10 ppm, CH_4: 10 ppm)

Based on the obtained radiolytic production yield or G values, the applied twofold difference in the dose rate during gamma irradiation did not result in a significant difference in the G values for gas production. Either there is no dose rate effect, or it would only be detectable at larger dose rate differences. The presence of oxygen resulted in an increase in the CO and CO_2 production but did not affect the H_2 production. Furthermore, the G_{CO} (though not statistically significant) and the G_{CO2} values increase with absorbed dose during oxic irradiation. In anoxic conditions, the G_{H2} and G_{CO} values decrease with absorbed dose, *i.e.* the gas production slows down when the dose increases, while the CO_2 production increases proportionally with the dose up to ~1.4 MGy.

2.1.3.2 Evolution of the physico-chemical properties of irradiated cellulosic tissues

To assess the evolution of the physico-chemical properties of irradiated cellulosic tissues, several analyses were performed on the gamma-irradiated tissues mentioned in Section 2.1.3.1 and *Table 4*: Scanning electron microscopy (SEM), size exclusion chromatography (SEC) coupled to a multi-angle light-scattering (MALS) detector to assess the molar mass distribution and polymerization degree, and WAXS (Wide-angle X-ray scattering) characterization to determine changes in the degree of crystallinity. Furthermore, a colorimetric bicinchoninic acid (BCA) assay was applied to determine the concentration of reducing (end) groups in the (irradiated) tissues. In this assay, the Cu(II) in the reagent is reduced to Cu(I) by the reducing (end) groups in the tissues at alkaline pH (pH ~10). Subsequently, the reduced Cu(I) is complexed by BCA, resulting in a purple coloration, which absorbs light at 560 nm. A UV-VIS spectrophotometer was used to determine the concentration of BCA-Cu(I), which is correlated to the concentration of reducing groups in the tissues. Finally, the water-soluble fraction of the tissues was determined by preparing suspensions of the tissues in water at a solid/liquid weight ratio 1/80. After 2 hours, the solution was sampled and filtered using a pre-washed Acrodisc syringe filter with a PTFE membrane and a pore size of 0.45 µm. Total dissolved organic carbon (DOC) concentrations were determined using a TOC/TIC analyzer with UV persulfate digestion. More details on the analysis techniques are provided by Bleyen *et al.* (2023).

When comparing the irradiated tissues to the non-irradiated ones, a clear yellow coloration was observed. The tissues had become darker and more brittle with absorbed dose. At 1.4 MGy, they seemed to have lost most of their mechanical strength. However, SEM analyses of non-irradiated and irradiated tissues did not show major differences due to irradiation. Although the tissues irradiated at 1.4 MGy under anoxic conditions contains more broken fibers than the non-irradiated tissues, the difference in the macrostructure is quite limited (*Figure 2-2*).

EURAD (Deliverables n° 3.6, 3.7 and 3.8) - Final Report of results generated in CORI
Dissemination level: PU
Date of issue of this report: **05/07/2024**

Page 34
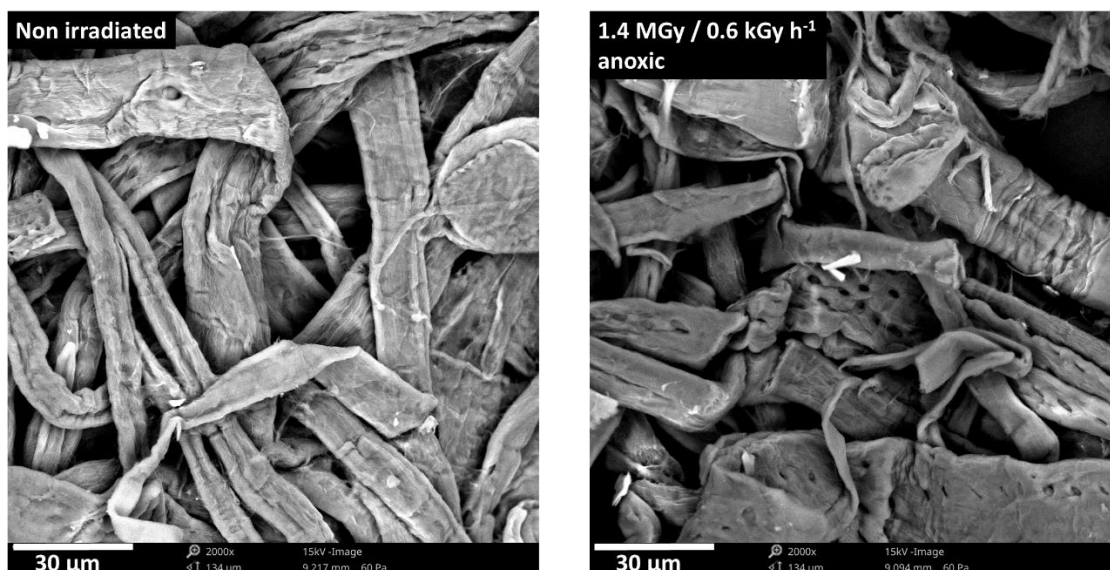
Figure 2-2:   *SEM images for non-irradiated (left) and irradiated (right) cellulosic tissues. Irradiation occurred under anoxic conditions by gamma rays at a dose rate of 0.6 kGy h^{-1} to a total absorbed dose of 1.4 MGy.*

The SEC-MALS (Size Exclusion Chromatography-Multi-Angle Light Scattering) analyses clearly show a shift in the MMD (molar mass distribution) towards smaller sizes with an increasing absorbed dose (*Figure 2-3*), *i.e.* the average molecular weight of the polymers in the tissues decreases with increasing dose. A small (though consistent) impact of the atmospheric conditions during irradiation on the MMD can be observed, *i.e.* for all tissue samples irradiated under oxic conditions (at 0.05 or 0.8 MGy), the relative abundance of the smallest chains is slightly higher.
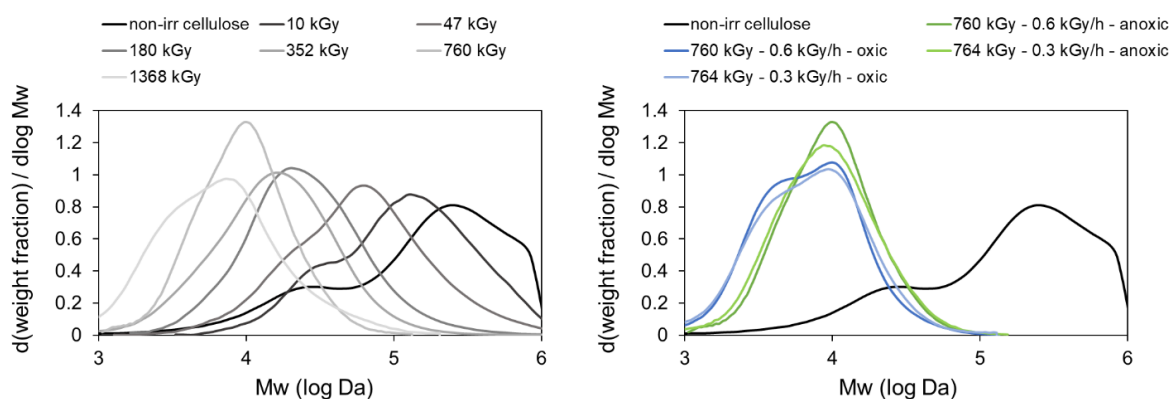
Figure 2-3:   *Evolution of the MMD of cellulosic tissues during gamma irradiation of cellulosic tissues as a function of absorbed dose and applied dose rate, under anoxic and oxic conditions. Left: effect of absorbed dose on the MMD, for tissues irradiated under anoxic conditions and with the highest dose rate (on average 0.6 kGy h^{-1}). Right: effect of dose rate and irradiation atmosphere on the MMD.*

WAXS (Wide-angle X-ray scattering) analyses show a significant decrease of the crystallinity index of cellulose in the tissues during irradiation. Furthermore, neither the dose rate nor the presence of oxygen during irradiation affect the decrease in crystallinity, *i.e.* the crystallinity indices for all samples irradiated at either 0.05, 0.2 or 0.8 MGy, do not differ significantly (*Table 5*).

EURAD (Deliverables n° 3.6, 3.7 and 3.8) - Final Report of results generated in CORI
Dissemination level: PU
Date of issue of this report: **05/07/2024**

Page 35

Table 5: Crystallinity indices (CI) of non-irradiated and irradiated tissues (irradiation conditions indicated in the first 3 columns), as determined by WAXS measurements. The indicated confidence intervals represent the uncertainty on the mean values based on the standard deviation and the t value (significance level α = 0.05).

Sample code	Absorbed dose (kGy)	Dose rate (kGy h^{-1})	Irradiation atmosphere	Number of measurements	CI
C0	-	-	-	5	0.55 ± 0.02
C2	47 ± 11	0.63 ± 0.14	Ar	3	0.53 ± 0.06
C3	47 ± 11	0.63 ± 0.14	Air	3	0.53 ± 0.10
C4	48 ± 7	0.34 ± 0.05	Ar	3	0.56 ± 0.08
C5	48 ± 7	0.34 ± 0.05	Air	3	0.54 ± 0.04
C6	180 ± 40	0.69 ± 0.16	Ar	4	0.54 ± 0.03
C7	352 ± 56	0.67 ± 0.11	Ar	3	0.49 ± 0.09
C8	760 ± 92	0.62 ± 0.08	Ar	3	0.47 ± 0.04
C9	760 ± 92	0.62 ± 0.08	Air	3	0.43 ± 0.04
C10	764 ± 91	0.31 ± 0.04	Ar	3	0.47 ± 0.02
C11	764 ± 91	0.31 ± 0.04	Air	3	0.47 ± 0.08
C12	1368 ± 160	0.55 ± 0.06	Ar	3	0.39 ± 0.02

A clear increase in the concentration of reducing groups measured by BCA assay is observed with increasing dose and this for both irradiation atmospheres ('REGm'; *Table 6*). Significantly higher concentrations of reducing groups are obtained when the tissues were irradiated under oxic conditions compared to anoxic irradiation ('REGm', *Table 6*). These results thus indicate that the presence of oxygen during irradiation results in an increased amount of oxidized functional groups. A comparison between the measured amount of reducing groups and the theoretical number of reducing end groups based on the number-average molecular weight (Mn, derived by SEC-MALS) under the assumption that each polymer contains 1 reducing end group ('REGt', *Table 6*), shows a good agreement between both values for non-irradiated tissues and tissues irradiated under anoxic conditions. This suggests that most of the reducing groups found for non-irradiated tissues and tissues irradiated under anoxic conditions are indeed end groups, likely formed from radiolytic chain scission. On the other hand, for tissues irradiated under oxic conditions, also reducing groups along the polymer backbone are found, presumably formed by additional radio-oxidation (*Table 6*).

Table 6: Reducing (end) group concentrations, as measured by BCA analysis (REGm) or as theoretically calculated based on the number-average molecular weight Mn (and assuming only 1 reducing end group per polymer; REGt). REGad is the difference between REGm and REGt and indicates the concentration of reducing groups in the polymer backbone. The indicated confidence intervals represent the uncertainty on the mean values based on the standard deviation and the t value (n = 2-12 and significance level α = 0.05).

Absorbed dose (kGy)	Dose rate (kGy h^{-1})	Irradiation atmosphere	REGm	REGt	REGad
-	-	-	3.4 ± 0.1	13.6 ± 1.9	-10.2 ± 1.9
10 ± 2	0.63 ± 0.14	Ar	7.9 ± 0.7	16.2 ± 0.6	-8.4 ± 1.0
47 ± 11	0.63 ± 0.14	Ar	23.6 ± 3.1	30.4 ± 3.2	-6.8 ± 4.3
47 ± 11	0.63 ± 0.14	Air	37.4 ± 4.9	35.9 ± 3.4	1.5 ± 5.9
48 ± 7	0.34 ± 0.05	Ar	22.1 ± 1.1	26.1 ± 2.8	-4.0 ± 3.1
48 ± 7	0.34 ± 0.05	Air	38.6 ± 1.8	32.4 ± 3.6	6.1 ± 4.0
172 ± 39	0.65 ± 0.15	Air	112.6 ± 17.0	n.d.	n.d.
180 ± 40	0.69 ± 0.16	Ar	62.2 ± 14.5	60.9 ± 18.3	1.3 ± 23.3
352 ± 56	0.67 ± 0.11	Ar	85.7 ± 30.8	102.4 ± 16.4	-16.7 ± 34.9
760 ± 92	0.62 ± 0.08	Ar	203.9 ± 24.0	135.5 ± 18.3	68.4 ± 30.6

EURAD (Deliverables n° 3.6, 3.7 and 3.8) - Final Report of results generated in CORI
Dissemination level: PU
Date of issue of this report: **05/07/2024**

Page 36

760 ± 92	0.62 ± 0.08	Air	> LOL	238.1 ± 45.0	n.d.
764 ± 91	0.31 ± 0.04	Ar	189.8 ± 9.6	158.0 ± 69.5	31.7 ± 70.2
764 ± 91	0.31 ± 0.04	Air	679.8 ± 55.2	193.6 ± 36.8	486.2 ± 66.3
1368 ± 160	0.55 ± 0.06	Ar	301.3 ± 51.0	266.8 ± 114.7	34.4 ± 125.6

n.d.: not determined

> LOL: higher than the upper limit of linearity of the analysis technique, *i.e.* 735 µmol g^{-1}.

A clear linear relationship can be observed between the released amount of water-soluble DOC and the absorbed dose, *i.e.* the water-soluble fraction of the tissues increases with increasing absorbed dose. Furthermore, irradiation under oxic conditions results in a higher water-soluble organic concentration compared to irradiation under anoxic conditions (*Table 7*).

Table 7: Water-soluble DOC released after 2 hours in water for non-irradiated and irradiated tissues (irradiation conditions indicated in the first 3 columns), expressed in mg C per g tissue and in wt% C. The weight fraction of water-soluble DOC in tissues is estimated based on the amount of cellulose and hemicellulose per g of tissue (Table 2) and assuming that hemicellulose consists of xylose monomers. Note that the amount of lignin was considered negligible (< 1 wt%; Table 2). The indicated confidence intervals represent the combined uncertainty (95% confidence), taking into account the measurement uncertainty of the DOC value, the volume of solution and the weight of the tissue.

Absorbed dose (kGy)	Dose rate (kGy h^{-1})	Irradiation atmosphere	DOC (mg C per g tissue)	Water-soluble fraction (wt% C)
-	**-**	-	1.0 ± 0.3	0.2
47 ± 11	0.63 ± 0.14	Ar	4.6 ± 1.4	1.1
47 ± 11	0.63 ± 0.14	Air	7.0 ± 2.1	1.7
48 ± 7	0.34 ± 0.05	Ar	5.1 ± 1.5	1.2
48 ± 7	0.34 ± 0.05	Air	8.6 ± 2.3	2.0
172 ± 39	0.65 ± 0.15	Air	21.0 ± 6.5	3.5
180 ± 40	0.69 ± 0.16	Ar	14.6 ± 4.1	5.0
760 ± 92	0.62 ± 0.08	Ar	55.6 ± 16.9	13.2
760 ± 92	0.62 ± 0.08	Air	119.2 ± 38.6	28.4
764 ± 91	0.31 ± 0.04	Ar	59.5 ± 18.2	14.2
764 ± 91	0.31 ± 0.04	Air	115.0 ± 32.5	27.4
1368 ± 160	0.55 ± 0.06	Ar	104.1 ± 30.1	24.8

A combination between data on the gas production and on the physico-chemical changes provides sufficient data to build hypotheses on ongoing processes. Firstly, under an anoxic atmosphere, radiation-induced degradation of cellulosic tissues follows the general radiolytic degradation mechanism for polymers, causing mostly production of H_2 and random chain scission by cleavage of the glycosidic bond. To a lesser extent, decomposition of the monomers rings of cellulose and hemicellulose occurs, thereby producing CO and CO_2. Finally, trace amounts of CH_4 are formed during irradiation as well, though with a much lower yield compared to H_2 (3 orders of magnitude lower). The chain scission is accompanied by a decrease in the polymerization degree and at higher doses (≥ 0.8 MGy) and also a decrease in amorphisation of the cellulose microstructure. Some crosslinking may occur, but it seems only to be important at low doses. For each chain scission in cellulose, two polymer chains are generated, predominantly each with a non-reducing and reducing end group, which thereby results in an overall increase in the reducing end group concentration. Formation of reducing groups along the polymer backbones does not occur significantly. Finally, additional chain scission of smaller chains results in an increasing degree of solubilization with an increasing absorbed dose.

EURAD (Deliverables n° 3.6, 3.7 and 3.8) - Final Report of results generated in CORI
Dissemination level: PU
Date of issue of this report: **05/07/2024**

Page 37

When oxygen is present during irradiation, additional oxidation processes occur on top of the degradation processes that take place under anoxic conditions and that are unaffected by the presence of oxygen (*e.g.* chain scission, monomer ring cleavage and H_2 production). This results in a partially oxidized polymer backbone without causing considerably more chain scission or amorphisation. In addition, more water-soluble organic molecules are formed compared to under anoxic conditions. Further radiolytic degradation of the partially oxidized polymer chain and/or smaller organic radiolytic degradation products results in a significant production of additional CO and CO_2. The secondary degradation processes could explain the increase in the G_{CO} and G_{CO2} values with an increased absorbed dose. Under these conditions, cleavage of (partially oxidized) monomers in (hemi)cellulose and of smaller organic compounds becomes more important than radiolytic chain scission and CO_2 is the most dominant radiolytic gaseous end product. In addition, irradiation under oxic conditions also results in a 10-fold increase in the radiolytic yield of CH_4 with the absorbed dose.

2.1.3.3 Alkaline degradation of pre-irradiated tissues

To study the release of organics from non-irradiated and irradiated cellulosic tissues, non-irradiated and irradiated samples were immersed in artificial young cement water (ACW; 0.114 M NaOH, 0.18 M KOH saturated with $Ca(OH)_2$, pH >13 (Glaus and Van Loon, 2008; Van Loon and Glaus, 1998)), with a ratio tissue-to-liquid (TL) of 10 or 1 wt% (*Table 8*). Note that the non-dissolved part of $Ca(OH)_2$ was not removed.

Table 8: Overview of all alkaline degradation tests performed with (non-)irradiated cellulosic tissues. Irradiation occurred as described in Section 2.1.3.1 and Bleyen et al. (2023).

Code test condition	Conditions during pre-irradiation of tissues			Tissue-to-liquid ratio (wt%) during alkaline degradation	Sampling times (days)	Sample codes*
	Absorbed dose (kGy)	Dose rate (kGy/h)	Irradiation atmosphere			
NI_ACW_TL10	-	-	-	10	0.04, 7, 28, 91, 92, 361, 362, 727	Cell_Rx_y
NI_ACW_TL1	-	-	Ar	1	0.04, 7, 91, 92, 361, 727	
C1_ACW	10 ± 2	0.63 ± 0.14	Ar	10	0.04, 91, 92, 361, 727	10_0.8_Ar_Rx_y
C2_ACW_TL10	47 ± 11	0.63 ± 0.14	Ar	10	0.04, 7, 91, 92, 361, 362, 727	50_0.8_Ar_Rx_y
C2_ACW_TL1	47 ± 11	0.63 ± 0.14	Ar	1	0.04	
C3_ACW	47 ± 11	0.63 ± 0.14	Air	10	0.04, 7, 91, 361, 362, 727	50_0.8_O2_Rx_y
C4_ACW	48 ± 7	0.34 ± 0.05	Ar	10	0.04, 362	50_0.4_Ar_Rx_y
C5_ACW	48 ± 7	0.34 ± 0.05	Air	10	0.04, 7, 91, 92, 361, 362, 727	50_0.4_O2_Rx_y
C6_ACW	180 ± 40	0.69 ± 0.16	Ar	10	0.04, 91, 92, 362, 727	200_0.8_Ar_Rx_y
C7_ACW	352 ± 56	0.67 ± 0.11	Ar	10	0.04, 7, 28, 91, 92, 362, 727	400_0.8_Ar_Rx_y
C8_ACW_TL10	760 ± 92	0.62 ± 0.08	Ar	10	0.04, 7, 91, 92, 361, 362, 727	800_0.8_Ar_Rx_y
C8_ACW_TL1	760 ± 92	0.62 ± 0.08	Ar	1	0.04, 939	
C9_ACW	760 ± 92	0.62 ± 0.08	Air	10	0.04, 12, 362, 727	800_0.8_O2_Rx_y

EURAD (Deliverables n° 3.6, 3.7 and 3.8) - Final Report of results generated in CORI
Dissemination level: PU
Date of issue of this report: **05/07/2024**

Page 38

C10_ACW	764 ± 91	0.31 ± 0.04	Ar	10	0.04, 362	800_0.4_Ar_Rx_y
C11_ACW	764 ± 91	0.31 ± 0.04	Air	10	0.04, 12, 362, 727	800_0.4_O2_Rx_y
C12_ACW_TL10	1368 ± 160	0.55 ± 0.06	Ar	10	0.04, 7, 28, 91, 92, 362, 727	1600_0.8_Ar_Rx_y
C12_ACW_TL1	1368 ± 160	0.55 ± 0.06	Ar	1	0.04, 7, 91, 92, 361, 727	

*: The sample codes consists of a reference to the target irradiation conditions, followed by 'Rx' indicating the replicate series number and 'y' as the time of sampling. x=1, 3 for TL 10 wt% and 2,4 for TL 1 wt%, with 1 and 2 being the series which is used for liquid sampling, and 3 and 4 the series with replicates which are sacrificed upon sampling.

Several series of suspensions were prepared for all (non-)irradiated tissues: for liquid sampling or with multiple replicates per test condition, in order to sacrifice one of them at their final sampling time and perform solid-phase analyses. For the first series, only a few mL of suspension was sampled at each sampling time. Sampling was performed after ~2 hours, after 1 week, 1 month, 3 months, 1 year, 2 years and 2.5 years (*Table 8*). For each sampling, the suspensions were filtered using a PTFE filter (0.45 µm pore size) inside a MILLICUP-FLEX™ filtration system (Merck Life Science) or in a syringe filtration system (Acrodisc One PSF wwPTFE membrane filter). Afterwards, DOC (dissolved organic carbon) and ISA concentrations were determined, with a TOC/TIC analyzer with a high temperature combustion technique, and with IC-PAD (ion chromatography equipped with a CarboPac PA1 anion-exchange column and a pulsed amperometric detector), respectively. The analysis method used in IC-PAD allows discriminating and quantifying the two ISA isomers (α and β). pH measurements were performed regularly. Furthermore, additional analyses were performed on some of the samples, in order to identify degradation products other than ISA: Ion chromatography (IC), size exclusion chromatography using a Superdex 200 10/300 GL column and a photodiode array detector and ESI-ToF-MS (electrospray ionization coupled to ultra-high resolution quadrupole Time-of-Flight mass spectrometry). More details are provided by Nushi et al (2023).

To assess the evolution of the physico-chemical properties of the cellulose in the tissues during alkaline degradation, the solid phase sampled when sacrificing certain test suspensions was neutralized, washed and dried. Afterwards, SEM, WAXS and SEC-MALS analyses were performed, in comparison to the analyses performed after irradiation (see Section 2.1.3.2).

2.1.3.3.1 Long-term DOC and ISA production

The results show a clear increase of the DOC and ISA concentrations for all test cases with time (Figure 2-4). In addition, for each sampling time, the DOC and ISA concentrations increased with increasing absorbed dose. After 2 years, ISA makes up ~30% of the DOC concentration in the solution with non-irradiated cellulose. For the tissues irradiated at higher doses (≥ 800 kGy, under anoxic conditions), the percentage of ISA is higher (up to ~45 to 55% after 2 years). More or less equal amounts of alpha and beta ISA are produced by cellulosic tissues under all test conditions, based on the IC-PAD analyses (average alpha/beta ratio = 0.98).

An effect of oxygen during irradiation on the ISA production is observed only for tissues irradiated at 50 kGy, *i.e.* a higher DOC and ISA production and relatively more ISA is produced after irradiation under oxic conditions. This effect is not observed at higher doses, though this may be related to the observed pH decrease (down to pH ~11 within 2 years) for tissues irradiated under oxic conditions at 0.8 MGy in ACW (*Figure 2-5*). In all other suspensions, the pH remained around pH 13, though a slight decrease is observed as well, especially for suspensions with tissues irradiated at high doses (*Figure 2-5*). This small pH decrease can be attributed to the fast peeling reaction observed in these tests, which results in the

EURAD (Deliverables n° 3.6, 3.7 and 3.8) - Final Report of results generated in CORI
Dissemination level: PU
Date of issue of this report: **05/07/2024**

Page 39

production of ISA and protons. However, the stronger pH decrease (down to pH ~11 in 2 years) in suspensions with tissues irradiated under oxic conditions (and especially at the highest absorbed dose) cannot be explained by the produced amount of ISA, but may be attributed to the radiolytic oxidation of the cellulose, *i.e.* production of carboxyl and carbonyl functional groups along the backbone structure, as discussed in Section 2.1.3.2.
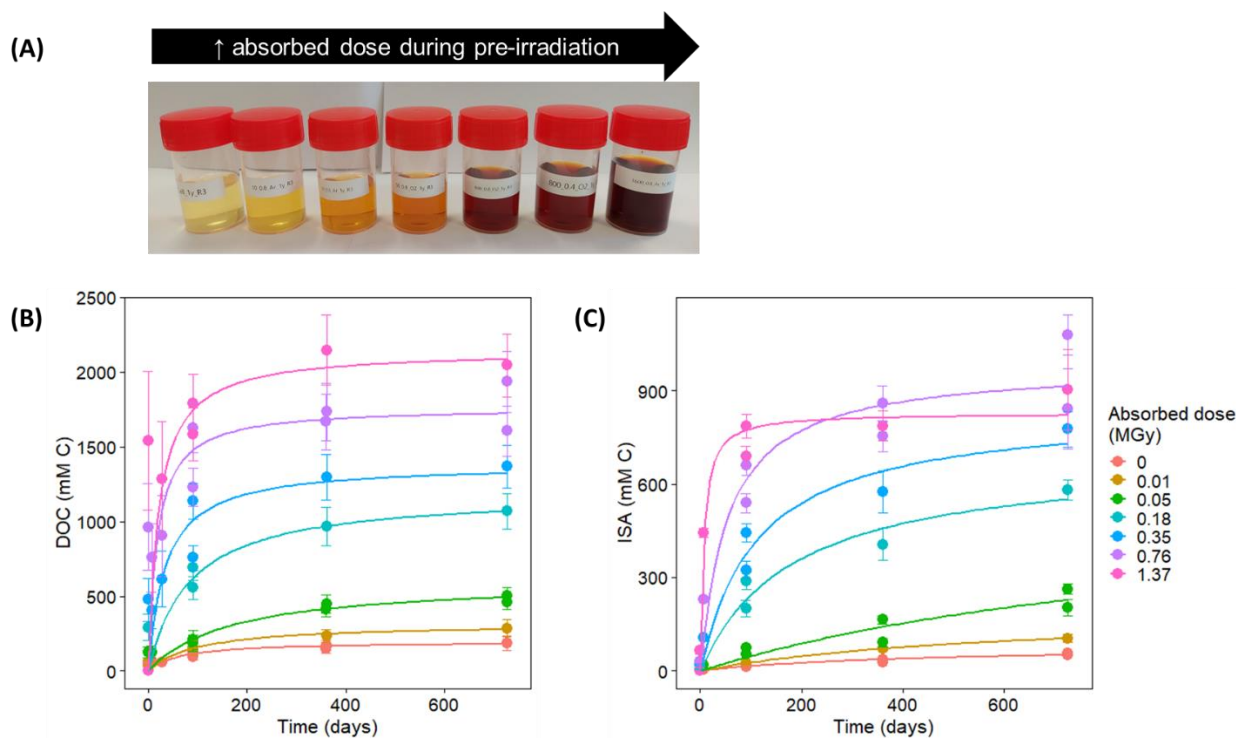
Figure 2-4: *A: Sampled solutions from suspensions of (non-)irradiated tissues in ACW, with an absorbed dose during pre-irradiation increasing from left to right. B,C: Evolution of DOC (B) and ISA (C) concentrations as a function of time, in suspensions of (non-) irradiated cellulose in ACW (TL = 10 wt%). Pre-irradiation was performed under anoxic conditions at different absorbed doses (see legend) and at a dose rate of ~0.6 kGy/h (see Table 8). The error bars represent the measurement uncertainty for a 95% confidence interval.*
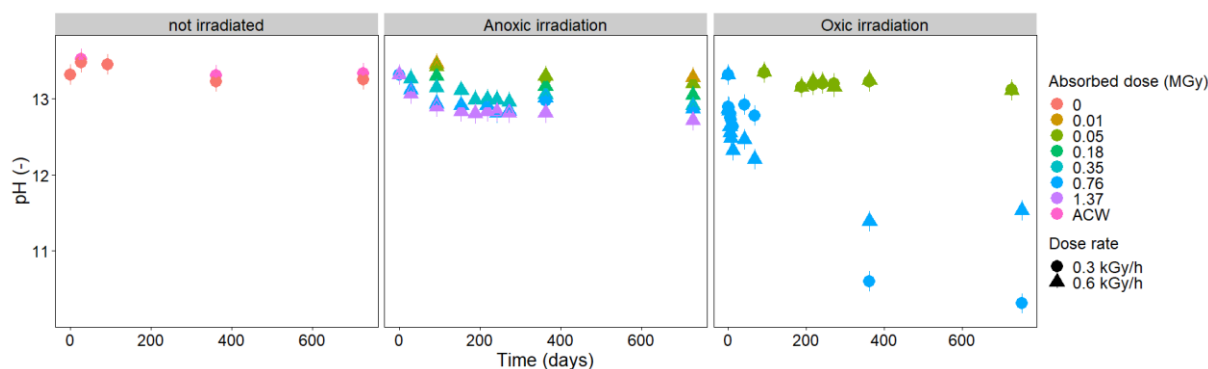
Figure 2-5: *pH evolution in suspensions of (non-)irradiated tissues in ACW (TL = 10 wt%) as a function of absorbed dose and the average dose rate during pre-irradiation, as indicated in the legend. The measurement uncertainty was estimated to be 0.1 and is represented by the error bars. Note that the results for suspensions with cellulosic tissues pre-irradiated at 0.8 MGy under oxic conditions during the first weeks of degradations were obtained in an additional small-scale study, specifically started in 2023 to follow-up the initial pH decrease.*

EURAD (Deliverables n° 3.6, 3.7 and 3.8) - Final Report of results generated in CORI
Dissemination level: PU
Date of issue of this report: **05/07/2024**

Page 40

Over time, the Ca concentration in the solutions has been increasing. Higher Ca concentrations were measured in solutions with higher ISA concentrations as shown in *Figure 2-6*. In the past few months, additional modelling was performed to assess a possible precipitation of $Ca(ISA)_2$ complexes. Given the highly alkaline environment and the fact that the Ca concentrations increase above the solubility limit of $Ca(ISA)_2$, significant precipitation of $Ca(ISA)_2$ is not expected. This is in agreement with the observations of Glaus and Van Loon (2008), who assessed the potential formation of Ca-ISA precipitates in the suspensions of pure cellulose powder in ACW after 4 and 12 years of degradation. In none of the samples, the amount of α-ISA that could be extracted from the solid phase by washing it in water, exceeded 1% of the total ISA concentration. This indicates that under the test conditions applied by Glaus *et al.* (2008), which are also applied in our work, Ca-ISA precipitates are not significantly formed.
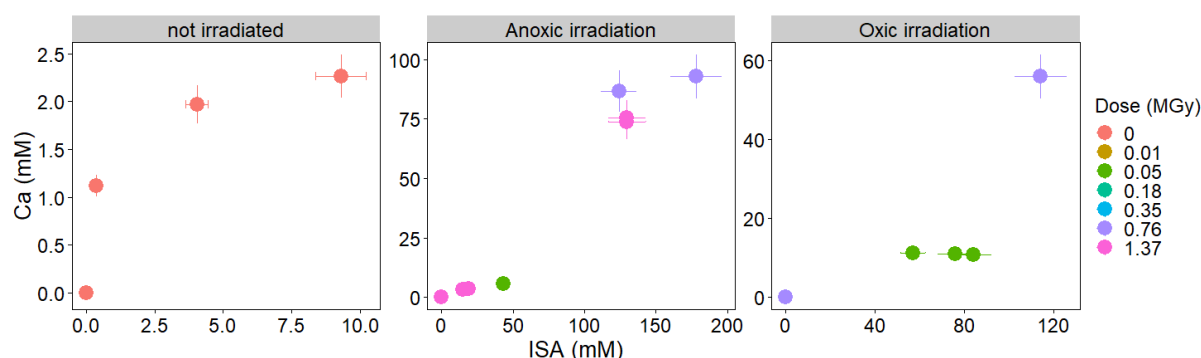
Figure 2-6:   *Calcium concentrations as a function of time, as measured in filtered solution from suspensions of (non-)irradiated tissues in ACW (irradiation conditions indicated on top of each graph and in the legend). The error bars represent the measurement uncertainty for a 95% confidence interval.*

The model developed and described by Glaus & Van Loon (2008) was used to fit the data from this hydrolytic degradation study (Figure 4). This model includes the rate constants of the peeling (k_1), stopping (k_t) and possible mid-chain scission (k_h) reactions to explain the production of ISA and DOC and takes into account the initial reducing end group concentration (measured by colorimetric bicinchoninic acid analysis (BCA)) of the cellulosic material [or $(G_r)_0$], according to Equation 1:

$$(celdeg)_t = 1 + e^{-k_h t}\left[\frac{k_1}{k_t}(G_r)_0(1 - e^{-k_t t}) - 1\right]$$

Equation 1

with $(celdeg)_t$ being the extent of cellulose degradation at time t, which can be derived from the measured ISA concentrations (or $[ISA]_t$) using Equation 2:

$$[ISA]_t = f_{ISA}(celdeg)_t = \frac{1000\ W_{cel}}{Mw\ V}(celdeg)_t$$

Equation 2

with f_{ISA} being a conversion factor from mole fraction to molar concentration, W_{cel} the weight of cellulose in the tissue suspensions (*i.e.* 88.1% of the dry weight of the tissues), Mw the molecular weight of the monomeric unit in cellulose (*i.e.* 162 g mol^{-1}) and V the volume of solution (Van Loon and Glaus, 1998).

Combining *Equations 1* and *2* results in Equation 3, which is used to fit the reaction rate constants based on the ISA concentrations measured in the solutions:

EURAD (Deliverables n° 3.6, 3.7 and 3.8) - Final Report of results generated in CORI
Dissemination level: PU
Date of issue of this report: **05/07/2024**

Page 41

$$[ISA]_t = \frac{1000 \, W_{cel}}{Mw \, V} \left[1 + e^{-k_h t} \left[\frac{k_1}{k_t} (G_r)_0 (1 - e^{-k_t t}) - 1 \right] \right] \qquad \text{Equation 3}$$

Best-fit first-order reaction rate constants (values not shown) were obtained using a non-linear regression (nls) function following Equation 3 in R. Up to now, only data from suspensions with anoxically irradiated tissues were fitted. Figure 2-7 shows that the data can be fitted using this model, suggesting that pre-irradiation does not affect the ongoing reactions, but rather their reaction rates.
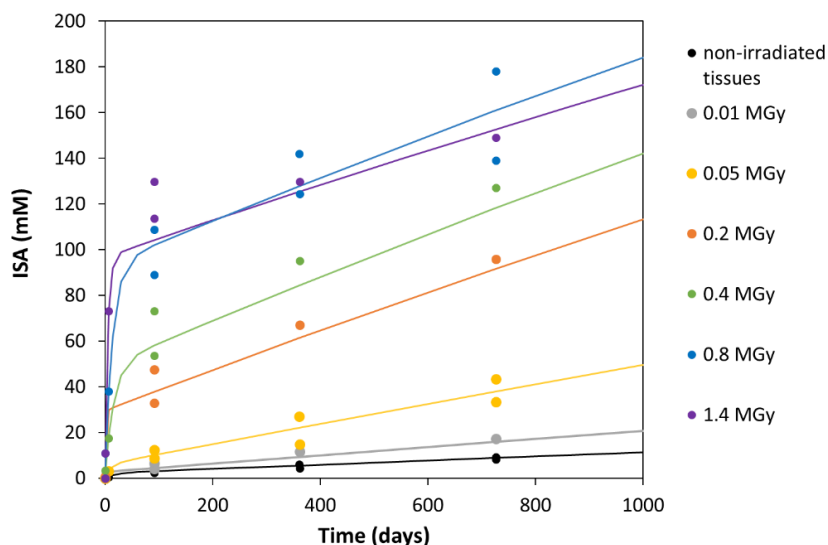
Figure 2-7:   *Fitting of the produced ISA evolution for suspensions of gamma irradiated tissues in ACW, using the model described by Glaus et al. (2008). Pre-irradiation was performed under anoxic conditions at different absorbed doses (see legend) and at a dose rate of ~0.6 kGy h^{-1} (see Table 4).*

2.1.3.3.2 Identification of degradation products

Although for pure cellulose, ~80 to 90% of the released organic compounds is ISA (Glaus and Van Loon, 2008), ISA only made up to ~30 to 60% of the dissolved organic carbon after 2 years of alkaline degradation of irradiated cellulosic tissues (see Section 2.1.3.3.1). Ion chromatography was performed to assess the concentrations of small organic acids in the degradation solutions sampled after 1 year (see Table 9). These results indicate that lactic and formic acid are produced in significant concentrations as well, mostly making up 1 to 3% of the DOC concentration. Also glycolic acid and acetic acid were found, though at lower concentrations and not in the suspensions with non-irradiated samples. The concentrations of these organic acids (formic, acetic, glycolic and lactic acid) increase with an increasing absorbed dose during pre-irradiation and even more in suspensions with tissues irradiated in an oxic environment. The concentrations of valeric, butyric and malonic acid were below the detection limit, while the concentrations of oxalic and propionic acid were always low (≤ 0.3% of the DOC), suggesting that these organics were not major degradation products of (irradiated) cellulosic tissues.

Additionally, a more detailed ESI-ToF MS molar mass distribution study has been performed to screen the solutions for differences in degradation products linked to certain test conditions (absorbed dose or presence of oxygen during pre-irradiation) (Nushi et al., 2023). Similar to the ion chromatography

EURAD (Deliverables n° 3.6, 3.7 and 3.8) - Final Report of results generated in CORI
Dissemination level: PU
Date of issue of this report: **05/07/2024**

Page 42

results, the MS analysis suggests that the main degradation compounds from alkaline degradation of cellulosic tissues is ISA. Although this technique cannot be used for quantitative analyses in complex organic mixtures, an increase in intensity of the base peak of ISA (at m/z 179) can be found for solutions with an increasing ISA concentration (*i.e.* suspensions with tissues irradiated at a high absorbed dose and/or irradiated under oxic conditions). Furthermore, based on the MS spectra and literature data, xylo-isosaccharinic acid (XISA) was suggested as a major degradation product of cellulosic tissues as well. It is likely formed during alkaline degradation of hemicellulose, using the same reaction mechanism as the production of ISA from cellulose. It also behaves in a similar way as ISA, *i.e.* increasing intensity of its main MS peak with time and for suspensions with tissues irradiated at an increasing absorbed dose. However, for tissues irradiated at a dose higher than 0.2 MGy, no difference in intensity of the XISA peaks could be found, neither with increasing dose nor with hydrolysis time. Finally, lactic acid can be detected in all alkaline degradation solutions as well.

To gain further insights, ESI-ToF MS was used to study the organics formed in aqueous leachates of irradiated cellulosic tissues to observe the compounds formed solely as a result of irradiation. Analysis of highly irradiated samples revealed the presence of sugars and oligosaccharides such as glucose, cellobiose, cellotriose, cellotetraose, and cellopentaose. Note that the presence of such oligomers was not observed in the ACW solutions with (irradiated) cellulosic tissues. Either they are not present in significant amounts or the low-molecular-weight organics produced during alkaline degradation of cellulose are preferentially ionised over the oligomers.

Finally, size exclusion chromatography was performed on one of the degradation solutions sampled after 1 year of hydrolysis ("C10_ACW" of Table 9), to investigate the presence of oligosaccharides in the degradation solutions. Based on this first analysis, oligosaccharides (or other organic molecules with molecular weights up to 3500 Da) seem to be present in the degradation solution as well. If so, these compounds may make up a significant part of the DOC fraction as well, which was not yet identified by ion chromatography or ESI-MS. However, additional analyses are required to investigate this in detail.

EURAD (Deliverables n° 3.6, 3.7 and 3.8) - Final Report of results generated in CORI
Dissemination level: PU
Date of issue of this report: **05/07/2024**

Page 43

Table 9: Concentrations of ISA and other organic acids measured by ion chromatography in degradation solutions sampled after 1 year (test codes according to Table 8; tissue codes according to Table 4). The total ISA concentration is the sum of the measured alpha and beta ISA concentrations measured by IC-PAD. All other carboxylic acids were measured by ion chromatography. The relative concentrations of each organic acid compared to the total DOC are provided in between brackets.

Test code	Sample code	DOC (mM C)	ISA (mM)	Formic acid (mM)	Oxalic acid (mM)	Acetic acid (mM)	Valeric acid (mM)	Malonic acid (mM)	Propionic acid (mM)	Glycolic acid (mM)	Butyric acid (mM)	Lactic acid (mM)
NI_ACW_TL10	Cell_R3_1y	167 ± 33	4.4 ± 0.4 (16%)	<0.7	<0.8	<1.0	<0.5	<0.2	<0.2	<0.3	<0.9	0.8 ± 0.08 (1%)
C2_ACW_TL10	50_0.8_Ar_R3_1y	442 ± 58	14.9 ± 2.2 (20%)	6.2 ± 0.2 (1%)	0.6 ± 0.10 (0.3%)	n.a.	n.a.	n.a.	n.a.	n.a.	n.a.	n.a.
C3_ACW	50_0.8_O2_R3_1y	750 ± 108	54.7 ± 3.8 (44%)	12.3 ± 0.2 (2%)	0.5 ± 0.04 (0.1%)	n.a.	n.a.	n.a.	n.a.	n.a.	n.a.	n.a.
C5_ACW	50_0.4_O2_R3_1y	775 ± 108	57.0 ± 4.7 (44%)	12.1 ± 0.2 (2%)	0.6 ± 0.10 (0.2%)	n.a.	n.a.	n.a.	n.a.	n.a.	n.a.	n.a.
C8_ACW_TL10	800_0.8_Ar_R3_1y	1717 ± 192	124.3 ± 7.9 (43%)	24.9 ± 2.5 (1%)	<0.8	2.9 ± 0.3 (0.3%)	<0.5	<0.2	0.19 ± 0.02 (0.03%)	2.1 ± 0.2 (0.2%)	<0.9	8.7 ± 0.9 (2%)
C9_ACW	800_0.8_O2_R3_1y	2075 ± 217	114.0 ± 9.2 (33%)	58.0 ± 5.8 (3%)	<0.8	5.5 ± 0.6 (0.5%)	<0.5	<0.2	0.29 ± 0.03 (0.04%)	7.2 ± 0.7 (0.7%)	<0.9	12.2 ± 1.2 (2%)
C10_ACW	800_0.4_Ar_R3_1y	1767 ± 200	131.0 ± 9.2 (44%)	n.a.	n.a.	n.a.	n.a.	n.a.	n.a.	n.a.	n.a.	n.a.
C11_ACW	800_0.4_O2_R3_1y	2050 ± 217	145.0 ± 16.6 (42%)	47.2 ± 0.6 (2%)	<0.3	n.a.	n.a.	n.a.	n.a.	n.a.	n.a.	n.a.
C12_ACW_TL10	1600_0.8_Ar_R3_1y	2125 ± 233	129.8 ± 7.9 (37%)	33.6 ± 3.4 (2%)	<0.8	3.3 ± 0.3 (0.3%)	<0.5	<0.2	0.28 ± 0.03 (0.04%)	2.8 ± 0.3 (0.3%)	<0.9	10.4 ± 1.0 (1%)

n.a.: not analyzed; * not measurable due to presence of multiple peaks

EURAD (Deliverables n° 3.6, 3.7 and 3.8) - Final Report of results generated in CORI
Dissemination level: PU
Date of issue of this report: **05/07/2024**

Page 44

2.1.3.3.3 Evolution of the physico-chemical properties of cellulose during alkaline degradation

SEM analyses showed no significant degradation of the fiber structure in the non-irradiated tissues after 1 year of hydrolysis. On the other hand, for tissues pre-irradiated at ~1.4 MGy (under anoxic conditions; C12 in *Table 4*), 1 year in ACW resulted in a severe reduction of the fiber structure. This seems to be in line with the preliminary results of the WAXS analysis (*Figure 2-8*), *i.e.* alkaline degradation results in a decrease of the crystallinity of the cellulose in tissues irradiated at 1.4 MGy under anoxic conditions. However, note that only one measurement was performed, and further analyses are needed to determine the variability of the results and draw conclusions. Furthermore, a clear conversion of the natural cellulose I to the cellulose II polymorph was noticed in the WAXS patterns for tissues pre-irradiated at high absorbed doses (*Figure 2-9*). Such a conversion occurs normally when treating natural cellulose fibers with highly concentrated NaOH solutions to increase *e.g.* its dye-ability. Since cellulose II is supposed to have a more open crystal structure, its reducing end groups may be more accessible. This it may therefore also explain the degradation rates of the tissues pre-irradiated at high absorbed doses in ACW.
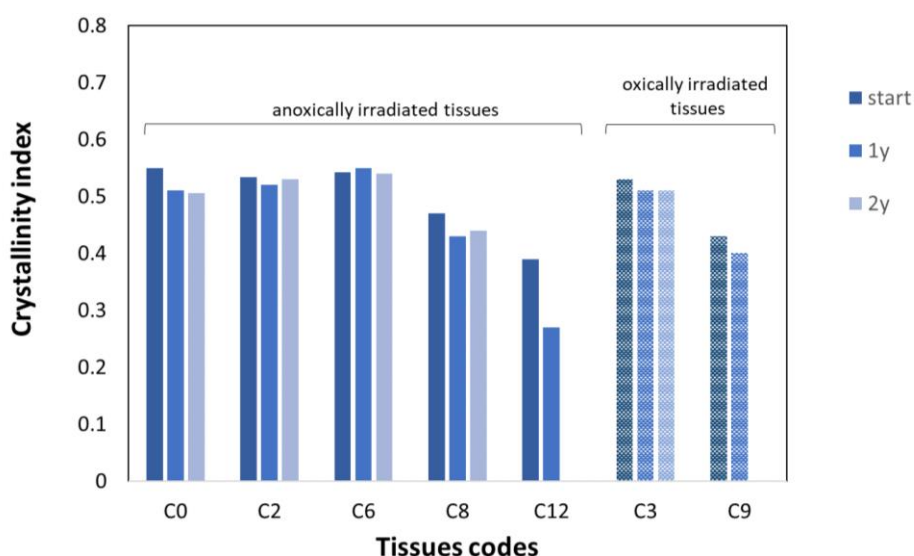
Figure 2-8:   *Crystallinity index of cellulose in tissues after gamma-irradiation, before hydrolysis ("start"), after 1 year of hydrolysis ("1y") and after 2 years of hydrolysis ("2y") in ACW (TL = 10 wt%). Note that only 1 measurement was performed per sampling period, and more measurements are needed to determine the variability of the results. The codes of the tissues in the X-axis correspond to the is correspond to the is correspond to the irradiation codes in Table 4.*

EURAD (Deliverables n° 3.6, 3.7 and 3.8) - Final Report of results generated in CORI
Dissemination level: PU
Date of issue of this report: **05/07/2024**

Page 45
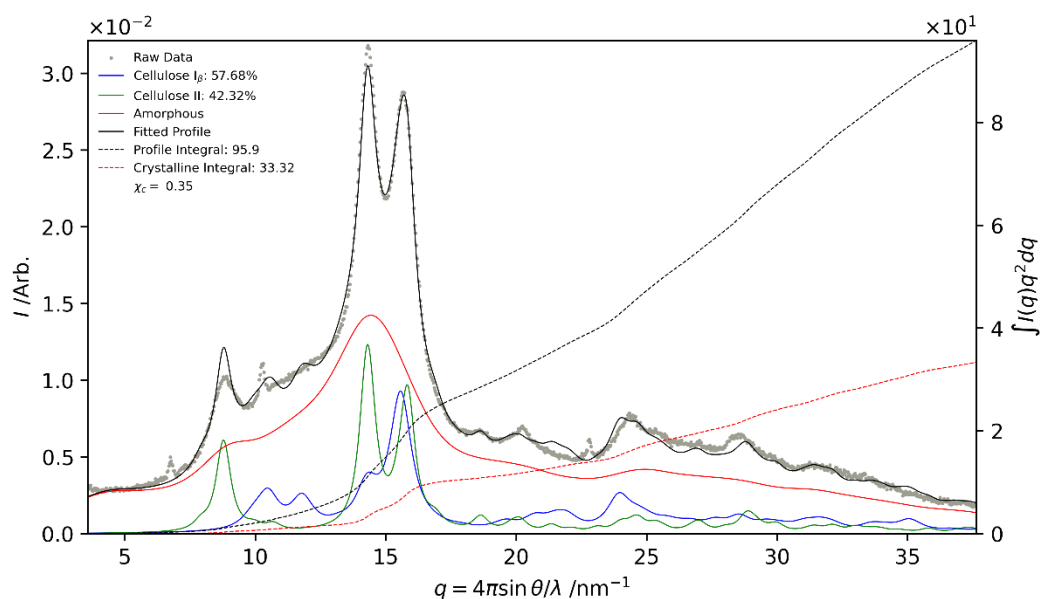
Figure 2-9:   *WAXS diffraction pattern of the cellulose in the solid phase of C12_ACW_TL10 after 1 year in ACW, including peak deconvolution for cellulose I (blue), cellulose II (green) and an amorphous fraction (red).*

Furthermore, SEC-MALS analyses show a shift of the molar mass distribution of all tissues in ACW in function of time. A larger shift towards smaller molecules is found for the tissues pre-irradiated at the highest absorbed doses (*Figure 2-10*). Furthermore, when the irradiation occurred under oxic conditions, the shift is also more extensive compared to irradiation (at the same dose) under anoxic conditions. Nevertheless, overall, the shifts remain rather small, which is in line with the peeling reaction being the most dominant reaction during alkaline degradation of cellulose.

EURAD (Deliverables n° 3.6, 3.7 and 3.8) - Final Report of results generated in CORI   Page 46
Dissemination level: PU
Date of issue of this report: **05/07/2024**
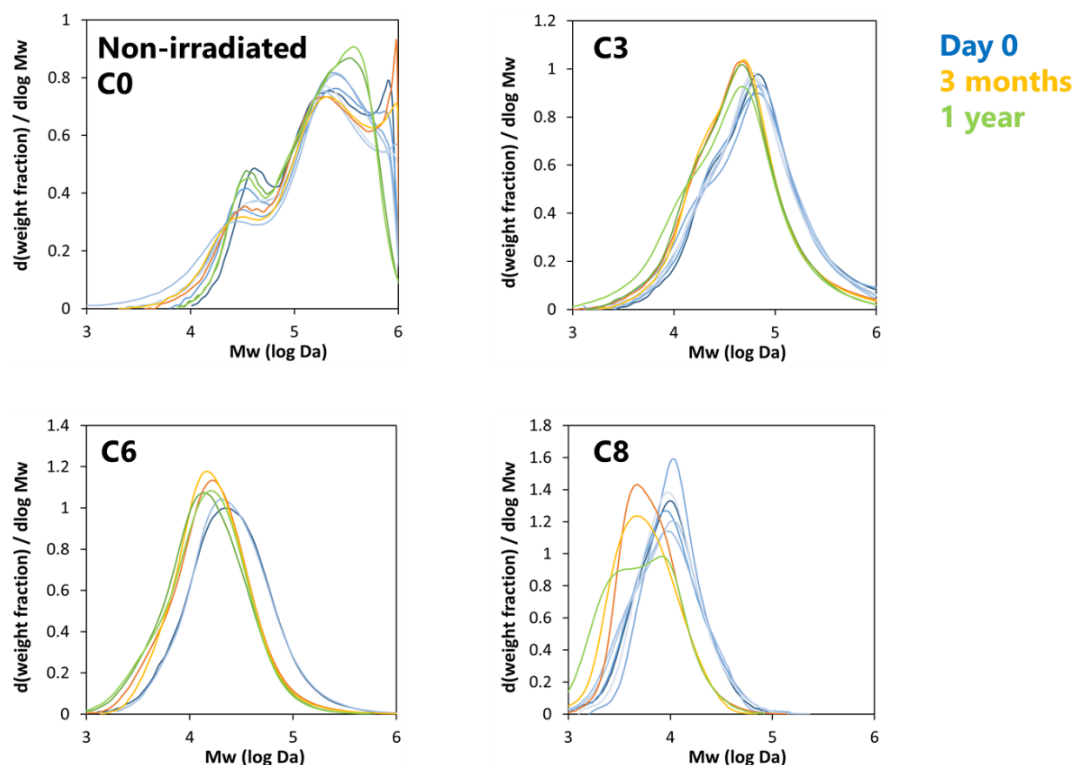
Figure 2-10:   *MMD profiles for non-irradiated and irradiated cellulosic tissues before (blue curves) and after contact with ACW (TL = 10 wt%) for 3 months (yellow curves) or 1 year (green curves). The tissue codes are indicated in the graph and refer to Tables 4 and 8.*

2.1.3.4 Long-term alkaline degradation of cellulose

2.1.3.4.1 Long-term DOC, ISA production and other degradation products

[PSI] performed recent sampling campaigns in the long-term experiments of anaerobic alkaline hydrolysis of cellulose at ambient temperature (22 ±2°C) that has been running for 28 years. These sampling campaigns were carried out after 19.2, 21.0 and 28 years of degradation in order to confirm the results previously made and to be able to unambiguously verify the potential further degradation also in the Aldrich cellulose sample. The preparation of the degradation samples and the monitoring of the concentration of various soluble degradation products and their influence on radionuclide sorption during the first 3 years of degradation has been described in a **[PSI]** report (Van Loon and Glaus, 1998).

The analytical results are summarised in *Table 10* for the sampling campaign after ~21 years and in *Table 11* for the one after ~28 years. The raw data were divided by correction factors (F_{evap}) where necessary in order to take into account the volume reduction caused by water evaporation.

EURAD (Deliverables n° 3.6, 3.7 and 3.8) - Final Report of results generated in CORI
Dissemination level: PU
Date of issue of this report: **05/07/2024**

Page 47

Table 10: Overview of analyses of cellulose degradation suspensions in artificial cement pore water (ACW-I) after degradation time ~21 years. Shown are the average values from four independent samples, except for the analysis of ISA where only the results of a single sample is given. The results of the other replicate samples were neglected owing to excessive instabilities of the signal drift. All results are corrected for the estimated evaporation of water (cf. the text), with the exception of those of Na^+, K^+ and Ca^{2+} which are uncorrected raw data.

Sample [a]	Time (days)	pH	F_{evap}	a-ISA (mM)	b-ISA (mM)	ISA [b] (mM)	LMW-CA [b,c] (mM C)	DOC$_{ident}$ [b,d] (mM C)	DOC [e] (mM C)	Na^+ (mM)	K^+ (mM)	Ca^{2+} (mM)
A15_5	7678	12.96	1.00	82.4	74.0	156 (82%)	32.8 (3%)	971 (85%)	1140	111	181	61
D_5	7678	12.95	1.00	81.9	73.9	156 (80%)	31.4 (3%)	966 (83%)	1171	108	179	65
C1.5_5	7677	13.18	1.07	14.9	13.5	28.4 (75%)	10.1 (4%)	181 (80%)	226	124	189	6.3
C2.5_5	7677	13.22	1.00	2.5	2.7	5.2 (60)	3.3 (6%)	34.5 (66%)	53.0	115	176	3.0
C3.5_5	7677	13.12	1.00	16.7	17.5	34.2 (61%)	33.2 (10%)	238 (71%)	336	114	177	12.1
A2 filtrate	7608 [f]	13.22	1.13	11.6	11.1	22.7 (84%%)	4.4 (3%)	141 (87%)	162	132	199	5.6
A6 filtrate	749 [f]	13.09	1.07	53.8	50.0	104 (81)	19.8 (3%)	643 (83%)	770	122	193	20
A9 filtrate	7301 [f]	12.99	1.15	70.6	61.8	132 (81%)	28.3 (3%)	823 (84%)	982	131	205	38
Blank	7678	n.d.		n.d.	n.d.	n.d.	0.2	0.2	1.2	122	190	2.0

[a] A.i: Purified cellulose (Aldrich); C1.i: Tela tissues; C2.i: Cotton; C3.i: Recycling paper; the filtrates of samples A2, A6 and A9 (Aldrich cellulose) were stored to investigate the stability of the compounds. All experiments were carried out at 100 g dm^{-3} cellulose. [b] Values in parentheses represent the fraction (%) of DOC$_{ident}$ related to the measured DOC values given in the next column. [c] Sum of identified carboxylic acids (viz. formic, acetic, glycolic, lactic acid. Succinic, oxalic and fumaric acid were also analysed but only detected in negligible amounts compared to the previous acids. [d] Sum of ISA+LMW-CA. [e] After correction for the initially extractable organic carbon (16, 70, 4, 200 mM C, cf. Glaus and Van Loon (2008)). [f] Time elapsed since filtration of the samples

EURAD (Deliverables n° 3.6, 3.7 and 3.8) - Final Report of results generated in CORI
Dissemination level: PU
Date of issue of this report: **05/07/2024**

Page 48

Table 11: Overview of analyses of cellulose degradation suspensions in artificial cement pore water (ACW-I) after degradation time ~28 years. Shown are the average values from three independent samples. All results are corrected for the estimated evaporation of water (cf. the text), with the exception of those of Na^+, K^+ and Ca^{2+} which are uncorrected raw data.

Sample [a]	Time (days)	pH	F_{evap}	a-ISA (mM)	b-ISA (mM)	ISA[b] (mM)	LMW-CA [b,c] (mM C)	DOC$_{ident}$ [b,d] (mM C)	DOC [e] (mM C)	Na^+ (mM)	K^+ (mM)	Ca^{2+} (mM)
A15_5	10302	12.95	1.0	79.5	85.4	165 (85%)	29 (3%)	1018 (87%)	1166	113	174	63
C1.5_5	10301	13.16	1.13	14.2	15.4	29.6 (64%)	9.6 (4%)	187 (68%)	276	125	187	7.2
C2.5_5	10301	13.15	1.0	2.8	3.2	6.0 (69)	2.7 (4%)	38.1 (73%)	61.0	114	173	2.9
C3.5_5	10301	12.96	1.0	17.2	20.4	37.6 (68%)	29 (9%)	238 (71%)	328	116	175	13.0
Blank	10302	n.d.	n.d.	n.d.	n.d.	n.d.	0.2	0.2	4.3	120	187	1.6

[a] A.i: Purified cellulose (Aldrich); C1.i: Tela tissues; C2.i: Cotton; C3.i: Recycling paper; the filtrates of samples A2, A6 and A9 (Aldrich cellulose) were stored to investigate the stability of the compounds. All experiments were carried out at 100 g dm^{-3} cellulose. [b] Values in parentheses represent the fraction (%) of DOC$_{ident}$ related to the measured DOC values given in the next column. [c] Sum of identified carboxylic acids (viz. formic, acetic, glycolic, lactic acid. Succinic, oxalic and fumaric acid were also analysed but only detected in negligible amounts compared to the previous acids. [d] Sum of ISA+LMW-CA. [e] After correction for the initially extractable organic carbon (16, 70, 4, 200 mM C, cf. Glaus and Van Loon (2008)). [f] Time elapsed since filtration of the samples

EURAD (Deliverables n° 3.6, 3.7 and 3.8) - Final Report of results generated in CORI
Dissemination level: PU
Date of issue of this report: **05/07/2024**

Page 49

The evolution of the concentration of ISA (sum of α-ISA and β-ISA) and the concentration of DOC is shown in (*Figure 2-11*). As can be seen from these plots, the progressive trend of a slow continuation of cellulose degradation remained similar as observed after 12 years of degradation (Glaus and Van Loon, 2008). For illustration purposes, the model curves are based on the assumption of complete dominance of the peeling-off process as hypothesised in previous work (Van Loon *et al.*, 1999), in order to emphasise the significance of the slow continuation of cellulose degradation compared to the level of cellulose degraded after ~3 years. The increase of DOC after this first phase of reaction is of rather similar magnitude in all samples. On a relative scale, the effect of the slow cellulose degradation is therefore largest for cotton. In the case of Aldrich cellulose, the potential increase of these concentrations cannot be discriminated unequivocally from the experimental uncertainties. Despite the broader scope of low-molecular weight carboxylate analytes in the present analysis compared to previous sampling campaigns (Glaus & Van Loon, 2008; Glaus *et al.*, 1999), substantial parts (~10 – 30%) of the organic matter produced from the alkaline degradation of cellulose remained unidentified. No conclusions can be drawn regarding the chemical nature of the unidentified degradation products. The observation that the fraction of ISA relative to the measured DOC remained almost constant along the entire observation phase, suggests that the primary and secondary phases of reaction produce rather the same product mixtures. The hypothesis that a slow secondary peeling-off process proceeds in the secondary degradation phase (Glaus & Van Loon, 2008), was therefore confirmed by the new experimental data.

Figure 2-12 shows the extent of cellulose degradation calculated from the measured ISA concentrations (cf. *Figure 2-11*). The model curves are based on a formal description of the co-action of the peeling-off process and the midchain scission reaction (Van Loon and Glaus, 1998), in which the time scales for the two degradation mechanisms are well separated. Alternatively, this behavior may be explained by a secondary slow peeling-off process, in which reducing end groups become available for peeling-off presumably by a slow conversion of crystalline to amorphous domains (Glaus and Van Loon, 2008). According to the previous (Glaus and Van Loon, 2008) and the present observations (t > 12 years), this reaction phase is characterized by a zero-order kinetics during which the amount of reduced end groups remains constant. The law of reaction proposed in Glaus and Van Loon (2008) for the slow secondary peeling-off process cannot be distinguished formally from the combination of the fast peeling-off process and the alkaline midchain scission during the experimental phase of observation. During that phase, both reaction schemes are equivalent. For simplicity – and in agreement with the evaluation done in Glaus and Van Loon (2008) – the latter reaction scheme is applied here for data evaluation according to the Equation 1 (Section 2.1.3.3.1). The plots show the predictions made on the basis of the parameter values proposed by Pavasars *et al.* (2003) and the best-fit parameter values obtained from all data available up to degradation times of ~28 years. The latter values are summarised in *Table 12*. As can be seen from this comparison, the best-fit parameter values remained merely unchanged compared to the previous analysis of the data. A formal estimate for k_h is available now also for Aldrich cellulose. As already previously concluded in Glaus and Van Loon (2008), the parameter values proposed by Pavasars *et al.* (2003), clearly overestimate the extent of cellulose degradation.

EURAD (Deliverables n° 3.6, 3.7 and 3.8) - Final Report of results generated in CORI
Dissemination level: PU
Date of issue of this report: **05/07/2024**

Page 50
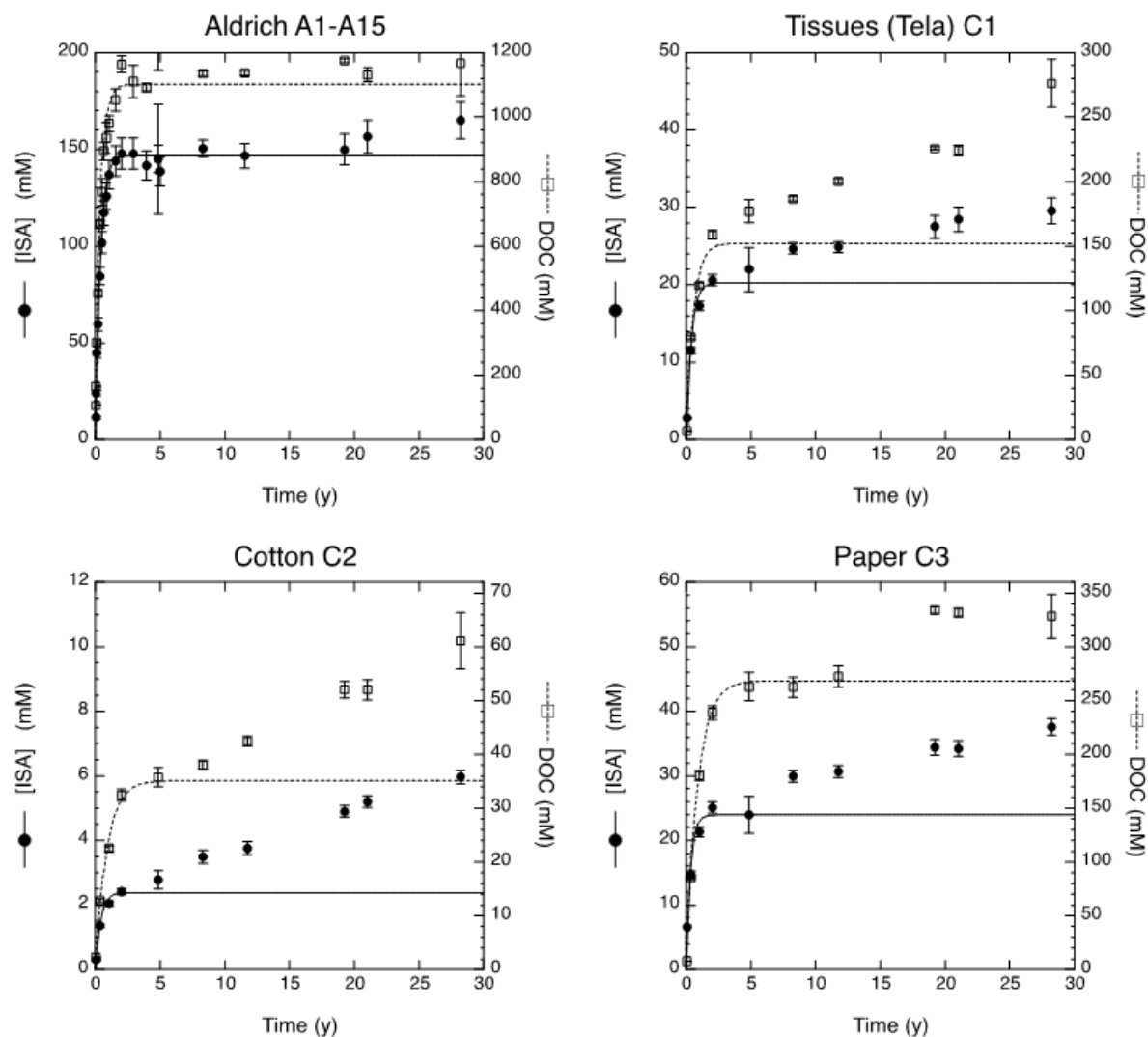
Figure 2-11:   *Evolution of concentrations of ISA and DOC (corrected for extractable compounds) as a function of time during degradation of various cellulose types in ACW-I. The model lines are based on the reaction rate constants given in Van Loon et al. (1999) for the peeling-off process only.*

EURAD (Deliverables n° 3.6, 3.7 and 3.8) - Final Report of results generated in CORI
Dissemination level: PU
Date of issue of this report: **05/07/2024**

Page 51
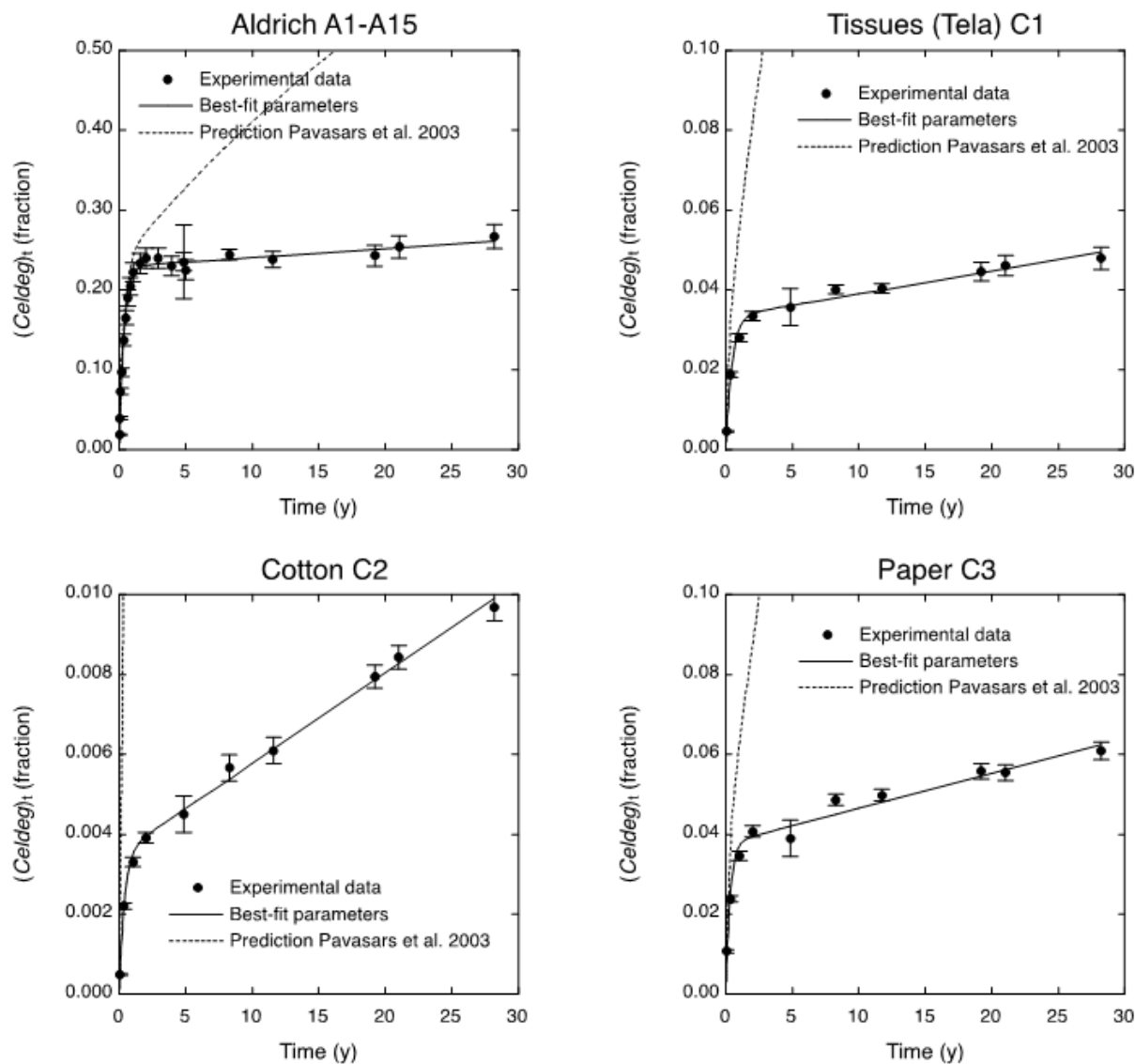
Figure 2-12:   *Extent of cellulose degradation based on ISA data as a function of time during the degradation of various cellulose types in ACW-I. The model curves show the comparison of the prediction of Pavasars et al. (2003) with the best-fit parameter values given in Table 12.*

Table 12: Comparison between the best-fit parameter values obtained for all data obtained during the ~28 years observation period and those previously published for a degradation time of ~12 years.

	Present data			Glaus and Van Loon (2008)		
Cellulose type	k_1 (h^{-1})	k_t (h^{-1})	k_h (h^{-1})	k_1 (h^{-1})	k_t (h^{-1})	k_h (h^{-1})
Aldrich cellulose	$(8.9 \pm 0.4) \cdot 10^{-3}$	$(3.3 \pm 0.2) \cdot 10^{-4}$	$(1.7 \pm 0.4) \cdot 10^{-7}$	$(8.8 \pm 0.4) \cdot 10^{-3}$	$(3.2 \pm 0.2) \cdot 10^{-4}$	-
Tela tissues	$(9.2 \pm 1.1) \cdot 10^{-3}$	$(2.5 \pm 0.3) \cdot 10^{-4}$	$(6.8 \pm 0.8) \cdot 10^{-8}$	$(1.0 \pm 0.1) \cdot 10^{-2}$	$(2.9 \pm 0.5) \cdot 10^{-4}$	$(1.0 \pm 0.2) \cdot 10^{-7}$
Cotton	$(1.9 \pm 0.2) \cdot 10^{-3}$	$(3.0 \pm 0.4) \cdot 10^{-4}$	$(2.6 \pm 0.1)\ 10^{-8}$	$(2.0 \pm 0.3) \cdot 10^{-3}$	$(3.3 \pm 0.5) \cdot 10^{-4}$	$(2.9 \pm 0.3) \cdot 10^{-8}$
Recycling paper	$(3.8 \pm 0.9) \cdot 10^{-3}$	$(3.6 \pm 0.9) \cdot 10^{-4}$	$(1.1 \pm 0.2) \cdot 10^{-7}$	$(4.3 \pm 1.3) \cdot 10^{-3}$	$(4.3 \pm 1.5) \cdot 10^{-4}$	$(1.6 \pm 0.5) \cdot 10^{-7}$

EURAD (Deliverables n° 3.6, 3.7 and 3.8) - Final Report of results generated in CORI
Dissemination level: PU
Date of issue of this report: **05/07/2024**

Page 52

2.1.3.4.2 Evolution of the physico-chemical properties of cellulose during alkaline degradation

The molecular mass distribution functions (MMD) obtained from the GPC measurements for ~21 years degraded cellulose samples are shown in Figure 2-13. The viscosity measurements were also performed. The degree of polymerization DP estimated based on GPC and viscosity measurement were estimated. All results including those of the initial state of the cellulose materials where available, is given in *Table 13*. The comparison between the values for the starting materials and the preparations obtained after 21 years of alkaline degradation rather indicates a slight increase of DP instead of the expected decrease. This inconsistency is most probably related to difficulties related to compare results from different laboratories and methods of evaluation (Potthast *et al.*, 2015). Note that a certain increase of DP of natural cellulose materials can be expected in situations in which DP of cellulose does not alter. The explanation for such an increase can be found in the initial presence of hemicelluloses which dissolve and degrade rather rapidly under alkaline conditions.
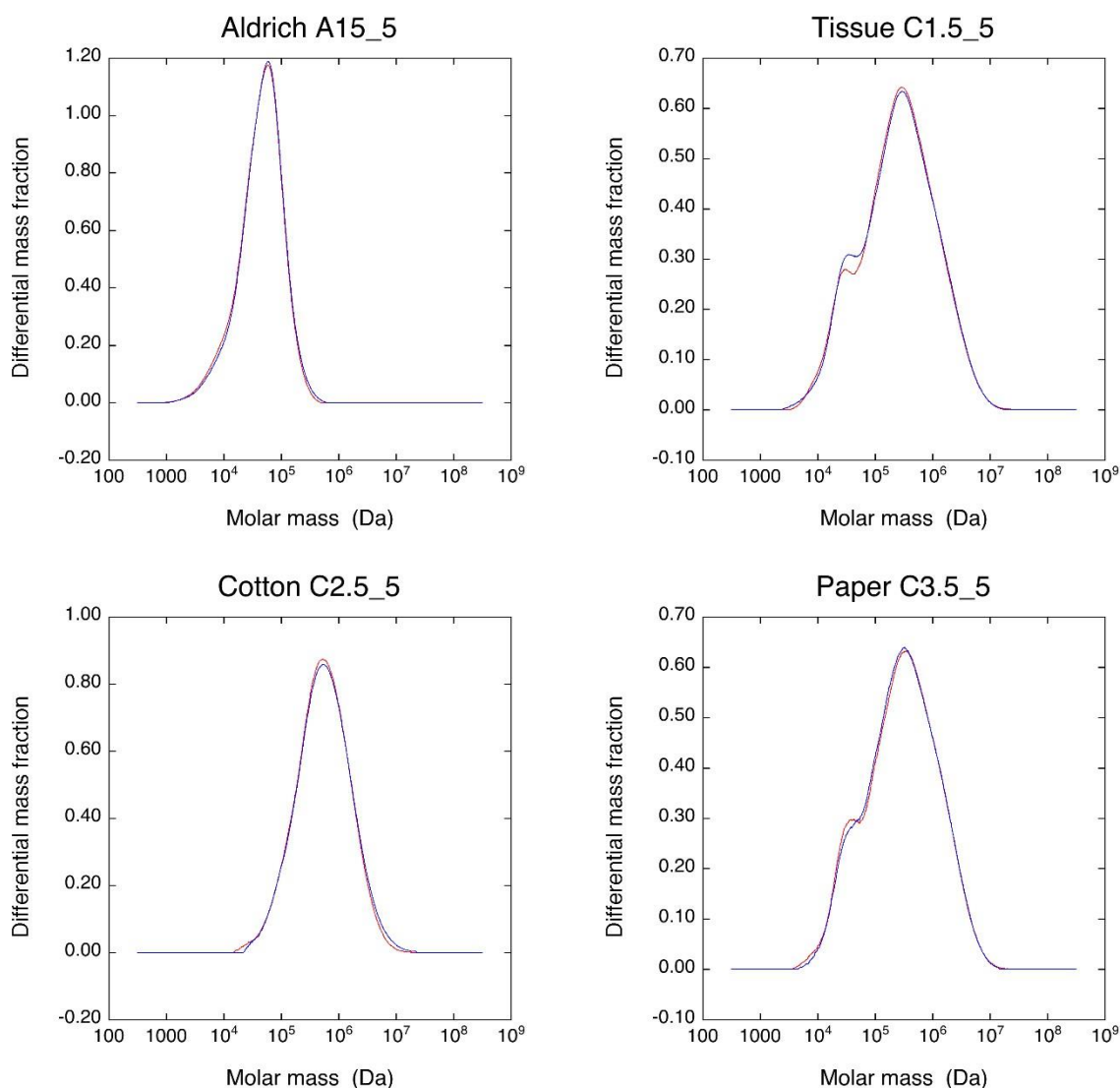
Figure 2-13:   *GPC elution profiles of the samples harvested after a reaction time of ~21 years, represented as histograms for the distribution of molecular mass. The two colours represent the results of duplicate tests.*

EURAD (Deliverables n° 3.6, 3.7 and 3.8) - Final Report of results generated in CORI
Dissemination level: PU
Date of issue of this report: **05/07/2024**

Page 53

Table 13: Overview of average degree of polymerization of the cellulose before and after alkaline degradation at room temperature. Values given in italics were measured at Cellulose Attisholz (Switzerland) in 1997 and published in (Van Loon et al., 1999b). Values given with straight numbers were measured at Aalto University (Finland) in 2016.

Cellulose	Time (years)	DP$_v$ #1 [a]	DP$_v$ #2 [b]	DP$_{reg}$ [c]	DP$_{GPC-Mw}$ [d]
Aldrich cellulose (A)	*0*	*117*	*236*	*128*	
	0	145	287		361
	21	144	286		379
Tela tissues (C1)	*0*	*1110*	*2087*	*417*	
	21	1160	2200		4097
Cotton (C2)	*0*	*1800*	*3712*	*3125*	
	21	1987	4176		5737
Recycling paper (C3)	*0*	*290*	*422*	*83*	
	0	328	489		2755
	21	458 / 476 / 480	727 / 762 / 769		4388 / 4018

[a] DP values were calculated from the limiting viscosity number using the Mark-Houwink equation, using the evaluation coefficients of Sihtola *et al.* (1963)

[b] DP values were calculated from the limiting viscosity number using the Mark-Houwink equation, using the evaluation coefficients of (Marx-Figini, 1978)

[c] Calculated from the reciprocal of the measurement of reducing end groups

[d] Calculated from the differential mass distribution (Mw) from size exclusion chromatography by dividing the calculated Mw values by the unit mass of anhydrous glucose monomer units (162 g mol 1).

2.1.3.4.3 Implications for long-term predictions of the alkaline degradation of cellulose

In view of the presumably small changes of molecular sizes of the cellulose molecules during the 28 years of degradation, it can be concluded that the contribution of the midchain scission to the anaerobic alkaline degradation of cellulose can indeed be neglected for degradation at room temperature. Note that a significant decrease of DP was observed at elevated temperatures of 60°C and 90°C (Glaus and Van Loon, 2004). At these temperatures, the effect of the mid-chain scission was obviously noticeable. The strong correlation between the ISA and the DOC concentrations in the present experiments suggests that the secondary slow degradation reaction is dominated by a slow peeling-off process. Whether this process is caused by a chemical conversion of stopped end groups to reactive end groups or by a minor equilibrium between crystalline and amorphous forms of cellulose, cannot be answered conclusively from the experimental observations. Either way, if it is assumed that the midchain scission is negligible in the overall anaerobic alkaline degradation of cellulose, a substitute kinetic expressions has to be applied for an adequate description of the intermediate-term degradation of cellulose. Such a formal expression has been proposed in Glaus and Van Loon (2008) with k_0 representing the reaction rate constant for the slow peeling-off process:

$$\left(celdeg\right)_t = k_1 / k_t \left(G_r\right)_0 \left(1 - e^{-k_t t}\right) + \left(k_1 / k_t \cdot k_0\right)t \qquad \text{Equation 4[1]}$$

---

[1] Note the typos in eqs. (6) and (7) in Glaus, M.A., Van Loon, L.R., 2008. Degradation of cellulose under alkaline conditions: new insights from a 12 years degradation study. Environ. Sci. Technol. 42, 2906–2911. The multiplikation with *t* went missing.

EURAD (Deliverables n° 3.6, 3.7 and 3.8) - Final Report of results generated in CORI
Dissemination level: PU
Date of issue of this report: **05/07/2024**

Page 54

As noted in the cited work, this equation has only a limited scope of applicability regarding large time values. For infinite values of t, $(celdeg)_t$ would also reach infinity which shows the limited scope of applicability of this equation. Because of the lack of any evidence of a stopping of this process, it has to be assumed that cellulose may be completely degraded under the pertinent conditions on a long term. Eq. (4) can, however, only be used in qualitative terms for the purpose of such predictions. For provisional purposes, it might be more appropriate to formally use eq. (1) in combination with the parameter values given in *Table 12* for the present data. The advantage of such an approach is that the $(celdeg)_t$ won't exceed the limiting value of 1 for infinitely large t values. However, the k_h values used have only a formal character and should not be misinterpreted as a rather fast progressing of the midchain scission reaction.

2.1.4 Stability of a-ISA in the presence of portlandite and Fe(0) powder

2.1.4.1 α-ISA stability experiments in gas-tight pressure reactors

The stability of α-ISA at 90°C in ACW in the presence of portlandite and Fe(0)-powder were studied by PSI in gas-tight pressure reactors. The results of experiments in which the stability of a $5 \cdot 10^{-4}$ M α-ISA solution was tested as a function of time in the presence of two different portlandite concentrations and 2 different concentrations of Fe(0) powder are shown in *Figure 2-14*.

HP-IEC-MS (Hyphenation of capillary high-performance ion-exchange chromatography with mass spectrometry) analysis of the solutions shows that the α-ISA concentrations decreased only slightly with time in the reactors with a Fe(0) powder concentration of 2.5 g·L^{-1} (*Figure 2-14*a). A much more significant decrease of the α-ISA concentration was observed in the presence of 25 g·L^{-1} iron powder (*Figure 2-14*a). $\Sigma(C)$ is identical to the α-ISA concentration, meaning that no LMW CAs (low molecular weight carboxylic acids) were formed during the observation period (*Figure 2-14*b). NPOC concentrations were approximately 100 μM higher than $\Sigma(C)$, as exemplified in *Figure 2-14*b for the experiment with 25 g·L^{-1} Fe(0) powder, suggesting the presence of impurities originating from the reactor.

The experiments show that α-ISA concentrations in alkaline cement pore water solutions decrease in the presence Fe(0) powder. Otherwise, the presence of solid portlandite in absence of Fe(0) does not cause any significant decrease in the α-ISA concentration in contrast to earlier reported observations Glaus and Van Loon (2008). This observation thus supports the assumption made by the latter authors that the decrease of α-ISA concentration might be due to oxidation reactions caused by traces of O_2 sorbed on the portlandite surfaces. A detailed examination of the aged α-ISA solutions and the corresponding gas phases in the present experiments did not lead to the detection of significant amounts of LMW organic degradation products. This observation suggests that the decrease in α-ISA concentration observed in the present experiments is not caused by abiotic degradation processes but rather by a sorption process involving the metallic Fe(0) or newly formed iron corrosion products. Indeed, the decrease of the α-ISA concentration with increasing amounts of iron powder indicates that the latter material plays a key role in the fate of α-ISA. The slow decrease in α-ISA concentration with time (*Figure 2-14*a) may be explained by sorption onto increasing amounts of iron corrosion products rather than by the metallic Fe(0).

The main conclusion is that the α-ISA is stable in ACW at pH = 13.3 under reducing conditions and a temperature of 90°C over a period of up to 120 days, both in absence and in presence of portlandite and Fe(0) powder. This conclusion is based on the absence of detectable concentrations of organic degradation products in both solution and gas phase. The decrease of the α-ISA concentration with time and with increasing amounts of Fe(0) powder might be explained by a sorption and/or co-precipitation process involving iron or its corrosion products growing on the surface of the Fe particles.

European Joint Programme on Radioactive Waste Management

EURAD (Deliverables n° 3.6, 3.7 and 3.8) - Final Report of results generated in CORI
Dissemination level: PU
Date of issue of this report: **05/07/2024**

Page 55
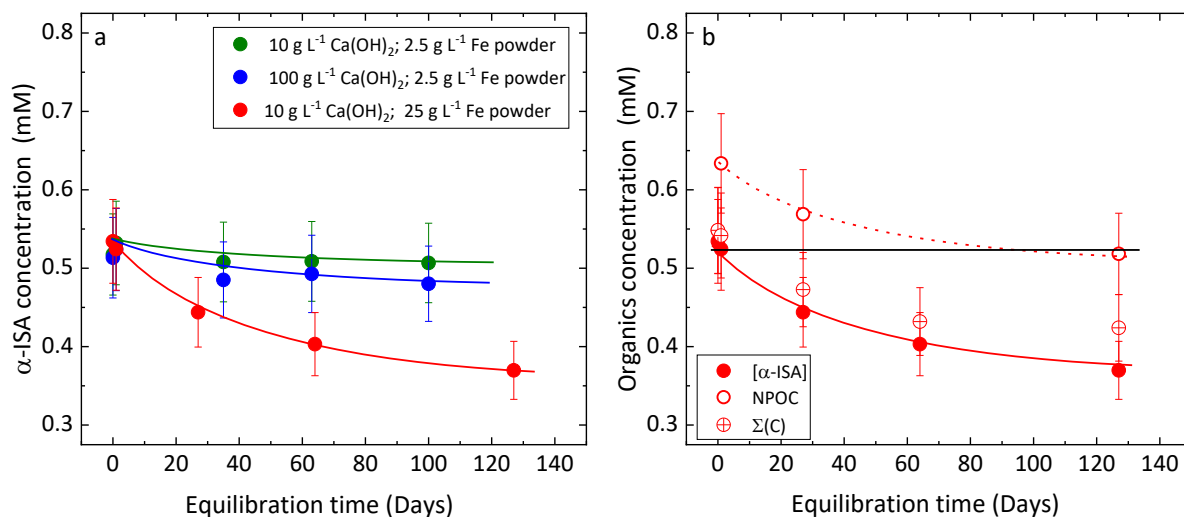
Figure 2-14:   *α-ISA stability in ACW at pH = 13.3 at 90°C in the presence of portlandite and Fe(0) powder measured in gas-tight pressure reactors under N_2 atmosphere. The starting pressure was 3.0 bar. The starting a-ISA concentration was 5.3 mM. a) Effect of the amount of portlandite and Fe(0) powder on the evolution of the α-ISA aqueous concentration with time. b) Evolution of the α-ISA concentration, NPOC and $\Sigma(C)$ in the aqueous phase as a function of time in the presence of 10 g L^{-1} portlandite and 25 g L^{-1} Fe(0) powder.*

2.1.5 Degradation of cellulose in the presence of portlandite and Fe(0) powder

2.1.5.1.1 Cellulose degradation experiments in gas-tight pressure reactors

The degradation of Aldrich cellulose in the presence of portlandite and Fe(0) powder was investigated in detail in gas-tight pressure reactors allowing to obtain a complete picture of the degradation processes including degradation products in both the liquid and gas phase. Degradation experiments were carried out in ACW at 90°C with two cellulose concentrations: 10.0 g L^{-1} and 0.1 g L^{-1} (*Figure 2-15* and *Figure 2-16*). As the main purpose of this project was to test whether the presence of portlandite and Fe(0) powder has an influence of the cellulose degradation processes, the degradation experiments were only run for a relatively short time of ~90 days. The progress of the degradation process in these experiments was monitored by regular measurements of the NPOC and ISA concentrations in solution (*Figure 2-15a to d*). These results were then used to calculate the fraction of cellulose that was degraded in terms of NPOC and in terms of ISA (%) (*Figure 2-15e* and *f*). *Figure 2-16* show the evolution of the LMW CAs produced in solution. Gaseous organic degradation products could not be detected by GC-MS analysis of the gas phase in the reactors in the course of the degradation experiments.

In the experiment with 10 g L^{-1} cellulose, the NPOC concentration, the ISA concentration and the fraction of degraded cellulose, show a strong increase during the first day of the experiment. During the following ~20 days, the degradation process continues at a much slower rate. Beyond 20 days reaction time the NPOC and ISA concentrations remain approximately constant suggesting that the degradation process may have stopped. The ISA concentrations in the presence of portlandite and Fe(0) powder appear to be slightly higher in the presence of portlandite and Fe(0) powder, but this effect is not confirmed by the NPOC and CAs concentrations and are therefore, probably, just coincidence. The NPOC and ISA concentrations and the fraction of cellulose degraded agree roughly with the values reported by Glaus & Van Loon (2004) for similar degradation experiments with 10 g L^{-1} cellulose in ACW at 90°C carried out in Teflon containers. The degree of cellulose degraded expressed in terms of total ISA concentrations (% celdeg-ISA) is lower than the degree of cellulose degradation expressed in terms of NPOC concentrations (% celdeg-NPOC) indicating that besides α-ISA and β-ISA, significant amounts of minor degradation products are formed (*Figure 2-15e* and *f*). These include mainly the LMW CAs:

EURAD (Deliverables n° 3.6, 3.7 and 3.8) - Final Report of results generated in CORI
Dissemination level: PU
Date of issue of this report: **05/07/2024**

Page 56

FA, AA, LA and OA (*Figure 2-16*). The concentration evolution of these CAs during cellulose degradation is similar to that observed for the NPOC concentration and the ISA concentration; i.e., a strong increase during the first day of reaction followed by a levelling to reach a plateau after approximately 20 days. The concentrations of some of the CAs decreases significantly in the presence of solids suggesting sorption on the solid surfaces. This effect seems to be stronger in the presence of the Fe(0) powder.

The cellulose degradation proceeds in a similar way in the experiments with a cellulose concentration of 0.1 g L^{-1}.

EURAD (Deliverables n° 3.6, 3.7 and 3.8) - Final Report of results generated in CORI
Dissemination level: PU
Date of issue of this report: **05/07/2024**

Page 57
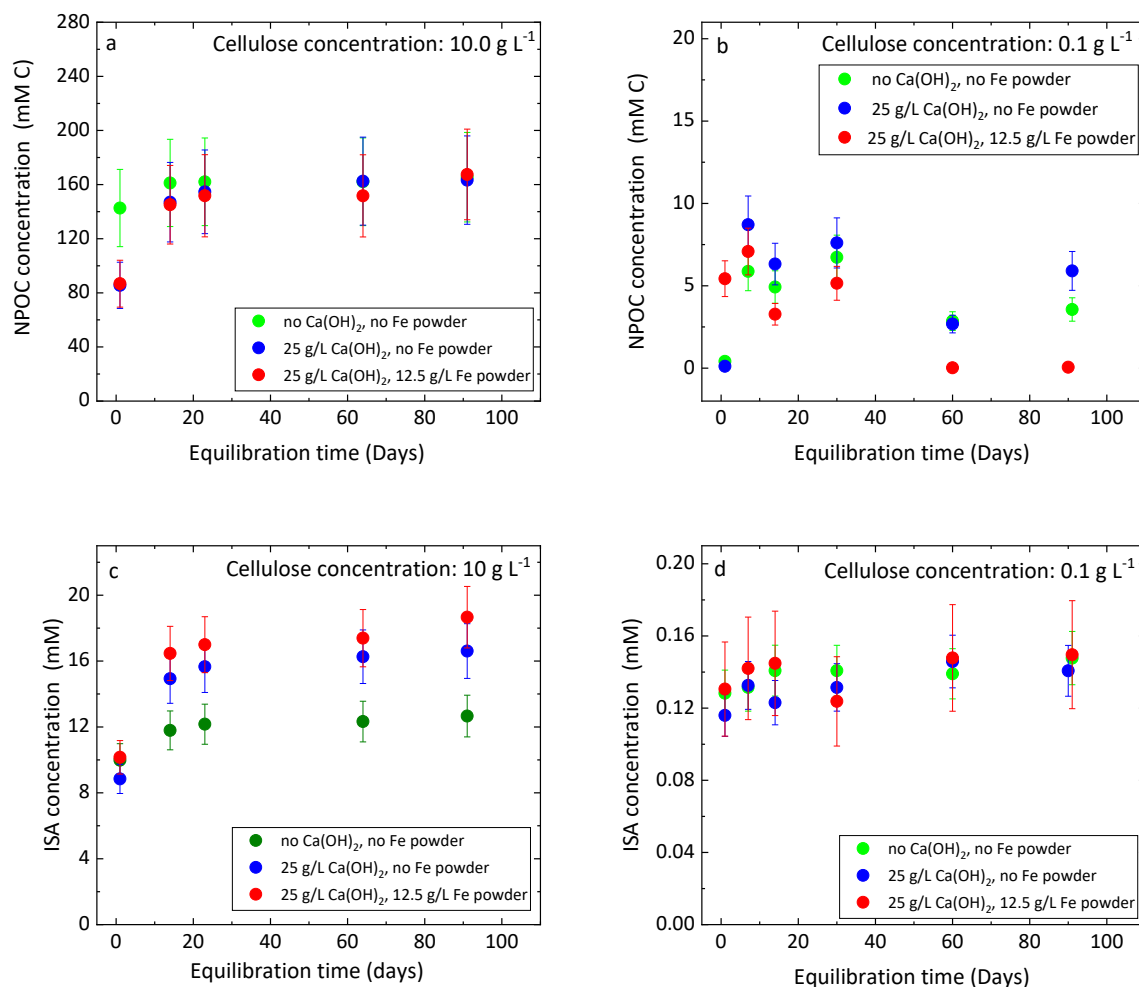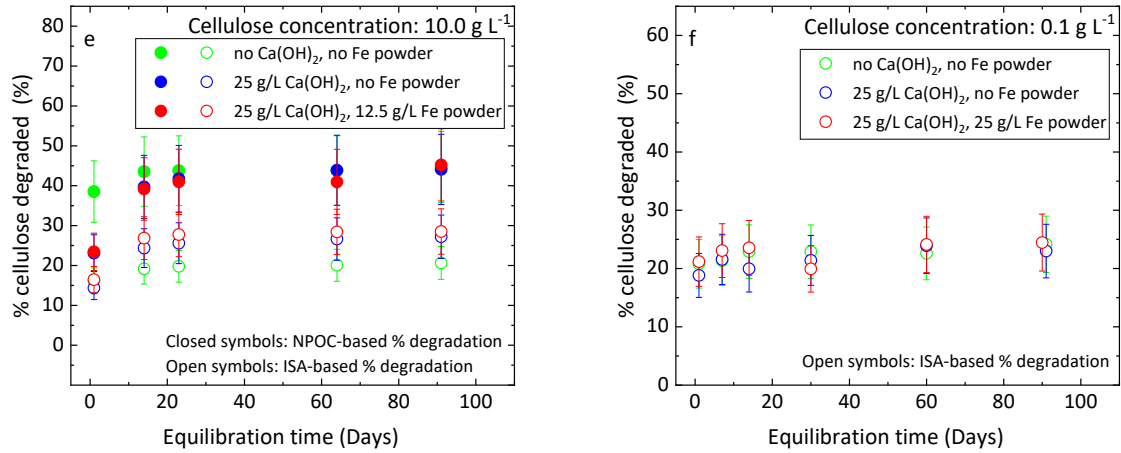
Figure 2-15: *Evolution of Aldrich cellulose degradation in the presence of ACW in gas-tight pressure reactors at 90°C. Aldrich cellulose concentrations were 10.0 g L^{-1} (Figs. a, c, e) and 0.1 g L^{-1} (Figs. b, d and f). NPOC concentrations (a, b), ISA concentrations (c, d) and % cellulose degraded (e, f).*

EURAD (Deliverables n° 3.6, 3.7 and 3.8) - Final Report of results generated in CORI
Dissemination level: PU
Date of issue of this report: **05/07/2024**

Page 58
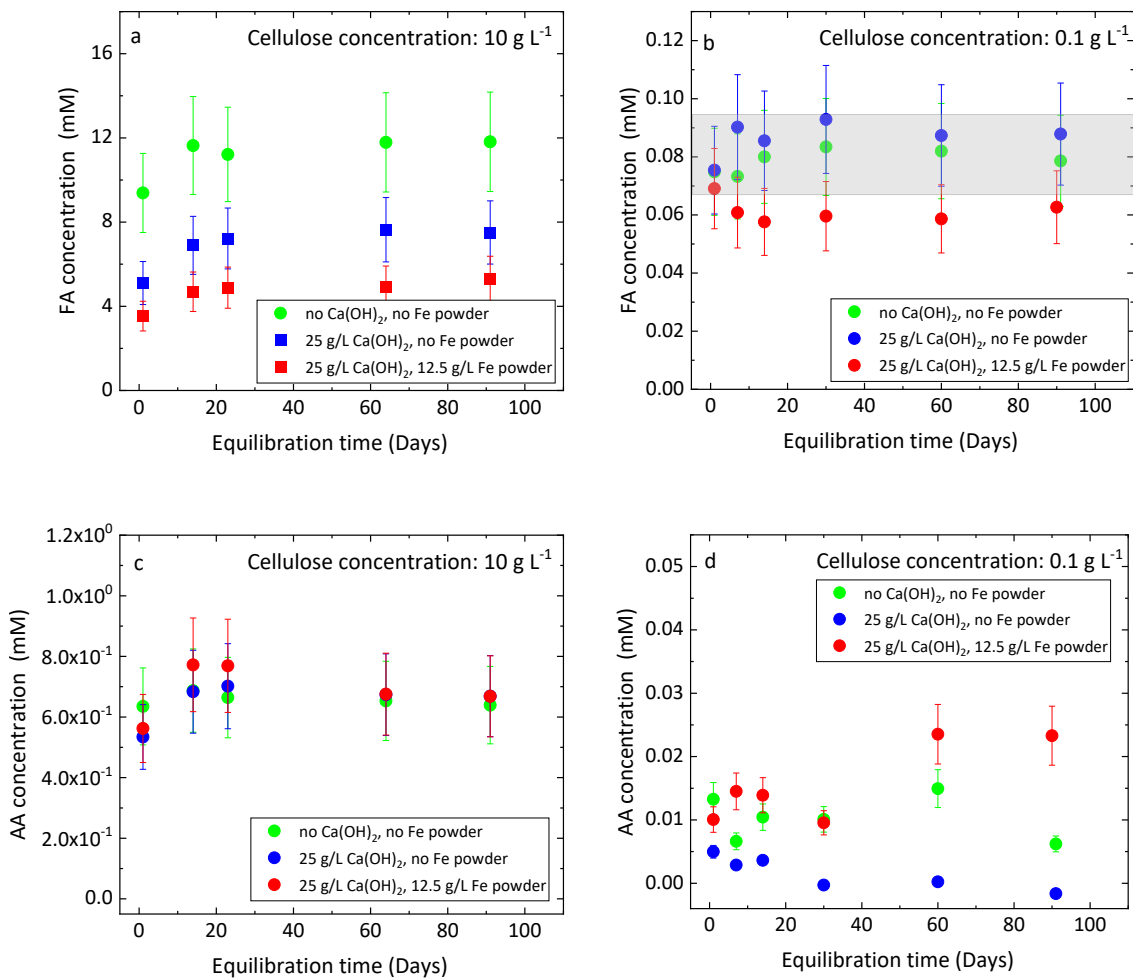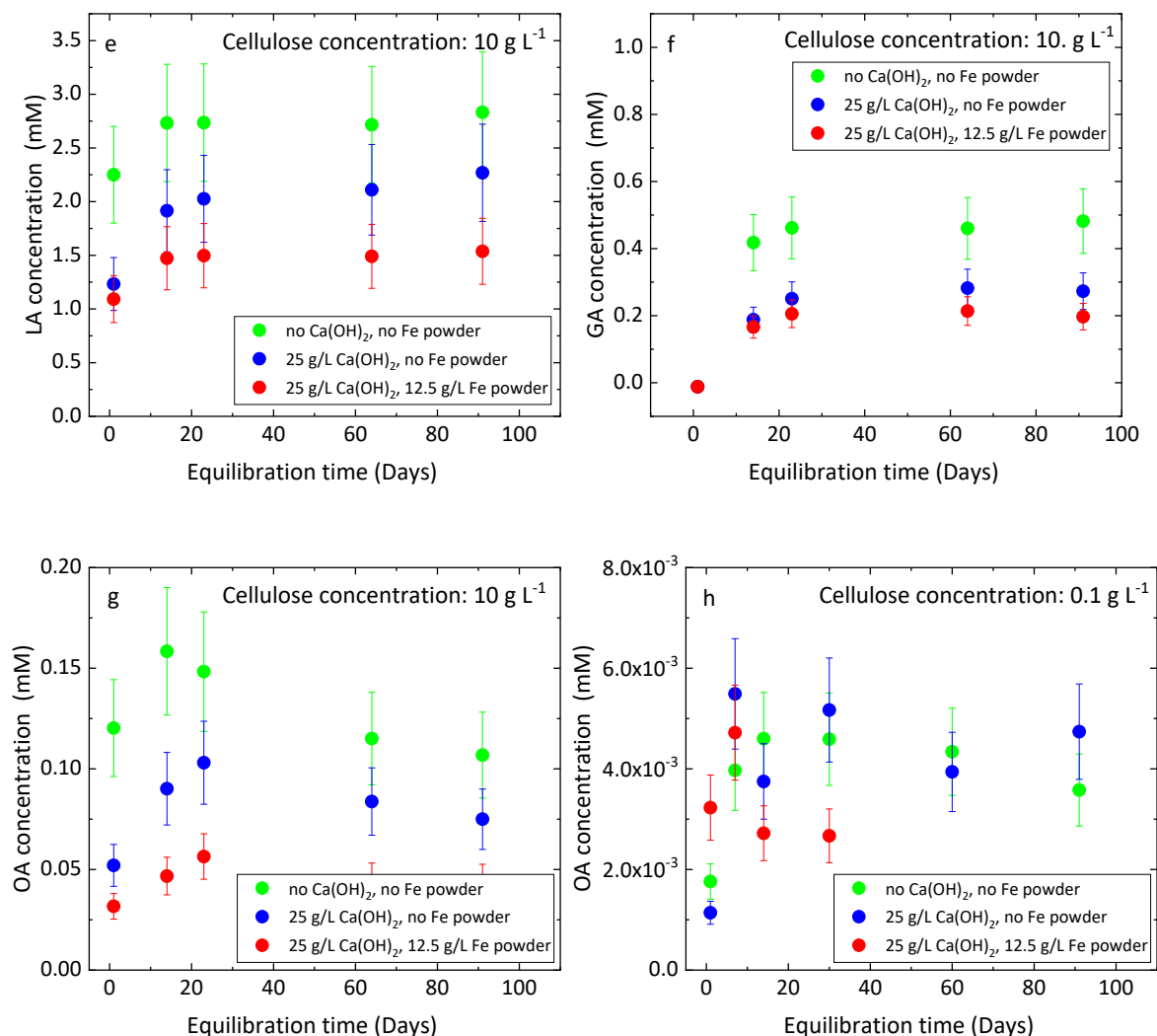
Figure 2-16:   *Evolution of the LMW CA concentrations during Aldrich cellulose degradation in the presence of ACW in gas-tight pressure reactors at 90°C. Aldrich cellulose concentrations were 10.0 and 0.1 g L^{-1}. Formic acid (FA), acetic acid (AA), glycolic acid (GA), lactic acid (LA) and oxalic acid (OA) concentrations are shown.*

Degradation experiments with Aldrich cellulose under alkaline conditions in ACW at 90°C carried out in simple autoclaves and gas-tight pressure reactors, in the absence and in the presence of portlandite and Fe(0) powder showed that the presence of these solids have no significant influence neither on the degradation rate nor on the type of degradation products formed. Cellulose degradation was monitored over a period of up to 90 days. During this relatively short reaction time, the degradation rate was similar to that observed by Glaus & Van Loon (2004). The degradation products detected were predominantly ISA together with minor amounts of carboxylic acids (FA, AA, GA, LA, OA) in agreement with the observations of Glaus & Van Loon (2004). Gaseous degradation products were not detected.

2.1.6 General conclusions

The results of the radiolytic gas production of **[SCK CEN]** show that H$_2$ and CO are the most important gaseous degradation products under gamma irradiation of cellulosic tissues. Significantly higher CO$_2$ and CO production was observed during irradiation of tissues under air.

Pre-irradiation of cellulosic tissues under any of the conditions leads to a significant formation of degradation products other than those observed for non-irradiated tissues. It leads to a significantly faster DOC and ISA production during subsequent hydrolytic degradation in artificial cement water. The

EURAD (Deliverables n° 3.6, 3.7 and 3.8) - Final Report of results generated in CORI
Dissemination level: PU
Date of issue of this report: **05/07/2024**

Page 59

organics released from cellulosic tissues in ACW form a complex mixture, consisting of mainly ISA, but also formic, glycolic, butyric, lactic, xylo-isosaccharinic acid and possibly oligosaccharides.

Pre-irradiation of cellulosic tissues does not seem to alter the alkaline degradation pathways, but rather accelerates the overall degradation. The model previously proposed by **[PSI]** (Glaus and Van Loon, 2008) to predict cellulose degradation and ISA production is still applicable.

[PSI] performed sampling campaigns carried out after 19.2, 21.0 and 28 years of degradation in the long-term experiments of anaerobic alkaline hydrolysis of cellulose at ambient temperature confirm the earlier observation that cellulose degradation slowly progressed after a rather short (~3 years) first phase of fast removal ("peeling-off") of glucose units from the reducing end of the cellulose chain. The secondary slow phase of peeling-off is assumed to proceed via the same reaction paths as the fast process. However, it is slowed down by the strongly reduced availability of reducing end groups in the cellulose chain compared to the initial phase of reaction.

Degradation experiments carried out by **[PSI]** shows that α-ISA is stable in ACW at pH = 13.3 under reducing conditions and a temperature of 90°C over a period of up to 120 days, both in absence and in presence of portlandite and Fe(0) powder. Aldrich cellulose under alkaline conditions in ACW at 90°C, in the absence and in the presence of portlandite and Fe(0) powder showed that the presence of these solids have no significant influence neither on the degradation rate nor on the type of degradation products formed.

2.2 Degradation of polyvinyl chloride PVC

The PVC materials studied are presented in *Table 14*. These studies are carried out by **[ISTO/BRGM]**. Besides PVC material, **[ISTO/BRGM]** are also studying degradation of polyethylene PE. PE is a material with a simple structure (only C-H bonds), so prediction of degradation of this material should be easier.

Table 14: PVC and PE materials studied in Task 2

Type	Origin	Partner
PVC	Industrial materials: sanitary pipe (San.), nuclear glovebox filter (Nuc.), HP pipe (HP)	**[ISTO/BRGM]**
PE	Pure PE (Sigma-Aldrich)	**[ISTO/BRGM]**

[ISTO/BRGM] looked at the degradation of hard polyvinyl chloride (PVC) polymers that could potentially be found in low- and intermediate-level radioactive waste. The degradation products emitted (gases, water-soluble organic products) from these two types of materials during hydrolysis and/or radiolysis are poorly documented.

2.2.1 Initial products characterization

The characterization of initial PVC and PE were carried out by **[ISTO/BRGM]**. The compositions of the initial products are reported in *Table 15*. The compositions especially of the industrial samples are obtained by combining chemical elementary analyses, XRD, TGA, FTIR and GC-MS. Pure PVC doesn't contain additives, but for pure PE, some alkan-2-ones and n-alkanes have been detected. For the industrial products, several inorganic additives are found by XRD, including carbonates (both calcite $CaCO_3$ and dolomite $(Ca,Mg)(CO_3)_2$). Rutile is present in Nuc. and San. samples, which could be added as a stabilizer to prevent chloride release. ICP-MS also reveals the presence of Sn (128 ppm) which could be added as organo-Sn stabilizer compound.

For the organic additives, GC-MS analyses show the presence of phthalates esters (diethylhexyl phthalate, DEHP; diisononylphthalate, DINP, diethylhexylterephthalate, DEHT), alkanes (isomers from

EURAD (Deliverables n° 3.6, 3.7 and 3.8) - Final Report of results generated in CORI
Dissemination level: PU
Date of issue of this report: **05/07/2024**

Page 60

nC_{14} to nC_{40}) in all industrial PVCs and adipates esters in Nuc and San (*Table 15*). With respect to previous studies on soft PVC (Baston *et al.*, 2017; Chantreux *et al.*, 2021; Colombani, 2006), the amounts of phthalates are strongly lower and the presence of alkanes seems to be specific to hard PVC, as such compound had not be found so far in soft PVC compositions.

Table 15: Initial composition of the PVC and PE samples, including industrial samples (sanitary pipe (San. PVC), nuclear glovebox filter (Nuc. PVC), HP pipe (HP- PVC).

	Pure PE	Pure PVC	Nuc. PVC	San. PVC	HP PVC
Main molecule (PE or PVC ; %)	99.5	100	84.9	54	90.2
Minerals (%)	-	-	6.7	32.3	3.7
Carbonates (Calcite/Dolomite)	-	-	3.2	32	3.7
Rutile	-	-	2.3	0.3	-
Hydrotalcite	-	-	1.2	-	-
Organics (%)	-	-	8.4	14.3	6.4
Phthalates	-	-	0.6	1.1	0.7
Alkanes	0.1	-	7	10.2	5.7
Adipates	-	-	0.8	3	-
Alkan-2-ones	0.4	-	-	-	-
Total additives (%)	0.5	-	15.1	46	9.8

2.2.2 Radiolysis under wet conditions

2.2.2.1 Gas production

[ISTO/BRGM] performed irradiation experiments of PE and PVC samples, in pure water (liquid to solid ratio L/S = 10) and NaOH pH 13 solutions (L/S = 10), with air atmosphere. The samples were irradiated to gamma ^{60}Co, with a dose rate of 0.55 $kGy.h^{-1}$ and a final dose close to 2.5 MGy. The main gases observed after 6 months of radiolysis were O_2 and H_2, but not CO_2 or HCl. Problems with vial tightness prevented quantification of these gases.

Another set of irradiations were carried out using low-dose irradiations (< 50 kGy) with a ^{137}Cs source with a dose rate of between 1 and 10 $Gy.min^{-1}$. These doses are considered low regarding the expected total absorbed dose reached in ILW disposal (some MGy). These irradiation experiments were gas-tight and enabled us to observe the decrease in O_2 during the first few hours of irradiation indicating oxidation of polymer materials. O_2 decrease was particularly observed for PE, pure PVC and San PVC, which lose 50% of their O_2 after irradiation at 40 kGy (*Figure 2-17*a), whereas Nuc PVC loses only 20%. Hydrogen formation is also confirmed, but the presence of this gas in the control vial (*Figure 2-17*b) indicates that radiolysis of water contributes to H_2 formation. Finally, these experiments showed the formation of CO_2 (*Figure 2-17*c). This is very significant with PE and pure PVC, but the quantities become zero after a dose of 40 kGy.

EURAD (Deliverables n° 3.6, 3.7 and 3.8) - Final Report of results generated in CORI
Dissemination level: PU
Date of issue of this report: **05/07/2024**

Page 61
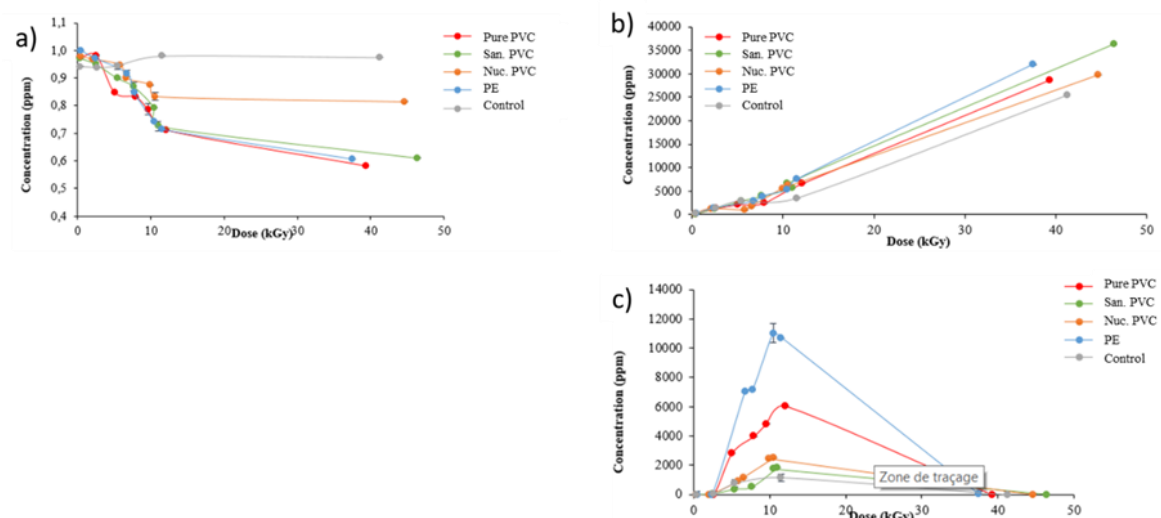
Figure 2-17: *Evolution of the amount of a) O_2, b) H_2 and c) CO_2 during the low-dose irradiation experiments at pH 13.*

2.2.2.2 Radiolytic degradation of PVC and PE

Evolution of the concentration of organic in solution is practically the same after the radiolysis at pH 8 and pH 13 for all polymers studied. Concentrations in alkanes, phthalate, adipate and some alcohols on the plastic decrease during the irradiation, while carboxylic acids (butenedioic, octadecatrienoic…) are formed (*Table 16*), which is consistent with previous studies (Chantreux, 2021). Among these acids, palmitic (C_{16}) and stearic (C_{18}) are highly "produced" in San. PVC (increase of 0.54µg/g to 4.70 µg/g for C_{16} and 0.80 to 6.10µg/g for C_{18}), HP PVC (increase of 0.77µg/g to 2.40 µg/g for C_{16} and 0.11 to 4.77µg/g for C_{18}) and Nuc PVC (increase of 2.70 µg/g to 3.10 µg/g for C_{16} and 0.47 to 2.51µg/g for C_{18}) but are not detected in pure PVC. They most certainly come from additives present in industrial plastics (Simon *et al.*, 1989; Putrawan *et al.*, 2022) and were released during radiolysis. Although the concentration of alkanes decreases after 7 months of irradiation, 2 n-alkanes (pentadecane and heptadecane) show an increase of their concentration, most probably due to the decarboxylation of the palmitic and stearic acids released during the radiolysis.

Table 16: *Concentration of organic in solution (µg/g of plastics) after an irradiation of 2.5 MGy.*

	Pure PVC		San. PVC		HP PVC		Nuc PVC		PE	
	initial	irradiated	initial	irradiated	initial	irradiated	initial	irradiated	initial	irradiated
n-Alkanes	-	-	14.22	10.62	3.1	3.04	0.39	0.15	894	2413
ketones	-	0.68	-	-	-	-	-	-	4527	9628
Alcohols-phenols	-	0.69	0.39	0.14	-	-	0.07	0	31	90
Phthalates esters	-	-	0.91	0.43	0.07	0.01	0.17	0.06	-	-
Adipates esters	-	-	2.7	0.51	-	-	-	-	-	-
Carboxylic acids	-	8.43	1.37	12.27	0.88	7.17	3.68	6.25	-	162

The pH of the solutions after irradiation of PVCs is shown in *Figure 2-18*. Globally, a severe drop in pH is observed, correlated with a strong increase of the chloride concentration. This is especially clear for the pure PVC resin while, for the industrial products, the drop in pH is limited, principally due to the presence of carbonate and rutile in polymers.

These pH drops are mainly due to the formation of gaseous HCl during radiolysis (Colombani, 2006). No HCl has been detected in gaseous phase, so it would be solubilized immediately into solution, releasing large quantities of chlorides (*Figure 2-18*). However, this release would be limited or prevented to a certain extent in industrial samples at this dose because of the presence of stabilizers, while the presence of carbonates would buffer the pH drop.

EURAD (Deliverables n° 3.6, 3.7 and 3.8) - Final Report of results generated in CORI
Dissemination level: PU
Date of issue of this report: **05/07/2024**

Page 62
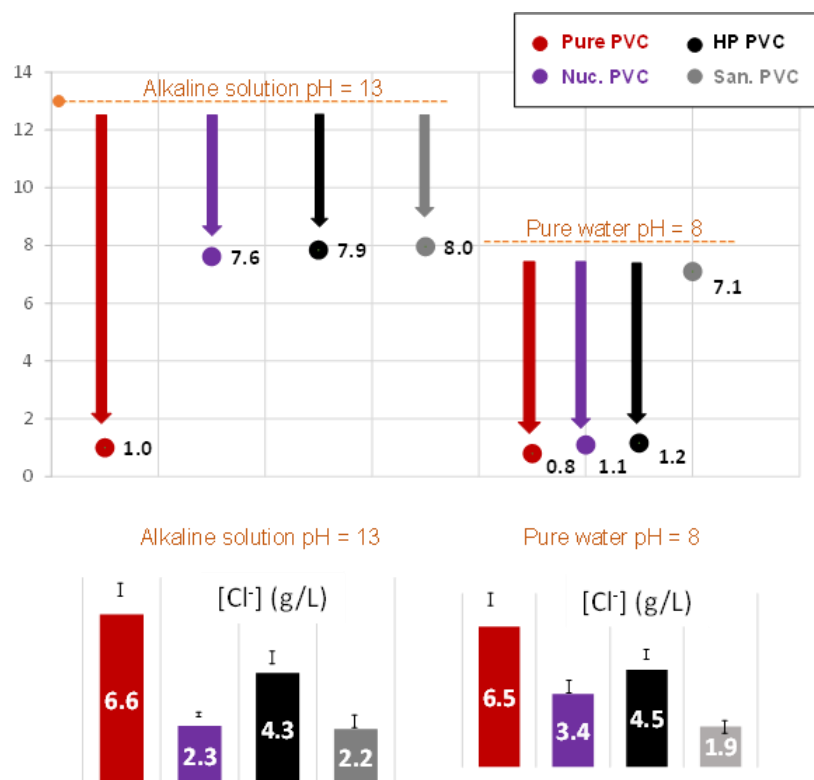
Figure 2-18: pH and chloride concentration [Cl⁻] of the solutions after a 2.5 MGy irradiation.

During radiolysis, pure PVC and PE release large quantities of dissolved organic carbon at pH 13 (around 120mg/l; *Figure 2-19*a). The release of dissolved organic carbon is very fast during the first hours of irradiation for these two pure plastics (30 mg/l of DOC after 40 kGy of irradiation; *Figure 2-18*). For industrial PVC, DOC release doesn't vary with dose of 40 kGy (*Figure 2-19c*) and is lower than the DOC of pure plastics after 2.5 MGy of irradiation. This can be explained by the presence of additives that protect the polymer chain and slows down its degradation. At pH 8, DOC release from industrial PVC and PE is practically identical to that at pH 13, whatever the dose received by the plastics (*Figure 2-19*a and b). However, pure PVC releases more organic carbon in solution (170 mg/l after 2.5 MGy; *Figure 2-19*a).

Determining the degradation products present was initially complicated by high salt concentrations ([Cl⁻ from 2 to 6 g/l), making analysis by ion chromatography or GC-MS impossible. The analysis of water-soluble degradation products was nevertheless carried out by LC/MS/MS, targeting compounds described in the literature (Colombani, 2006; Chantreux et al., 2021), particularly small organic acids, alcohols and phenols. Only the organic acids have been identified during the analysis. The concentrations of the small carboxylic acids released into the solution are practically identical, whatever the pH of the solution in which radiolysis has taken place (*Table 17*), which is consistent with the DOC quantities described above. Pure PVC releases mainly chloroacetic, dichloroacetic and succinic acids (at pH 13: 832 ng/l, 2320 ng/l, 710 ng/l, respectively; *Table 17*), resulting from the recombination of acetic acid produced during radiolysis with other radicals (Cl°, carboxylic acid; Chantreux, 2021).

Among the commercial PVCs, San. PVC shows the highest concentrations of total acid that is associated to fewest amount of additives when compared with the other two industrial materials.

EURAD (Deliverables n° 3.6, 3.7 and 3.8) - Final Report of results generated in CORI
Dissemination level: PU
Date of issue of this report: **05/07/2024**

Page 63
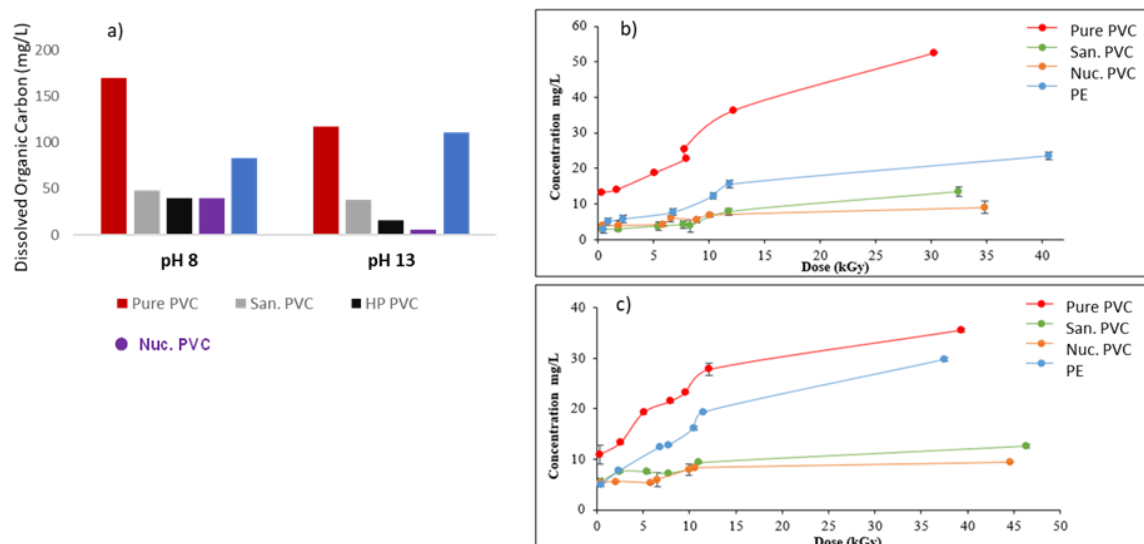
Figure 2-19:   *a) Concentration of DOC during 2.5MGy irradiation experiment at pH 8 and 13. Evolution of DOC with the irradiation dose at b) pH 8 and c) pH 13.*

Table 17: Concentration of small organic acids (ng/l) released in solution by the PVC after 2.5 MGy of irradiation.

	Pure PVC		San. PVC		HP PVC		Nuc. PVC	
	pH 8	pH 13	pH 8	pH 13	pH 8	pH 13	pH 8	pH 13
Acetic acid	88.2	92.2	394	420	110	165	45.9	55.1
Chloroacetic acid	761	832	623	717	117	183	79.2	92.2
Dichloroacetic acid	1960	2320	17.8	21.2	61.5	78.4	24.9	29.5
Malonic acid	12.9	15	35.3	38.3	19.4	24	12.5	17.3
Succinic acid	673	710	68.6	79.2	213	231	207	218
Glutaric acid	8.2	9.7	1.8	2.9	3.6	5.2	3.7	7.3
Adipic acid	-	-	0.3	0.6	-	-	4	4.8
Pimelic acid	-	-	-	-	-	0.1	0.4	0.9
Phthalic acid	-	-	3.5	5.2	-	-	-	-
Total	3503.3	3978.9	1144.3	1284.4	524.5	686.7	377.6	425.1

However, all the compounds detected and quantified represent only a very small part of the DOC released into solution. Heavier molecules, or macromolecules, must certainly be part of the composition of these DOC. Other analytical methods will have to be developed to determine the total composition of these DOC.

2.2.2.3 Hydrolysis of PVC and PE materials

2.2.2.3.1 Non-irradiated plastics

Hydrolysis of non-irradiated materials was conducted at 25°C and 90°C. Gas analyses were conducted during hydrolyses experiments. At pH 13, gas analyses revealed a decrease of the amount of O_2 for all 3 polymers, very low at 25°C and very high in the experiments at 90°C, but no trace of CO_2 was observed in each experiment. However, an increase of the quantity of H_2 has been demonstrated in hydrolyses involving PE (*Figure 2-20*): at 25°C, H_2 is non-existent after 180 days of incubation, but 0.3 mmol is produced at 45°C and reach 1 mmol at 90°C. This H_2 production would be the result of a radical reaction following homolytic breaking of the C-C bond, similar to that observed during thermal degradation of PE at higher temperatures (Murata *et al.*, 2002), but with much slower kinetics in the case of our experiments. In addition, traces of methane were detected during PE hydrolysis at 90°C.

EURAD (Deliverables n° 3.6, 3.7 and 3.8) - Final Report of results generated in CORI   Page 64
Dissemination level: PU
Date of issue of this report: **05/07/2024**
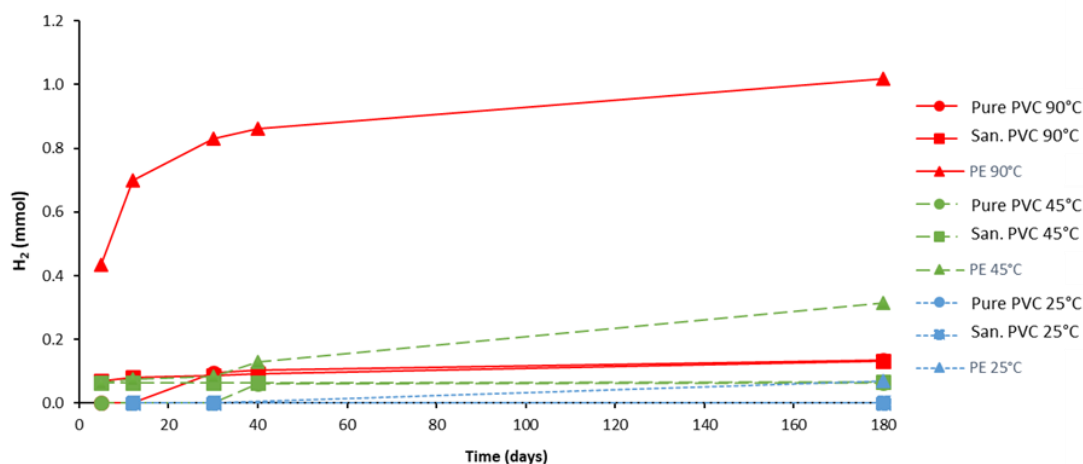
Figure 2-20:   Evolution of H_2 during hydrolysis experiments at pH 13.

Analysis of the composition of organic species in the 6 months leaching solution increased compared to the composition in the beginning of the leaching, with these increases being most pronounced at 90°C (*Table 18*). For San. PVC, the quantities of alkanes increase significantly, particularly at 90°C. In addition, carboxylic acids, and particularly, hexadecanoic and octadecanoic acid were detected with amounts equal to 2.38 and 15.29 µg/g of PVC respectively. Phthalates and adipates decrease after 6 months of hydrolysis, which is consistent with previous studies reported in the literature (Chantreux et al., 2021). In the case of PE, all additives increase sharply during hydrolysis, and a series of carboxylic acids (C8 to C30 isomers) appear in higher concentrations at 90°C.

Table 18: Composition of organic molecules on San. PVC and PE (µg/g of polymer) after 6 months of hydrolysis at pH 13.

	PVC San.				PE			
	initial	25°C	45°C	90°C	initial	25°C	45°C	90°C
n–Alkanes	150	185	214	239	893.7	528.2	1279.3	1762.3
Alkan-2-ones	-	-	-	-	4527	1825	5987	6117
Alcohols	8.88	9.02	8.53	10.92	30.80	11.00	24.60	34.30
Carboxylic acids	-	8.34	10.23	17.67	-	6.30	31.50	72.50
Phthalates and adipate (DEHP, DINP, DEHA, DEHT...)	54.28	46.29	37.56	31.48	-	-	-	-
Other compounds	14.64	19.01	45.02	48.62	-	-	-	-

During the hydrolysis at pH 13, DOC concentrations increase rapidly for the three materials at high temperatures (45 and 90°C) and reach 250, 280, and 550 mg/L after 6 months at 90°C for PE, San. PVC and pure PVC respectively, while at pH 8 and at 90°C, these increases are more modest (20, 33, and 80 mg/L for PE, San. PVC and pure PVC respectively).

After hydrolysis at pH 13, LC/MS analyses on the liquid phase reveal the presence of mostly small carboxylic acids in solution (phthalic, succinic and adipic) for San. PVC and PE (*Table 19*). In pure PVC and PVC, no chlorinated carboxylic acids are observed during the experiments at 90°C, but a small amount of dichloroacetic acid was observed, indicating that this acid could also be an adjuvant released during hydrolysis.

EURAD (Deliverables n° 3.6, 3.7 and 3.8) - Final Report of results generated in CORI
Dissemination level: PU
Date of issue of this report: **05/07/2024**

Page 65

Table 19: Concentration of small organic acids (ng/l) after 6 months of hydrolysis at pH 13.

	Pure PVC			San. PVC			PE		
	25°C	45°C	90°C	25°C	45°C	90°C	25°C	45°C	90°C
Dichloroacetic acid	-	-	-	-	-	6.7	-	-	-
Malonic acid	-	-	2.9	-	-	6.5	-	-	3.1
Succinic acid	-	-	45.2	-	35.2	76.5	-	-	68.5
Glutaric acid	-	-	2.1	-	-	4.9	-	-	24.4
Adipic acid	-	-	-	-	45.6	115.9	-	-	11.9
Pimelic acid	-	-	-	-	-	0.8	-	-	2.3
Phthalic acid	-	-	-	-	21.2	39	-	-	-

2.2.2.3.2 Analyses of irradiated materials

Pure PVC and the 3 industrial PVCs were irradiated for 6 months (2.5 MGy), then placed in a solution at pH 13 and 45°C (to approach storage conditions) for 1 month. The irradiated plastics formed a kind of solid that stuck to the walls of the bottles and could not be recovered. As a result, analysis of the solids (FTIR, GC/MS adjuvant) could not be carried out.

After 6 months of hydrolysis, DOCs are very high for all PVCs, with concentrations well above 1 g/L for pure PVC, San PVC and HP PVC (1.39, 1.61 and 1.38 g/L, respectively), which is far higher (10 to 30 times) than what was observed during radiolysis in solution or simple hydrolysis. As with solution radiolysis, Nuc PVC remains the PVC that emits the least DOC (0.57 g/L).

The small acids released during hydrolysis of irradiated PVCs are the same as those detected during radiolysis in solution (more specifically, acetic, chloro- and dichloroacetic, malonic, succinic, glutaric, adipic, pimelic and phthalic acids; *Table 20*), but in larger quantities. Succinic acid is one of the acids released by most PVCs, with the exception of San PVC, which releases much more acetic and chloroacetic acids. This is consistent with what was observed during radiolysis in a basic medium. However, as with radiolysis in solution, the concentrations measured represent only a small fraction of the DOC released into solution. Other characterization methods (ultrafiltration, high-resolution mass spectrometry) are needed to better describe the soluble compounds released from this experiment.

Table 20: Concentration of small organic acids released by irradiated plastics (ng/l) after 1 month of hydrolysis.

	Pure PVC	San. PVC	HP PVC	Nuc. PVC
Acetic acid	282.24	2403.4	484	96.39
Chloroacetic acid	2587.4	1370.6	280.8	118.8
Dichloroacetic acid	3920	78.32	153.75	77.19
Malonic acid	78.69	254.16	46.56	76.25
Succinic acid	3028.5	370.44	937.2	662.4
Glutaric acid	33.62	9.72	21.96	20.72
Adipic acid	-	1.95	-	12
Pimelic acid	-	-	0.96	-
Phthalic acid	-	120.25	-	-

2.2.3 Modelling approach

Based on experimental results a mechanism for the PVC degradation is proposed, with the release of HCl first in a gaseous state, before being dissolved in solution. Such release would be limited or prevented to a certain extent in sanitary PVC samples because of the presence of stabilizers, while the presence of carbonates would buffer the pH drop following the dissolution of gaseous HCl. This hypothesis has been further tested by [**Andra (BRGM)**] using a geochemical modelling approach. The modeling is processed using PhreeqC Parkhurst and Appelo (2013) and with the following conditions:

EURAD (Deliverables n° 3.6, 3.7 and 3.8) - Final Report of results generated in CORI
Dissemination level: PU
Date of issue of this report: **05/07/2024**

Page 66

- Kinetic degradation reactions

  - Degradation products HCl_g, H_{2g} Colombani (2006), acetate, formate, oxalate and phthalates Lamouroux and Cochin (2012).

  - Each degradation product is provided with one specific rate law

  - Reaction are not stoichiometric: Ex PVC (C_2H_3Cl) ⇨ HCl_g

- Parameters

  - Global parameter: p_{total} ; chemical parameters: pH, Eh, Cl^-, Ca^{2+}

- Process

  - 1st step: Calibration based on literature data

  - 2nd step: Carrying out the calculations by modifying the PVC/additives proportions in the input data and the composition of the solution (pure water or NaOH 0.1M) according to the experimental conditions

Results are shown in for pure PVC *Figure 2-21* and *2-22* for the sanitary PVC samples. The modeling succeeded in reproducing the results of the experiments, provided the HCl release is decreased by 2 to 5 times in the sanitary samples. It confirms the buffering of the pH drop by the carbonate dissolution and the role of stabilizers in decreasing the HCl release rate.

Figure 2-21:   Modelling of the degradation by irradiation of pure PVC.
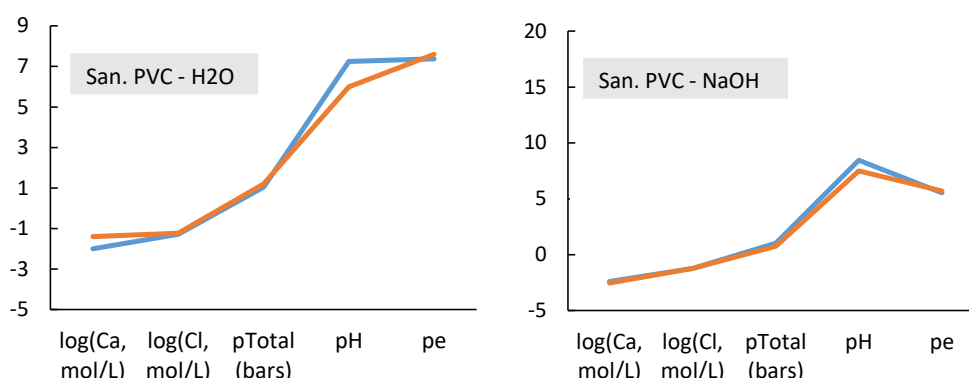
Figure 2-22:   Modelling of the degradation by irradiation of sanitary PVC.

2.2.4 General conclusions

Studies carried out by **[ISTO/BRGM]** indicates the production of H_2 and CO_2 gases during radiolysis in alkaline media. HCl is not observed, but increase of chloride concentrations in PVC radiolysis solutions, and pH decreases indicate its dissolution.

EURAD (Deliverables n° 3.6, 3.7 and 3.8) - Final Report of results generated in CORI
Dissemination level: PU
Date of issue of this report: **05/07/2024**

Page 67

Organic carboxylic acids are produced from radiolysis degradation in solution: (i) acids with long carbon chains (C16 and C18) are observed during solid analysis and (ii) small organic acids (acetic, chloro- and dichloroacetic, succinic) are mainly formed and transferred to the solution.

Alcohols, ketones and carboxylic acids are formed during hydrolysis of pre-irradiated materials, and succinic acid is mainly released into solution for the degradation of PVC. Alkaline hydrolysis of radiolysed PVCs releases ten times more organic carbon into solution than radiolysis in solution.

2.3 Degradation of Ion exchanges resins IER

The Ion Exchange Resins (IER) studied in framework of Task 2 were based on Polyacrylonitrile PAN. These kind of IERs are found in the waste inventories of WMO and not a lot of available information was reported in the literature before CORI studies. The details about the studied materials and partners involved in these actions are listed Table 21 and available chemical structure are presented in the *Figure 2-23*.

Table 21: Ion Exchange Resins studied in TASK 2 "Organic Degradation".

Type	Origin	Partner	Physical properties
PAN based IER	filter aid (UP2)	**[KIT]**	
PAN based IER	AMP-PAN*, KNiFC-PAN**, PAN-based	**[SURAO], [CTU], [CV REZ], [UJV]**	bead size 0.3 – 0.8 mm PAN (pH = 6.24), AMP-PAN (pH = 0,41), KNiFC-PAN (pH = 6.32),

* Ammonium molybdophosphate (AMP) - polyacrylonitrile (PAN)

** Potassium-nickel hexacyanoferrate resin in a polyacrylnitrile matrix
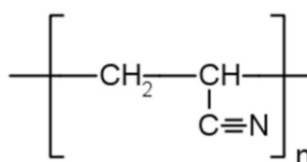
Figure 2-23: *Chemical structure of PAN based IER studied.*

2.3.1 Filter aid (UP2)

[KIT], in collaboration with **[SKB]**, has investigated the hydrolytic degradation of UP2W (Task 2), the interaction of the resulting degradation products with cement (Task 3) and the corresponding impact on radionuclide retention (Task 4). UP2W is a filter aid based on polyacrylonitrile (PAN), which is widely used in nuclear plants for particle removal and as support material for ion exchange resins. Significant amounts of used UP2W fiber mass are therefore disposed of in underground repositories for low and intermediate level nuclear waste (LILW), *e.g.* in SFR, Sweden.

The hydrolytic degradation has been studied under different conditions. The UP2W material provided by SKB was previously washed with Milli-Q water at T = 65°C, filtered and dried under ambient conditions. *Table 22* summarizes the experimental conditions for the batch degradation experiments conducted in this work.

EURAD (Deliverables n° 3.6, 3.7 and 3.8) - Final Report of results generated in CORI
Dissemination level: PU
Date of issue of this report: **05/07/2024**

Page 68

Table 22: Experimental conditions applied in the degradation batch samples containing UP2 resin material.

#	Degradation conditions	pH_c	Volume dm^3	S:L (Ca(OH)$_2$) g·dm^{-3}	S:L (UP2) g·dm^{-3}	S:L (Fe(0)) g·dm^{-3}	T °C
1	Ca(OH)$_2$-saturated sol.	12.5	1	50	50	-	22
2	Ca(OH)$_2$-saturated sol., with iron(0)	12.5	1	50	50	5	22
3*	Ca(OH)$_2$-saturated sol. at elevated T	11.5	1	50	50	-	80
4	Dilute NaOH solution	12.5	0.5	-	50	-	22
5	0.10 M NaOH	~ 13	0.5	-	50	-	22
6	1.00 M NaOH	~ 14	1	-	50	-	22

*Stirring was not possible for this sample, which was placed in an oven inside a glovebox.

2.3.1.1 Hydrolytic degradation

The evolution of NPOC values show that degradation kinetics at T = 25 °C in Ca(OH)$_2$-buffered media are substantially slower compared to the Ca-free systems (NaOH) at pH = 12.5 (*Figure 2-24*). Detected organic-carbon content in NaOH solutions increased also with increasing concentration of NaOH, whilst pH values of the degradation leachates substantially decreased over time. After ~700 days of contact time, however, the leached organic content for the Ca(OH)$_2$-buffered case showed an increase for the systems equilibrated at room temperature under continuous stirring. As for the system at T = 80 °C, detected NPOC values in the filtrates were in the range of the background level even after 1000 days of contact time, indicating that chain scission did not take place to a relevant extent at this temperature.

EURAD (Deliverables n° 3.6, 3.7 and 3.8) - Final Report of results generated in CORI
Dissemination level: PU
Date of issue of this report: **05/07/2024**

Page 69
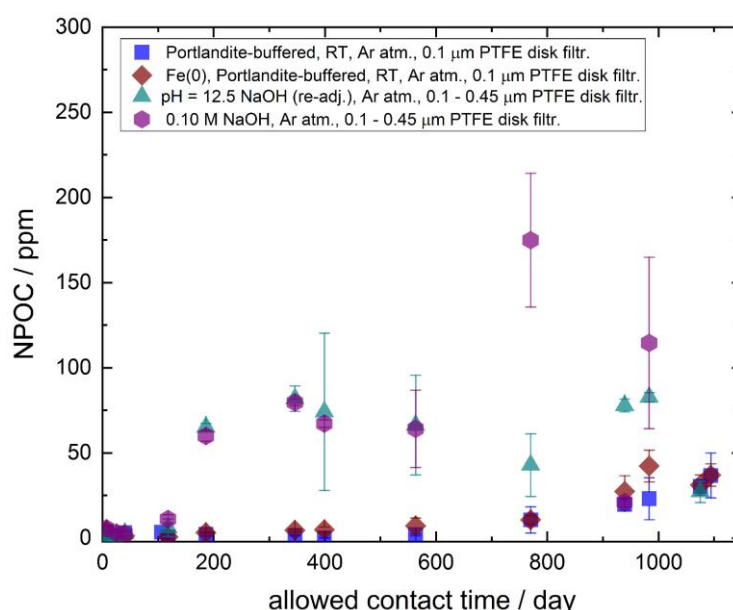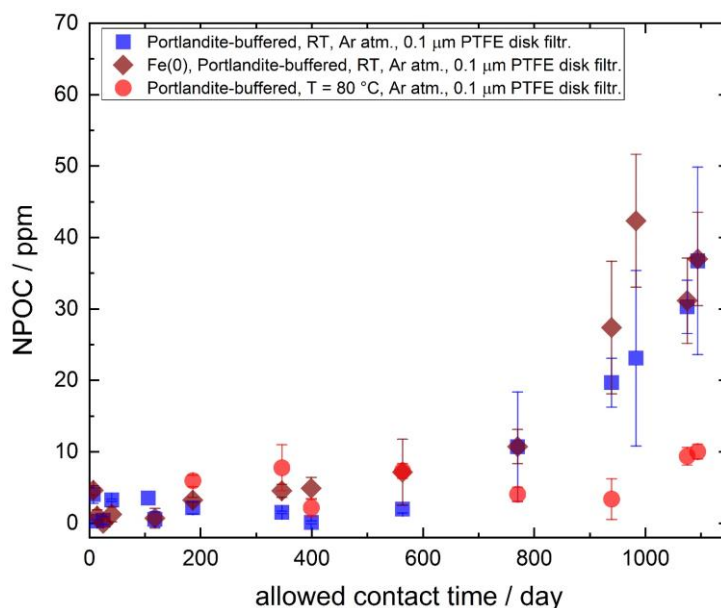
Figure 2-24: *Leached organic-content in solution quantified by NPOC measurements after filtration through 0.1 µm syringe PTFE disk filters as a function of allowed contact time for UP2W degradation samples equilibrated in 0.1 M NaOH, pH = 12.5 NaOH solutions (top) and Ca(OH)$_2$-saturated solutions with or without Fe(0) at T = 22 ± 3 °C or 80°C (bottom).*

Figure 2-25 exemplifies ^{13}C NMR data of the supernatant in the degradation experiment with 1.0 M NaOH gained on the filtered leachate after 2.5 years of contact time. In agreement with the evolution of the solid phase in the degradation process, the spectra shown in the figure underpins the presence of amide and carboxylate groups. Based on ^{1}H NMR data and in accordance with other experimental observations, three proxy ligands were proposed to simulate the chemical characteristics of the UP2W degradation products: glutaric acid (GTA) represents the bulk chain of the generated polymer fragments, whilst α-hydroxyisobutyric acid (HIBA) and 3-hydroxybutyric acid (HBA) simulate the effect of the end groups. *Figure 2-26* shows the SEC-OCD-UVD-OND (size-exclusion chromatography with organic carbon, ultraviolet and organic nitrogen detectors) spectra collected for the eluates of the UP2W degradation leachates after degradation times of 1200 days, for systems equilibrated at T = 22 °C in the presence of portlandite and portlandite + Fe(0). The values of total organic content determined for the degradation leachates at t = 1200 days are in good agreement with NPOC measurements discussed above. Degradation leachates obtained after 701 days in NaOH systems are characterized by significantly large molecular weights, *i.e.* > 33 kDa. These values translate in *ca.* 220 equivalent monomer units, calculated as units of polyacrylic acid. In contrast to this, manifestly smaller fragments are observed for the degradation leachates obtained at 701 days in portlandite systems, *i.e. ca.* 3 kDa (*ca.* 40 equivalent monomer units). *Figure 2-24* showed a significant increase in the NPOC values of portlandite systems at degradation times t > 800 days. In connection with this observation, the degradation leachates in portlandite systems collected at t = 1200 days are characterized by significantly enhanced molecular weights, *i.e.* ~ 14 kDa (~ 190 equivalent monomer units) and ~ 8 kDa (~ 110 equivalent monomer units) in the absence and presence of Fe(0), respectively.

EURAD (Deliverables n° 3.6, 3.7 and 3.8) - Final Report of results generated in CORI
Dissemination level: PU
Date of issue of this report: **05/07/2024**

Page 70
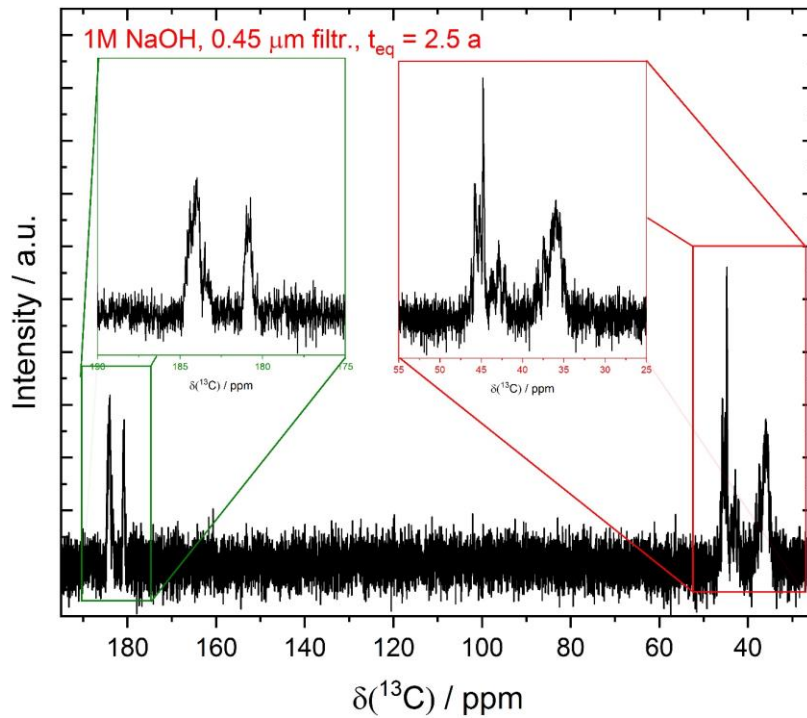
Figure 2-25: ^{13}C NMR spectrum of the UP2W degradation leachates after filtration (through 0.45 µm Teflon syringe filter) taken from the degradation experiment with UP2W in 1.0 M NaOH (with 20% D_2O).
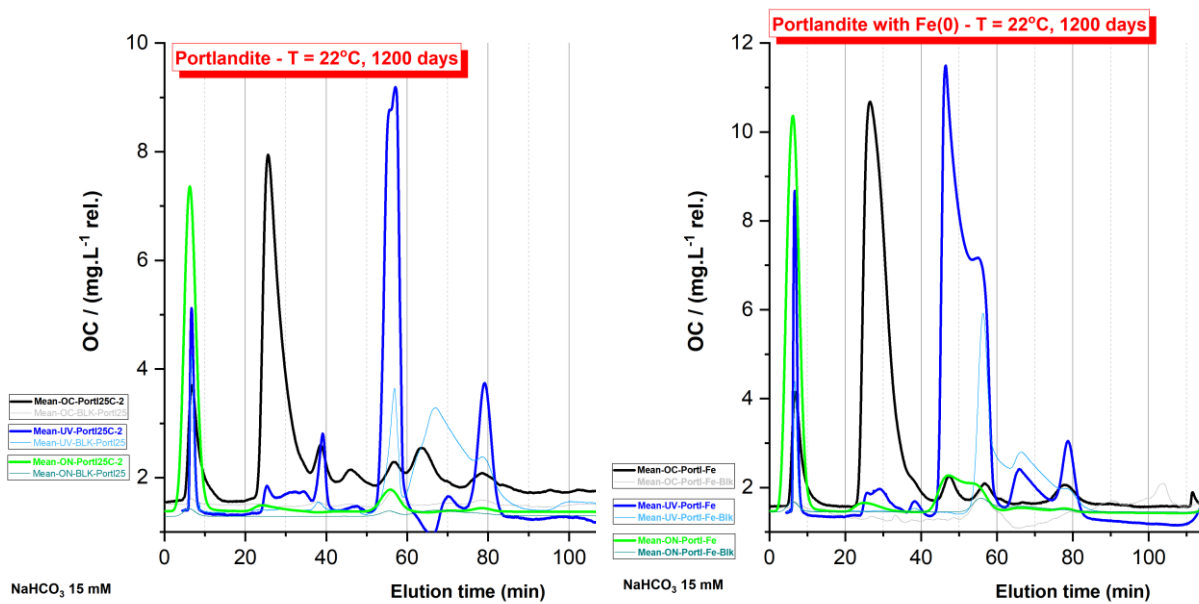
Figure 2-26:   SEC-OCD-UVD-OND spectra obtained after chromatographic separation of the UP2W degradation leachates collected after a degradation time of 1200 days. Figures correspond to degradation leachates obtained in portlandite (left) and portlandite + Fe(0) (right) systems, in both cases at T = 22°C.

EURAD (Deliverables n° 3.6, 3.7 and 3.8) - Final Report of results generated in CORI
Dissemination level: PU
Date of issue of this report: **05/07/2024**

Page 71

2.3.2 PAN based IER

The construction of three new nuclear power plants is planned in the Czech Republic. It is assumed that the reactors will be a different type than already existing reactors in Czech Republic. In the new types of NPPs, there may be ion exchange resins with higher activities than we have worked with so far. For this reason, Czech partners are interested in the properties of ion exchange resins and their degradation.

Radiolysis and hydrolysis of polyacrylonitrile materials synthesized in **[CTU]** (PAN, KNiFC-PAN and AMP-PAN), potentially present in RAW, have been studied by **[CTU]** and **[CV REZ]**. PAN samples in different types of solution (water, $Ca(OH)_2$ and NaOH) were irradiated to gamma irradiation (^{60}Co source), with a dose rate of 1.5 kGy·hour^{-1} and total dose of 1, 2, 4, 6, 8 and 12 MGy.

Data obtained from FT-IR and HRMS indicated degradation of PAN matrix. In recorded spectral data as the first step imidic acid formation was confirmed, which is tautomerized to amide and subsequently undergoes in nucleophilic attack of OH- to carboxylic acid after deprotonation. FT-IR spectrum of PAN hydrolysed in NaOH solution for 1 year is presented in *Figure 2-27*. The course of the hydrolysis is also schematically shown in this figure. It proceeds via intermediates (-C=N) and amide (-CONH2) and leads to the formation of a carboxyl functional group (-COOH). The presence of intermediates in the reaction mixture is manifested by characteristic bands of vibrations in the infrared spectrum of the examined samples. The hydrolysed samples show a characteristic decrease in band intensity of around 1455 cm^{-1}, which can be assigned to the nitrile functional group in polyacrylonitrile. This is also related to the decrease in the intensity of valence vibration of the nitrile group at 2250 cm^{-1}. The bands around 1565 cm^{-1} correspond to the vibrations -COO- alternatively -CONH$_2$. The wide intense band at a wavelength of 1637 cm^{-1} corresponds to the vibrations of the intermediate with the functional group –C=NH. The presence of PAN fragments after hydrolysis was also confirmed by MS spectra.
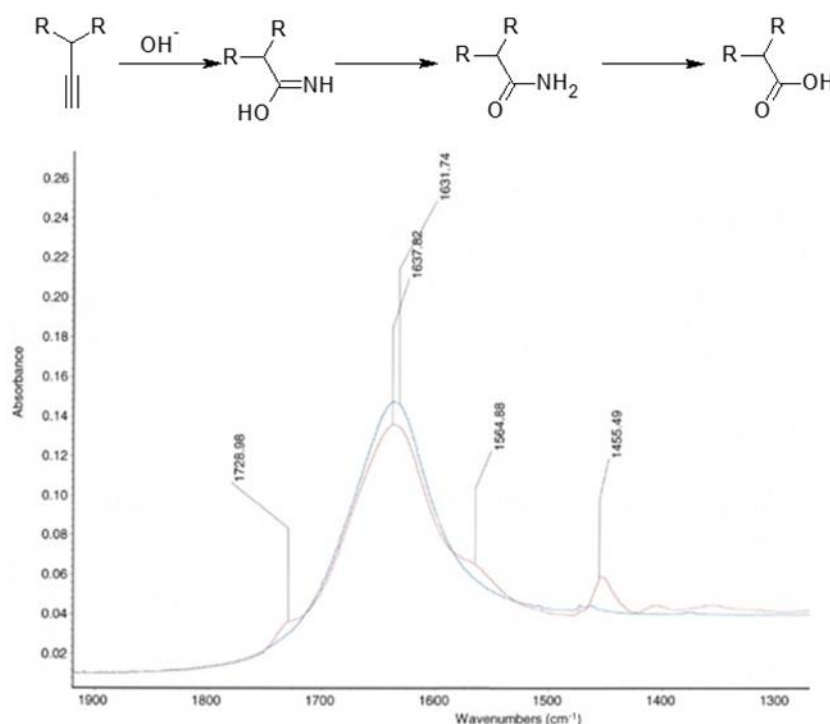
Figure 2-27:   FTIR spectra of hydrolysed PAN samples.

Physico-chemical changes are also observed from irradiation experiments. We can conclude that significant conversion of nitrile to amino groups occurred after irradiation of PAN.

EURAD (Deliverables n° 3.6, 3.7 and 3.8) - Final Report of results generated in CORI
Dissemination level: PU
Date of issue of this report: **05/07/2024**

Page 72

2.3.3 General conclusions

Studies carry out by **[KIT]** about the hydrolytic degradation UP2W filter show a differential behavior of the degradation in NaOH- and Ca(OH)$_2$-buffered systems. The key role of Ca is revealed in the degradation experiments. NPOC values determined in Ca(OH)$_2$-buffered systems experience a significant increase after a contact time of ca. 800 days.

Based on the analysis of solid phase and degraded leachates three proxy ligands were proposed to simulate the chemical characteristics of the UP2W degradation products: GTA, HIBA and HBA.

PAN based materials synthesized by CTU seems to be degraded by hydrolysis. The course of the hydrolysis proceeds via intermediates (-C=N) and amide (-CONH2) and leads to the formation of a carboxyl functional group (-COOH).

2.4 Degradation of superplasticizers

Several groups have studied the degradation of surperplasticizers as indicated in *Table 23*. The categories of superplasticizers studied are PolyCarboxylate Ether PCE, LignoSulfonate LS, PolyAryl Ether PAE and PolyMelamine Sulfonate PMS in order to consider different kinds of superplasticizers used or expected to be used in the formulation of cementitious matrices for radioactive waste packages.

Table 23: Superplasticizers studied in TASK 2 "Organic Degradation".

Type	Origin	Partner	Physical properties
PCE	Home-made	**[CNRS-SUBATECH]**	Polydispersity: M_w/M_n = 7.4 Refractive index increment: d_n/d_c = 0.151 +/- 0.02 mL/g
PCE/LS	Commercial CX ISOPLAST 531	**[SURAO], [CTU], [CV REZ], [UJV]**	pH ~ 2.7, density (20 °C): 1.03 ± 0.03 g/cm^2; Cl content: ≤ 0.10 mol. %; Na$_2$O equivalent: ≤ 1.50 mol. %
PCE	Commercial TEMPO 9, SIKA	**[BRGM/ISTO]**	pH (33 wt% aqueous solution +/- 1.5) = 4.5 +/- 1.0, Density (20°C) = 1.070 +/- 0.020, Polydispersity = 1.27, Cl content: ≤ 0.10 %, Na2O equivalent: ≤ 1.00 %
PCE, PAE	Commercial MasterEase 3000 from BASF, and CH210 and CH266 from TKK d.o.o.	**[JSI]**	Na content: 15 – 23 g/L, S content: 7 – 9 g/L; P content :1 – 20 g/L
LS	Commercial ISOLA BV	**[SURAO], [CTU], [CV REZ], [UJV]**	pH: 4.5 ± 1.0, density (20 °C): 1.17 ± 0.03 g/cm^2; Cl content: ≤ 0.10 mol. %, Na$_2$O equivalent: ≤ 2.50 mol. %
PMS	Commercial Peramin SMF10	**[CPST]**	pH (5% aqueous solution) ~ 8.8, density 4.50-6.50 g/cm^3 Cl content ≤ 0.004 %, Na$_2$O 0.021%

2.4.1 PCE homemade superplasticizer

In geological disposal facilities, low- and intermediate-level radioactive waste are conditioned in cementitious materials as confinement and stabilisation barrier. Superplasticizers (SPs) are widely used as organic chemical admixtures in the cement to improve the mechanical strength and workability of concrete or the dispersion and hydration of cement particles.

EURAD (Deliverables n° 3.6, 3.7 and 3.8) - Final Report of results generated in CORI
Dissemination level: PU
Date of issue of this report: **05/07/2024**

Page 73

Among the SPs, ether polycarboxylate based compound (PCE) is the last generation of polymer used by cement manufacturers. The chemical structure of PCE investigated by [**CNRS-SUBATECH**] is represented in *Figure 2-28*. The homemade PCE synthesis is based on a previous work in the laboratory (Androniuk, 2017) and originally adapted from (Plank *et al.*, 2008). Degradation under alpha and gamma irradiation was studied.
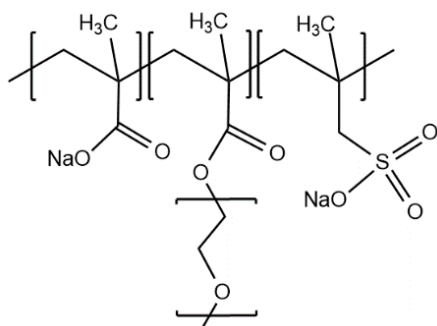
Figure 2-28:   *Ether Polycarboxylate (PCE) chemical structure.*

During disposal of nuclear waste, PCE undergoes degradation by the radiation emitted by material nearby. The resulting radiolytic degradation products can affect the radionuclide sorption and migration behavior in the waste package. In order to improve knowledge of degradation of organic wastes in conditions representative of disposal facilities, degradation of homemade synthesized PCE (*Figure 2-28*) is proposed by alpha and gamma irradiation. Gaseous and soluble organic degradation products will be characterized and quantified using micro-gas chromatography, ion chromatography, UV-visible spectrophotometry. It is worth noting that no data in the literature was found about the radiolytic degradation of PCE superplasticizer polymer.

2.4.1.1 Initial products characterization

Two PCE synthesis batches was prepared for this study; the mass-average molecular mass and polydispersity of these materials is presented in the Table 24. The polydispersity is quite high, between 5.8 and 7.4.

Table 24: SEC characterization of homemade PCE synthesis. M_W = mass-average molecular mass and M_n = number-average molecular mass.

Synthesis	Mass (g)	M_w (g.mol^{-1})	M_n (g.mol^{-1})	Polydispersity (M_w/M_n)
PCE2	0.9	98 350	16 980	5.8
PCE5	3.9	73 560	9 940	7.4

2.4.1.2 Gas production

Gas production of PCE homemade superplasticizer were studied in solution in different mediums under alpha and gamma irradiation. Irradiation was performed using a helium ion beam $_2^4He$ delivered by the ARRONAX cyclotron (E = 60.7 MeV, dose rate = 844 and 887 Gy.min^{-1}) and by gamma irradiation with a ^{137}Cs source (E = 0.66 MeV, dose rate = 6 – 8 Gy.min^{-1}). Hydrogen initial yields have been estimated, the results are presented in Table 25.

The irradiation of pure water lead to hydrogen formation yields of G(H_2)=(0.69± 0.05)×10^{-7} mol.J^{-1} and G(H_2)=(0.25 ± 0.02)×10^{-7} mol.J^{-1} for alpha and gamma radiolysis respectively. These yields are consistent with the ones given in the literature in the same radiolytic conditions. Moreover, this result

EURAD (Deliverables n° 3.6, 3.7 and 3.8) - Final Report of results generated in CORI
Dissemination level: PU
Date of issue of this report: **05/07/2024**

Page 74

shows also a higher formation of H_2 for alpha radiolysis compared to gamma radiolysis pointing out a linear energy transfer (LET) effect. Increasing the LET increases the energy deposition density within the track of the incident particle or the beam in the solution, increases the concentration of radicals, and therefore the probability of radical-radical recombination reactions, producing a higher concentration of molecular species in solution. Comparing H_2 formation with the presence of PCE superplasticizer in the 3 different studied mediums demonstrate a higher production of H_2 with the polymer in solution compared to the blank solutions. Indeed, this overproduction of H_2 can be explained by hydrogen abstraction reactions on the PCE molecule, $H^\bullet$ radicals react with the polymer by taking a hydrogen atom leading to the formation of an organic PCE radical and H_2.

Table 25: Hydrogen initial yields values for pure water and PCE 1 g·L^{-1} solutions in different mediums under alpha and gamma irradiation. PCE2 was used for alpha radiolysis and PCE5 for gamma radiolysis. ACW medium corresponds to Artificial Cement pore Water.

Medium	pH	Alpha radiolysis $G(H_2)$ ($\times 10^{-7}$ mol·J^{-1})	Gamma radiolysis $G(H_2)$ ($\times 10^{-7}$ mol·J^{-1})
H_2O *(this work)*	6.9	0.69 ± 0.05	0.25 ± 0.02
H_2O *(literature Crumière et al. (2013))*	5.6	0.64 ± 0.06	0.26 ± 0.03
PCE 1 g.L^{-1} H_2O	8.5	1.34 ± 0.09	1.12 ± 0.05
K^+	13.7	0.75 ± 0.05	0.42 ± 0.03
PCE 1 g.L^{-1} K^+	13.7	0.84 ± 0.08	0.71 ± 0.03
ACW	13.7	0.67 ± 0.04	0.43 ± 0.03
PCE 1 g.L^{-1} ACW	13.7	0.90 ± 0.08	0.70 ± 0.04

CO_2 has been measured as well for each irradiated solutions described in *Table 25*. The carbon dioxide production reaches, for a gamma irradiated PCE 1 *g.L^{-1}* solution in water, $G(CO_2)=(0.44 \pm 0.04)\times 10^{-7}$ mol.J^{-1}. CO_2 can be formed by indirect radiolysis of PCE carboxylate moieties by reaction with a hydroxyl radical $HO^\bullet$ leading to the formation of a $RCOO^\bullet$ radical (Equation 5). This radical can then release a CO_2 molecule by electronic rearrangement (Equation 6).

$$HO^\bullet + RCOO^- \rightarrow HO^- + RCOO^\bullet$$
<div align="right">Equation 5</div>

$$RCOO^\bullet \rightarrow R^\bullet + CO_2$$
<div align="right">Equation 6</div>
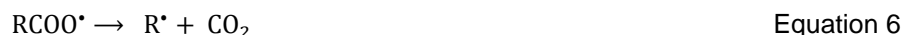
On the other side, a PCE water solution has also been irradiated by alpha radiolysis but there was no significant formation of CO_2 in the medium, no yield can be given. Less or no carbon dioxide is formed by alpha radiolysis compared to gamma radiolysis. Two hypotheses may explain this result: 1/ a LET effect exists, hydroxyl radical $HO^\bullet$ are more disseminated in gamma irradiated solutions and therefore have a higher probability to interact with the PCE molecule to form CO_2 and 2/ gamma radiolysis favours another way of carboxylate moiety radiolysis like the formation of formate or acetate ions.

For alkaline medium, in both K^+ and ACW solutions (with and without PCE) measurements of CO_2 were always under the detection limit, no carbon dioxide formation yields can be given. Either no CO_2 is produced during irradiation or the alkaline medium has an influence on the CO_2 accumulation. It may be possible all CO_2 formed under irradiation is rather dissolved in the pH 13.7 aqueous solutions in the form of CO_3^{2-}.

EURAD (Deliverables n° 3.6, 3.7 and 3.8) - Final Report of results generated in CORI
Dissemination level: PU
Date of issue of this report: **05/07/2024**

Page 75

2.4.1.3 Carboxylate anions degradation products

After gas measurements, the alpha and gamma irradiated solutions were analyzed by ion chromatography to quantify carbonates and small organic anions coming from the radiolytic degradation of PCE superplasticizer in solution. Results for carbonate, formate and acetate ions yield determination under alpha radiolysis were given in *Figure 2-29* and alpha and gamma radiolytic yields are presented in *Table 26*. If there is no yield given, either the species are not concentrated enough (very low concentration measured) or its formation does not follow any tendency with the dose.
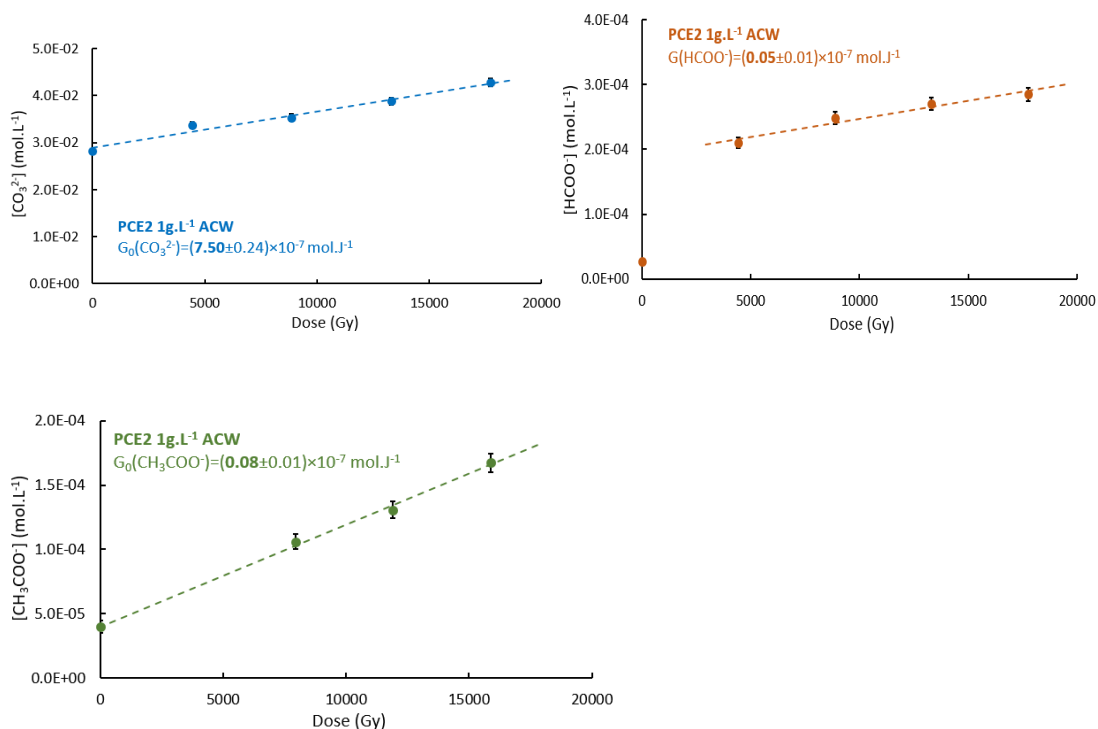
Figure 2-29:   *Carbonate, Formate, Acetate yield measurements for alpha irradiation in ACW media.*

EURAD (Deliverables n° 3.6, 3.7 and 3.8) - Final Report of results generated in CORI
Dissemination level: PU
Date of issue of this report: **05/07/2024**

Page 76

Table 26: Formation yields of carbonate, formate and acetate ions after alpha (α) and gamma (γ) radiolysis of PCE superplasticizer in various solutions and mediums without PCE. PCE2 was used for alpha radiolysis and PCE5 for gamma radiolysis.

Systems	pH	$G_0(CO_3^{2-})$ $(\times 10^{-7}\ mol \cdot J^{-1})$	$G_0(HCOO^-)$ $(\times 10^{-7}\ mol \cdot J^{-1})$	$G_0(CH_3COO^-)$ $(\times 10^{-7}\ mol \cdot J^{-1})$
PCE 1 g·L^{-1} H$_2$O	8.2	α: -0.24 ± 0.001 γ: -0.42 ± 0.01	α: 0.71 ± 0.04 γ: 1.32 ± 0.05	α: 0.023 ± 0.001 γ: -
H$_2$O	6.9	α: - γ: -	α: - γ: -	α: - γ: -
PCE 1 g·L^{-1} K$^+$	13.7	α: 8.85 ± 0.24 γ: 6.50 ± 0.33	α: 0.10 ± 0.01 γ: 1.13 ± 0.07	α: 0.07 ± 0.03 γ: 0.42 ± 0.03
K$^+$	13.7	α: 9.70 ± 0.34 γ: 8.01 ± 0.40	α: 0.039 ± 0.001 γ: -	α: - γ: -
PCE 1 g·L^{-1} ACW	13.7	α: 7.50 ± 0.24 γ: -	α: 0.35 ± 0.01 γ: 1.19 ± 0.08	α: 0.08 ± 0.01 γ: 0.47 ± 0.03
ACW	13.7	α: 7.57 ± 0.24 γ: 8.13 ± 0.40	α: 0.017 ± 0.001 γ: -	α: 0.026 ± 0.001 γ: -

It can be seem from the *Table 26* that formate and acetate ions formation yields after PCE solution irradiation are always in favor of gamma radiolysis compared to alpha radiolysis. PCE superplasticizer is more degraded in formate and acetate ions by gamma radiolysis highlighting a LET effect. A simple explanation is that the species that lead to the degradation of PCE into formate and acetate ions like $HO^\bullet$ / $O^{\bullet-}$ or $H^\bullet$ / e_{aq}^- (depending on the pH), are more spread in the solution in gamma radiolysis and therefore have a higher probability to interact with the PCE molecule to form formate and acetate ions.

2.4.2 Commercial PCE

2.4.2.1 Tempo 9

The **[BRGM]**'s contribution is focused on the degradation by radiolysis and hydrolysis of PCE superplasticizer Tempo 9 (from SIKA^{TM} cement supplier company) in contact with aqueous phase (water and alkaline solutions).

2.4.2.1.1 Hydrolysis

The hydrolysis of Tempo 9 superplasticizer was studied in pure water and in alkaline solutions. In pure water, structural analyses made by ^{1}H NMR show no change in the characteristic chemical shifts of the initial poly(PEG-co-methacrylic acid). The molecular weights of the copolymer are unchanged over time. The residual monomer content of PEG methacrylate is not altered.

In conclusion, prolonged exposure of the copolymer to an aqueous medium does not seem to have an impact on the chemical structure of the initial poly(methacrylate PEG-co-acid methacrylic). No hydrolysis reaction of the copolymer was observed by the techniques used.

However, in alkaline conditions structural changes in the copolymer were observed by ^{1}H NMR and FTIR analyses which suggest the presence of an ionic form of the copolymer. It is possible that

EURAD (Deliverables n° 3.6, 3.7 and 3.8) - Final Report of results generated in CORI
Dissemination level: PU
Date of issue of this report: **05/07/2024**

Page 77

polymethacrylic acid appears after 1 month of hydrolysis. Indeed, SEC analysis show that the concentration of low-molecular-weight organic compounds increases significantly from this deadline. A degradation by-product, probably methoxy PEG (mPEG), has formed, representing about 1.5 g/L explaining the jump from 2.1 to 3.6 g/L of mPEG and PEGMA content (*Figure 2-31*).
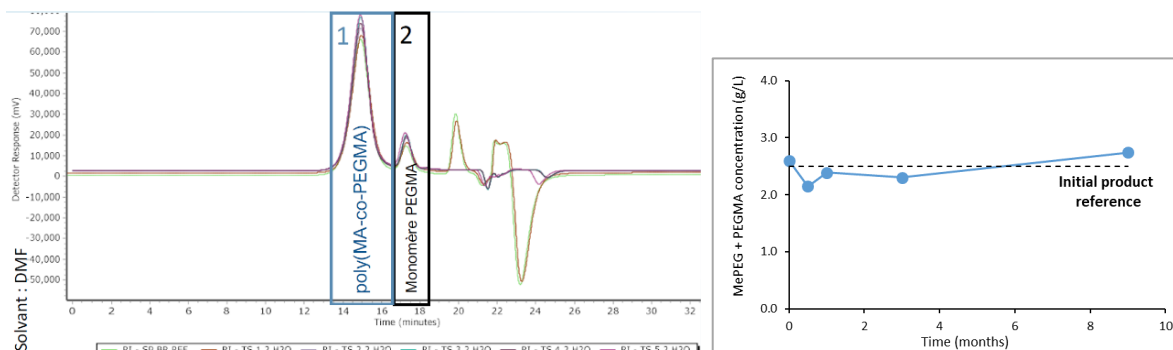
Figure 2-30:   *SEC analysis of hydrolysed PCE in water. Left: spectra obtained at different times. Right: variations of mPEG and PEGMA concentrations according to time estimated from the surface area under respective peaks. An extern calibration is used for this estimation of concentrations.*
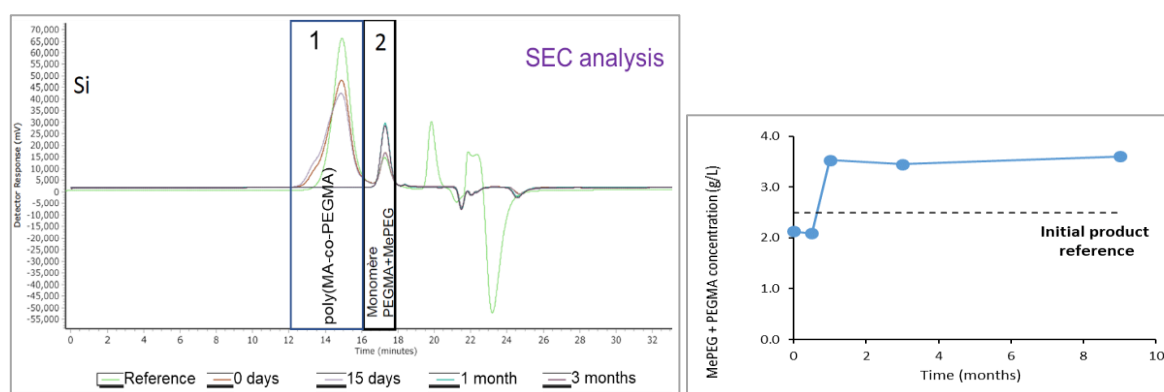
Figure 2-31:   *SEC analysis of hydrolysed PCE in alkaline solution. Left: spectra obtained from alkaline solutions at different times. Right: variations of mPEG and PEGMA concentrations according to time estimated from the surface area under respective peaks. An extern calibration is used for this estimation of concentrations.*

Results of pH-titrations used to measure the concentration of polymethacrylic acid (PMA) show that the chemical composition of the superplasticizer is unchanged after up to 1 month of experiment (*Figure 2-32*). After this period, the chemical composition of the superplasticizer is significantly modified. The copolymer seems to be richer in polymethacrylic acid and depleted in polymethacrylate of PEG. The sample has a higher concentration of methoxy polyethylene glycol (mPEG), a degradation product of the copolymer, which is consistent with the change in the chemical composition of the copolymer. For the following samples (3 and 6 months), the chemical composition of the superplasticizer seems to no longer change significantly compared to the 1-month sample.

EURAD (Deliverables n° 3.6, 3.7 and 3.8) - Final Report of results generated in CORI   Page 78
Dissemination level: PU
Date of issue of this report: **05/07/2024**
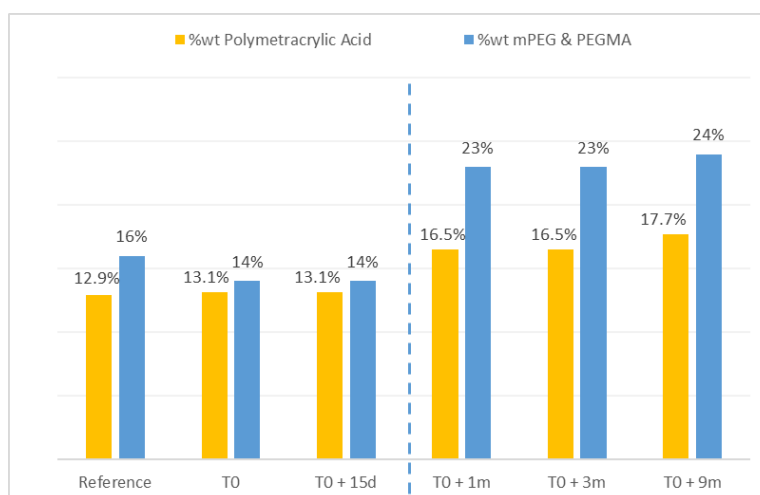
Figure 2-32:   *Polymetacrylic acid concentrations according to pH-titrations (yellow histograms). "Reference" referred to the commercial product. T0 corresponds to the start of the experiments, i.e. the time when commercial product was diluted in alkaline solution. For comparison of analytical techniques, blue histograms are mPEG and PEGMA concentrations estimated with SEC titrations.*

In conclusion, the poly(methacrylate PEG-co-acid methacrylic) degrades in alkaline solutions. The hydroxide ions (OH⁻) can react on two potential reaction sites of the molecule: *(i)* an acid-base reaction on the carboxylic group and (ii) a saponification reaction on the ester group.
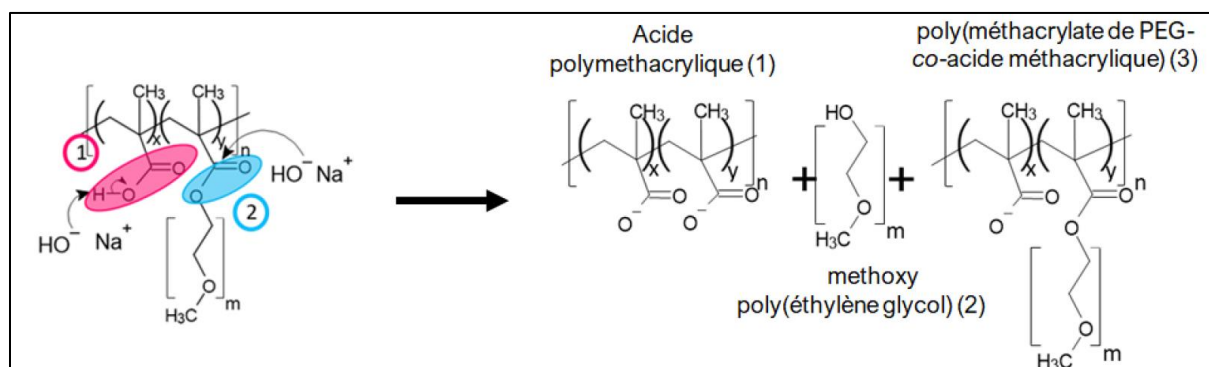
Figure 2-33:   *Degradation way of PCE superplastizer with the formation of polymetacrylic acid and methoxy polyethylene glycol (mPEG). The carboxylic groups (1) and ester group (2) reaction sites are indicated in the figure in pink and blue color.*

2.4.2.2 Radiolysis of PCE superplasticizer

After irradiation, the aqueous part of the irradiated samples (PCE in H_2O) and (PCE + NaOH) are exposed to hydrolysis. A set of analysis of the solution composition was performed on radiolysed samples before and after hydrolysis:

- For both systems (irradiated samples in H_2O and in NaOH solution), the pH decreases with hydrolysis, but it seems to reach a plateau relatively quickly. For irradiated solutions in water for example, initial pH is 8.35 and it decreases to 3.27 and 3.37 after 3 and 6 months of hydrolysis, respectively.
- For both systems, IR-TF spectra show drastic differences with the initial sample before radiolysis: apparition of a larger signal for the pic representative of C=O bonds, apparition of a signal characteristic of OH function (carboxylic acid or alcohol), and important decrease of the –C-O-

EURAD (Deliverables n° 3.6, 3.7 and 3.8) - Final Report of results generated in CORI
Dissemination level: PU
Date of issue of this report: **05/07/2024**

Page 79

C- signal. In contrast, spectra of irradiated samples compared to hydrolyzed pre-irradiate are quite similar. The spectra related to the irradiated samples in H_2O are showed in *Figure 2-34.*

- SEC analysis after radiolysis and before hydrolysis shows different signals that seems to indicate degradation of the initial product formation of smaller molecules (*Figure 2-35*).
- pH titration shows an increase of the methacrylic acid PMA content after the radiolysis (*Figure 2-36*), this concentration remains stable during the post-hydrolysis. This increase of PMA content could indicate a potential degradation of the PCE. This degradation seems to be higher than in the case of a simple hydrolysis. After 6 months of hydrolysis, the PMA concentration seems to slightly decrease but this measurement is uncertain due to the low amount of remaining solution.
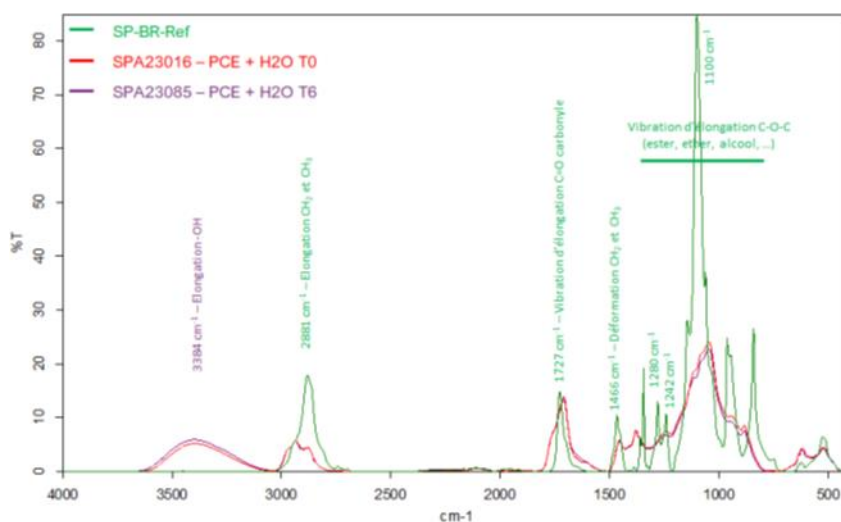
Figure 2-34: ^1H NMR (top) and IR-TF (bottom) spectra of irradiated PCE superplasticizer before (Reference) and after irradiation in water and alkaline solutions.

SEC analysis shows signals different than the ones of the reference sample with increasing retention times synonymous of the formation of smaller molecules not identified (*Figure 2-35*). At last, pH-titration were done on the two irradiated samples (PCE + H_2O) and (PCE + NaOH). If the hydrolysis of PCE diluted in water show no variation, the irradiated PCE in water contains a concentration of polymetacrylic acid higher than in the reference. This increase could indicate a potential degradation of the PCE. In the case of PCE in NaOH solutions, the irradiation seems to be higher as revealed by the measured concentration (21.9 %wt against 12.9 %wt in the reference).
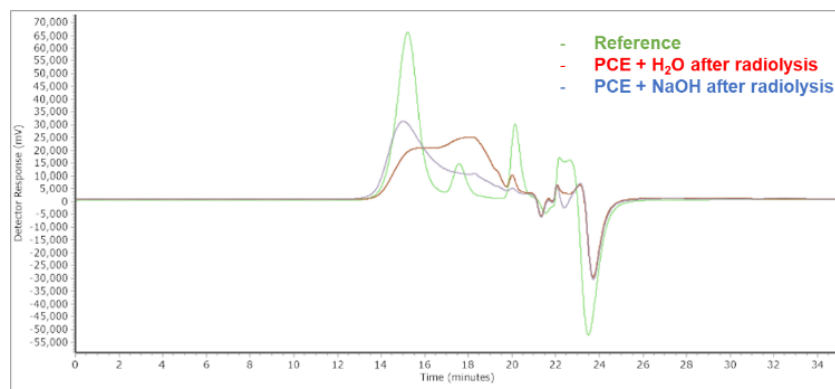
Figure 2-35:   SEC spectra of irradiated PCE superplasticizer before (Reference) and after irradiation in water and alkaline solutions.

EURAD (Deliverables n° 3.6, 3.7 and 3.8) - Final Report of results generated in CORI   Page 80
Dissemination level: PU
Date of issue of this report: **05/07/2024**
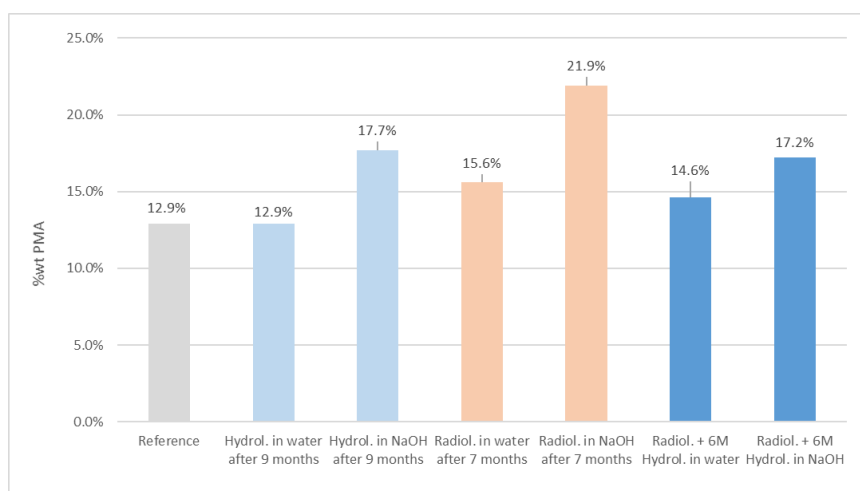
Figure 2-36   *Polymetacrylic acid (PMA) concentrations according to pH-titrations. "Reference" referred to the commercial product. "Hydrol." refers to hydrolysis experiments performed during 9 months in pure water and alkaline solutions. "Radiol." corresponds to radiolysis experiments in water and alkaline solutions. "Radiol.+ 6 months Hydrol." refers to the 6 month-hydrolysis performed on irradiated solutions.*

2.4.2.3 Cementol Hiperplast 210 (CH210)

[UVJ] studied the radiolysis and hydrolysis of the commercial PCE Cementol Hiperplast 210 (CH210) from TKK company. This kind of superplasticizers is intended to be used in the Slovenian radioactive waste disposal programme.

Under irradiation, the gelation of the sample has occurred between 0.6-0.8 MGy of irradiation dose. However, analysis of these gases was not possible in this experimental setup. At irradiation dose of 3.2 MGy, part of sample turned back from a gel into a liquid. This behavior could not be explained;

Analysis of its FTIR spectrum revealed the presence of O-H functional groups, ether functional groups, carboxylate functional groups, as well as C-H stretching from sp^3 hybridized carbons *(Figure 2-37)*. It can be seen that there is no significant difference between the irradiated sample (1.1 MGy dose) and the non-irradiated sample. NMR analysis also indicated no significant differences between the irradiated and non-irradiated samples.
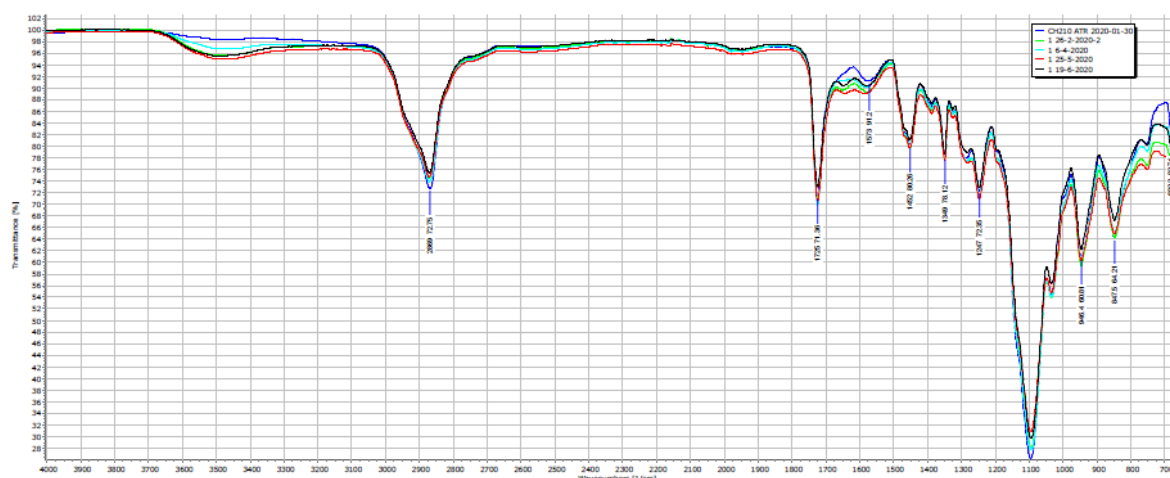
Figure 2-37:   *FTIR spectra comparing original and irradiated CH210 PCE sample. Band assignment: O-H: 3100 – 2700 cm^{-1}, C=O: 1726 cm^{-1}, C-O-H: 1422 cm^{-1}, C-O: 1247 cm^{-1}*

EURAD (Deliverables n° 3.6, 3.7 and 3.8) - Final Report of results generated in CORI
Dissemination level: PU
Date of issue of this report: **05/07/2024**

Page 81

Size exclusion chromatography revealed an increase in molecular weight after irradiation (*Table 27*), which is consistent with visual observation of gelation of the irradiated sample. In addition, only 47% of the sample remained soluble, and the results for the irradiated sample correspond only to the soluble part. It can be assumed that the PU molecular weight of the insoluble part is even larger.

Table 27: Molecular weight of not irradiated and irradiated sample CH210

Sample	M_w	M_n	M_w/M_n
CH210	63000	30500	2.069
CH210 irradiated	125400	22600	5.561

The irradiate sample to 1.1 MGy was submitted to basic hydrolysis in NaOH solution for 3 days. It seems that hydrolysis induced cleavage of ester bonds and cleavage of PEG sidechains from the backbone of the PCEs. These appear as visible peaks at 12-13 min elution time in the SEC chromatogram (Figure 2-38). In addition, the C=O stretch (1700 cm^{-1}) disappears from the FTIR spectra (Figure 2-37).
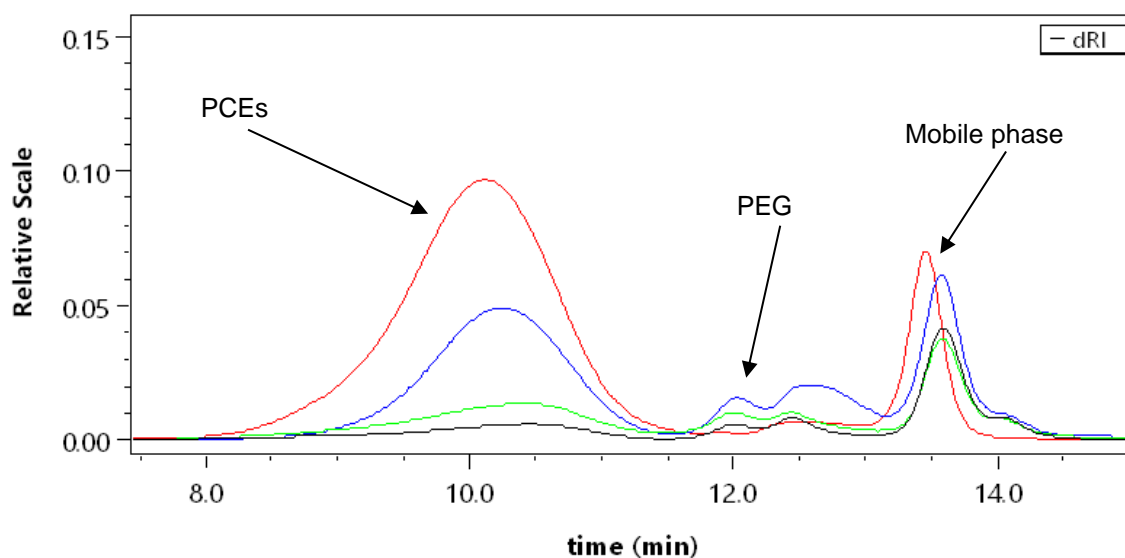
Figure 2-38:   *SEC chromatogram of original and irradiated CH210 PCEs sample after hydrolysis. Red – original, blue – original hydrolyzed in 0.1 M NaOH, green – insoluble fraction of irradiated to 1.1 MGy and hydrolyzed in 0.1 M NaOH, black – soluble and insoluble fraction of irradiated to 1.1 MGy and hydrolyzed in 0.1 M NaOH.*

EURAD (Deliverables n° 3.6, 3.7 and 3.8) - Final Report of results generated in CORI
Dissemination level: PU
Date of issue of this report: **05/07/2024**

Page 82
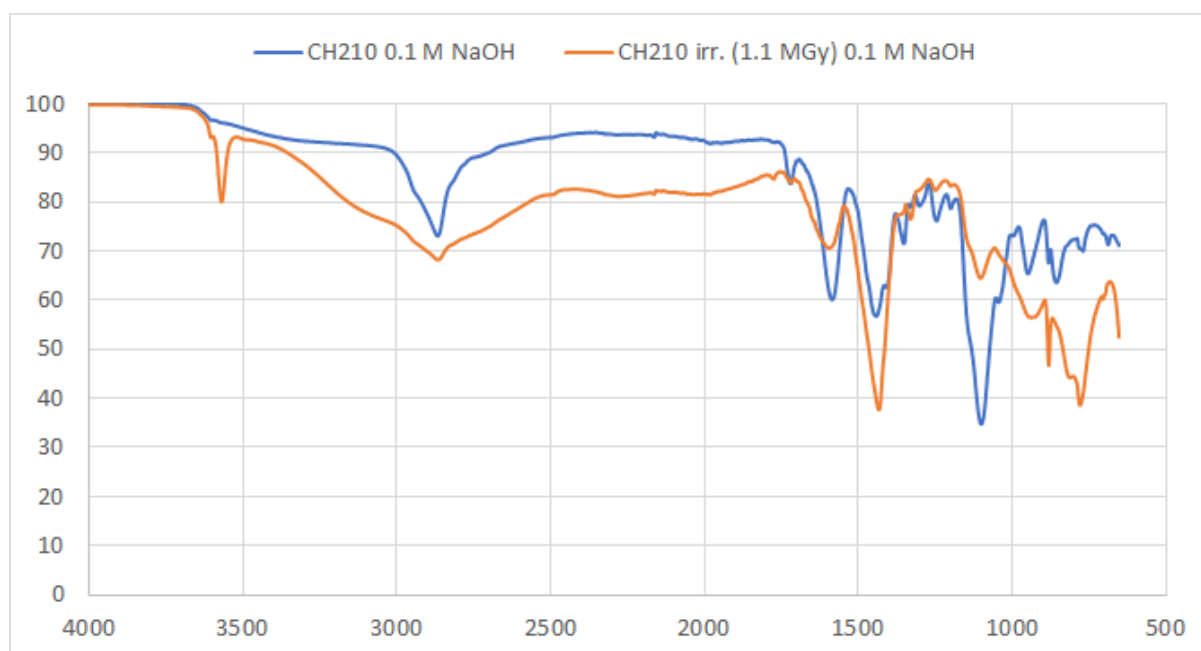
Figure 2-39:   *FTIR spectra of original and irradiated CH210 PCEs sample (1.1 MGy) fter hydrolysis in 0.1 M NaOH.*

2.4.3 Polycarboxylic ether and lignosulfonate SP

Radiolysis of superplasticizer CX ISOPLAST 531 based on polycarboxylic ether and lignosulfonate, have been studied by **[CTU]**. The chemical structure is presented in Figure 2-40. This superplasticizer was irradiated to gamma irradiation by **[CV REZ]** under different conditions (original sample, addition of solid or solution of NaOH, addition of solid or solution of $Ca(OH)_2$), with the dose rate of 1.5 kGy·hour^{-1} and absorbed dose of 1, 2, 4, 6 and 8 MGy.

LC-MS analysis was performed for different samples. The presence 6 main regions: m/z 223, peak with max around m/z 548, m/z 664, m/z 808, m/z 1029, m/z 1816 (all reveal constant repeating mass differences). All peaks can be attributed to product ions of CX ISOPLAST 531, where mass differences represent the elimination of functional groups from the structure of original plasticizer. *Figure 2-41* shows the spectrum of the sample of CX ISOPLAST 531 irradiated to 4 MGy in presence of sodium hydroxide. This sample gelatinized during irradiation indicating the crosslinking of the chains. MS studies of the fraction dissolved in water indicates the present of low molecular fragments m/z 141, 185, 241 and 580 that might be attributed to decompositions products of plasticizer. Most of them might be assigned to molecules loss of sulphonyl moieties which were repeated several times.

Formula Weight   = $1025.972127 + [27.04522]_n$

Figure 2-40:   *Chemical structure of commercial PCE/LS CX ISOPLAST 531.*

EURAD (Deliverables n° 3.6, 3.7 and 3.8) - Final Report of results generated in CORI
Dissemination level: PU
Date of issue of this report: **05/07/2024**

Page 83

Figure 2-41:   HRMS of superplasticizer CX ISOPLAST 531: A non-irradiated sample, B – sample with received dose of 2 MGy (pH 12.5), C – sample with received dose of 4 MGy (pH 12.5).

On the other side the LC-MS analysis of irradiated CX ISOPLAST 531 with partial separation, indicates presence of several products of radiolysis which differ each other on molecular weight. As can be seen on *Figure 2-42* the most abundant mass and shape of polymers can be observed at m/z 559, 708, 1073, 1183 and 1816. This means that CX ISOPLAST 531 polymer is being degraded by cleavage of long carbon/alkyl-sulphono moieties form the structure. Differences corresponds to 100 – 200 Da (low molecular fragments) or 500-600 Da (high molecular fragments).

EURAD (Deliverables n° 3.6, 3.7 and 3.8) - Final Report of results generated in CORI
Dissemination level: PU
Date of issue of this report: **05/07/2024**

Page 84

Figure 2-42:   LC-MS of superplasticizer CX ISOPLAST 531: irradiated sample 4 MGy.

LC-MS results showed no difference regarding nature of basic solution (sodium hydroxide or calcium hydroxide) considered for irradiation of CX ISOPLAST 531. The effect of basic conditions may help the degradation of polymeric chains and formation of low molecular fragments.

2.4.4 SP based on polymelamine sulphonate

The commercial cement SP based on polymelamine sulphonate (PMS) Peramin SMF10 (Peramin AB, Sweden) was chosen by **[CPST]** for hydrolysis investigations. Chemical structure of PMS is presented in *Figure 2-43*.

Figure 2-43:   Chemical structure of PMS.

The detailed chemical composition of the initial product was obtained by Wavelength dispersive X-Ray Fluorescence. Major constituent was found to be a polymer of PMS ($C_3N_3(NH)_3(CH_2)_3SO_3Na$ unity structure) in quantity over 99.8%. Minor constituents present in the PMS were determined (P_2O_5, ZnO, CaO, Na_2O etc.) (*Table 28*).

Table 28: Detailed chemical composition of commercial product Peramin SMF10.

Compound	Percentage
PMS	**99.824**
Na_2O	0.021
Al_2O_3	0.017
SiO_2	0.021
P_2O_5	0.054

EURAD (Deliverables n° 3.6, 3.7 and 3.8) - Final Report of results generated in CORI
Dissemination level: PU
Date of issue of this report: **05/07/2024**

Page 85

K$_2$O	0.006
CaO	0.017
Fe$_2$O$_3$	0.005
ZnO	0.033
Cl	0.004

2.4.4.1 Hydrolysis of SP

Hydrolysis experiments of PMS superplasticizer in different aqueous solutions at room temperature were conducted by **[CPST]**. No difference was observed by UV/Vis and Raman spectrometric (*Figure 2-44*) of PMS hydrolytic after 2 years and 6 months show no modification compared to the initial PMS solutions.
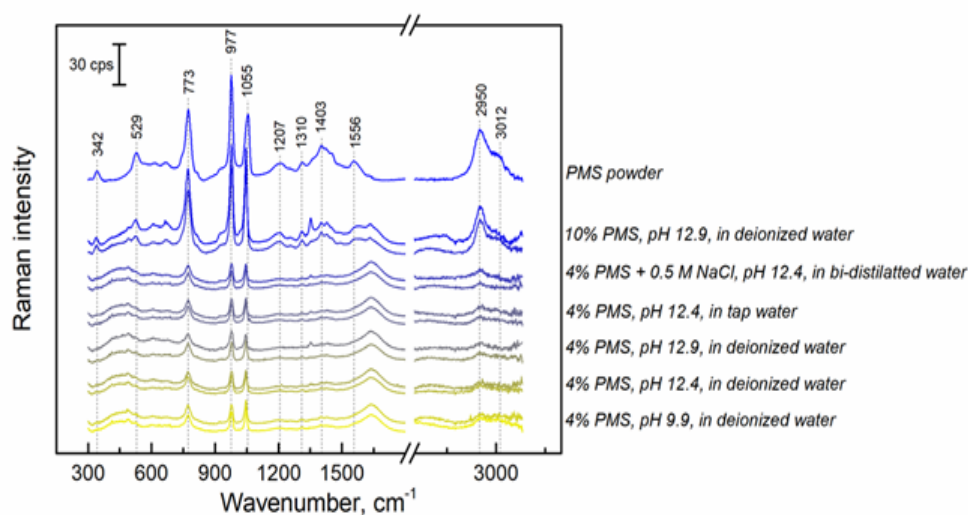
Figure 2-44:   *Raman spectra of different polymelamine sulphonate (PMS) hydrolytic solutions during time. The upper curves indicate solutions after 2.5 years, the lower ones – of just prepared samples*

2.4.5 ISOLA superplasticizer

The degradation by radiolysis and hydrolysis of superplasticizer ISOLA were studied by **[UVJ]**. ISOLA superplasticizer samples was submitted to hydrolysis at elevated temperature.

Proton and carbon NMR spectra of samples with ISOLA superplasticizer in different environments were measured to determine the structure of the plasticizer. It was found that the water in which the ISOLA samples has a significant signal in the spectrum, even though the sample was diluted with D$_2$O. The interpretability of the ^{1}H NMR spectrum is so difficult due to significant solvent shielding. A NMR spectra of ISOLA superplasticizer hydrolyzed in alkaline Ca(OH)$_2$ solution at 60 °C is presented in *Figure 2-45*. Comparison with original materials shows that the signal related to methyl group is missing in the sample of ISOLA in alkaline solution. It could be associated to a kind of degradation of superplasticizer structure.

For carbon NMR a chemical shift of 146 ppm, 122 ppm, 115 ppm and 112 ppm indicate the presence of aromatic and heteroaromatic nuclei of different types. Chemical shifts that lie between 55-69 ppm can be attributed to ether, ester and alcohol functional groups.

EURAD (Deliverables n° 3.6, 3.7 and 3.8) - Final Report of results generated in CORI
Dissemination level: PU
Date of issue of this report: **05/07/2024**

Page 86
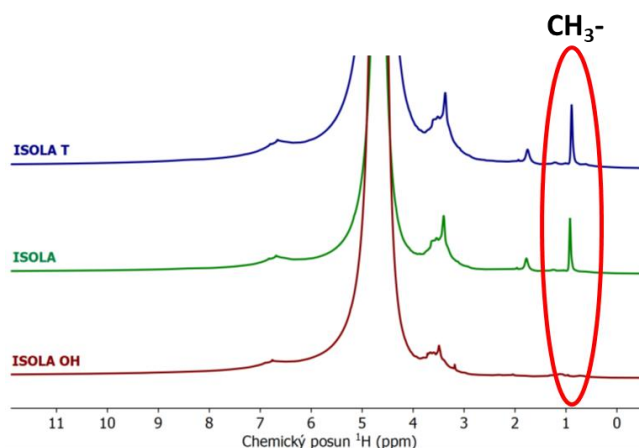
Figure 2-45:   *Part of ISOLA superplasticizer 1H NMR spectra – comparison of original material (green, ISOLA), hydrolyzed material at elevated temperature of 60°C (blue, ISOLA T) and material in alkaline $Ca(OH)_2$ solution (brown, ISOLA OH).*

2.4.6 General conclusions

The studies carried with [**CNRS-SUBATECH**] homemade PCE showed that the major gas formed under radiolysis was H_2 and carbon dioxide CO_2. The presence of PCE superplasticizer in the 3 different studied mediums always demonstrates a higher production of H_2 with the polymer in solution compared to the blank solutions without PCE. CO_2 formation was only observed for the gamma radiolysis of PCE in ultrapure water. In solution, the major species formed were carbonate, formate and acetate anions and small amounts of oxalate and sulfate anions. A higher formation of formate and acetate ions has been observed in the presence of PCE in solution. These species are certainly formed by the degradation of the carboxylate moieties of the PCE polymer.

Studies performed by [**BRGM**] with PCE tempo 9 superplasticizers showed that the concentration of superplasticizer in solution and conditions of irradiation can highly change the behavior of PCE under irradiation. Dilution of superplasticizer leads to the degradation of the polymer and formation of small molecules while the irradiation in higher concentration leads to the cross-linking. Irradiated PCE diluted in water or in NaOH pH 13 solutions degrades significantly. The alkaline media seem to favour the degradation. Indeed, the irradiation of the material tends to increase the degradation of the initial copolymer with respect to only hydrolysis. An increase of about 3% of the by-products (polymethacrylic acid and methoxy polyethylene glycol) content is observed. The post-hydrolysis of the irradiated solutions seems to not influence the concentrations of by-products.

JSI results indicate that backbone crosslinking is the main process during irradiation of investigated commercial PCE Cementol Hiperplast 210, with gelation occurring at 0.6 – 0.8 MGy of gamma irradiation dose. The result is a notable increase in the molecular weight of the sample. At irradiation doses of 3.2 MGy, cleavage of PEG sidechains occurs, a process that is also dominant during NaOH hydrolysis.

CX ISOPLAST 531 superplasticizer based on polycarboxylic ether and lignosulfonate gelatinized during irradiation indicating the crosslinking of the chains. The analysis of soluble fraction showed the formation of low molecular fragments that might be associated to the degradation of the superplasticizer products and loss of sulphonyl sideway backbone.

Spectroscopy analysis of Peramin SMF10SP superplasticizer based on polymelamine sulphonate did not highlight structural changes after 2.5 year of hydrolysis in pure water.

Basic hydrolysis of ISOLA superplasticizer at 60 °C showed some structural change when compared to non-aged material that might be associated to some kind of superplasticizer degradation.

EURAD (Deliverables n° 3.6, 3.7 and 3.8) - Final Report of results generated in CORI
Dissemination level: PU
Date of issue of this report: **05/07/2024**

Page 87

2.5 Summary for Task 2

Long-term alkaline hydrolytic degradation of cellulose (up to 28 years) at ambient temperature confirms that cellulose degradation slowly progressed after a rather short (~3 years) first phase of fast removal ("peeling-off") of glucose units from the reducing end of the cellulose chain. The secondary slow phase of peeling-off is assumed to proceed via the same reaction paths as the fast process.

Hydrolytic cellulose degradation studies also indicated that the presence of portlandite and Fe(0) powder have no significant influence neither on the degradation rate nor on the type of degradation products formed. Furthermore, α-ISA is stable in artificial cement water at pH = 13.3 under reducing conditions and a temperature of 90°C over a period of up to 120 days, both in absence and in presence of portlandite and Fe(0) powder.

Pre-irradiation of cellulosic tissues leads to a significant formation of degradation products other than those observed for non-irradiated tissues. It leads to a significantly faster DOC and ISA production during subsequent hydrolytic degradation in artificial cement water. This pre-irradiation of cellulosic tissues does not seem to alter the alkaline degradation pathways, but rather accelerates the overall degradation. The model previously proposed by PSI to predict cellulose degradation and ISA production is still applicable.

Degradation of hard PVC under radiolysis followed by hydrolysis have showed similar results as the ones described in the literature for soft PVC. The main difference is that phthalate is one the most important degradation product of soft PVC and not found as degradation product of hard PVC. This can be explained by the fact that phthalate is added in high concentration to the commercial soft PVC as plasticizer additive and is found in very low concentration in formulation of the hard one.

Organic carboxylic acids produced from radiolysis degradation of PVC in solution are: (i) acids with long carbon chains (C16 and C18) are observed during solid analysis and (ii) small organic acids (acetic, chloro- and dichloroacetic, succinic) are mainly formed and transferred to the solution. Alcohols, ketones and carboxylic acids are formed during hydrolysis of pre-irradiated materials, and succinic acid is mainly released into solution for the degradation of PVC.

Basic hydrolytic degradation of PAN based material (UP2W filter and IER) leads to the degradation of the material. For UP2W filter, the release of organic molecules in solution significant increase after a contact time of ca. 800 days. Three proxy ligands were proposed to simulate the chemical characteristics of the degradation products: glutaric acid, α-hydroxyisobutyric acid and 3-hydroxybutyric acid.

Irradiation of different kinds of pure superplasticizer showed unexpected results. In fact, superplasticizers backbone crosslinked under irradiation. This crosslinking led to difficulties of characterization and furthermore behavior cannot be extrapolated to bulk cement in disposal conditions. In the cement, superplasticizer will be present in lower concentration and cement particles would probably reduce the possibility that large amounts of superplasticizers could come into contact for crosslinking.

Dilution of superplasticizer solution seems to avoid chain crosslinking, favouring some degradation of the polymer chains and formation of small molecules in solution. Analysis of soluble fraction of partial crosslinked systems seems indicate some degree of degradation of superplasticizers and release of low molecular weight molecules in solutions. Radiolytic degradation of homemade PCE led to the release of formate and acetate.

Degraded solutions were provided to Task 3 and 4 in order to analyse the effect real leachates in the interaction with cement material and radionuclide. These results are discussed in the Task 3 and Task 4 dedicated sections of this document.

![eurad logo] European Joint Programme on Radioactive Waste Management

EURAD (Deliverables n° 3.6, 3.7 and 3.8) - Final Report of results generated in CORI
Dissemination level: PU
Date of issue of this report: **05/07/2024**

Page 88

3. Materials and methods dedicated to Task 3 and Task 4

3.1 Organic preparation, degradation and characterization

3.1.1 ISA

Most of the organizations analyzing the effects of the cellulose degradation products used the isosaccharinic acid, α-ISA, synthesized in the laboratory using a standard procedure (Whistler and BeMiller, 1963 Van Loon *et al.*, 1997; Vercammen, 2000). The method starts with the preparation of Ca-ISA, dissolving α- lactose in Ca(OH)$_2$, which is further converted it in the Na-ISA using an ion exchange resin (**[KIT (Amphos21)]**, **[JGU]**, **[UHelsinki]**, **[CIEMAT]**).

[CNRS-SUBATECH] has used crystalline calcium α-D-isosaccharinate purchased from Alfa Aesar (>98% purity) as precursor. The ISA was purified following the CEA protocol modified from Whistler and BeMiller (1963) before using in migration experiments. For Stage III, ISA was used as Na-ISA prepared by converting Ca(ISA)$_2$ solutions into NaISA solutions using an ion exchange (Amberlite IR 120, Na-form, Supelco).

[SCK CEN] has applied this preparation protocol with some minor modifications: reflux was used during the first boiling step to maintain volume; filtration was performed on 0.8 µm Nylon filters and a final purification step with acetone was added. The Ca- α -(ISA)$_2$ was then converted to Na-α-ISA using a Chelex®-100 BioRad resin with *ca*. 25 g of resin for 1 g of Ca-α-(ISA)$_2$. The suspension was filtered with 0.2 µm Nylon filters to remove the resin and the filtrate was evaporated until a syrup was obtained. Finally, the water was removed by washing with di-ethylether and drying at 50°C. The molal yield of the whole procedure was 12-13%. The purity was controlled by Electrospray Ionization Mass Spectrometry (ESI-MS) and no impurities were identified. In addition, the concentration of solutions further prepared from the solid Na-α-ISA was always checked with IC-PAD analysis.

Commercial ISA (Isosaccharinic acid-1,4-lactone, by Biosynth Carbosynth®; CAS 7397-89-9, formula C$_6$H$_{10}$O$_5$) has been used by **[CIEMAT(CSIC)]**.

In addition, some organizations made additional experiments with real degradation products (RDP) of cellulosic materials obtained by hydrolysis **[PSI]** and/or irradiation by **[SCK CEN]** working in Task 2 (see section 2.1).

3.1.2 EDTA

EDTA (C$_{10}$H$_{14}$N$_2$Na$_2$O$_8$·2H$_2$O, EDTA disodium salt dihydrate, CAS number 6381-92-6, Sigma-Aldrich) has been used by **[CEA]**. Stock-solutions were prepared by dissolving pure salt in ultrapure water (Milli-Q water, 18.2 MΩ cm, Millipore) to reach 10^{-1} mol/L. Aliquots of solution are diluted in Milli-Q water and Total Carbon (TC) and Total Inorganic Carbon (TIC) concentrations were measured using Variotoc Cube analyzer, (Elementar). The Total Organic Carbon (TOC) concentration is then calculated from TIC and TC concentrations. Also, C-14 radiolabelled EDTA stock solution was prepared from a radioactive source containing 9.25 MBq and an initial EDTA concentration of 1.8 mM (initially packaged in sterile water and stored in a refrigerator at 4°C, purchased from American Radiolabeled Chemicals. Inc).

EDTA (C$_{10}$H$_{14}$N$_2$O$_8$·2H$_2$O, EDTA (Ethylenediaminetetraacetic acid) disodium salt dihydrate (by Scharlau), CAS 6381-92-6, Scharlau) has been used by **[CIEMAT(CSIC)]**.

[KIT(JGU)] prepared a tracer solution by diluting a stock solution of 3.7 MBq·mL^{-1} of ^{14}C-EDTA (Hartmann Analytic, Germany) in degassed Milli-Q water. Additionally, stock solutions of inactive EDTA were prepared using an appropriate amount of Na$_4$EDTA·2(H$_2$O) (VWR International GmbH, Germany) diluted with degassed Milli-Q water and ACW, respectively. The concentrations of the stock solutions ranged from 0.1 to 0.4 M, as specified in the experiments.

EURAD (Deliverables n° 3.6, 3.7 and 3.8) - Final Report of results generated in CORI
Dissemination level: PU
Date of issue of this report: **05/07/2024**

Page 89

3.1.3 Phthalic acid

PHTHAL (HOOCC$_6$H$_4$COOK, Potassium phthalate monobasic, CAS number 877-24-7, Sigma-Aldrich) has been used by **[CEA]**. Similarly to EDTA, stock-solutions were prepared by dissolving pure salt in ultrapure water (Milli-Q water, Millipore, 18.2 MΩ cm) to reach 10^{-1} mol/L. C-14 radiolabelled PHTHAL stock solution is prepared from a radioactive source containing 9.25 MBq and an initial PHTHAL concentration of 1.8 mM (initially packaged in ethanol and stored in a freezer at -18°C, purchased from American Radiolabeled Chemicals. Inc). Some tests using a H-3 radiolabelled PHTHAL solution have been performed. The H-3 radiolabelled PHTHAL was also purchased from the same supplier and correspond to a radioactive source containing 37 MBq and an initial PHTHAL concentration of 1.7 mM.

For phthalate studies performed by **[KIT** (**Amphos21]**, reagent was obtained from commercial phthalic (Sigma-Aldrich, ACS reagent) acids. Given the low solubilities of phthalic acid in water, to achieve the higher concentrations in their experiments, stocks were made by dissolving solids in ethanol (96%, Pharmpur, Scharlab).

Commercial phthalic acid (Sigma-Aldrich, ACS reagent) has been used by **[CIEMAT]**. Given the low solubility of phthalic acid in water, to achieve the higher concentrations in our experiments, stocks were made by dissolving solids in ethanol (96%, Pharmpur, Scharlab).

3.1.4 Adipic acid

Commercia adipic acid ((CH$_2$)$_4$(COOH)$_2$, Sigma-Aldrich, BioXtra) has been used by **[CIEMAT]**. Given the low solubility of adipic acid in water, to achieve the higher concentrations in our experiments, stocks were made by dissolving solids in ethanol (96%, Pharmpur, Scharlab).

For adipate studies performed by **[KIT** (**Amphos21**)**]**, reagent was obtained from commercial adipic (Sigma-Aldrich, BioXtra) acids. As for phthalic acid, the adipic-acid-stock solutions were made by dissolving solids in ethanol (96%, Pharmpur, Scharlab).

3.1.5 Gluconate

Stock solutions of ^{14}C-GLU (Hartmann Analytic, Germany) and sodium gluconate (Sigma Aldrich, United States) were prepared and diluted **[KIT(JGU)]**.

3.1.6 Citrate

Concerning **[HZDR]** studies, citrate stock solutions were prepared by weighing and dissolving appropriate amounts of commercial reagents either citric acid (VWR Chemicals, > 99.8%) or trisodium citrate (Roth, p.a.).

[KIT(EMPA)] used the citrate form as precursor in their studies, either the commercial Na$_3$-citrate or K$_3$-citrate (Na$_3$C$_6$H$_5$O$_7$·H$_2$O or K$_3$C$_6$H$_5$O$_7$·H$_2$O, Sigma-Aldrich, ≥99.0 %).

3.1.7 Formate

[RATEN] used formate in their studies as ^{14}C labelled formic acid without stable formate solution addition. [**KIT(EMPA)**] used the stable commercial one (Sigma-Aldrich, ≥99.0 %).

3.1.8 NTA

Nitrilotriacetic acid (H$_3$NTA) is a typical representative of aminopolycarboxylic acids. For **[HZDR]** studies, stock solutions were prepared by weighing and dissolving appropriate amounts of commercial Na$_2$HNTA reagent (≥99%, Sigma-Aldrich).

3.1.9 Superplasticizer

Two superplasticizers were selected by **[CIEMAT]**. The SIKAMENT™ 200 R, SIKA, (Spain), based on modified melamine; that it is a dark brown product, with a density of approximately 1.15 kg·L^{-1} and a pH of approximately 8. The recommended dose for cement preparation is between 1% and 1.5% in cement

EURAD (Deliverables n° 3.6, 3.7 and 3.8) - Final Report of results generated in CORI
Dissemination level: PU
Date of issue of this report: **05/07/2024**

Page 90

weight, proportion that can be increased if the ambient temperature is high. The second product (MG) is the Master Glenium SKY 886 (BASF). This is an innovative superplasticizer based on latest generation of polycarboxylate ether (PCE) polymers. This is a milky product with a pH of 5.6 and a density of 1.02 kg·L^{-1}. It is used as unique additive in a percentage of approximately 0,5 – 2,0% on cement weight depending on the type of concrete.

An image of the two products (diluted 1:20) is shown in *Figure 3-1*. Both superplasticizers come in a liquid form, diluted in water. The quantity that must be added to the cement (few %) is calculated based on the liquid product. They were analyzed to determine their total mass and total organic carbon (TOC). The dispersed solid was measured by gravimetry weighting a known mass of the initial liquid before and after drying it overnight at 100ºC. SIKA had a dry residue of 363±6 g·L^{-1} with a TOC of approximately 153.8 g·L^{-1} (42 %). MG contained a dry residue of approximately 228±1 g·L^{-1} and a TOC of 117 g·L^{-1} (51%). For the experiments, the *as-received* products must be diluted 1:10 or 1:20.
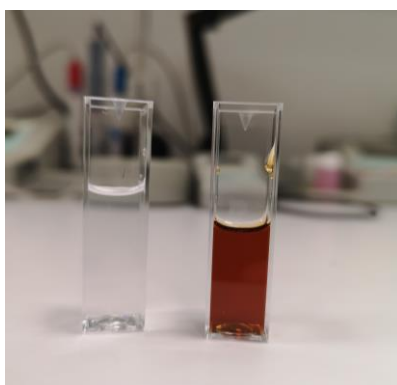
Figure 3-1:   *Image of the two superplasticizers used in the experiments.*

[UJV] analyzed the effects of the superplasticizer ISOLA on Ni migration. The characteristics of this SP is detailed in *Table 23* and the characterization of the degraded product is reported in Task 2 (see section 2.4.5).

3.1.10 GTA, HIBA, HBA and real leachate

[KIT] studies the effect of α-hydroxyisobutyric acid (HIBA); 3-hydroxybutyric acid (HBA) and glutaric acid (GTA) and UP2W degradation products onto RN retention. Glutaric acid ($C_5H_8O_4$, 99%), α-hydroxyisobutyric acid ($C_4H_8O_3$, 99%) and 3-hydroxybutyric acid ($C_4H_8O_3$, 99%) were purchased from Sigma-Aldrich. Some dedicated experiments were performed using ^{14}C-labelled glutaric acid [1,5-^{14}C-GTA](s) was obtained from American Radiolabeled Chemical. The specific activity of the tracer was 50 mCi/mmol–60 mCi/mmol, with a total activity of 50 µCi *i.e.* 1.85 MBq.

UP2W material provided by **[SKB]** was prepared and degraded as described by Szabo *et al.* (2023).

3.2 Preparation and characterization of cementitious matrices (Task 3 and Task 4)

3.2.1 RCM and HCP

The reference cement material (RCM) is a CEM I hardened cement paste (HCP) that was provided by **[UJV]** from the Czech team to the interested organizations for different experimental tests. The reference cement samples (RCM) have been prepared from a CEM I cement (producer CEMEX Prachovice, Czech Republic) and with a cement/water ratio of 0.45 in 2021. After the initial cure, a certain volume of Stage II solution at pH 12.5 (S2, corresponding to a filtrated portlandite saturated

EURAD (Deliverables n° 3.6, 3.7 and 3.8) - Final Report of results generated in CORI
Dissemination level: PU
Date of issue of this report: **05/07/2024**

Page 91

solution) has been added to cover the HCP cylinder to avoid desiccation during the shipment to the partners.

For **[KIT** (**Amphos21**)**]** experiments, the received RCM was grinded and sieved to obtain a particle size lower than 200 µm. RCM was degraded up to Stage II by contacting it with milli-Q water with a S:L ratio 4 g·L^{-1} for 2 weeks.

For **[CNRS-SUBATECH]**, the HCP samples were prepared in December 2014 and provided by **[CEA]**. It was prepared from a CEM V/A (Rombas, Calcia, France), with a water-to-cement ratio (w/c) of 0.4, casted as cylinders (50 mm in height; 50 mm in diameter), cured in a wet chamber (RH > 98%, T= 22°C during 200 days) and finally stored in containers covered with an artificial cement pore water (ACW) ([K] = 291 mmol·L^{-1}, [Na] = 79 mmol·L^{-1}, [Ca] = 2.1 mmol·L^{-1}, [SO$_4^{2-}$] = 0.96 mmol·L^{-1}, [Cl] = 0.57 mmol·L^{-1}, pH = 13.5).

For batch experiments, one HCP cylinder was grinded (ball grinder) and entirely sieved (< 200 µm).For diffusion experiments, HCP cylinders were sawn (with a diamond wire saw) into 2-2.2 mm thick disks (18 disks/cylinder) and stored in ACW up to their use. For Stage II, eight disks stored in Stage II solution (S2) for 2 years were selected for the diffusion experiments. For Stage III, the degradation was performed in a specific setup designed for leaching eight HCP samples simultaneously. This degradation step lasted 16 months. HCP disks were submerged in 2 L ultrapure water and the (stirred) solution was renewed once a week during this period. The composition of the leachate solution was regularly analyzed for pH and major components (by IC and ICP-MS) in order to estimate the quantity of the released elements. The composition of the Stage III solution (S3) was analyzed and found to be very similar to the one reported in Pointeau *et al.* (2004) for a degraded CEM V HCP with a Ca/Si ratio close to 1 ([Ca] = 1.5 mmol·L^{-1},[Si] = 0.15 mmol·L^{-1}, pH = 11.6).

One disk was removed from the solution and a fraction was abraded with a SiC sand paper (peeling technique). 50 µm-thick layers of HCP were successively removed and the disk was characterized by XRD after each step of abrasion. No Portlandite nor Ettringite was detected in the first 100 µm-thick layer, but Ettringite reappears from 150-200 µm in depth. This means that Ettringite was still present over a large fraction (more than 90%) of the degraded HCP disk. The reappearance of Portlandite at 450-500 µm in depth strongly indicated the existence of an intact zone (core). This means that probably the degraded zone represents around 50% of the total thickness (2 mm) of the S3 HCP disk (*Figure 3-2* (right)). In addition, water porosity measurements (drying step at T=60°C) showed that the global porosity of S3 HCP disks was about (42.4±0.4) % vol. compared to (36.1±0.4) % vol. measured for intact S2 HCP disks. Based on these data, one can estimated that the porosity of the degraded zone is about 50% vol.

Laser Ablation-ICP-MS (Element XR HR-ICP MS spectrometer, Thermo Electron coupled with a Nd:YAG laser UP 213 nm, New wave Research) analyses were performed in order to characterize the distribution of elements (Ca, Si, Al,..) along the thickness of the S3 HCP disk.

Elemental profiles confirmed the presence of degradation fronts up to a depth of 500 µm on both sides of the disk and hence highlighted its heterogeneous structure consisting in two external degraded zones sandwiching an intact zone (non-degraded core). These results are consistent with XRD data. In the degraded zones, the global Ca/Si molar ratio is 0.8±0.1 which a bit lower than expected. Note that for in-diffusion experiments, each S3 disk was dedicated to LA HR ICP-MS characterizations at the end of the diffusion step.

EURAD (Deliverables n° 3.6, 3.7 and 3.8) - Final Report of results generated in CORI
Dissemination level: PU
Date of issue of this report: **05/07/2024**

Page 92
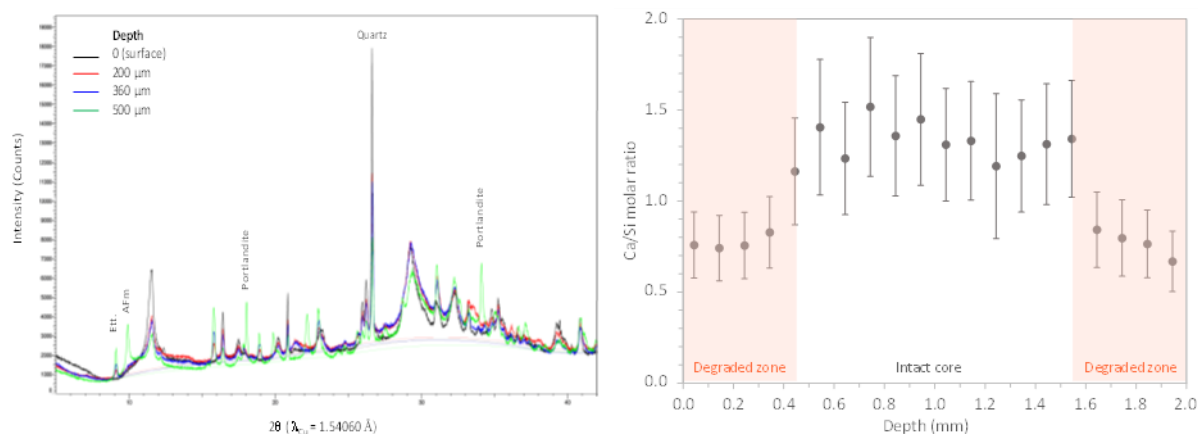
Figure 3-2:   *Degraded S3 HCP disk characterization vs depth: (Left) Evolution of the mineralogy (XRD patterns), (Right) Ca/Si profile (each point = average data of 500 µm-long ablation lines; laser spot = 30 µm).*

[JGU] prepared HCP from a Portland cement (PZ Doppel N CEM 1 42.5 N, Dyckerhoff, Germany). The cement was mixed with Milli-Q water to achieve a water-to-cement ratio (w/c) of 0.5. The paste was used to fill cylindrical moulds and hardened for 48 h before the blocks were demoulded and further stored in Milli-Q water for at least 28 d. For batch sorption experiments, the preparation of HCP powder (particle size of Ø < 63 µm) as the solid phase was based on DIN EN 196–3. The obtained HCP was crushed with a vibrating disk mill and sieved to a particle size with a diameter of Ø < 63 µm. The HCP powder was characterized by XRF, XRD, XPS, N_2-BET, and CEC measurements. A detailed description of these measurements and of the results can be found in Stietz *et al.* (2023a). For sorption experiments, the HCP powder was then suspended in ACW with a pH of 13.3 (0.114 NaOH and 0.18 KOH). ACW with a pH > 13 (containing 0.003 M NaN_3) was used for the diffusion experiment with Pu(IV) and ISA.

[CEA] used the HCP RCM materials and prepared HCP samples are prepared from a CEM V/A composite cement (CEM V/A (S-V) 42.5N CE PM-ES-CP1 NF "PMF3"– ROMBAS, Calcia), with a cement/water ratio of 0.40 in 2016. During 5 years, these samples were hydrated in individual-cylindrical-polyethylen-plastic container (*c.a.* 50 mm in diameter and 55 mm in height) with some artificial cement pore water (ACW) at Stage I (pH 13.5) on the top of the HCP block. A part of the HCP samples was crushed and sieved at < 250µm for HCP CEM V/A and for two fraction sizes *i.e.* <250 µm and <63µm for the RCM.

Another part of the HCP blocks were sliced *c.a.* 3 mm thick and placed individually in a container filled with S2 solution. After 1 month, the leachate is removed and replaced by freshly filtrated S2 solution. This is repeated every few weeks until ORGA or RN-ORGA addition. The estimated sufficient leaching time is 50 days in order to extract more that 99% of initial alkalis content by diffusion from the pore solution of the 3-mm-thick discs. Calculations were performed using the analytical equation provided by Crank (1975) and an arbitrary value of apparent coefficient diffusion (D_a) for alkalis (*e.g.* K^+) of $7.5 \cdot 10^{-13}$ m^2/s and factor capacity, α of 0.33. The result of this simulation is presented in *Figure 3-3*.

EURAD (Deliverables n° 3.6, 3.7 and 3.8) - Final Report of results generated in CORI
Dissemination level: PU
Date of issue of this report: **05/07/2024**

Page 93
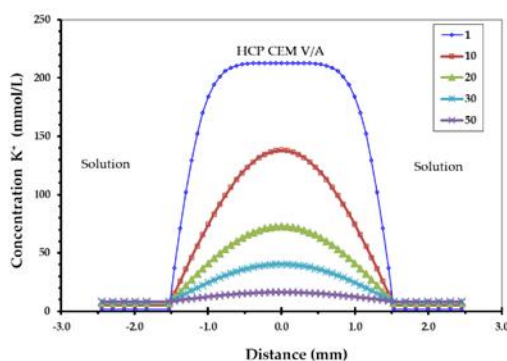
Figure 3-3:   *Calculated K+ diffusion profiles and concentration in solution as a function of lixiviation time in ACW-Stage-II solution: at 1, 10, 20, 30 and 50 days for a 3-mm-thick-HCP sample.*

[SCK CEN] prepared cement samples from Type I ordinary Portland cement (CEM I 52.5 N) with a composition as reported in *Table 29*. The cement paste was prepared at a water/cement ratio of 0.5. The cement powder was mixed with water and transferred to a PVC tube. Gas was evacuated by vibration and the tube was closed and sealed (with glue). Segregation was prevented by rotating the tube containing the cement paste for 12 to 24 h. The tube was then stored in a hydration chamber (relative humidity: 95%, T = 20-22°C) for the entire hydration period which lasted for a minimum of 3 months. The mineralogical composition of the hardened cement paste (HCP) was characterized by XRD and SEM-EDX. The content of natural Ni was also determined by digestion followed by ICP-MS analyses.

Table 29: Chemical composition (wt%) of the cement (from manufacturing fact sheet).

CaO	63.0%	Chromium (VI)	$< 2 \cdot 10^{-4}\%$
SiO_2	20.0%	Cl^-	0.06%
Fe_2O_3	3.0%	Na_2O eq.	0.85%
Al_2O_3	5.0%	Loss on ignition	1.60%
Sulfate SO_3	2.9%	Insoluble residue	0.50%

After 3 months of cure, the HCP was retrieved from the PVC tube with the use of a diamond saw. The HCP pieces were then introduced in a glovebox under inert atmosphere (N_2), crushed and sieved to < 74 μm. The obtained HCP powder was then conditioned to Stage III by leaching in degassed ultrapure water (pH 8.7). Two types of leaching procedures were tested in parallel, *i.e.* dynamic and static leaching, to evaluate which one was the most efficient in terms of the experimental time and the amount of leached material.

The static leaching tests were performed in the same conditions as reported by Pointeau *et al.* (2004) to reach a cement paste with a corresponding pH of ~11.5 and a C/S ratio of 1. The authors used a solid/liquid ratio of 0.4 g/L in ultrapure water and a contact time of 15 days. The tests were here performed in inert atmosphere and in plastic bottles of 1L. Three replicate suspensions were prepared. The suspensions were shaken manually every day. After regular time intervals, the HCP powder was left to settle for at least 1h and the pH of the solutions was measured on 2 mL aliquots. Five mL of each solution was also sampled, filtered (0.2 μm, PP, VWR) and analyzed by ICP-OES for cation

EURAD (Deliverables n° 3.6, 3.7 and 3.8) - Final Report of results generated in CORI
Dissemination level: PU
Date of issue of this report: **05/07/2024**

Page 94

concentrations. The last samples, *i.e.* after 15 days, were also analyzed by IC. The leached HCP was filtered out and analyzed by SEM-EDX.

The dynamic leaching tests were performed in inert atmosphere at a solid/liquid ratio of 5.4 g/L. A total of seven Oak-ridge-PPCO-Nalgene tubes were each filled with 0.2 g of cement powder and 37 mL of degassed ultrapure water. The suspensions were agitated continuously in a glovebox under inert atmosphere. At time intervals of 3 days, the tubes were taken out of the glovebox, centrifuged at 5 000 rpm for 1h15 and carefully reintroduced in the glovebox, paying attention not to resuspend the cement powder. Thirty mL of the supernatants was removed and replaced by fresh degassed ultrapure water. 2 mL of the sampled supernatants was used for pH measurements. The rest was taken out of the glovebox, filtered (0.2 µm, PP, VWR) and analyzed by ICP-OES. The suspensions were put again under agitation until the next sampling point. After 7 steps, the tests were stopped, the leached solids recovered and freeze-dried and analyzed further by SEM-EDX to determine the bulk C/S ratio.

For the Stage III sorption experiments performed by **[SCK CEN]**, a synthetic pore solution was prepared based on the composition of the equilibrium solution obtained during the conditioning of the cement powder. It was indeed assumed that at the end of the last step of the dynamic leaching, taken here as the reference conditioning approach, the solution was in equilibrium with the cement powder and representative of its degradation stage. The composition of the synthetic solution is reported in *Table 30*. The solution was prepared in an inert atmosphere according to the recipe reported in *Table 30*. It was stirred overnight and further filtered at 0.2 µm on PVDF filters.

Table 30: Composition of the synthetic Stage III cement water used in sorption experiments and recipe for preparation.

pH	Ca (mol/L)	Si (mol/L)	Al (mol/L)	SO_4^{2-} (mol/L)
11.5	$2.4 \cdot 10^{-3}$	$4 \cdot 10^{-4}$	$6 \cdot 10^{-5}$	$4 \cdot 10^{-4}$
	$Ca(OH)_2$	SiO_2	$Al_2(SO_4)_3, 18H_2O$	$CaSO_4, 2H_2O$
$g \cdot L^{-1}$	$1.5 \cdot 10^{-1}$	$2.6 \cdot 10^{-2}$	$2.0 \cdot 10^{-2}$	$5.8 \cdot 10^{-2}$

For diffusion experiments, a first series of HCP discs were cut with a precision diamond saw to dimensions of 47.5×6 mm² (diameter × thickness). These discs were used to test two leaching methods: accelerated leaching in 6 M NH_4NO_3 and leaching in ultrapure water. The discs were placed in contact with 1L of a solution of 6 M NH_4NO_3 or 2.5 L of ultrapure water in a glovebox under an inert atmosphere in the set-up depicted in *Figure 5-1*. Four leaching experiments were launched in 6 M NH_4NO_3. The evolution of the pH of the leaching solutions was followed up in time. The cement discs were retrieved after 15, 24, 32 and 48 h. The solutions were analyzed by ICP-OES and IC and the average bulk Ca/Si in the discs was determined by SEM-EDX. Three leaching experiments were launched in ultrapure water. The evolution of the pH and the composition (measured by ICP-OES) of the leaching solutions were followed up in time. The cement discs were retrieved after 77, 113 and 196 days, freeze-dried and analyzed by XRD and SEM-EDX. During the leaching experiments, the water was renewed after 41, 92 and 113 days. After 113 days, the leaching solution was replaced with only 1.8 L of ultrapure water.

EURAD (Deliverables n° 3.6, 3.7 and 3.8) - Final Report of results generated in CORI
Dissemination level: PU
Date of issue of this report: **05/07/2024**

Page 95
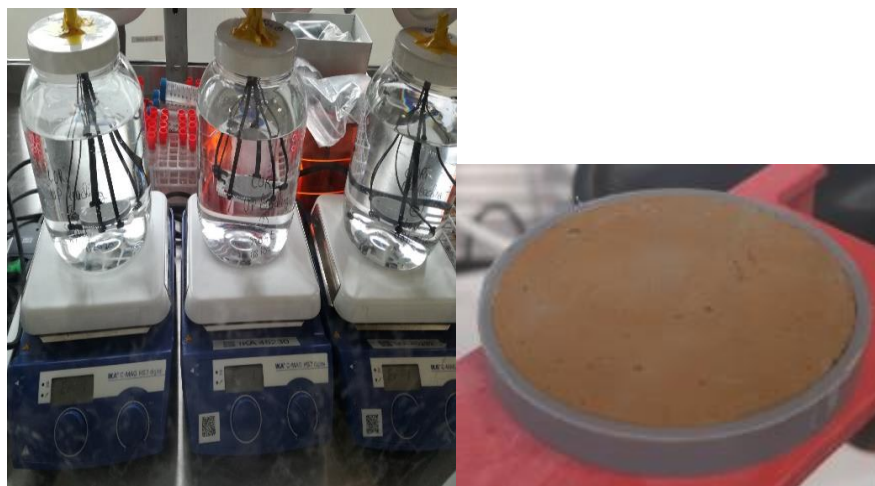
Figure 3-4:   Leaching set-up of the 6 mm cement discs used by **[SCK CEN]**.

[SCK CEN] prepared a second series of HCP discs cut with a precision diamond saw to dimensions of ~ 47.5 × 3 mm² (diameter × thickness). Six samples were cut. The discs were put into contact with 100 mL of degassed ultrapure water in a glovebox under an inert atmosphere. The solution was renewed approximatively every week with fresh water. The evolution of the pH and the composition (measured by ICP-OES and/or IC) of the leaching solutions was followed up in time. The cement discs were retrieved after 114, 198 and 268 days, freeze-dried and analyzed by XRD and SEM-EDX. One sample was retrieved at 268 days and further stored to be used in the diffusion experiment. Two samples were leached for a total of 345 days with weekly water renewal. Afterwards, they were left to equilibrate into solution for 210 more days. The solution was then sampled, filtered at 0.45 µm and analyzed by ICP-OES, ICP-MS and IC. One of the two sample was further freeze-dried and analyzed by XRD and SEM-EDX. The two other degraded cement discs of 2.3 and 3.4 mm thickness, respectively, were resined and loaded into stainless steel diffusion cells

The evolution of the pH of the leaching solutions is reported in *Figure 3-5*. The leaching tests in NH_4NO_3 were performed over a very short time, *i.e.* maximum 2 days. The 6 M NH_4NO_3 solution has a pH of ~4.5, which significantly accelerates the degradation of the cement powder in comparison to degassed ultrapure water.
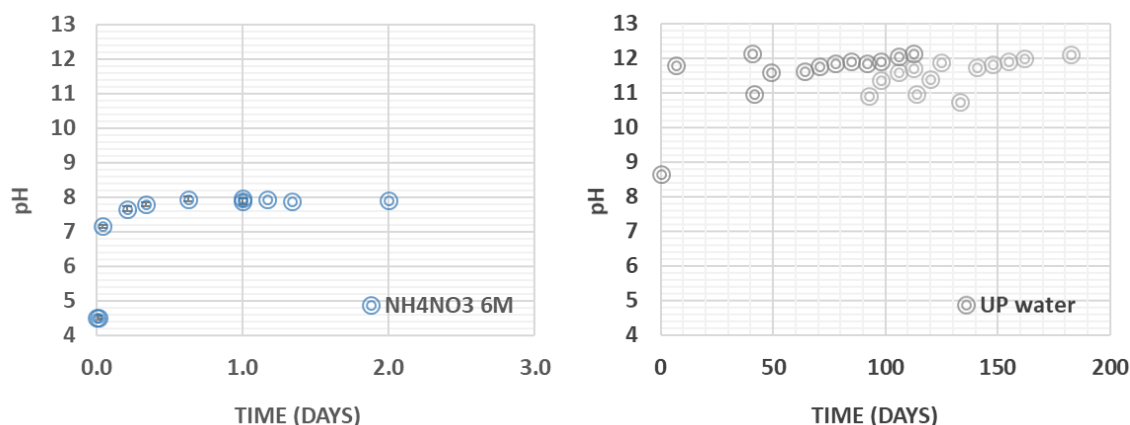
Figure 3-5:   Evolution of the pH of the leaching solution. Left: accelerated leaching with 6 M NH_4NO_3 and right: leaching with ultrapure water.

EURAD (Deliverables n° 3.6, 3.7 and 3.8) - Final Report of results generated in CORI
Dissemination level: PU
Date of issue of this report: **05/07/2024**

Page 96

The pH of the equilibrium solution never rose above 8 and over a period of 2 days, already $4 \cdot 10^{-2}$ mol/L of Ca^{2+} (*Figure 3-6*) had leached from the cement disc indicating a significant degradation of the sample.
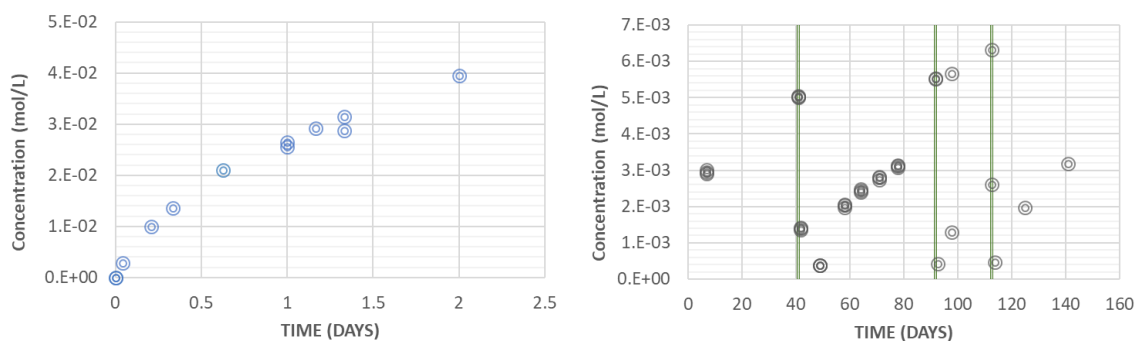
Figure 3-6: *Evolution of the concentration of Ca^{2+} in the leaching solution. Left: accelerated leaching with 6 M NH₄NO₃ and right: leaching with ultrapure water. Green lines indicate the renewal of the leaching solution.*

Indeed, based on the initial amount of portlandite in the sample (*Table 31*) and considering a cement density of 1.8 g/cm³, the maximum amount of Ca^{2+} that could dissolve from the portlandite would be $3 \cdot 10^{-2}$ mol. The advanced degradation degree is further confirmed by the bulk Ca/Si measured by SEM-EDX and reported in *Table 31*. After 15 hours, the bulk Ca/Si had dropped from 1.5 to 0.8 indicating the dissolution of the portlandite and ettringite and a partial decalcification of the C-S-H phases. Unfortunately, XRD measurements were not performed to confirm the change of the mineralogy.

Table 31: Bulk Ca/Si ratio (± standard deviation) measured by SEM-EDX on the HCP before and after leaching in 6 M NH₄NO₃

Time (hours)	Ca/Si
0	1.5 ± 0.2
15	0.8 ± 0.3
32	0.9 ± 0.2

On the other hand, the cement degradation in ultrapure water progressed much slower and even after 196 days, the pH of the solution was still ~12. The total amount of Ca^{2+} leached over the entire test reached only $2.1 \cdot 10^{-3}$ M, which is more than 10 times less than the estimated maximum amount of Ca^{2+} that could come from the portlandite.

EURAD (Deliverables n° 3.6, 3.7 and 3.8) - Final Report of results generated in CORI
Dissemination level: PU
Date of issue of this report: **05/07/2024**

Page 97

The limited degradation was confirmed by the XRD measurements (*Table 32*), which show the slow dissolution of portlandite, *i.e.* only 45% of the initial amount had dissolved after 196 days. This indicates that only a part of the sample was degraded while the rest had remained mostly unaltered.

Table 32: Bulk mineralogical composition of the HCP before and after leaching in ultrapure water at different leaching times determined from XRD measurements.

	t= 0 d	t= 77 d	t= 113 d	t=196 d
Hydrogarnet	1.7	1.6	1.3	1.4
Ettringite (AFt)	0.6	2.2	1.5	0.0
Portlandite	14.7	9.3	8.0	6.6
Amorphous	75.7	75.7	75.7	75.7
Quartz	0.1	0.3	0.2	0.4
AFm	3.4	3.0	1.7	0.6
Clinker	3.8	4.0	3.1	5.2

It appears therefore that, as could be expected, leaching in 6 M NH_4NO_3 is much more efficient than in ultrapure water. However, the degradation of the cement discs progresses so fast, that it is difficult to control. Less concentrated NH_4NO_3 solutions would therefore better be used to fine tune the degradation extent. On the other hand, the use of NH_4NO_3 might affect the chemistry of the cement by inducing the formation of nitrate phases. Since chemistry is important when one looks at the sorption properties, it was decided to proceed by conditioning of the samples for the diffusion experiments in ultrapure water. However, to accelerate the conditioning step and limit the chemical gradient in the samples, it was decided to reduce the thickness of the cement discs to 3 mm.

The leaching of the 3 mm cement discs in ultrapure water was monitored for about a year with weekly renewal of the leaching solution. Over this period, the cement discs were retrieved one after the other and analyzed to follow-up the progression of the degradation. After 345 days, the renewal of the solution was stopped and the two remaining discs were left to equilibrate. The follow-up during this last period was reduced but some pH and ICP-OES measurements were still performed from time to time. The evolution of the pH and the Ca^{2+} concentration over the entire leaching period is reported in *Figure 3-7*.
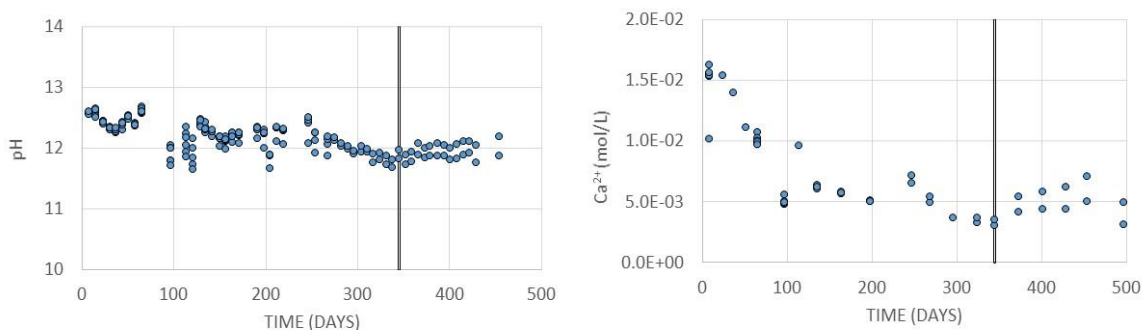
Figure 3-7:   *Evolution of the leaching solution during the leaching in ultrapure water of 3 mm HCP discs. On the left: evolution of pH. On the right: evolution of the Ca^{2+} concentration. The black line indicate the end of the solution renewal.*

EURAD (Deliverables n° 3.6, 3.7 and 3.8) - Final Report of results generated in CORI
Dissemination level: PU
Date of issue of this report: **05/07/2024**

Page 98

For the first 100 days, the rate of leaching was slow but significant. The pH decreased from ~12.6 to ~12 and the Ca^{2+} released in solution decreased further with each water renewal. This shows the leaching of soluble phases like portlandite and ettringite. Indeed, the XRD results show that over 114 days, 66 % of the initial portlandite had leached out of the samples. After that period, the degradation progressed slower and was mainly controlled by the diffusion of the Ca^{2+} out of the discs and the slow decalcification of the C-S-H. After 268 days, XRD results revealed that the totality of the portlandite and ettringite had leached out. This results should however be considered as an approximation more than a true value. Indeed, the XRD method as applied here is semi-quantitative and traces of both phases could still be present (*Table 33*).

Table 33: Bulk mineralogical composition of the 3 mm HCP discs before and after leaching in ultrapure water at different leaching times.

	t= 0 d	t= 114 d	t= 198 d	t=268 d
Hydrogarnet	1.6	2.6	3.3	3.7
Ettringite (Aft)	3.9	0.4	2.3	0.0
Portlandite	12.1	4.4	1.2	0.0
Amorphous	79.7	85.8	85.9	82.5
Quartz	0.1	0.2	0.5	0.6
AFm	1.4	1.1	1.1	1.4
Clinker	1.1	5.8	5.8	6.4

However, it shows that most of the two phases were removed. The final pH was measured around 11.8 for a concentration of Ca^{2+} of ~$4 \cdot 10^{-3}$ M. The bulk Ca/Si ratio measured by SEM-EDX along the thickness of the sample and after different leaching times is reported in *Figure 3-8*.
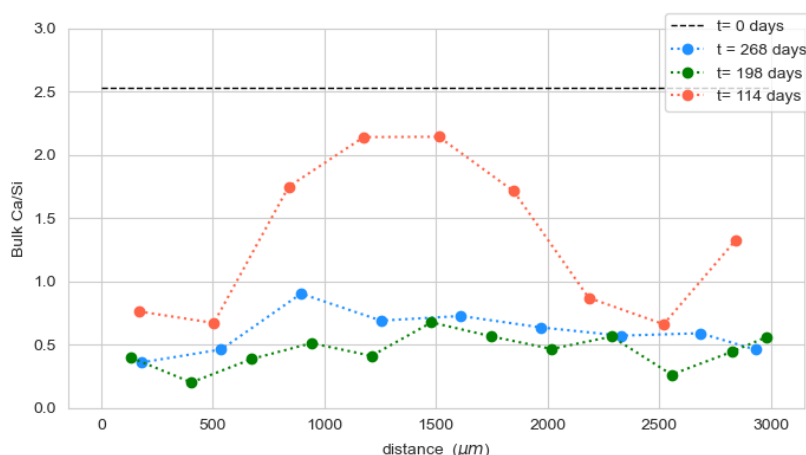
Figure 3-8:   *Evolution of the bulk Ca/Si ratio measured by SEM-EDX along the sample thickness and as a function of leaching time.*

Note that as for XRD, the SEM-EDX method is only semi-quantitative and the calculated Ca/Si values should be considered as an approximation. Nevertheless, the evolution of the Ca/Si values shows that after 198 days, the leaching of the portlandite was mostly complete, which is in agreement with the XRD results. After that time, no obvious change in the bulk Ca/Si values can be noticed and the measured

EURAD (Deliverables n° 3.6, 3.7 and 3.8) - Final Report of results generated in CORI
Dissemination level: PU
Date of issue of this report: **05/07/2024**

Page 99

values were homogeneous along the sample thickness. The cement discs used in the sorption experiments were leached for 268 and 345 days, for Diff1 and Diff2, respectively. It can therefore be expected that, at least in terms of the Ca/Si ratio, the samples were homogeneous with a bulk Ca/Si ratio of around 0.5-0.7

Only a few partners did some investigations with concrete samples. **[SÚRAO]** operates three ILW repositories. In order to better understand the behavior of components and materials used in the repositories, **[SÚRAO]** provided concrete samples from the Richard repository for testing and comparison with other types of concrete within CORI (*Figure 3-9*) Concrete Richard (CEM III) was designed during the international EC Phare project in 2006 and is an important material used in the Richard repository. Witness samples are intended for the approved concrete aging program in the repository.

Figure 3-9:   *Witness samples of structural concrete from the Richard repository*

3.2.2 Portlandite

Portlandite ($Ca(OH)_2$) was prepared for **[CIEMAT]** studies by recrystallization dissolving CaO in desionized water, purged with N_2, in a glove box under anoxic conditions. Upon precipitation the solid was filtered and left drying in the glove box. After drying the solid was crushed and, for the experiments suspended in 20 mM $Ca(OH)_2$. The solid obtained was analyzed by different techniques (N_2-BET, scanning electron microscopy, SEM, and energy dispersive X-ray spectroscopy (EDX or EDS); Fourier-transform infrared (FTIR) spectroscopy).

3.2.3 C-S-H

[KIT (EMPA)] used CaO and SiO_2 as precursors of C-S-H phases. C-S-H phases were synthesized with an initial solid-to-liquid (S/L) ratio of 55 g/dm^3. The C-S-H phases were equilibrated for one month under continuous shaking (~ 100 rpm) before characterizations and use in sorption experiments.

For **[CIEMAT]**, the preparation of the C-S-H phases was carried out in an anoxic glove box, under N_2 atmosphere (O_2<1 ppm). For their synthesis by the "direct method" (Missana *et al.* (2017)) CaO (Alfa Aesar 99.95% purity) and SiO_2 (Aldrich 99,8% purity). Both solids were weighed to obtain the requested molar Ca/Si ratios and solid to liquid ratio. They were mixed to 1L deionised water previously boiled and bubbled with N_2 to minimize the CO_2 contamination. The suspensions were prepared in HDPE dark bottles and maintained under stirring to obtain a homogeneous product. Conductivity and pH were periodically measured until the steady state was reached (10-15 days approximately), indicating the completion of the synthesis process.

The C-S-H phases used in **[UCYPRUS]** studies were also synthesized according to Maddalena *et al.* (2019) by which Ludox (50%, Aldrich) is mixed with CaO (Aldrich) in de-ionized water under N_2. The product was cast in cubes and left for one month under water-vapour saturated N_2-atmosphere. Finally, the C-S-H cubes have kept overnight in dried acetone to remove excess water and then dried under vacuum at 70°C for 24 h.

EURAD (Deliverables n° 3.6, 3.7 and 3.8) - Final Report of results generated in CORI   Page 100
Dissemination level: PU
Date of issue of this report: **05/07/2024**

The phases were characterized by different techniques (N_2-BET, scanning electron microscopy, SEM, and energy dispersive X-ray spectroscopy (EDX or EDS); atomic force microscopy or Fourier-transform infrared (FTIR) spectroscopy).

3.2.4 C-A-S-H

[KIT (Amphos21)] prepared two different C-A-S-H phases according to Olmeda *et al.* (2019). These phases are referred to as C-A-S-H x1-x2 where x1 refers to the theoretical Ca/Si ratio and x2 refers to the theoretical Al/Si ratio. **[KIT (Amphos21)]** studies are considering the theoretical Ca/Si and Al/Si ratios: 1.2-0.05 and 1.2-0.02 as proposed by Olmeda *et al.* (2019), the synthesis was performed in an anaerobic chamber under a N_2 atmosphere (CO_2 < 10 ppm and O_2 < 10 ppm) to prevent carbonation. Samples were prepared by adding deoxygenated deionized water (DDW) to weighed amounts of reagent grade CaO, SiO_2, and $Al(NO_3)_3 \cdot 9H_2O$. The mass of each solid was chosen to achieve both the desired Ca:Si and Al:Si ratios and a solid:liquid ratio of 10 g·L^{-1}. Synthesis was considered complete when there was no significant change in these values, typically a period of 28 days.

After the synthesis period, aliquots of the suspension were transferred to 15 mL centrifuge tubes. The tubes were removed from the glovebox for centrifugation (2600 g, 10 minutes: nominal particle size cut-off 0.5 µm) then returned to the glovebox, and the supernatant passed through a 0.22 µm nylon syringe filter. The filtrate was acidified, and the solid phase left to dry inside the glovebox for 72 h before characterization. The concentration of Ca in the filtrate was determined with ion chromatography (ICS-2000 system, Dionex), Si and Al were measured with ICP-MS (model 7500cx, Agilent Technologies Inc.).

For solid phase characterization, scanning electron microscopy (SEM; FE-SEM - ZEISS Ultraplus) was used to obtain images of the sample surfaces. Energy Dispersive X-ray Spectroscopy (EDX; X-Max EDX detector, OXFORD Instruments) was used to obtain semi-quantitative chemical composition analysis of the solid. The crystalline and semi-crystalline phase composition of solid samples was determined via XRD (PANalytical X'Pert PRO MPD). The characterization of the samples was consistent with that observed in a previous study with C-A-S-H solids (Olmeda *et al.*, 2019) The zeta potential of the C-A-S-H 1.2-0.05 suspension was determined with a Zetasizer Nano ZS (Malvern Panalytical). The results of the aqueous, solid, and suspension characterization are summarized in Table 34.

Table 34*: Aqueous and solid phase characterization of C-A-S-H phases used in* **[KIT (Amphos21)]** *experiments. Reported Ca:Si and Si:Al molar ratios* are *taken from semi-quantitative EDX measurements.*

Sample	Ca (mol/L)	Al (mol/L)	Si (mol/L)	pH	Ca:Si	Si:Al	ζ potential (mV)
C-A-S-H 1.2-0.05	$6.40 \cdot 10^{-3}$	$9.44 \cdot 10^{-6}$	$2.73 \cdot 10^{-4}$	11.24	1.13	0.04	-2.35 ± 0.73
C-A-S-H 1.2-0.2	$1.38 \cdot 10^{-2}$	$6.06 \cdot 10^{-7}$	$1.77 \cdot 10^{-3}$	10.24	0.74	0.41	-

[HZDR] also prepared some C-A-S-H phases with Ca/Si molar ratios of 0.8, 1.2 and 1.6, representing different alteration stages of concrete, and with increasing Al/Si molar ratios of 0, 0.06 and 0.18 in each series.

3.2.5 AFm/AFt

For **[KIT(EMPA)]**, C_3A (3CaO Al_2O_3), $CaCO_3$, CaO (obtained by heating $CaCO_3$ at 1000ºC for 12 h), $Ca(OH)_2$, $CaSO_4 \cdot 2H_2O$, $Al_2SO_4 \cdot 16.3 H_2O$ were used as precursors for the synthesis of AFm phases and ettringite. Ms (monosulfolauminate), Mc (monocarboaluminate), Hc (hemicarboaluminate) and ettringite phases were synthesized with an initial solid-to-liquid (S/L) ratio of 44.2, 46.3, 43.5 and 41.8 g/dm^3, respectively. All cement phases were equilibrated for one month under continuous shaking (~ 100 rpm) before characterizations and use in sorption experiments.

EURAD (Deliverables n° 3.6, 3.7 and 3.8) - Final Report of results generated in CORI
Dissemination level: PU
Date of issue of this report: **05/07/2024**

Page 101

[CIEMAT] prepared the ettringite mixing $Al_2(SO_4)_3 \cdot 18H_2O$, $Ca(OH)_2$ and $Na(OH)$ in 1 L of deionized water under anoxic conditions (N_2). The solution was sealed in a polyethylene bottle, heated to 60°C and stirred for 48 hours. The solid was separated by the aqueous phase with a Büchner vacuum filtration funnel, with a 0.2 µm filter. The solid obtained was analyzed by different techniques (N_2-BET, scanning electron microscopy, SEM, and energy dispersive X-ray spectroscopy (EDX or EDS); Fourier-transform infrared (FTIR) spectroscopy).

3.3 Speciation, solubility experiments

For **[CEA]**, the operational solubility of U in ACW Stage II and Stage IV in the presence of organic (EDTA and phthalate) have been determined to investigate the starting parameters for the sorption and diffusion experiments. The assumption is that the solubility increases by the addition of organics. The U was added in excess compared to the theoretical solubility, in a concentration of $8.4 \cdot 10^{-5}$ M in the stage II system and $6.8 \cdot 10^{-5}$ M in the Stage IV system. The pH was adjusted to 9.5 by adding NaOH in the Stage IV samples. The organics were added in a concentration range of $5 \cdot 10^{-10} – 1 \cdot 10^{-3}$ M and $1 \cdot 10^{-7} – 1 \cdot 10^{-2}$ M in resp. Stage II and IV. All manipulations of the samples in ACW Stage II are performed in the N_2 filled glovebox to avoid atmospheric carbonation. All manipulations of the samples in ACW Stage IV were performed in air. The operational solubility of Ni was studied with similar the experimental conditions. Ni was added to all tubes in $3.5 \cdot 10^{-5}$ mol/L, in combination with 800 Bq/mL ^{63}Ni. The organics Na-EDTA or K-phthalate were added in a concentration range of $2 \cdot 10^{-7} – 2 \cdot 10^{-2}$ mol/L. The operational solubility of Eu was investigated using the reference solutions prepared for the diffusion experiments. Reference solutions were prepared in ACW Stage II solution by adding a spike of Eu-152 standard solution and different concentration of degraded cellulose solutions expressed in mg of C per kg of solid, $i.e$ ppm^C (0 ppm^C; 70 ppm^C; 1 500 ppm^C and 15 000 ppm^C).

[JUELICH] investigated the effect of phthalate and TMA on the solubility of Eu(III)/Am(III) under highly alkaline conditions. The solubility tests were carried out in a glove box under a controlled Ar atmosphere (O_2 and CO_2 concentrations < 5 ppm) following the experimental procedure of Tits and Wieland (2018). The batch solubility tests were carried out in 40 mL polypropylene centrifuge tubes, which were thoroughly washed and left overnight in a solution of 0.1 M HCl, then rinsed with Milli-Q® water. For the solubility tests three different concentrations of ^{241}Am and ^{152}Eu (between ~$1 \cdot 10^{-8}$ M and ~$1 \cdot 10^{-10}$ M; stock solutions of the radionuclides were obtained from Eckert & Ziegler Nuclitec GmbH) were employed in CEM V/A water in the presence and absence of the organics. Stock solutions of phthalic acid (99.5% Sigma-Aldrich) and tri-methyl-amine (Alfa Aesar) of 0.1 M were be prepared and diluted to obtain the required initial concentrations in the experiments. The concentration of the organics in the solubility tests ranged between $1 \cdot 10^{-3}$ and $1 \cdot 10^{-5}$ M. After selected times, aliquots were withdrawn from the solutions before and after centrifugation (6,000 rpm ,1 hour) and analyzed for ^{241}Am and ^{152}Eu with liquid scintillation counting (TriCarb 3100 TR, Perkin Elmer, Freiburg, Germany) using Ultima Gold (Perkin Elmer) as scintillation cocktail.

3.4 Retention experiments

This section describes the retention studies proposed by the organizations participating in WP3 CORI Task 3 and Task 4. In the Task 3, it involves organic retention by cementitious matrices while in Task 4, one considers the radionuclide (RN) retention in cement matrices (CEM) $i.e.$ hardened cement pastes (HCP) or cementitious phases in the presence of organics. The uptake of a species, X, is usually quantified by a solid liquid distribution coefficient noted K_d (or distribution ratio R_d) (generally in $L \cdot kg^{-1}$) and defined by:

$$K_d = \frac{[X]_{solid}}{[X]_{solution}} = \left(\frac{[X]_{initial}}{[X]_{solution}} - 1 \right) \frac{V}{m} \qquad \text{Equation 7}$$

EURAD (Deliverables n° 3.6, 3.7 and 3.8) - Final Report of results generated in CORI
Dissemination level: PU
Date of issue of this report: **05/07/2024**

Page 102

where $[X]_{solid}$ [mol·kg^{-1}] is the concentration of the sorbed species per mass of sorbent, $[X]_{solution}$ [mol·L^{-1}] is the concentration of the species X in solution at equilibrium, $[X]_{initial}$ [mol·L^{-1}] is the initial concentration of the species X introduced in the suspension, V [L] is the volume of solution and m [kg] is the dry mass of the solid sorbent. The higher the K_d value, the higher is the uptake.

In ternary systems, including ORGA-RN-CEM, one can also express the effect of the ORGA onto the RN retention using reduction factor capacity, RFC, which corresponds to the ratio of the K_d obtained in the presence of the organic and the K_d under the same conditions in the absence of the organic:

$$RFC = \frac{K_d(RN + ORGA)}{K_d(RN)}$$

Equation 8

A value of 1 for the RFC means therefore no effect of the ORGA onto the RN retention.

As mentioned in the CORI SOTA "State-of-the-art report on cement-organic- radionuclide- interactions in the content of L/ILW disposal (Deliverable 3.1)", the distribution coefficient is an experimentally determined parameter, therefore the experimental conditions must be controlled, including the attainment of constant aqueous concentrations of the species of interest. This parameter represents the sum of all the phenomena able to remove an element from the aqueous phase, *i.e.* by adsorption on the surface of the solid matrix, incorporation inside some of the solid matrix mineral phases or precipitation in solution with other species. The most relevant retention process is adsorption however, to isolate the contribution of adsorption processes on radionuclide retention, precipitation must be avoided in sorption experiments, considering the solubility limits.

3.4.1 Sorption experiments performed by [**CNRS-SUBATECH**]

Sorption/desorption isotherms and/or time-series (kinetics) experiments were performed on binary and ternary systems for both cement degradation stages in the following experimental conditions (Table 35).

Table 35: *Experimental conditions for wet chemistry experiments.*

	Systems		**[ISA] range (mol·L^{-1})**	**Solid/liquid (kg·L^{-1})**	**Sampling time (days)**
Stage II	ISA/HCP	Isotherms	$1 \cdot 10^{-3}$ to $3 \cdot 10^{-2}$	$2.5 \cdot 10^{-2}$	32
		Kinetics	$1 \cdot 10^{-2}$	$2.5 \cdot 10^{-2}$	1, 3, 7, 14, 28, 91
Stage III	ISA/HCP	Isotherms	$5 \cdot 10^{-4}$ to $3 \cdot 10^{-2}$	$5 \cdot 10^{-3}$, $17 \cdot 10^{-3}$	28
		Kinetics	$1 \cdot 10^{-2}$	$5 \cdot 10^{-3}$	1, 3, 7, 14, 28, 64

Sampling of solutions were performed by weighting. At the end of experiments, suspensions were centrifuged (2650 g, 15 min), then supernatants were filtered and sampled for analysis. For desorption experiments, after removing the supernatants, 20 mL of fresh S2/S3 solutions (without U(VI) nor ISA) were added to each tube, agitated during the adequate duration and, at the end, sampled as previously described.

Sorption/desorption isotherms are expressed and quantified by a solid-liquid distribution ratio (R_d in m^3·kg^{-1}), defined as by Equation 7. If the sorption process is found to be reversible, R_d becomes K_d (solid-liquid distribution coefficient).

Different analytical techniques have been used for the characterization of solutions: Quadrupolar ICP-MS (ThermoElectron X serie 2) for Uranium (Limit of Quantification (LQ) = 10 ng·L^{-1}, Bi as internal standard) and Si (LQ = 10 µg·L^{-1}, In as internal standard), TOC meter (Analytik Jena NC2100S) for ISA (Non Purgeable Organic Carbon method, LQ = 1 mg^C·L^{-1}), Ion Chromatography (Metrohm 850 Professional IC) for cations (eluent mixture of PDCA 1.3 mM/HNO$_3$ 8 mM ; LQ = 0.25 mg·L^{-1}) and pH values were measured with a microelectrode calibrated at pH 7.00 and 12.45 (IUPAC Standard, Hach).

EURAD (Deliverables n° 3.6, 3.7 and 3.8) - Final Report of results generated in CORI
Dissemination level: PU
Date of issue of this report: **05/07/2024**

Page 103

3.4.2 Sorption experiments performed by [**SCK CEN**]

The sorption kinetics of α-ISA on the degraded cement powder was assessed at an α-ISA concentration of $1.0 \cdot 10^{-3}$ mol/L and at a fixed solid/liquid ratio of 26 g/L. Sorption was measured after five different contact times over a period of 21 days and for four replicates.

The sorption samples were prepared under inert conditions in 10 mL Nalgene tubes (PPCO) for a total volume of 7 mL. A quantity of 0.18 g of cement powder was first added to the tubes followed by the synthetic Stage III cement water. The cement powder was left to equilibrate with the solution for 48h under agitation. The 'equilibrium' pH of the suspensions was 11.5 ± 0.1. α-ISA was then added either as a solid or as a solution freshly prepared in $3 \cdot 10^{-3}$ M NaOH. The pH of the suspension was measured again and if needed adjusted to the pH before α-ISA addition. The suspension was placed back on the shaker afterwards. After 1, 3, 7 and 14 days, the suspensions were taken out of the glovebox and centrifuged for 2 h at 20000 g. After centrifugation, the tubes were gently reintroduced in the glovebox and 70 μL of the supernatants was sampled, diluted in $3 \cdot 10^{-3}$ M NaOH and analyzed by IC-PAD. The tubes were then put back on the shaker until the next sampling point. For the last sampling point, *i.e.* after 21 days, 2.5 mL of the supernatants was sampled after centrifugation and were directly analyzed by IC-PAD. The pH of the supernatants was also measured.

The sorption of α-ISA on the degraded cement powder was assessed at an α-ISA concentration ranging from $2.7 \cdot 10^{-6}$ to $1.4 \cdot 10^{-1}$ mol/L and at a fixed solid/liquid ratio of 26 g/L. A total of 10 concentration points were investigated in two different batches and two or three repetitions were performed per point. The sorption protocol was the same as the one followed to investigate the sorption kinetics and the contact time was 21 days. At the end of the contact time and after centrifugation, 2.5 mL of the supernatants was sampled and analyzed by IC-PAD and the equilibrium pH was measured. For each experimental batch, three blanks were performed in parallel to follow the stability of α-ISA in the time and conditions of the experiments. The blank samples consisted of α-ISA in synthetic Stage III cement water at concentration of $3.9 \cdot 10^{-3}$ and $1.4 \cdot 10^{-3}$ mol/L in the first and second batch, respectively. They were treated and analyzed as the sorption samples.

3.4.3 Sorption experiments performed by [**CSIC**]

Adsorption experiments were carried out in polysulfonate centrifuge tubes, that are known to have good resistance to basic solutions and organics do not sorb on the tube walls (Pointeau *et al.* (2006). Adsorption isotherms have been carried out on powdered cement paste samples at a Solid/Liquid (S/L) ratio of 20 g/L for cement paste during 15 days in equilibrium with different concentrations of the organic compounds in both distilled water (DW) and in the corresponding simulated pore water solution (PW) for each degradation stage, to analyze the sensitivity of the adsorption process of the same species in the same matrix in different media. After the corresponding time of contact, samples were centrifuged for 20 min at 4000 rpm. Then, the supernatant liquid was filtered, pH, Ca and the content in total organic carbon (TOC) was measured, using a TOC/TN XPERT equipment by Hach Lange.

3.4.4 Sorption experiments performed by [**CEA**]

All batch sorption experiments were carried out in duplicate in polysulfone polymer (PSF) centrifuge tubes (Nalgene) with polypropylene screw closure. The solid:liquid ratio of 0.1:25 g/mL was used for each HCP suspensions. In general, for all sorption studies the powdered cement and ACW solution were equilibrated for 2 weeks with three changes of equilibrium solution by ACW-Stage II to obtain a stable starting point. The organics were spiked into the suspension as a joined addition of stable organics (EDTA or phthalate) and ^{14}C labelled organics to reach an initial concentration ranging from 10^{-5} to 10^{-2} M and 10 Bq·mL^{-1}. The radionuclide ^{63}Ni or ^{238}U was spiked in the suspension to achieve initial concentration below the operational solubility limit. For some cases, the order of addition of the RN-ORGA was tested. The supernatant was sampled after centrifugation at 20000 RPM for 30 min at several time points to determine the kinetics and the sorption isotherms.

EURAD (Deliverables n° 3.6, 3.7 and 3.8) - Final Report of results generated in CORI
Dissemination level: PU
Date of issue of this report: **05/07/2024**

Page 104

3.5 Diffusion experiments

Diffusion is the most important mechanism for RN transport in HCP. The determination of diffusion coefficients in these materials is important not only for describing RN migration, but also for the prediction of the migration of the main ions present in the porewater which contributes to its main chemical properties during its degradation.

The mathematic treatment of diffusion is widely addressed in the literature (*e.g.* Crank, 1975) and it is mainly based on the first and second Fick's laws (see the Equation 9 and the Equation 10).

$$F = -D \frac{\partial C}{\partial x}$$

Equation 9

The first Fick's law (expressed in Equation 9 in its one-dimensional form) indicates that the mass flux per unit cross-sectional area, F [kg m^{-2}·s^{-1}], is directly proportional to the concentration, C [kg·m^{-3}], gradient. The diffusion coefficient, D [m^2·s^{-1}] represents the proportionality constant between concentration gradient and flux and indicates the rate at which ions and/or molecules spread.

The Fick's second law (see Equation 10) indicates that the concentration of ions/molecules in the pore water, C, depends on time t [s] and distance x [m] as:

$$\frac{\partial C}{\partial t} = D \frac{\partial^2 C}{\partial x^2}$$

Equation 10

Diffusion in porous media is affected by the porous structure of the material, in term of *tortuosity* (τ) or *constrictivity* (δ). The volume available for diffusion and contributing to solute transport in materials is related to connected pores: the cross-sectional area available for diffusion is limited by the material porosity (ε). The diffusion coefficient of a species in free water, D_w, can be related to the diffusion coefficient in a porous media, D_p, using the following relation: $D_p = \frac{\delta}{\tau^2} D_w$. In a porous media, the effective diffusion coefficient, D_e, is defined by:

$$D_e = \varepsilon \cdot D_p$$

Equation 11

The retention on the solid surfaces is another mechanism that can affect RN diffusion. To account for retention processes, the apparent diffusion coefficient, D_a, is defined:

$$D_a = \frac{D_e}{(\varepsilon + \rho \cdot K_d)} = \frac{D_e}{\alpha}$$

Equation 12

Where ρ is the dry density of the solid and α is the "capacity factor", which includes retention through the distribution coefficient, K_d. If a solute is non-sorbing ($K_d = 0$ m^3·kg^{-1}) then the capacity factor is equivalent to the porosity.

To determine these transport parameters different experimental set-ups can be designed, based on the characteristic of the system to be studied. Depending on the constraint of the experiment, different analytical solutions to the Ficks' laws exists (Crank, 1975) but experimental results can also be analyzed by numerical methodologies. The most used classical experimental techniques to measure the diffusion coefficients of chemical species are: Through-Diffusion (TD); In-Diffusion (ID) and Out-Diffusion (OD) (Flury and Gimmi, 2002).

As mentioned in the "State-of-the-art report on cement-organic- radionuclide- interactions in the content of L/ILW disposal (Deliverable 3.1)" diffusion studies in cements are quite scarce end even scarcer are studies in the presence of organics. Thus, to obtain quantitative data about diffusive transport of RN-organic complexes in cementitious materials is a particularly important issue. Different organizations are

EURAD (Deliverables n° 3.6, 3.7 and 3.8) - Final Report of results generated in CORI
Dissemination level: PU
Date of issue of this report: **05/07/2024**

Page 105

involved in diffusion/transport studies: **[CEA]**, **[CIEMAT]**, **[JGU]**, **[JUELICH]**, **[SCK CEN]**, **[CNRS-SUBATECH]**, **[UJV], [UHELSINKI],** and **[CSIC]**. Regarding these two latter, electro-diffusion experiments have been conducted on organic molecules as accelerated-diffusion technique due to the low motion of these species in solution. Consequently, the treatment of the electro-diffusion data requires relevant tools which are not based on the Fick law as cited above, but based on the Nernst-Planck equation defining J_i, the ionic flux of the species i under an applied voltage:

$$J_i = -D_{E,i} \left(\frac{\partial c_i}{\partial x} + c_i \frac{\partial \ln \gamma_i}{\partial x} + \frac{z_i c_i F}{RT} \frac{\partial \psi}{\partial x} \right)$$ Equation 13

Where $D_{E,i}$ is the effective diffusion coefficient of the species i, c_i is the molar concentration of the species i, z_i is the valence of the species i, γ_i is the activity coefficient of the species i, and ψ is the applied electrical potential. F is the Faraday contant, R is the ideal gas constant, and T is the temperature.

The following sections provided details about specific diffusion set-up used by those partners in Task 3 and/or Task 4.

3.5.1 Diffusion experiments performed by [**CEA**]

Different set-ups of diffusion cells have been used by **[CEA]**. The first type corresponds to a classical through-diffusion set-up with two 100-mL-reservoirs in PVC (*Figure 3-10* A) or with two 10-mL-reservoirs in PMMA (*Figure 3-10* B). After leaching, the edge of the HCP disks is glue using an epoxy resin (sikadur-31-EF, Sika, France) and placed in a specific sample holder in PVC.

(A)   (B)

(C)
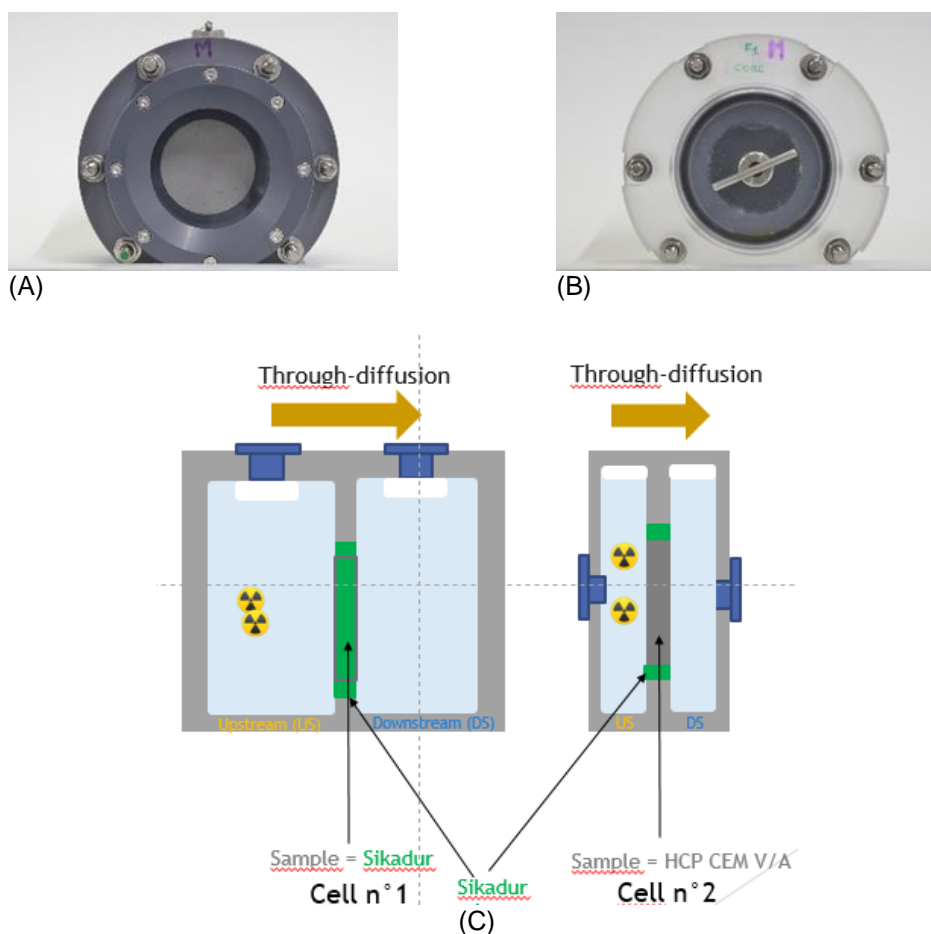
Figure 3-10: *Picture of the 100-mL-through-diffusion cell (A) and the 10-mL-through-diffusion cell (B). Schematic of both type of through diffusion set-up used by **[CEA]**.*

EURAD (Deliverables n° 3.6, 3.7 and 3.8) - Final Report of results generated in CORI
Dissemination level: PU
Date of issue of this report: **05/07/2024**   Page 106

The second type of diffusion cell, consist in using the cell n°2-type (*Figure 3-10* C) as an in-diffusion set-up. To achieve it, one of the two compartment is filled with the epoxy resin (sikadur-31-EF, Sika, France). Then, only one surface of the HCP disk is remaining in contact with the radioactive Stage II solution.

The last type of diffusion set-up is an –in-diffusion set-up with only one 10-mL-reservoir in PMMA, adapted from the set-up proposed by Legand (2023), see *Figure 3-11*. The aim of such a set-up is to avoid the presence of exogenous organic species in contact with the HCP sample in the artificial cement porewater (ACW). In the other concept, the exogenous organic species mainly come from glue used to fix the sample in sample holder or the alkaline degradation of the plastic used in the diffusion vessel.

(A)   (B)
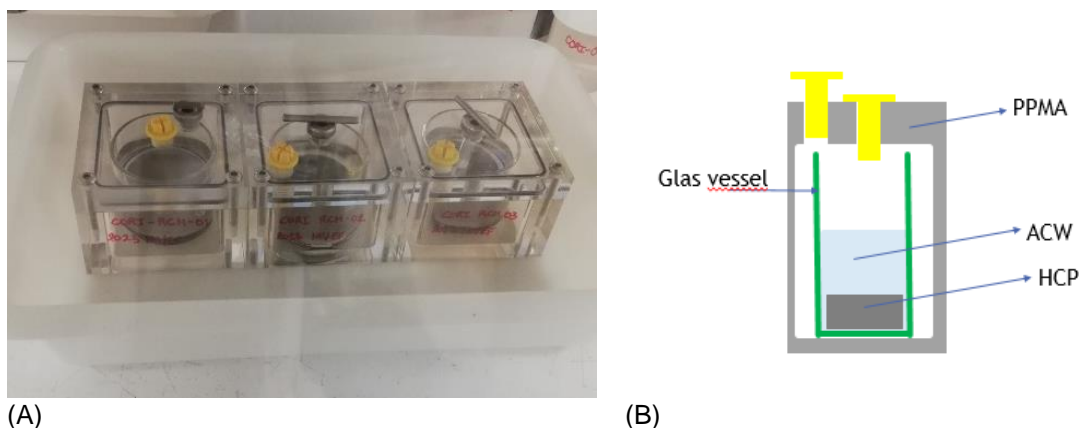
Figure 3-11:   (A) *Picture of the 10-mL-through-diffusion cells. (B) Schematic of the in- diffusion set-up used by [CEA].*

The compartments labelled "upstream reservoir" were filled with the Stage II solution then the stable organic solution is added with eventually some radioactive solution containing HTO and/or C-14 labelled organic and/or stable organic and/or ^{238}U(VI) or ^{63}Ni. In the through-diffusion set-up, the second side was labelled "downstream reservoir" and filled with only Stage II solution.

The HTO data for the cell n°1 (Sikadur) was interpreted by modelling and a D_a(HTO) value of $6.4 \cdot 10^{-14}$ m^2/s can correctly describe the activity evolution in both compartments, resulting to a very low diffusivity of this tracer through this matrix (cf. *Figure 3-12*).

(A)   (B)
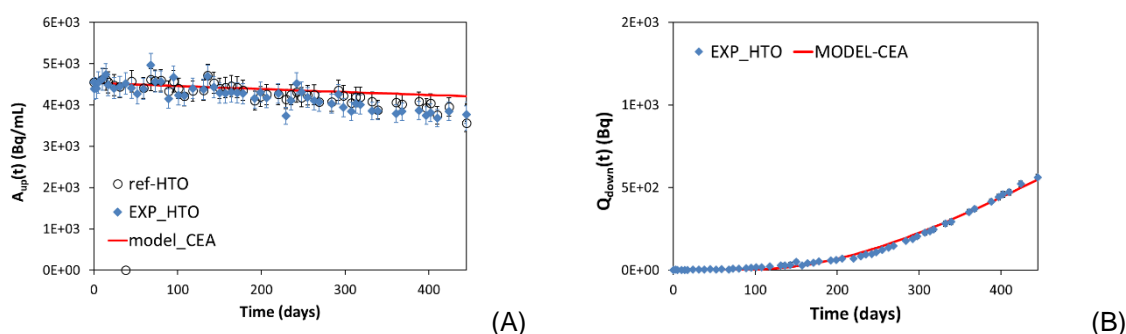
Figure 3-12:   *Through-diffusion of HTO in a SIKADUR glue disk in Stage II ACW solution over time. (A) Evolution of the activities of HTO in the upstream compartment. (B) Evolution of the cumulative activity of HTO in the downstream compartment.*

In the cell n°2, containing the CEM V/A disk, the upstream compartment was spiked with HTO solution (4.52 kBq/mL) at the beginning of the through diffusion experiment and after 110 days, the second radioactive tracer (^{14}C-EDTA) was added (5.18 kBq/mL). The HTO concentration changed much more significant (*Figure 3-13*A) compared to the initial activity (see series "HTO-REF" in *Figure 3-13*A). The concentration in the downstream compartment rises above the detection limit after only 25 days (*Figure 3-13*B). The HTO data was interpreted before the addition of ^{14}C –EDTA. The model leads to give a D_a(HTO) value of $4.2 \cdot 10^{-13}$ m^2/s ($\alpha = 0.33$), which can correctly describe the activity evolution in both

EURAD (Deliverables n° 3.6, 3.7 and 3.8) - Final Report of results generated in CORI
Dissemination level: PU
Date of issue of this report: **05/07/2024**

Page 107

compartments, resulting to and higher diffusivity of this tracer through this matrix compared to the one obtained for the SIKADUR sample.
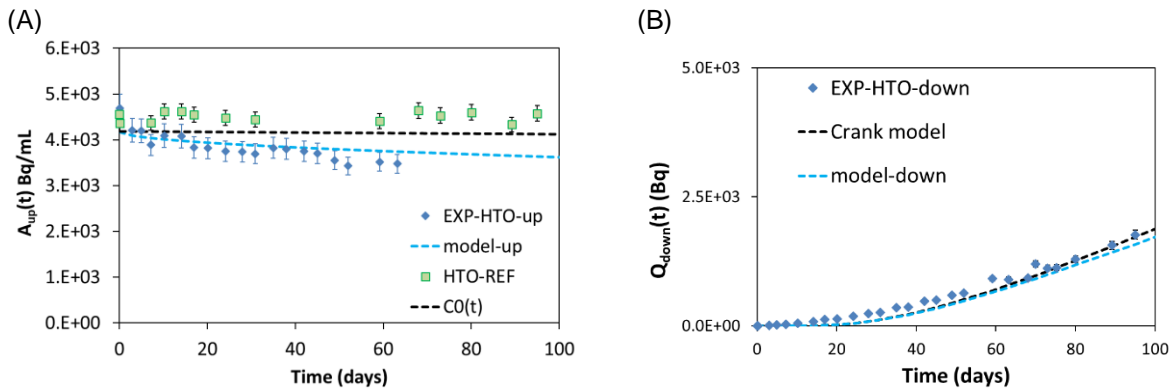
Figure 3-13: *Through diffusion of HTO in a CEM V/A disk in Stage II ACW solution over time (F1 cell) before the addition of ^{14}C-EDTA in the upstream compartment. (A) Evolution of the activities in the upstream compartment compared to the reference solution (B) Evolution of the cumulative activity in the downstream compartment.*

3.5.2 Diffusion experiments performed by [**CIEMAT**]

[**CIEMAT**] performed diffusion tests with α-ISA synthesized in the laboratory and Ni diffusion in the presence of α-ISA using classical through-diffusion cells with circulating solution in the inlet and outlet resevoirs. The schematic of through-diffusion experiments and a picture of tests mounted in the anoxic glove box are shown in *Figure 5-3*.
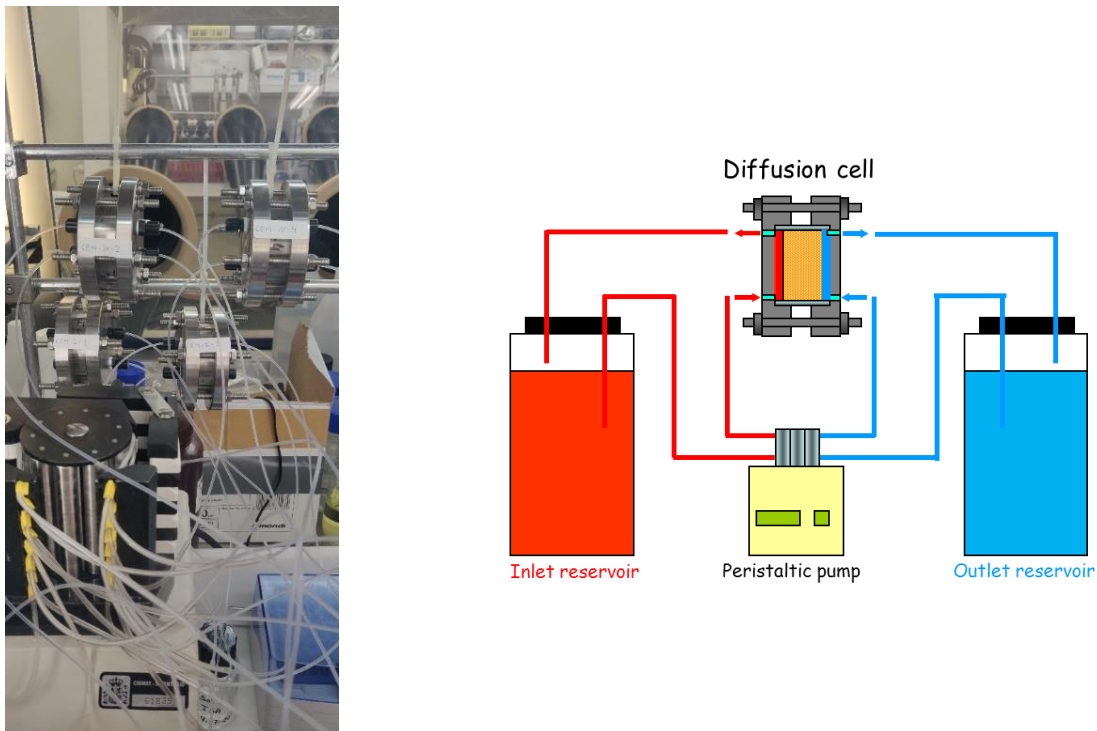
Figure 3-14: *Schematic of through diffusion tests and experimental set-up mounted in the anoxic glove box used by [**CIEMAT**].*

EURAD (Deliverables n° 3.6, 3.7 and 3.8) - Final Report of results generated in CORI
Dissemination level: PU
Date of issue of this report: **05/07/2024**

Page 108

3.5.3 Diffusion experiments performed by [**JGU**]

[**JGU**] performed also in-diffusion experiments of ^{238}Pu(IV) into HCP at Stage I (pH > 13) in the absence and presence of ISA ([ISA]$_0$ = 1 10^{-2} M) in ACW (with 0.003 M NaN$_3$). The experiment was conducted in two in-house, filter-free, and tubeless diffusion cells made of Perspex. The cells were designed based on the setup by Tits *et al.* (2003), as described in Bott (2022). Prior to characterization, the HCP cores (diameter: 25 mm, thickness: 6 mm) were pre-equilibrated with ACW for one week. The cement cores were first characterized using through-diffusion of HTO ([HTO]$_0$ ≥ 2 10^{-9} M). The determination of the diffusion parameters, porosity ε and the effective diffusion coefficient D$_e$, are presented in *Table 36* and compared with available literature data (Tits *et al.* (2003), Bott (2022)).

Table 36: Diffusion parameters of HTO through-diffusion test of both cells compared with literatures

	Cell I	**Cell II**	**Bott (2022)**	**Tits *et al.* (2003)**
D$_e$ (m^2 s^{-1})	(1.73±0.005)·10^{-11}	(1.66 ± 0.005)·10^{-11}	(1.3 ± 0.2)·10^{-11}	2.72·10^{-10}
ε	0.65 (± 0.02)	0.68 (± 0.02)	0.68 (± 0.01)	0.63

3.5.4 Diffusion experiments performed by [**JUELICH**]

[**JUELICH**] proposed a dedicated experimental set-up combining through-diffusion of HTO with in-diffusion of Am (III) and Eu (III). The diffusion experiment was conducted inside an Ar glovebox. Cylindrical diffusion cells were constructed based on the design of Ait-Mouheb (2021). The diffusion cells are made from transparent polymethyl methacrylate (PMMA) (*Figure 3-15*) permitting an easy visual check of processes occurring during the experiments. The diffusion cell comprised a thin hardened cement disk (diameter = 3 cm, thickness = 1 cm) sealed with resin and mounted between the two reservoir compartments, called high and low concentration reservoirs, with total volumes of 50 mL and 3.8 mL, respectively. After saturating the disks with the CEM V water, the diffusion experiments were initialised by replacing the solution inside the high concentration reservoir by CEM V water labelled with HTO and Am (III)/Eu (III); the low concentration reservoir was filled with fresh tracer-free CEM V water. The initial concentrations of the radionuclides in the high reservoir were (Am(III) / Eu(III) = 10^{-8} M; HTO = 10^{-9} M) in the presence and absence of phthalate and TMA. Openings located on both reservoirs allowed for regular sampling of both reservoirs. From the obtained solution samples the pH value was determined and the HTO, Am(III) and Eu(III) activities were measured by liquid scintillation counting (LSC, 1220 Ultra low-level Quantulus™, Perkin Elmer). After each sampling, the low concentration reservoirs were again refilled with tracer-free CEM V water.
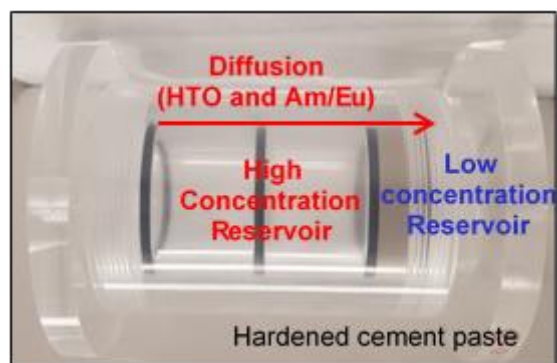
Figure 3-15:   Diffusion cell used in the combined in-diffusion (Am(III) / Eu (III)) and through-diffusion (HTO) experiments based on the design of Ait-Mouheb (2021).

EURAD (Deliverables n° 3.6, 3.7 and 3.8) - Final Report of results generated in CORI
Dissemination level: PU
Date of issue of this report: **05/07/2024**

Page 109

Transport parameters for HTO are obtained by inverse modelling of the diffusive flux data determined at the low reservoirs by measuring the accumulated activity (details on flux calculations are given, *e.g.*, in Tits *et al.* (2003a)). RNs concentration profiles in the HCP disks are performed using laser ablation ICP-MS. The laser ablation ICP-MS (Perkin Elmer NexION2000 combined with a UV YAG LA System von New Wave Research Inc) provides a highly sensitive multi-element technique with a wide analytical dynamic range from the part per trillion (ppt) to the part per million (ppm) level directly in the solid. For Eu(III) and Am(III), the effective diffusion coefficients will be determined by fitting the experimental tracer distribution profiles in the HCP.The finite element code COMSOL Multiphysics v.5 (COMSOL, 2018) is used for solving the partial differential equations and for the evaluation and modelling of the experiments.

3.5.5 Diffusion experiments performed by [**SCK CEN**]

The diffusion set-up used by [**SCK CEN**] is presented in *Figure 3-16*.
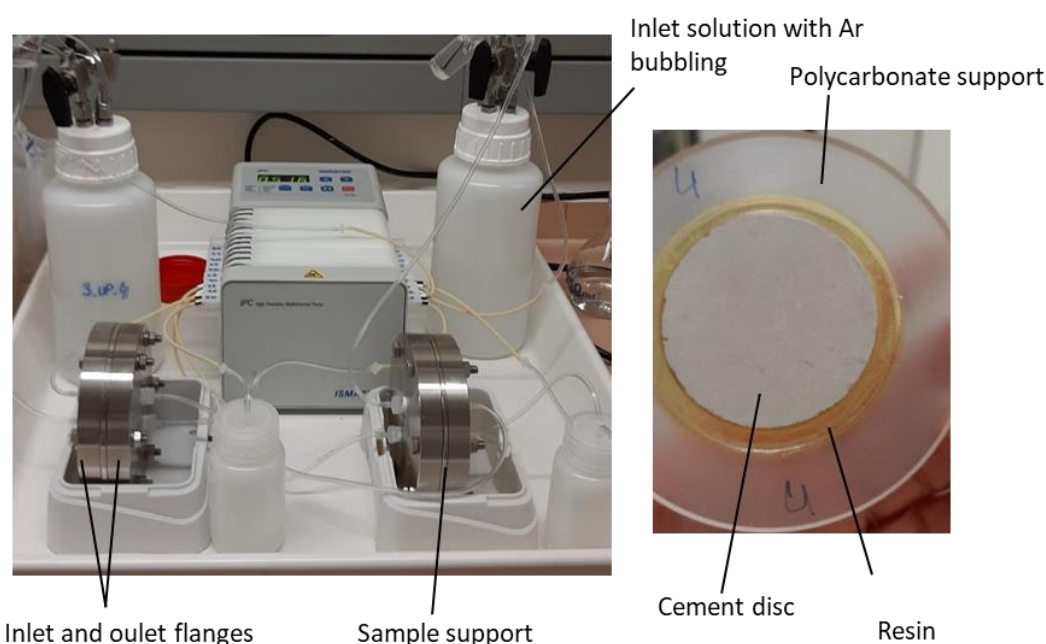
Figure 3-16:   *Diffusion experimental set-up used by [**SCK CEN**].*

The polycarbonate supports in which the cement discs were resined, were placed into a stainless steel ring, which was itself screwed in between the inlet and outlet stainless steel flanges as shown in *Figure 3-16*. The inlets of the diffusion cells were each connected to a 1 L bottle containing the synthetic diffusion water with argon bubbling to avoid CO_2 and O_2 contamination. The outlets were connected each to a 20 mL liquid scintillation vial filled with synthetic diffusion water. The vials were bathing in 1M NaOH to avoid CO_2 contamination. The inlet and outlet solutions were circulating with the use of a peristaltic pump.

The composition of the solution used in the diffusion experiments, referred to as synthetic diffusion water, was based on the composition of the equilibrium solution measured after 210 days of contact with the two cement discs obtained after 345 days of leaching (see Section 3.2.1). The synthetic diffusion water was prepared in an inert atmosphere following the recipe reported in *Table 37*. The solution was stirred overnight and subsequently filtered with PVDF filters (pore size 0.2 µm).

EURAD (Deliverables n° 3.6, 3.7 and 3.8) - Final Report of results generated in CORI
Dissemination level: PU
Date of issue of this report: **05/07/2024**

Page 110

Table 37: Composition of the synthetic diffusion water and recipe for preparation.

pH	Ca (mol/L)	Si (mol/L)	Al (mol/L)	SO_4^{2-} (mol/L)
11.8	$4 \cdot 10^{-3}$	$6 \cdot 10^{-5}$	$7 \cdot 10^{-5}$	$2 \cdot 10^{-4}$
	$Ca(OH)_2$	SiO_2	$Al_2(SO_4)_3, 18H_2O$	$CaSO_4, 2H_2O$
$g \cdot L^{-1}$	$2.9 \cdot 10^{-1}$	$4 \cdot 10^{-3}$	$2.3 \cdot 10^{-2}$	$1.6 \cdot 10^{-2}$

The cement discs used in the diffusion experiments were leached as part of the second leaching series as described in Section 3.2.1. The details of the two cement discs used for the diffusion experiments are reported in *Table 38*. To perform the diffusion experiments on CEM I HCP degraded to Stage III, first the cement discs needed to be degraded to that stage. For this, cement discs of ~3 mm thickness and 47.5 mm diameter were leached in ultrapure water and the degradation was followed over time by analyzing the contact solution. In addition, samples were stopped at different time intervals and the solids were analyzed. The leaching in ultrapure water was slow and the two samples further used for the diffusion experiments were leached for 264 and 345 days. XRD analyses performed on the cement discs after that leaching period showed a total removal of portlandite and ettringite. The evolution of the bulk C/S ratio along the thickness of the sample measured by SEM-EDX revealed relatively homogeneous ratios. The composition of the solution in equilibrium with the cement discs was taken as a reference to prepare the solution for the diffusion experiments. This solution had a pH of 11.8 for a concentration of Ca^{2+} of $4 \cdot 10^{-3}$ M. The two degraded cement discs of 2.3 and 3.4 mm thickness, respectively, were resined and loaded into stainless steel diffusion cells.

The transport properties of the samples were evaluated by through-diffusion of HTO coupled to 1D transport modelling. Though it was initially the intention to dedicate an experiment to the diffusion of α - ISA, the technical constraints related to the degradation of the cement discs pushed us to limit ourselves to perform only two experiments: one to follow the diffusion of Ni and one to follow the combined diffusion of Ni and α-ISA.

Table 38: Cement samples used for diffusion experiments*.*

	Test 'Diff1'	Test 'Diff2'
Leaching time	268 days	345 days
Dimensions (Ø × L)	47.5 × 2.3 mm²	47.5 × 3.4 mm²

The cement discs were equilibrated with the synthetic diffusion water for about two weeks in an inert atmosphere. After what they were resined on a polycarbonate support adjusted to their dimensions (*Figure 3-16*). Care was taken to avoid the formation of bubbles in the resin. After hardening of the resin, which was done in a closed plastic box to avoid carbonation, the samples were left to (re)saturate with the synthetic diffusion water for ~24 h under vacuum.

The through-diffusion of HTO was investigated in both cells. For this, the inlet solution was prepared by spiking 500 mL of synthetic diffusion water with HTO to an activity of 4.5 and 6.8 Bq/mL for Diff1 and Diff2, respectively. The outlet solutions were sampled regularly, analyzed by LSC and replaced by fresh synthetic diffusion water. 200 µL of the inlet solutions was also sampled at regular intervals and analyzed by LSC. The experiments were followed until a steady-state regime was reached in the outlet. The

EURAD (Deliverables n° 3.6, 3.7 and 3.8) - Final Report of results generated in CORI
Dissemination level: PU
Date of issue of this report: **05/07/2024**

Page 111

experimental results were modelled with a 1D diffusion transport model with COMSOL Multiphysics. The evolution of the experimental and modelled inlet HTO activities and outlet flux in the two diffusion experiments are reported in *Figure 3-17*.

(A)   (B)
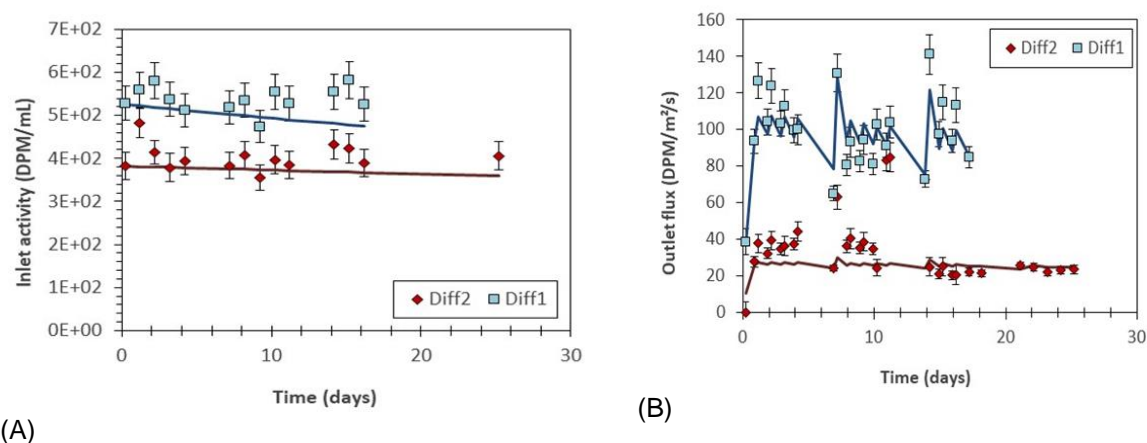
Figure 3-17:   *HTO diffusion through HCP Stage III – Results from* **[SCK CEN]**.

As it can be seen in *Figure 3-17*B, the plateau of the outlet flux in test "Diff2" is significantly lower than in test "Diff1", which indicates a lower effective diffusion coefficient in "Diff2". Indeed, the best fit to the experimental data is obtained for the effective diffusion coefficient values reported in *Table 39* with DeHTO (Diff1) about twice DeHTO(Diff2). Note that the thickness of the two samples differs with Diff1 being thinner than Diff2. Although the thickness of the sample is not expected to affect the diffusion coefficient, at the low sample thickness used here, the presence of some small preferential paths could play a role (but expected to be very limited). Nevertheless, the two experiments show diffusion coefficients of the same order of magnitude.

Table 39: HTO diffusion parameters obtained for 'Diff1' and 'Diff2' experiments **[SCK CEN]**.

	Test 'Diff1'	**Test 'Diff2'**
D_e (m^2/s)	$(5.4 \pm 0.7) \cdot 10^{-11}$	$(2.8 \pm 7.3) \cdot 10^{-11}$

The through-diffusion of HTO was followed up in the two diffusion experiments with Ni in presence and absence of α-ISA. At the end of the HTO through-diffusion experiments, the inlet solution of Diff2 was discarded and replaced by ~1 L of synthetic diffusion water containing $3 \cdot 10^{-7}$ M of stable Ni and 10^{-2} M of α-ISA. The solution was first left to circulate without the cement disc to 'saturate' the tubing and bottle walls with Ni (in case of Ni sorption on the tubings and the bottles). An aliquot of the inlet solution was then sampled and analyzed for Ni by ICP-MS. The starting Ni concentration was measured to be $1.3 \cdot 10^{-7}$ M. Afterwards, the cement disc was placed in the circulation.

The outlet solutions have been sampled regularly, analyzed by ICP-MS and IC-PAD and replaced by fresh synthetic diffusion water. The outlet pH has also been measured regularly. Furthermore, 200 µL of the inlet solutions has been sampled at regular intervals and analyzed by ICP-MS (and IC-PAD). The pH of the inlet solution has been measured from time to time.

EURAD (Deliverables n° 3.6, 3.7 and 3.8) - Final Report of results generated in CORI
Dissemination level: PU
Date of issue of this report: **05/07/2024**

Page 112

3.5.6 Diffusion experiments performed by [**CNRS-SUBATECH**]

Diffusion experiments performed by **[CNRS-SUBATECH]** were carried out with classical 2-compartments PVC diffusion cells. HCP disks (50 mm in diameter and 2 mm thick) were glued in PVC sample holders with an epoxy resin and let equilibrated during at least one month in either saturated lime water (Stage II) or solution from degradation experiment (Stage III). Beforehand any addition of U(VI) and ISA, four HTO through-diffusion experiments were performed for each stages (II and III) in order to check the set-ups (absence of leak or fracking of HCP samples,…); this HTO step lasted up to 160 days. Diffusion results (HTO cumulative activity in the downstream compartment *vs* time) were interpreted by resolving Fick's diffusion law with a semi-infinite 1D-analytical solution in order to determine HTO effective coefficients (D_e(HTO)) (Crank, (1975)).

For Stage II, HCP disks, the average value for D_e(HTO) was $(3.9\pm0.6)\cdot10^{-13}$ $m^2.s^{-1}$ which is very consistent with values obtained from previous studies and literature data on similar CEM V HCP (Landesman *et al.* (2018), Bejaoui&Bary (2007))

For Stage III, since the HCP disks are structurally heterogeneous due to the water degradation step, D_e(HTO) values cannot be rigorously derived from the analytical solution which supposes homogeneous samples. Keeping that in mind, the interpretation gives D_e(HTO) estimated values ranging from 1.4 to $2.4\cdot10^{-12}$ $m^2\cdot s^{-1}$ *i.e.* 3 to 6 times higher than those obtained for S2 HCP disks. Thus as expected, the opening of the porosity (due to the dissolution of some mineral phases) facilitates the diffusion pathway of water through S3 HCP samples.

Diffusion experiments were carried out on binary and ternary systems for both degradation stages in the following experimental conditions (*Table 40*).

Table 40: Experimental conditions for diffusion experiments

	Systems	[U] in upstream compartment $(mol \cdot L^{-1})$	[ISA] in upstream compartment $(mol \cdot L^{-1})$	Duration (days)
Stage II	U(VI)/HCP	$5.6\cdot10^{-6}$ *	-	505
	U(VI)/ISA/HCP	10^{-4}	$3.3\cdot10^{-2}$	400
Stage III	U(VI)/HCP	$2\cdot10^{-6}$	-	275
	U(VI)/ISA/HCP	$2.1\cdot10^{-6}$	$3\cdot10^{-2}$	275

* Controlled by Ca-Uranate solubility in S2 solution $(5.60 \pm 0.84)\cdot10^{-8}$ $mol\cdot L^{-1}$

3.5.7 Diffusion experiments performed by [**UJV**]

[UJV] performed laboratory leaching tests based on ANSI/ANS 16.1 were performed by applying surface/volume (S/V) = 1/10 cm^2/ml for different liquid phases: distilled water, portlandite water (saturated Ca(OH)$_2$ solution) and synthetic granitic water. The release of ^{63}Ni fixed in the pure CEM I paste and CEM I paste with ISOLA superplasticizer was studied by these specific leaching tests.

3.5.8 Electromigration experiments performed by [**UHelsinki**]

Migration experiments performed by **[UHelsinki]** were carried out using two set-ups. The first one consisted in classical through-diffusion tests and the second one in development of electromigration tests.

HCP (CEM V) fresh and at Stage II, provided by **[ANDRA]**, were used for classical through-diffusion tests (*Figure 3-18*). The samples were sent in saturation with cement water simulant. However, to facilitate the samples preparations for the electromigration device, they were air-dried for a couple of days to achieve surface dryness for gluing the samples into the through diffusion device. After drying, the cement samples were fitted in a poly methylmethacrylate (PMMA) cylindrical shell which has a 2 mm larger inner diameter than the diameter of the HCP sample. The gaps between the PMMA shell and the cement samples were carefully glued with epoxy (suitable for pH > 12) to make sure that all the

EURAD (Deliverables n° 3.6, 3.7 and 3.8) - Final Report of results generated in CORI
Dissemination level: PU
Date of issue of this report: **05/07/2024**

Page 113

tracer ions can only migrate through the cement sample by its connected pore network. Then, the sample holder was left in the open air for 2 days to guarantee the total strength of the epoxy. After the samples were placed to the diffusion cells and before the through-diffusion experiment, they were saturated with the cement water simulant for 3 days.

Figure 3-18:   Left: Original samples received from **[ANDRA]**; Middle: the cement sample (5 cm length) that was fitted in a PMMA cylinder; Right: the cut and polished cement sample with 1 cm length.
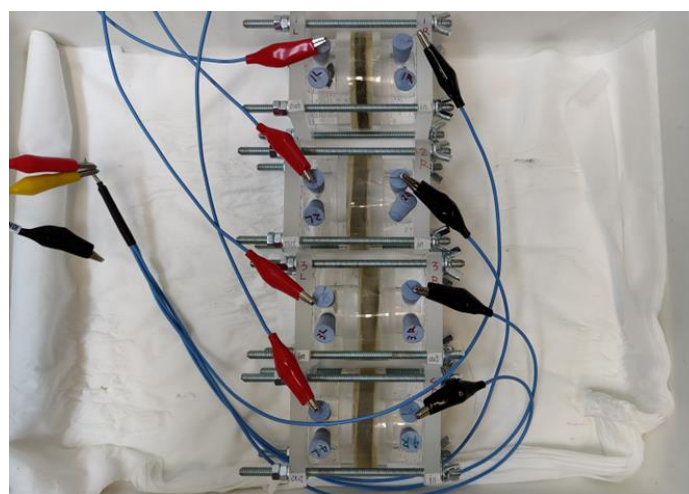
Figure 3-19:   New electromigration device with 4 parallel running cells.

A new device which can run several electromigration cells in parallel was developed by **[UHelsinki]**. *Figure 3-19* above shows the new device that has 4 cells running in parallel in one time. In this new electromigration setup, the tracers tested in different cells are summarized in *Table 41*. A cement sample with No. 6.2 was tested with three tracers (Cl-36, C-14-gluconate and Cs-134), while for the second sample with No. 2.3, Cl-36 was tested. The four cells were run in parallel under the same experimental conditions. The voltage applied over the samples was kept being 5 V for all the four samples and kept being constant (±0.01 V) during the experimental time.

EURAD (Deliverables n° 3.6, 3.7 and 3.8) - Final Report of results generated in CORI
Dissemination level: PU
Date of issue of this report: **05/07/2024**

Page 114

Table 41 summarizes all the tested samples by electromigration in the CORI project.

Table 41: Summary of the analyzed samples by the electromigration device. The table lists cell number, sample number, tracers, voltages and time used in the experiment.

Cell number	Sample number	Tracers	Voltage (V)	Time (d)
1*	5.6	HTO	4	60
1*	5.6	Cl-36	4	21
1*	6.6	HTO	4	51
1*	6.6	Cl-36, C-14 Gluconate	10	16
1*	3.4	Cl-36, C-14 Gluconate	10	20
1**	6.2	Cl-36	5	40
2**	6.2	C-14 Gluconate	5	40
3**	6.2	Cs-134	5	40
4**	2.3	Cl-36	5	40

*one sample device

** four sample device

3.5.9 Diffusion experiments performed by [**CSIC**]

3.5.9.1 Diffusion method

Diffusion coefficients of the organic species through samples C1 and C1-Fe have been carried out by [**CSIC**]. To do so, small classical diffusion cells have been used, as shown in *Figure 3-20*. In them, the specimens separate two compartments, one containing the solution with the target compound (source compartment) and the other initially free of the organic compound (downstream compartment). The compounds diffuse through the aqueous phase in the pores of the specimen and go from the source compartment to the downstream compartment, where they are analyzed.

*Figure 3-20:   Natural diffusion set-up performed at [**CSIC**].*

The specimens consisted of thin discs (around 5 mm), in order to achieve as soon as possible a quasi-steady state in the diffusion through the cement pastes. This assumption implies a flux, J (g/cm^2·sec) constant with time, so that Fick's first law can be applied:

$$J = -D \frac{dc}{dx}$$

Equation 14

Considering that the flow J can be defined as:

EURAD (Deliverables n° 3.6, 3.7 and 3.8) - Final Report of results generated in CORI
Dissemination level: PU
Date of issue of this report: **05/07/2024**

Page 115

$$J = \frac{V}{A} \frac{dc}{dt}$$

Equation 15

In steady state conditions:

$$J = - D_{ef} \frac{C_2 - C_1}{\Delta x} = \frac{D_{ef}}{l} (C_1 - C_2)$$

Equation 16

Where:

V = Volume of the downstream compartment (cm^3).

A = Effective area of the specimen (cm^2).

Def = Effective diffusion coefficient (cm^2/s).

C1= Concentration of the species in the source compartment (g/cm^3).

C2= Concentration of the species in the downstream compartment (g/cm^3).

l = Thickness of the specimen (cm).

t = Time (sec).

Combining the above equations:

$$\frac{D_{ef}}{l}(C_1 - C_2) = \frac{V}{A} \frac{dC_2}{dt}$$

Equation 17

Integration of the above equation for constant C1 leads to:

$$\ln(C_1 - C_2) = - \frac{D_{ef} A}{Vl} (t - t_o) + \ln C_1$$

Equation 18

Thus, from the slope of the straight line obtained by plotting ln (C1-C2) versus time, the value of the effective diffusion coefficient, Def, is obtained.

3.5.9.2 Electromigration method

Migration tests have been carried out at **[CSIC]** according to the method given in Castellote *et al.* (2001) for chloride ions, adapted for organic compounds. The test consists of applying a voltage drop to a test specimen between two compartments containing, upstream, a solution with the target compound and, downstream, a solution without it. Provided dissociated ISA has a negative charge, the negative electrode was placed within the upstream compartment and therefore the external electrical potential applied forced it to migrate through the specimen towards the downstream compartment.

These tests have been quite difficult to perform, as no references in literature were found. Several preparatory tests were carried out in order to assure that the organic compound migrating towards the positive electrode would not be oxidized on it. To do so, cyclic voltammetry tests were carried out to have a safe margin for oxidation of ISA. In addition, before finding the optimum method, several trials have been performed using several electrodes (stainless steel, aluminium, titanium) and forcing the electrodes to specific absolute potential values. After several attempts, the optimum test was designed, that was carried out successfully on sample C2-E2, using distilled water in the anolyte and a solution of ISA 1g/L in the catholyte. The ΔV applied was 12 V DC and both electrodes were activated titanium wires. *Figure 3-21* shows a migration test during the run.

EURAD (Deliverables n° 3.6, 3.7 and 3.8) - Final Report of results generated in CORI
Dissemination level: PU
Date of issue of this report: **05/07/2024**

Page 116
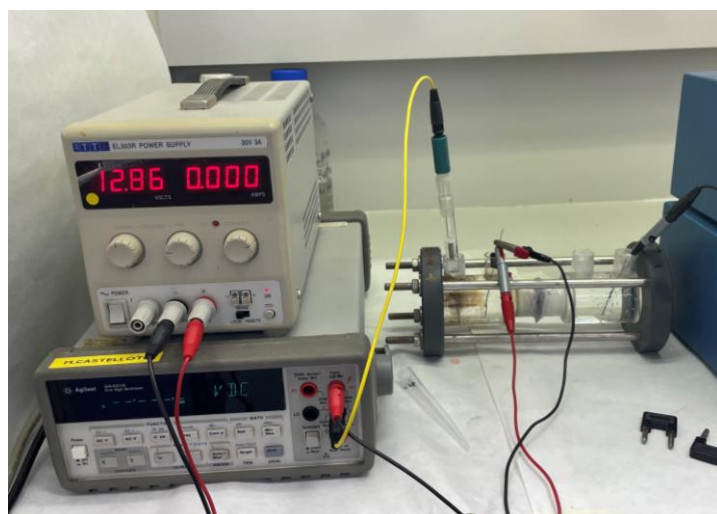
*Figure 3-21   Migration tests performed at **[CSIC]**.*

The steady-state diffusion coefficient, Ds, is calculated using the period in which the passage of ISA reach the steady state (linear behavior with time) from the Modified Nernst-Planck equation:

$$D_s = \frac{A \cdot R \cdot T \cdot l}{z \cdot S.F \cdot Cl \cdot \gamma \cdot \Delta\Phi_{ss}}$$

Equation 19

Where:

D_s: steady-state diffusion coefficient (cm^2/s).

A: slope of the linear regression during the steady-state period (mol/s)

S: surface area of test specimen available for transport (cm^2)

Cl: concentration of ISA in the catholyte (mol/cm^3)

γ = Activity coefficient of the catholyte solution (-).

$\Delta\Phi ss$= Averaged effective voltage (V) through the specimen during the steady-state period

l = thickness of the sample (cm)

R : perfect gas constant (1.9872 cal/mol K)

T: Average temperature during the test (K)

z: ion valence, for ISA, z = 1;

F: Faradays constant = 23060 (cal/ Veq)

The non-steady-state diffusion coefficient, Dns, is calculated from the time-lag, obtained by the intersection of the straight line of chloride flux characteristic of the steady state with the X axis.

EURAD (Deliverables n° 3.6, 3.7 and 3.8) - Final Report of results generated in CORI
Dissemination level: PU
Date of issue of this report: **05/07/2024**

Page 117

4. Results obtained in Task 3

It is reminded here that Task 3 aims to improve knowledge of the organic molecule behavior in cement-based materials in terms of transport and retention properties. The organic molecules studied in the Task 3 are the following: polyvinyl chloride PVC, cellulose, ion exchange resins (IER) and superplasticizers (cementitious additives). The cement-based materials are hardened cement pastes in various degradation stages: Stage II in equilibrium with portlandite, Stage III related to the C-S-H decalcification, and Stage IV corresponding to a carbonated material.

CORI Task 3 is co-leaded by **[Andra]** and **[KIT** (**Amphos21**)**]**, and the work performed in Task 3 on binary system (CEM/ORGA) is part of the studies proposed by the following CORI partners: **[Andra]**, **[KIT (Amphos21)]**, **[CEA]**, **[CIEMAT]**, **[CIEMAT (CSIC)]**, **[CNRS-SUBATECH]**, **[CV REZ]**, **[JSI]**, **[KIT]**, **[PSI (EMPA)]**, **[RATEN]**, **[SCK CEN]**, **[SURAO (CTU)]**, **[SURAO (UJV)]** and **[UHelsinki]**. *Table 42* shows the systems that have been studied by the different organizations in Task 3.

Table 42: Summary of the system studied by each organization in Task 3

Organization	Type of experiment	Material	Organic
[KIT (Amphos21)]	Sorption	C-A-S-H, RCM	ADI, PHT, ISA
[CEA]	Sorption Diffusion	HCP (CEMV), RCM	EDTA, PHT, RDP
[CIEMAT]	Sorption Diffusion	HCP (CEM I, IV, V), RCM C-S-H, POR, ETT	SP (Master Glenium, SIKAMENT), ISA, RDP
[CIEMAT (CSIC)]	Diffusion Electromigration	HCP	ISA
[CTU]	Sorption	HCP (CEM I/ III) C-S-H	PHT, ADI, EDTA
[CV REZ]	Irradiation and ultrasonic	HCP (CEM I), Richard Concrete	SP ISOLA, SP ISOPLAST
[HZDR]	Sorption	C-A-S-H HCP (CEM I)I	GLU, PBTC, RDP, CIT, NTA
[JGU]	Sorption Diffusion	HCP (CEM I) C-S-H	GLU, ISA, EDTA
[JUELICH]	Sorption Diffusion	HCP (CEM V) C-A-S-H	PHT, TMA
[KIT (EMPA)]	Sorption Solubility	HCP (CEMI) C-S-H	FOR, CIT, GLU
[KIT]	Sorption Solubility	HCP (CEMI)	UP2 resins real leachate, GTA, HIBA, HBA Degraded cellulose leachate
[RATEN]	Sorption Solubility	HCP (CEM I, V)	FOR
[SCK CEN]	Sorption diffusion	HCP (CEM I)	ISA
[CNRS-SUBATECH]	Sorption diffusion	HCP(CEM V)	ISA
[SURAO]	Sorption	Richard Concrete	EDTA

EURAD (Deliverables n° 3.6, 3.7 and 3.8) - Final Report of results generated in CORI
Dissemination level: PU
Date of issue of this report: **05/07/2024**

Page 118

[UJV]	Sorption, Diffusion, Leaching	HCP (CEM I) Richard Concrete	SP (ISOLA)
[UCYPRUS]	Sorption	C-S-H	EDTA
[UHelsinki]	Electromigration	HCP (CEM V)	GLU

EURAD (Deliverables n° 3.6, 3.7 and 3.8) - Final Report of results generated in CORI
Dissemination level: PU
Date of issue of this report: **05/07/2024**

Page 119

4.1 Isosaccharinic acid and cellulose degraded products

ISA and degraded products from cellulose were studied by **[KIT]**, **[KIT (Amphos21]**, **[KIT(JGU)]**, **[CIEMAT]**, **[CNRS-SUBATECH]**, **[SCK CEN]** and **[CIEMAT (CSIC)]**.

[KIT(JGU)] performed batch sorption experiments in binary systems HCP/ISA and C-S-H/ISA**.** The uptake of ISA on HCP (pH >13) and C-S-H (pH ~10) was investigated through two types of batch sorption experiments (see Stietz *et al.* 2023b). One experiment was performed at a constant ligand concentration ($[ISA]_0 = 10^{-3}$ M) while varying the S/L ratio (S/L = 0.5 – 50 g·L^{-1}), and as sorption isotherm of ISA ($[ISA]_0 = 4 \cdot 10^{-10}$ M – 10^{-1} M) at constant S/L ratio (S/L = 5 g·L^{-1}). Both experiments had a contact time of 72 hours. The determination of ISA in the supernatants was done by Total Organic Carbon (TOC) analysis in collaboration with **[KIT]**. *Figure 4-1* (A) shows that the sorption behavior of ISA has a very high sorption, ranging from 63% to 92% at 50 g·L^{-1}.

A
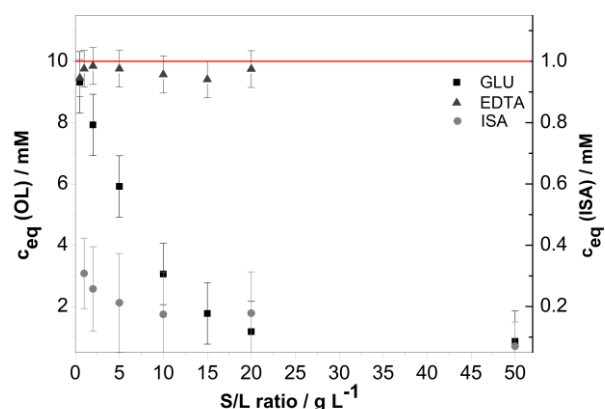
B
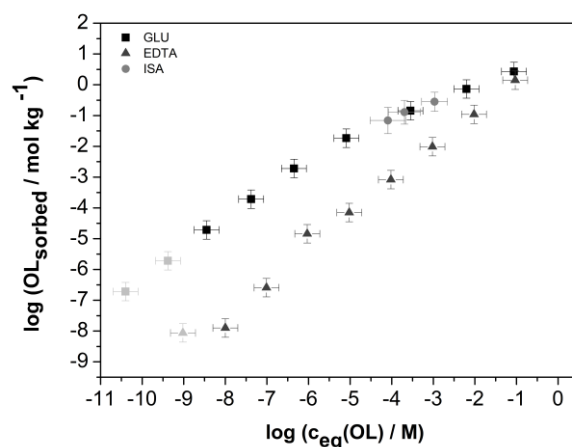
Figure 4-1   *Batch sorption experiments of the binary system at HCP / Organic Ligand (OL = GLU, EDTA or ISA) after a contact time of 72 h at pH = 13.3. A) at constant OL concentration ($[Glu]_0$ and $[EDTA]_0$ = $1 \cdot 10^{-2}$ M, $[ISA]_0 = 1 \cdot 10^{-3}$ M) and varying S/L ratio (S/L = 0.5 – 50 g·L^{-1}). The red line marks the initial concentration of OL. B) sorption isotherms with initial OL concentrations from $4 \cdot 10^{-10}$ – $1 \cdot 10^{-1}$ M at S/L = 5 g·L^{-1}. Data from Stietz et al. 2023b.*

Sorption isotherms (*Figure 4-1* B) were obtained by varying the ISA concentration. As can be seen, the curves flattened at high concentrations $[ISA]_0 \geq 10^{-3}$ M, indicating a saturation of the sorption sites of HCP.

Analogous experiments with the C-S-H phases (C/S = 0.8) at pH~10 were performed. In the first experiment, shown in *Figure 4-2* left, the S/L ratio was varied between 0.5 and 50 g/L at a constant OL ($[Glu]_0$ resp. $[EDTA]_0 = 10^{-2}$ M) concentration. In the second experiment, the sorption isotherm of OL on

EURAD (Deliverables n° 3.6, 3.7 and 3.8) - Final Report of results generated in CORI
Dissemination level: PU
Date of issue of this report: **05/07/2024**

Page 120

C-S-H phases was determined by varying the concentration over eight orders of magnitude ($[OL]_0 = 10^{-9} - 10^{-1}$ M) at constant S/L value of 5 g L^{-1}. As can be seen, in all experiments the sorption of GLU (< 5%) and EDTA (< 10%) is very low (*Figure 4-2* left). For sorption isotherm experiments, a linear fit was used for both GLU (Dettmann *et al.* (2023)) and EDTA. In the case of GLU, the determined R_d value of 2.02 ± 1.3 L·kg^{-1} is slightly lower compared to the value ($R_d = 4.5$ L·kg^{-1}) from the study of Androniuk (2017). Regarding EDTA, the resulting R_d value was 5.8 ± 1.6 L·kg^{-1}, a little higher than the value obtained for GLU. The sorption of GLU and EDTA on the C-S-H phase was found to be very low at a C/S ratio of 0.8, and there was no blocking of sorption sites by GLU on the C-S-H. No sorption experiments with ISA have been conducted to date.
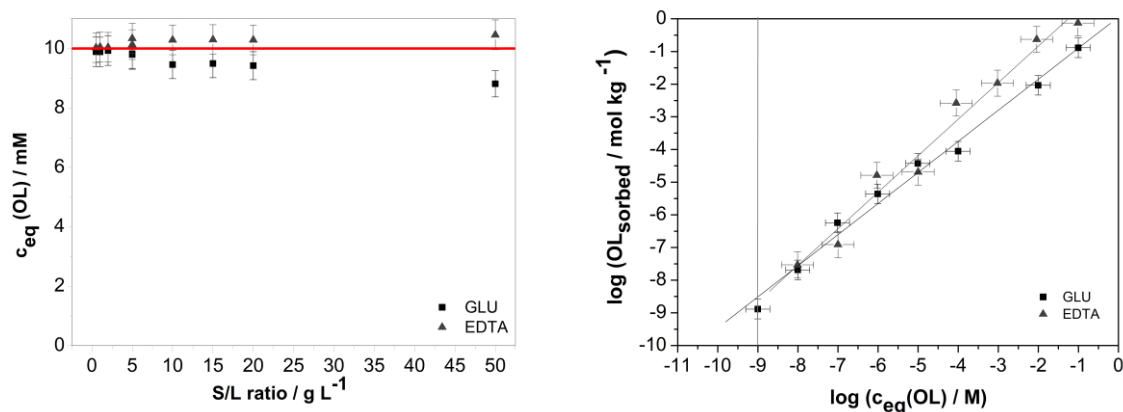
Figure 4-2   *Batch sorption experiments of the binary system at C-S-H / OL (GLU, EDTA) after a contact time of 72 h at pH = 10. Left) at constant OL concentration and varying S/L ratio (S/L = 0.5 – 50 g·L^{-1}). The red line marks the initial concentration of OL. Right) sorption isotherms.*

[KIT (Amphos21)] studied the ISA sorption in C-A-S-H systems and on RCM suspensions. Regarding the sorption experiments of ISA on RCM provided by the Czech partners, the extent of sorption is greater than for C-A-S-H phases. Results for ISA sorption to C-A-S-H 1.2-0.05, C-A-S-H 1.2-0.2, and RCM are plotted alongside existing literature values for cementitious materials in *Figure 4-3*.
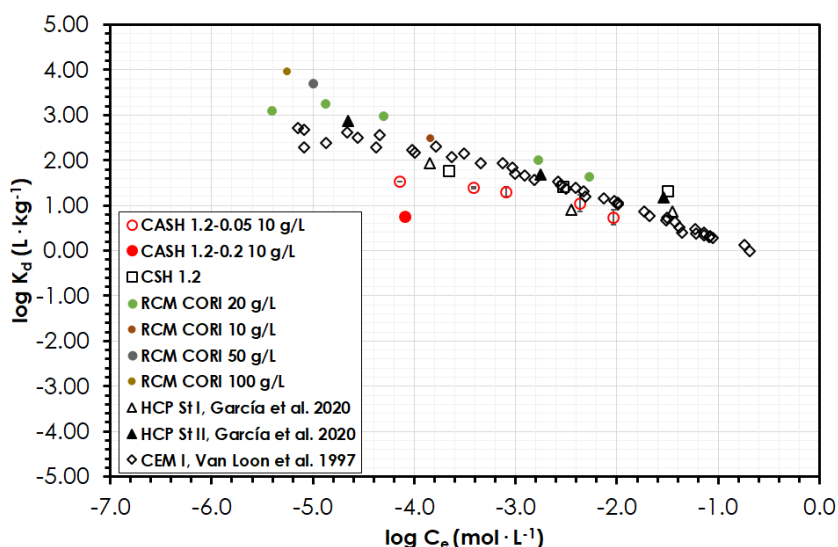
Figure 4-3   *Sorption of ISA to C-S-H 1.2 (Garcia et al., 2020), C-A-S-H 1.2-0.05 and 1.2-0.2 (current work), hardened cement paste at Stage I (HCP_I) and Stage II (HCP_II) (García et al., 2020), CEM I (Van Loon et al., 1997), and Reference Cement Material (RCM) at different solid solutions (as indicated). Data are plotted as solution concentration (mol/L) against calculated solid concentration (mol/kg).*

![eurad logo] European Joint Programme on Radioactive Waste Management   EURAD (Deliverables n° 3.6, 3.7 and 3.8) - Final Report of results generated in CORI
Dissemination level: PU
Date of issue of this report: **05/07/2024**   Page 121

[CNRS-SUBATECH] investigated ISA sorption in CEM I HCP at Stage II and Stage III. Uptake results are reported in *Figure 4-4*. R_d(ISA) values diminish from 180 to 14 L·kg^{-1} for ISA concentrations in solution ranging from 10^{-4} up to 2·10^{-2} mol L^{-1}. Literature data for R_d(ISA) values on CEM V HCP are very limited (only one dataset from García *et al.* (2020)), but the same trend has been already reported for CEM I HCP (Jo *et al.* (2022)).

The comparison with García's data (obtained on the exact same CEM V HCP) is reasonably good for ISA concentration in solution above 10^{-4} mol·L^{-1}. The observed decrease of R_d(ISA) values with increasing [ISA]$_{aq}$ is consistent with a progressive saturation of a sorption site. ISA data sorption have been successfully fitted using a one-site Langmuir isotherm as described below:

$$[ISA]_{solid} = \frac{K_{ads} \times S_{max} \times [ISA]_{aq}}{1 + K_{ads} \times [ISA]_{aq}}$$

Equation 20

where [ISA]$_{solid}$ is the concentration of ISA sorbed on HCP (mol·kg^{-1}), [ISA]$_{aq}$ is the concentration of ISA in the aqueous phase after sorption (mol·L^{-1}), K_{ads} and S_{max} stand for the adsorption affinity constant (L·mol^{-1}) and the adsorption capacity (mol·kg^{-1}) respectively.
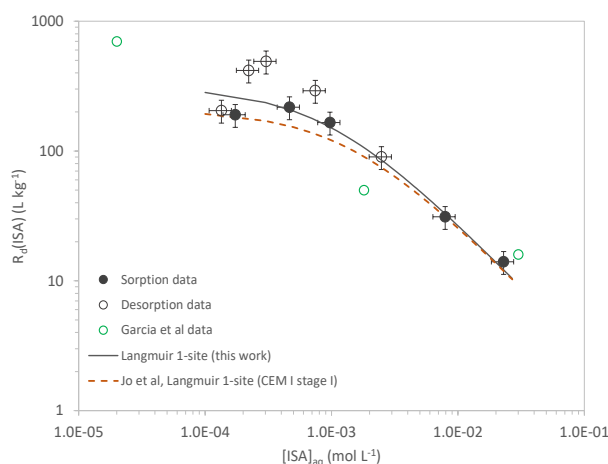
Figure 4-4   Sorption isotherm of ISA in HCP at Stage II

The fit, reported as the black solid line in *Figure 4-4*, results in K_{ads} = (1081 ± 330) L·mol^{-1} and S_{max} = (0.29 ± 0.02) mol·kg^{-1} and shows a good description of ISA sorption data.

Comparison with literature data shows that García *et al* did not succeed in fitting their ISA sorption data with a one-site Langmuir isotherm, especially at low ISA concentration (below 10^{-4} mol·L^{-1}) probably because of a too limited number of data points. Jo *et al* proposed the same model for fitting ISA sorption data on a CEM I HCP at Stage I (Jo *et al.* 2022). The fitted values obtained for the sorption parameters are close to ours (K_{ads} = (714 ± 266) L·mol^{-1} and S_{max} = (0.29 ± 0.04) mol·kg^{-1}) and are reported on *Figure 4-4* as a dashed line.

Nevertheless, desorption experiments consecutively performed to the sorption step show that an irreversible sorption process seems to occur. This result clearly prevents the use of Langmuir isotherm (based on a reversible sorption process) for interpreting ISA sorption data. A more detailed model is then needed. The role of Ca as a bridge between the surface of cement (or C-S-H) and polyhydroxocarboxylic acids (ISA or gluconic acid) has been already reported (Androniuk&Kalinichev, 2020; Jo *et al.* 2022, Pointeau *et al.* 2008) and the model proposed by Pointeau *et al.* (2008) for CEM I HCP assuming the formation of a surface complex with a Ca-bridging (>SOCaISA) was successfully applied for a CEM I HCP (Stage II) by Bruno *et al.* (2018). We plan to use this model for interpreting our ISA sorption data on CEM V HCP (Stage II).

For the Stage III, results obtained from the sorption experiment ([ISA]$_{eq}$ ranging from 4.6·10^{-4} to 3·10^{-2} mol·L^{-1}; S/L = 5·10^{-3} kg·L^{-1}; pH = 11.7) gave low and unfortunately not very precise R_d(ISA) values

EURAD (Deliverables n° 3.6, 3.7 and 3.8) - Final Report of results generated in CORI
Dissemination level: PU
Date of issue of this report: **05/07/2024**

Page 122

(<10 L·kg^{-1}). Nevertheless, a punctual experiment performed at a higher S/L value ($1.7 \cdot 10^{-2}$ kg·L^{-1}) confirmed this trend. However, these results are consistent with data reported by Pointeau *et al* for ISA sorption on a CEM I HCP (Pointeau *et al.* 2008). For pH values ranging from 11.5 to 11.8 (*i.e.* corresponding to **[CNRS-SUBATECH]** Stage III conditions), R$_d$(ISA) values ranged from 0 to (25 ± 15) L·kg^{-1}. Assuming the formation of a surface complex with a Ca-bridging (>SOCaISA) as the process for ISA sorption on HCP, the decrease of R$_d$(ISA) at Stage III (compare to Stage II) is interpreted to be due to the progressive decrease or even absence of calcium in solution.

[SCK CEN] studied the sorption of ISA on degraded HCP at the Stage III. The sorption isotherms obtained in the two performed experimental sets are reported in *Figure 4-5*. The equilibrium pH measured in the two sets were 11.59 ± 0.03 and 11.49± 0.04, respectively. In both experimental sets, the blank samples shows a recovery of α-ISA above 96 % confirming the stability of α-ISA in the experimental conditions, at least for the 21 days of the experiments. The two experimental sets show relatively good reproducibility when taking into account the initial α-ISA concentration as measured by IC-PAD and all the obtained data points are modelled together using a Langmuir isotherm. The best fit to the data is obtained with a one-site isotherm with a capacity of 0.016 mol/kg and an affinity of 5552 L/mol. The optimised Langmuir isotherm compared to the two-site isotherm reported for fresh cement by Van Loon *et al.* (1997), revealed the lower sorption obtained here and suggests that with degradation, cement tends to retain less α-ISA.
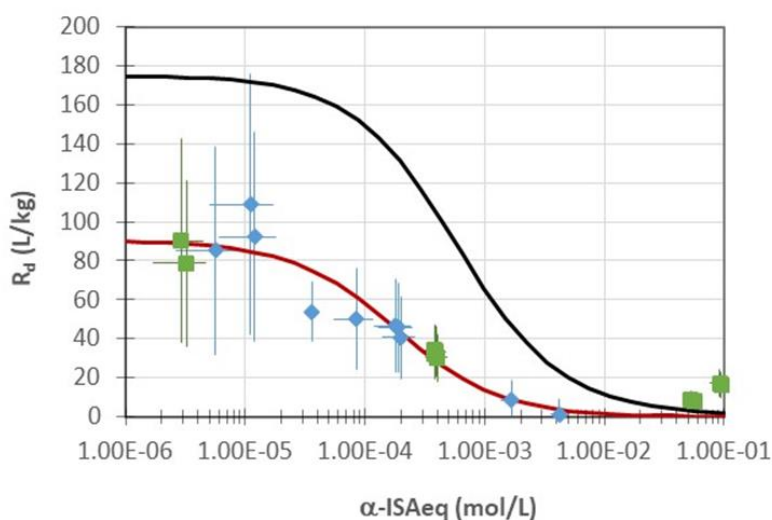
Figure 4-5   *Experimental sorption isotherms and Langmuir isotherm of α-ISA on degraded HCP powder at 26 g/L in synthetic Stage III cement water. Blue and green markers: experimental data points from set1 and set2, respectively. Red line: one-site Langmuir isotherm optimised on the experimental data. Black line: two-site Langmuir isotherm reported by Van Loon et al. (1997) on fresh cement.*

[CIEMAT (CSIC)] studied ISA sorption in CEM V HCP at Stage I (as reference) and Stage II. *Figure 4-6* presents the experimental data for the systems equilibrated with the cement pore water for both degradation stages. These results show a slight decrease of ISA sorption for Stage II.

EURAD (Deliverables n° 3.6, 3.7 and 3.8) - Final Report of results generated in CORI
Dissemination level: PU
Date of issue of this report: **05/07/2024**

Page 123
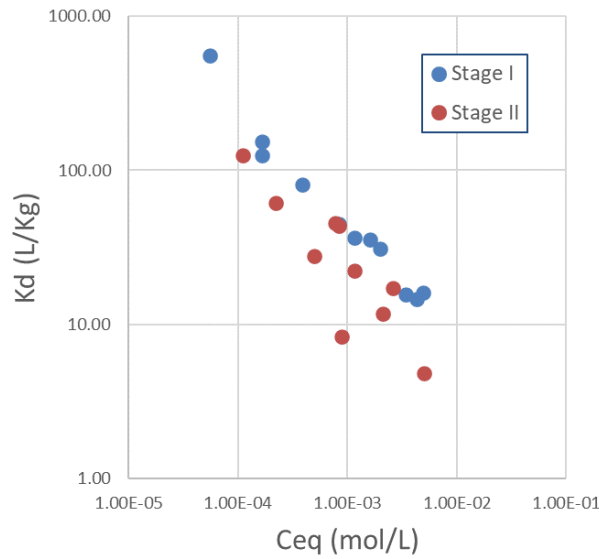
Figure 4-6   *Sorption isotherms of ISA in CEM V HCP at Stage I and Stage II.*

[CIEMAT] studied the sorption of ISA in C-S-H and portlandite. *Figure 4-7* shows a similar sorption for portlandite and C-S-H(1.4) which have similar surface properties. For C-S-H(0.8) having a negatively charged surface, the lower sorption would confirm the surface adsorption mechanism for explaining the ISA sorption in these cement hydrates.
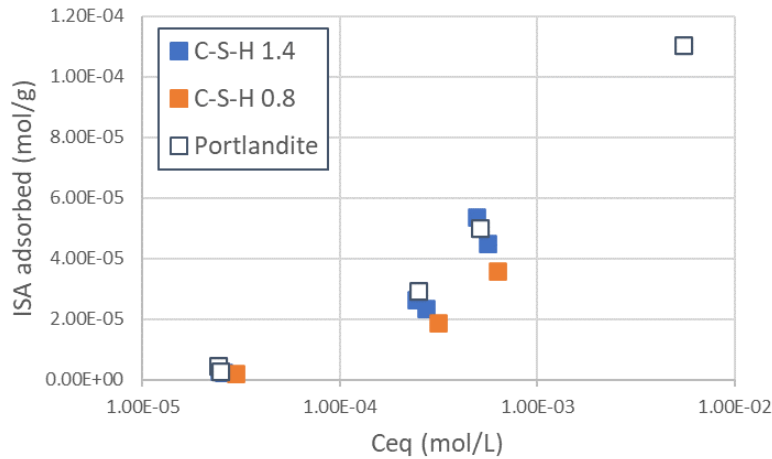
Figure 4-7   *Sorption isotherms of ISA in C-S-H (C/S = 0.8 and 1.4) and portlandite.*

The results from *Figure 4-7* could be compared with zeta potential measurements from portlandite suspensions as a function of ISA concentration (*Figure 4-8*). The zeta potential decreases as ISA concentration increases which is in agreement with a ISA adsorption at the surface.

EURAD (Deliverables n° 3.6, 3.7 and 3.8) - Final Report of results generated in CORI
Dissemination level: PU
Date of issue of this report: **05/07/2024**

Page 124
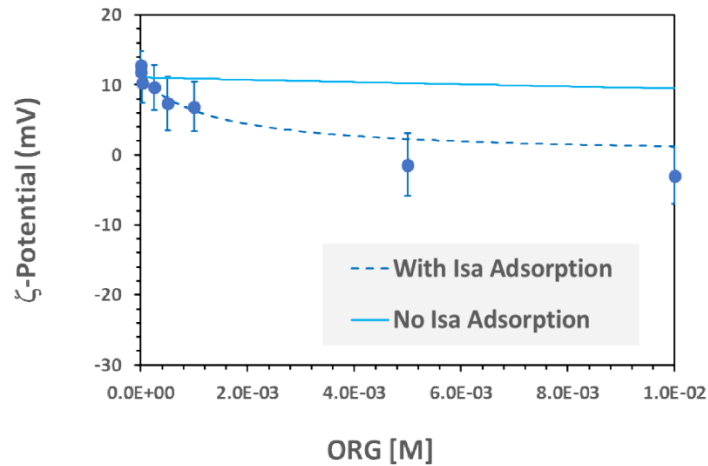
Figure 4-8   Zeta potential measurements of portlandite suspensions as a function of the ISA concentration

4.2 GTA, HIBA, HBA and real leachate

[KIT] investigated the sorption in CEM I HCP of various proxy ligands (GTA, HIBA, HBA) in the context of the degradation of filter aids UP2W (see § 2.3.1). Also, sorption studies with some leachates provided by Task 2 have been studied. Most of the results given in this section have been published in Szabo *et al.* (2022).

Figure 4-9 shows that in the experiments at organic concentration $[L]_0 \sim 10^{-3}$ M and 0.2 $g \cdot L^{-1} \leq$ S/L $\leq$ 50 $g \cdot L^{-1}$, a decrease in the initial concentration of proxy ligands HBA and HIBA occurs only at the highest S/L, *i.e.* 50 $g \cdot L^{-1}$. HBA and HIBA have a very weak sorption with Rd values around 1.6 $L \cdot kg^{-1}$ and 2.2 $L \cdot kg^{-1}$ respectively.
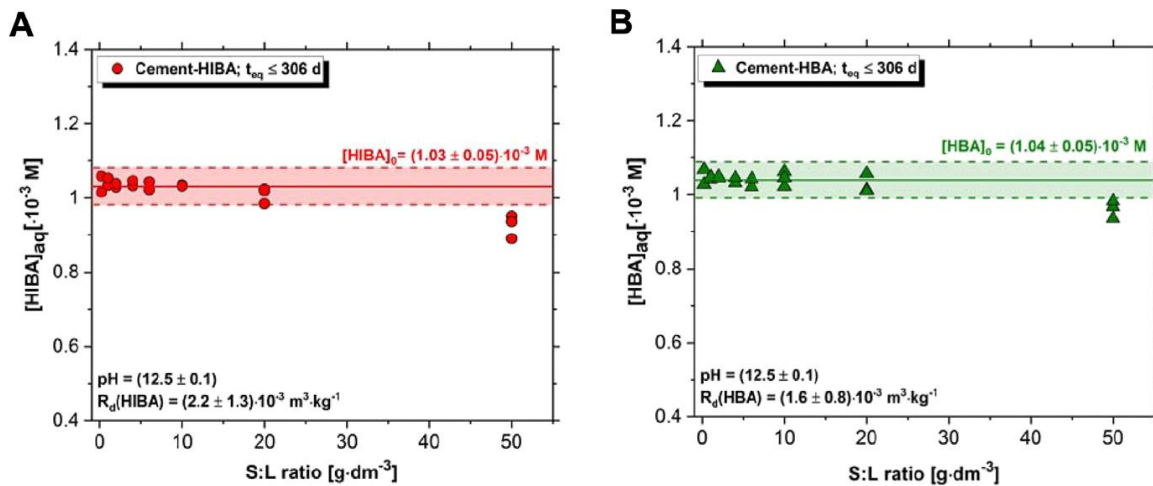
Figure 4-9   Uptake of (A) HIBA and (B) HBA by HCP at Stage II. Data represented as $[L]_{aq}$ vs. S:L ratio. Shadowed red and green areas correspond to the experimentally measured initial concentrations of HIBA and HBA, respectively. The uncertainty of individual measurements is within the size of the symbols.

On the other hand, glutaric acid (GTA) shows higher interactions with the cementitious matrix as illustrated in *Figure 4-10* with a significant decrease of the initial GTA concentration ($[GTA]_0$) as the solid-to-liquid ratio increases. This experiment has been performed with stable GTA ($[GTA]_0 \sim 10^{-3}$ M) and radiolabelled ^{14}C-GTA ($[GTA]_0 \sim 10^{-7}$ M); the Rd values for GTA have determined at 11.5 ± 2 $L \cdot kg^{-1}$.

EURAD (Deliverables n° 3.6, 3.7 and 3.8) - Final Report of results generated in CORI
Dissemination level: PU
Date of issue of this report: **05/07/2024**

Page 125
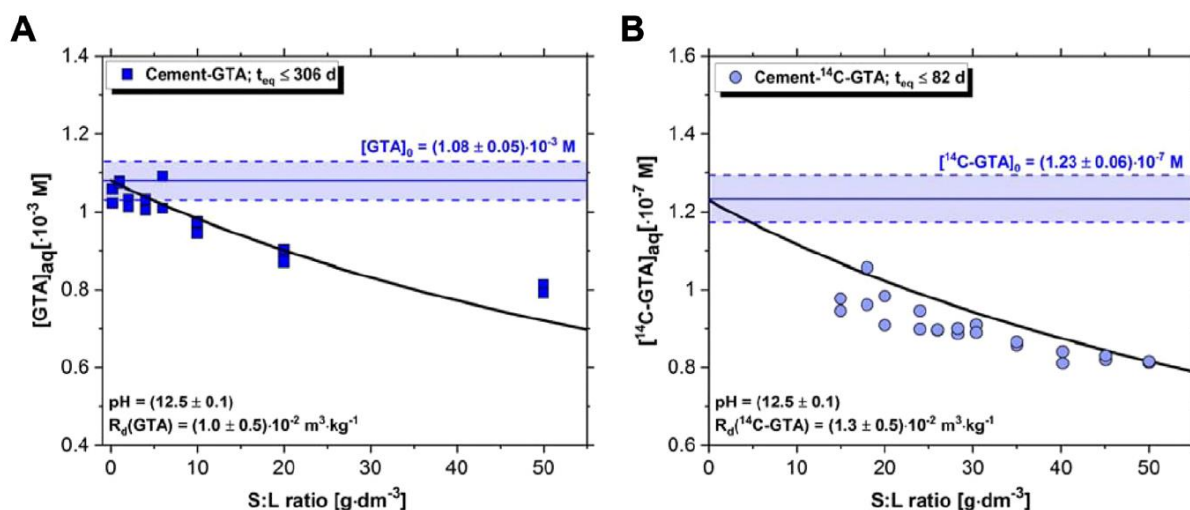
Figure 4-10　*Uptake of (A) GTA and (B) ^{14}C-GTA by HCP at Stage II. Data represented as [GTA]$_{aq}$ or [^{14}C-GTA]$_{aq}$ vs. S/L ratio. Shadowed blue region corresponds to the experimentally measured initial concentrations of GTA and ^{14}C-GTA. Solid black lines correspond to the GTA concentration calculated using the one-site Langmuir isotherm derived in this work. The uncertainty of individual measurements is within the size of the symbols.*

The interactions between have also been characterized by zeta potential measurements as a function of organic concentration. HIBA and GTA systems were compared to published data on ISA (*Figure 4-11*). HIBA proxy molecules have a very low effect on the zeta potential of HCP suspensions while the system with GTA molecules showed a significant decrease from [GTA] ~ 10^{-3} M. This threshold value remains high compared the influence of ISA for which a drop of the zeta potential starts around [GTA] ~ 10^{-5} M.

EURAD (Deliverables n° 3.6, 3.7 and 3.8) - Final Report of results generated in CORI
Dissemination level: PU
Date of issue of this report: **05/07/2024**

Page 126
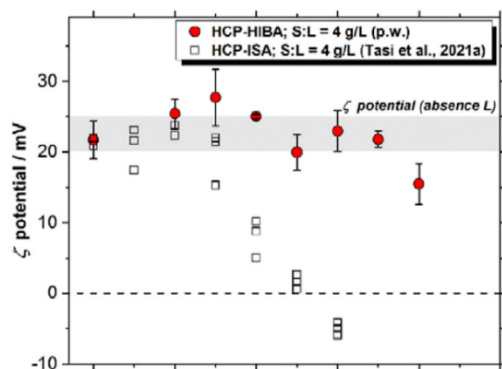
(A)
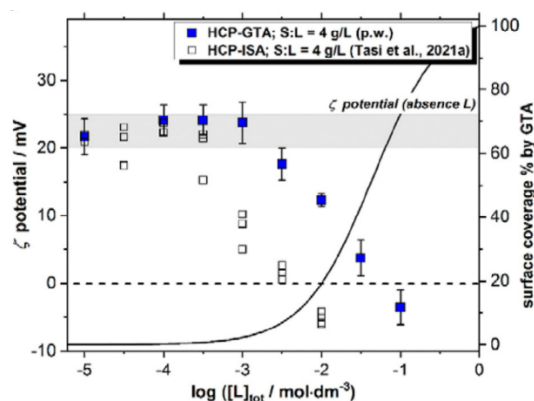
(B)

Figure 4-11   *Zeta potentials of suspended HCP particles in the presence of proxy ligands at 10^{-5} M ≤ [L]tot ≤ 0.1M: (A) HIBA and (B) GTA, compared with those obtained for ISA in similar conditions. Zeta potentials reported in the literature for the HCP-ISA system are included for comparison (Tasi et al., 2021). Grey zone in the figures correspond to the zeta potentials representative of HCP (CEM I) at Stage II and absence of organic ligands (see text). Solid line in figure c corresponds to the surface coverage of HCP and is calculated with the one-term Langmuir isotherm.*

Finally, a significantly stronger uptake was observed in *Figure 4-12* for the degradation leachate generated in Task 2, as compared to the proxy ligands HIBA, HBA and GTA. This observation indicates that several functional groups of the UP2W degradation leachate are involved in the interaction with the surface of cement, and that such interaction is not fully described by the considered proxy ligands. These results of the sorption experiments on UP2W degradation leachate and proxy ligand GTA (using inactive and ^{14}C-GTA at *S:L* = 20 g·dm^{-3} and 10^{-7} M ≤ [GTA]$_0$ ≤ 0.1 M), were compared in *Figure 4-12* with the sorption isotherm reported in the literature for the uptake of ISA by HCP (Van Loon *et al.* 1997).

EURAD (Deliverables n° 3.6, 3.7 and 3.8) - Final Report of results generated in CORI
Dissemination level: PU
Date of issue of this report: **05/07/2024**

Page 127
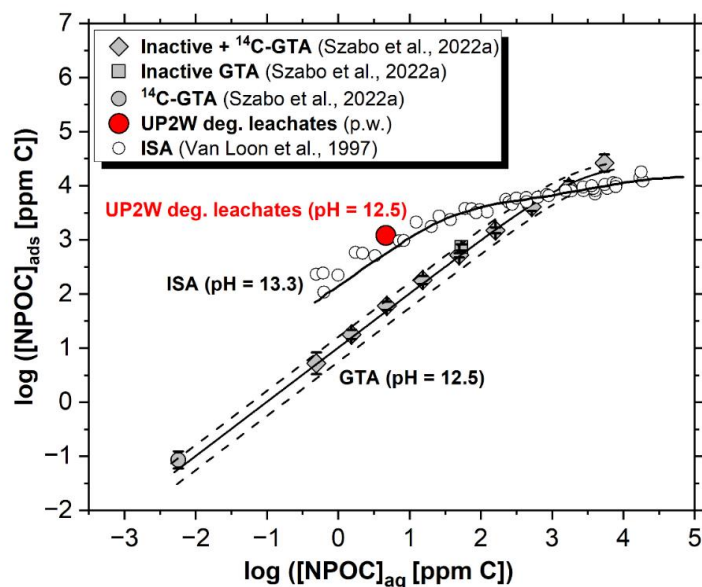
Figure 4-12   *Uptake of GTA and the UP2W degradation leachate by HCP at Stage II. Data represented as log [NPOC]solid vs. log [NPOC]aq, with concentrations reported in ppm of C. Experiments performed at S/L = 20 g·dm⁻³. Empty symbols show the sorption data reported for ISA in Van Loon et al. (1997).*

4.3 EDTA, NTA

[CEA] studied EDTA sorption by degraded HCP at Stage II and III/IV. The first series of sorption experiments focused on the interactions of EDTA to HCP CEMV/A at Stages II and III/IV (resp. in contact with S2 and S3 solution). The sorption isotherm are given in *Figure 4-13*. The sorption isotherms were fitted with a 1-site-Langmuir-type isotherm. The results of the duplicates are both given in the graphs rather than an average and standard deviation.

The CEM V/A - ^{14}C-EDTA distribution coefficient (R_d) decreases from [EDTA]$_{solution}$ = 10^{-4} M and above in the S2 and S3 solutions. The R_d is a factor 1.3 to 2 lower for resp. S2 and S3 in 10^{-2} M EDTA compared to the samples with concentrations below 10^{-5} M. The R_d in the S2 solution is a factor 4 higher compared to the S3 over the full range of the sorption isotherm. The ^{14}C-EDTA R_d values increases over time even after the apparent equilibrium at 28-30 days. The R_d is a factor 2.7 to 4.7 higher at 113-117 days compared to 48 hours. R_d increases with time faster in the S2 solution than in S3 solution.

EURAD (Deliverables n° 3.6, 3.7 and 3.8) - Final Report of results generated in CORI
Dissemination level: PU
Date of issue of this report: **05/07/2024**

Page 128
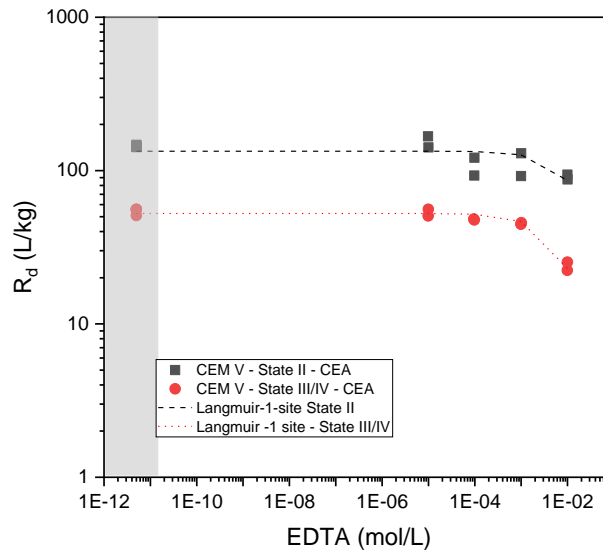
Figure 4-13   *Uptake of EDTA by CEM V HCP at Stage II and Stage III/IV. The grey zone corresponds to sorption data obtained in absence of organic species.*

In addition, RCM (CEM I HCP) has been studied at Stage II, and compared with the previous results on CEM V (*Figure 4-14*). No differences have been observed between the EDTA sorption in CEM I and CEM V HCPs.
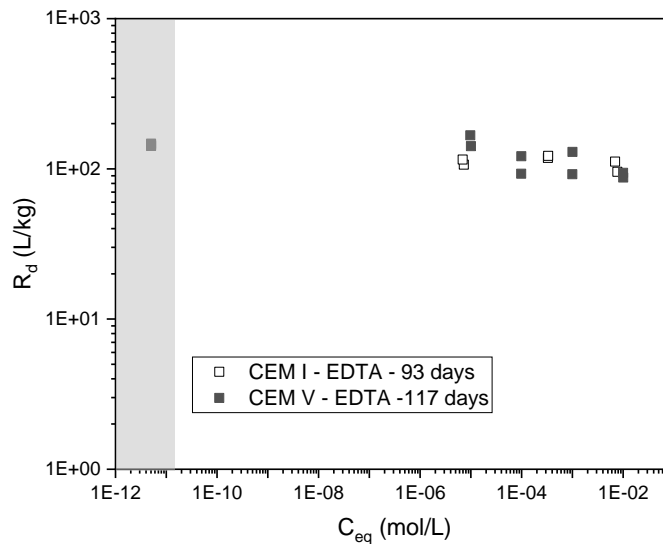
Figure 4-14   *Uptake of EDTA by CEM V and CEM I HCP at Stage II after 117 days and 93 days of contact time, respectively. The grey zone corresponds to sorption data obtained in absence of organic species.*

In the framework of the studies on RCM, the sorption of EDTA has been investigated for different particle sizes as shown in *Figure 4-15*. No effect of the particle size was observed.

EURAD (Deliverables n° 3.6, 3.7 and 3.8) - Final Report of results generated in CORI
Dissemination level: PU
Date of issue of this report: **05/07/2024**

Page 129
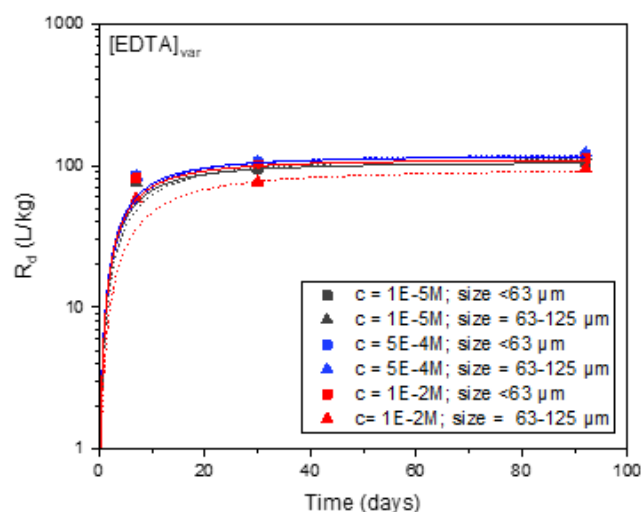
Figure 4-15 *Uptake of EDTA by HCP RCM – Stage II for various particle sizes.*

[CEA] investigated the diffusion of stable EDTA in S2 solution through a CEM V/A HCP sample (cell F2). This diffusion cell is the same as the one described in the Task 4 (see section 5.2). The data presented in *Figure 4-1* corresponds to the period from the addition of stable EDTA at 50 mM (*cf.* the black line) and before the HTO and ^{63}Ni addition in the upstream solution. The EDTA concentration were determined by COT measurements. During 230 days of diffusion, data show no major difference between the concentrations of EDTA measured in the upstream solution and in the reference solution. The only difference comes from the presence of a precipitate in the upstream solution of the F2 cell. It was not possible to separate and characterize the precipitate. The data presented in *Figure 4-16* can be interpreted by a low diffusive behavior and low retention of EDTA in this condition. In the downstream compartment, due to the initial COT background coming from the alkaline leaching of the PCV diffusion cell and due to the detection limit of the COTmeter, no significant amount of EDTA was measured. This result is consistent with the evolution in the upstream compartment.
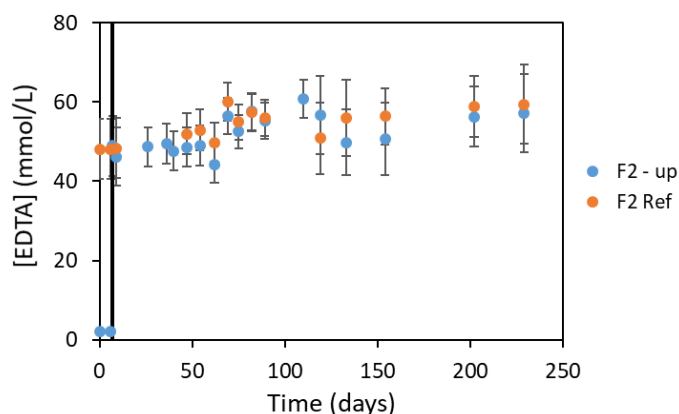
Figure 4-16 *Evolution of the EDTA concentration in the upstream solution of the F2 cell ("F2-up" series) compared to the reference S2 solution containing 50 mM of EDTA ("F2 Ref" series). The black line marks the initial addition of EDTA in the upstream solution.*

EURAD (Deliverables n° 3.6, 3.7 and 3.8) - Final Report of results generated in CORI
Dissemination level: PU
Date of issue of this report: **05/07/2024**

Page 130

[KIT(JGU)] studied EDTA sorption in CEM I HCP and C-S-H(0.8). The results given in *Figure 4-17* show similar sorption between HCP and C-S-H(0.8). These latter simulate a degraded HCP. The sorption values depend on the mass of HCP or C-S-H, then it is important to note that they are not directly comparable. However, these results would show an additional solid phase than C-S-H for sorbing EDTA.
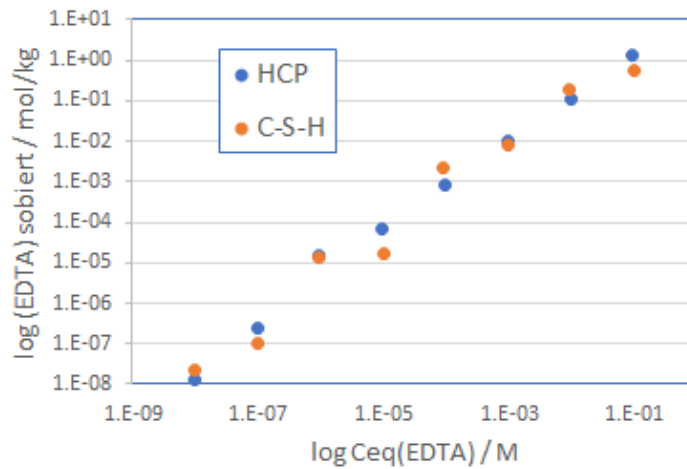
Figure 4-17   *Uptake of EDTA by CEM I HCP and C-S-H(0.8).*

[JSI] studied EDTA and NTA sorption by CEM I HCP (CEM I ULTRASAL 52.5 R from Salonit Anhovo, Slovenia) and by the CORI reference material (RCM) casted by UJV (CEM I Prachovice 42.5 R from CEMEX, Czechia). The measurements for EDTA showed a significant number of negative values for the sorbed content, *i.e.* a higher equilibrium concentration than the initial concentration reflecting the data uncertainties; also, the results were very dependant on the S/L ratio as seen in *Figure 4-18*. Consequently, no K_d values for EDTA are proposed.
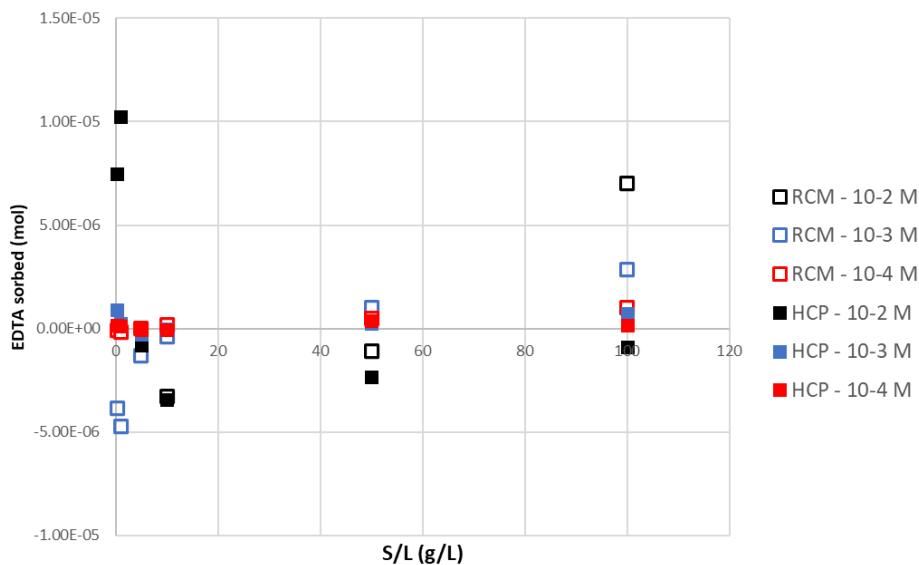
Figure 4-18   *Uptake of EDTA by CEM I HCP and RCM at Stage III.*

However, NTA showed a better sorption with clear trend (*Figure 4-19*). Nevertheless, there is still an influence of the S/L on K_d values which is not clearly explained at this moment.

EURAD (Deliverables n° 3.6, 3.7 and 3.8) - Final Report of results generated in CORI
Dissemination level: PU
Date of issue of this report: **05/07/2024**

Page 131
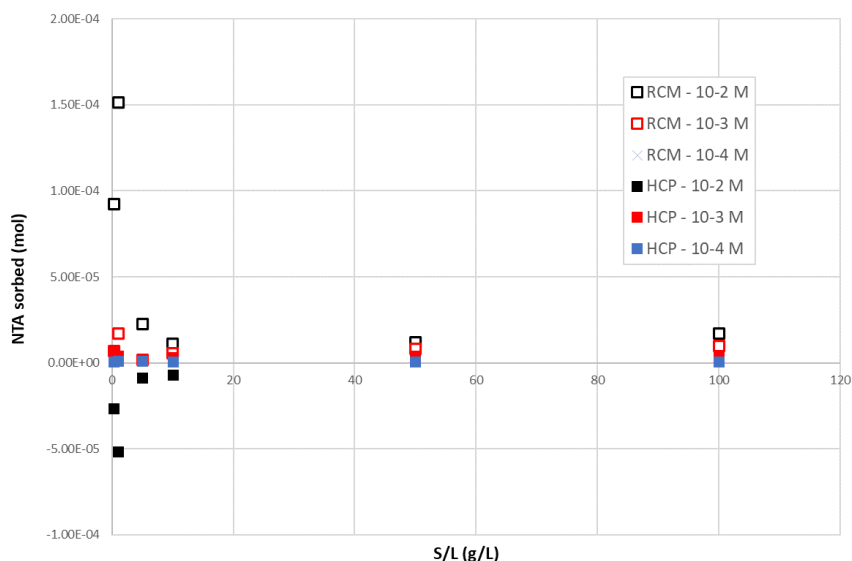
Figure 4-19   *Uptake of NTA by CEM I HCP and RCM at Stage III.*

Figure 4-20 presents the measured K_d values of NTA for CEM I HCP with initial concentrations equal to 10^{-3} M and 10^{-4} M. These results still show an unexpected influence of the S/L ratio. However, the sorption seems to be high for the lowest concentration; possibly, that would significate a saturation mechanism on the adsorption sites. This assumption needs to be confirmed by additional investigations.
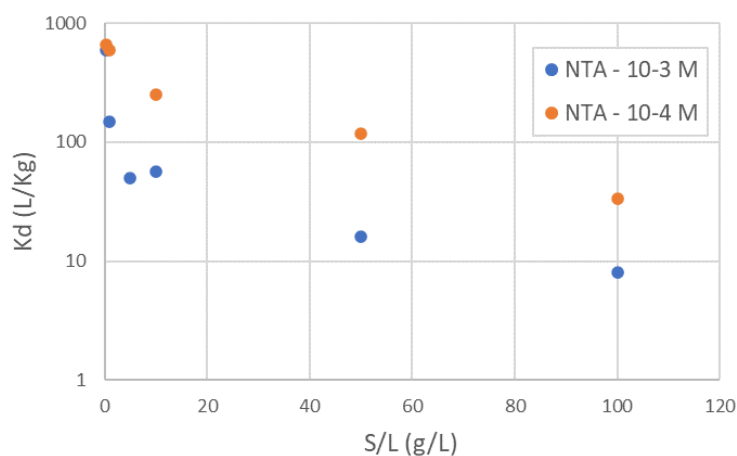
Figure 4-20   *K_d values for NTA in CEM I HCP at Stage III as a function of S/L ratio.*

[CIEMAT(CSIC)] performed batch sorption experiments on EDTA with CEM V HCP at Stage I and Stage II. The results are given in terms of K_d values in *Figure 4-21*. The sorption of EDTA has been found significantly lower at the Stage II. Zeta potential measurements seems to show a higher zeta potential for the Stage II compared to Stage I, which would be in agreement with the sorption results (a higher sorption of EDTA would involve a lower zeta potential due to the negative charge of EDTA species); however, the trend of zeta potential measurements is not clear and would need to be confirmed.

EURAD (Deliverables n° 3.6, 3.7 and 3.8) - Final Report of results generated in CORI
Dissemination level: PU
Date of issue of this report: **05/07/2024**

Page 132
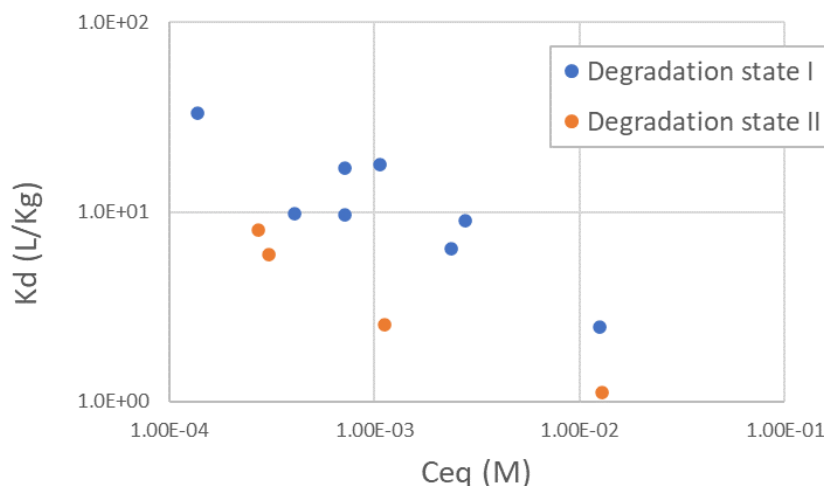
*Figure 4-21 K_d values of EDTA in CEM V HCP at Stage I and Stage II (data obtained by **[CIEMAT (CSIC)]**).*

4.4 Citrate, formate, adipate, phthalate

[KIT] and **[EMPA]** investigated citrate and formate adsorption onto fresh Portland cement (PC), AFm/AFt and C-S-H phases through a Ph.D. study performed in collaboration between both institutions. Formate adsorption was also investigated by **[RATEN]** and **[UJV]** on Portland Cement (CEM I and CEM V types).

Na-citrate and Na-Formate was used as organic re-agent in these experiments while AFm phases, Monosulfoaluminate (Ms), Hemicarboaluminate (Hc) and Monocarboaluminate (Mc), were synthesized by using appropriate amounts C_3A and $Ca_2SO_4 \cdot 2H_2O$, C_3A, CaO and $CaCO_3$, and C_3A, CaO and $CaCO_3$, respectively. Ettriginte (AFt) was synthesized by using appropriate amounts of $Al_2(SO_4)_3 \cdot 18H_2O$ and CaO. Gluconate concentration in the adsorption experiments ranged from 10^{-4} to 10^{-1}M, being the solid to liquid ratio (S/L) in the experiments variable from 40 to 55 g/L (Ms=55.3, Mc=46.3, Hc=43.5, AFt=41.8)). C-S-H synthesis was performed mixing the necessary amounts of CaO and SiO_2 to obtain representative C-S-H members with Ca/Si ratio of 0.8, 1.0, 1.2 and 1.4. Portland Cement (PC) was a CEM I type and experiments were performed at fresh conditions, *i.e.* pH=13.3. The S/L used in both C-S-H and PC adsorption experiments was 50 g/L.

EURAD (Deliverables n° 3.6, 3.7 and 3.8) - Final Report of results generated in CORI
Dissemination level: PU
Date of issue of this report: **05/07/2024**

Page 133

Results of the adsorption experiments for Ms, Mc, Hc and AFt are presented in *Figure 4-22*, while results for formate and citrate adsorption on C-S-H and PC are shown in *Figure 4-23*.

(a)   (b)
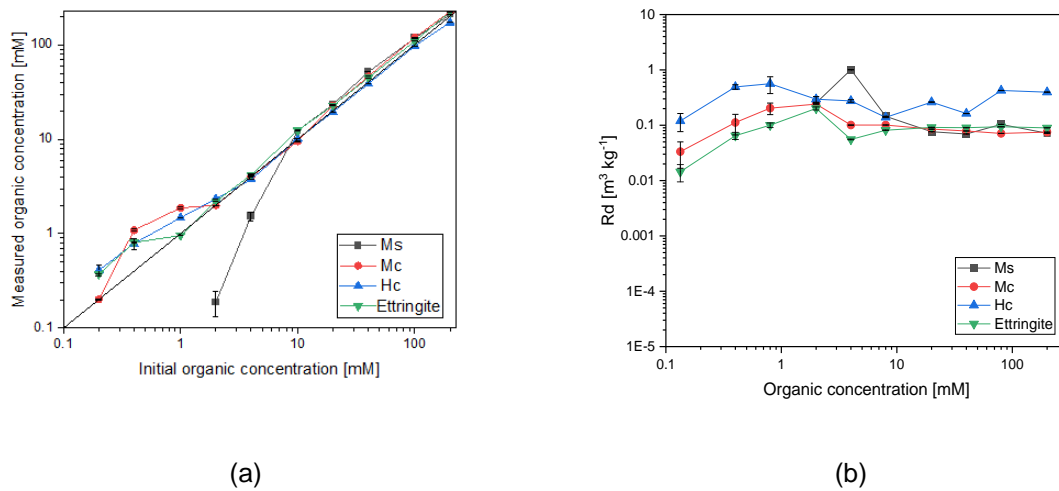
Figure 4-22   *Uptake of formate (a) and citrate (b) by Ms (Monosulfoaluminate), Mc (Monocarboaluminate), Hc (Hemicarboaluminate) and AFt (Ettriginte) as a function of the organic concentration.*

Formate, as expected, presented a very weak uptake in all concentration range for all the investigated phases. In the case of citrate, a higher adsorption is observed, with similar results for all investigated phases at higher organic concentration.

(a)   (b)
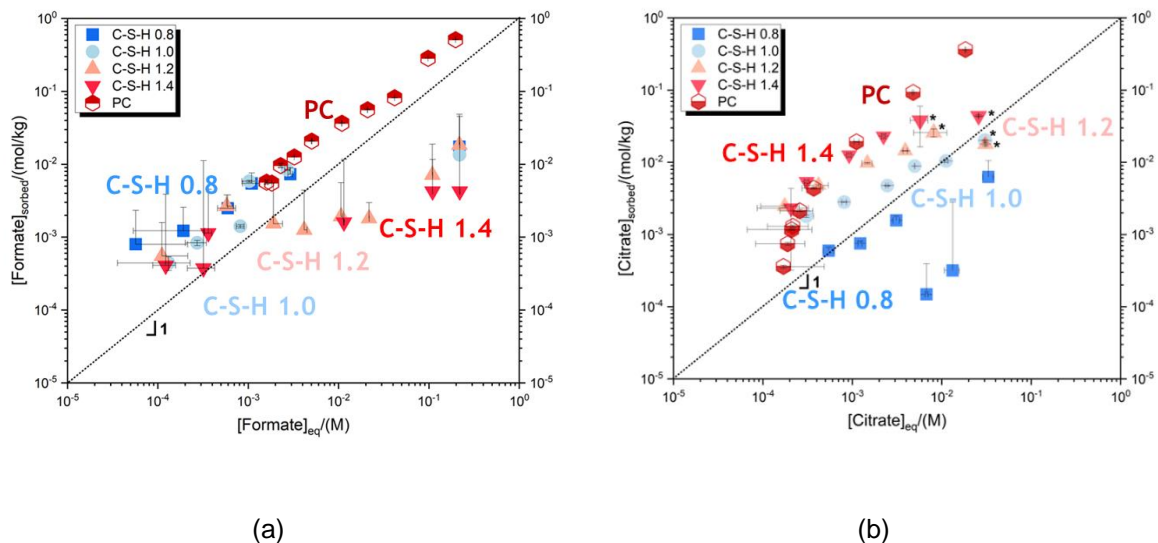
Figure 4-23   *Uptake of formate (a) and citrate (b) by several C-S-H phases and PC (Portland Cement) as a function of organic equilibrium concentration.*

In the case of C-S-H and PC, formate adsorption is again very weak although slightly higher for PC than for C-S-H. The variation of Ca/Si ratio in C-S-H does not have an impact in formate sorption behavior. For citrate, as identified for other organic compounds like gluconate, an effect of Ca ions is observed. Higher Ca/Si ratio in C-S-H phase implies a higher adsorption values. PC adsorption results are higher than those obtained for all C-S-H, indicating the role of multiple sorption phase in complex materials.

[RATEN] investigated the uptake of ^{14}C labelled formate on Portland Cement, including both CEM I and CEM V samples. In the case of CEM I samples, both fresh (pH=13.3) and carbonated cement were studied while for CEM V, only fresh samples (pH=13.3) were investigated. A solid to liquid ratio of 100g/L

EURAD (Deliverables n° 3.6, 3.7 and 3.8) - Final Report of results generated in CORI
Dissemination level: PU
Date of issue of this report: **05/07/2024**

Page 134

was used in these experiments. **[UJV]** studied CEM I paste with and without the presence of superplasticizer in the formulation at Stage II. The solid to liquid ratio in these experiments was 0.1 g/L.

Results obtained by **[RATEN]** indicated a weak adsorption of formate in both CEM I and CEM V fresh samples (R_d ranging from 1.0 to 2.0L/kg). In the other hand, results obtained for the carbonated CEM I samples shown a higher adsorption (R_d ranging from 3.0 to 3.5 L/kg) in comparison with CEM V samples. This fact may indicate that cement degradation might have an important effect on formate adsorption. Nevertheless, additional test are required to confirm this extent. Results obtained by **[UJV]**, even using concentrations with three orders of magnitude less than those used by **[RATEN]**, are in the same line with R_d values ranging from 1.7 to 4.8 L/kg.

The sorption of adipate and phthalate in C-A-S-H phases has been investigated by **[KIT (Amphos21)]**. C-A-S-H correspond to C-S-H phases with some aluminium incorporated in the structure. In particular, C-A-S-H are the cement hydrate in CEM V HCP. *Figure 4-24* presents the results on adipate and phthalate. The observations show no significant sorption for all the studied organic molecules.
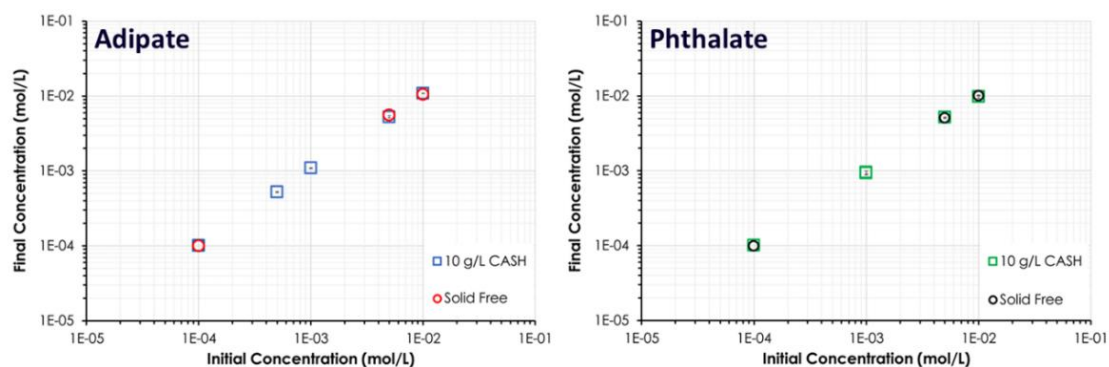
Figure 4-24   *Sorption isotherms of adipate and phthalate on C-A-S-H phases.*

Phthalate adsorption was also investigated by **[CEA]** onto the RCM, *i.e.* a CEM I cement type and also onto a CEM V cement, at Stage II (*i.e.* pH=12.5) and III-IV (pH=11.5). [14]C labelled radiotracers were used by **[CEA]**. CEM V/A Rombas (Ciments Calcia) and CEM I CEMEX Prahovice were used in this study. Details about the hardened cement paste characterization are provided in the material section of this report. R_d results obtained for phthalate adsorption on CEM V cement at different degradation stages are presented in *Figure 4-25*.
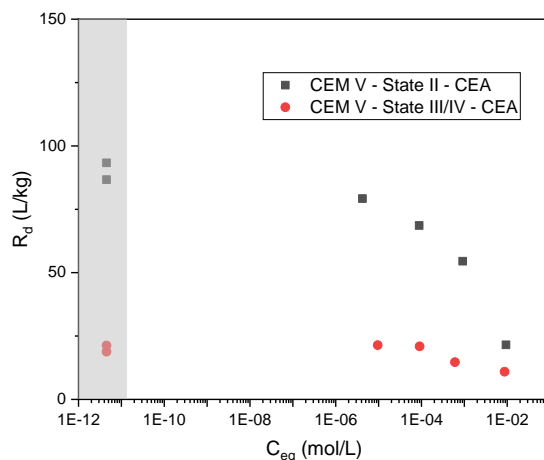
Figure 4-25   *R_d values for phthalate in degraded CEM V HCP at Stage II and Stage III/IV. The grey zone corresponds to sorption data obtained in absence of organic species.*

EURAD (Deliverables n° 3.6, 3.7 and 3.8) - Final Report of results generated in CORI
Dissemination level: PU
Date of issue of this report: **05/07/2024**

Page 135

In general, R_d values increase with increasing time. Stage II seems to have greater adsorption properties, presenting R_d values 4 times higher than those from Stage III/IV. This might be related with the role of high Ca/Si ratios in C-S-H at Stage II and the effect of Ca-phthalate complexes. Results obtained for CEM I at different particle size are presented in *Figure 4-26*. These results show a significant influence of the particle size on the sorption process of phthalate contrary to results on EDTA (*Figure 4-15*).
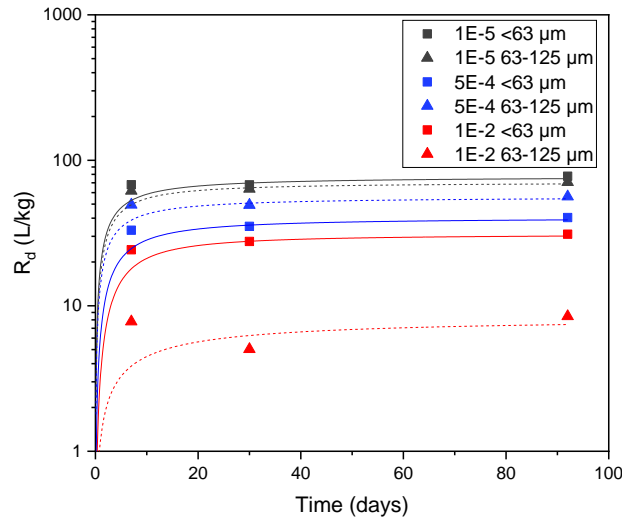
Figure 4-26   Sorption isotherms of phthalate on CEM I – Stage II at different particle size.

For both solid phases, CEM I and CEM V, in the same degradation stage R_d results are similar. This is indicative of similar phases being responsible for the adsorption process (*Figure 4-27*).
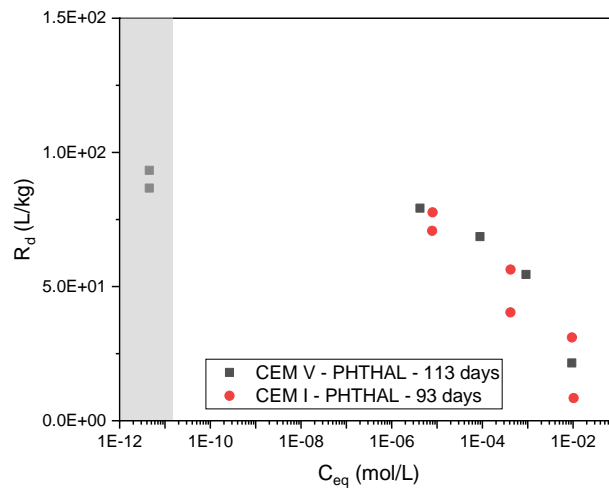
Figure 4-27   Sorption isotherms of phthalate on CEM I and CEM V at Stage II after 93 days and 113 days of contact time, respectively. The grey zone corresponds to sorption data obtained in absence of organic species.

[CEA] investigated the diffusion of stable phthalate in S2 solution through a CEM V/A HCP sample (cell F3). This diffusion cell is the same as the one described in the Task 4 (see section 5.3.5). The data presented in the *Figure 4-28* corresponds to the period from the addition of stable phthalate at 50 mM (*cf.* the black line) and before the HTO and ^{63}Ni addition in the upstream solution. The phthalate

EURAD (Deliverables n° 3.6, 3.7 and 3.8) - Final Report of results generated in CORI
Dissemination level: PU
Date of issue of this report: **05/07/2024**

Page 136

concentration were determined by COT measurements. During 230 days of diffusion, data show no major difference between the concentrations of phthalate measured in the upstream solution and in the reference solution, except a slight decrease to 35-40 mM, which has remained constant after 26 days of diffusion. Moreover, in the case of phthalate and contrary to what has been observed for EDTA (see section 4.2), a precipitate is observed in the reference solution and not in the diffusion cell. It was not possible to separate and characterize the precipitate. The data presented in *Figure 4-28* can be interpreted by a precipitation of phthalate followed by a low diffusive behavior and low retention in the HCP for this condition. In the downstream compartment, due to the initial COT background coming from the alkaline leaching of the PCV diffusion cell and due to the detection limit of the COTmeter, no significant amount of phthalate was measured. This result is consistent with the evolution in the upstream compartment.
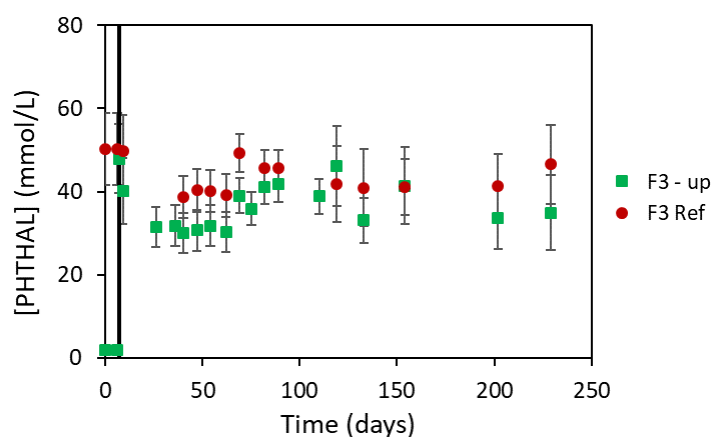
Figure 4-28   *Evolution of the phthalate concentration in the upstream solution of the F3 cell ("F3-up" series) compared to the reference S2 solution containing 50 mM of phthalate ("F3 Ref" series). The black line marks the initial addition of phthalate in the upstream solution.*

4.5 Gluconate

[KIT] and **[EMPA]** investigated gluconate adsorption onto fresh Portland cement (PC), AFm/AFt and C-S-H phases through a Ph.D. study performed in collaboration between both institutions. Na-Gluconate was used as organic re-agent in these experiments while AFm phases, Monosulfoaluminate (Ms), Hemicarboaluminate (Hc) and Monocarboaluminate (Mc), were synthesized by using appropriate amounts C_3A and $Ca_2SO_4 \cdot 2H_2O$, C_3A, CaO and $CaCO_3$, and C_3A, CaO and $CaCO_3$, respectively. Ettriginte (AFt) was synthesized by using appropriate amounts of $Al_2(SO_4)_3 \cdot 18H_2O$ and CaO. Gluconate concentration in the adsorption experiments ranged from 10^{-4} to 10^{-1}M, being the solid to liquid ratio (S/L) in the experiments variable from 40 to 55 g/L (Ms=55.3, Mc=46.3, Hc=43.5, AFt=41.8)). C-S-H synthesis was performed mixing the necessary amounts of CaO and SiO_2 to obtain representative C-S-H members with Ca/Si ratio of 0.8, 1.0, 1.2 and 1.4. Portland Cement (PC) was a CEM I type and experiments were performed at fresh conditions, *i.e.* pH=13.3. The S/L used in both C-S-H and PC adsorption experiments was 50 g/L.

EURAD (Deliverables n° 3.6, 3.7 and 3.8) - Final Report of results generated in CORI
Dissemination level: PU
Date of issue of this report: **05/07/2024**

Page 137

Results of the adsorption experiments for Ms, Mc, Hc and AFt are presented in *Figure 4-29*, while results for gluconate adsorption on C-S-H and PC are shown in *Figure 4-30*.
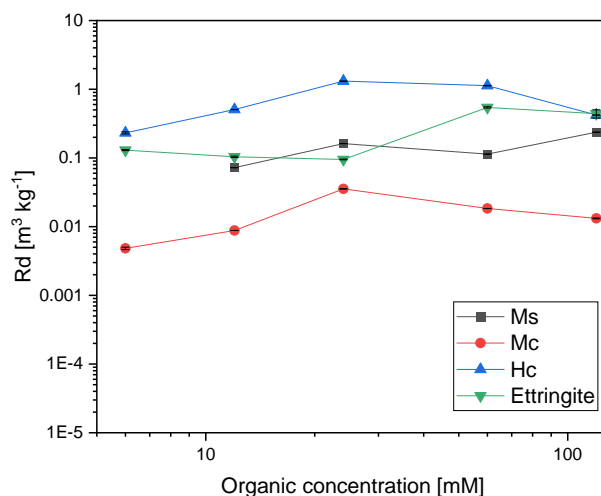
Figure 4-29   *Uptake of gluconate by Ms (Monosulfoaluminate), Mc (Monocarboaluminate), Hc (Hemicarboaluminate) and AFt (Ettriginte) as a function of the organic concentration.*

In general, a weak adsorption behavior is observed for Ms, Mc, Hc and AFt, investigated by **[KIT(EMPA)]**, being Monocarboaluminate the solid phase presenting the lowest adsorption values. A tendency could be also seen from this plot indicating higher adsorption with increasing organic concentration.
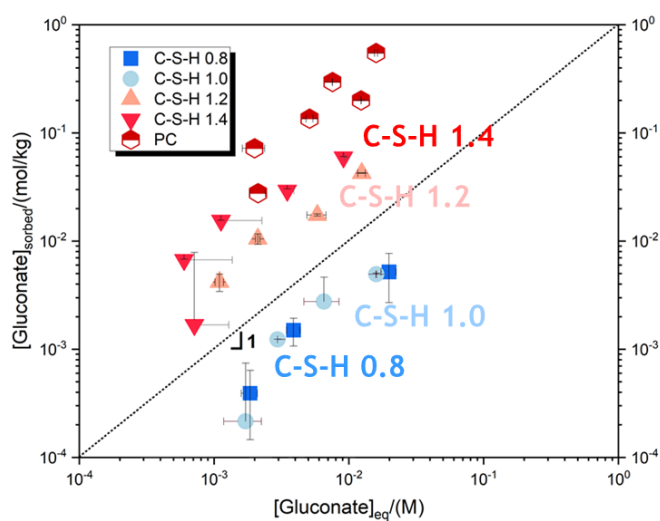
Figure 4-30   *Uptake of gluconate by several C-S-H phases and PC (Portland Cement) as a function of organic equilibrium concentration.*

Adsorption results for C-S-H phases indicate a higher adsorption of Gluconate as Ca/Si ratio increase in the solid phase. This is clearly related with the role of Ca ions at the surface of C-S-H phases and the formation of Ca-gluconate species. Interestingly, adsorption results for PC are higher than the ones obtained for C-S-H, indicating the role of more than one phase in gluconate adsorption process.

[KIT(JGU)] studied also gluconate sorption in HCP and C-S-H(0.8). These results are compared with the previous results by **[KIT(EMPA)]**. *Figure 4-31* presents the results on C-S-H(0.8) and *Figure 4-32* shows the gluconate sorption in CEM I HCP. In both cases, the measurements by **[EMPA]** and **[JGU]** are in good agreement.

EURAD (Deliverables n° 3.6, 3.7 and 3.8) - Final Report of results generated in CORI
Dissemination level: PU
Date of issue of this report: **05/07/2024**

Page 138
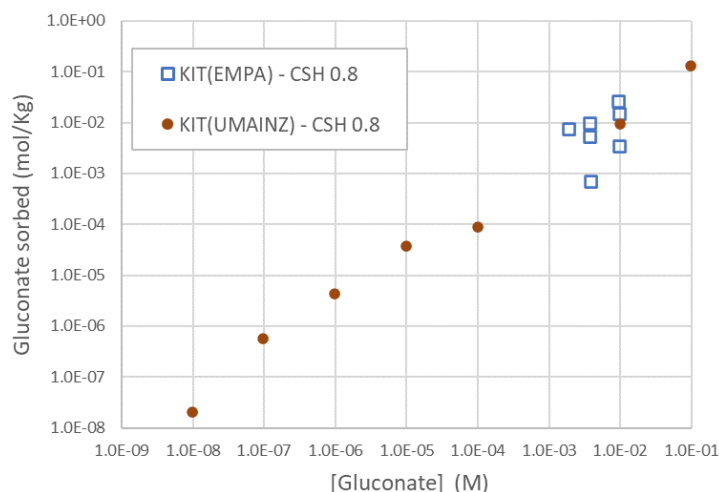
*Figure 4-31   Gluconate sorption isotherm for C-S-H(0.8) by **[KIT(JGU]** and **[KIT(EMPA)]**.*
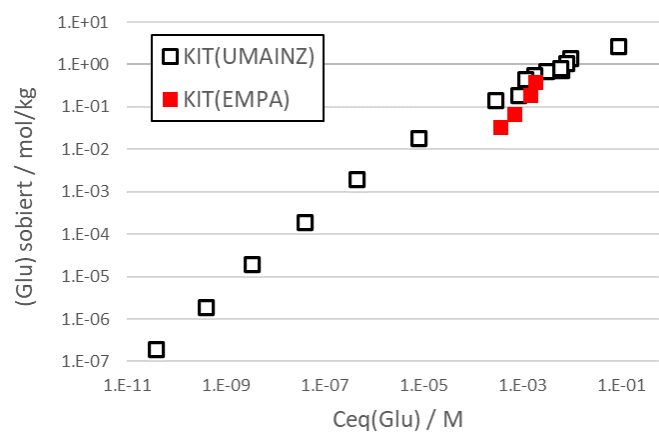
*Figure 4-32   Gluconate sorption isotherm in CEM I HCP by **[KIT(JGU]** and **[KIT(EMPA)]**. Data extracted from Stietz et al. (2023b)*

4.6 Superplasticizers

Superplasticizers adsorption on different cementitious phases have been investigated by **[CIEMAT]** and **[CIEMAT (CSIC)]**. **[CIEMAT (CSIC)]** studied the adsorption of a polycarboxylate superplasticizer onto two different CEM I formulations, with and without iron, and at two different degradation stages (fresh or Stage I and Stage II). Overall, results obtained at Stage I (R_d ranging between 10 and 100) presented higher adsorption values than those obtained at Stage II (R_d ranging between 5 and 50). Nevertheless, the scaterring of the results is quite high and thus additional tests might be needed to draw exact conclusions. The effect of Fe in the system seems to be relatively low with adsorption values for the superplasticizer very similar.

[CIEMAT] investigated the adsorption of two superplasticisers, SIKAMENT™ 200 R (Sika) and Master Glenium SKY 886 (BASF). The first one (SIKA)) is a melamine based superplasticizer while the second one (MG) is a polycarboxylate ether (PCE) superplasticizer. The solids investigated were cement samples, in fresh and degraded stage as well as C-S-H, portlandite and ettringite.

Adsorption of MS on C-S-H is relatively strong depending on the initial concentration (K_d values ranging from 250 to 450 L/Kg). Its adsorption, as seen for other organics, is highly depending on the Ca/Si ratio

EURAD (Deliverables n° 3.6, 3.7 and 3.8) - Final Report of results generated in CORI
Dissemination level: PU
Date of issue of this report: **05/07/2024**

Page 139

of the C-S-H phases, with higher adsorptions for higher Cs/Si ratios. Zeta potential measurements confirmed this effect (*Figure 4-33*).
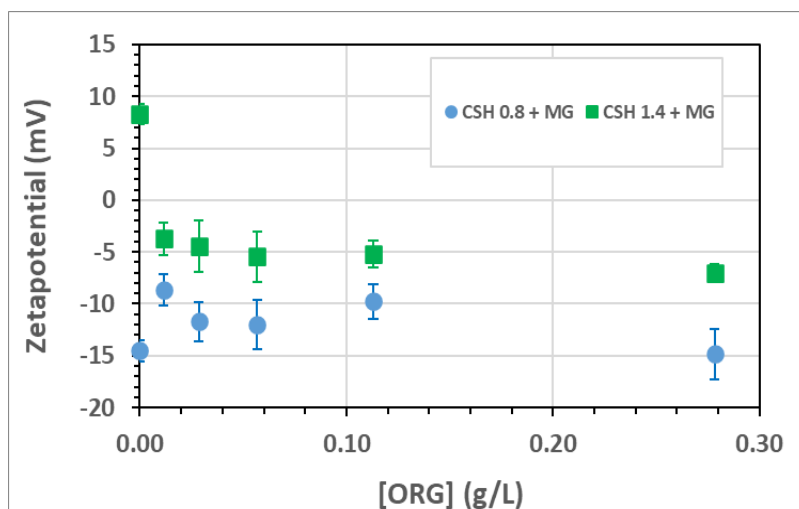
Figure 4-33   *Zeta potential measurements of C-S-H surface as a function of the organic concentration.*

Similar results and trends are obtained for SIKA with K_d values ranging from 125 to 550 L/kg depending on the Ca/Si ratio used.

In the case of portlandite and ettringite, the adsorption of SIKA is relatively low, 86 and 66 L/kg respectively, in comparison with the values obtained for C-S-H. Although the surface potential is completely dominated by the superplasticizer, regardless the type of it.

4.7 Summary for Task 3

As presented in the previous sections, the behavior of various organic molecules in presence of cement-based materials or individual cement hydrates were studied in the framework of the Task 3 with a specific focus on sorption properties. In the present part, a summary of the most relevant observed behaviors is proposed in order to highlight some trends depending on the type of organic molecules or depending on the type of materials or solid phases.

One of the main outcomes is the discrepancies between the type of organics in terms of K_d values as illustrated in *Figure 4-34*. ISA and gluconate are significantly sorbed while glutaric acid (GTA), citrate and formate have a very weak sorption. It confirms some previous works on binary systems ORG/cement and would support K_d values for organics in the cement-based materials in the context of safety assessments.

EURAD (Deliverables n° 3.6, 3.7 and 3.8) - Final Report of results generated in CORI
Dissemination level: PU
Date of issue of this report: **05/07/2024**

Page 140
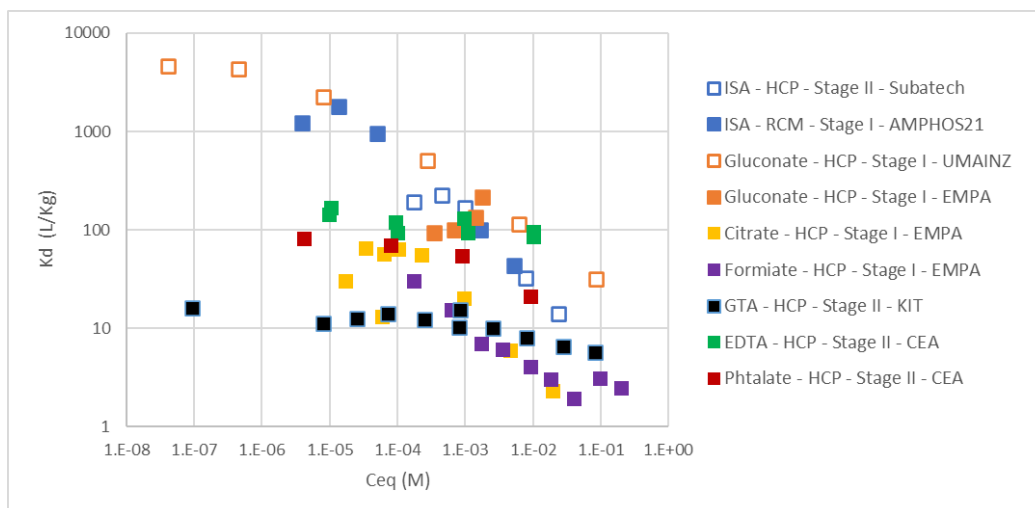
Figure 4-34 K_d *measurements of various organic molecules in HCP at different degradation stages (fresh and Stage II).*

Figure 4-35 shows sorption isotherms of ISA, EDTA and phthalate for HCP at Stage III compared with Stage I and/or Stage II. For each molecule, the sorption is lower at the Stage III. Also, the trend as a function of the equilibrium concentration (Ceq) remains the same whatever the degradation stage; indeed, for ISA, the K_d value decreases as Ceq increases from Ceq = 10^{-5} M at Stage I and Stage III while for EDTA, K_d slightly evolves for Stage II, and Stage III/IV. Apparently, the chemical degradation of the cement-based materials does not modify the threshold concentrations related to the decrease of the sorption due to the possible saturation of the adsorption sites.
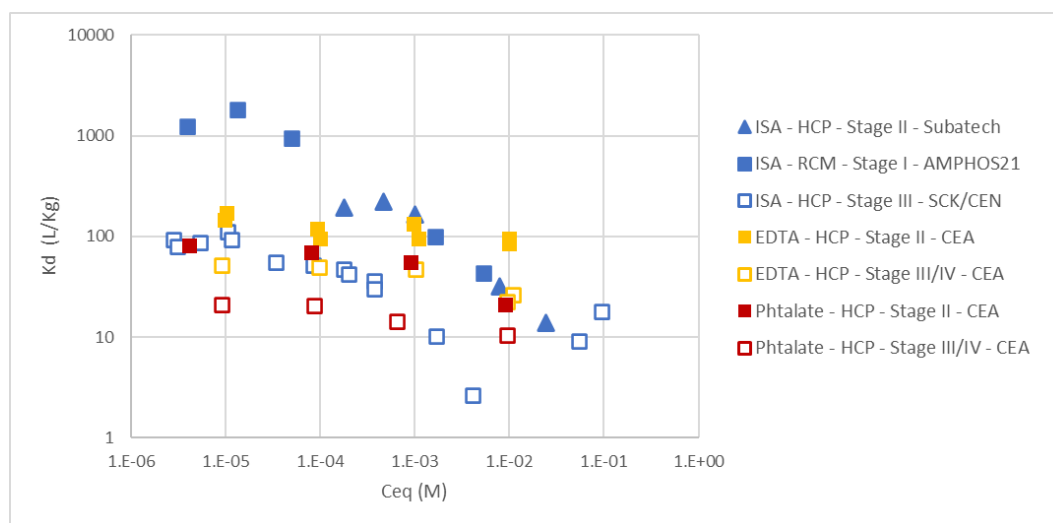
Figure 4-35 K_d *measurements of various organic molecules in HCP at different degradation stages.*

ISA has been one of the most studied molecules due to the high amount of cellulose in the chemical inventory of radioactive waste (from low level to intermediate level waste). *Figure 4-36* presents the K_d values measured for the various systems in the framework of Task 3. All values can be associated to a general trend regarding the evolution of K_d values as a function of the ISA concentration; in particular there is a remarkable agreement with existing data.

EURAD (Deliverables n° 3.6, 3.7 and 3.8) - Final Report of results generated in CORI
Dissemination level: PU
Date of issue of this report: **05/07/2024**

Page 141
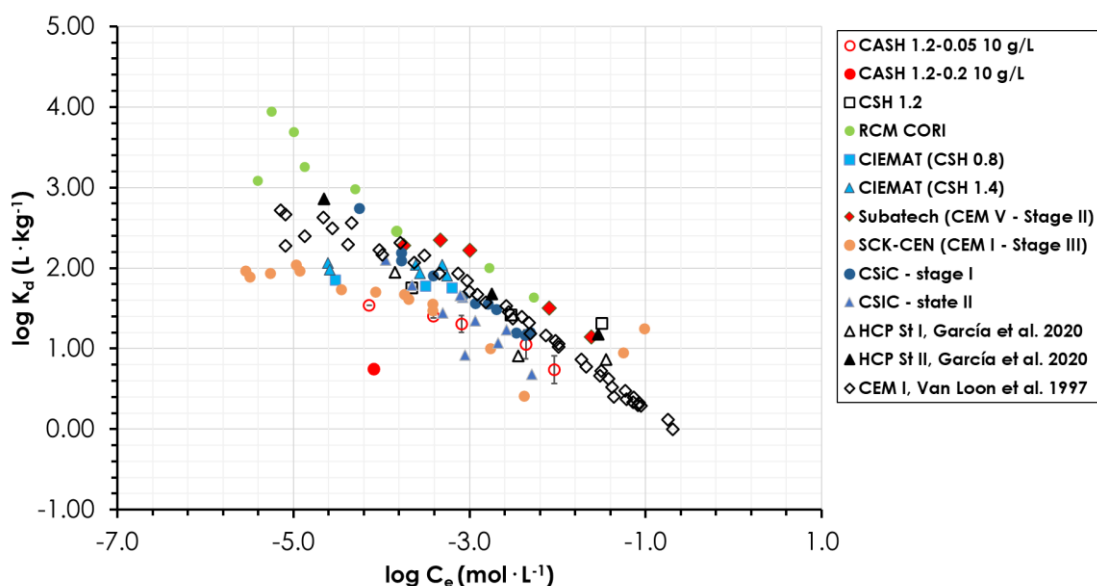
Figure 4-36   *Various K_d measurements of ISA in the different systems studied in TASK 3 in comparison with some existing results from Literature.*

Also, the measurements of gluconate sorption in C-S-H phases provided by **[KIT(EMPA)]** were compared with the results given in Androniuk (2017) (*Figure 4-37*). There is a quite agreement between both studies which validate the acquired data on C-S-H but also on the other cement hydrates.
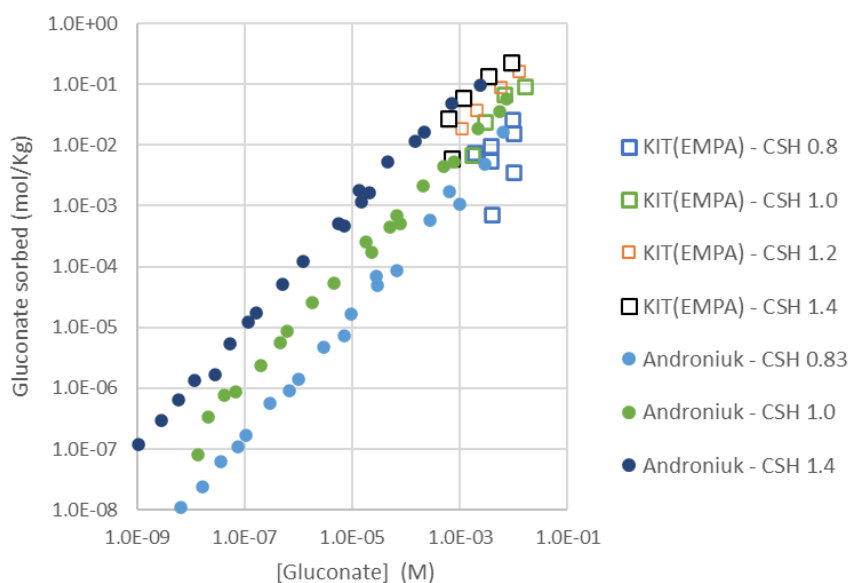
Figure 4-37   *Gluconate sorption in C-S-H phases at various Ca/Si ratios. Results from [KIT(EMPA)] compared to Androniuk (2017).*

In addition, one of the relevant outcomes is the determination of sorption properties for cement hydrates other than C-S-H phases. Indeed, **[KIT(EMPA)]** and **[CIEMAT]** have clearly shown that AFm/AFt phases and portlandite can sorb with high affinities organic molecules in the case of citrate (*Figure 4-38*) and ISA respectively (*Figure 4-7*). The sorption properties of some of individual phases (AFm, HC for ex.) can have similar K_d values than C-S-H. Consequently, this outcome can confirm and explain the higher K_d

EURAD (Deliverables n° 3.6, 3.7 and 3.8) - Final Report of results generated in CORI
Dissemination level: PU
Date of issue of this report: **05/07/2024**

Page 142

values in HCP than in C-S-H, and provides a consistent information in terms of mechanistic knowledge and understanding of the processes involved in the sorption of organic molecules in cement-based-materials.
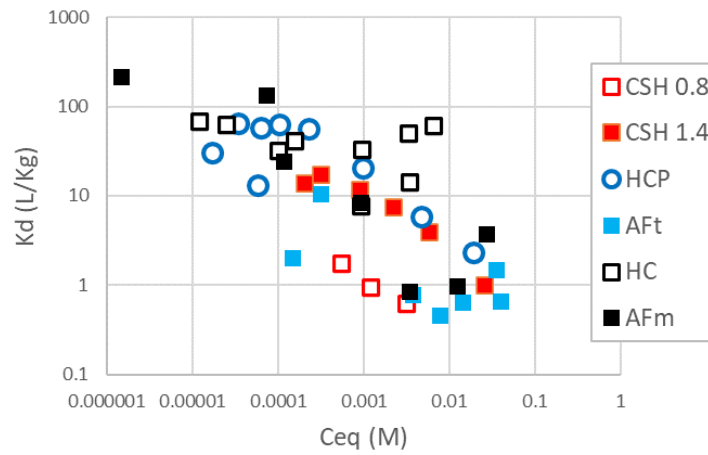
Figure 4-38   Sorption of citrate in various cement hydrates and CEM I HCP.

EURAD (Deliverables n° 3.6, 3.7 and 3.8) - Final Report of results generated in CORI
Dissemination level: PU
Date of issue of this report: **05/07/2024**

Page 143

5. Results obtained in Task 4

The work performed in Task 4 on ternary systems (CEM/ORGA/RN) extends knowledge beyond the already published data in the literature. Different organizations are involved in speciation, sorption and/or diffusion experiments: **[KIT (Amphos21)], [CEA], [CIEMAT], [CTU], [CPST], [JGU], [JUELICH], [HZDR], [KIT (EMPA)], [KIT], [SCK CEN], [CNRS-SUBATECH], [RATEN], [SURAO], [UJV], [UHelsinki], [UCYPRUS]** and **[UPPC]**. Table 43 shows the systems that have been studied by the different organizations in Task 4.

Table 43: *Summary of the system studied by each organization in Task 4*

Organization	Type of experiment	Material	Element	Organic
[KIT (Amphos21)]	Sorption	C-A-S-H, RCM	U	ISA, PHT
[CEA]	Sorption Diffusion	HCP (CEMV/A), RCM	U, Ni, Eu	Cellulose RDP, EDTA,PHT
[CIEMAT]	Sorption Diffusion	HCP (CEM I, IV, V), RCM C-S-H, POR, ETT	Ni, Eu, Pu, U	ISA, cellulose RDP; SPs (Master Glenium, SIKAMENT) and SP RDP
[CPST]	Sorption	CEM I	*Am, Pu*	ADI (DOA), PHT (DIOP), OXA, Acetate
[CTU]	Sorption	HCP (CEM I/ III) C-S-H	Eu, U, Pb	EDTA, ADI, PHT, SP (CX ISOPLAST 531)
[HZDR]	Sorption	C-A-S-H HCP (CEM I)I	U	CIT, GLU, PBTC, cellulose RDP, NTA
[JGU]	Sorption Diffusion	HCP (CEM I) C-S-H	Th, Pu	ISA, EDTA, GLU
[JUELICH]	Sorption Diffusion	HCP (CEM V) C-A-S-H	Eu, Am	PHT, TMA
[KIT (EMPA)]	Sorption Solubility	HCP (CEMI) C-S-H	Pu, Eu, Cm	FOR, CIT, GLU
[KIT]	Sorption Solubility	HCP	Ca(II), Ni(II), Nd(III), Eu(III) and Pu(IV)	UP2 resins (proxy ligands and RDP)
[RATEN]	Sorption Solubility	HCP (CEM I, V)	C, Ni	FOR
[SCK CEN]	Sorption diffusion	HCP (CEM V)	Ni	ISA, cellulose RDP
[CNRS-SUBATECH]	Sorption diffusion	HCP(CEM V)	U	ISA
[SURAO]	Sorption	Richard Concrete	Eu	EDTA
[UJV]	Sorption, diffusion, leaching	HCP (CEM I) Richard Concrete	Ni	SP (ISOLA)
[UCYPRUS]	Sorption	C-S-H	U	EDTA
[UHelsinki]	Diffusion	HCP (CEM V)	Cs, C, Cl	GLU
[UPPC]	Speciation Sorption	C-S-H	Eu	GLU, NTA

EURAD (Deliverables n° 3.6, 3.7 and 3.8) - Final Report of results generated in CORI
Dissemination level: PU
Date of issue of this report: **05/07/2024**

Page 144

5.1 Isosaccharinic acid and cellulose degradation products

The effects of the presence of cellulose degradation products on radionuclide (RN) sorption and/or migration in different cementitious materials have been studied by many organizations (**[KIT (Amphos21)], [CEA], [CIEMAT], [JGU], [SCK CEN], [CNRS-SUBATECH], [HZDR]**). Most of the organizations analyzed the effect of the α-ISA, Na exchanged (Na-(αISA)) synthesized in the laboratory using a standard procedure (Van Loon *et al.*, 1997; Vercammen, 2000). Other institutions additionally analyzed real degradation products (RDP) of cellulose, produced in experimental tests in Task 2.

[KIT (Amphos21)] analyzed the effects of Na-(αISA) on uranium retention in the C-A-S-H phases (C-A-S-H1.2-0.05 and C-A-S-H 1.2-0.02) and the reference cement material (RCM) by batch sorption experiments under anoxic atmosphere.

Solubility tests with [U] = 10^{-6} M were also made in the presence of ISA, at initial concentrations of 10^{-3} and 10^{-2} M, and the measured concentration of uranium was higher than in the absence of ISA. The measured concentration in the presence of 10^{-3} M ISA was $(8.5 \pm 0.3) \cdot 10^{-7}$ M and $(7.7 \pm 0.5) \cdot 10^{-7}$ M with $1 \cdot 10^{-2}$ M ISA, compared to $(4.3 \pm 1.8) \cdot 10^{-7}$ M when ISA was not present.

The modelled speciation of U in the presence of ISA, for both C-A-S-H experiments is shown in *Figure 5-1* One noticeable change in the speciation of U is the increasing fraction of U present as $UO_2(OH)_3(HIsa)_2^{3-}$ at the pH of the experiment (11.2) as the concentration of ISA increases. This suggests that the formation of this species leads to the increased solubility of uranium in the system.
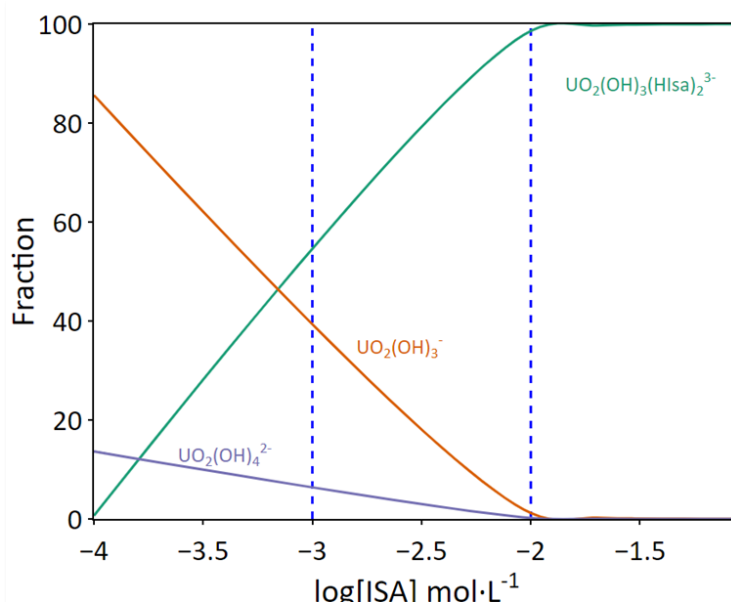
Figure 5-1:   *U speciation at [U] = 10^{-8} M as a function of ISA concentration under the solution conditions of the experiments with C-A-S-H 1.2- 0.05 (pH = 11.24). Calculations were performed using GibbsStudio code coupled with ThemoChimie v12 database (Nardi A. & de Vries, 2017; Giffaut et al., 2014). For clarity, species whose contribution never rises above 0.05 are not shown.*

In sorption experiments with C-A-S-H phases at 10 g·L^{-1} and initial uranium concentrations ranging from 10^{-8} to 10^{-6} M, the solution concentration in all samples after 14 days of equilibration was below the instrument detection limit ($4 \cdot 10^{-10}$ M). Despite the observation that ISA could increase the measured concentration of uranium in solid-free experiments, its presence, even at 10^{-2} M, did not lead to measurable concentrations of U in the sorption experiments. Taking the 10^{-7} M initial U sample (the 10^{-6} M sample was excluded because of potential precipitation of U solids) and the instrument detection limit, at the solid solution ratios in these experiments (10 g·L^{-1}) a minimum log R$_d$ of 4.8 was estimated for uranium sorption to C-A-S-H 1.2-0-05 and 1.2-0.2.

Following these results, a set of sorption experiments were performed with C-A-S-H 1.2-0.2 at a solid:solution ratio of 0.5 g·L^{-1} and uranium at an initial concentration of $4 \cdot 10^{-7}$ M (*cf. Figure 5-2*). These

EURAD (Deliverables n° 3.6, 3.7 and 3.8) - Final Report of results generated in CORI
Dissemination level: PU
Date of issue of this report: **05/07/2024**

Page 145

resulted in measurable uranium solution concentrations and a calculated log R_d of 5.5, which is broadly comparable to previously obtained values for U sorption to C-S-H at a pH value < 12 (Tits *et al.*, 2014). The addition of 10^{-3} M ISA decreased the log R_d value to 4.7, indicating that its presence can lead to a slight increase in the mobility of U in cementitious systems.
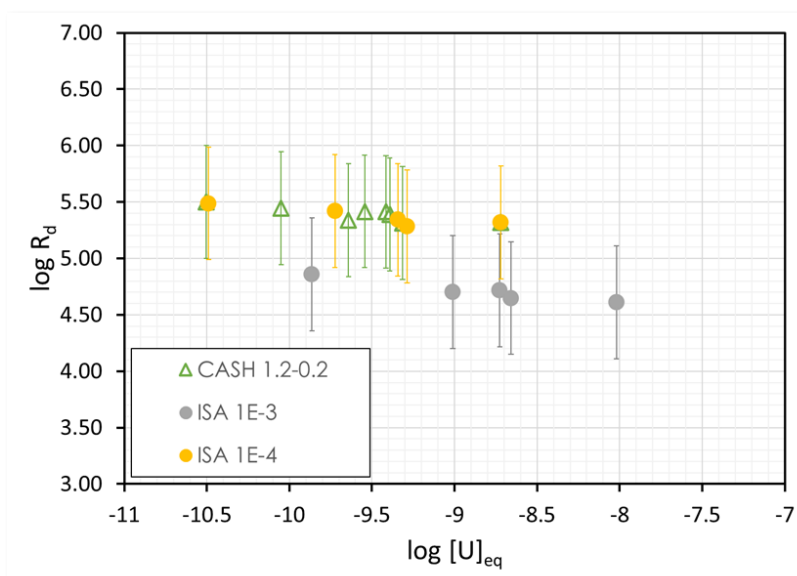
Figure 5-2:   *Sorption isotherms obtained for C-A-S-H 1.2-0.2 without the presence of ISA (green triangles) and in the presence of ISA: 10^{-4} M (yellow circles) and 10^{-3} M (grey circles).*

[CEA] analyzed the effects of real cellulose degradation products (RDP) provided by **[PSI]** and **[SCK CEN]** on the migration of europium in RCM degraded at Stage II. Cellulose degradation product provided by **[PSI]** corresponds to the long-term hydrolysis experiment performed within the Task 2. The solution was used without any dilution to reach a sufficient initial TOC concentration *i.e.* close to 70 ppm of C. Concerning the solution provided by **[SCK CEN]**, the TOC content was estimated to 15000 ppm of C with an initial ISA concentration of 65 mM (α-ISA and β-ISA were reported in the composition of this RDP). A dilution of a factor 10 was applied for two systems; a dilution of 200 for one system to be comparable to the initial concentration in the **[PSI]**-degraded-solution.

Eu-152 was measured in solution using a γ-counter (WIZARD^2, Perkin Elmer) or a γ-spectrometer (ultrapure germanium detector, HITEC Instrument and interwinner 6.0 as software) using classical 5-mL-vial or in-house-normalized-50-mL-vial (SG50, CEA). The quantification of the Eu-152 activity in the solid was also performed using these techniques. Efficiency of the germanium detector was determined using a commercial multi-γ standard solution (LEA, Orano, France).

The composition of the contact solution was checked after preparation or after migration experiments by routine analytical characterizations (ionic chromatography and pH measurements). Concerning the stable organic content in solution, TC, TIC and TOC concentration measurements have been performed using a Variotoc Cube analyser (Elementar) at least to check initial stock solution.

Before sorption/diffusion experiments, the operational solubility of Eu was investigated using the reference solutions prepared for the diffusion experiments. Reference solutions are prepared in the water representative of Stage II of cement degradation solution by adding a spike of Eu-152 standard solution and different concentration of degraded cellulose solutions ([C]=0 ppm; 70 ppm; 1500 ppm and 15000 ppm). The activity of Eu-152 was measured at least once a week during the diffusion experiment. Preliminary results indicate a major difference in the presence of the organic species in solution. For TOC content ranging from 70ppm^C to 1500 ppm^C, the activity of Eu-152 remained comparable. When no TOC is added in the solution representing the Stage II, S2, after 3 days of contact, only 3% of the

EURAD (Deliverables n° 3.6, 3.7 and 3.8) - Final Report of results generated in CORI
Dissemination level: PU
Date of issue of this report: **05/07/2024**

Page 146

initial activity was measured, indicated an increase of the solubility in the presence of the cocktail of organics species present in the degraded cellulose solution.

For studying Eu diffusion in the presence of organics, in-diffusion set-up was used with the reference cement material (RCM). The RCM disks were directly placed into the S2 solution in a glass container to avoid RN interactions with exogenous organic from glue or plastic alkaline degradation as proposed by Legand (2023)

The summary of the experiments is as follow:

- cell-RCM-01: in-diffusion – 1x30mL – cellulose degraded by long-term hydrolysis ([**PSI]**) at 70ppm^C in S2**+ ^{152}Eu**
- cell-RCM-02: in-diffusion – 1x30mL – cellulose degraded by radiolysis ([**SCK CEN]**)+ 1y of hydrolysis at 1500ppm^C in S2**+ ^{152}Eu**
- cell-RCM-03: in-diffusion – 1x30mL – cellulose degraded by radiolysis ([**SCK CEN]**)+ 2y of hydrolysis at 1500ppm^C in S2**+ ^{152}Eu**
- cell-RCM-04: in-diffusion – 1x30mL –no ORGA in S2**+ ^{152}Eu**

Periodically, the solution in compartments was sampled and analysis to determine the activity of the investigated RN. Except for the reference experiment containing only the epoxy glue (Cell-SIKADUR), at the end of the diffusion experiments, the sample was removed from the sample holder and the diffusion profile was acquired by a step-by-step multi grinding procedure (see Macé *et al.* 2019).

The evolution of the residual activity of ^{152}Eu in solution during the diffusion experiment and the profile determined in the solid are presented in the following figures. *Figure 5-3* represents data for RCM01 in-diffusion experiment; *Figure 5-4*, data for RCM02 in-diffusion experiment; *Figure 5-5*, data for RCM03 in-diffusion experiment and *Figure 5-6*, data for RCM04 in-diffusion experiment.

EURAD (Deliverables n° 3.6, 3.7 and 3.8) - Final Report of results generated in CORI
Dissemination level: PU
Date of issue of this report: **05/07/2024**

Page 147
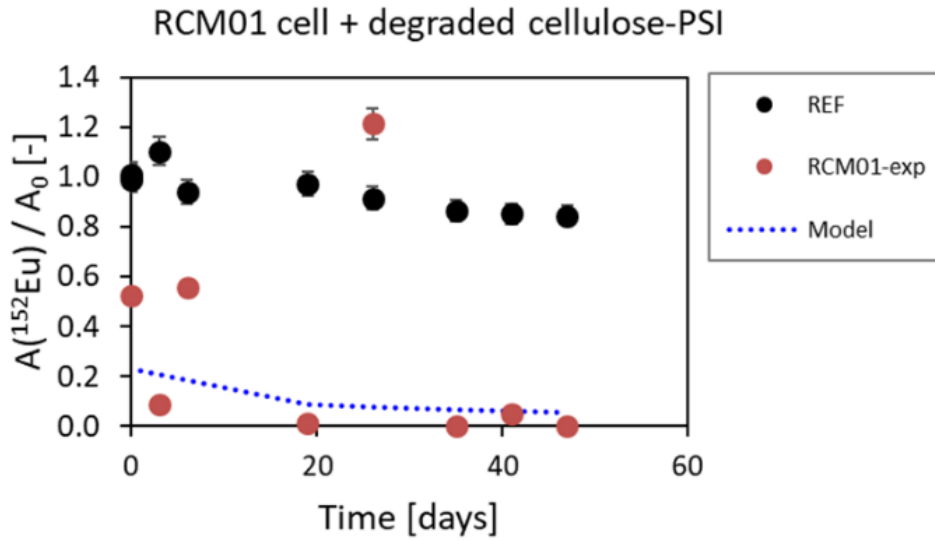
(a)
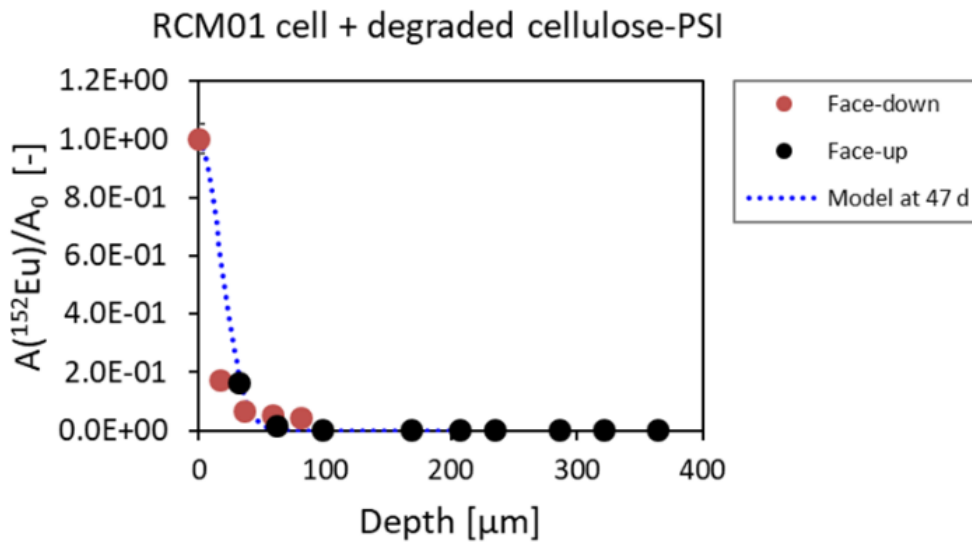
(b)

Figure 5-3: Experimental and modelled data obtained for the RCM01 cell (a) residual activity in solution (b) diffusion profile- ^{152}Eu diffusion in RCM-Stage II in presence of degraded cellulose leachate provided by **[PSI]**.

EURAD (Deliverables n° 3.6, 3.7 and 3.8) - Final Report of results generated in CORI
Dissemination level: PU
Date of issue of this report: **05/07/2024**

Page 148

(a)

(b)
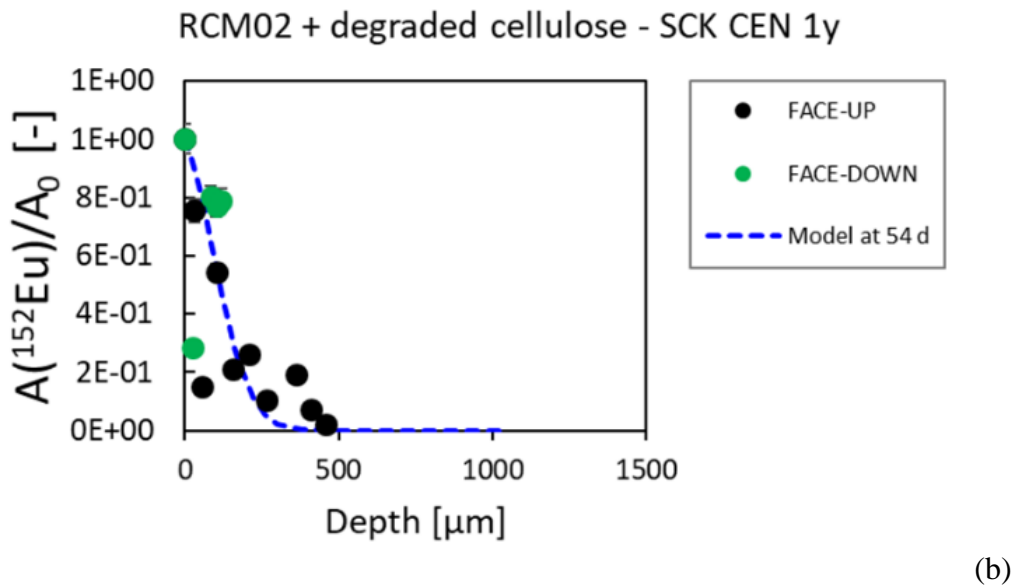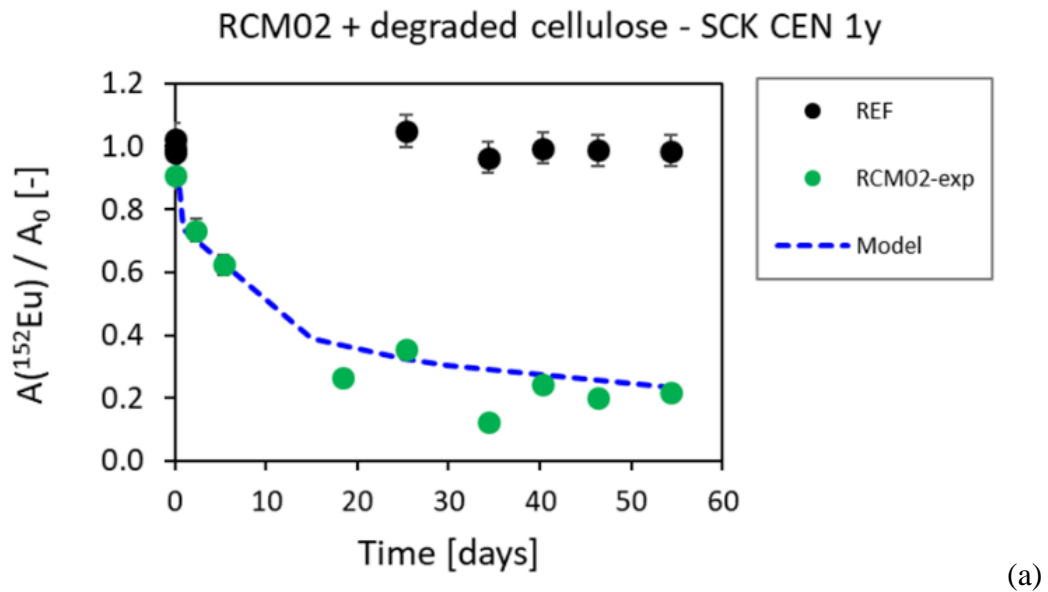
Figure 5-4: Experimental and modelled data obtained for the RCM02 cell (a) residual activity in solution (b) diffusion profile- ^{152}Eu diffusion in RCM-Stage II in presence of 1y-degraded cellulose by radiolysis provided by **[SCK CEN]**.

EURAD (Deliverables n° 3.6, 3.7 and 3.8) - Final Report of results generated in CORI
Dissemination level: PU
Date of issue of this report: **05/07/2024**

Page 149
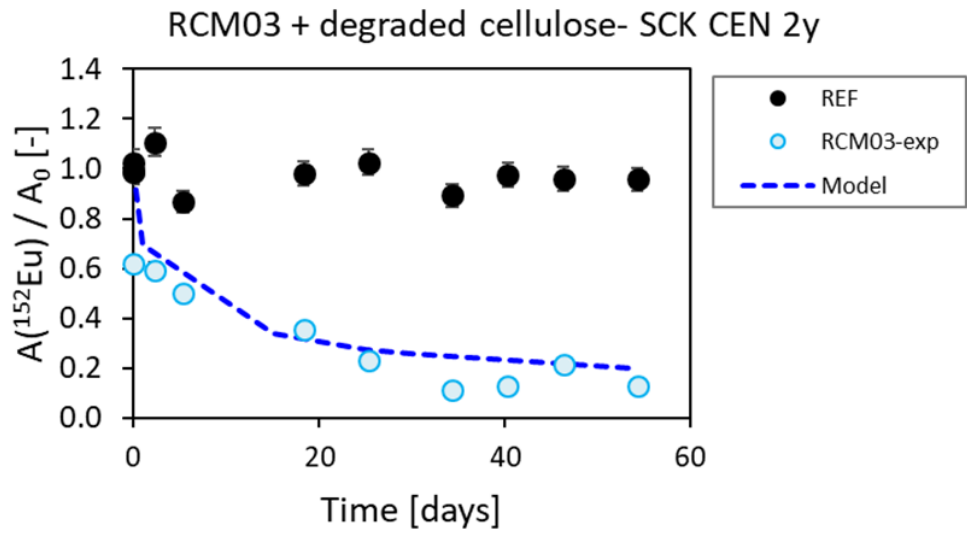
(a)
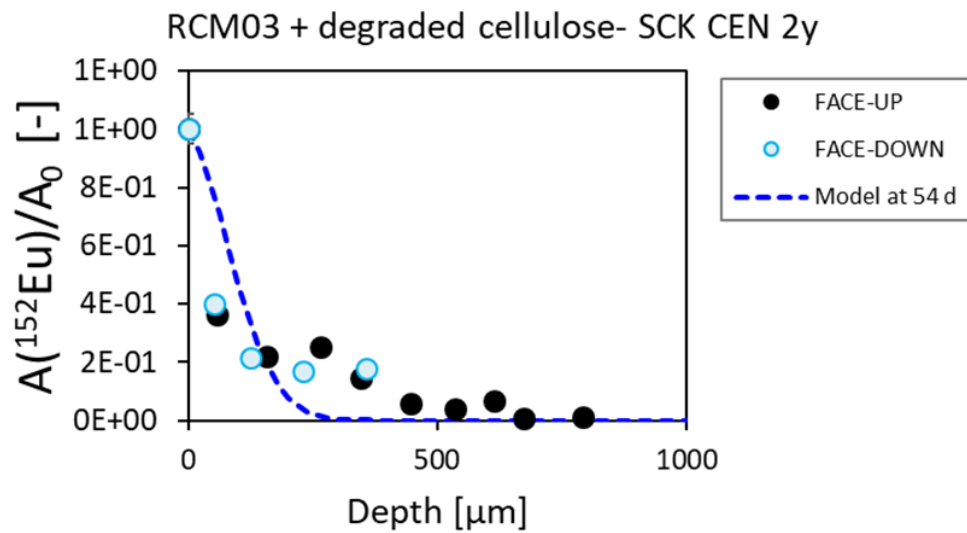
(b)

Figure 5-5:   *Experimental and modelled data obtained for the RCM03 cell (a) residual activity in solution (b) diffusion profile- ^{152}Eu diffusion in RCM-Stage II in presence of 2y-degraded cellulose by radiolysis provided by **[SCK CEN]**.*

EURAD (Deliverables n° 3.6, 3.7 and 3.8) - Final Report of results generated in CORI
Dissemination level: PU
Date of issue of this report: **05/07/2024**

Page 150
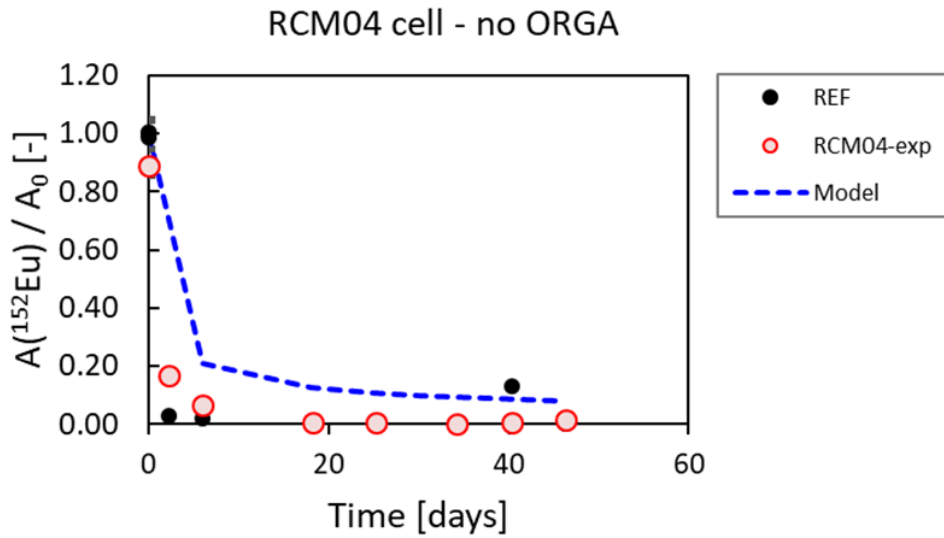
(a)
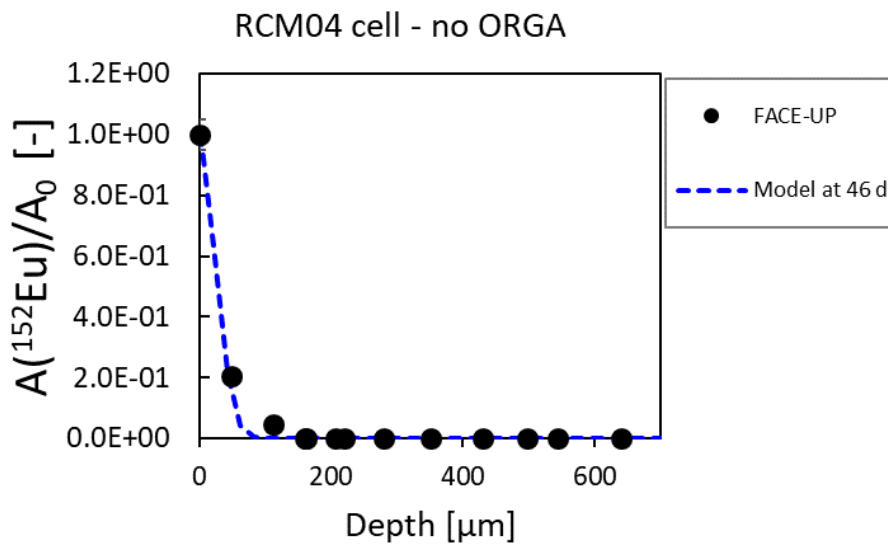
(b)

Figure 5-6:   *Experimental and modelled data obtained for the RCM04 cell (a) residual activity in solution (b) diffusion profile- ^{152}Eu diffusion in RCM-Stage II without organic species.*

Table 44 gives an overview of the values of apparent diffusion coefficient obtained ^{152}Eu in RCM sample at Stage II. There is a clear effect of the TOC content onto the diffusivity of ^{152}Eu, by increasing the D_a value by a factor *ca.* 250. It means that the complexing agent present in high quantity in the real leachate obtained after hydrolysis and radiolysis after irradiation can strongly affect the mobility of Eu. This effect is lower for cellulose degraded only by hydrolysis since the TOC content is lower in this system.

EURAD (Deliverables n° 3.6, 3.7 and 3.8) - Final Report of results generated in CORI
Dissemination level: PU
Date of issue of this report: **05/07/2024**

Page 151

Table 44: Summary of the effect of TOC content onto apparent diffusion coefficient obtained for ^{152}Eu in RCM Stage II

	$[TOC]_{ini}$ ppm^C	$D_a(^{152}Eu)$ $[m^2/s]$
RCM04	0	$8 \cdot 10^{-17}$
RCM01	70	$4 \cdot 10^{-17}$
RCM02	1350	$1.5 \cdot 10^{-15}$
RCM03	1700	$1.0 \cdot 10^{-15}$

[CIEMAT] analyzed the effects cellulose RDP, provided by [**SCK CEN**], on the adsorption of Ni, Eu, U and Pu on RCM fresh and degraded to Stage II and, compared the results on those obtained with Na-αISA synthesized in the laboratory. Diffusion experiments in degraded HCP in the presence of Na-αISA were carried out with Ni and Pu. Finally, the adsorption behavior of Ni on C-S-H phases in the presence of Na-αISA was analyzed and modelled.

Batch adsorption tests with the RCM in the presence of the cellulose degradation product provided by [**SCK CEN**] were carried out on at a solid to liquid ratio of 1 g/L on powdered material, fresh or degraded to Stage II under anoxic environment (N_2-atmosphere). The solution in contact with the solid was synthetic water mimicking the cement porewater at the fresh and Stage II. The contact time was 7 days, and the usual separation was performed by centrifuging ($22000 \cdot g$, 30 min). To check for the possible existence of bias on the results, due to the presence of organic colloids and low centrifugation, some experimental points were repeated using ultracentrifugation ($405000 \cdot g$, 30 min). No significant difference was observed in the two sets of experiments.

Sorption isotherms were carried out without the organic ligand, to establish the extent of adsorption in both the fresh and degraded RCM, to evaluate possible precipitation and the initial [RN] concentration

EURAD (Deliverables n° 3.6, 3.7 and 3.8) - Final Report of results generated in CORI
Dissemination level: PU
Date of issue of this report: **05/07/2024**

Page 152

to be used in the experiments with the organics. The plots in
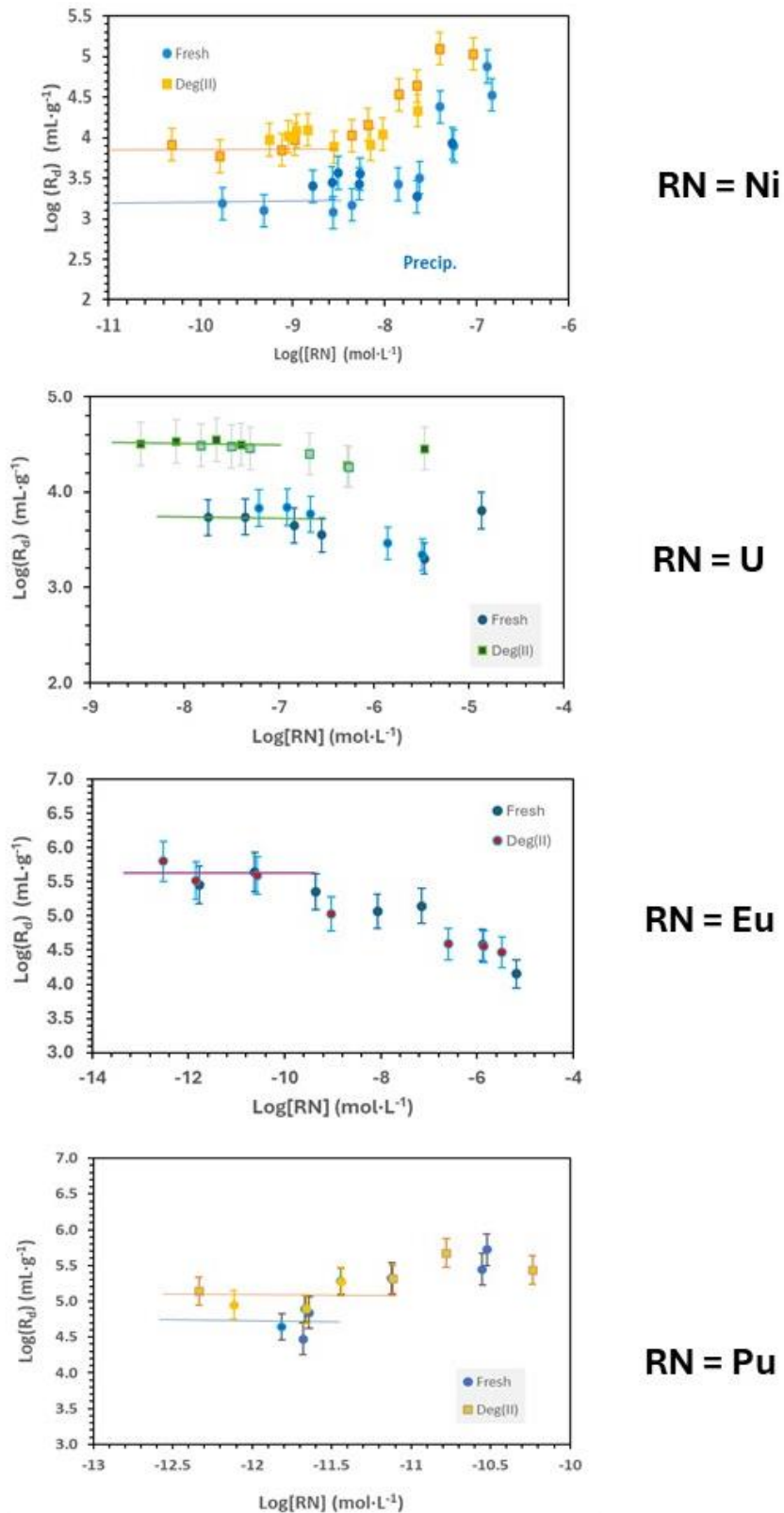
Figure 5-7 show the sorption isotherms, expressed as the logarithm of the R_d ($Log(R_d)$) values *vs.* the logarithm of the final RN concentration in solution ($Log[RN]$), obtained at [**CIEMAT**] for Ni, U, Eu and Pu without the organics. Tests were carried out in the RCM fresh and degraded to stage II. Results showed that for Ni and U the adsorption in the RCM degraded to Stage II was almost 1 order of magnitude higher

EURAD (Deliverables n° 3.6, 3.7 and 3.8) - Final Report of results generated in CORI
Dissemination level: PU
Date of issue of this report: **05/07/2024**

Page 153

than in fresh cement, whereas in case of Eu and Pu significant difference could not be observed. Clear signals of precipitation were observed for Ni and Pu at low RN concentration.

EURAD (Deliverables n° 3.6, 3.7 and 3.8) - Final Report of results generated in CORI
Dissemination level: PU
Date of issue of this report: **05/07/2024**

Page 154
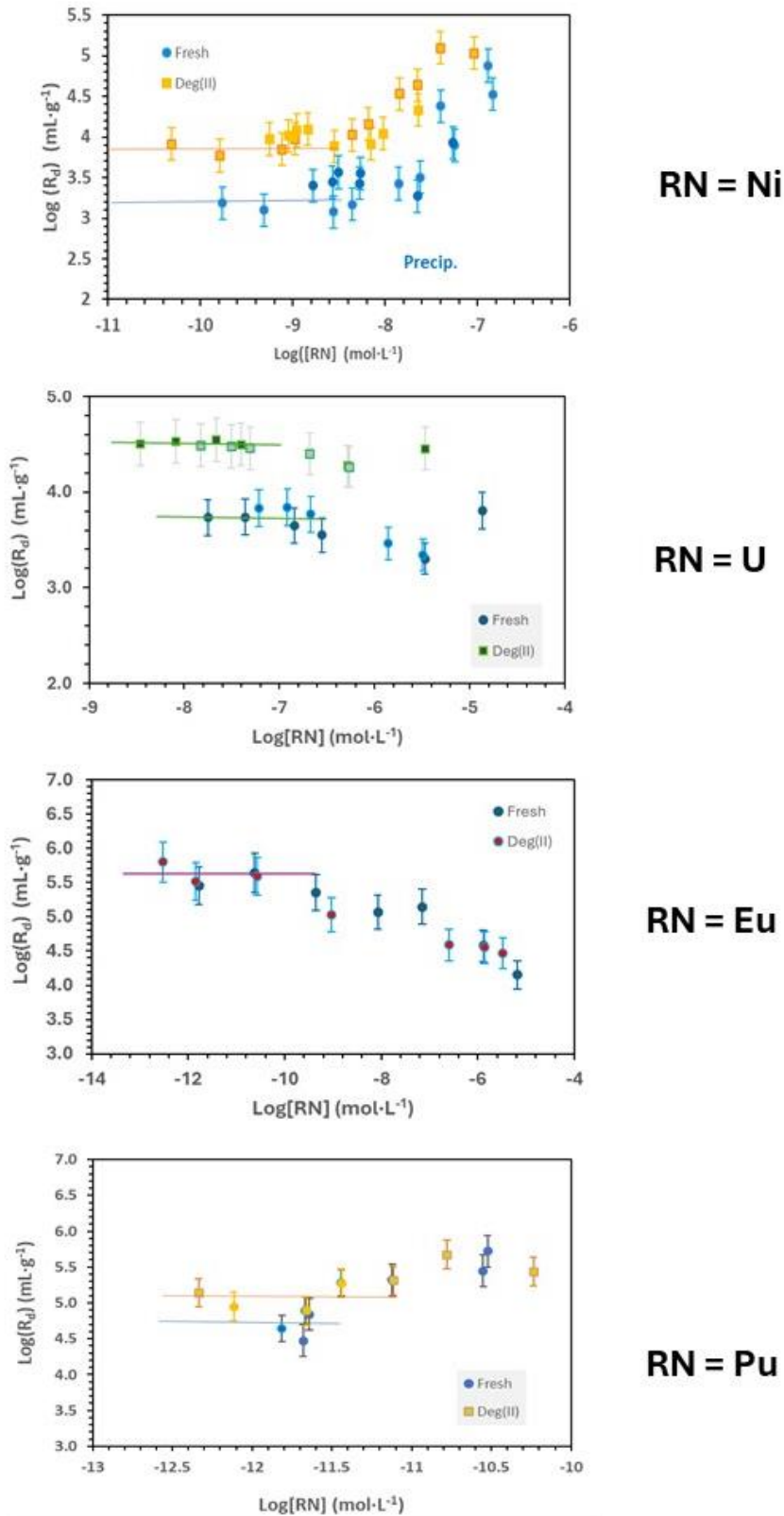
Figure 5-7:   *Sorption isotherms without the presence of organics for Ni, U, Eu and Pu in the RCM fresh and degraded to Stage II. The solid lines represent the region where the R_d values are constant (adsorption region).*

EURAD (Deliverables n° 3.6, 3.7 and 3.8) - Final Report of results generated in CORI
Dissemination level: PU
Date of issue of this report: **05/07/2024**

Page 155

Complementary, [**CIEMAT**] studied the adsorption of Ni, U, Eu and Pu in the presence of the cellulose RDP obtained from [**SCK CEN**], which was irradiated before alkaline degradation (Bleyen *et al.* 2023). The plots in *Figure 5-8* express the measured $\log(R_d)$ as a function of the total ISA content, considering the α-ISA and β-ISA content reported by SCK-CEN in the solution provided. Tests were carried out in the RDP for two systems (fresh and degraded HCP). For all the cases, in respect to the sorption values obtained without RDP, the R_d value was observed to decrease. In the case of Ni the decrease of R_d was around 1.5 orders of magnitude in both the fresh HCP and the degraded to stage II.

This result is quite interesting as previous studies carried out at [**CIEMAT**] indicated that the effect of the α-ISA synthesized in the laboratory was very slight for Ni adsorption in degraded HCP (CEM I and CEM IV, 10 g/L) and observable only at concentrations above $\sim$0.01 M. This is probably an indication that some of the not yet identified cellulose degradation products obtained by hydrolysis and radiolysis may have stronger effect than α-ISA on Ni retention.

In the case of U, a clear decrease in R_d was observed for the degraded HCP (two orders of magnitude at the higher ISA concentration, $> 3 \cdot 10^{-3}$ M). Nevertheless, the effect of the RDP on uranium adsorption in fresh cement was negligible.

In the case of Eu, the effect of the RDP was similar in both RCM degraded stages, with a significant decrease of sorption (up to three orders of magnitude). Previous studies carried out at [**CIEMAT**] with degraded HCP (CEM I and CEM IV, 10 g/L) also indicated that the effect ISA on Eu was relatively important with a decrease of 1 to 1.5 orders of magnitude in R_d values, above α-ISA concentration of $\sim$10^{-3} M.

The effect of RDP on Pu retention is higher in the degraded HCP where, above ISA concentration of 10^{-3} M, the activity of Pu drops under the detection limit. In the case of fresh RCM, the $\log(R_d)$ of Pu decreases about two orders of magnitude. Previous studies carried out at [**CIEMAT**] with degraded HCP (CEM I and CEM IV, 10 g/L) indicated that the effect ISA on Pu was also important with a decrease of more than 2 orders of magnitude in R_d α-ISA concentration of $\sim$10^{-3} M.

Thus, the RDP have a very important effect on the retention of all the investigated RN (except for U in fresh RCM), and the results are especially interesting for Ni, because no effects were seen on sorption by the presence of α-ISA.

[Ni] =1.4·10^{-8}M   **[U]=2.8·10^{-7} M**

EURAD (Deliverables n° 3.6, 3.7 and 3.8) - Final Report of results generated in CORI
Dissemination level: PU
Date of issue of this report: **05/07/2024**

Page 156

[Eu]= 4.6·10⁻¹⁰ M   **[Pu] =5·10⁻¹⁰ M**
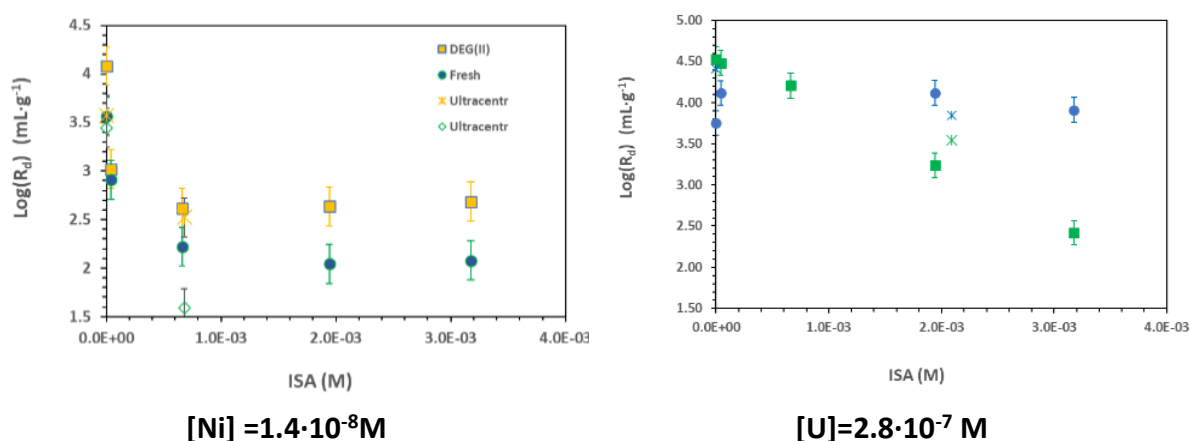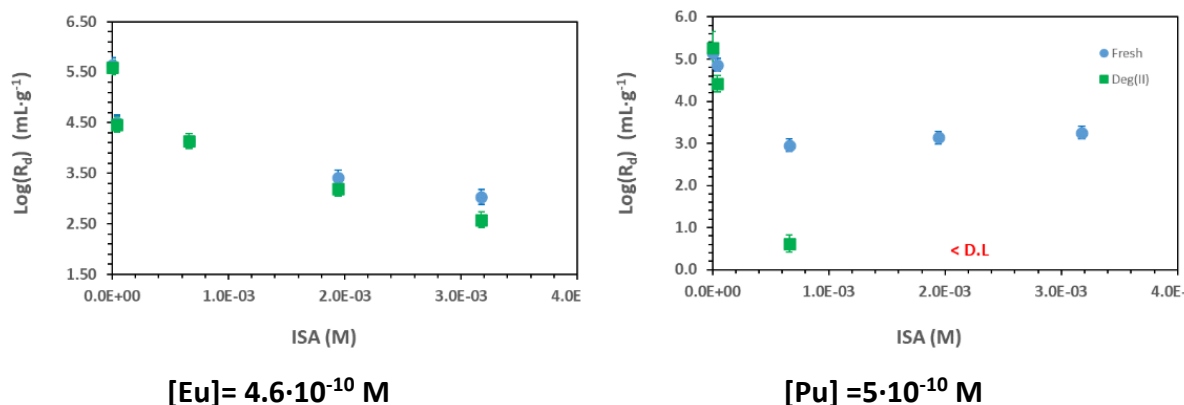
Figure 5-8:   *Sorption for for Ni, U, Eu and Pu in the RCM fresh and degraded to Stage II in the presence of cellulose RDP from [SCK CEN]. Data are expressed as a function of the concentration of ISA measured in the RDP.*

[CIEMAT] also studied the adsorption of Ni on C-S-H at different Ca/Si ratios and the data have been also successfully modelled (Missana *et al.* (2022a)). A summary of the adsorption results and their modelling without the presence of organics is shown in *Figure 5-9*, which shows Ni adsorption data as a function of the Ca/Si ratio and the modelling obtained. This experimental and modelling work on the binary C-S-H-Ni system represented the basis for the sorption studies in the presence of organics. The effect of Na-αISA on Ni adsorption in the C-S-H has been published in Missana *et al.* (2022b). Result showed that the presence of ISA at a concentration up to $1 \cdot 10^{-2}$ M only moderately affected Ni adsorption in the C-S-H, causing a diminution of K_d(Ni) by less than 1 order of magnitude. To interpret the experimental dataset, surface complexation modelling was successfully used in this system for the first time. The modelling was based on a double layer approach, which accounts for the properties of the binary Ni/C-S-H system and includes the formation of Ni-ISA aqueous complexes as well as ISA adsorption on the C-S-H, under the specific chemical conditions generated by the solids. The results of Ni adsorption on C-S-H (0.8) and C-S-H (1.4) in the presence of ISA are shown in *Figure 5-10*.
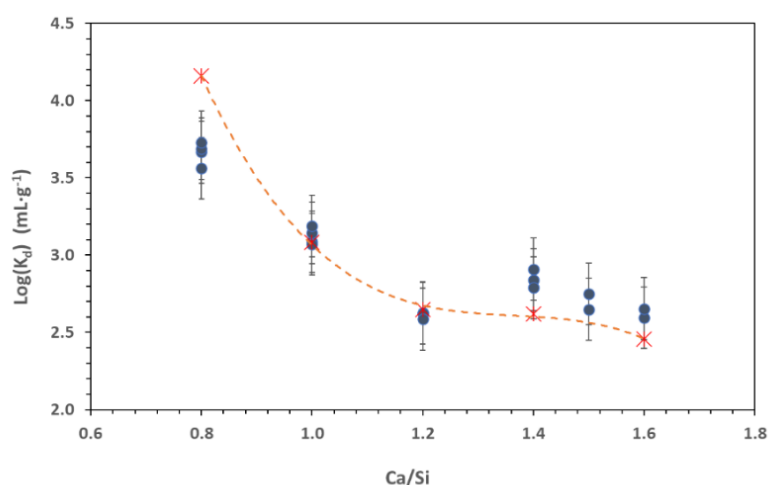
Figure 5-9:   *Ni adsorption in C-S-H as a function of the Ca/Si ratio. The red curve represents the modelling with the parameters and methodology detailed in Missana et al. (2022a).*

EURAD (Deliverables n° 3.6, 3.7 and 3.8) - Final Report of results generated in CORI
Dissemination level: PU
Date of issue of this report: **05/07/2024**

Page 157
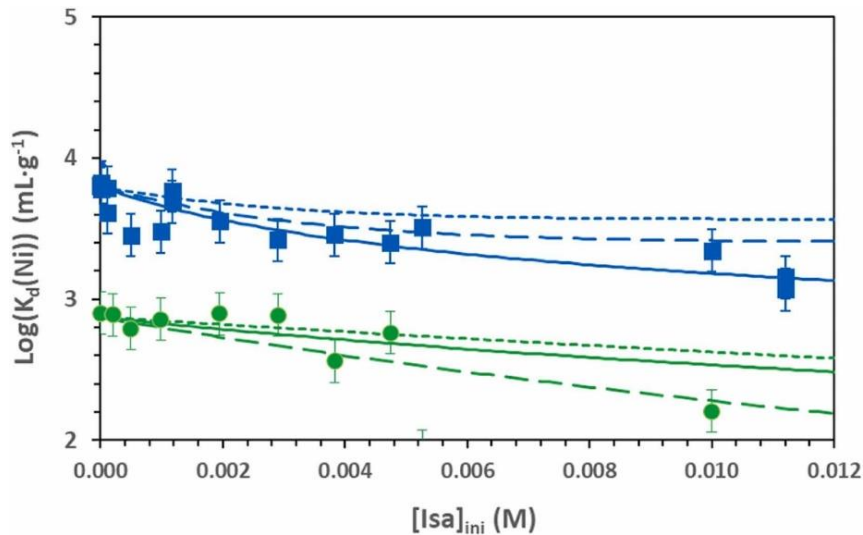
Figure 5-10: *Logarithm of Ni distribution coefficient vs. initial ISA concentration. Squares correspond to C-S-H(0.8), and circles correspond to C-S-H(1.4) (10 g·L⁻¹). The lines correspond to the modelling of the distribution coefficients. Continuous line: no adsorption of Isa on the C-S-H; dotted line: Isa adsorption only in the weak site; dashed line: Isa adsorption on strong and weak sites*

Finally, **[CIEMAT]** performed diffusion tests with α-ISA synthesized in the laboratory. Ni diffusion in the presence of α-ISA has been analyzed by means of through-diffusion tests with variable concentration, TDV test, to test experimental methodologies different from the classical in-diffusion and through diffusion and comparing two different analytical solutions available in the literature (Bharat, 2014 and Takeda *et al.* 2008). Both the selected analytical solutions are based on the fit of the RN evolution in the inlet and outlet reservoirs, and considers as fit parameters the effective diffusion coefficients, D_e, and the distribution coefficient K_d.

Even after more than 200 days, no Ni could be measured in the out reservoir, than the simulation of the curves was carried out considering [Ni] = 0 M. This partial information may not be enough for a correct interpretation of the RN activity curves. An example of the evolution of Ni in the inlet reservoir, in a TDV experiment in degraded HCP (left CEM I and right CEM IV) and in the presence of ISA, is shown in *Figure 5-11*. These curves could be successfully simulated with both the equations, but similar simulations of the same profile. As those shown in the *Figure 5-12*, the modelled curves lead to similar K_d values (30-150 L/kg) but systematically higher D_e values for Bharat's than Takeda's equation (0.9-1.5·10⁻⁹ m²/s *vs.* 3-4·10⁻¹⁰ m²/s), which is something not clear at present and must be analyzed in more details. No difference was observed on the Ni diffusion behavior without ISA.
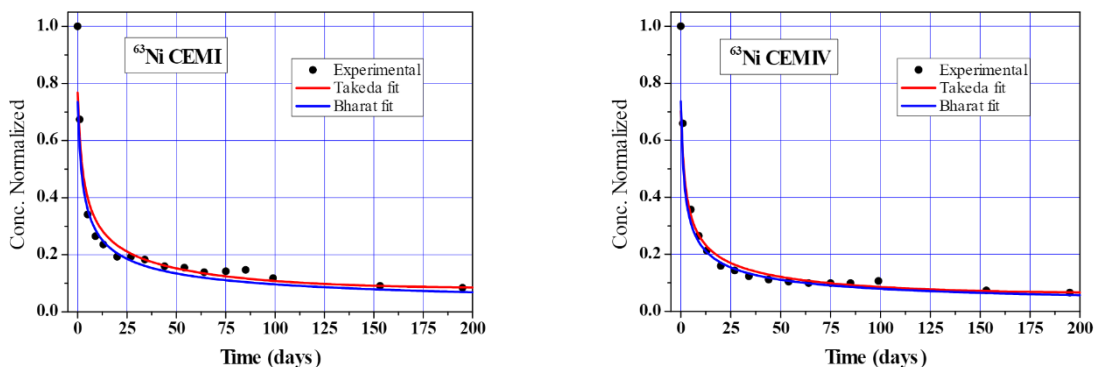
Figure 5-11: *Results of TDV experiments of Ni in the presence of ISA: evolution of Ni in the inlet deposit and comparison of the simulations obtained by the two selected analytical methods. These tests lasted 200 days.*

EURAD (Deliverables n° 3.6, 3.7 and 3.8) - Final Report of results generated in CORI
Dissemination level: PU
Date of issue of this report: **05/07/2024**

Page 158

Additional tests were also carried out for Ni by the in-diffusion method in degraded HCP (CEM I and CEM V), with a duration of approximately 400 days. The range of apparent diffusion coefficients, D_a, determined by in-diffusion test, with and without the organic was similar ~ $(3\text{-}4)\cdot10^{-15}$ m^2/s and no large differences were seen amongst the two HCPs.

In-diffusion tests were carried out with degraded HCP (CEM I) to determine the D_a for Pu in the presence of ISA. The measured D_a were between $(9.2\pm0.8)\cdot10^{-14}$ m^2/s to $(1.5\pm0.8)\cdot10^{-13}$ m^2/s. An example of the results obtained in CEM I is shown in *Figure 5-12*.
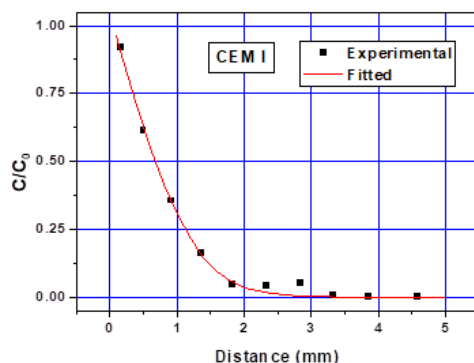
Figure 5-12:   *In diffusion profile for Pu in the presence of ISA in degraded HCP (CEM I)*

[JGU] studied the effect of ISA on the retention of actinides Th(IV) and Pu(IV) by fresh CEM I HCP (pH>13) by means of batch sorption experiments. Additionally, diffusion experiments with Pu(IV) in intact cement cores were conducted to gain further insights into the transport behavior in the presence and absence of ISA. The experimental conditions for adsorption experiments were: $[^{239}Pu(IV)]_0$ or $[^{232}Th(IV)]_0$ = $1\cdot10^{-8}$ M, $[ISA]_0 = 1\cdot10^{-2}$ M, pH = 13.3, and S/L = 5 g·L^{-1}. The same procedure was followed for all three different additions as previously described. *Figure 5-13* (left) shows the result of ^{232}Th(IV) sorption experiments in dependence of order of addition and contact time up to 194 d. As can be seen, ISA and the order of addition significantly influenced the sorption behavior of ^{232}Th(IV) on HCP. The R_d values obtained were two orders of magnitude smaller compared to the sample without ISA. Depending on the contact time, it was observed that equilibrium could be reached after 194 days, with an R_d value of 10^2 L·kg^{-1}.

Wieland *et al.* (2002) observed reduced Th(IV) uptake by HCP at high ISA concentrations (≥10^{-4} M). Their obtained R_d values were similar to those at lower S/L ratios of 5 g·L^{-1}. The decrease may be due to the formation of Ca-Th(IV)-OH-ISA complexes at high pH values, as described elsewhere [(Tits *et al.* 2001, 2005; Vercammen *et al.* 2001)]. Additionally, sorption isotherms of $^{232/234}$Th(IV) on HCP were conducted at different Th concentrations ($[^{232/234}Th(IV)]_0$ =10^{-6} M - 10^{-13} M at S/L=0.1 g·L^{-1}) in the absence and presence of ISA ($[ISA]_0 = 10^{-2}$ M) in an ACW solution at pH 13.3 (*Figure 5-13*, right). Both Th(IV) and ISA were added simultaneously and allowed to interact for 72 hours. In the absence of ISA, a R_d value of $4\cdot10^4$ L·kg^{-1} was determined using a linear fit with a slope of one. This indicates an uptake of > 99%, which is consistent with values reported in the literature (Goudarzi, 2023) and the results of the experiment shown without ISA.

In the presence of ISA, R_d value of $5\cdot10^2$ L·kg^{-1} was determined using the same linear fit. This value is in the same order of magnitude (R_d~$5\cdot10^2$ L·kg^{-1}) as the value obtained in the experiment with different addition orders (see *Figure 5-13* (left)). It is important to note that the presence of ISA led to a significant increase in the solubility of Th(IV) due to the possible formation of Th-OH-ISA [Vercammen *et al.* (2001), Tits *et al.* (2005), Colás *et al.* (2014)] and Ca-Th-OH-ISA (Vercammen *et al.* (2001), Tits *et al.* (2002, 2005)) complexes.

EURAD (Deliverables n° 3.6, 3.7 and 3.8) - Final Report of results generated in CORI
Dissemination level: PU
Date of issue of this report: **05/07/2024**

Page 159
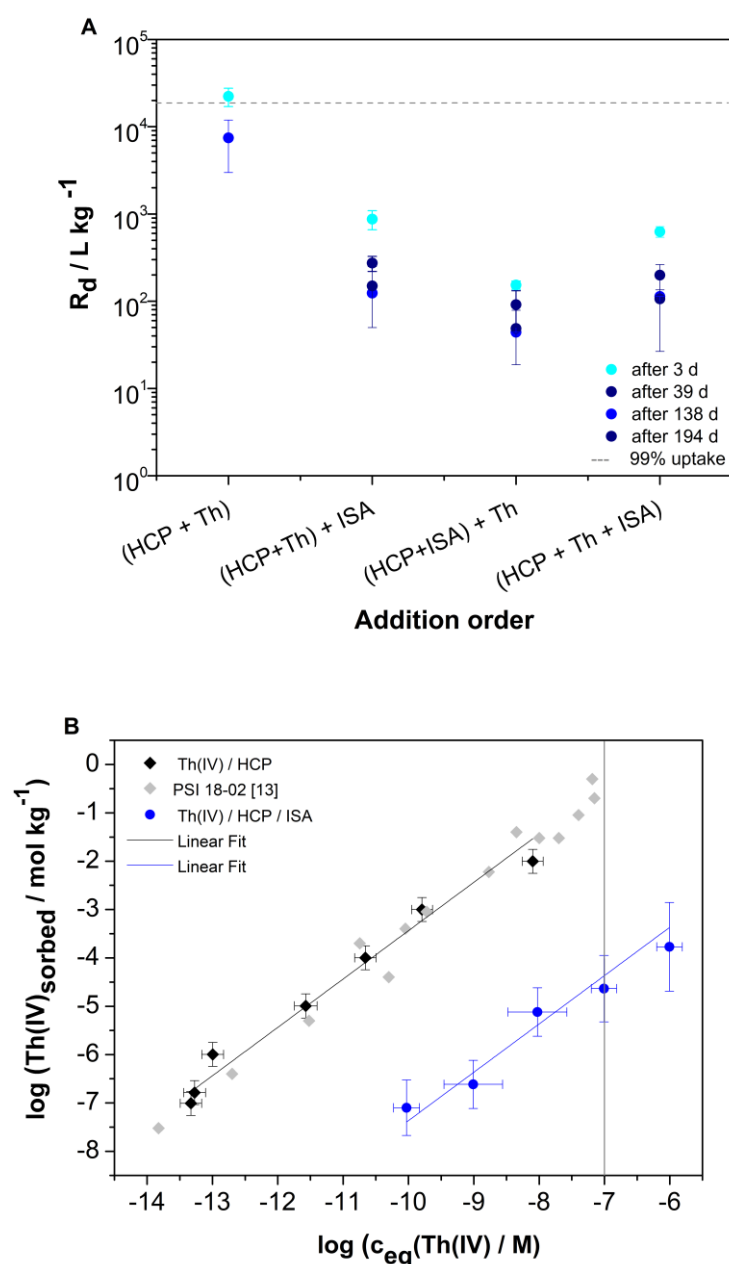
Figure 5-13:   *A) Sorption isotherm of HCP / $^{232/234}$Th(IV) ([Th(IV)] =1·10^{-6} M – 1·10^{-13}M; S/L=0.1 g·L^{-1}) in the absence (black) and presence (blue) of ISA ([ISA] =1·10^{-2} M) with corresponding fit. The grey dots are values from the literature [Wieland et al. (2002)]. The solubility limit of Th(IV) at high pH values of > 13 is shown by the grey line [Fanghänel & Neck, 2002]. B) Distribution coefficients R_d (L·kg^{-1}) determined for Th(IV) ([^{232}Th(IV)] =1·10^{-8} M) uptake on HCP (S/L=5 g·L^{-1}) in presence and absence of ISA ([ISA] =1·10^{-2} M) after a contact time of 3 d, 39 d, 138 d and 194 d in ACW at pH 13.3. The order of addition of An(IV) and ISA to the HCP suspensions is indicated at the abscissa. The dashed line represents an uptake of 99%.*

Furthermore, analogous experiments were conducted to investigate the influence of the order of addition and contact time on Pu(IV) sorption on HCP. The experimental conditions were [^{239}Pu(IV)]$_0$ = 10^{-8} M, [ISA] = 1·10^{-2} M, pH = 13.3, S/L = 5 g·L^{-1}, contact time 72 h to 119 days. The calculated R_d values are shown in *Figure 5-14*. In the absence of ISA the uptake of Pu(IV) on HCP is > 99%, consistent with existing literature [Ochs *et al.* (2016), Tasi *et al.* (2021)]. The observed effect of the order of addition agree well with the results of Tasi *et al.* (2021). The strong affinity of ISA for the HCP surface hinders

EURAD (Deliverables n° 3.6, 3.7 and 3.8) - Final Report of results generated in CORI
Dissemination level: PU
Date of issue of this report: **05/07/2024**

Page 160

the sorption of Pu(IV) on HCP, similar to the results obtained in the HCP/Pu(IV)/GLU system. After 119 days of contact, the uptake of Pu(IV) in the presence of ISA decreased in all cases. The effect is most noticeable in the (HCP + Pu) + ISA addition sequence.
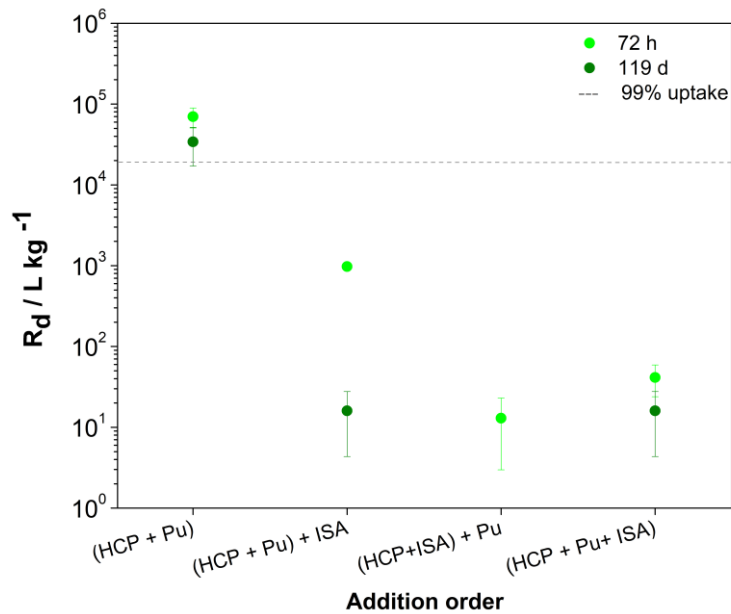
Figure 5-14: Distribution coefficients R_d (L·kg^{-1}) determined for Pu(IV) ([^{239}Pu(IV)] =1·10^{-8} M) uptake on HCP (S/L=5 g· L^{-1}) in presence and absence of ISA ([ISA] =1·10^{-2} M) after a contact time of 72 h and 119 d in ACW at pH 13.3. The dashed line represents an uptake of 99%.

The sorption of ISA on HCP is observed to dominate, resulting in the desorption of Pu(IV) from HCP. Tasi *et al.* (2021) reported that even after 490 days of contact time in systems with S/L ≤ 8 g·L^{-1} at Stage II (pH ≈ 12), the log [Pu]$_{eq}$ was found to be comparable to the [Pu]$_0$.

The in-diffusion of 7·10^{-10} M of ^{238}Pu(IV) into HCP at Stage I (pH > 13) in the absence and presence of ISA ([ISA]$_0$ = 1·10^{-2} M) in ACW (with 0.003 M NaN$_3$) was investigated (see section 3.5.3). Following a diffusion period of 118 days, the HCP samples were removed from the diffusion cells, dried, and then mounted on a sample holder for abrasive peeling. The abrasive peeling technique employed was described by Van Loon & Eikenberg (2005). The activities of ^{238}Pu(IV) present in the HCP layers were directly measured using α-spectroscopy.

Figure 5-15 shows the profile of ^{238}Pu in the HCP in absence (left) and presence (right) of ISA.
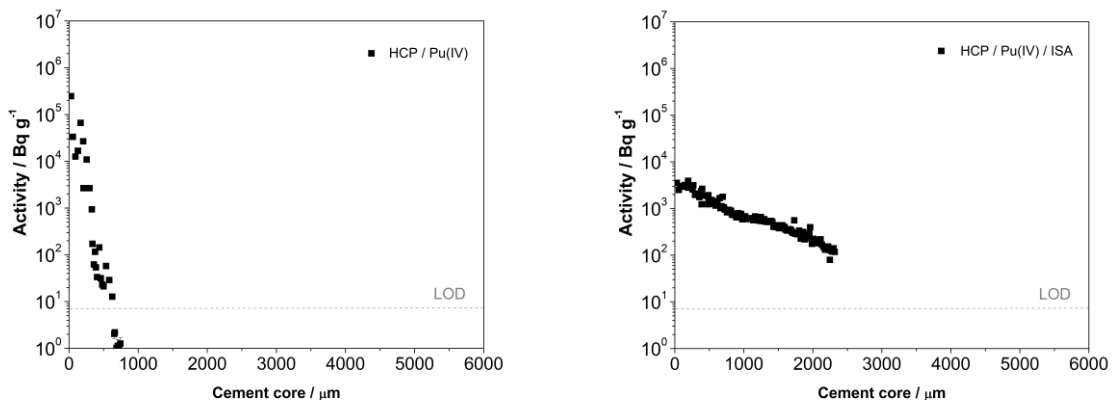
Figure 5-15: In-diffusion profile of ^{238}Pu(IV) in the absence (left) and the presence (right) of ISA in the cement core.

EURAD (Deliverables n° 3.6, 3.7 and 3.8) - Final Report of results generated in CORI
Dissemination level: PU
Date of issue of this report: **05/07/2024**

Page 161

As shown in *Figure 5-15*, the diffusion profile of the core from cell I in the absence of ISA (*Figure 5-15* left) reveals that ^{238}Pu(IV) exhibits strong sorption at the HCP core, only diffusing up to a depth of 627 µm within 118 days. In contrast, the diffusion profile of the HCP core from cell II in the presence of ISA (*Figure 5-15* right) demonstrates that Pu diffuses much deeper into the core, up to 2.5 mm (further grinding was not possible to avoid removing material from the sample holder). These results suggest that ISA has a significant influence on the diffusion of Pu(IV) into HCP as already shown by batch sorption experiments. The high uptake of 10^{-2} M ISA by HCP leads to the blocking of sorption sites. Additionally, a Ca-Pu-OH-ISA complex forms in solution, potentially exhibiting different uptake behavior by HCP.

[SCK CEN] has investigated the sorption of ^{63}Ni on hardened cement paste (HCP) powder degraded to different stages in presence and absence of α-isosaccharinic acid (α-ISA) and cellulose degradation products obtained in CORI Task 2. The diffusion of Ni in CEM I hardened cement paste (HCP) degraded to Stage III in the absence and presence of α-ISA was also studied.

Sorption experiments were performed on three different powdered (< 74 µm) CEM I HCP, *i.e.* fresh HCP prepared from CEM I 52.5 N, HCP prepared from the same batch but further degraded to Stage III by leaching in ultrapure water and the CORI reference HCP degraded to Stage II also by leaching in ultrapure water. The three HCP powders were characterized by XRD and unexpectedly both the Stage II and Stage III HCPs were found to contain neither portlandite nor ettringite. Extra analysis on the Stage II CORI reference HCP is still to be performed to confirm this result. Synthetic solutions were prepared as proxies of the pore water of each degradation stage.

For Stage I, the composition was based on the literature (Van Loon *et al.* 1997) while for Stage II and III, it was based on the composition of the solutions measured at the end of the leaching experiments. The sorption experiments were performed in an inert atmosphere at a solid/liquid ratio of 5 g/L in the corresponding synthetic pore water and for a contact time of 7 days. Sorption of ^{63}Ni in the absence of organics was investigated on the three HCP powders. The sorption was linear with constant calculated $\log(R_d)$ values until a ^{63}Ni equilibrium concentration of $2 \cdot 10^{-9}$ M. At higher concentrations, Ni started to precipitate in the fresh cement system (pH 13.1). ^{63}Ni sorption was strong on all materials with $\log(R_d)$ values > 2.8 but depended on the degradation level of the HCP. The lowest values were obtained on the fresh cement with an average $\log(R_d)$ of 2.99 [2.85-3.09], while average values of 3.94 [3.73-4.07] and 4.26 [4.14-4.35] were obtained for the HCP Stage III and CORI reference HCP Stage II, respectively. The presence of α-ISA was found to have no impact on the sorption of ^{63}Ni on fresh HCP while it showed a limited effect on both degraded HCPs. This limited effect was only visible for α-ISA concentrations higher than 10^{-3} M for the CORI HCP Stage II and higher than $4 \cdot 10^{-4}$ M for the HCP Stage III.

The induced decrease of $\log(R_d)$ was only limited in both cases to 0.3-0.5 log unit for $1 \cdot 10^{-2}$ M of α-ISA. On the other hand, the effect of cellulose degradation products obtained in Task 2 appeared quite strong for both fresh and HCP Stage III (not investigated on CORI HCP Stage II) and much stronger in comparison to pure α-ISA with a decrease of $\log(R_d)$ of more than 2 log units for $1 \cdot 10^{-2}$ M of α-ISA. This result could suggest the involvement of cellulose degradation products other than α-ISA in the ^{63}Ni sorption reduction.

The results of the previous solubility studies are shown in *Figure 5-16*, which reports the Ni equilibrium concentration measured after centrifugation at 20000 g in comparison with the introduced Ni concentration. A slight deviation from linearity is observed at a concentration higher than $1 \cdot 10^{-8}$ mol/L but no clear precipitation front is visible. This result suggests that in synthetic Stage III cement water and after a week of contact, Ni is mostly soluble up to at least $1 \cdot 10^{-4}$ mol/L. However, the formation of colloids or sorption of Ni on the centrifuge tube could in some cases partially reduce the concentration of Ni in solution.

EURAD (Deliverables n° 3.6, 3.7 and 3.8) - Final Report of results generated in CORI
Dissemination level: PU
Date of issue of this report: **05/07/2024**

Page 162
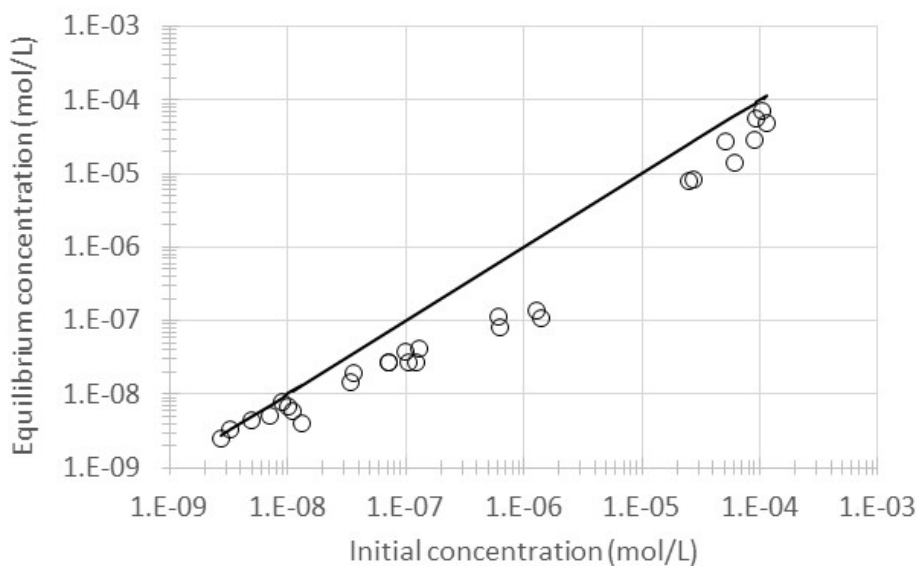
Figure 5-16:   *Ni solubility in synthetic Stage III cement water after 7 days of contact. The initial concentration corresponds to the concentration measured in solution after 7 days of contact before centrifugation and the equilibrium concentration to the concentration measured after centrifugation at 20000 g for 2 h.*

The sorption isotherms of ^{63}Ni obtained on the different HCP powders are reported in *Figure 5-17*. The equilibrium pH was found to be 13.34 ± 0.02, 12.14 ± 0.02 and 11.64 ± 0.02 for fresh, Stage II and Stage III HCP, respectively. The calculated R_d values show a lower sorption in the fresh cement compared to the more degraded stages. At equilibrium concentrations higher than $2 \cdot 10^{-9}$ mol/L, in the fresh cement system, an increase of R_d values can be observed. This suggests that at these concentrations, Ni precipitation starts to play a role. It should be mentioned that the plotted equilibrium concentration represents only the concentration of ^{63}Ni. The total concentration of Ni would indeed be higher since HCPs contain and release natural Ni in solution. The measurements of the stock cement suspensions showed that up to $5 \cdot 10^{-8}$ mol/L could be present in the solution at equilibrium.
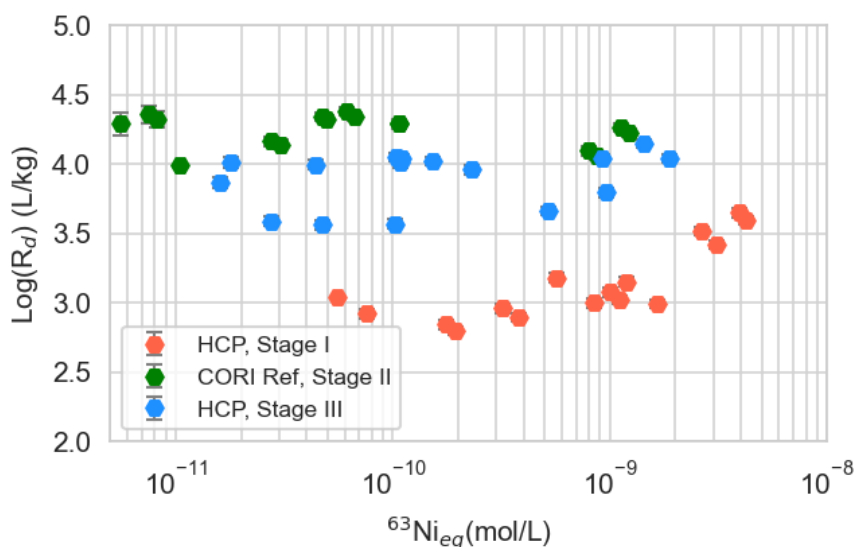
Figure 5-17:   *Sorption isotherms of ^{63}Ni on HCP at different degradation stages at 5 g/L and in the corresponding synthetic cement waters.*

EURAD (Deliverables n° 3.6, 3.7 and 3.8) - Final Report of results generated in CORI
Dissemination level: PU
Date of issue of this report: **05/07/2024**

Page 163

The sorption isotherms of [63]Ni obtained on the different HCP powders in the presence of α-ISA are reported in *Figure 5-18*. The equilibrium pH was found to be 13.17 ± 0.01, 12.13 ± 0.01 and 11.69 ± 0.03 for fresh, Stage II and Stage III HCP, respectively. The calculated R_d values show no impact of α-ISA on the sorption of [63]Ni on fresh cement while it shows a limited effect on both degraded cements. This effect is only visible for α-ISA concentrations higher than 10^{-3} M for the CORI HCP degraded to Stage II and higher than $4 \cdot 10^{-4}$ M for the HCP degraded to Stage III. Hence, with degradation of the cement phases, the effect of α-ISA on the [63]Ni sorption would become more pronounced.
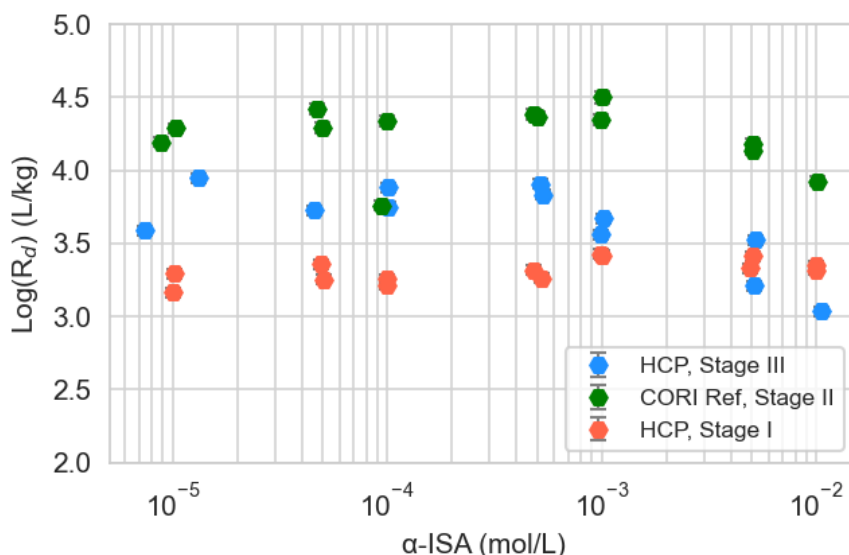
Figure 5-18: *Sorption isotherms of [63]Ni in presence of α-ISA on HCP at different degradation stages at 5 g/L and in the corresponding synthetic cement waters.*

The sorption isotherms of [63]Ni obtained on the different HCP powders in the presence of cellulose degradation products are reported in *Figure 5-19*. The equilibrium pH was found to be 13.30 ± 0.02 and 11.44 ± 0.07 for fresh and Stage III HCP, respectively. For comparison, the results obtained with pure α-ISA are also reported in *Figure 5-19*. The effect of cellulose degradation products is visible for both degradation stages even from low concentrations of α-ISA. It is moreover quite strong for both fresh and degraded cement and much stronger in comparison to pure α-ISA. This result could suggest the involvement of cellulose degradation products other than α-ISA in the [63]Ni sorption reduction. Indeed, the solution of cellulose degradation products obtained after irradiation and hydrolytic degradation contains a large variety of organics as shown in Section 2.1 of Task 2 and α-ISA represents only 43% of the total TOC in the sample used here.

EURAD (Deliverables n° 3.6, 3.7 and 3.8) - Final Report of results generated in CORI
Dissemination level: PU
Date of issue of this report: **05/07/2024**

Page 164
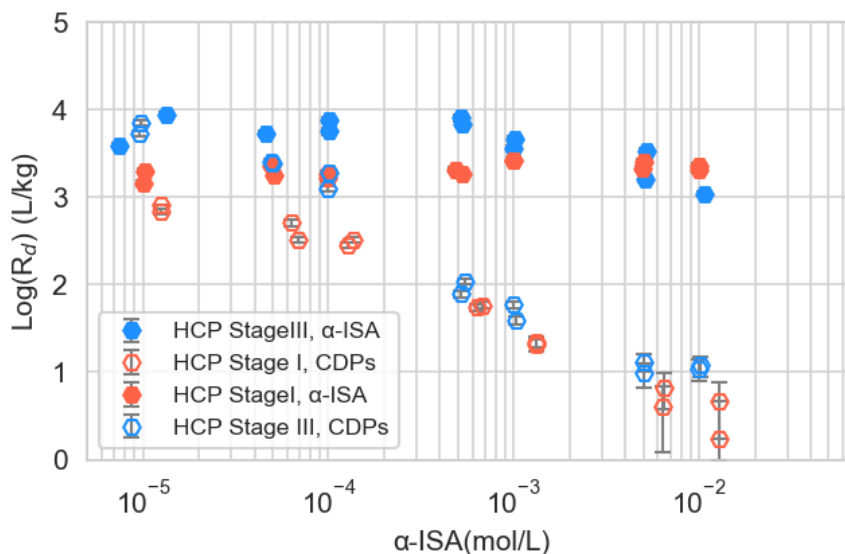
Figure 5-19: *Sorption isotherms of [63]Ni in presence of pure α-ISA and cellulose degradation products on HCP at different degradation stages at 5 g/L and in the corresponding synthetic cement waters. The data are here plotted as a function of α-ISA concentration through the cellulose degradation products contains also other organics.*

[SCK CEN] also investigated diffusion tests of Ni in presence of a-ISA and cellulose degradation products on HCP (see section 3.5.5). The two diffusion experiments, Diff1 and Diff2, performed on the degraded cement discs were stopped after about 200 days. The evolution of inlet and outlet Ni concentration over time are reported for the two experiments in *Figure 5-20*. The discs were cut in pieces, freeze-dried, embedded in resin and polished to be further analyzed by LA-ICP-MS. Due to some technical issues, this analysis could unfortunately not be performed in the time frame of the project. Diffusion profiles of Ni in the cement discs could therefore not be acquired. Over the experimental time, the outlet concentrations of Ni both in presence and absence of $\alpha-$ISA did not rise above the background concentration, *i.e* the natural Ni concentration of the HCP, which was between $5\cdot10^{-9}$ and $8\cdot10^{-9}$ mol/L. Only the evolution of the inlet concentration could therefore be modelled limiting the output of the model. Indeed, by fitting the inlet concentration, only the product $\alpha(D\_app)^{1/2}$ could be determined. Moreover, in the experiment performed in presence of α-ISA (Diff2), the low amount of data points and their scatter (*Figure 5-20*, right) did not allow a reasonable estimate of the transport parameters. Hence only the value of $\alpha(D\_app)^{1/2}$ for pure Ni can be reported here: $8.6\cdot10^{-5}$ m·s$^{-0.5}$.
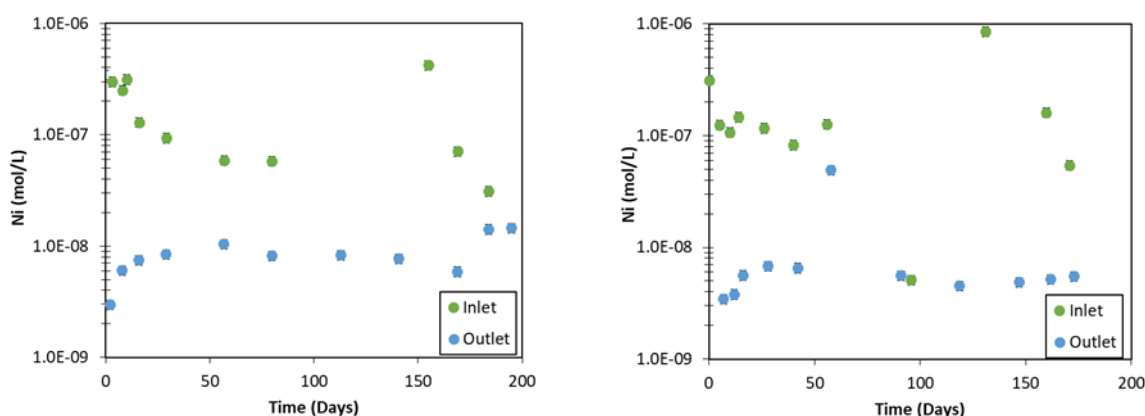
Figure 5-20: *Evolution of stable Ni concentration in the inlet and outlet reservoirs in diffusion experiments performed on the degraded cement discs. On the left: pure Ni in Diff1. On the right: Ni in presence of α-ISA in Diff2.*

EURAD (Deliverables n° 3.6, 3.7 and 3.8) - Final Report of results generated in CORI
Dissemination level: PU
Date of issue of this report: **05/07/2024**

Page 165

[CNRS-SUBATECH] contribution to Task 4 aims at understanding the effect of ISA on the migration of uranium(VI) in a CEM V HCP. Two degradation stages were investigated: Stage II, buffered by the dissolution of Portlandite resulting in pH ≈ 12.5 and [Ca] ≈ 22 mmol.L^{-1}, and Stage III, dominated by the incongruent dissolution of C-S-H phases with a global solid Ca/Si ratio of 1-1.2 and a pH value ≈ 11.7. The experimental methodology is based on transport (diffusion) experiments combined with wet chemistry experiments (batch) either on binary U(VI)/HCP and ISA/HCP (as reference systems) or ternary U(VI)/ISA/HCP systems for both degradation stages. Solutions and solids are analyzed in order to characterize the degradation stages and to acquire pertinent data for determining retention and transport parameters. The interpretation of data is firstly based on the application of simple models (K_d, Langmuir isotherm, Fick laws) in order to get a global understanding of these complex systems.

Preparation steps, batch and diffusion experiment and sampling steps were all performed in a glove box (under Argon) at room temperature (T=22°C) to prevent any atmospheric carbonation. All solutions were prepared with degassed ultrapure water (Milli-Q, Millipore, 18.2 MΩ·cm). Uranyl nitrate stock solutions (99.99% purity) were provided by SCP Science as 1000 mg·L^{-1}and 10000 mg·L^{-1} ICP-MS standard solutions. Saturated lime water solution (S2 solution) was prepared by dissolving 25 g·L^{-1} of CaO (Alfa Aesar, 99.95%) in degassed ultrapure water followed by a filtration step (0.2 µm PTFE Millipore). For ISA preparation and purification, see section 3.1.1.

For Stage II, prior to wet chemistry experiments, an equilibration step was performed. Appropriate amounts of HCP powder were mixed in 35 mL PPCO Nalgene tubes with 20 mL of S2 solution and agitated for a week. These suspensions were centrifuged (2650 g, 15 min) and supernatants were discarded. This step was repeated twice. Appropriate amounts of U(VI) and/or ISA were then added to S2 solution to obtain the appropriate experimental conditions.

For Stage III, degraded HCP powder was prepared by mixing a certain amount of HCP powder with degassed ultrapure water at a solid/liquid ratio of 9·10^{-4} kg·L^{-1} and agitated for 2 weeks. Solid and liquid phases were then separated by filtration. The solution was characterized by ion chromatography (for major cations and anions), pH and single quadrupolar ICP-MS (for Si) and the solid by X-Ray Diffraction (Bruker D8 Advance) in order to identify the mineral phases. Both solution and solid were used for batch experiments.

Sorption/desorption isotherms and/or time-series (kinetics) experiments were performed on binary and ternary systems for both degradation stages in the following experimental conditions (*Table 45*).

Table 45: Experimental conditions for wet chemistry experiments

	Systems		[U] range (mol·L^{-1})	[ISA] range (mol·L^{-1})	Solid/liquid (kg·L^{-1})	Sampling time (days)
Stage II	U(VI)/HCP	Isotherms	1·10^{-8} to 1·10^{-4}	-	1·10^{-3}	28
		Kinetics	3·10^{-7}, 3·10^{-6}, 1·10^{-4}	-	1·10^{-3}	3, 7, 14, 28
	ISA/HCP	Isotherms	-	1·10^{-3} to 3·10^{-2}	2.5·10^{-2}	32
		Kinetics	-	1·10^{-2}	2.5·10^{-2}	1, 3, 7, 14, 28, 91
	U(VI)/ISA/HCP	Isotherms	1·10^{-7} and 1·10^{-4}	1·10^{-4} to 2·10^{-2}	1·10^{-3}	33
Stage III	U(VI)/HCP	Isotherms	7.5·10^{-9} to 1·10^{-4}	-	1·10^{-3}	32
		Kinetics	1·10^{-6}	-	1·10^{-3}	1, 3, 7, 14, 28, 91
	ISA/HCP	Isotherms	-	5·10^{-4} to 3·10^{-2}	5·10^{-3}, 17·10^{-3}	28
		Kinetics	-	1·10^{-2}	5·10^{-3}	1, 3, 7, 14, 28, 64
	U(VI)/ISA/HCP	Isotherms	9.7·10^{-8} and 3·10^{-5}	1·10^{-4} to 4.8·10^{-2}	1·10^{-3}	28

EURAD (Deliverables n° 3.6, 3.7 and 3.8) - Final Report of results generated in CORI
Dissemination level: PU
Date of issue of this report: **05/07/2024**

Page 166

At the end of experiments, suspensions were centrifuged (2650 g, 15 min), then supernatants were filtered and sampled for analysis. For desorption experiments, after removing the supernatants, 20 mL of fresh S2/S3 solutions (without U(VI) nor ISA) were added to each tube, agitated during the adequate duration and, at the end, sampled as previously described.

Different analytical techniques have been used for the characterization of solutions. Quadrupolar ICP-MS (ThermoElectron X serie 2) was used for uranium quantification (Limit of Quantification (LQ) = 10 ng·L^{-1}, Bi as internal standard) and for Si quantification (LQ = 10 µg·L^{-1}, In as internal standard). TOC meter (Analytik Jena NC2100S) for ISA determination (Non Purgeable Organic Carbon method, LQ = 1 mg^{C}·L^{-1}). Ion Chromatography (Metrohm 850 Professional IC) for cations quantification (eluent mixture of PDCA 1.3 mM / HNO$_3$ 8 mM; LQ = 0.25 mg·L^{-1}). The pH values were measured with a microelectrode calibrated at pH 7.00 and 12.45 (IUPAC Standard, Hach).

Uptake results of the binary system U(VI)/HCP are presented in *Figure 5-21*. R_d(U(VI)) values range from 300 to 70 m^3·kg^{-1} for U(VI) concentrations in solution (at equilibrium) from $3 \cdot 10^{-11}$ to $2 \cdot 10^{-6}$ mol·L^{-1}. These high R_d values are consistent with what is known about U(VI) uptake on HCP in literature data (Pointeau *et al.* (2004), Wieland *et al.* (2010) and references therein]. R_d values are constant up to $[U]_{eq} = 4 \cdot 10^{-9}$ mol·L^{-1} ($[U]_{init} = 3 \cdot 10^{-6}$ mol·L^{-1}) which corresponds to the linear part of the isotherm ($[U(VI)]_{solid} = f([U(VI)]_{solution})$). Beyond this point, R_d values decrease indicating the progressive saturation of a sorption site.
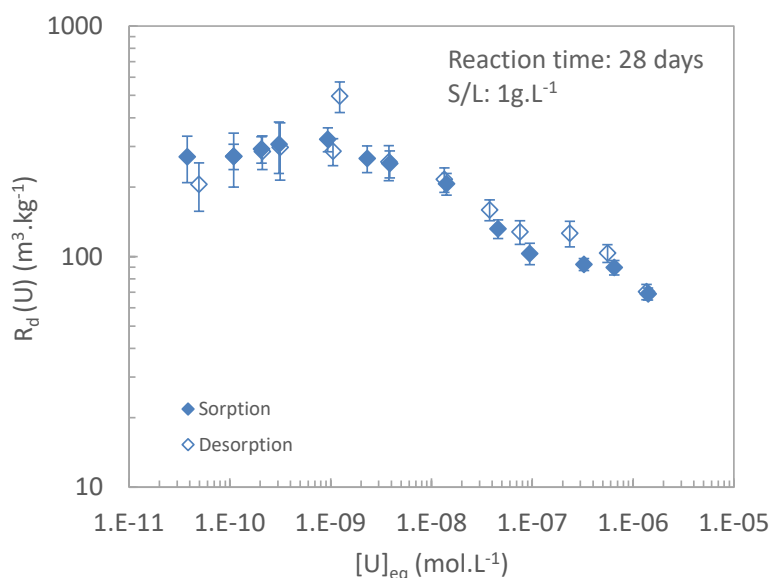
Figure 5-21:   U(VI) sorption and desorption isotherms on HCP Stage II.

Desorption experiment shows that sorption and desorption isotherms exhibit similar R_d values which indicates that uranium uptake seems to be reversible. This is confirmed by kinetics experiments (*Figure 5-22*). Taking into account uncertainties, Uranium uptake shows a reversible behavior up to, at least 28 days of sorption. This suggests that, for these (rather) short-term experiments, uranium uptake is dominated by a surface sorption process.

EURAD (Deliverables n° 3.6, 3.7 and 3.8) - Final Report of results generated in CORI
Dissemination level: PU
Date of issue of this report: **05/07/2024**

Page 167
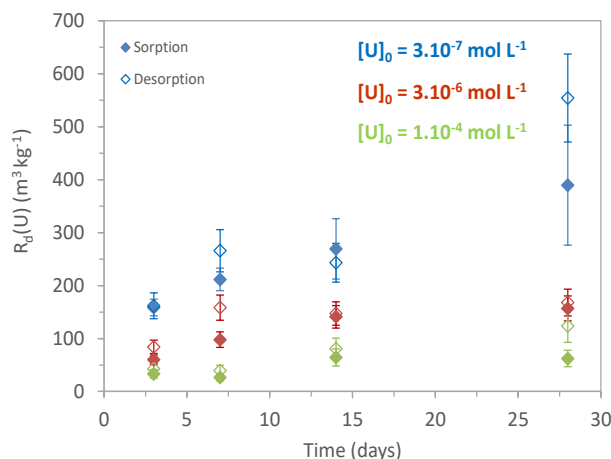
Figure 5-22:   *U(VI) sorption and desorption isotherms on HCP Stage II.*

U(VI) uptake by cementitious materials has been already explained in terms of inner-sphere complexation on the surfaces of the cement particles (Pointeau *et al.* (2004), Sutton *et al.* (2003)). In addition, C-S-H phases are described as the uptake-controlling phases for U(VI) immobilization.

In particular, Tits *et al.* (2015) have demonstrated from TRLFS studies that U(VI) complexes can be either sorbed as inner-sphere complexes on C-S-H surface silanol sites or incorporated into C-S-H interlayers Tits *et al.* (2015). Moreover, Macé *et al.* (2013) have shown from EXAFS data that U(VI) is taken up as $UO_2(OH)_4^{2-}$ type species by C-S-H surface. Androniuk *et al.* (2017) have also shown, by performing Molecular dynamics (MD) simulations, that U(VI) can sorb on several sites onto C-S-H surface (as mono- or bidentate species) and that a competition with calcium for these sorption sites should be expected.

More recent MD simulations have shown that, in presence of calcium (in alkaline solutions), a strong interaction between U(VI) hydroxyl species and Ca^{2+} exists suggesting the formation of a stable Ca-uranyl complex at the C-S-H aqueous interfaces (Androniuk and Kalinchev, (2020)). The stabilisation of complexes by Ca^{2+} ions, in alkaline solutions, have been already observed for other actinides (Altmaier *et al.* (2008); Tasi *et al.*, (2018)) and thus may be expected for U(VI) complexes.

The uptake results for the ISA/HCP binary system are reported in *Figure 5-23*. R_d(ISA) values diminish from 180 to 14 L·kg^{-1} for ISA concentrations in solution ranging from 10^{-4} up to $2\cdot10^{-2}$ mol·L^{-1}. Literature data for R_d(ISA) values on CEM V HCP are very limited (only one dataset from Garcia *et al.* (2020)), but the same trend has been already reported for CEM I HCP (Jo *et al.* (2022)).
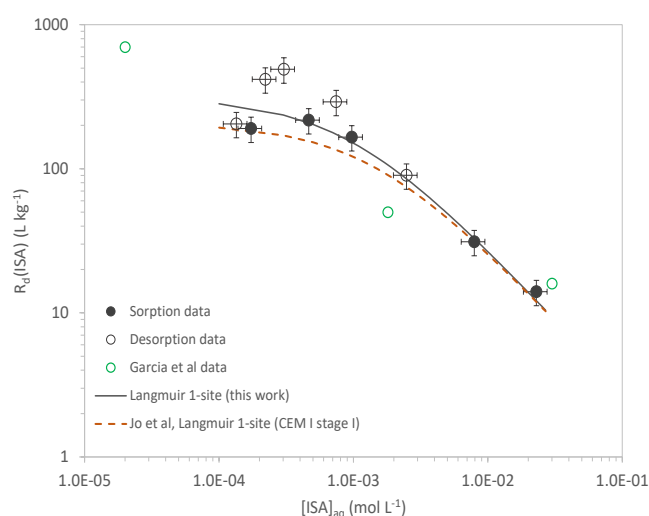
Figure 5-23:   *ISA sorption/desorption isotherms on HCP Stage II (contact time 32 days; S/L = 1 g·L^{-1}).*

EURAD (Deliverables n° 3.6, 3.7 and 3.8) - Final Report of results generated in CORI
Dissemination level: PU
Date of issue of this report: **05/07/2024**

Page 168

The comparison with Garcia's data (obtained on the exact same CEM V HCP) is reasonably good for ISA concentration in solution above 10^{-4} mol·L^{-1}. The observed decrease of R_d(ISA) values with increasing [ISA]$_{aq}$ is consistent with a progressive saturation of a sorption site. ISA data sorption have been successfully fit using a one-site Langmuir isotherm as described below:

$$[ISA]_{solid} = \frac{K_{ads} \times S_{max} \times [ISA]_{aq}}{1 + K_{ads} \times [ISA]_{aq}}$$

Equation 21

where [ISA]$_{solid}$ is the concentration of ISA sorbed on HCP (mol·kg^{-1}), [ISA]$_{aq}$ is the concentration of ISA in the aqueous phase after sorption (mol·L^{-1}), K_{ads} and S_{max} stand for the adsorption affinity constant (L·mol^{-1}) and the adsorption capacity (mol·kg^{-1}) respectively.

The fit, reported as the black solid line results in K_{ads} = (1081 ± 330) L·mol^{-1} and S_{max} = (0.29 ± 0.02) mol·kg^{-1} and shows a good description of ISA sorption data.

Comparison with literature data shows that Garcia *et al.* (2020) did not succeed in fitting their ISA sorption data with a one-site Langmuir isotherm, especially at low ISA concentration (below 10^{-4} mol·L^{-1}) probably because of a too limited number of data points. Jo *et al* proposed the same model for fitting ISA sorption data on a CEM I HCP at Stage I (Jo *et al.* (2022)). The fitted values obtained for the sorption parameters are close to ours (K_{ads} = (714 ± 266) L·mol^{-1} and S_{max} = (0.29 ± 0.04) mol·kg^{-1}) and are reported on *Figure 5-23* as a dashed line.

Nevertheless, desorption experiments consecutively performed to the sorption step show that an irreversible sorption process seems to occur. This result clearly prevents the use of Langmuir isotherm (based on a reversible sorption process) for interpreting ISA sorption data. A more detailed model is then needed. The role of Ca as a bridge between the surface of cement (or C-S-H) and polyhydroxocarboxylic acids (ISA or gluconic acid) has been already reported (Androniuk and Kalinchev, (2020); Jo *et al.* (2022); Pointeau *et al.* (2008)). The model proposed by Pointeau *et al.* (2008) for CEM I HCP assuming the formation of a surface complex with a Ca-bridging (>SOCaISA) was successfully applied for a CEM I HCP (Stage II) by Bruno *et al* (2018). This model would be then a good option for interpreting the ISA sorption data on CEM V HCP (Stage II).

For the U(VI)/ISA/ HCP ternary system the results of uranium in presence of ISA are reported *Figure 5-24*. R_d(U(VI)) values range are from 1000 to 3 m^3·kg^{-1} and from 50 to 0.9 m^3·kg^{-1} for initial U(VI) concentrations of 10^{-7} and 10^{-4} mol·L^{-1} respectively. For both U(VI) initial concentrations, the presence of ISA has a strong impact on uranium behavior. In fact, for ISA concentrations above $2 \cdot 10^{-4}$ mol·L^{-1}, R_d(VI) values decrease almost linearly by a factor of 330 or 60 for initial U(VI) concentrations of 10^{-7} and 10^{-4} mol·L^{-1} respectively.
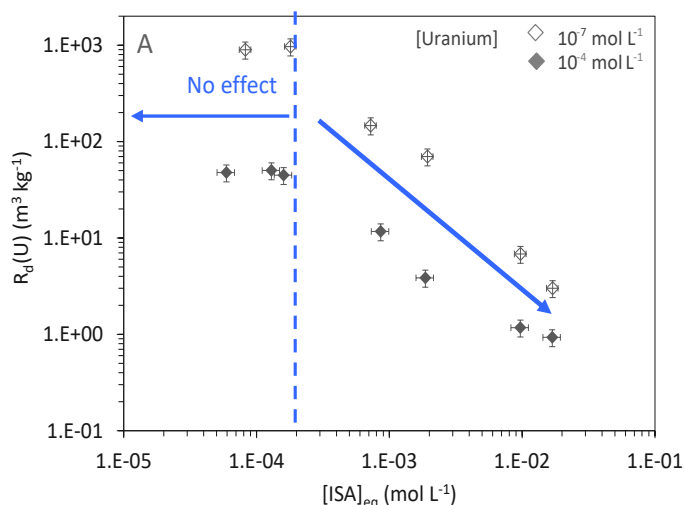
Figure 5-24: U(VI) sorption isotherm in presence of ISA (Solid/Liquid = 10^{-3} kg·L^{-1}).

EURAD (Deliverables n° 3.6, 3.7 and 3.8) - Final Report of results generated in CORI
Dissemination level: PU
Date of issue of this report: **05/07/2024**

Page 169

The same behavior has already been reported by Pointeau *et al.* (2018) for a CEM I HCP at Stage I and III for which the ISA threshold concentration stands in the same order of magnitude even a bit higher, *i.e.* about 10^{-3} mol·L^{-1} compare to of $2 \cdot 10^{-4}$ mol·L^{-1}. Similar observations have been recently reported for the uptake of Nb(V) (CEM I HCP Stage I) by Çevirim-Papaioannou *et al.* (2023) and Pu(IV) (CEM I HCP Stage II) by Tasi *et al.* (2021).

ISA is found to decrease the uptake of these radionuclides for concentration above 10^{-3} mol·L^{-1}. This effect is explained by the possible formation of stable Ca-RN-ISA complexes in the aqueous phase. The same observation was reported by Wieland *et al.* (2002) for Th(IV). Similarly, the formation of a stable aqueous ternary complex Ca-U(VI)-ISA is expected for explaining U(VI) sorption behavior in presence of ISA.

[CNRS-SUBATECH] studied the U(VI)/HCP binary system also by means of diffusion experiments. The experiment lasted 505 days. As expected for an in-diffusion experiment, no uranium was measured in the downstream compartment. The follow-up of U(VI) concentration in the upstream compartment was, as designed, consistent with a control by the solubility of Ca-Uranate phase (CaUO$_4$·H$_2$O) *i.e.* $(5.60 \pm 0.84) \cdot 10^{-8}$ mol·L^{-1}. Uranium distribution profiles in the HCP sample were quantified by Laser ablation HR-ICP-MS at two different locations (*Figure 5-25*).
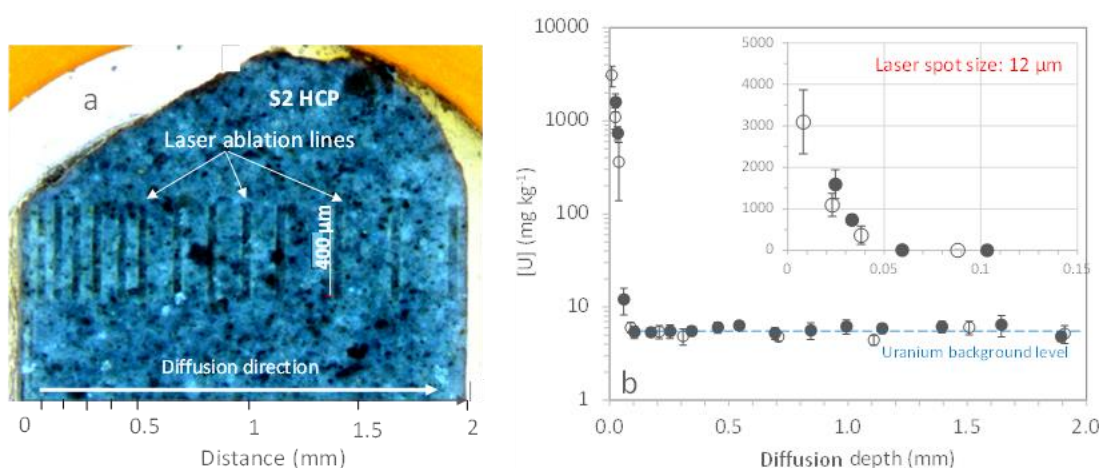
Figure 5-25:   *Uranium distribution in a S2 disk after 505 days of diffusion: (a) Laser ablation HR-ICP-MS analyses; (b) Uranium profiles (each point = average of data from 400 μm-long ablation line; quantification NIST 610).*

Results show that uranium is heterogeneously distributed as it is mostly located close to the surface. Nevertheless, the two distribution profiles can be superimposed meaning that the radial diffusion of uranium is homogenous. Uranium concentration in solid decreases from 3000 mg·kg^{-1} (at the surface) to 5.5 mg·kg^{-1} (HCP background concentration) over about 40 μm (*Figure 5-25*b). This very short distance of penetration is consistent with either the strong sorption of U(VI) onto HCP and/or a very slow diffusion process.

A similar observation was reported by Wieland *et al* (2010) from an in-diffusion experiment of U(VI) through a CEM I HCP (Stage I). The authors found a penetration depth of about 10 μm after 9 months of diffusion.

To move a bit further, we plan to interpret the uranium distribution profiles with a 1D-analytical solution based on the resolution of Fick 2nd law to obtain an estimation of uranium apparent diffusion coefficient.

Diffusion tests were carried out also in the ternary U(VI)/ISA/HCP system. The experiment lasted 400 days. The follow-up of U(VI) and ISA concentration is reported *Figure 5-26*. A very slight diminution of both concentrations is observed but there is no visible precipitation in the upstream compartment. As expected, no uranium is measured in the downstream compartment.

EURAD (Deliverables n° 3.6, 3.7 and 3.8) - Final Report of results generated in CORI
Dissemination level: PU
Date of issue of this report: **05/07/2024**

Page 170
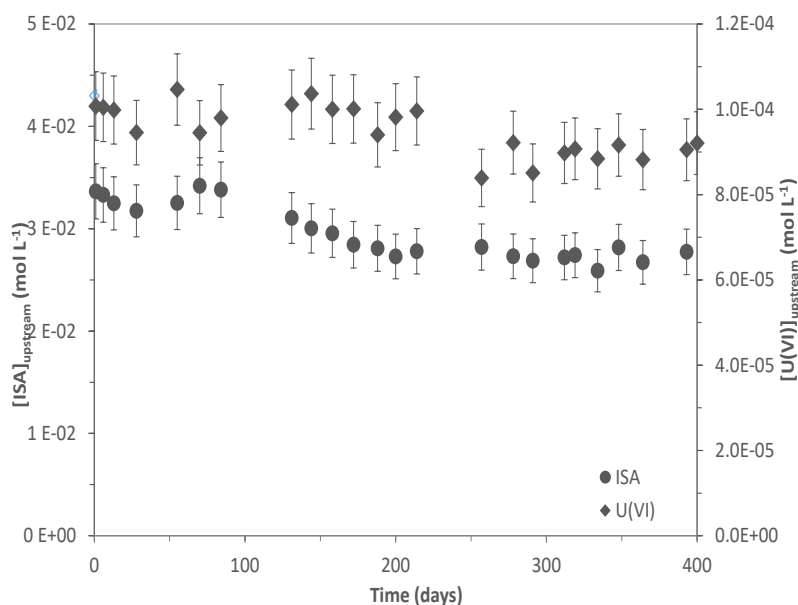
Figure 5-26:   *In-diffusion on ternary U(VI)/ISA/HCP at Stage II: Follow-up of U(VI) and ISA concentrations in the upstream compartment.*

A uranium distribution profile acquired after 400 days of diffusion by laser ablation HR-ICP-MS, is reported in *Figure 5-27*. This result shows that uranium is located at or very close to the surface (penetration depth around 10 µm only) with a very sharp decrease reaching the HCP background concentration after only 40 µm. Uranium profile in presence of ISA (ternary system) seems to be sharper than in absence of ISA (binary system) which could mean that ISA may reduce the penetration of uranium inside HCP.
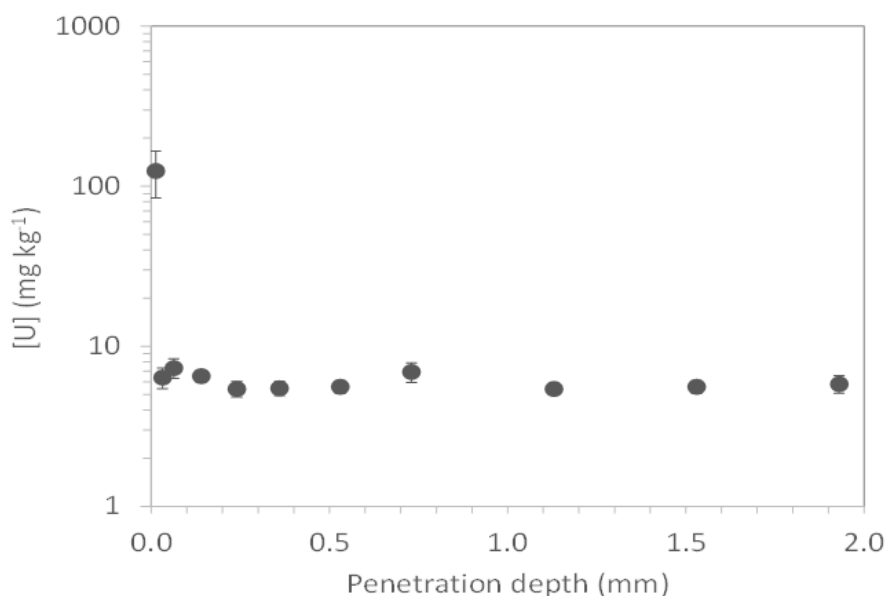
Figure 5-27:   *In-diffusion profile of uranium in presence of ISA and in S2 solution after 400 days (each point = average of data from a 400 µm-long ablation line; quantification NIST 610).*

Regarding Stage III, the uptake results for the U(VI)/HCP binary system are presented in *Figure 5-28*.

EURAD (Deliverables n° 3.6, 3.7 and 3.8) - Final Report of results generated in CORI
Dissemination level: PU
Date of issue of this report: **05/07/2024**

Page 171
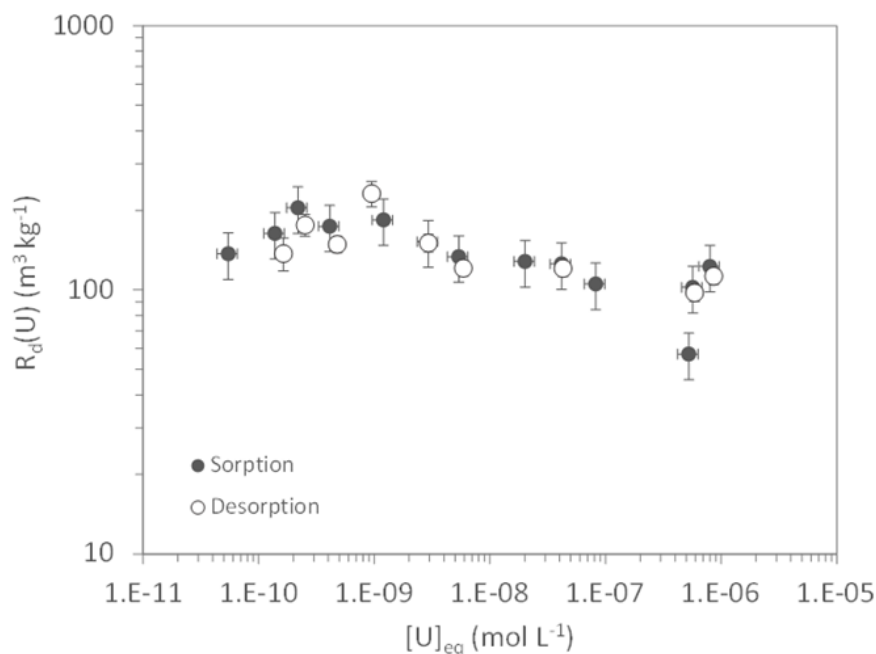
Figure 5-28:   *U(VI) uptake on HCP Stage III (duration 32 days ; S/L = 10^{-3} kg·L^{-1}).*

R_d(U(VI)) values range from 190 to 60 m^3· kg^{-1} for U(VI) concentrations in solution (at equilibrium) from $6\cdot10^{-11}$ to $8\cdot10^{-7}$ mol·L^{-1}. The pH value is constant at 11.7. These high R_d values are consistent with R_d values reported by Pointeau *et al.* (2004) for a CEM V HCP at Stage III.

R_d values are constant up to $[U]_{eq} = 8.2\cdot10^{-8}$ mol·L^{-1} ($[U]_{init} = 8.7\cdot10^{-6}$ mol·L^{-1}), then slightly decrease up to $[U]_{eq} = 5.2\cdot10^{-7}$ mol·L^{-1} and start to increase again above this concentration meaning that a precipitation process might occur. The operational solubility limit for uranium at Stage III was beforehand measured to be $[U]_{lim} = (2.7 \pm 0.4)\cdot10^{-6}$ mol·L^{-1} which is consistent with the value reported by Pointeau *et al* (2004) *i.e.* $[U]_{lim} = (4 \pm 1)\cdot10^{-6}$ mol·L^{-1} at pH 11.7. Taking into account uncertainties, uranium uptake shows a reversible behavior up to, at least 32 days of sorption.

For the ISA/HCP binary system, results obtained from the sorption experiment ($[ISA]_{eq}$ ranging from 4.6 10^{-4} to $3\cdot10^{-2}$ mol·L^{-1}; S/L = $5\cdot10^{-3}$ kg·L^{-1}; pH = 11.7) gave low and unfortunately not very precise R_d(ISA) values (<10 L·kg^{-1}). Nevertheless, a punctual experiment performed at a higher S/L value ($1.7\cdot10^{-2}$ kg·L^{-1}) confirmed this trend. However, these results are consistent with data reported by Pointeau *et al.* (2008) for ISA sorption on a CEM I HCP. For pH values ranging from 11.5 to 11.8 (*i.e.* corresponding to the Stage III conditions), R_d(ISA) values ranged from 0 to (25 ± 15) L·kg^{-1}. Assuming the formation of a surface complex with a Ca-bridging (>SOCaISA) as the process for ISA sorption on HCP, the decrease of R_d(ISA) at Stage III (compare to Stage II) is interpreted to be due to the progressive decrease or even absence of calcium in solution.

For the U(VI)/ISA/ HCP ternary system, the results obtained for uranium in presence of ISA and in Stage III are reported *Figure 5-29*. R_d(U(VI)) values range are from 100 to 0.3 m^3· kg^{-1} for initial U(VI) concentrations of 10^{-7} and $3\cdot10^{-5}$ mol·L^{-1}. As for Stage II, for both U(VI) initial concentrations, the presence of ISA has a strong impact on uranium behavior. In fact, for ISA concentrations above $3\cdot10^{-4}$ mol·L^{-1}, R_d(U(VI)) values decrease almost linearly by a factor of 330. All these results are consistent with the change of uranium speciation in presence of ISA (formation of U/ISA complexes) which prevents the sorption of uranium on HCP.

EURAD (Deliverables n° 3.6, 3.7 and 3.8) - Final Report of results generated in CORI   Page 172
Dissemination level: PU
Date of issue of this report: **05/07/2024**
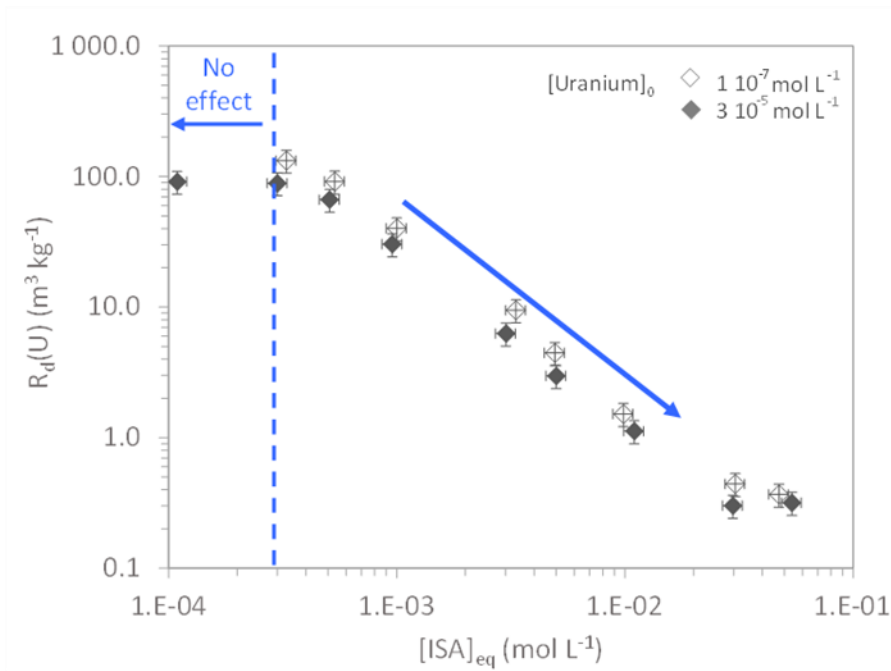
Figure 5-29: U(VI) uptake on HCP Stage III in presence of ISA (contact time = 28 days; S/L = 10^{-3} kg·L^{-1}).

For what concerns diffusion experiments in U(VI)/HCP binary system, the in-diffusion experiment has been completed after a diffusion time of 275 days. The initial uranium concentration (upstream compartment) was $2 \cdot 10^{-6}$ mol·L^{-1} (below the operational solubility of uranium in S3 solution). As expected, no uranium is measured in the downstream compartment. The follow-up in the upstream compartment is reported in *Figure 5-30*. A clear decrease of uranium concentration is observed down to a constant value at $4 \cdot 10^{-9}$ mol·L^{-1} (plateau zone) which is reached after 100 days. The decrease shows an initial fast step (after one day) where uranium concentration falls to $7 \cdot 10^{-7}$ mol·L^{-1} then a more progressive step over the next 50 days for reaching the plateau zone. No visible precipitation is observed in the compartment. The initial rapid diminution of uranium concentration may be attributed to the strong interaction of uranium at the solid/solution interface.
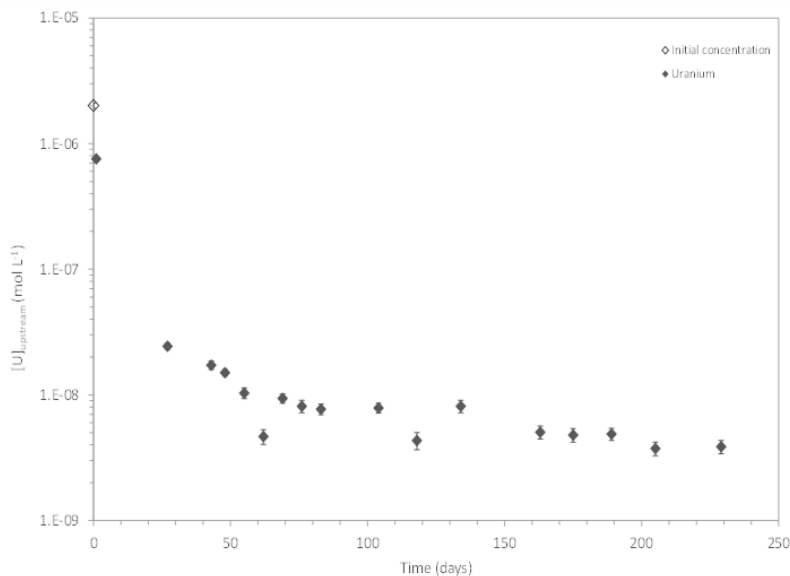
Figure 5-30: In-diffusion experiment on binary U(VI)/HCP (Stage III): Follow-up of U(VI) concentration in the upstream compartment.

EURAD (Deliverables n° 3.6, 3.7 and 3.8) - Final Report of results generated in CORI
Dissemination level: PU
Date of issue of this report: **05/07/2024**

Page 173

Finally, for the U(VI)/ISA/HCP ternary system in-diffusion experiment has been completed after 275 days. The initial concentrations in the upstream compartment were $2\cdot10^{-6}$ mol·L^{-1} and $3\cdot10^{-2}$ mol·L^{-1} for uranium and ISA respectively. As expected, no uranium is measured in the downstream compartment.
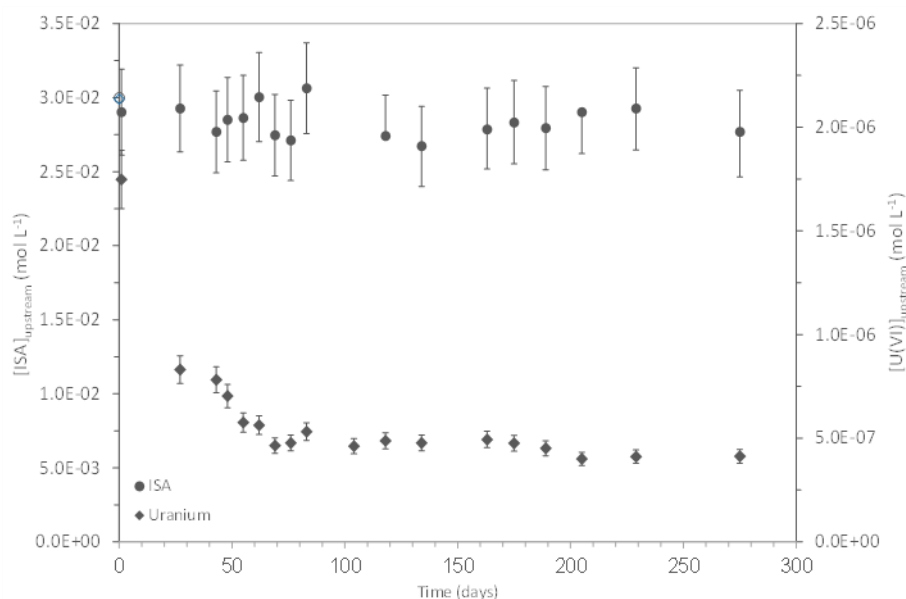
Figure 5-31:   *In-diffusion experiment on ternary U(VI)/ISA/HCP (Stage III): Follow-up of U(VI) and ISA concentrations in the upstream compartment.*

The follow-up in the upstream compartment is reported *Figure 5-31*. For ISA, no variation is observed, and the upstream concentration has been staying equal to the initial value over the whole duration of the experiment. This was expected as it is consistent with batch experiment results which showed a low (or absent) sorption of ISA on HCP in S3 conditions.

Uranium exhibits a trend quite similar to what has been reported for the binary U(VI)/HCP system. A decrease of its concentration is observed down to a constant value at $4\cdot10^{-7}$ mol·L^{-1} (plateau zone) which is reached after 70 days. No visible precipitation occurs in the compartment. These first observations suggest that the presence of ISA in excess towards uranium has a strong impact on the interaction between uranium and the solid sample (S3 HCP disk) by keeping uranium in the aqueous phase probably as U-ISA complexes.

Two uranium distribution profiles (acquired by laser ablation HR-ICP-MS) located at two different zones of the S3 HCP disk (centre and edge) are reported in *Figure 5-32*. As a first observation, the radial diffusion of uranium in the S3 disk appears to be homogeneous as the two profiles can be superimposed. Uranium concentration in solid decreases from 150 mg·kg^{-1} (at the surface) to 5.5 mg·kg^{-1} (HCP background concentration) over about 720 µm. Complementary XRD analysis (data not shown), performed on the same S3 HCP disk allowed to estimate the depth of the degraded zone [670-720 µm] and the position of the degradation fronts (upstream side): [170-220 µm] for ettringite and [670-720 µm] for portlandite. These first observations are consistent with a deep penetration of uranium inside the degraded zone which could be (at least partly) linked to the change of mineralogy in the degraded zone and the presence of ISA (to be confirmed).

EURAD (Deliverables n° 3.6, 3.7 and 3.8) - Final Report of results generated in CORI
Dissemination level: PU
Date of issue of this report: **05/07/2024**

Page 174
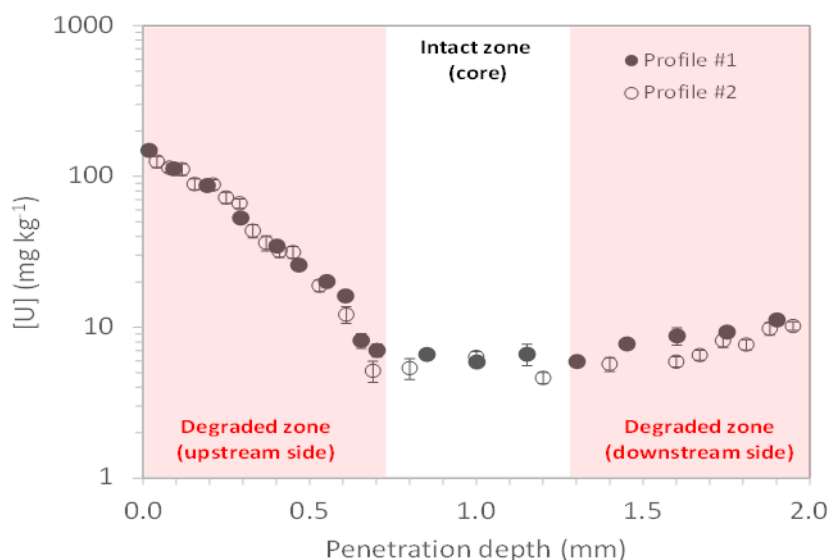
Figure 5-32: In-diffusion experiment on ternary U(VI)/ISA/HCP (Stage III): uranium distribution profiles located at the centre (profile #1) and the edge (profile #2) in the S3 HCP disk.

5.2 EDTA, NTA

The effect of EDTA on RNs retention/migration processes has been analyzed by [**CEA**], [**CTU**], [**JGU**], [**SURAO**] and [**UCYPRUS**]. [**HZDR**] and [**UPPC**] studied NTA.

[**CEA**] analyzed the migration of ^{63}Ni(II) and ^{238}U(VI) through altered cement pastes at Stage II in presence of EDTA**.** The operational solubility of U in the water representing the cement Stage II and Stage IV in the presence of the organic was determined first to investigate the starting parameters for the sorption and diffusion experiments. The assumption is that the solubility increases by the addition of organics. The U is added in a concentration of $8.4 \cdot 10^{-5}$ M in the Stage II system and $6.8 \cdot 10^{-5}$ M in the Stage IV system. The pH is adjusted to 9.5 by adding NaOH in the Stage IV samples. The organics are added in a concentration range of $5 \cdot 10^{-10} – 10^{-3}$ M and $10^{-7} – 10^{-2}$ M in Stage II and Stage IV, respectively. All manipulations of the samples in the Stage II water are performed in the N_2 filled glovebox to avoid atmospheric carbonation. All manipulations of the samples in Stage IV water are performed in air.

The operational solubility of Ni is determined with similar the experimental conditions. Ni is added to all tubes in $3.5 \cdot 10^{-5}$ M, in combination with 800 Bq/mL ^{63}Ni. The organic Na-EDTA is added in a concentration range of $2 \cdot 10^{-7} – 2 \cdot 10^{-2}$ M.

Figure 5-33 represents the effect of the presence of organics on the evolution of U concentration in Stage II water for different contact times, ranging from 49 days to 238 days.

EURAD (Deliverables n° 3.6, 3.7 and 3.8) - Final Report of results generated in CORI
Dissemination level: PU
Date of issue of this report: **05/07/2024**

Page 175
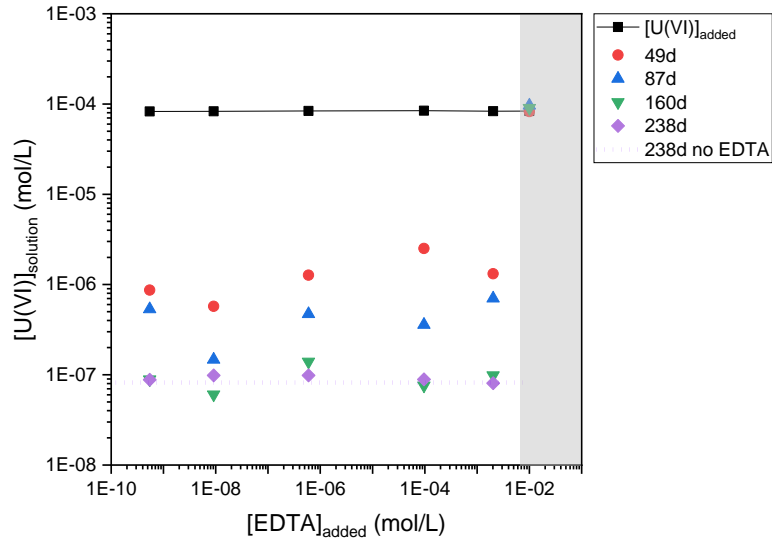
Figure 5-33:   Effect of the presence of EDTA on the evolution of U concentration in Stage II solution for different contact times. Data in the grey zone should be discarded due to uncontrolled experimental conditions.

The U concentration decreases over time from 10^{-6} M to 10^{-7} M in the presence of EDTA. No significant difference in the U concentration is noted between 160 and 238 days. The solubility for the longer contact time investigated is similar to one without organics. After equilibration, the U concentration is too low for TRLFS measurements.

Figure 5-34 represents the effect of the presence of EDTA on the evolution of U concentration in Stage IV water for different contact times, ranging from 1 day to 28 days. The U concentration in the presence of organics is lower than without organics. With the highest EDTA concentration, an increase in the U concentration is observed. pH decreases in the presence of EDTA, with 9.2, 8.5 and 7.1 at respectively 5, 15 and 28 days. It is suspected that the increase in solubility over time is a pH effect.
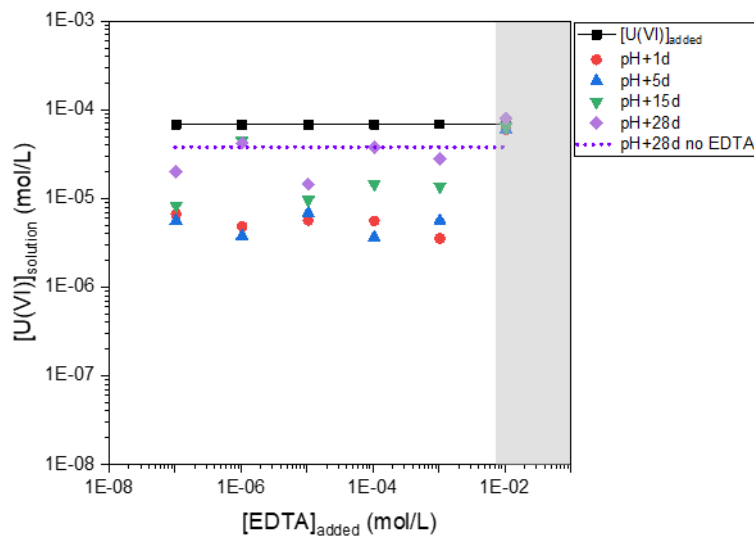
Figure 5-34:   The effect of the presence of EDTA on the evolution of U concentration in Stage IV solution for different contact times. Data in the grey zone should be discarded due to uncontrolled experimental conditions.

EURAD (Deliverables n° 3.6, 3.7 and 3.8) - Final Report of results generated in CORI
Dissemination level: PU
Date of issue of this report: **05/07/2024**

Page 176

The TRLFS spectra presented in the *Figure 5-35* suggest that the EDTA interacts with the complexes at the highest concentration.
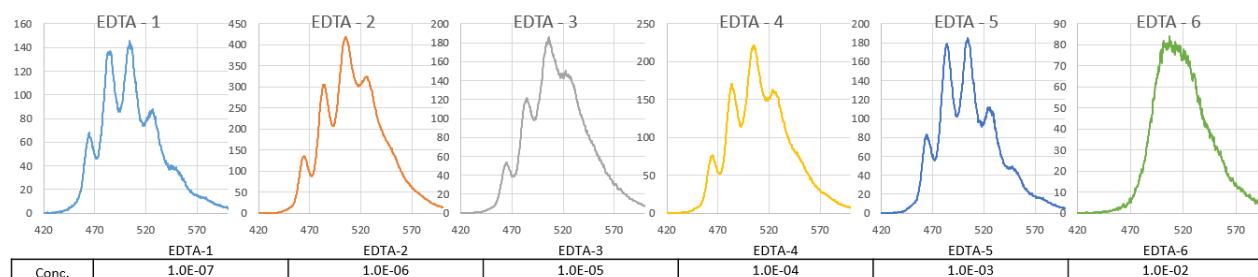
Figure 5-35:   *TRLFS spectra of the U- EDTA solubility experiment in Stage IV solution.*

Figure 5-36 represents the effect of the presence of organics on the evolution of Ni concentration in ACW Stage II for different contact times, ranging from 2 days to 449 days.
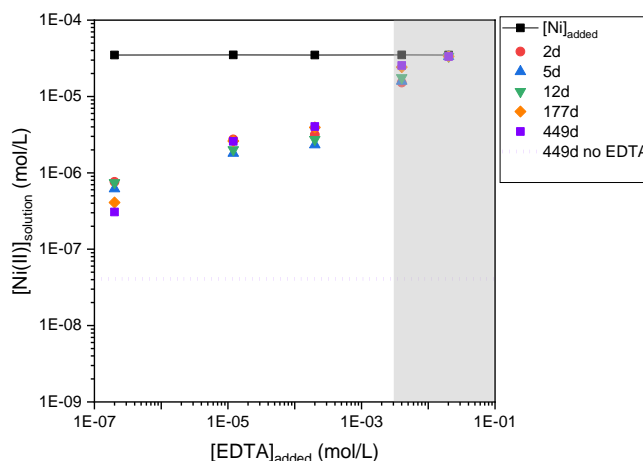
Figure 5-36:   *The effect of the presence of EDTA on the evolution of Ni concentration in Stage II solution for different contact times. Data in the grey zone should be discarded due to uncontrolled experimental conditions.*

The residual Ni concentration after 449 days in the absence of organics is $4 \cdot 10^{-8}$ M. In the presence of small amount of EDTA, the Ni concentration increases in solution and with higher EDTA concentrations, the Ni concentration in solution reach $4 \cdot 10^{-6}$ M (*Figure 5-36*).

The measured residual Ni concentration as a function of time and organic species concentration is presented in the *Figure 5-37* for the Stage IV solution.

EURAD (Deliverables n° 3.6, 3.7 and 3.8) - Final Report of results generated in CORI
Dissemination level: PU
Date of issue of this report: **05/07/2024**

Page 177
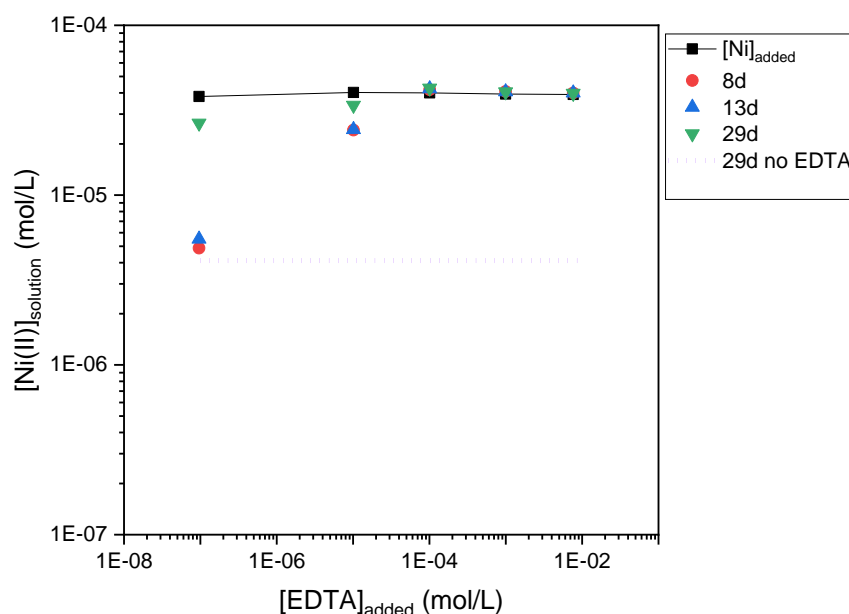
Figure 5-37:   The effect of the presence of EDTA on the evolution of Ni concentration in Stage IV solution for HCP CEM V/A and different contact times.

Ni concentration in solution increase with time and for most investigated organic concentration and tend to reach a plateau at $4 \cdot 10^{-5}$ M, *i.e.* the Ni added concentration. As many pH adjustments were necessary before and after sampling, and some solid precipitation occurs with time in the filtrated oversaturated calcite solution, these solubility results are difficult to interpret. Due to its low amount, it was not possible to characterize the solid. Data obtained after 29 days of contact time are strongly influenced by change in pH.

Figure 5-38 represents the U(VI) retention results obtained in the presence of EDTA on HCP CEM V/A at Stage II and for and different contact times, ranging from 2 days to 33 days. The U(VI) sorption is still significant ($R_d \sim 10^5$ L/kg) independently of the introduced EDTA concentration and contact time.
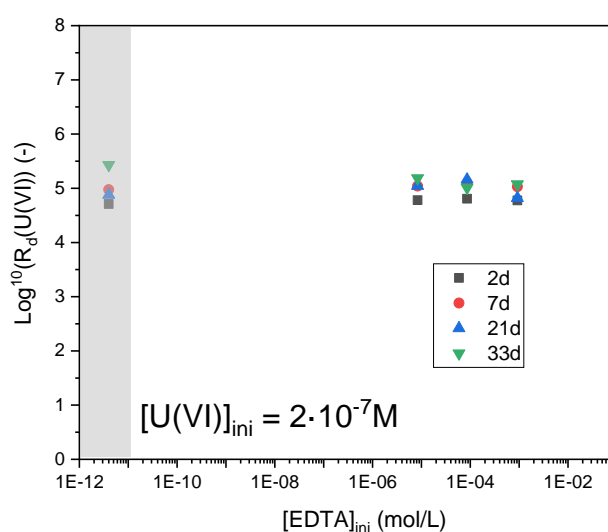
Figure 5-38:   The effect of the presence of EDTA on the retention of U(VI) in HCP CEM V/A at Stage(II) and different contact times. The grey zone corresponds to sorption data obtained in absence of organic species.

EURAD (Deliverables n° 3.6, 3.7 and 3.8) - Final Report of results generated in CORI
Dissemination level: PU
Date of issue of this report: **05/07/2024**

Page 178

Figure 5-39 represents the experimental U(VI) retention results obtained in the presence of EDTA on the RCM sample degraded at Stage II, for different contact times, ranging from 2 days to 92 days. In both cases, there is an increase of the R_d value with time. For the highest organic concentration addition, pH of the resulting supernatant was not checked, and the data should not be included in the interpretation. For an initial U(VI) concentration of $5 \cdot 10^{-7}$M, there is a limited effect of the nature of the organic species onto the U(VI) retention.
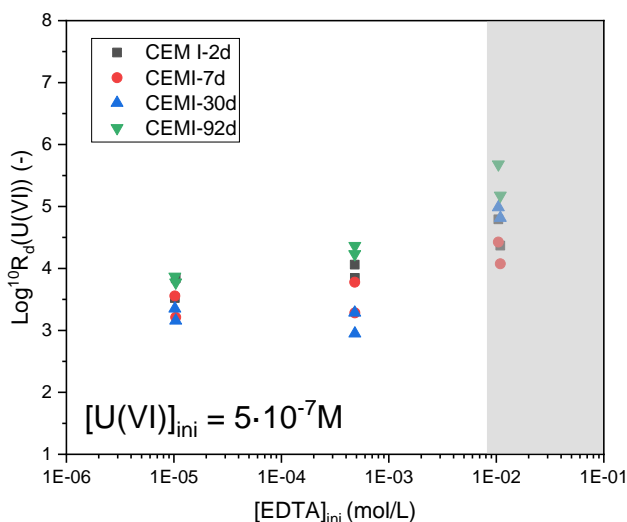
Figure 5-39: *The effect of the presence of EDTA on the retention of U(VI) in for RCM at Stage II and different contact times. Data in the grey zone should be discarded due to uncontrolled experimental conditions.*

Figure 5-40 represents the experimental U(VI) retention results obtained in the presence of EDTA on HCP CEM V/A at Stage III/IV and for and different contact times, ranging from 2 days to 33 days. For the EDTA system, the U(VI) sorption is still significant ($R_d \sim 10^5$ L/kg) and is higher with the contact time. For an initial EDTA concentration up to 10^{-3}M, the R_d value tends to decrease, suggesting a saturation of sorption site.
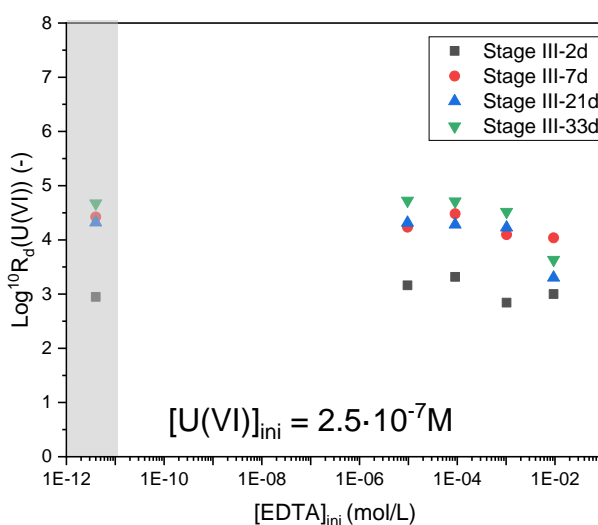
Figure 5-40: *The effect of the presence of EDTA on the retention of U(VI) at Stage III/IV for HCP CEM V/A and different contact times. The grey zone corresponds to sorption data obtained in absence of organic species.*

EURAD (Deliverables n° 3.6, 3.7 and 3.8) - Final Report of results generated in CORI
Dissemination level: PU
Date of issue of this report: **05/07/2024**

Page 179

Figure 5-41 represents the experimental Ni(II) retention in the presence of EDTA on HCP CEM V/A at Stage II and different contact time, ranging from 2 days to 33 days. No effects are observed on Ni retention in the presence of EDTA. Ni retention is significant and R_d values are ranging between 10^3 and 10^4 L/kg.
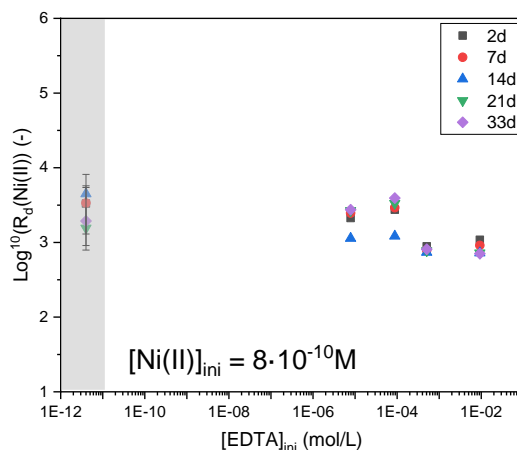
Figure 5-41:   *The effect of the presence of EDTA on the retention of Ni(II) HCP CEM V/A at Stage II and different contact times. The grey zone corresponds to sorption data obtained in absence of organic species.*

Figure 5-42 represents the experimental Ni(II) retention in the presence of EDTA on HCP CEM V/A in water at Stage III/IV with different contact time, ranging from 2 days to 33 days. In the presence of EDTA, the evolution of the R_d values with the organic concentration suggests a competition effect and/or a saturation of the sorption site for EDTA concentration higher than 10^{-4} M.
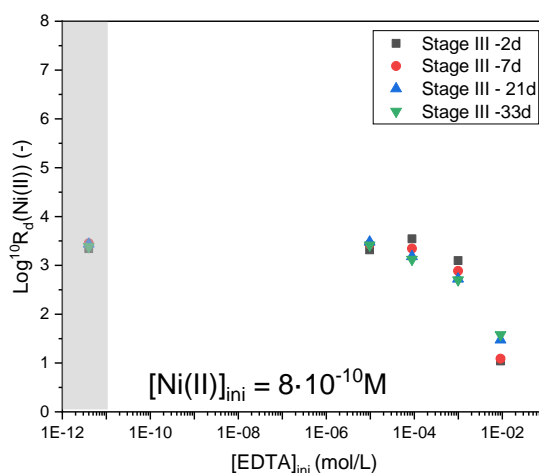
Figure 5-42:   *The effect of the presence of EDTA on the retention of Ni(II) on HCP CEM V/A Stage III/IV and different contact times. The grey rectangle corresponds to sorption data obtained in absence of organic species.*

For what concerns diffusion studies, different set-ups of diffusion cells have been used by **[CEA]** as described in Section 3.5.1. Three diffusion cells have been investigated with EDTA as organic species: two through-diffusion experiments and one in-diffusion experiment (see

Table 46).

EURAD (Deliverables n° 3.6, 3.7 and 3.8) - Final Report of results generated in CORI
Dissemination level: PU
Date of issue of this report: **05/07/2024**

Page 180

Table 46: Diffusion studies in presence of EDTA investigated by CEA

Name	Type of set-up	Material	System investigated
Cell-SIKADUR	through-diffusion – 2x100mL	Epoxy glu	HTO + ^{14}C-EDTA at $5 \cdot 10^{-2}$M in S2 + ^{238}U
Cell-F1	through-diffusion – 2x10mL	HCP CEM V/A Stage II	HTO + ^{14}C-EDTA at $5 \cdot 10^{-2}$M in S2 + ^{238}U
Cell-F2	in-diffusion – 1x10mL	HCP CEM V/A Stage II	EDTA at $5 \cdot 10^{-2}$M in S2+ ^{63}Ni

The compartments labelled "upstream reservoir" are filled with the Stage II solution then the stable organic solution is added with eventually some radioactive solution containing HTO and/or C-14 labelled organic. In the through-diffusion set-up, the second side is labelled "downstream reservoir" and filled with only Stage II solution.

In the cell containing the glue, SIKADUR, the upstream compartment was spiked with HTO solution (4.52 kBq/mL) at the beginning of the through diffusion experiment, after 192 days, the second radioactive tracer (^{14}C-EDTA) is added (320 Bq/mL) and finally after 445 days the last tracer (^{238}U) is added to the solution. The HTO and ^{14}C activities in the upstream and downstream compartments are not affected by the addition of the other tracers over all investigated diffusion times (see Figure 5-43).

(A) (B) (C) (D)
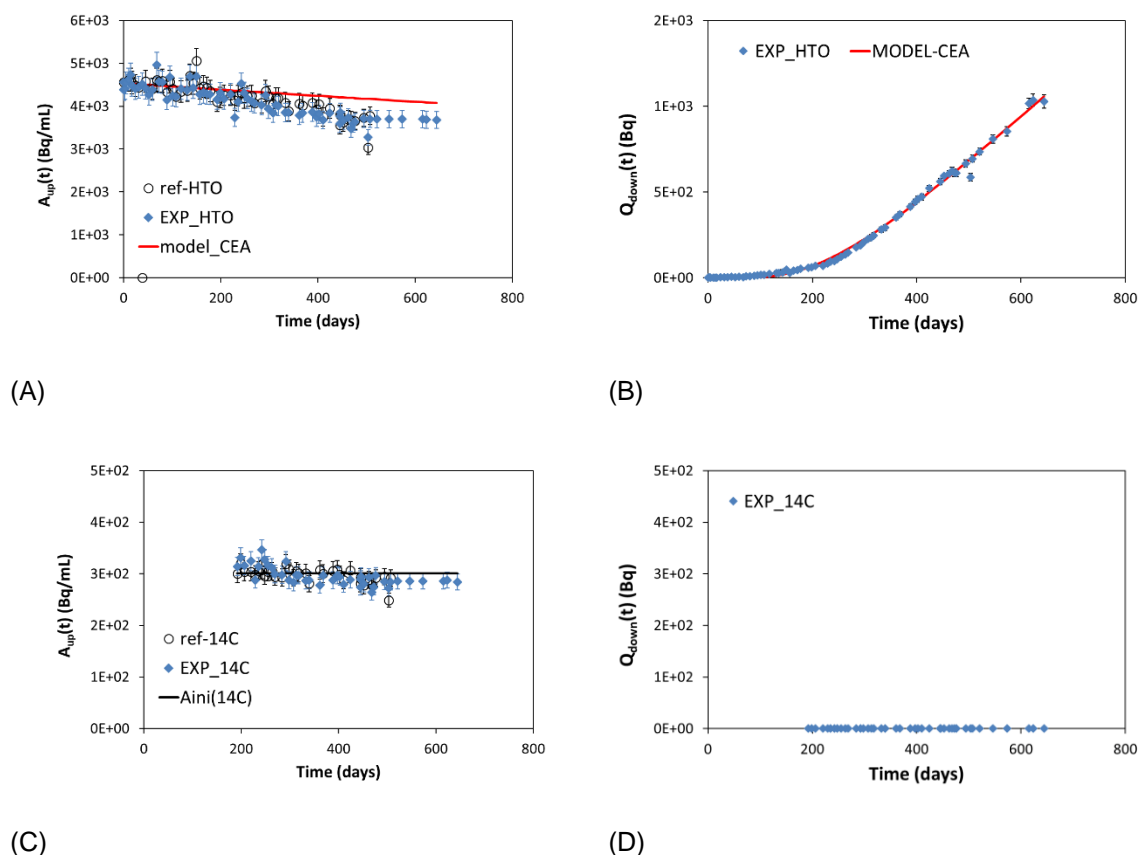
Figure 5-43: *Through-diffusion of HTO and ^{14}C-EDTA in a SIKADUR glue disk in stage II ACW solution over time. (A) Evolution of the activities of HTO in the upstream compartment (B) Evolution of the cumulative activity of HTO in the downstream compartment (C) Evolution of the activities of ^{14}C*

EURAD (Deliverables n° 3.6, 3.7 and 3.8) - Final Report of results generated in CORI
Dissemination level: PU
Date of issue of this report: **05/07/2024**

Page 181

in the upstream compartment (D) Evolution of the cumulative activity of ^{14}C in the downstream compartment.

The HTO diffusion parameter ($D_{a(HTO)}$ = 6.4·10^{-14} m^2/s) proposed in Task 3 to interpret the experimental data until the addition of ^{238}U is still acceptable in that case till the end of the diffusion experiments. Before and after the addition of ^{238}U, the measured ^{14}C activities follow the same trend: no ^{14}C activity is measured in the downstream compartment. Finally, the U(VI) concentration was measured in solution as a function of time by ICP-MS. Data are under treatment. Figure 5-44 corresponds to the HTO and ^{14}C-EDTA through-diffusion data for the HCP CEM V/A sample at Stage II. After 445 days, *i.e.* when the ^{238}U solution was added in the upstream compartment, the activities of HTO and ^{14}C were affected in the upstream compartment and the current model was not adjusted to fit the data. The major observation is the fact that the slight tracer uploading didn't affect their behavior in the downstream compartment.

(A)   (B)
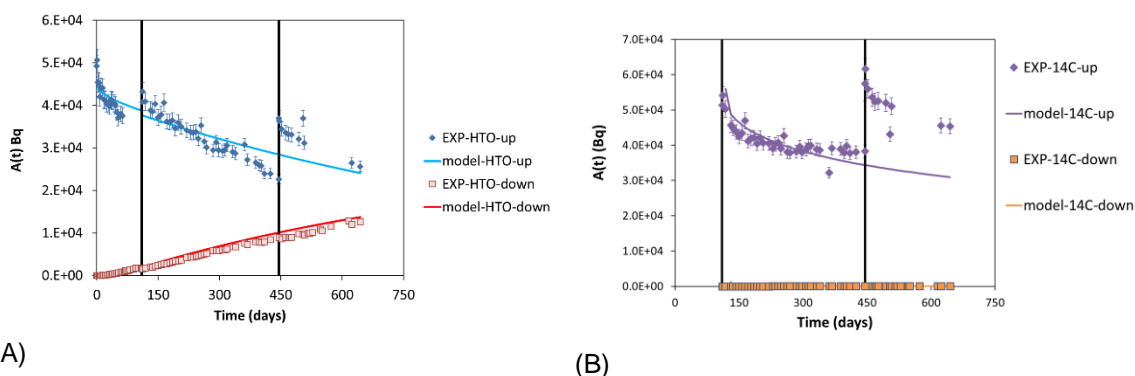
Figure 5-44:   Through diffusion of HTO (A) and ^{14}C-EDTA (B) in a CEM V/A disk in Stage II solution over time (F1 cell) – the black straight line at 110 days corresponds to the addition of ^{14}C-EDTA and the one at 445 days corresponds to the addition of ^{238}U in the upstream compartment.

[**CEA**] investigated the uranium diffusion in presence of EDTA in S2 solution and for two samples: epoxy resin (SIKADUR cell) and a CEM V/A HCP (F1 cell). For both experiments, the U(VI) concentration was measured in solution as a function of time by ICP-MS.

The results obtained for the SIKADUR cell are presented in *Figure 5-45*. From these results, 3 main observations can be highlighted: i) considering the measurements uncertainties, there is no uranium diffusion through the epoxy resin during *ca*. 200 days of investigation, ii) the organic species present in the upstream compartment, which is a mixture of EDTA and hydrolysis degradation product of the SIKADUR increased the solubility of uranium, compared to what was measured in the solution S2 with only EDTA (see "U-EDTA-S2-op.solubility" series in *Figure 5-45*) and iii) no sorption of U is observed on the surface of the SIKADUR sample.

EURAD (Deliverables n° 3.6, 3.7 and 3.8) - Final Report of results generated in CORI
Dissemination level: PU
Date of issue of this report: **05/07/2024**

Page 182
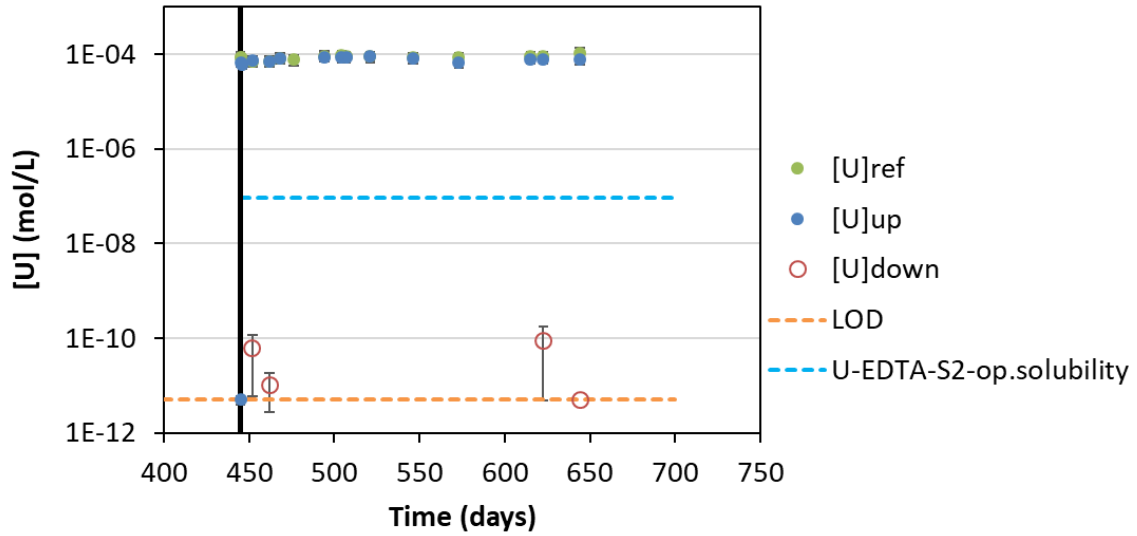
Figure 5-45: *Evolution of U(VI) in the upstream, downstream and reference solutions of cell containing the SIKADUR disk in Stage II solution and with an initial concentration of $5 \cdot 10^{-2}$ M of EDTA (SIKADUR cell)*

The results obtained for the F1-cell are presented in *Figure 5-46*. The results are quite different to what have been measured for the SIKADUR cell. In the upstream solution, the concentration of uranium decreased rapidly after the tracer addition and reached a plateau at $2.8 \cdot 10^{-7}$ M, which is higher than the value obtained in S2 solution in presence of only EDTA. This observation could be explained by a significant retention of U at the surface of the HCP sample and an increase of solubility of uranium due to the presence of the EDTA and SIKADUR degradation products in solution. From these results, it's difficult to consider that the amount of U measured in the downstream compartment is explained by its diffusion from the upstream compartment.
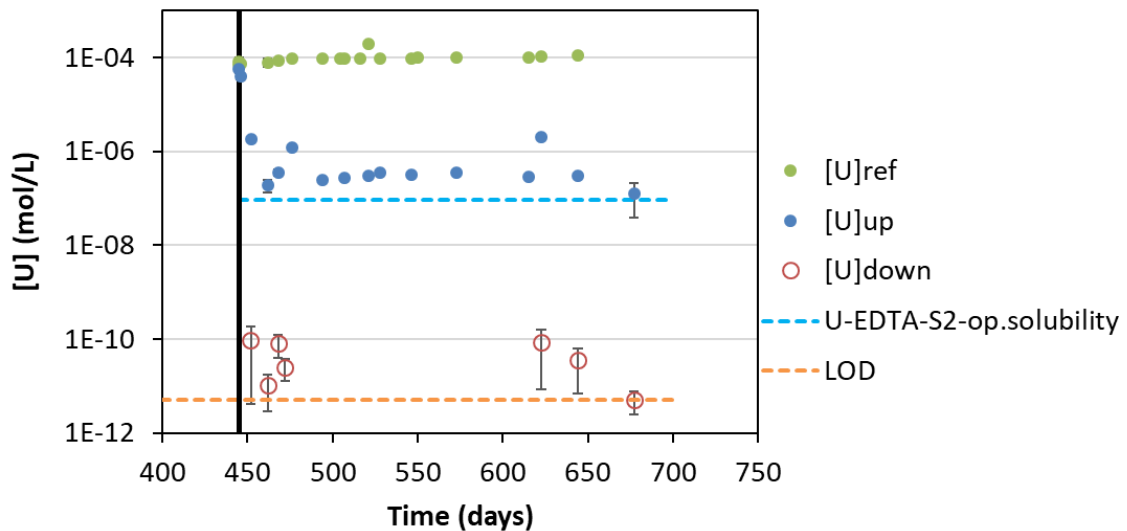
Figure 5-46: *Evolution of U(VI) in the upstream, downstream and reference solutions of cell containing the CEM V/A HCP disk in Stage II solution and with an initial concentration of $5 \cdot 10^{-2}$ M of EDTA (F1 cell)*

EURAD (Deliverables n° 3.6, 3.7 and 3.8) - Final Report of results generated in CORI
Dissemination level: PU
Date of issue of this report: **05/07/2024**

Page 183

For the F1 cell, 677 days after the initial addition of HTO and 232 days after the addition of U, the solid has been dismantled from the sample-holder. Then, the sample has been dried overnight before U diffusion profile determination. First, the dried-HCP sample has been abraded in 3 successive steps from the downstream surface to the core of the sample, corresponding to 0.1 mm of depth. Then, the second face of sample has been treated in a similar procedure *i.e.* from the upstream surface to the core of the sample corresponding to 17 successive abrasive steps and 0.27 mm of depth. After, each abrasive-step, the powder was leached twice by acid solution (HNO$_3$, 2%) to release the uranium in solution and U concentration was determined by ICP-MS. The U diffusion profile is presented in *Figure 5-47*. The penetration depth is around 0.13 mm, suggesting a very low diffusivity of the U-ORGA species. It's also interesting to notice that the U content of the HCP was not zero and corresponds to a background concentration of $1.1 \cdot 10^{-5}$ mol/kg^{HCP}. This result could explain the small amount of U measured in the downstream compartment, corresponding to the leaching of the HCP surface.
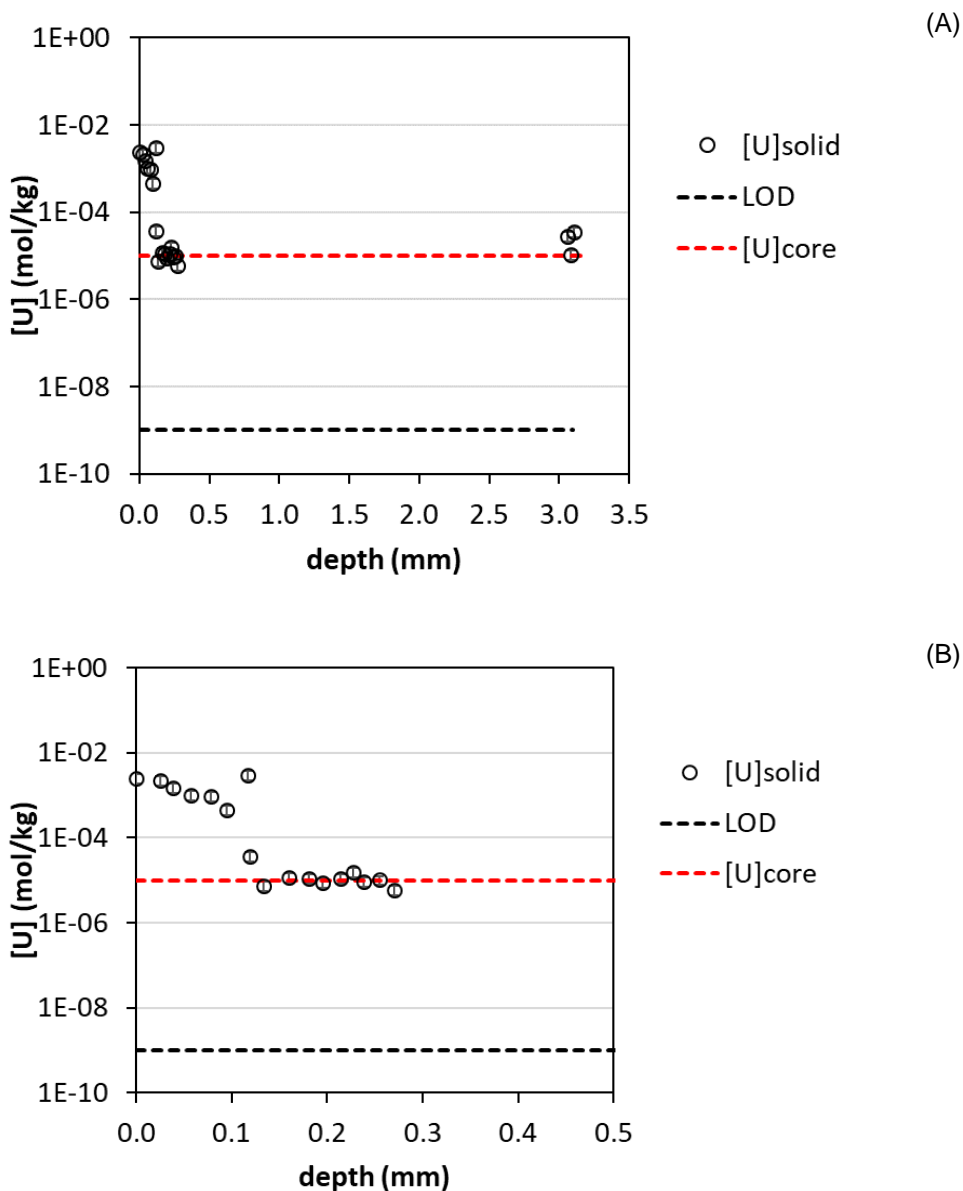
Figure 5-47: *Diffusion of U in a CEM V/A HCP disk in Stage II solution with initially $5 \cdot 10^{-2}$ M of EDTA (F1 cell) (A): U diffusion profile obtained after 232 days of in-diffusion (B) focus of the diffusion profile to a max depth of 0.5 mm*

EURAD (Deliverables n° 3.6, 3.7 and 3.8) - Final Report of results generated in CORI
Dissemination level: PU
Date of issue of this report: **05/07/2024**

Page 184

[CEA] performed in-diffusion tests for the system ^{63}Ni/EDTA/HCP CEM V/A at Stage II (F2 cell). The activity of ^{63}Ni in the solution was measured during 109 days of diffusion and represented around 80% of the initial activity introduced in the upstream compartment (see *Figure 5-48*a). After 109 days, the HCP sample has been removed from the solution, dried overnight and cut in two pieces in order to access the two diffusion profiles. Unfortunately, one part has been broken during the preparation. Prior to the multi-abrasive steps /leaching procedure, the remained part has been measured by digital autoradiography (DA) in order to directly access the diffusion profile (see "DA-profile-F2-EDTA" series in *Figure 5-48*b) and compared to the ^{63}Ni profile after the abrasive peeling procedure (see "MG-profile" series in *Figure 5-48*b). There are some discrepancies between the two techniques and no explanation can be given for the moment. The penetration of ^{63}Ni (or ^{63}Ni-EDTA complex) in the solid is quite limited close to the surface of the HCP sample. In respect with what has been observed for phthalate, the presence of EDTA does slightly enhance the ^{63}Ni diffusion. For a similar diffusion time, the response of the DA showed a longer ^{63}Ni profile in presence of EDTA.

(A)

(B)
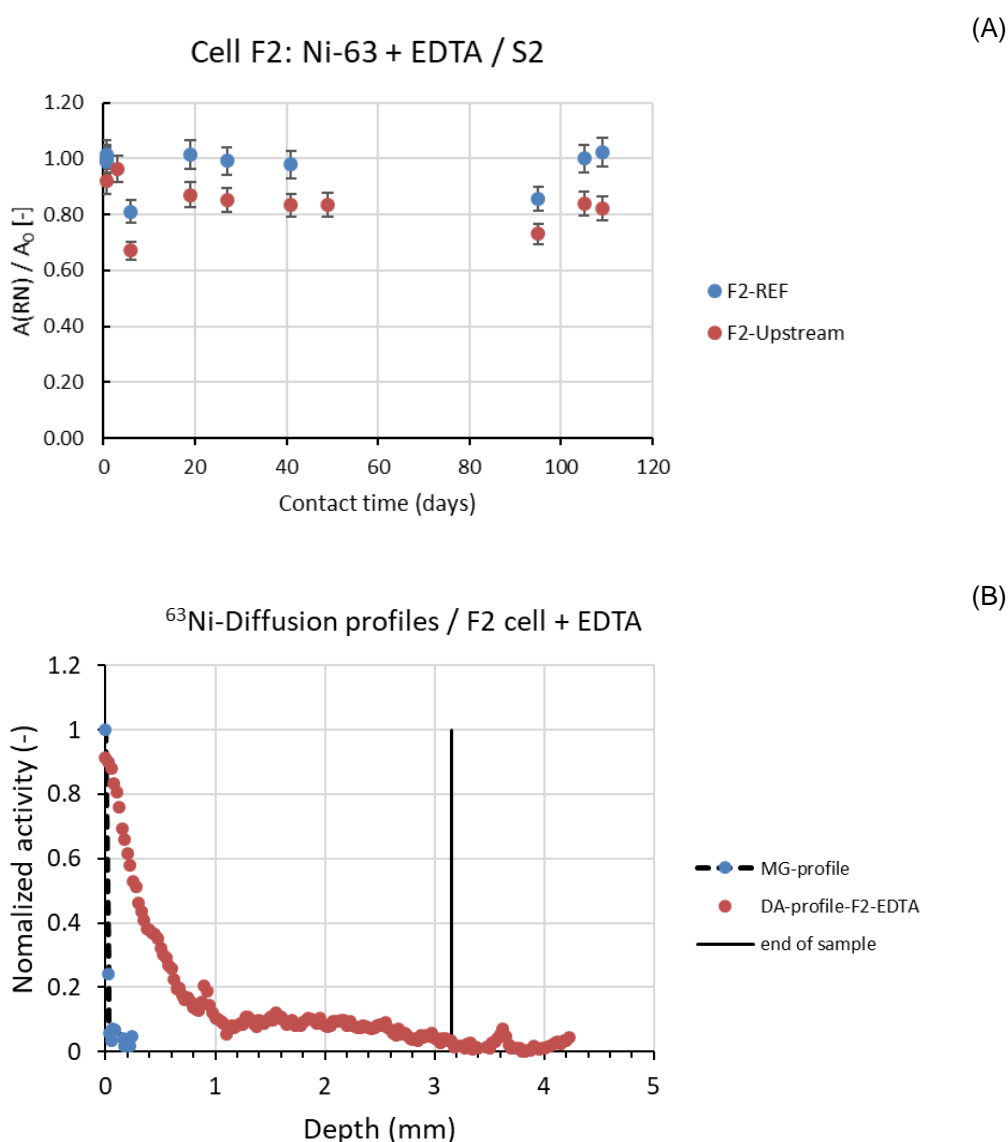
Figure 5-48:   *In-diffusion of ^{63}Ni in HCP CEM V/A at Stage II in presence of EDTA (A) evolution of the activity of ^{63}Ni in S2 solution containing initially with $5 \cdot 10^{-2}$ M of EDTA (B) Diffusion profiles obtained by two methods: multi-abrasive steps/leaching in a CEM V/A disk in Stage II solution over time (F2 cell) – the black straight line corresponds to the end of the sample.*

EURAD (Deliverables n° 3.6, 3.7 and 3.8) - Final Report of results generated in CORI
Dissemination level: PU
Date of issue of this report: **05/07/2024**

Page 185

[CTU] performed batch sorption experiments with U, Pb, and Eu in HCP (CEM I and CEM III) and in C-S-H phases in the presence of EDTA, determining the R_d values and sorption reduction factor values (SRF).

Table 47 shows the average values of uncertainty of the R_d determination and sorption on experimental ampoules walls for studied radionuclides.

Table 47: Average values of uncertainty of the R_d determination and sorption on experimental ampoules walls for studied radionuclides.

	Uncertainty [%]	Sorption on walls [%]	Uncertainty [%]	Sorption on walls [%]
	HCP		C-S-H	
U	13	36 ±12	12	< 5.4
Pb	5	< 3.7	23	5-80
Eu	19	min 40 dependent on L/S	not determined	not determined

Table 48 indicates the average values of R_d for each studied radionuclide and the sorption reduction factor (SFR) after organic species addition.

EURAD (Deliverables n° 3.6, 3.7 and 3.8) - Final Report of results generated in CORI
Dissemination level: PU
Date of issue of this report: **05/07/2024**

Page 186

Table 48: Average values of distribution ratios R_d (L·kg^{-1}) and SRF for U, Eu, and Pb in systems with EDTA in different solids.

Material	System	Average R_d [L·kg^{-1}]	SRF
HCP CEM I	^{152}Eu (2.9·10^{-9} mol·L^{-1})	(11.9 ± 2.2)·10^3	-
HCP CEM I	^{152}Eu + EDTA 5·10^{-5} mol·L^{-1}	(31.9 ± 6.0)·10^3	0.37 ± 0.10
HCP CEM I	^{152}Eu + EDTA 5·10^{-3} mol·L^{-1}	(25.7 ± 4.8)·10^3	0.47 ± 0.12
HCP CEM I	^{233}U (7·10^{-8} mol·L^{-1})	(2.7-12.5)·10^{3*}	-
HCP CEM I	^{233}U + EDTA 5·10^{-5} mol·L^{-1}	(2.0-12.9)·10^{3*}	1.05 ± 0.40
HCP CEM I	Pb (5·10^{-4} mol·L^{-1})	(0.8-1.6)·10^{3*}	-
HCP CEM I	Pb + EDTA 5·10^{-5} mol·L^{-1}	(0.9-1.5)·10^{3*}	1.0 ± 0.1
HCP CEM I	Pb + EDTA 5·10^{-3} mol·L^{-1}	(1.4-2.3)·10^{3*}	0.7 ± 0.1
HCP CEM III	^{152}Eu (2.9·10^{-9} mol·L^{-1})	(14.1 ± 1.5)·10^3	-
HCP CEM III	^{152}Eu + EDTA 5·10^{-5} mol·L^{-1}	(44.6 ± 4.6)·10^3	0.41± 0.04
HCP CEM III	^{152}Eu + EDTA 5·10^{-3} mol·L^{-1}	(106.7 ± 11.1)·10^3	0.150 ± 0.003
HCP CEM III	Pb (5·10^{-4} mol·L^{-1})	(1.8-2.3)·10^{2*}	-
HCP CEM III	Pb + EDTA 5·10^{-5} mol·L^{-1}	(1.8-2.6)·10^{2*}	0.9 ± 0.1
HCP CEM III	Pb + EDTA 5·10^{-3} mol·L^{-1}	(2.5-3.6)·10^{2*}	0.6 ± 0.1
C-S-H 1.0	^{233}U (7·10^{-8} mol·L^{-1})	(85.8 ± 23.2)·10^3	-
C-S-H 1.0	^{233}U (7·10^{-8} mol·L^{-1}) EDTA 5·10^{-5} mol·L^{-1}	(72.4 ± 19.6)·10^3	1.2 ± 0.3
C-S-H 1.0	^{233}U (1·10^{-5} mol·L^{-1}) EDTA 5·10^{-3} mol·L^{-1}	(13.9-128.6)·10^{3*}	≥ 1.7
C-S-H 1.0	Pb (5·10^{-4} mol·L^{-1})	(37.7 ± 8.7)·10^3	-
C-S-H 1.0	Pb + EDTA 5·10^{-5} mol·L^{-1}	(9.5 ± 2.2)·10^3	4.0 ± 0.9
C-S-H 1.0	Pb + EDTA 5·10^{-3} mol·L^{-1}	110 ± 30	340 ± 80
C-S-H 1.2	Pb (5·10^{-4} mol·L^{-1})	(37.5 ± 8.6)·10^3	-
C-S-H 1.2	Pb + EDTA 5·10^{-5} mol·L^{-1}	(10.9 ± 2.5)·10^3	3.4 ± 0.8
C-S-H 1.2	Pb + EDTA 5·10^{-3} mol·L^{-1}	70 ± 20	540 ± 120
C-S-H 1.4 fresh	Pb (5·10^{-4} mol·L^{-1})	(17.2 ± 4.0)·10^3	-
C-S-H 1.4 fresh	Pb + EDTA 5·10^{-5} mol·L^{-1}	(14.4 ± 3.3)·10^3	1.2 ± 0.3
C-S-H 1.4 fresh	Pb + EDTA 5·10^{-3} mol·L^{-1}	(9.3 ± 2.1)·10^3	1.8 ± 0.4

*range of R_d for non-linear dependences of R_d on L/S

EURAD (Deliverables n° 3.6, 3.7 and 3.8) - Final Report of results generated in CORI
Dissemination level: PU
Date of issue of this report: **05/07/2024**

Page 187
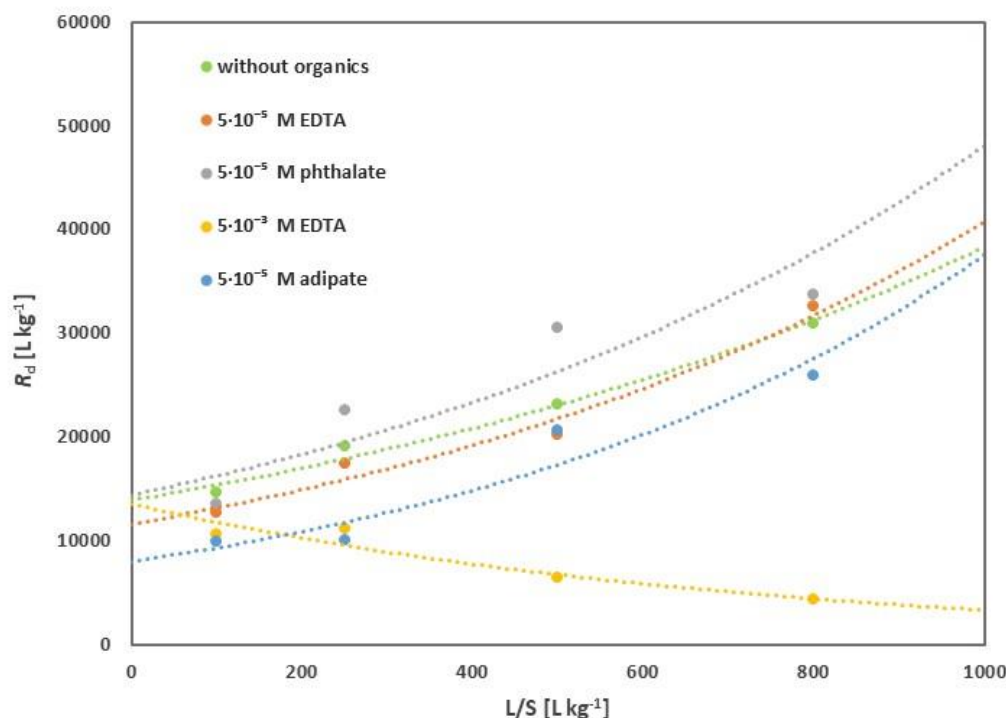
Figure 5-49:   *Dependence of R_d ($L \cdot kg^{-1}$) on the phase ratio L/S at a uranium concentration of $1.2 \cdot 10^{-6}$ $mol \cdot L^{-1}$ for different compositions of the liquid phase in presence of HCP CEM I.*

[CTU] also analysed the adsorption of uranium at different solid to liquid ratio in HCP (CEM I) in the presence of EDTA (*Figure 5-49*). The data without EDTA, showed an increasing trend of sorption as the liquid to solid ratio increased; the data at the lower ligand the concentration ($5 \cdot 10^{-5}$ M) was very similar to that obtained without the ligand; nevertheless, in the presence of $5 \cdot 10^{-3}$ M of EDTA, the R_d decreases significantly as the liquid to solid ratio increased.

[JGU] carried out studies on the fresh HCP An(IV) /EDTA system. The experiments were conducted at concentration of ^{232}Th(IV) and ^{239}Pu(IV) of $1 \cdot 10^{-8}$ M with S/L-ratio of 5 $g \cdot L^{-1}$, and an initial concentration of EDTA of $1 \cdot 10^{-2}$ M and a pH of 13.3. The effect of different addition order (RN & ligand) was also investigated.

Figure 5-50 shows the calculated R_d values for both Th(IV) and Pu(IV) uptake on HCP in the presence and absence of EDTA after 72 hours of contact time. These values are in the range of 10^5 to 10^6 $L \cdot kg^{-1}$.

EURAD (Deliverables n° 3.6, 3.7 and 3.8) - Final Report of results generated in CORI
Dissemination level: PU
Date of issue of this report: **05/07/2024**

Page 188
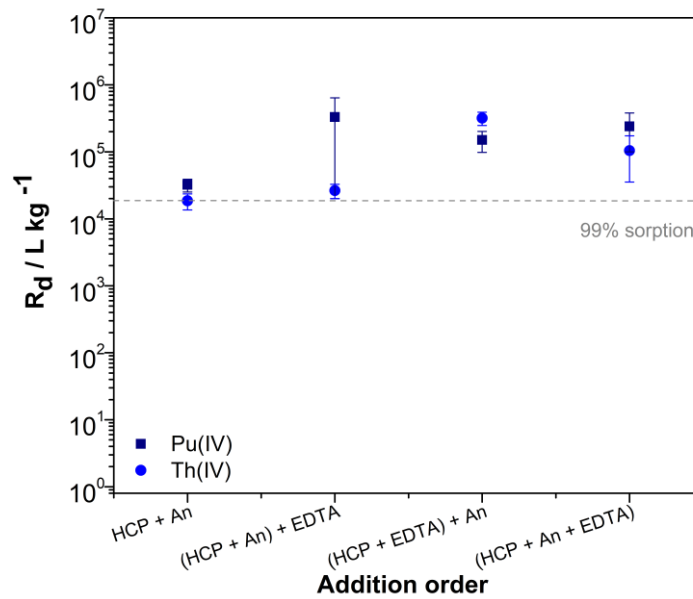
Figure 5-50: *The distribution coefficients R_d (L·kg^{-1}) determined for Th(IV) and Pu(IV) ([^{232}Th(IV)] and [^{239}Pu(IV)] = 1·10^{-8} M) uptake on HCP in presence and absence of EDTA [EDTA] = 1·10^{-2} M, S/L = 5 g·L^{-1}) at pH 13.3 after a contact time of 72 h. The dashed line represents an uptake of 99%.*

The quantitative uptake of Th(IV) and Pu(IV) on HCP observed in this study suggests that the order of reactant addition and the presence of EDTA did not influence retention of Th and Pu on HCP after 72 hours of contact time, which is consistent to the values of the literature (Ochs *et al.*, 2016; Tasi *et a*l. 2021).

[SURAO] studied europium adsorption in concrete based on CEM III, which is an important material used in the Richard repository (Richard Concrete) in the presence of EDTA. Figure 5-51 shows the kinetics of Eu adsorption in Richard cement, in portlandite water in absence and presence of EDTA (or adipate) at two different concentrations. No significant differences were observed for all investigated systems.
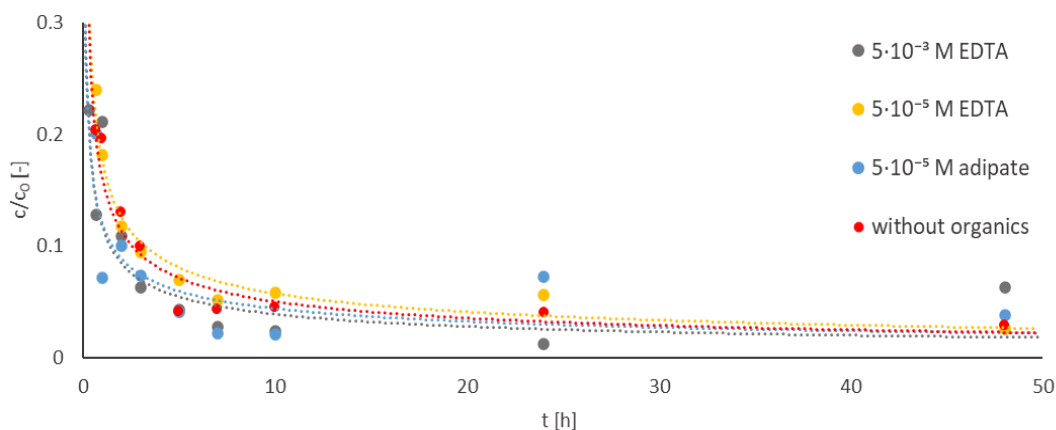
Figure 5-51: *Kinetics of ^{152}Eu (2.9·10^{-9} mol·L^{-1}) sorption on CEM (III) in portlandite water with and without organics (5·10^{-5} and 5·10^{-3} mol·L^{-1}).*

EURAD (Deliverables n° 3.6, 3.7 and 3.8) - Final Report of results generated in CORI
Dissemination level: PU
Date of issue of this report: **05/07/2024**

Page 189

[UCYPRUS] investigated the effect of EDTA on the adsorption and desorption of U(VI) by C-S-H (C:S ratio of 1.27) under N_2, ambient and 1% CO_2-atmosphere. In all experiments, analytical grade reagents and de-ionized water were used. The ^{232}U-tracer solution, which was added for the uranium quantification, was obtained from NPL (National Physical Laboratory, Teddington, UK). EDTA solutions of different concentration (0.0001, 0.001, 0.01 and 0.1 M) have been prepared by dissolution of disodium EDTA dihydrate ($C_{10}H_{14}N_2O_8$ 2Na·2H_2O, Aldrich) in de-ionized water.

Solid calcium-silicate-hydrate (C-S-H) has been synthesized according to Maddalena *et al.* (2019) at a C:S ratio of 1.27 and the solid product has been characterized by FTIR spectroscopy (FTIR, FTIR-ATP 8900, IR Prestige-2, Shimadzu, Europa GmbH, Duisburg, Germany) and X-Ray diffraction Shimadzu XRD-6000 Series). The preparation of C-S-H was carried out by mixing 12.02 g Ludox (50%, Aldrich) with 8.52 g CaO (Aldrich) in 35 mL de-ionized water under N_2. The product was cast in cubes and left for one month under water-vapour saturated N_2-atmosphere. Finally, the C-S-H cubes were kept overnight in acetone to remove excess water and then dried under vacuum at 70°C for 24 h.

In solutions of increased EDTA concentration ([EDTA] > 0.1 M) calcium is complexed and extensively extracted from C-S-H, which results in the dissolution of the $Ca(OH)_2$ phase and deterioration of C-S-H. Hence, only in solutions of lower EDTA concentrations (0.0000 < [EDTA] ≤ 0.0100 M) and U(VI) investigation were possible. The sorption experiments were carried out using constant U(VI) concentrations ([U]= 5·10^{-5} M) and the desorption of U(VI) from C-S-H was carried out by coprecipitating U(VI) during C-S-H formation C-S-H/U). Under N_2 atmosphere, the presence of EDTA in solution results in lower sorption efficiency (*e.g.* lower K_d values) due to stabilization of U(VI) in solution in the form of EDTA complexes. However, lower desorption efficiency (e.g. higher K_d values) are observed when EDTA solutions are contacted with the C-S-H/U phase, because of the formation of ternary C-S-H/U(VI)/EDTA surfaces complexes, which stabilize U(VI) onto the C-S-H phase. On the other hand, under ambient atmosphere the U(VI) carbonate complexes govern the U(VI) chemistry in solution, resulting generally in lower K_d values. Similarly, under 1% CO_2 U(VI)-carbonate complexes govern the U(VI) chemistry in solution and result in the formation of ternary carbonate solid phases.

The effect and sorption of EDTA on the C-S-H solid was investigated by contacting a certain amount of the solid (0.2 g) with 20 mL aqueous solution of EDTA (0, 0.0001, 0.001, 0.01 and 0.1 M). After 30 days contact time, the calcium concentration in solution was determined by flame-photometry (PFP7 flame photometer, Jenway) and after solid–liquid phase separation the solids have been analyzed by X-ray diffraction (XRD-6000 Series, Shimadzu), thermo-gravimetric analysis (TGA-50, Shimadzu) and FTIR (FTIR-ATR 8900, IR Prestige-21 Shimadzu).

Sorption studies were performed in batch type experiments using 0.2 g C-S-H in 20 mL aqueous solution of EDTA (0, 0.0001, 0.001 and 0.01 M), at a U(VI) concentration of 5·10^{-5} M and pH 11 and pH 10.3 for the experiments under 1% CO_2. The experiments were performed under ambient conditions 1% CO_2 and N_2 atmosphere to investigate the effect of carbonate on the sorption capacity of U(VI) in the studied system. After 30 days contact time, aliquots of the solution have been obtained, filtrated using membrane filters (pore size: 450 nm) and the uranium concentration in solution was determined by alpha-spectroscopy (Alpha Analyst Integrated Alpha Spectrometer, Canberra) after electrodeposition on a stain-less steel planchet. Prior to electrodeposition, the sample-electrolyte mixture was traced with 50 mBq of the U-232 isotope to account for any uranium losses during electrodeposition.

The desorption investigations were performed in batch type experiments using 0.2 g C-S-H/U in 20 mL aqueous solution of EDTA (0, 0.0001, 0.001 and 0.01 M), at a U(VI)/Ca(II) ratio of 1/10000 and pH 11. The experiments were performed under ambient conditions (*e.g.* 23 ± 2 °C, 0.03% and 1% CO_2) and N_2 atmosphere to investigate the effect of carbonate on the desorption of U(VI) from the studied system. The uranium levels were determined as described above and the measurements were performed in triplicate and the mean value (m) is given in the related graphs and tables.

Figure 5-52 summarizes the K_d values determined for the sorption of U(VI) by C-S-H in the presence of varying concentrations of EDTA and under N_2, ambient and 1% CO_2-atmosphere. Under N_2 atmosphere increasing EDTA concentration in solution results generally in decreasing K_d values, which can be

EURAD (Deliverables n° 3.6, 3.7 and 3.8) - Final Report of results generated in CORI
Dissemination level: PU
Date of issue of this report: **05/07/2024**

Page 190

attributed to the complexation of U(VI) with EDTA and stabilization of the uranium in solution. According to the data in Figure 5-52, the K_d value ($\log_{10}K_d = 4.6 \pm 0.1$) obtained for the C-S-H in the absence of EDTA is close to K_d values obtained for similar systems (Androniuk *et al.*, 2017). However, when EDTA is added in solution the K_d values ($\log_{10}K_d = 4.3 \pm 0.2$) decrease with increasing EDTA concentration in solution. This could be attributed to the stabilization of U(VI) in the aqueous phase basically through complex formation between EDTA and U(VI). However, at 0.01 M EDTA the K_d value increases, which is not clear if it is a real effect, or an artifact attributed to uranium analysis at increased EDTA concentration by the applied analysis method.

Comparison of the K_d values obtained under ambient and 1% CO_2-atmosphere, and N_2-atmosphere show that generally the K_d values corresponding to CO_2 presence are generally lower ($\log_{10}K_d = 3.9 \pm 0.2$) assuming further stabilization of U(VI) in solution through the formation of U(VI) carbonate complexes which are formed because of the elevated carbonate concentration in solution under the given conditions.
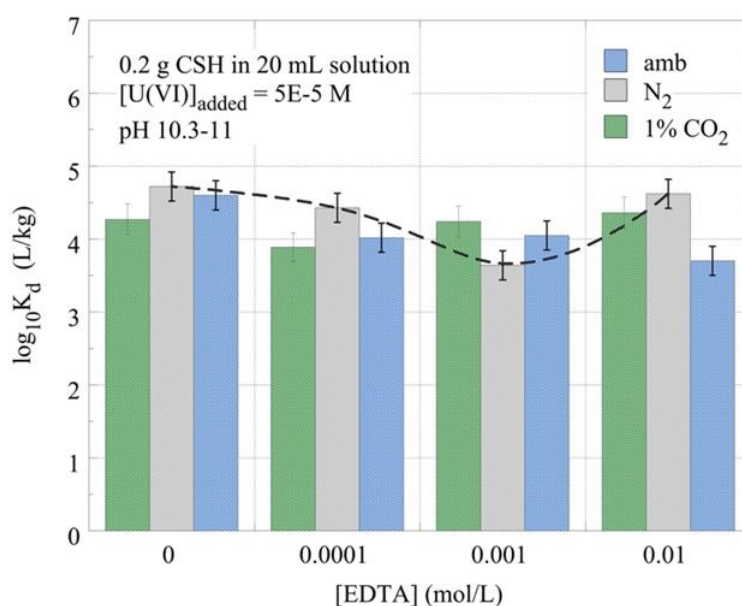
Figure 5-52:   *The $\log_{10}K_d$ values obtained for the U(VI) sorption by C-S-H under N_2, ambient and 1% CO_2 atmosphere and varying EDTA concentration in solution. The dash line corresponds to the evolution of the $\log_{10}K_d$ values under N_2 atmosphere.*

Figure 5-53 summarizes partition coefficient values as a function of the EDTA concentration in solution under N_2- and ambient and 1% CO_2-atmosphere. In the systems under N_2-atmosphere the K_d values increase with increasing EDTA concentration in solution and are generally higher ($4.9 < [\log_{10}Kd] < 5.8$) than the corresponding K_d value ($\log_{10}K_d = 4.9$) determined in the EDTA-free suspension. This is in contradiction with the results obtained from sorption experiments, which revealed the opposite effect due to stabilization of U(VI) in solution in the form of U(VI)-EDTA complexes (Marangou and Pashalidis, 2021). The increased K_d values, which are associated higher U(VI) amounts adsorbed by the C-S-H phase could be ascribed to enhanced sorption of EDTA through an interaction with calcium and uranium ions present at the C-S-H surface and the formation of ternary surface complexes (Nalet and Nonat, 2016).

It is notable that the highest K_d value ($\log_{10}K_d = 5.8$) and lowest U(VI) desorption from the C-S-H phase is observed at an initial concentration of 0.001 M EDTA under the existing experimental conditions (*e.g.*, 0.2 g C-S-H in 20 mL solution). A similar effect was observed in a previous study, where increased EDTA sorption by the C-S-H phase was observed under similar experimental conditions (Marangou and

EURAD (Deliverables n° 3.6, 3.7 and 3.8) - Final Report of results generated in CORI   Page 191
Dissemination level: PU
Date of issue of this report: **05/07/2024**

Pashalidis, 2021). In the latter case the retardation of EDTA was ascribed to the sorption of EDTA through an interaction with calcium ions at the C-S-H surface (Nalet and Nonat, 2016). Similarly, EDTA could be sorbed in the C-S-H phase via interaction with the U(VI) cations present in the solid phase. This interaction retards U(VI) in the solid phase resulting in lower U(VI) levels in solution compared to EDTA-free solutions.
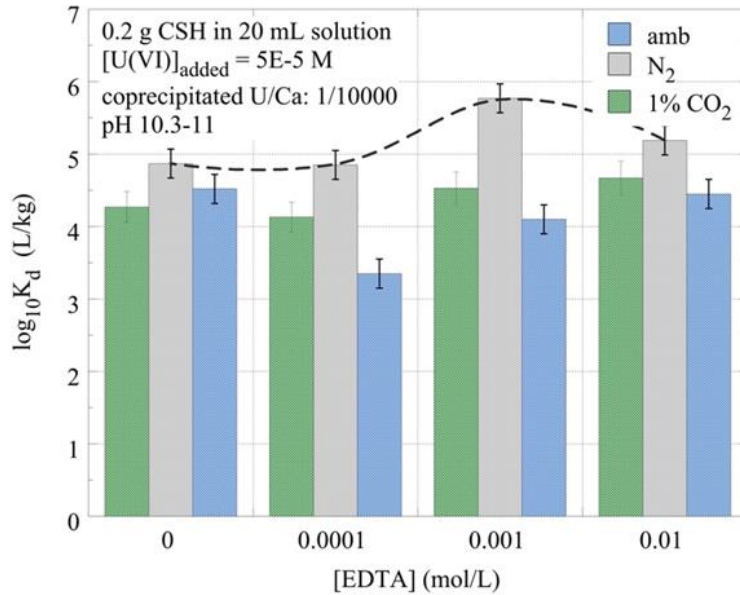
Figure 5-53: *The $\log_{10}K_d$ values obtained for the U(VI) desorption by C-S-H under N_2, ambient and 1% CO_2 atmosphere and varying EDTA concentration in solution. The dash line corresponds to the evolution of the $\log_{10}K_d$ values under N_2 atmosphere.*
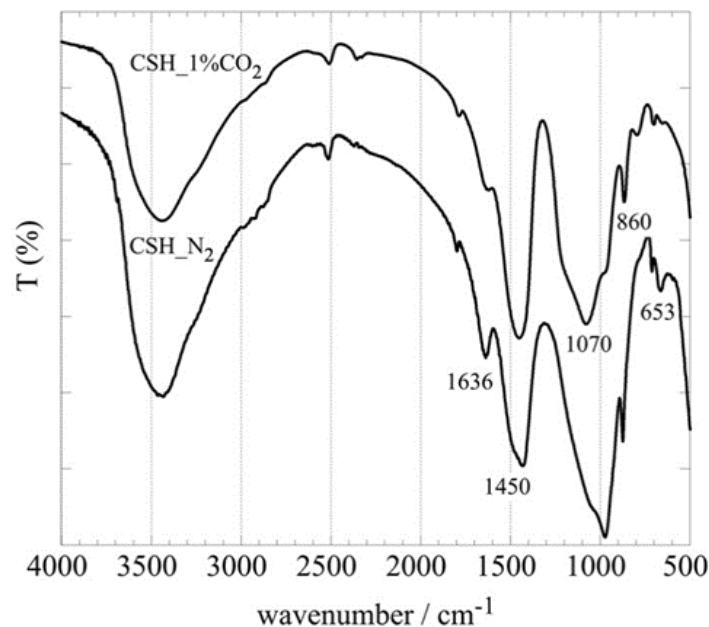
Figure 5-54: *IR-spectrum of C-S-H under 1% CO_2 and N_2 atmosphere.*

On the contrary, under ambient and 1% CO_2 atmosphere the K_d values ($3.4 < [\log_{10}K_d] < 4.5$) obtained are generally lower than the K_d value determined in the EDTA-free suspension and significantly lower than the corresponding K_d values obtained under N_2-atmosphere. This indicates that in the presence of CO_2 the equilibrium is shifted towards the U(VI) species in solution. Under ambient atmospheric conditions (pH 11) and 1% CO_2, CO_2 is extensively dissolved in the aqueous phase and exists

EURAD (Deliverables n° 3.6, 3.7 and 3.8) - Final Report of results generated in CORI
Dissemination level: PU
Date of issue of this report: **05/07/2024**

Page 192

predominantly in the form of the carbonate anion (CO_3^{2-}). U(VI) forms with carbonate anions very stable complexes (*e.g.* $UO_2(CO_3)_3^{4-}$, logβ= 19.5) (Pashalidis *et al.*, 1997), which compete the U(VI) sorption by C-S-H, resulting in lower K_d values. Similar behavior was observed also in the case of experiments related to the U(VI) sorption by C-S-H in the presence of varying EDTA concentrations and the higher U(VI) levels had been ascribed to the formation of U(VI)-carbonato species (Pashalidis *et al.*, 1997), which compete the sorption by C-S-H and stabilize U(VI) in solution. Moreover, secondary solid phases are formed ($CaCO_3$) under 1% CO_2 atmosphere. The latter is indicated by IR spectra obtained prior C-S-H contact with 1% CO_2 atmosphere (Figure 5-54).

Nitriloacetate (NTA) was studied by **[HZDR]** in collaboration with **[UPPC]** and **[JGU]**. The complexation of Eu(III) or Cm(III) by NTA was studied applying spectroscopic/analytical methods and quantum chemical calculations. Complex formation constants were determined, and complex structures were identified. The results have been published in (Kretzschmar *et al.*, 2020, 2021 and Friedrich *et al.*, 2023). Experiments (background electrolyte 10 mM NaCl) investigating the complexation of Eu(III) by organic ligands (OL = NTA) in the presence of C-S-H phase (pH 9.8 and C/S = 0.8 as well as pH 11.7 and C/S = 1.65) were carried out. The influence of OL was investigated for a large concentration range (for NTA up to 750 µM). Time-resolved laser fluorescence spectroscopy (TRLFS) was used as analytical method. The raw TRLFS data (IL, λ_{em}, t) are further analyzed using parallel factor analysis (PARAFAC) in order to deconvolute the different luminescent Eu(III) species. For both C/S ratios the TRLFS data (and subsequently the PARAFAC deconvoluted data of the Eu(III) species) were collected for the spectral range covering the Eu(III) luminescence transitions up to the $^5D_0$-$^7F_4$ band allowing a Judd-Ofelt (JO) analysis. Based on the JO analysis the emission quantum efficiencies of the species were accessible and were used to determine the concentrations of the species in the respective samples. It has been shown that NTA has only a minor influence on the sorption of Eu(III) by C-S-H_1.65 (0 < [NTA] < 750 µmol/L).

5.3 Citrate, formate, adipate, oxalate, acetate, phthalate

5.3.1 Citrate

The effects of citric acid on RN behavior was analyzed by **[HZDR]** and [**KIT(EMPA)]**.

[HZDR] studied the U(VI) citrate system (U(VI)−Cit), by means of extensive spectroscopic studies (NMR, UV-Vis, ATR-FT-IR, EXAFS) in the pH range 2−10. The experimental findings were also supported by a variety of quantum chemical calculations at the level of density functional theory (DFT). The focus was on both the (pH- and concentration-dependent) molecular structures and the thermodynamic complex formation constants (Kretzschmar *et al.*, 2020, 2021; Friedrich *et al.*, 2023). The dominant complex species under the measurement conditions are species with U(VI):Cit ratios of 2:2, 3:3, and 3:2. The combination of methods revealed that a) different isomers of the 2:2 complexes coexist and interconvert; b) U(VI) hydrolysis gives rise to ternary 2:2 U(VI) citrate-hydroxo species; c) above a concentration threshold determined as 3 mM, two molecules of the 3:3 species form a so-called sandwich complex that includes metal ions (Na^+, Ca^{2+}, or La^{3+}); and d) the 3:2 species also forms a superstructure, namely a 9:6 macrocycle, which shows distinct intra- and intermolecular dynamics.

[KIT] in collaboration with **[EMPA]** carried out sorption experiments with Cm(III), Pu(III/IV) and Eu(III) in presence and absence of citrate in the C-S-H phases (Ca/Si = 0.8, 1.4), AFm phases and ettringite. Results showed a strong uptake of Pu(IV/III) and Eu(III) by C-S-H phases and a strong uptake of Pu(IV/III) by AFm phases and ettringite. Citrate had a negligible impact on the Pu and Eu retention by C-S-H phases, and it was observed to reduce Pu retention by AFm phases and ettringite only at [CIT]$_{tot}$ > 10^{-2} M.

5.3.2 Formate

The effect of formate on RN retention has been analyzed by **[RATEN]** and **[KIT(EMPA)]**.

EURAD (Deliverables n° 3.6, 3.7 and 3.8) - Final Report of results generated in CORI
Dissemination level: PU
Date of issue of this report: **05/07/2024**

Page 193

[RATEN] analyzed ^{63}Ni solubility and adsorption in fresh and degraded (Stage II and Stage III) CEM I HCP and CEM V, in the absence and presence of formic acid. The powdered HCP samples were obtained, inside a glove box, in N_2 atmosphere, by crushing and grinding followed by sieving to collect fraction with particle size less than 63 µm. The extent of calcium content in the non-degraded CEM I cement pastes was determined by emission spectrometry ICP-OES (iCAP 6000 series) carried out on samples resulted by cement pastes dissolution (microwave digestion in HNO_3, HCl and HF). The HCP samples were also characterized by SEM-EDS to gather information on the chemical composition of the material and TGA/DTA to investigate sample weight change and the different compositional trends.

The composition of the solution in equilibrium with HCP was prepared according to the procedure of Wieland *et al.* (2006). Before sorption experiments solubility studies in the cement porewater were carried out with and without formic acid. Three types of laboratory experiments have been performed:

- Evaluation of the solubility limit of ^{63}Ni in artificial cement pore water corresponding to Stage I (ACW), at pH 13.3, without organic molecules addition in the system;
- Evaluation of the solubility limit of ^{63}Ni in artificial cement pore water corresponding to Stage I (ACW), at pH 13.3, with organic molecules (formic acid -HCOOH) addition in the system.
- Evaluation of the solubility limit of ^{63}Ni in cement pore water resulted from de degradation test of the HCP based on CEM I (DCW), at pH 11.3.

Table 49 presents the general experimental conditions applied in the tests performed to evaluate the solubility of ^{63}Ni in cement pore waters, for the binary system (radionuclide-cement) and for ternary system (radionuclide-cement-organics). All solubility tests have been conducted in duplicate, in pre-washed centrifuge tubes, inside of a glove box with nitrogen atmosphere ($O_2 <$ 0.1%), at room temperature (22 ± 3°C). Considering the findings of Wieland *et al.* (2006), upon contacting the HCP with ACW, the nickel bound to cement based material could be released into solution. This solubility tests were conducted using ^{63}Ni labelled solutions. The total nickel concentration in the experiments ranged between 10^{-8} M – 10^{-5} M. For this concentration domain, four nickel concentrations have been selected and obtained by preparing stock solution of 10^{-4} M $NiCl_2$ and a stock of ^{63}Ni tracer solution. Appropriate volumes from the stock solutions have been added in ACW and DCW (the total volume in a centrifuge tube was 40 mL).

The total concentration of formic acid used in the tests designated to evaluate the influence of short carboxylic acids (HCOOH) on ^{63}Ni solubility limit, was kept constant in all experiments (10^{-3} M). The centrifuge tubes have been intermittently shaken for 30 days. At the end of the testing period, the solutions were sampled and after centrifugation aliquots were withdrawn from each test tube, acidified and analyzed for total nickel concentration in the system, by Inductively Coupled Plasma – Optical Emission Spectrometry (ICP-OES iCAP 6000 series)/InductivelyCoupled Plasma-Mass Spectrometry (ICP-MS).

*Table 49: Experimental conditions for the solubility study **[RATEN]***

Atmosphere	N_2
$[Ni]_{initial}$	$6 \cdot 10^{-8}$ M – 10^{-6} M
[ORG]	10^{-3} M
ACW	pH = 13.3
DCW	pH = 11.3
Equilibration time	30 days
Phase separation	Centrifugation+Filtration
Total Ni concentration measurement	ICP-OES/ICP-MS

EURAD (Deliverables n° 3.6, 3.7 and 3.8) - Final Report of results generated in CORI
Dissemination level: PU
Date of issue of this report: **05/07/2024**

Page 194

The results of [63]Ni solubility test in ACW (pH=13.3) and DCW (pH=11.3), with and without formic acid addition in the system, are presented in

Figure 5-55 and

Figure 5-56.

In cement pore water, ACW (pH 13.3), up to a total nickel concentration of $2 \cdot 10^{-7}$ M when formic acid was added to the system, nickel total and in solution concentrations are not significantly influenced when comparing these values with those obtained in the solubility test conducted without HCOOH addition (

Figure 5-55). Above this value, the formation of a precipitate or a fraction of colloidal nickel could have been occurred, determining lower nickel concentrations in ACW, after the centrifugation and filtration steps. Inside the testing tubes, visually no macroscopically nickel precipitate was observed.
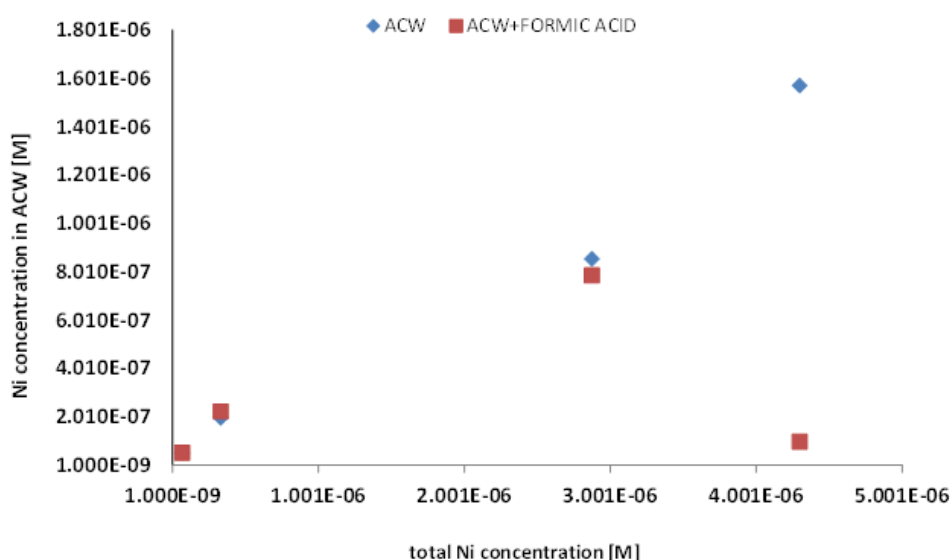
Figure 5-55:   Effect of organic molecules addition on nickel solubility limit in cement pore water at pH 13.3.

From this operational nickel solubility measurement in ACW, the concentrations for batch sorption test have been selected to be below $1 \cdot 10^{-7}$ M, to avoid precipitation phenomena that could occur in these complicated cement systems.

In the HCP degradation cement pore waters (DCW) at a pH of 11.3, total and in solution nickel concentrations are quite in good agreement up to a total nickel concentration of $5 \cdot 10^{-6}$ M when no formic acid is added (

Figure 5-56). Thus, the pore water composition and respectively the pH, have a significant influence on nickel solubility limit at pH 11.3 compared to what observed at pH 13.3. When formic acid is added to the system, the concentration measured in solution is higher. Experimental uncertainties have to be determined before further interpretations of the results.

EURAD (Deliverables n° 3.6, 3.7 and 3.8) - Final Report of results generated in CORI
Dissemination level: PU
Date of issue of this report: **05/07/2024**

Page 195
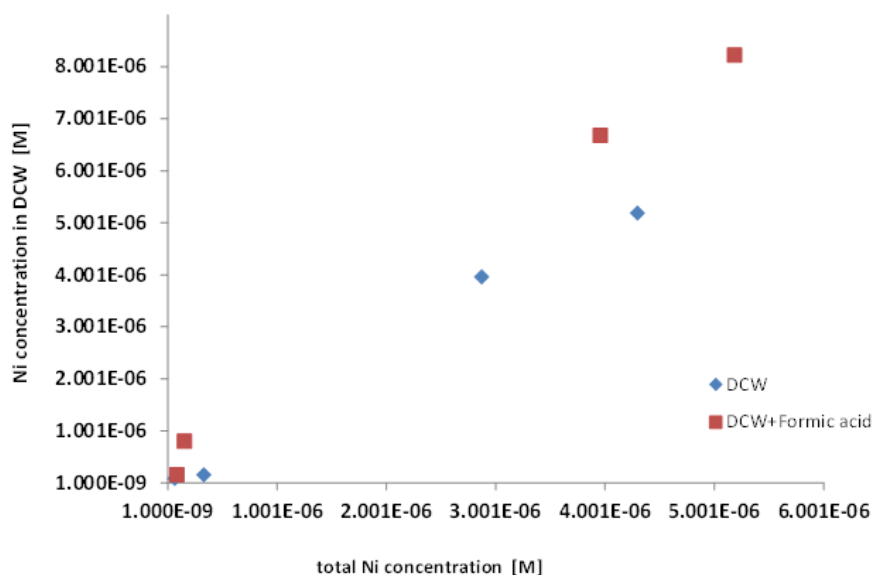
Figure 5-56:   *Nickel concentrations in cement pore waters at pH 11.3 (DCW) with and without formic acid.*

As a comparison with literature results, on can indicate that Wieland *et al.* (2006) determined $[Ni]_{aq} = 7 \cdot 10^{-7}$ M at pH 13.3. In their studies, Pilkington & Stone (1990) are reporting an experimental nickel solubility limit of $5 \cdot 10^{-8}$ mol/L, for a pH value of 13.2. Other experimental solubility study reports a nickel solubility limit between $6.5 \cdot 10^{-6}$ mol/L and $8.5 \cdot 10^{-8}$ mol/L, in cement pore waters with a pH of 12.94. Obviously, experimental conditions are different from one study to another, and the results obtained have been considered reasonable indications of nickel operational solubility limit in ACW and DCW, contributing to the selection of nickel concentrations for batch sorption experiments.

^{63}Ni uptake by HCP has been assessed by batch sorption experiments. The batch tests have been conducted for a solid to liquid ratio (S/L) of $2.5 \cdot 10^{-2}$ kg·L^{-1} (1 g of 63 μm crushed and sieved HCP in 40 mL ACW), at room temperature, inside a glove box, under nitrogen atmosphere. Sorption experiments were carried out in duplicate in 50 mL polypropylene centrifuge tubes. Before use, the centrifuge tubes were pre-washed and blank batches were prepared to assess nickel concentration in cement pastes. Also ^{63}Ni sorption on centrifuge tubes has been checked. Weighed amounts of dry crushed HCP were equilibrated with ACW prior addition of ^{63}Ni labelled solutions.

For uptake experiments a stock solution using carrier-containing ^{63}Ni radiotracer (NiCl$_2$ in 0.1 M HCl) has been prepared from a source with the total activity of $3.841 \ 10^6$ Bq. The total nickel concentration added in the system have been selected and calculated so that the ^{63}Ni plus carrier concentrations are well below the solubility limit. Nickel concentrations in the system ranged from 10^{-9} M to 10^{-8} M. The sorption kinetic test was performed, for an initial Ni-63 concentration of $1 \cdot 10^{-8}$ M. The evolution of Ni-63 concentration was analyzed in the aqueous phase at different time periods.

The sorption isotherm test was performed in similar conditions with kinetics test for three Ni-63 initial concentrations: $5 \cdot 10^{-9}$ M, $1 \cdot 10^{-8}$ M, $5 \cdot 10^{-8}$M.

The kinetics of ^{63}Ni sorption on CEM in the presence of organic molecules has been evaluated for a formic acid concentration in the system of 10^{-3} M. In all experiments with ^{63}Ni, stable formic acid was added in the system to avoid experimental difficulties in the LSC counting of ^{63}Ni.

During the equilibration periods the test tubes have been placed on a shaker at 170 rpm. After equilibration the test tubes have been centrifuged, the supernatant solutions were sampled and the residual activity of ^{63}Ni in the solutions has been measured by LSC counting, using Ultima Gold

EURAD (Deliverables n° 3.6, 3.7 and 3.8) - Final Report of results generated in CORI
Dissemination level: PU
Date of issue of this report: **05/07/2024**

Page 196

scintillation cocktail and Canberra Packard Tri-Carb 5110 TR liquid scintillation analyser. The samples counting was performed until the uncertainty of %σ ≤ 0.5 was achieved.

Figure 5-57 shows the results obtained from the ^{63}Ni sorption kinetic tests on fresh CEM I HCP with and without formic acid addition show a fast kinetic ^{63}Ni uptake. Organic molecules addition in the system influences the percentage uptake and R_d values (*Figure 5-58*). Lower R_d values were found in the ternary system cement -^{63}Ni – HCOOH.
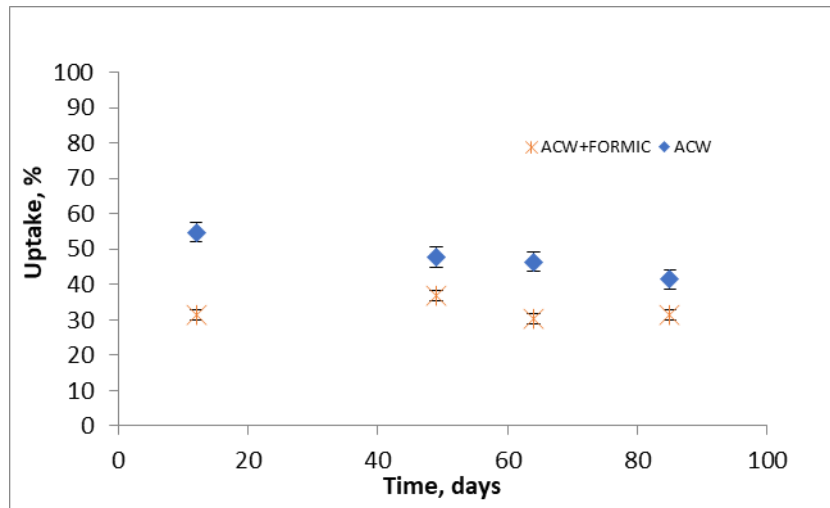
Figure 5-57:   Evolution of ^{63}Ni percentage uptake on CEM I HCP.
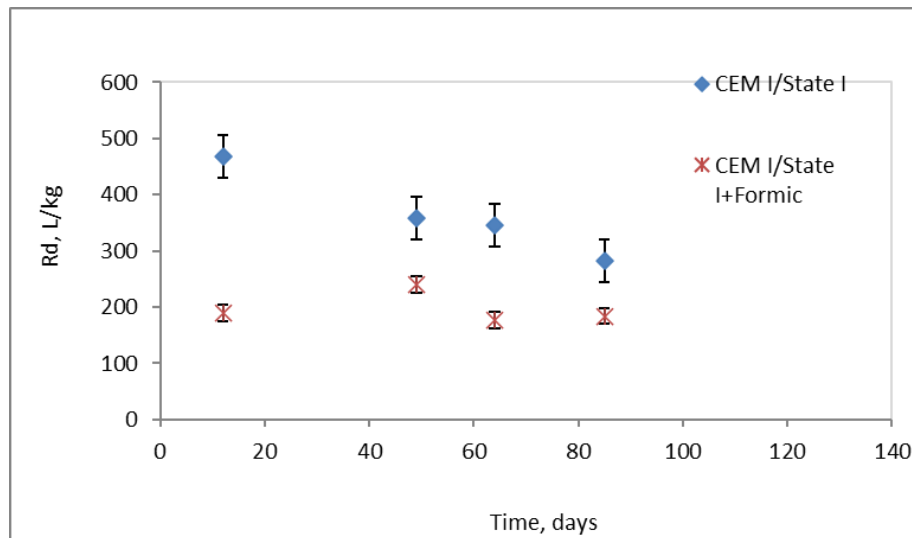
Figure 5-58: ^{63}Ni uptake by non-degraded CEM I HCP, in absence and presence of 10^{-3} M formic acid, as a function of time

Sorption kinetic tests of ^{63}Ni on HCP CEM I in Stage III of degradation with and without formic acid addition and R_d evolution show very high percentage sorption obtained for this degradation stage, characterized by a pH = 11.3. The effect of formic acid addition is visible, a slight influence on ^{63}Ni uptake on degraded CEM I HCP can be observed, lower sorption values being obtained in the ternary system (*Figure 5-59*). Organic molecules influence is moreover higher for the non-degraded CEM I HCP than for the Stage III of degradation.

EURAD (Deliverables n° 3.6, 3.7 and 3.8) - Final Report of results generated in CORI
Dissemination level: PU
Date of issue of this report: **05/07/2024**

Page 197
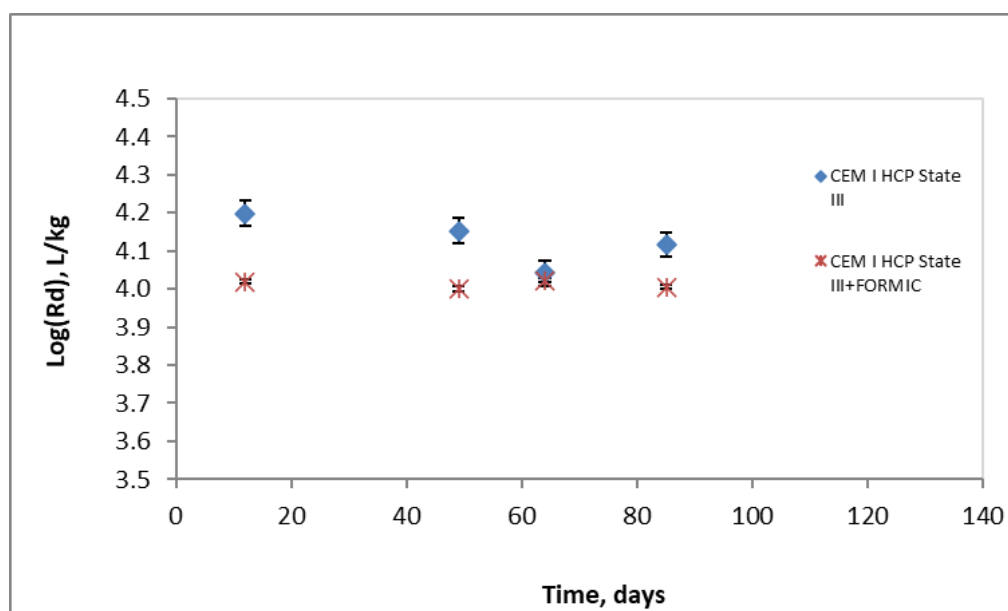
Figure 5-59:   [63]*Ni uptake by degraded stage III CEM I HCP, in absence and presence of 10^{-3}M formic acid, as a function of time*

Very high sorption values were also obtained for the carbonated stage of CEM I HCP samples (*Figure 5-60*), for both sorption test (total Ni initial concentrations in the system were $1 \cdot 10^{-7}$ M and $1 \cdot 10^{-8}$ M). No visible formation of a precipitate occurred in the test tubes.
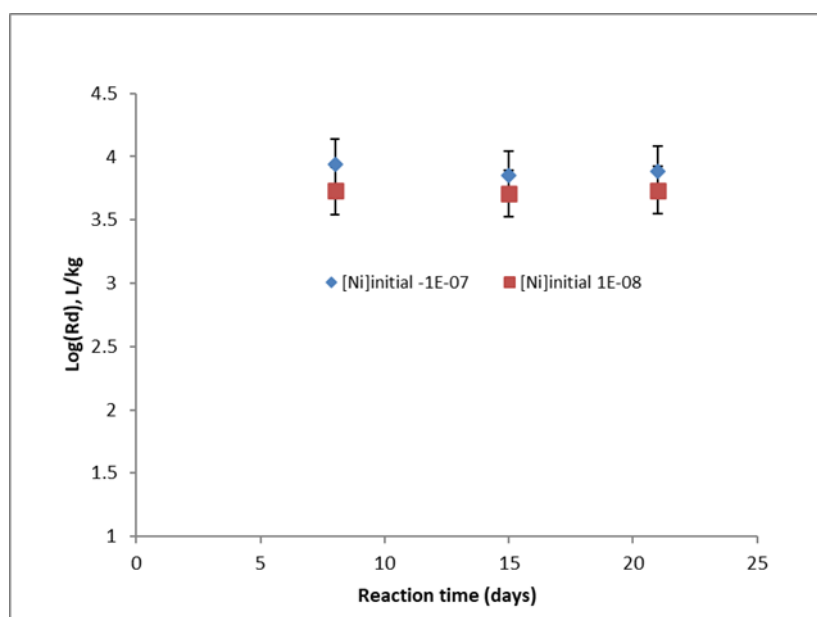
Figure 5-60:   [63]*Ni kinetic uptake on carbonated CEM I HCP as a function of time, for two initial total nickel concentrations in the system*

Results of the uptake kinetic tests on non-degraded CEM V HCP show that [63]Ni is retained to a greater extent than on non-degraded CEM I HCP. In opposite to the results obtained for CEM I HCP, in CEM V HCP ternary system, [63]Ni uptake seems to be favored by the presence of 10^{-3}M formic acid in the system, although the results were difficult to interpret, due to some discrepancies between the parallel samples (Figure 5-61).

EURAD (Deliverables n° 3.6, 3.7 and 3.8) - Final Report of results generated in CORI
Dissemination level: PU
Date of issue of this report: **05/07/2024**

Page 198
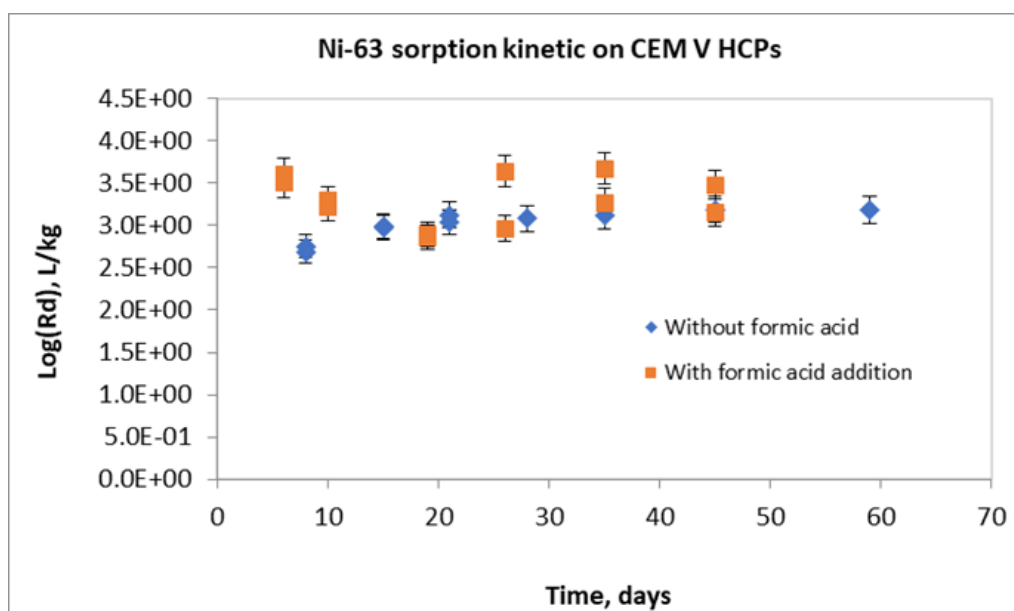
Figure 5-61: [63]Ni uptake on CEM V HCP, in absence and presence of 10^{-3} M formic acid, as a function of time

On the degraded CEM V HCP, [63]Ni uptake is also higher, when comparing the results obtained for R_d values in the experiment with the non-degraded CEM V HCP (*Figure 5-62*).
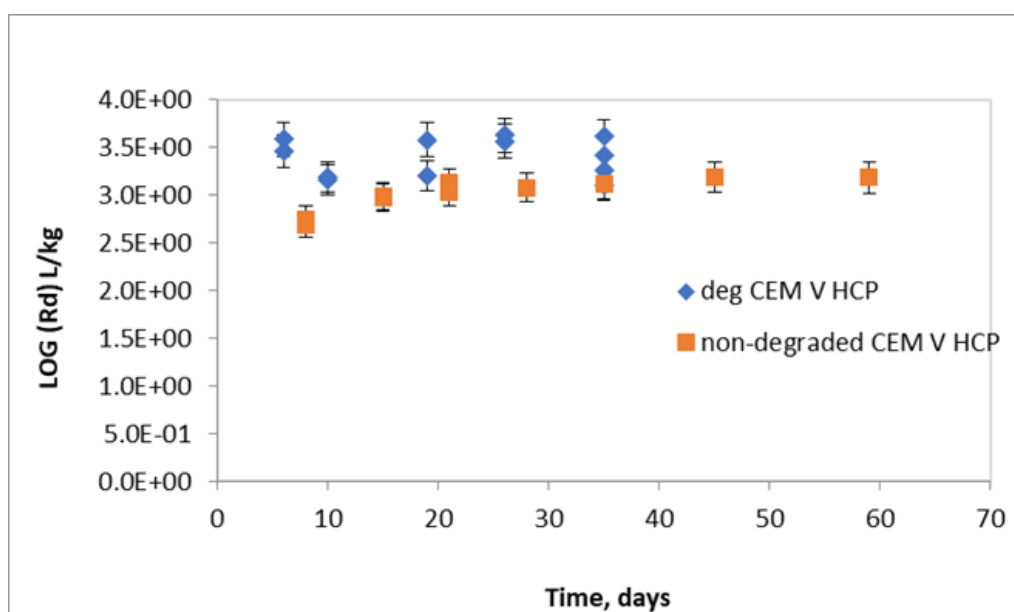
Figure 5-62: [63]Ni sorption uptake on degraded CEM V HCP, in the absence of organic molecules; compared with [63]Ni uptake on non-degraded CEM V HCP.

[KIT] in collaboration with **[EMPA]** analyzed the effect of formate on [242]Pu uptake by C-S-H phases (Ca:Si = 0.8, 1.4), AFm phases and ettringite. In all the cases, formate has no effect on the uptake of Pu. Also the analyzed the impact of formate on [152]Eu on C-S-H. High uptake of Eu(III) has been observed on C-S-H phases in the absence of organic ligands and hyper-alkaline conditions. Formate had a negligible impact on Eu(III) uptake on C-S-H phase with a Ca:Si ratio of 0.8 and 1.4.

EURAD (Deliverables n° 3.6, 3.7 and 3.8) - Final Report of results generated in CORI
Dissemination level: PU
Date of issue of this report: **05/07/2024**

Page 199

5.3.3 Adipate

The effect of adipate on RN mobility in cementitious materials has been studied by **[CPST]** by analysing the effect of adipate on Pu and Am adsorption on HCP. The parameters of the sorption experiments carried out at CPST are summarized in *Table 50*. Commercial Portland cement (CEM I 42.5 R, Heidelberg Cement Group, Sweden) cured 3 months with a water to cement ratio (S/L) of 0.5 under ambient conditions (20°C and relative humidity above 70%) in clogged plastic vials. Then the prepared hardened cement paste (HCP) was dried, crushed in a grinding-mill, and sieved out through 0.25 mm separator.

To achieve the HCP leachate with pH 12.5, the powdered HCP was poured with the deionized water at solid to liquid ratio (S/L) of 0.25 and allowed to shake for 7 days in the air (20°C and relative humidity above 70%). Subsequently, the solution was separated from the solid phase by centrifugation (5000 rpm, 10 min) and the pH of the equilibrium solution was measured. If the pH has not reached the required value, the fresh deionized water was poured into the solid phase and the procedure was repeated under above mentioned ambient conditions until the pH of the equilibrium solution was approximated to ~ 12.50, Eh varied from -323 to -328 mV (*Table 51*).

*Table 50: The experimental conditions carried out at **[CPST]** to investigate Pu and Am adsorption on HCP.*

Radionuclide concentration	[Pu (III/IV)] = $8.5 \cdot 10^{-8}$ M [Am(III)] = $2.0 \cdot 10^{-13}$ M
Organic	Adipic acid (0.1M, 0.2M) Dioctyl adipate (DOA) (0.006 M, 0.012M, 0.019M) Di-iso-octyl phthalate (DIOP) (0.006 M, 0.012M, 0.019M) NaOAc (0.01 M, 0.1M, 1M) Oxalic acid (0.01M, 0.1M, 1M) Citric acid (0.1M, 0.2M)
HCP (CEM I 42.5 R) water	pH ~ 12.5
S/L ratio	0.25
Contact time	3, 7, 14, 30 days
Phase separation	Centrifugation 5000 rpm, 1h
Analytical technique	XRF Alpha/gamma spectrometry Mösbauer spectroscopy
All experiments were performed in the air under ambient conditions	

Table 51: Final pH/Eh of the HCP leachate (S/L 0.25).

Sample	Eh (mV)	pH
D1 (3 days)	-325	12.50
D2 (7 days)	-323	12.48
D3 (14 days)	-327	12.54
D4 (30 days)	-327	12.56
D5 (3 days)	-327	12.54
D6 (7 days)	-328	12.56
D7 (14 days)	-325	12.51
D8 (30 days)	-326	12.53

EURAD (Deliverables n° 3.6, 3.7 and 3.8) - Final Report of results generated in CORI
Dissemination level: PU
Date of issue of this report: **05/07/2024**

Page 200

Solid phase was separated by centrifuging the suspension, dried at 105°C, and further used for batch sorption studies. Sorption kinetics experiments were started immediately to minimize possible changes in the cement caused by the ambient environment. For each series of experiments, fresh HCP was prepared.

For the sorption experiments, solutions of organic substances in deionized water at different concentrations were prepared. The pH of the solutions was adjusted to a value of 12.50 with 0.1 M sodium hydroxide.

A concentrated liquid (oil) of the dioctyl adipate (DOA) was used for the sorption experiment because it is sparingly soluble in water. There 2.5 mL, 5 mL and 7.5 mL of DOA corresponding to the molar concentration of 0.006 M, 0.012 M, 0.019 M were added to the HCP suspension, respectively.

The sorption kinetics tests of Pu(IV) and Am(III) without organic ligands (blank test) were performed under the same experimental conditions.

The tracer solutions of Pu^{4+} ($8.5 \cdot 10^{-8}$ M) and Am^{3+} ($2.0 \cdot 10^{-13}$ M) in 2 M HNO_3 were prepared using ^{239}Pu and ^{243}Am stock solutions (Eckert & Ziegler Isotope Products). The oxidation stage of Pu(IV) was maintained by adding 0.1 ml of 0.5 M $NaNO_2$ to the solution.

For sorption kinetics studies, 40 mL of each organic solutions with different concentrations (in deionized water) adjusted to pH 12.5 were added to 10 g of powdered HCP (S/L ratio 0.25), and the suspensions were allowed to equilibrate for 7 days before spiking with the appropriate amounts of ^{239}Pu and ^{243}Am. The centrifuge tubes were shaken end-over-end for an appropriate period (3, 7, 14, 30 days). After equilibration, the phases were separated by centrifugation, pH of the supernatant was monitored and then it was taken for further radiochemical analysis and preparation of ^{239}Pu sources for alpha spectrometry. Gamma-spectrometric measurements of ^{243}Am in the solid phase of HCP were carried out.

The concentration of ^{239}Pu was measured with the alpha-spectrometer Octete Plus (Ortec). Counting times ranged from 25 to 75 hours depending on the activity of the sample. The alpha counting efficiency was 25% and resolution 25–27 keV, the detection limit of ^{239}Pu for α counting time of 86400 s is 10^{-3} Bq.

Gamma-spectrometric measurements of ^{243}Am in the solid phase were carried out using a HPGe detector with Genie 2000 gamma-spectroscopy analysis software (Canberra Industries, USA). The detector itself was that of GMX series made by Ortec, USA, with relative efficiency of 30%. The detection limit for ^{243}Am is 12 mBq.

The results show high HCP retention capacity of the investigated actinides at pH 12.50 -12.56 in the presence of organics. Sorption kinetic studies showed little effect of adipic acid on Pu (III/IV) uptake by HCP at pH ~12.5 as can be seen in *Figure 5-63*.

Figure 5-63:   *Sorption of Pu(III/IV) on HCP in the presence of variable adipic acid concentration: data represent the residual percentage of Pu(III/IV) in solution at different contact times (3, 7, 14 and 30 days).*

EURAD (Deliverables n° 3.6, 3.7 and 3.8) - Final Report of results generated in CORI
Dissemination level: PU
Date of issue of this report: **05/07/2024**

Page 201

This is consistent with the sorption kinetics in the blank system without adipic acid: all these results have shown rapid sorption kinetics during the first 3 days. The sorption of Pu(III/IV) onto HCP in the absence of adipic acid has suggested that the process might be reversible. Regarding the quantitative uptake of Pu by HCP in the presence of adipic acid after 30 days, it is assumed that adipic acid may inhibit the desorption of Pu from the matrix. Compared to the blank test, the presence of adipic acid had some effect on the sorption of Am(III) onto hardened cement paste during the first seven days with no more than 2% Am(III) remaining in the solution (*Figure 5-64*). During the next 14-30 days, the amount of Am in the solution began to increase indicating the likely reversibility of the sorption.
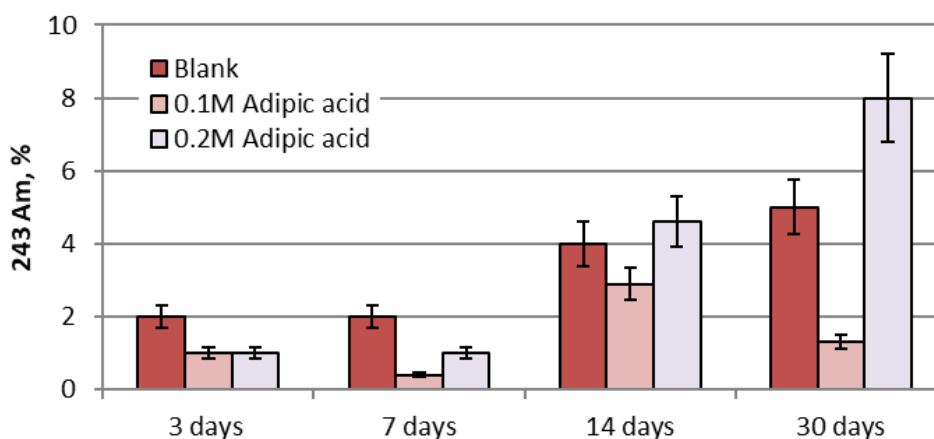
Figure 5-64:   *Sorption of Am(III) on HCP in the presence of variable adipic acid concentration: data represent the residual percentage of Am(III) in solution at different contact times (3, 7, 14 and 30 days).*

Similar tests were also carried out in HCP with Pu(III/IV)/Am(III) at pH~12.5 adding dioctyl adipate (DOA) and the results are shown in *Figure 5-65* and *Figure 5-66*. In this case, the effect is more evident, above all at the highest DOA concentration.

The concentration of di-octyl-adipate (DOA) in the experimental system had a relevant effect on the sorption of Pu and Am(III) to HCP. The sorption of Pu(III/IV) was slightly lower when the concentration of DOA in the system was higher (0.019 M), and the percentage of Pu(III/IV) remaining in the solution varied between 10-20%. The data showed that DOA inhibited the sorption of Am(III) to HCP under certain experimental conditions and this was dependent on the concentration of the organic ligands. The concentration of Am(III) in the solution varied from about 13% after 3 days to about 26% at the end of the experiment (30 days). The summary of the R_d obtained by CPST for Pu/Am sorption in HCP in the presence of adipates are summarized in *Table 52*.

EURAD (Deliverables n° 3.6, 3.7 and 3.8) - Final Report of results generated in CORI
Dissemination level: PU
Date of issue of this report: **05/07/2024**

Page 202
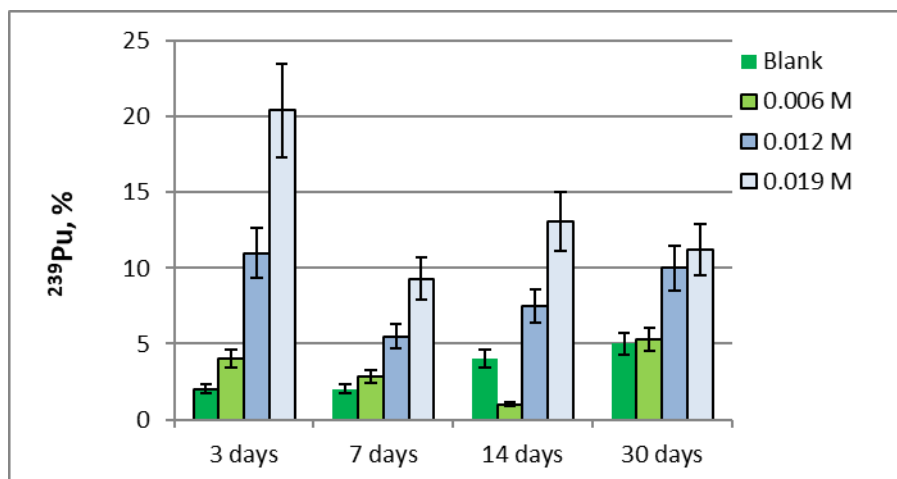
Figure 5-65:   Sorption of Pu(III/IV) on HCP in the presence of variable dioctyl adipate concentration: data represent the residual percentage of Pu(III/IV) in solution at different contact times (3, 7, 14 and 30 days).
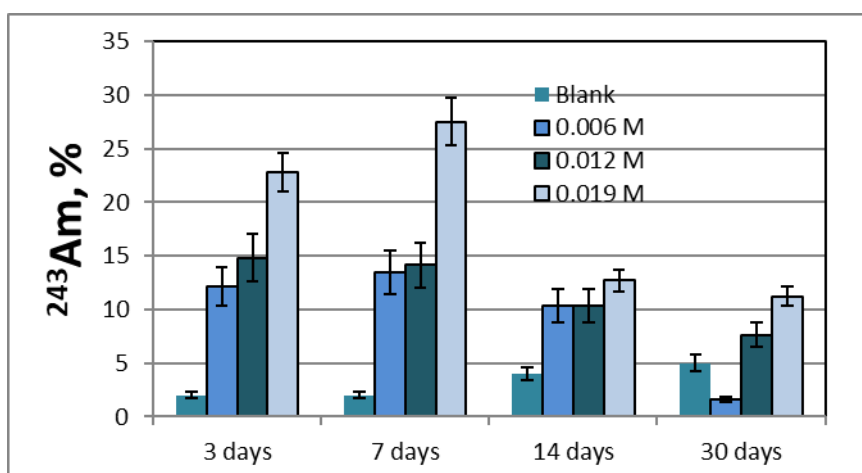
Figure 5-66:   Sorption of Am(III) on HCP in the presence of variable dioctyl adipate concentration: data represent the residual percentage of Am(III) in solution at different contact times (3, 7, 14 and 30 days)..

Table 52: Calculated K_d values for Pu(III/IV) and Am(III) sorption to HCP at pH ~ 12.5 in the presence of 0.1 M and 0.2 M adipic acid and 0.006 M, 0.012 M and 0.019 M dioctyl adipate (DOA)

Days	K_d [L/kg]						K_d [L/kg]					
	Pu(III/IV)			Am(III)			Pu(III/IV)			Am(III)		
	Adipic acid						DOA					
	blank	0.1 M	0.2 M	blank	0.1 M	0.2 M	0.006M	0.012M	0.019M	0.006M	0.012M	0.019M
3	396±20	2496±50	675±26	196±14	392±20	393±20	96±10	32±7	16 ± 4	29 ±5	23 ±5	13 ±4
7	496±22	2645±51	996±32	196±14	996±32	392±20	139±12	69 ±8	39 ±6	26 ±5	24 ±5	10 ±3
14	311±18	2101±46	1424±38	96±10	134±12	83 ±9	396±20	49 ±7	26 ±5	34 ±6	34 ±6	27 ±5
30	140±12	2218±47	1662±41	76 ±9	304±17	46 ±7	71 ±8	36 ±6	32 ±7	249±16	49 ±7	32 ±7

EURAD (Deliverables n° 3.6, 3.7 and 3.8) - Final Report of results generated in CORI
Dissemination level: PU
Date of issue of this report: **05/07/2024**

Page 203

5.3.4 Oxalate and Acetate

The effect of oxalate and acetate on Pu(III/IV)/Am(III) on HCP at pH=12.5 has been studied by **[CPST].**

The experimental details of sorption experiments are summarised in *Table 50*. *Figure 5-67* to *Figure 5-70* shows the results of sorption of Pu and Am in the presence of NaOAc and *Figure 5-71* to *Figure 5-74* shows the results in the presence of oxalic acid. The presence of acetate [NaOAc 0.01 M, 0.1M, 1 M], and oxalic acid [0.01M, 0.1M, 1 M] in the experimental system showed a little effect on HCP sorption of Pu(III/IV) and Am(III) under hyperalkaline conditions.

The kinetic study of both Pu(III/IV) and Am(III) showed that after 7 days equilibrium was reached in both systems with NaOAc and oxalic acid, so no further increase in the sorption values was observed: the residual amount of radionuclides in the supernatant did not exceed 5% after 30 days. However, the experimental distribution coefficient K_d values calculated for Pu(III/IV) and Am(III) in this work are significantly low and continued to decrease throughout the 30 days of the experiment.

It should be noted that in all experimental systems with different organic ligands, low values of Pu(III/IV) and Am(III) K_d and their large fluctuations were determined. There may be several reasons for the variation of K_d. One of the implicit assumptions regarding K_d may be sorption reversibility. On the other hand, during sorption, the sorbing solid is constantly changing, which affects the mechanisms of radionuclide retention by cementitious materials.
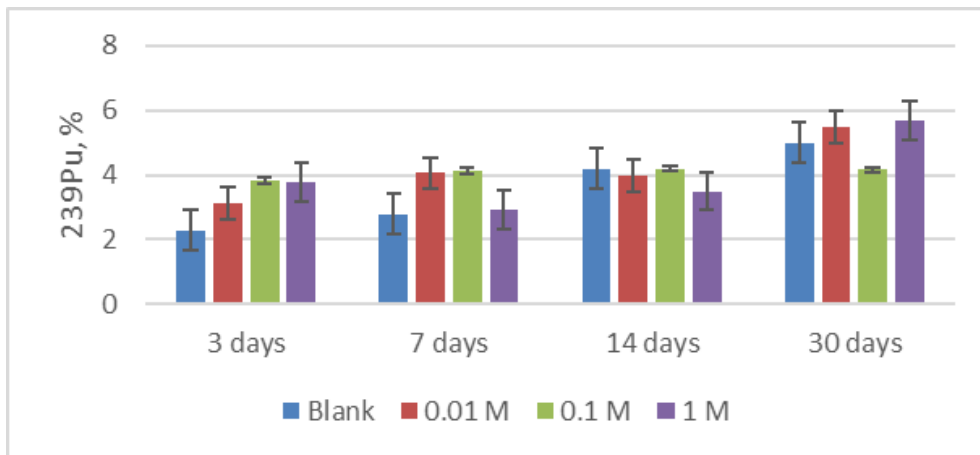
Figure 5-67:   *Sorption of Pu(III/IV) to HCP in the presence of variable NaOAc concentration: data represent the percentage of Pu(III/IV) remaining in solution after different contac times (3, 7, 14 and 30 days).*
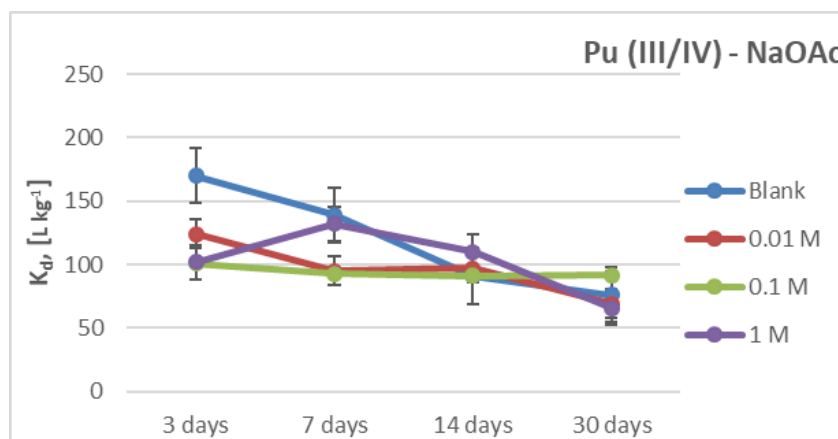
Figure 5-68:   *Evolution of Pu(III/IV) K_d values in HCP in the presence of NaOAc as a function of contact time and organic ligands concentration.*

EURAD (Deliverables n° 3.6, 3.7 and 3.8) - Final Report of results generated in CORI
Dissemination level: PU
Date of issue of this report: **05/07/2024**

Page 204
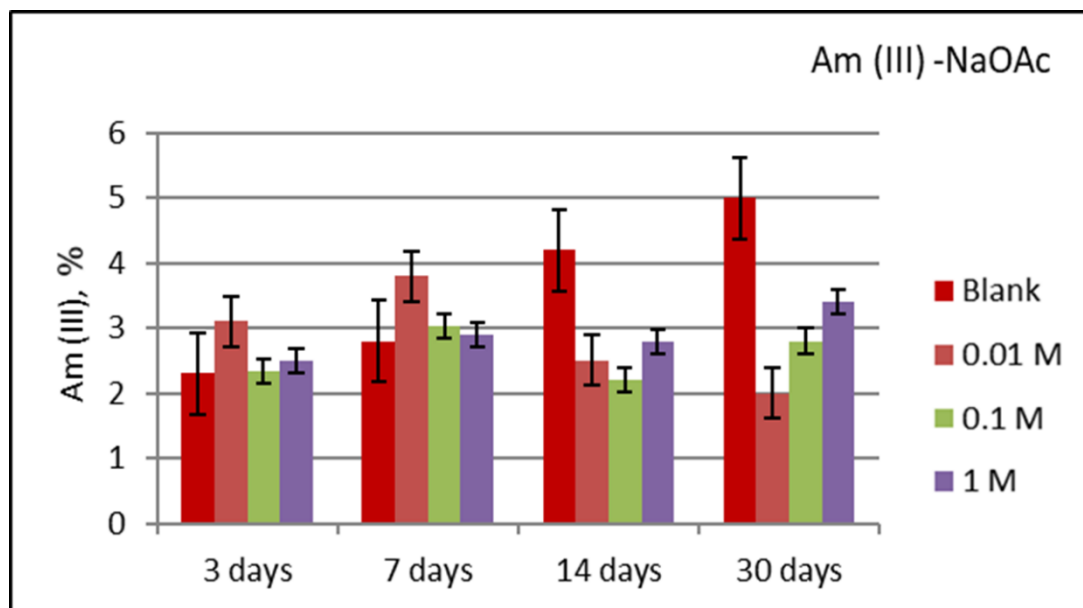
Figure 5-69:   Sorption of Am(III) to HCP in the presence of variable NaOAc concentration: data represent the percentage of Pu(III/IV) remaining in solution after different contact times (3, 7, 14 and 30 days).
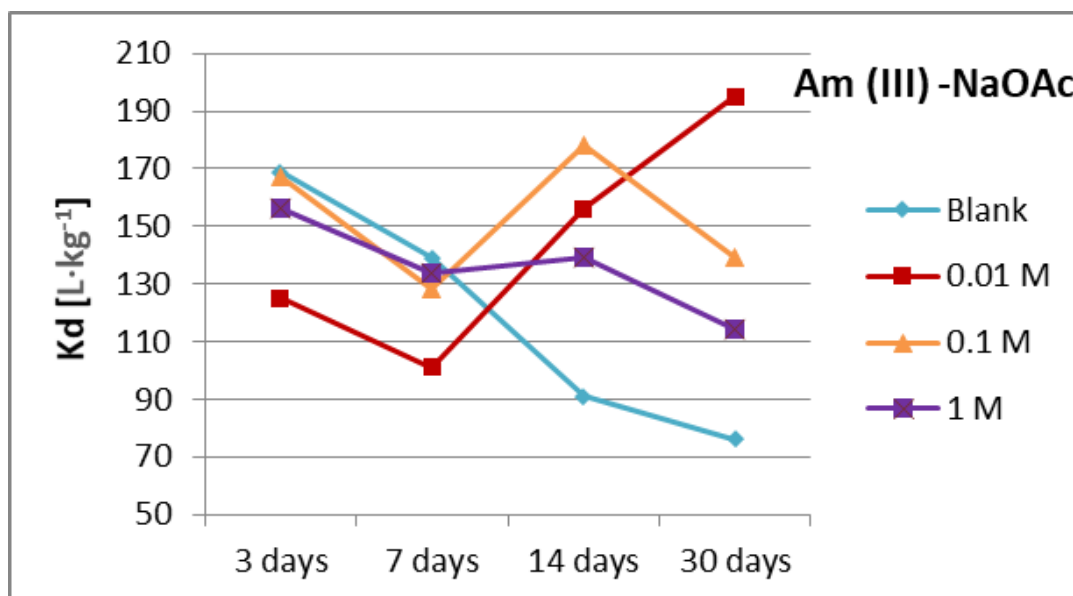
Figure 5-70:   Evolution of Am(III) K_d values in HCP in the presence of NaOAc as a function of contact time and organic ligands concentration.

EURAD (Deliverables n° 3.6, 3.7 and 3.8) - Final Report of results generated in CORI
Dissemination level: PU
Date of issue of this report: **05/07/2024**

Page 205
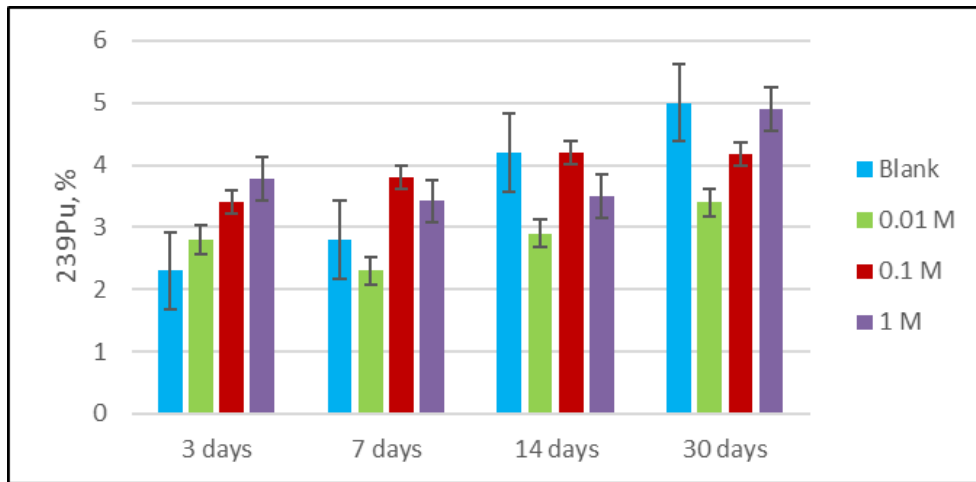
Figure 5-71:   Sorption of Pu(III/IV) to HCP in the presence of variable oxalic acid concentration: data represent the percentage of Pu(III/IV) remaining in solution after different contact times (3, 7, 14 and 30 days).
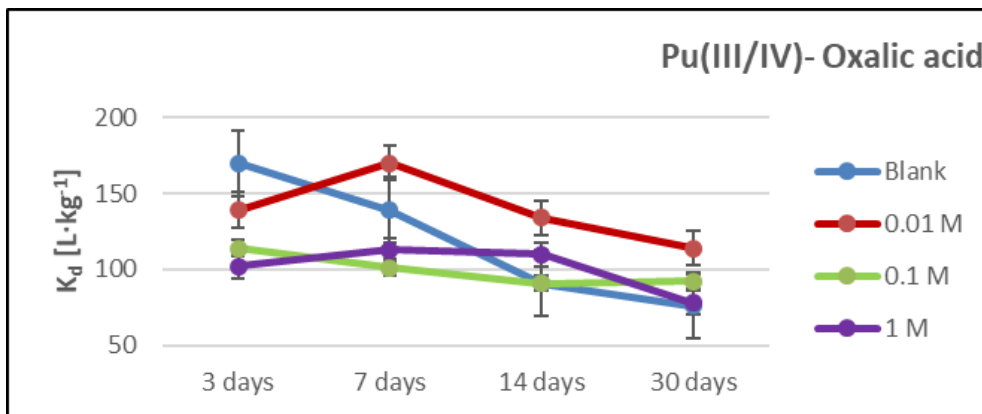
Figure 5-72:   Evolution of Pu(III/IV) K_d values in HCP in the presence of oxalic acid as a function of contact time and organic ligands concentration.
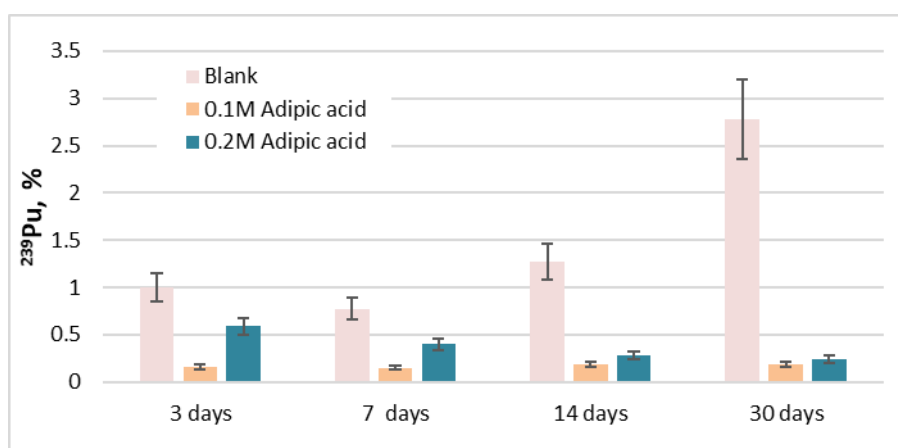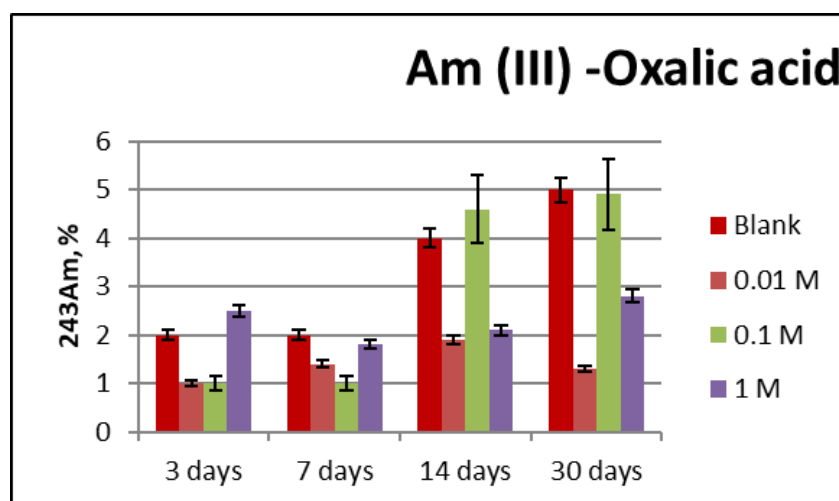

Figure 5-73:   Sorption of Am(III) to HCP in the presence of variable oxalic acid concentration: data represent the percentage of Pu(III/IV) remaining in solution after different contact times (3, 7, 14 and 30 days).

EURAD (Deliverables n° 3.6, 3.7 and 3.8) - Final Report of results generated in CORI
Dissemination level: PU
Date of issue of this report: **05/07/2024**

Page 206
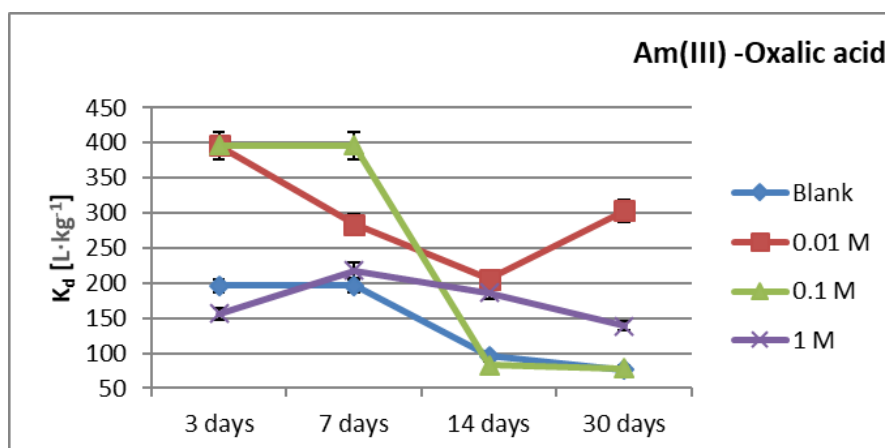
Figure 5-74: *Evolution of Am(III) K_d values in HCP in the presence of oxalic acid as a function of contact time and organic ligands concentration.*

The experiments performed in this study demonstrate the high retention capability of hardened cement paste at Stage II (pH 12.5) towards the investigated actinides in the presence of organic ligands. These results suggest that cement degradation may not have a significant effect on the uptake of actinides (Pu and Am) in the cementitious material in the short term. The organic ligands used to the experimental system had no significant effect on the sorption of radionuclides.

However, relatively low K_d of Pu and Am, which in this case indicates weak affinity of cement for Pu and Am, and its sudden decrease within 30 days of the study raised many questions: (i) contact time to achieve equilibrium of the system, (ii) solid to liquid ratio, because the volume of the solid phase defines the evolution of bulk density and porosity, which in turn define $K_d(R_d)$ value (iii) sufficient radionuclide concentration for reliable determination of K_d; (iv) chemical evolution of HCP under ambient conditions.

5.3.5 Phthalate

The effects of phthalic acid on RN migration in cementitious material has been investigated by **[KIT (Amphos21)]**, **[CEA]**, **[CPST]**, **[CTU]** and **[JUELICH]**.

[KIT (Amphos21)] performed adsorption isotherm for U in presence of phthalate. *Figure 5-75* show the evolution of the R_d values in log as a function of U(VI) in solution after equilibrium in absence or presence of phthalate. For all investigated systems (C-A-S-H1.2-0.005, C-A-S-H1.2-0.2 and RCM) the sorption of uranium is significant. The presence of phthalate until 1mM does not affect the R_d values.

EURAD (Deliverables n° 3.6, 3.7 and 3.8) - Final Report of results generated in CORI
Dissemination level: PU
Date of issue of this report: **05/07/2024**

Page 207

(a)

(b)

(c)
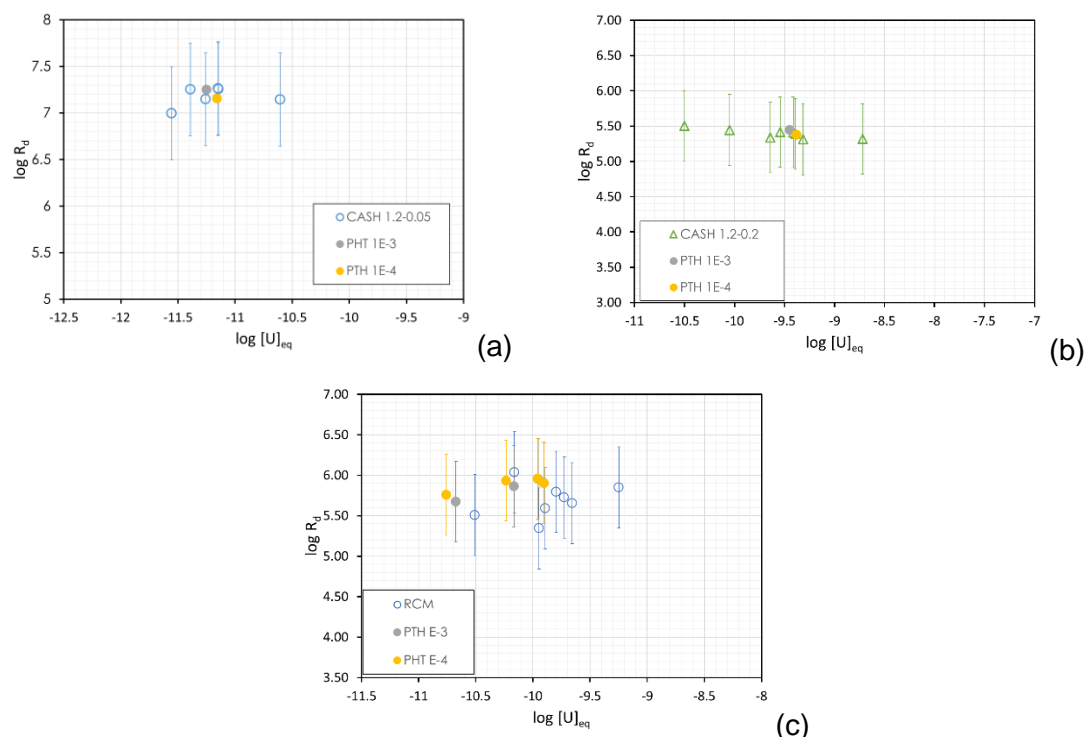
Figure 5-75:   *Sorption of uranium to (a) C-A-S-H 1.2-0.05, (b) C-A-S-H 1.2-0.2 and (c) RCM plotted as concentration of uranium in solution (in mol/L) against calculated log R_d in the presence (filled symbols) and absence (open symbols) of phthalate.*

[CEA] analyzed the migration of [63]Ni and [238]U(VI) in the presence of phthalate by means of sorption and diffusion tests. First, the operational solubility of the radionuclides (U and Ni) in the presence of PHT was analyzed. Figure 5-76 shows the effects on U solubility of the presence of PHT in Stage II solution at different contact times, ranging from 49 days to 238 days.
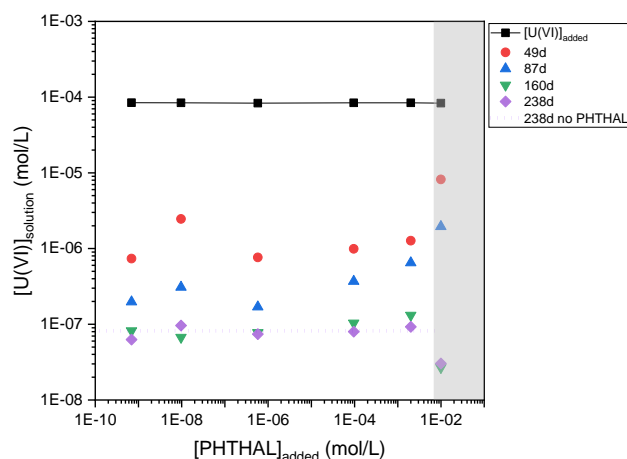
Figure 5-76:   *The effect of the presence of PHT on the evolution of U concentration in Stage II solution for different contact times. Data in the grey zone should be discarded due to uncontrolled experimental conditions.*

The U concentration decreases over time from 10^{-6} M to 10^{-7} M. No significant difference in the U concentration is noted between 160 and 238 days. The solubility for the longer contact time investigated is similar to one without organics. After equilibration, the U concentration is too low for TRLFS measurements. *Nota bene*: The grey rectangles in *Figure 5-76* corresponds to an increase of U

EURAD (Deliverables n° 3.6, 3.7 and 3.8) - Final Report of results generated in CORI
Dissemination level: PU
Date of issue of this report: **05/07/2024**

Page 208

concentration in solution for the highest organic addition. It appears that the pH value decreases to more acidic conditions due to the organic addition. Similarly, the operational solubility has been studied for the water representative of the Stage IV of HCP degradation. The results are shown in *Figure 5-77*, for different contact times, ranging from 1 day to 28 days.

The U concentration in the presence of organics is lower than without organics. Results show a decrease in the U concentration with highest phthalate concentration. The pH was not adjusted after the start of the experiment at pH 9. The pH decreases to 8.5, 7.7 and 7.0 at respectively 5, 15 and 28 days in the presence of phthalate. Therefore, it is suspected that the increase in solubility over time is a pH effect.
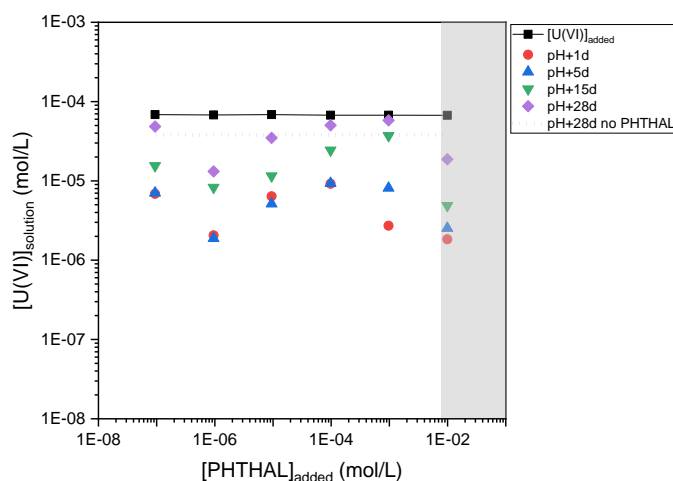
Figure 5-77:   *The effect of the presence of organics on the evolution of U concentration in Stage IV solution for different contact times. Data in the grey zone should be discarded due to uncontrolled experimental conditions.*

The TRLFS spectra presented in Figure 5-78 suggest that phthalate interaction is stronger at the lower concentration, with a cut-off between $9.5 \cdot 10^{-6}$ and $9.7 \cdot 10^{-5}$ M.
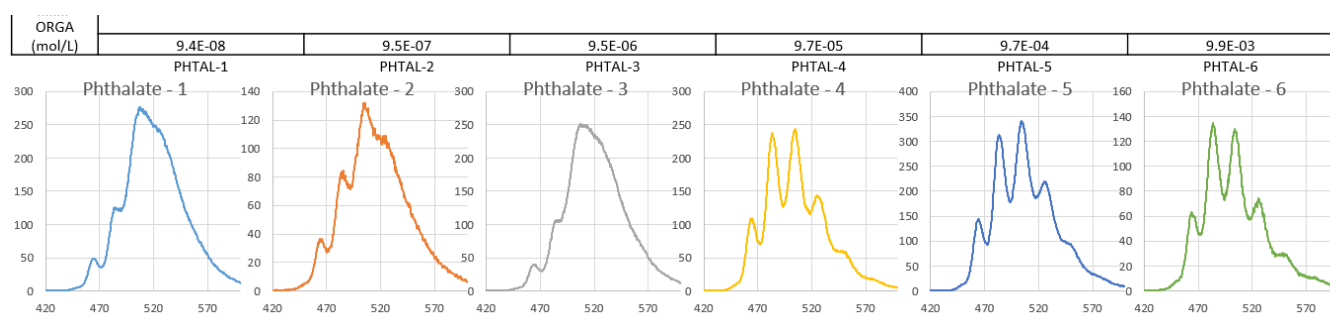
Figure 5-78:   *TRLFS spectra of the U - PHT solubility experiment in Stage IV water. There are clearly two different species present in the phthalate systems. Where the U-CO₃ complexes (distinguished by the '5 fingers') are present strongest in the highest concentration phthalate.*

For what concerns Ni solubility, Figure 5-79 represents the effect of the presence of organics on the evolution of Ni concentration in S2 solution for different contact times, ranging from 2 days to 449 days.

EURAD (Deliverables n° 3.6, 3.7 and 3.8) - Final Report of results generated in CORI
Dissemination level: PU
Date of issue of this report: **05/07/2024**

Page 209
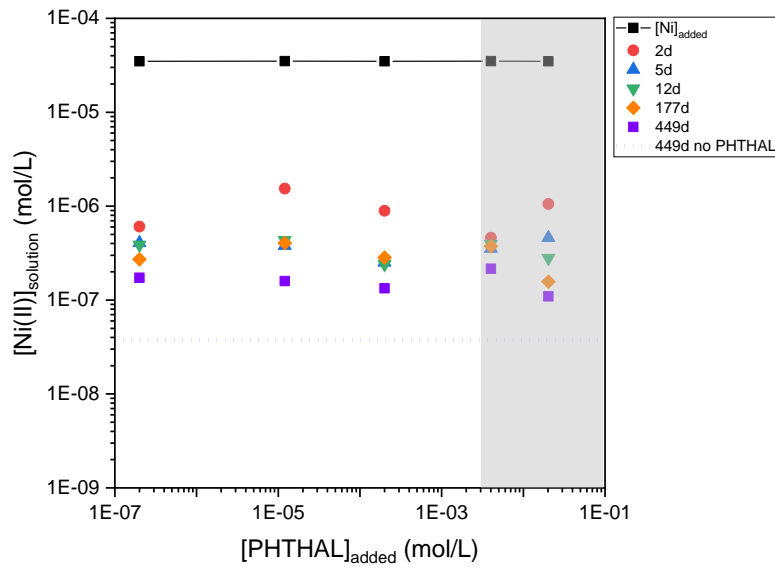
Figure 5-79:   *The effect of the presence of organics on the evolution of Ni concentration in S2 solution for different contact times. Data in the grey zone should be discarded due to uncontrolled experimental conditions.*

The residual Ni concentration after 449 days in the absence of organics is $4 \cdot 10^{-8}$ M. The addition of phthalate increases the Ni concentration in solution; however there is no effect of the phthalate concentration. The solubility of the PHT-Ni decreases over time and tend to $1.5 \cdot 10^{-7}$ M after 449 days of equilibration.

Figure 5-80 shows the effect of the presence of PHT on the evolution of Ni concentration in Stage IV solution.
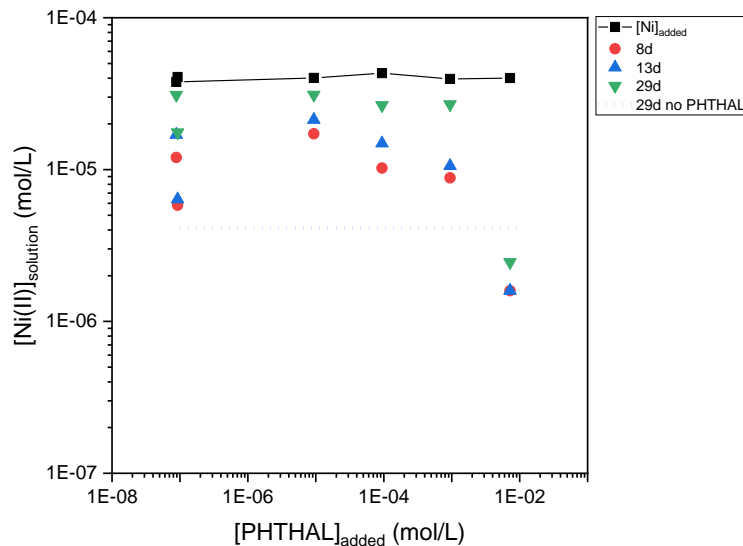
Figure 5-80:   *The effect of the presence of organics on the evolution of Ni concentration in Stage IV solution for HCP CEM V/A and different contact times.*

Except for the highest PHT concentration, the Ni concentration in solution increase with time and for most investigated organic concentration and tend to reach a plateau at $4 \cdot 10^{-5}$ M, *i.e.* the Ni added concentration. As many pH adjustments were necessary before and after sampling, and some solid

EURAD (Deliverables n° 3.6, 3.7 and 3.8) - Final Report of results generated in CORI
Dissemination level: PU
Date of issue of this report: **05/07/2024**

Page 210

precipitation occurs with time in the filtrated oversaturated calcite solution, these solubility results are difficult to interpret. Data obtained after 29 days of contact time are strongly influenced by change in pH.

Sorption studies were carried out in the ternary CEMV /PHT/ U system under Stage II conditions, different contact times, ranging from 2 days to 30 days, and the results are shown in *Figure 5-81*.
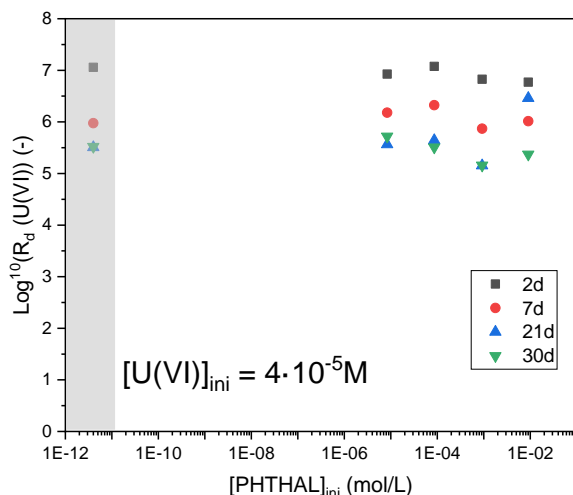
Figure 5-81: *The effect of the presence of PHT on the retention of U(VI) in S2 solution for HCP CEM V/A and different contact times. The grey rectangle corresponds to sorption data obtained in absence of organic species.*

In the phthalate system, the data cannot be interpreted as sorption data as far as the initial U(VI) concentration was set over the measured solubility limit. Experiments were also carried out with the RCM at Stage II. *Figure 5-82* represents the experimental U(VI) retention results obtained at different contact times, ranging from 2 days to 92 days. An increase of the R_d value with time is observed. For the highest organic concentration addition, pH of the resulting supernatant was not checked, and the data should not be included in the interpretation. For an initial U(VI) concentration of $5 \cdot 10^{-7}$ M, there is a limited effect of the nature of the organic species onto the U(VI) retention.
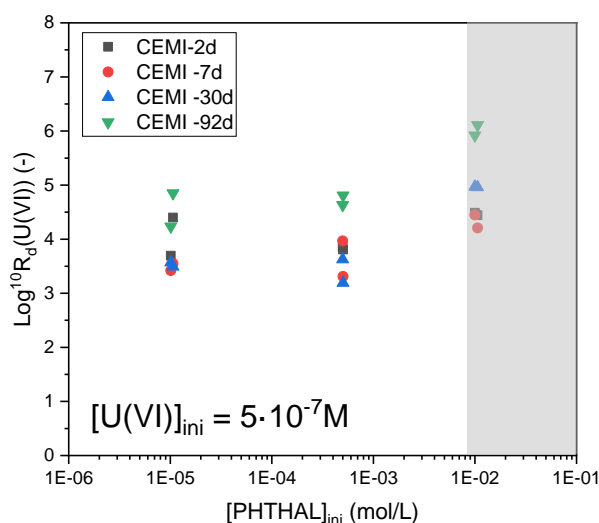
Figure 5-82: *The effect of the presence of organics on the retention of U(VI) in S2 solution for RCM and different contact times. Data in the grey zone should be discarded due to uncontrolled experimental conditions.*

EURAD (Deliverables n° 3.6, 3.7 and 3.8) - Final Report of results generated in CORI
Dissemination level: PU
Date of issue of this report: **05/07/2024**

Page 211
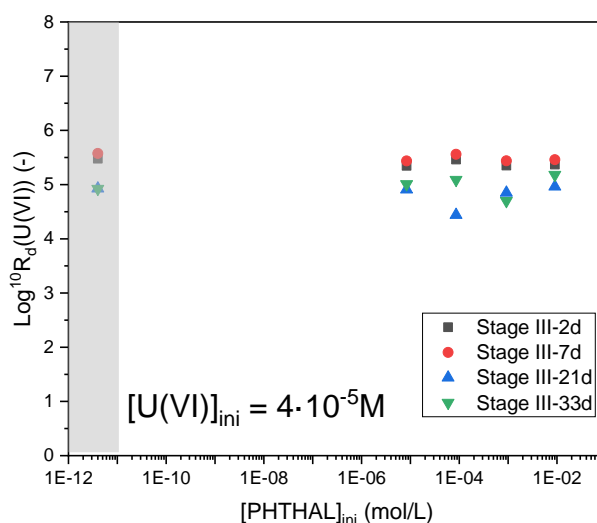
Figure 5-83: *The effect of the presence of organics on the retention of U(VI) in Stage III/IV solution for HCP CEM V/A and different contact times. The grey rectangle corresponds to sorption data obtained in absence of organic species.*

Figure 5-83 represents the experimental U(VI) retention results obtained for PHT on HCP CEM V/A in water representative of the stage III/IV and for and different contact times, ranging from 2 days to 33 days. In the PHT system, the data can not be interpreted as sorption data as far as the initial U(VI) concentration was set over the measured solubility limit.

Figure 5-84 represents the experimental Ni(II) retention results obtained for the organics species on HCP CEM V/A in Stage II solution with different contact time, ranging from 2 days to 33 days. From these data, one can conclude that there is no effect of the presence, the concentration or nature of the organic species onto the Ni(II) retention on the HCP at Stage II. The Ni retention is significant and R_d values are ranging between 10^3 and 10^4 L/kg.
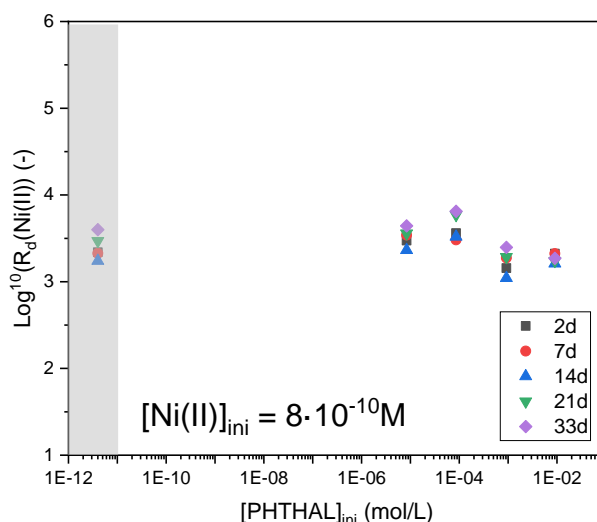
Figure 5-84: *The effect of the presence of PHT on the retention of Ni(II) in ACW Stage II for HCP CEM V/A and different contact times. The grey rectangle corresponds to sorption data obtained in absence of organic species.*

EURAD (Deliverables n° 3.6, 3.7 and 3.8) - Final Report of results generated in CORI
Dissemination level: PU
Date of issue of this report: **05/07/2024**

Page 212
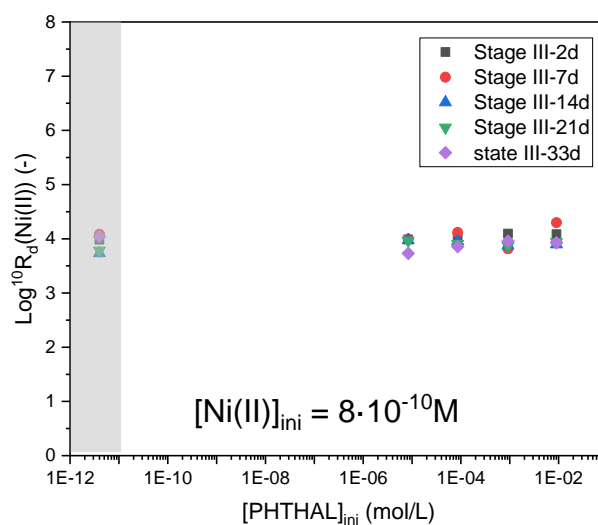
Figure 5-85:   *The effect of the presence of organics on the retention of Ni(II) in Stage III/IV solution for HCP CEM V/A and different contact times. The grey rectangle corresponds to sorption data obtained in absence of organic species.*

Figure 5-85 represents the experimental Ni(II) retention results obtained for PHT on HCP CEM V/A in stage III/IV at different contact time, ranging from 2 days to 33 days. From these data, one can conclude that there is no effect of the presence and the concentration of PHT species onto the Ni(II) retention. The Ni retention is significant, and a constant R_d values of *ca.* 10^4 L/kg have been determined.

[CEA] performed in-diffusion tests for the system ^{63}Ni/phthalate/HCP CEM V/A at Stage II (F3 cell). The activity of ^{63}Ni in the solution was measured during 109 days of diffusion. At the beginning of the experiment, the activity decreased to reach around 20% of the initial activity introduced in the upstream compartment (see *Figure 5-86*a). This can be linked to high retention (or precipitation) and low diffusive behavior of the Ni-phthalate species. After 109 days, the HCP sample has been removed from the solution and dried overnight and cut in two pieces. Prior to the multi-abrasive steps /lixiviation procedure, the two parts have been measured by digital autoradiography (DA) in order to directly access the diffusion profiles (see "DA-profile-1" and "DA-profile-2" series in *Figure 5-86*b). These DA-profiles have been compared to the one obtained after the abrasive peeling procedure (see "MG-profile" series in *Figure 5-48*b). As observed in the *Figure 5-86*b, there are some discrepancies between the two techniques and no explanation can be given for the moment. The penetration of ^{63}Ni (or ^{63}Ni-phthalate complex) in the solid is very limited close to the surface of the HCP sample. The black straight line in the *Figure 5-86*b corresponds to the end of the sample, so any data collected after this line is representative to the background intensity observed on the autoradiography screen. In respect with what has been observed for EDTA, the presence of phthalate does significantly reduce the ^{63}Ni migration. For a similar diffusion time, the response of the DA showed a shorter ^{63}Ni profile in presence of phthalate. This result is consistent with the operational solubility measurements. In that study case, the migration of ^{63}Ni seems to be limited by its precipitation at the surface.

EURAD (Deliverables n° 3.6, 3.7 and 3.8) - Final Report of results generated in CORI
Dissemination level: PU
Date of issue of this report: **05/07/2024**

Page 213

(a)

Cell F3: Ni-63 + PHTHALATE / S2

(b)

^{63}Ni-Diffusion profiles / F3 cell + PHTHALATE
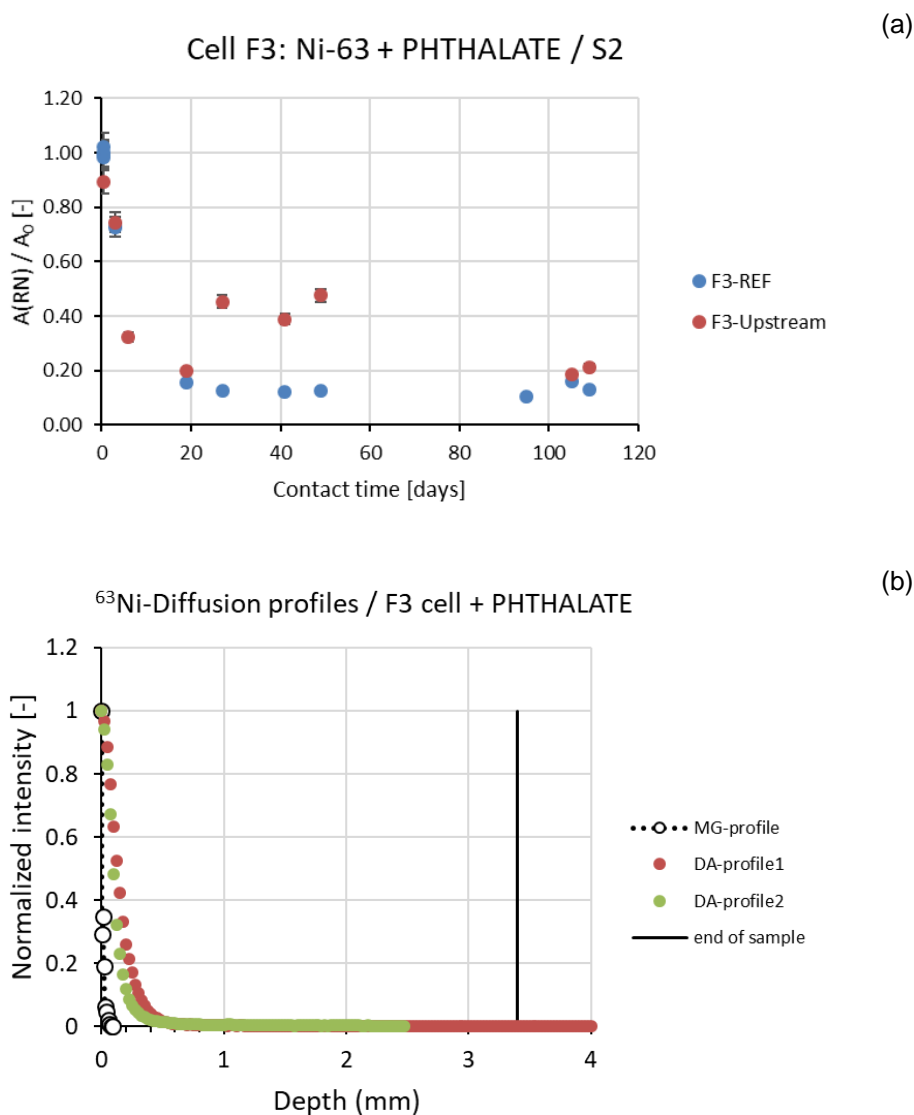
Figure 5-86:   *In-diffusion of ^{63}Ni in HCP CEM V/A at Stage II in presence of phthalate (A) evolution of the activity of ^{63}Ni in S2 solution containing initially with $5 \cdot 10^{-2}$M of phthalate (B) Diffusion profiles obtained by two methods: multi-abrasive steps/lixiviation in a CEM V/A disk in Stage II solution over time (F3 cell) – the black straight line corresponds to the end of the sample.*

[CPST] performed sorption experiments with Pu(III/IV) [$8.5 \cdot 10^{-8}$ M] and Am(III) [$2.0 \cdot 10^{-13}$ M] using diisooctyl phthalate (DIOP) (0.006 M, 0.012M, 0.019M) in HCP CEM I 42.5 R) at pH ~12.5. The contact water used was deionized water and the pH of the solutions was adjusted to a value of 12.50 with 0.1 M sodium hydroxide. The sorption kinetics tests of Pu(IV) and Am(III) without the organic (blank test) were performed under the same experimental conditions.

For sorption kinetics studies, 40 mL of each organic solutions with different concentrations (in deionized water) adjusted to pH 12.5 were added to 10 g of powdered HCP (S/L ratio 0.25), and the suspensions were allowed to equilibrate for 7 days before spiking with the appropriate amounts of ^{239}Pu and ^{243}Am. The centrifuge tubes were shaken end-over-end for an appropriate period (3, 7, 14, 30 days). After equilibration, the phases were separated by centrifugation, pH of the supernatant was monitored and then it was taken for further radiochemical analysis and preparation of ^{239}Pu sources for alpha

EURAD (Deliverables n° 3.6, 3.7 and 3.8) - Final Report of results generated in CORI
Dissemination level: PU
Date of issue of this report: **05/07/2024**

Page 214

spectrometry. Gamma-spectrometric measurements of ^{243}Am in the solid phase of HCP were carried out.

Figure 5-87 shows the results of Pu adsorption tests in the presence of DIOP obtained after different times (3 to 30 days). The percentage of Pu remained in solution is very low and, in general, is lower in the presence of DIOP. *Figure 5-88* shows the K_d values obtained for Pu at different times and DIOP concentration. As can be seen, within the experimental error, the concentration of DIOP does not affect the retention in the HCP.
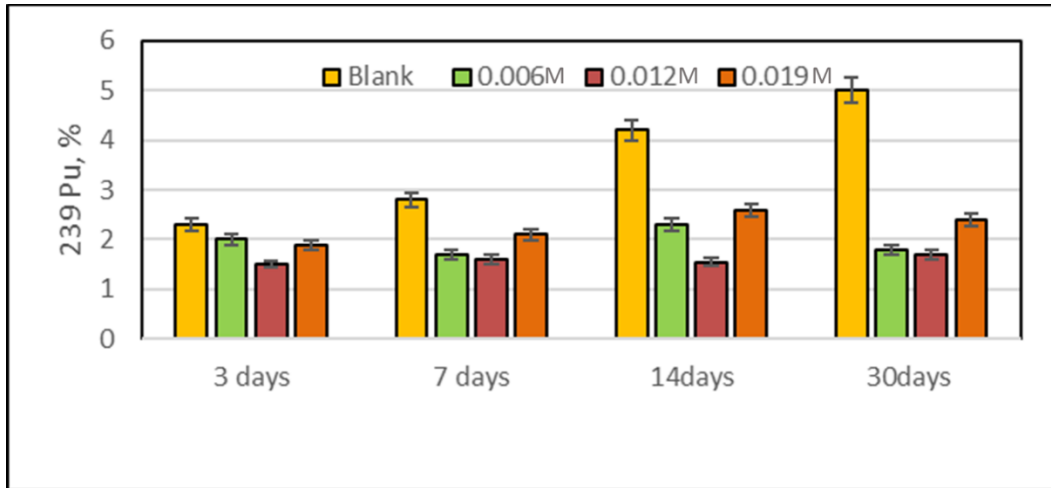
Figure 5-87:   Sorption of Pu(III/IV) on HCP in the presence of variable DIOP concentration: data represent the residual percentage of Pu(III/IV) in solution after different contact time (3, 7, 14 and 30 days).
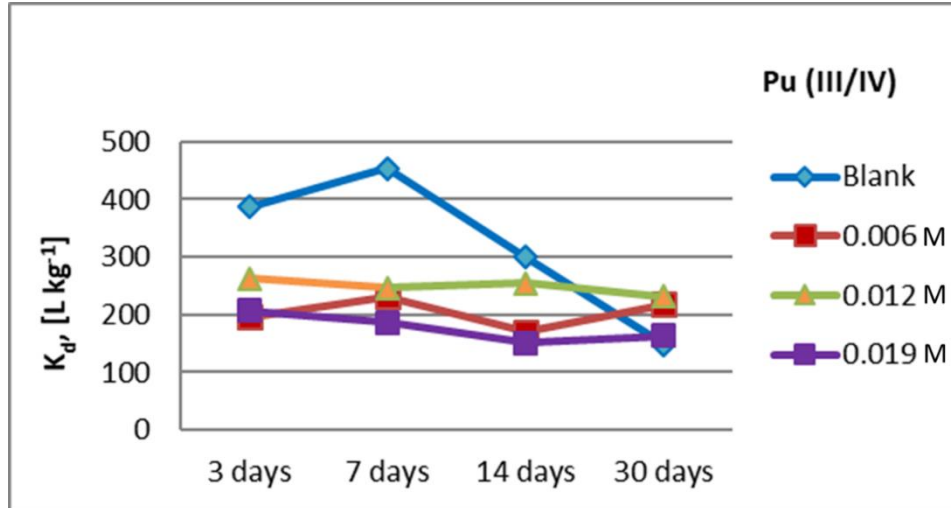
Figure 5-88:   Evolution of Pu(III/IV) K_d values in HCP in the presence of DIOP as a function of contact time and organic ligands concentration.

Figure 5-89 shows the results of Am adsorption tests in the presence of DIOP obtained after different times (3 to 30 days). The percentage of Am remained in solution increases with increasing the DIOP concentration.

EURAD (Deliverables n° 3.6, 3.7 and 3.8) - Final Report of results generated in CORI
Dissemination level: PU
Date of issue of this report: **05/07/2024**

Page 215
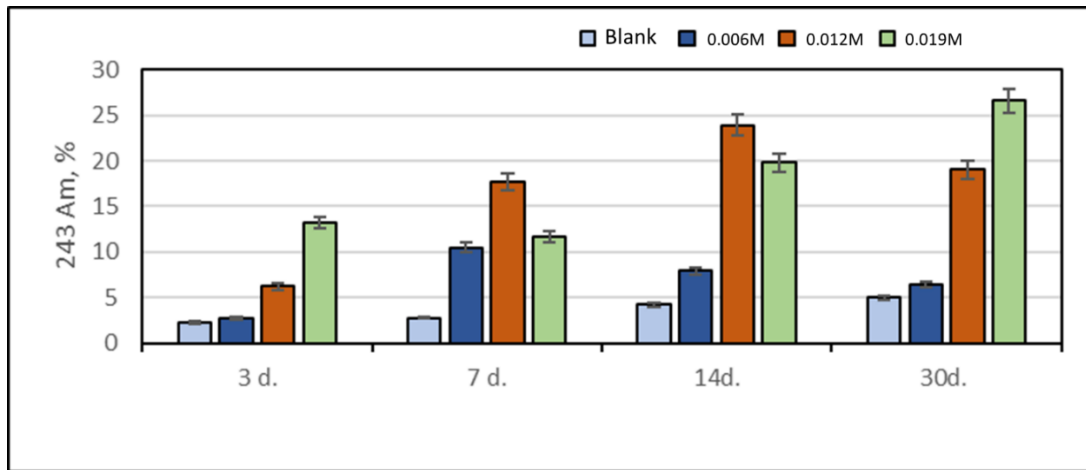
Figure 5-89:   *Sorption of Am(III) on HCP in the presence of variable DIOP concentration: data represent the residual percentage of Am(III) in solution after different contact time (3, 7, 14 and 30 days)..*

Figure 5-90 shows the K_d values obtained for Am at different times and DIOP concentration. K_d values tend to decrease with the presence of DIOP. However, K_d without the ligand also tend to decrease with time, which can be related to chemical evolution of the system.
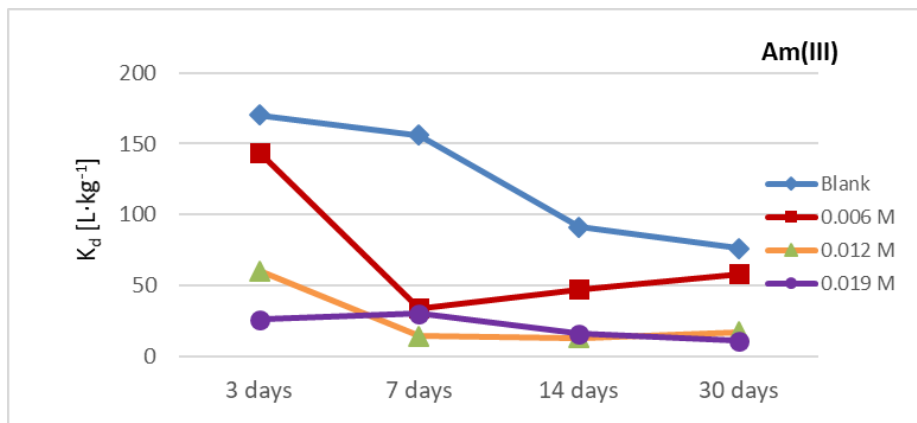
Figure 5-90   *Evolution of Am(III) K_d values in HCP in the presence of DIOP as a function of contact time and organic ligands concentration.*

These results show small effect of DIOP on Pu and Am retention in HCP.

EURAD (Deliverables n° 3.6, 3.7 and 3.8) - Final Report of results generated in CORI
Dissemination level: PU
Date of issue of this report: **05/07/2024**

Page 216

[CTU] determined R_d and sorption reduction factor values (SRF) for Eu, and Pb in HCP in the presence of PHT and the results are summarized in Table 53.

Table 53: Average values of distribution ratios R_d (L·kg^{-1}) and SRF for U, Eu, and Pb in systems with organics and C-S-H.

Material	System	Average R_d [L·kg^{-1}]	SRF
HCP CEM I	^{152}Eu (2.9·10^{-9} mol·L^{-1})	(11.9 ± 2.2)·10^3	-
HCP CEM I	^{152}Eu + phtalate 5·10^{-3} mol·L^{-1}	(29.1 ± 5.4)·10^3	0.59 ± 0.12
HCP CEM I	Pb (5·10^{-4} mol·L^{-1})	(0.8-1.6)·10^{3*}	-
HCP CEM I	Pb + phthalate 5·10^{-5} mol·L^{-1}	(0.9-1.9)·10^{3*}	0.9 ± 0.1
HCP CEM III	Pb (5·10^{-4} mol·L^{-1})	(1.8-2.3)·10^{2*}	-
HCP CEM III	Pb + phthalate 5·10^{-5} mol·L^{-1}	(2.3-3.0)·10^{2*}	0.7 ± 0.1

*range of R_d for non-linear dependences of R_d on L/S

[CTU] also analysed the adsorption of uranium at different solid to liquid ratio in HCP (CEM I) in the presence of PHT (*Figure 5-49*). The data without PHT, showed an increasing trend as the solid to liquid ratio increased; similar trend is observed in the presence of PHT.

[JUELICH] studied the uptake/retention and migration behavior of ^{241}Am and ^{152}Eu in the presence of phthalate on C-A-S-H phases and HCP (CEM V). The aim of the work was to provide insights into the role and significance of selected organic degradation products such as phthalates (degradation product of PVC additives and superplasticizers). The retention behavior of ^{241}Am and ^{152}Eu at tracer concentration on hardened cement pastes (HCP) prepared from a CEM V/A 42.5N was studied in batch sorption experiments and in diffusion experiments under anoxic conditions in the presence and absence of phthalate. Preparatory solubility tests showed that phthalate concentrations up to 10^{-3} mol·kg^{-1} have no impact on the dissolved and colloidal fractions of ^{241}Am and ^{152}Eu in cementitious waters. In the absence of organics, a strong uptake of ^{241}Am and ^{152}Eu on the CEM V/A HCP was observed with distribution ratios, R_d, in the order of 10^5 to 10^6 L·kg^{-1}. The uptake of ^{241}Am and ^{152}Eu uptake was found to be dependent on the aqueous phthalate concentration, leading to a distinct decrease of the R_d values at phthalate concentrations above 1·10^{-3} mol·kg^{-1}. The reduction of the ^{241}Am and ^{152}Eu uptake in the presence of phthalate is attributed to the destabilisation/dissolution of C-S-H/C-A-S-H due to increasing Ca-complexation by phthalate in solution.

Cylindrical HCP monoliths (diameter = 5 cm and height = 5 cm) were obtained from the *Commissariat à l'énergie atomique et aux énergies alternatives* (CEA). The hardened cement paste (HCP) was manufactured in February 2016 from a CEM V/A cement (CEM V/A (S-V) 42.5N CE PM-ES-CP1 NF, Calcia, Rombas) with a cement/water ratio of 0.40 as described by Macé *et al.* (2019). The CEM V/A is a ternary blended cement consisting of 54% Ordinary Portland cement (OPC), 23% blast furnace slag (BFS), and 23% fly ash (FA), and is expected to be used in the French nuclear waste disposal program (*cf.* Bildstein and Claret, 2015; Claret *et al.*, 2018). The HCP cylinders (were stored at room temperature in a glove box under controlled atmosphere (Ar) to avoid carbonation. The HCP was mechanically crushed for use in batch sorption experiments. The HCP was characterized with respect to the phase assemblage by XRD and TG-DSC, using crushed and powdered material. The hydration phases comprised predominately C-S-H phases (*ca.* 80 wt.%) and some ettringite (c. 10 wt.%); in addition, minor amounts of portlandite (*ca.* 6 wt.%) and unreacted clinker phases (alite/belite, *ca.* 3 wt.%) were found, as well as traces of calcite.

CEM V/A water was prepared by immersing crushed HCP in Milli-Q water (Millipore, 18.2 MΩ·cm at 25°C and total organic carbon TOC content = 2 ppb) at a solid-to-liquid ratio of 12 g·L^{-1} (Pointeau *et al.*,

EURAD (Deliverables n° 3.6, 3.7 and 3.8) - Final Report of results generated in CORI
Dissemination level: PU
Date of issue of this report: **05/07/2024**

Page 217

2004). The Stage III free of portlandite was obtained with a resulting pH of 12.2, which is regulated by the dissolution of C-(A)-S-H phases.

Previous solubility tests were carried out with ^{241}Am and ^{152}Eu in the CEM V/A water. Results are expressed as a function of the phthalate concentration for different initial radionuclide concentrations (*Figure 5-91*).

Already a first decrease of ^{241}Am and ^{152}Eu concentrations in comparison with the input concentrations can be observed before the centrifugation. This decrease of the concentrations of ^{241}Am and ^{152}Eu is due to the sorption on the walls of the centrifuge tubes. After centrifugation, a further decrease in the activity of ^{241}Am and ^{152}Eu is observed, which can be explained by the presence of ^{241}Am and ^{152}Eu colloids generated in CEM V/A water and settled during centrifugation. The presence of PHT at different concentrations shows no influence on the input and output concentrations of ^{241}Am and ^{152}Eu in CEM V/A water, *i.e.*, does not influence the solubility of the radionuclides and their sorption to the centrifugation tubes and colloids, respectively. Though PHT are strong complexing ligands at near neutral conditions, under cementitious conditions their impact on the speciation and solubility of ^{241}Am and ^{152}Eu is negligible, confirmed by thermodynamic calculations.

EURAD (Deliverables n° 3.6, 3.7 and 3.8) - Final Report of results generated in CORI
Dissemination level: PU
Date of issue of this report: **05/07/2024**

Page 218
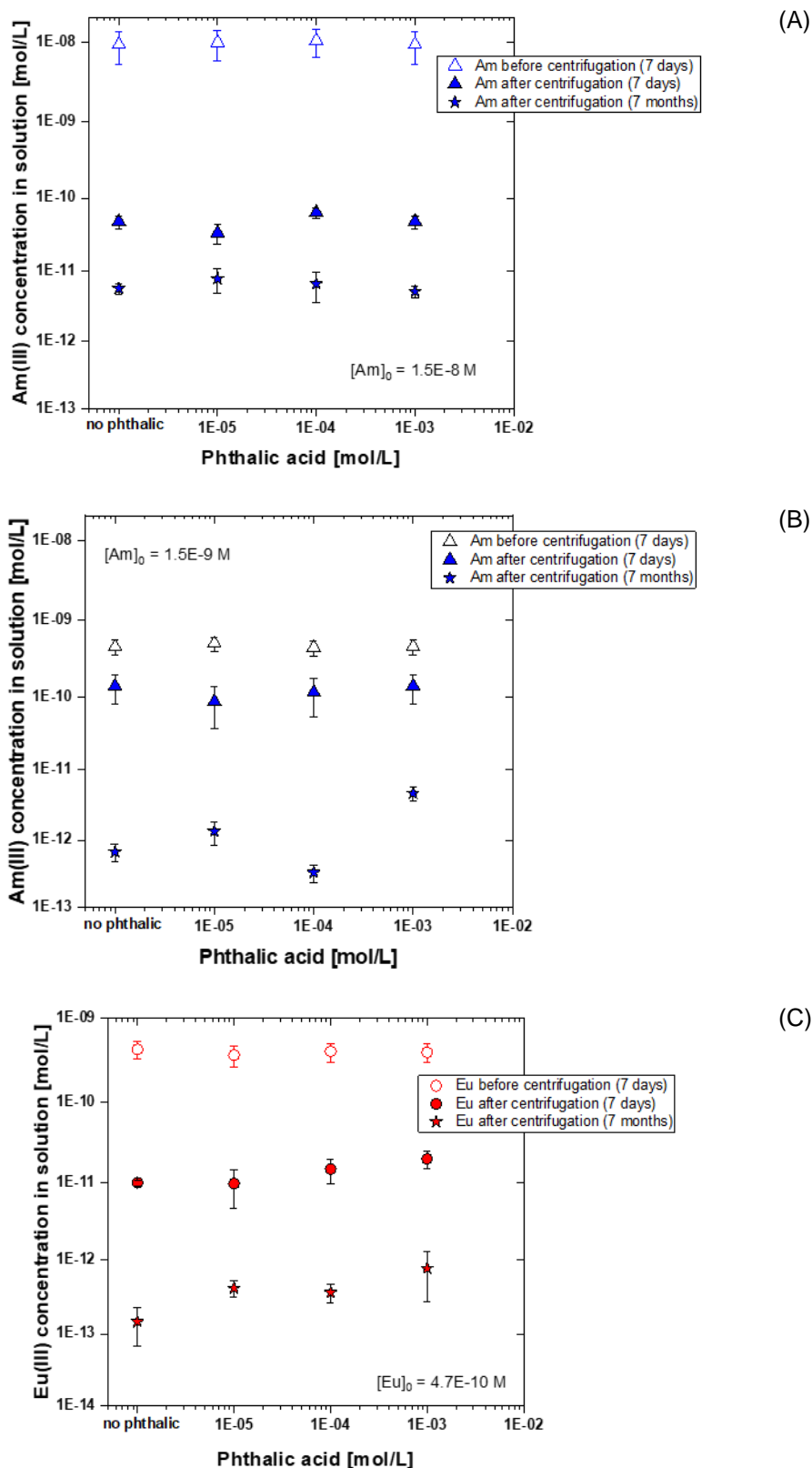
Figure 5-91: ^{241}Am and ^{152}Eu concentration in HCP CEM V/A equilibrated water as a function of the phthalic acid concentrations after 7 days and 7 months equilibration, at different initial concentrations of the RN: (A) for $[Am]_0 = 1.5 \cdot 10^{-8}$ M, (B) for $[Am]_0 = 1.5 \cdot 10^{-9}$ M and (C) for $[Eu]_0 = 4.7 \cdot 10^{-10}$ M. Background electrolyte is the CEM V/A water at equilibrium with the HCP at Stage III.

EURAD (Deliverables n° 3.6, 3.7 and 3.8) - Final Report of results generated in CORI
Dissemination level: PU
Date of issue of this report: **05/07/2024**

Page 219

The results of ^{241}Am and ^{152}Eu batch sorption experiments with CEM V/A HCP in absence and presence of PHT are shown in *Figure 5-92*. In the absence of phthalate, R_d values of ^{241}Am and ^{152}Eu are in the range 10^5 L·kg^{-1} < R_d < 10^6 L·kg^{-1}. These values are in good agreement with the results obtained in the literature (*cf.* Tits and Wieland, 2018; Pointeau *et al.*, 2001; Ochs *et al.*, 2016), considering that in absence of organics, the mentioned authors did not observe a distinct effect of the degradation stage on *An*(III)/*Ln*(III) sorption. The uptake of ^{241}Am and ^{152}Eu is associated with their incorporation into the C-S-H structure, substituting for Ca^{2+} in the C-S-H interlayer and in the Ca-octahedral layer (cf. Tits *et al.*, 2003b; Tits and Wieland, 2018). In the investigated systems, ^{241}Am and ^{152}Eu uptake by HCP CEM V/A was found to be strongly dependent on the aqueous phthalate concentration (*cf. Table 54*). The results in *Figure 5-92* show a plateau of the uptake at low phthalate concentrations (< 10^3 M), where the R_d values are like those in absence of PHT, followed by a distinct decrease in the R_d values above a so-called "concentration edge" (Tits *et al.*, 2005).

(A)

(B)
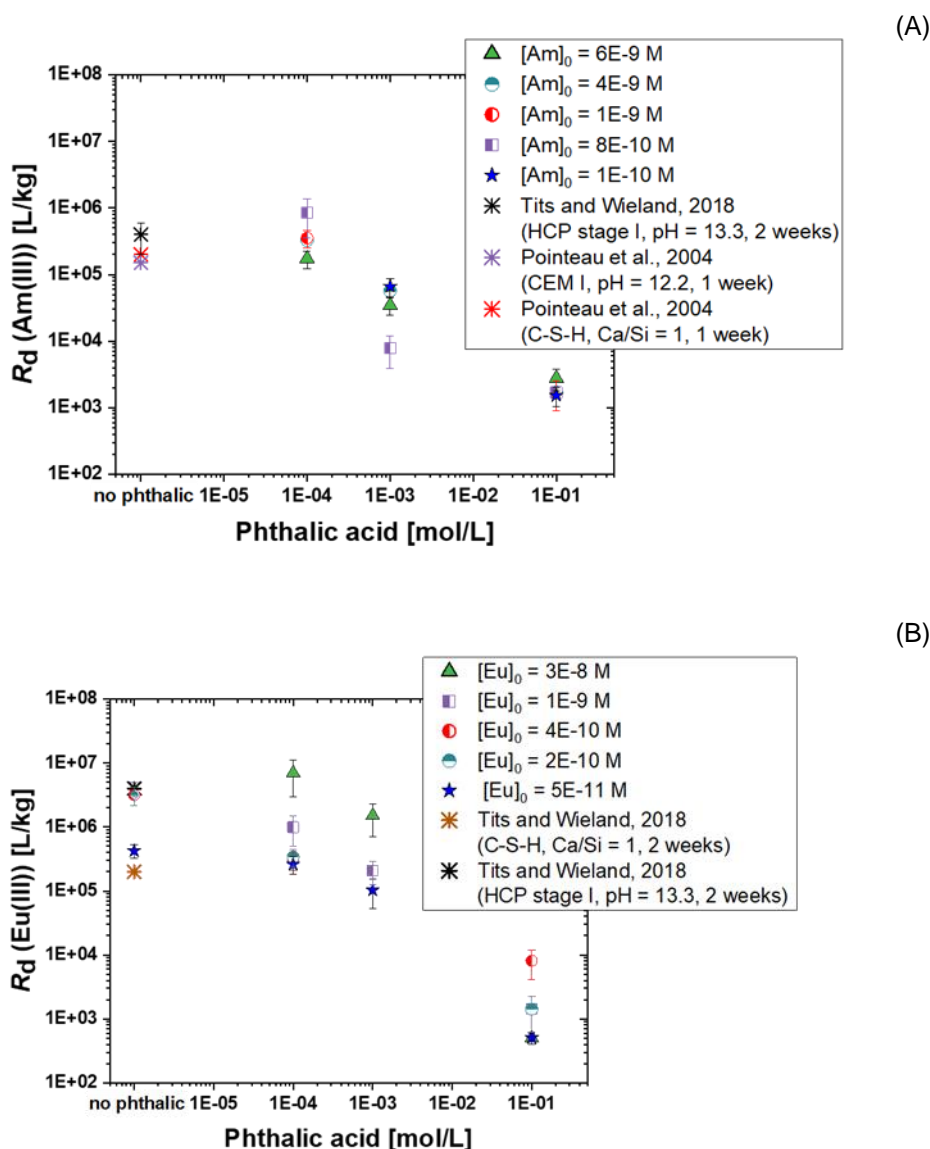
Figure 5-92:   *Effect of phthalate on ^{241}Am and ^{152}Eu uptake by CEM V/A HCP (solid/liquid ratio = 5·10^{-4} kg·L^{-1}, pH = 12.2, 1 week of equilibration: (A) $c_0(^{241}Am) = 10^{-8} – 10^{-10}$ mol·kg^{-1}, and (B) $c_0(^{152}Eu) = 3.0·10^{-8} – 5.0·10^{-11}$ mol·kg^{-1}).*

EURAD (Deliverables n° 3.6, 3.7 and 3.8) - Final Report of results generated in CORI
Dissemination level: PU
Date of issue of this report: **05/07/2024**

Page 220

Above the "concentration edge" the R_d values of ^{241}Am and ^{152}Eu decrease by several orders of magnitude to values of about 10^3 L·kg^{-1} < R_d < 10^4 L·kg^{-1}. Due to the negligible presence of phthalate complexes of ^{241}Am and ^{152}Eu under cementitious conditions, this "concentration edge" cannot be explained by complexation with the organic compound but rather suggests an effect of the phthalate addition on the cementitious material used in the sorption experiments.

Table 54: Distribution ratios R_d for sorption of Am(III) and Eu(III) by CEM V/A HCP in presence of phthalate.

Phthalate (mol·kg^{-1})	log R_d ^{241}Am (L·kg^{-1})	log R_d ^{152}Eu (L·kg^{-1})
0	6.123 ± 0.390	6.410 ± 0.451
10^{-4}	5.706 ± 0.413	6.186 ± 0.746
10^{-3}	4.780 ± 0.850	6.026 ± 0.836
10^{-1}	3.522 ± 0.641	3.388 ± 0.607

In *Figure 5-93*, the calculated aqueous speciation of Ca in the solution equilibrated with HCP CEM V/A is shown as function of the phthalate concentration. At phthalate additions above approximately 10^{-3} mol·kg^{-1} the contribution of the aqueous Ca-phthalate complex (Ca(C$_8$H$_4$O$_4$)^0) to the total Ca concentration increases sharply, becoming the dominant Ca-complex at phthalate concentrations above about 10^{-2} mol·kg^{-1}. The increasing organic complexation of Ca in solution causes the dissolution/ destabilisation of Ca-bearing phases in the cementitious material, leading in particular to a decalcification of C-S-H/C-A-S-H phases, which are the main sorbing phases for *An*(III)/*Ln*(III) in cementitious materials. The destabilisation of C-S-H is also indicated by the calculated saturation indices. As expected in the absence of the organic complexants and at low phthalate concentrations (≤ 10^{-3} mol·kg^{-1}), respectively, the solution equilibrated with CEM V/A is practically in equilibrium with C-S-H with low Ca/Si ratio (C-S-H0.8; saturation index SI ≈ 0). With increasing phthalate addition, the SI for C-S-H 0.8 decreases to about –0.8 (at 10^{-1} mol·kg^{-1} phthalate), indicating the increasing destabilisation of this phase.
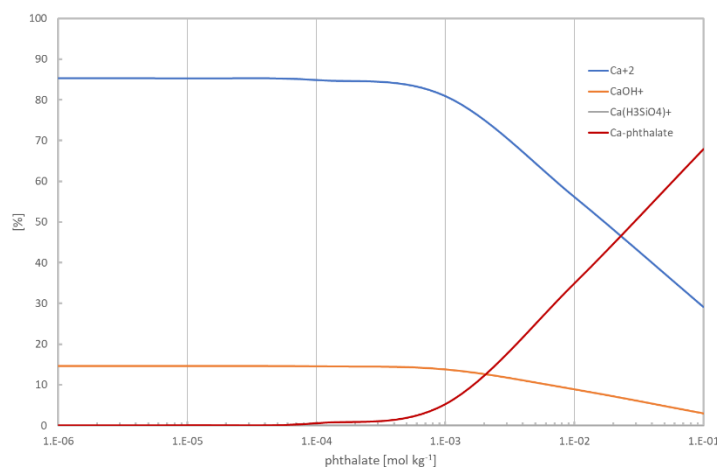
Figure 5-93:   *Calculated Ca-speciation in the solution equilibrated with HCP CEM V/A as function of the phthalate concentration ([Ca]$_{tot}$ = 6.5 mol·kg^{-1} and pH = 12.2).*

These results indicate that above a no-effect level of about 10^{-3} mol·kg^{-1}, the presence of phthalate ions will lead to a strong sorption reduction of trivalent actinides and lanthanides in a cementitious repository, increasing their mobility within the engineered barrier system.

EURAD (Deliverables n° 3.6, 3.7 and 3.8) - Final Report of results generated in CORI
Dissemination level: PU
Date of issue of this report: **05/07/2024**

Page 221

In contrast, in sorption experiments with pure synthesised C-(A)-S-H (Ca/Si ratio 1.6), only a minor effect of the phthalate addition on the retention behavior of Am and Eu was observed (see *Figure 5-94*). In the absence of organics and at phthalate concentrations up to 10 mM, the R_d values of Am and Eu were in the order of 10^5 to 10^7 L·kg^{-1}, in agreement with Pointeau *et al.* (2004) and Tits and Wieland (2018). Only at very high phthalate additions (10^{-1} mol·kg^{-1}), a slight decrease in the radionuclide uptake was found. Further investigations would help to understand this discrepancy between the sorption behavior of HCP CEM V and pure C-(A)-S-H.
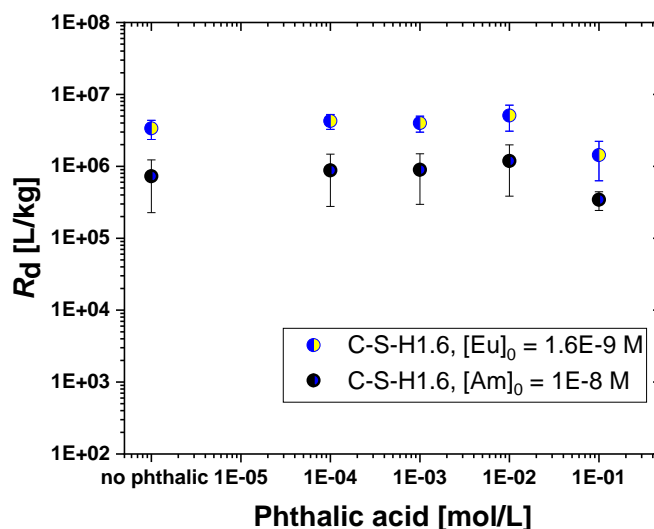
Figure 5-94:   *Effect of phthalate on ^{241}Am and ^{152}Eu uptake by C-(A)-S-H (Ca/Si = 1.6; solid/liquid ratio = $5 \cdot 10^{-4}$ kg·L^{-1}, pH = 12.2, 1 week of equilibration, $c_0(^{241}Am) = 1 \cdot 10^{-8}$ mol·kg^{-1}, $c_0(^{152}Eu) = 2.0 \cdot 10^{-9}$ mol·kg^{-1}).*

5.4 Gluconate and 2-phosphonobutane-1,2,4,-tricarboxylate (PBTC)

The effect of gluconic acid (GLU) on RN retention in cementitious materials has been investigated by **[HZDR]**, **[JGU]**, **[KIT(EMPA)]** and **[UHelsinki]**. **[HZDR]** also analyzed PBTC.

[HZDR] analyzed the U(VI) retention by calcium aluminosilicate hydrate (C-A-S-H), formed as binding phase in concrete due to aluminum-rich additives in cement formulations. For this, samples with Ca/Si molar ratios of 0.8, 1.2 and 1.6, representing different alteration stages of concrete, and with increasing Al/Si molar ratios of 0, 0.06 and 0.18 in each series, were applied. Furthermore, the impact of temperature (25°C, 100°C, 200°C) on both the C-A-S-H structure and the U(VI) retention mechanism was studied. Organics retention processes were also studied, both in the absence and presence of U(VI). Spectroscopic studies have been performed to identify retention mechanisms. R_d values have been determined for U(VI) retention by the cementitious materials in the absence and presence of organics as well as for organics retention. The results to the effect of gluconate on U(VI) retention by C-S-H have been published in (Dettmann *et al.*, 2023). After the C-A-S-H phase formation at room temperature, some of the sample suspensions were subjected to increased temperatures: 100°C to simulate the effect of heat generating nuclear waste on the C-A-S-H structure and even 200°C to obtain further samples for structure-related studies.

The objective was to study which effect a temperature increase would have on the structure of C-A-S-H phases and their retention behavior towards radionuclides and/or organics (please note: the temperature during the retention studies was not increased, but room temperature). Structural characteristics of the cementitious phases were obtained from powder X-ray diffraction (XRD) as well as solid-state ^{27}Al and ^{29}Si single-pulse (SP) and cross-polarization (CP) magic angle spinning nuclear

EURAD (Deliverables n° 3.6, 3.7 and 3.8) - Final Report of results generated in CORI
Dissemination level: PU
Date of issue of this report: **05/07/2024**

Page 222

magnetic resonance (MAS NMR) spectroscopy. Al tetrahedra were identified to occupy bridging positions of the Si chain and cross-linking positions. Elevated temperatures were found to enforce cross-linking between (alumino)silicate chains as well as and to increase the crystallinity of the material with the appearance of neo-formed crystalline phases.

Time-resolved laser-induced luminescence spectroscopy (TRLFS) was applied to characterize the U(VI) binding. Several U(VI) species (surface-sorbed or interlayer-sorbed) are forming in different amounts, depending on the composition of the C-A-S-H phases and history of temperature impacts on the C-A-S-H samples. The results showed a strong U(VI) retention by the C-A-S-H phases with log R_d values of about 5.

The influence of gluconate (GLU) on the U(VI) retention by a calcium-silicate-hydrate (C-S-H) phase with a C/S ratio of 0.8 was studied (Dettmann *et al.*, 2023), where it was shown that GLU has little to no effect on the overall sorption of Eu(III), Am(III), Th(IV), Pu(IV), and U(VI) by C-S-H (C/S = 0.8).

In the presence of $1 \cdot 10^{-2}$ M GLU, the log R_d only slightly decreases from 5.1 in absence of GLU to 4.8 ± 0.1. Regarding the U(VI) uptake, no clear trend can be seen in the tests with different addition sequences of U(VI) and GLU. That means, the organic ligand GLU has only a very small influence on the U(VI) retention by C-S-H under these conditions. To identify U(VI) and GLU species on the solid phase and in the supernatant, the samples were studied by luminescence and NMR spectroscopy, respectively.
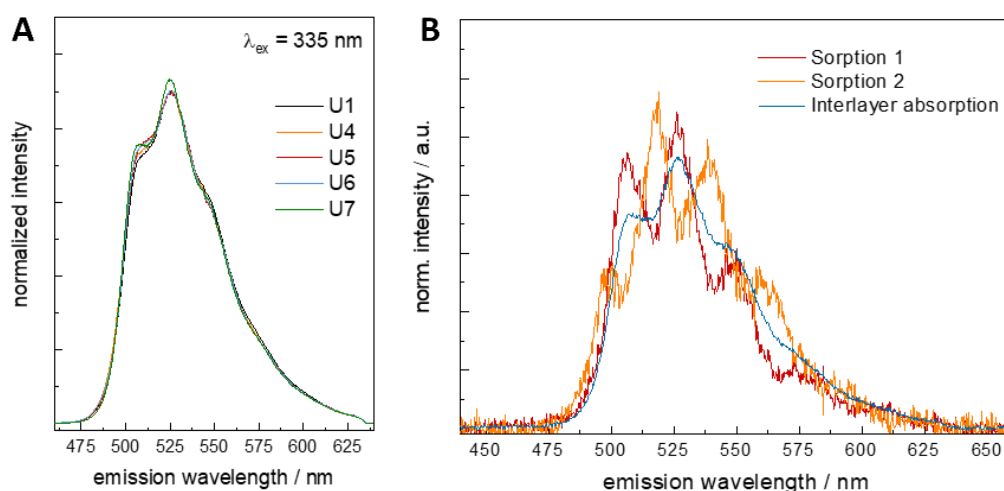
Figure 5-95: (A) U(VI) luminescence spectra obtained from U(VI)-loaded C-S-H phases U_1 ([U(VI)] =$2 \cdot 10^{-5}$ M, S/L = 24 g/L, pH 10.8) and $U_4 - U_7$ ([U(VI)] = $5 \cdot 10^{-7}$ M, S/L = 1 g/L, absence or presence of $1 \cdot 10^{-2}$ M GLU, pH ~10.9). (B) Emission spectra of extracted pure components from the decomposition of the measured U(VI) luminescence spectra obtained from U(VI)-loaded C-S-H phases.

EURAD (Deliverables n° 3.6, 3.7 and 3.8) - Final Report of results generated in CORI
Dissemination level: PU
Date of issue of this report: **05/07/2024**

Page 223
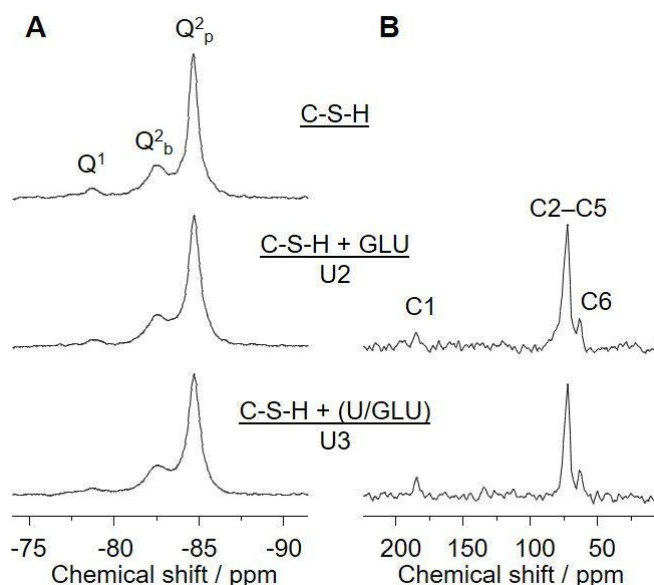
Figure 5-96: (A) ^{29}Si SP MAS NMR and (B) ^{13}C CP MAS NMR spectra of C-S-H as well as after sorption of GLU (U$_2$) or sorption of U(VI)/GLU (U$_3$) on C-S-H; ([U(VI)] =5·10^{-6} M, [GLU] =1·10^{-2} M, S/L=10 g/L).

The luminescence spectra of various U(VI)-loaded C-S-H samples are very similar to each other and independent of the presence or absence of GLU (*Figure 5-95*A). Three pure components can be extracted from each measured spectrum: two U(VI) species sorbed on the C-S-H surface and one U(VI) species sorbed into the interlayer region of C-S-H (*Figure 5-95*B). The effect of GLU on the fraction of the various species in the differently prepared U(VI)-containing C-S-H samples is very small.

^{29}Si SP MAS NMR spectra show that the short-range order of the C-S-H phase remains unaffected by U(VI) and/or GLU (*Figure 5-96*A). ^{13}C CP MAS NMR spectra of GLU containing samples U2 and U3 (*Figure 5-96*B), *i.e.*, C-S-H + GLU (top) and C-S-H + (U(VI)/GLU) (bottom), reveal the presence of GLU in the sorption samples. The quite low signal-to-noise ratio implies that only a fraction of the initial 10^{-2} M GLU is associated with the C-S-H phase which is in full agreement with findings from GLU sorption experiments.

[JGU] analyzed the effect of GLU on the retention of Th(IV) and Pu(IV) by hardened cement pastes (HCP) at Stage I (pH > 13) and calcium-silicate-hydrate (C-S-H) phase at Stage III (C/S = 0.8, pH ~ 10). They also analysed the order of addition (RN & ligand).

Batch sorption experiments were conducted in binary and ternary systems. In the binary system, two sorption isotherms were performed: one by varying the concentration of the ligand (10^{-9} - 10^{-1} M) at a constant solid-to-liquid ratio (S/L = 5 g·L^{-1}), and the other by varying the S/L ratio (S/L = 0.5 - 50 g·L^{-1}) at a constant ligand concentration (10^{-2} M). In the ternary systems, batch sorption experiments were conducted to investigate the influence of the order of addition of actinides and the ligand, as well as the contact time. For the experiments with GLU, stock solutions of ^{14}C-GLU (Hartmann Analytic, Germany) and sodium gluconate (Sigma Aldrich, United States) were prepared and diluted as described in Dettman *et al.,* (2023).

In the batch experiments with HCP/Pu(IV)/GLU the order of addition was varied while maintaining a constant contact time of 72 hours. The order of addition of An ([^{239}Pu(IV)] or [^{232}Th(IV)] = 10^{-8} M) and L ([GLU] = 10^{-2} M) on HCP (S/L=5 g·L^{-1}) was varied in three combinations as described above, (i) *(HCP +An) + GLU*, (ii) *((HCP + GLU)+ An)*: (iii) *(HCP +An + GLU).* Up to our knowledge, there is no literature data available for the ternary system of HCP / Pu(IV) / GLU. Table 55 summarizes the calculated R_d values obtained from batch experiments.

EURAD (Deliverables n° 3.6, 3.7 and 3.8) - Final Report of results generated in CORI
Dissemination level: PU
Date of issue of this report: **05/07/2024**

Page 224

Table 55: R_d (L·kg⁻¹) values of Pu(IV) in the binary and ternary systems in dependence of the order of addition under alkaline conditions (water at pH =13.3) after 72 h of contact time with ([²³⁹Pu(IV)] = 1·10⁻⁸ M) and ([GLU] = 1·10⁻² M).

Experiments	R_d L·kg⁻¹
HCP + Pu(IV)	$2.2 \cdot 10^6$
(HCP + Pu(IV)) + GLU	$1.1\ (\pm\ 0.1) \cdot 10^3$
(HCP + GLU) + Pu(IV)	$0\ (\pm\ 2)$
(HCP+ Pu(IV) + GLU)	$0\ (\pm\ 2)$

The results in Table 55 show much lower R_d values of Pu(IV) obtained in the ternary system than the binary HCP/Pu(IV) system. When Pu(IV) is added first, uptake is higher than with GLU present, but lower compared to the binary system, indicating Pu(IV) desorption after GLU addition. Adding GLU first or simultaneously prevents Pu(IV) uptake, suggesting GLU occupies sorption sites. The order of addition affects Pu(IV) uptake on HCP.

In the similar experiment with Th(IV) and GLU, a leaching effect of Th from HCP was observed, which was also confirmed in the ternary system Th(IV) / HCP / GLU ([²³²Th(IV)] = 10^{-8} M and [GLU] = 10^{-2} M at a pH of 13.3 and S/L ratio of 5 g·L⁻¹). The concentration of Th was determined by ICP-MS measurements in different samples with different order of addition and compared to the values of the binary systems of HCP/Th(IV) and HCP/GLU.

As shown in Table 56, in the absence of GLU, the uptake of ²³²Th(IV) on HCP was high (> 99%), resulting in very low ²³²Th concentration. However, unexpectedly, a high concentration of ²³²Th was detected in the samples of HCP + (GLU + Th(IV)) and HCP + GLU + Th(IV), indicating a leaching effect of Th from HCP. The presence of GLU significantly increased the concentrations of ²³²Th. Additional analysis of the HCP + GLU sample (S/L = 5 g·L⁻¹) in the binary system confirmed this leaching effect. As known, Ordinary Portland Cement typically contains around 2.8 ppm of Th based on XRF analysis (Stietz *et al* 2023a).

Table 56: ²³²Th concentrations determined by ICP-MS in the samples of ternary system HCP / Th(IV) / GLU compared to the values of the binary systems HCP / Th(IV) or HCP /GLU with [²³²Th(IV)]₀ = 10^{-8} M and [GLU] = 10^{-2} M, S/L ratio of 5 g·L⁻¹ at a pH of 13.3 and contact time of 72 h.

Sample	[²³²Th]$_{eq}$ mol/L
HCP + Th(IV)	$(3.9 \pm 0.1) \cdot 10^{-11}$
(HCP + Th(IV)) + GLU	$(7.7 \pm 0.3) \cdot 10^{-9}$
(HCP + GLU) + Th(IV)	$(1.8 \pm 0.1) \cdot 10^{-8}$
(HCP + Th(IV) + GLU)	$(1.7 \pm 0.1) \cdot 10^{-8}$
HCP + GLU	$(1.4 \pm 0.1) \cdot 10^{-8}$

[HZDR] studied also the influence of 2-phosphonobutane-1,2,4,-tricarboxylate (PBTC) on U(VI) retention by C-A-S-H phases was studied following various procedures: i) U(VI)-doped C-A-S-H phases, which were prepared by direct synthesis of C-A-S-H phases in the presence of U(VI), were subjected to leaching experiments with PBTC-containing supernatant solutions ([U(VI)]₀ = $2 \cdot 10^{-5}$ M, [PBTC] =$1 \cdot 10^{-2}$ M, S/L=10 g/L) to study whether U(VI) can be remobilized due to U(VI)−PBTC complexation in solution. ii) U(VI) sorption onto C-S-H (C/S = 0.8) was studied in the absence of organics and in the presence of increasing amounts of PBTC ([U(VI)]₀ = $5 \cdot 10^{-7}$M, [organics] = $5 \cdot 10^{-4}$ M to $1 \cdot 10^{-2}$M, S/L = 5 g/L, pH 10.9). The sorption of PBTC onto C-S-H in the absence of U(VI) was studied in the same

EURAD (Deliverables n° 3.6, 3.7 and 3.8) - Final Report of results generated in CORI
Dissemination level: PU
Date of issue of this report: **05/07/2024**

Page 225

concentration range by means of ^{31}P or ^{13}C NMR as well as by ICP-MS. Moreover, under the same experimental conditions, retention experiments with CEM I HCP instead of C-S-H were performed. Luminescence and NMR spectroscopy was applied to identify the retention mechanisms. The R_d values determined for U(VI) retention by the cementitious materials in the presence of organics as well as for organics retention must be validated using further experiments.

[KIT] in collaboration with **[EMPA]** studied the effect of GLU on Cm(III), Pu(III/ IV) and Eu(III) adsorption by C-S-H (Ca/Si 0.8 and 1.4) and AFm phases and ettringite, under the alkaline conditions representative of the Stage I of hydrated cement. Sorption experiments have been carried out on solid phases synthesized in laboratory (see section **Erreur ! Source du renvoi introuvable.**) varying the organic ligand concentration (10^{-4} M ≤ $[L]_{tot}$ ≤ $10^{-1.5}$ M) and by keeping the sodium concentration constant and equal to $[Na]_{tot}$ = 0.2 M (pH ≈ 13.3). C-S-H samples have been synthesized with both S:L ratios of 1 and 25 g·dm^{-3} while AFm phases and ettringite with a S:L of 5 g·dm^{-3}.

Pu sorption experiments have been carried out with $[Pu]_{tot,in}$= 10^{-8} M (C-S-H) - $10^{-8.5}$ M (AFm phases and ettringite) and in presence of $2\cdot10^{-3}$ M of redox buffer (hydroquinone (HQ) or Sn(II)Cl$_2$ (Sn(II)). The use of two different redox buffers allows to investigate the retention behavior of Pu(IV) expected for the HQ-buffered system and of Pu(III/IV) for the Sn(II) buffered system (Tasi *et al.* 2018). Eu sorption experiments have been carried out using both inactive ($[Eu]_{tot,in}$ = 10^{-7} M) and active isotopes ($[Eu]_{tot,in}$= 10^{-9} M). Sorption samples have been monitored for equilibration time of 90 days (Pu sorption experiments) and 120 days (Eu sorption experiments).

^{242}Pu and ^{152}Eu concentrations have been quantified by SF-ICP-MS and gamma counting respectively. Time Resolved Laser Fluorescence Spectroscopy (TRLFS) analysis has been performed on ^{248}Cm-C-S-H (Ca:Si=0.8,1.4) GLU system, by using an initial curium concentration $[Cm]_{tot,in}$= 10^{-7} M and in the absence and presence of gluconate (10^{-3} M ≤ $[GLU]_{tot}$ ≤ $10^{-1.5}$M). The TRLFS analysis has been performed on two different samples: the 'solution sample' to study the aqueous speciation of Cm in solution, and the 'suspension sample' (comparable to the batch sorption experiment) to measure the emission fluorescence of both solid and solution.

Results indicated that, in the case of the ^{242}Pu-C-S-H-GLU system, gluconate decreases the uptake of Pu at [Gluconate]tot > 10^{-4} M for both C-S-H phases with high (1.4) and low (0.8) Ca:Si ratio and redox buffer (*i.e.* HQ and Sn(II)). The only difference is evidenced for the Sn(II)-buffered system (Pu-C-S-H 1.4-Gluconate) at $[Gluconate]_{tot}$ = $10^{-1.5}$ M, where the higher R_d value (respect the HQ buffered system) is tentatively explained in terms of stable surface complex formation (> Pu(III)-OH-GLU).

In the case of ^{242}Pu-AFm phases/ettringite-GLU system, in the absence of any organic ligands, a strong Pu uptake by AFm phases and ettringite has been observed, with log R_d of (5.6 ± 1.0) and (5.7 ± 1.1) (with R_d values reported in L/kg), respectively. Gluconate decreases the uptake of Pu by AFm phases and ettringite at gluconate concentrations higher than 10^{-4} M (Figure 5-97), both for Sn(II) and HQ redox buffers. The impact of gluconate on the retention of Pu by AFm phases and ettringite was stronger than for C-S-H phases, which possibly reflects the influence of gluconate both on the aqueous speciation of Pu as well as on the structural and surface properties of the solid phases.

EURAD (Deliverables n° 3.6, 3.7 and 3.8) - Final Report of results generated in CORI
Dissemination level: PU
Date of issue of this report: **05/07/2024**

Page 226
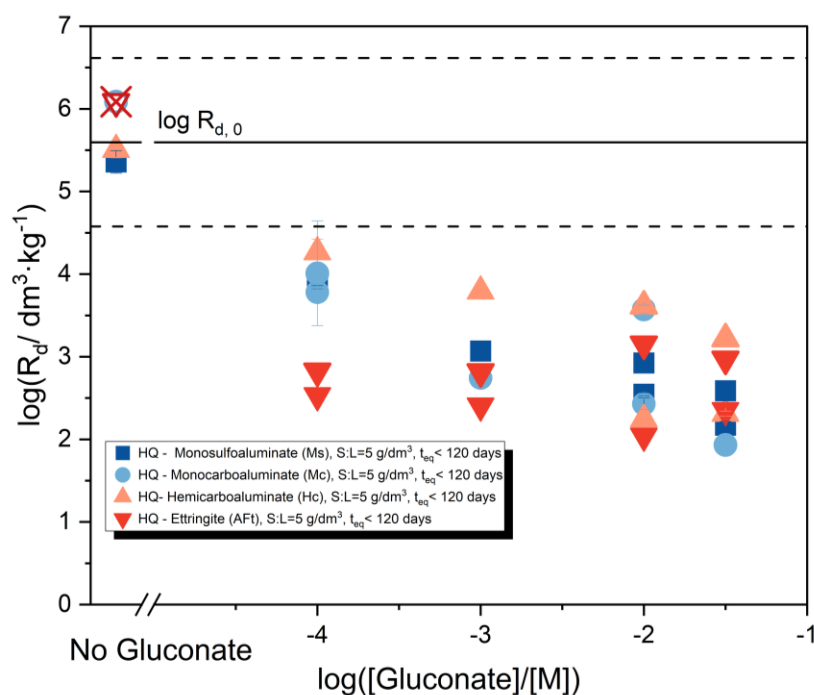
Figure 5-97: *Distribution ratios, R_d, determined for the HQ-buffered systems (AFm+ Pu) + GLU and (AFt+ Pu) + GLU. In both cases data corresponding to pH ≈ 13.3, S/L = 5 g·dm^{-3} and 120 days of contact time. X crossed symbols refers to values at the detection limit.*

In the case of the ^{152}*Eu-C-S-H-GLU* system, high uptake of Eu(III) has been observed on C-S-H phases in the absence of organic ligands and hyper-alkaline conditions, in agreement with Wieland (2014). Gluconate has a negligible effect on ^{152}Eu retention on C-S-H 0.8 at [Gluconate]$_{tot}$ < 10^{-2} M, whereas a moderate decrease in the retention is observed for gluconate concentrations [Gluconate]$_{tot}$ = 10$^{-1.5}$ M and for longer equilibration times. For C-S-H 1.4, a strong decrease of Eu retention has been observed for [Gluconate]$_{tot}$ > 10^{-3} M (Figure 5-98), supporting the formation of more stable Eu(III)-gluconate complexes for the Eu(III)-C-S-H 1.4-Gluconate ternary system.

For the ^{248}Cm-C-S-H-GLU system, TRLFS (Time Resolved Laser Fluorescence Spectroscopy) analysis has been carried out as a complementary study on the sorption mechanism of An(III)/Ln(III) on C-S-H phases in the presence of gluconate and on the role of Ca concentration in the complex formation. For the system with low Ca:Si ratio (C-S-H 0.8), the determination of the lifetime and comparison with data available in the literature (Tits at al., 2003b), indicated that Cm(III) is mostly incorporated in the C-S-H phase structure both in the presence and in absence of gluconate. Conversely, for C-S-H 1.4, the formation Ca-Cm(III)-gluconate-(OH) aqueous complexes is observed at [Gluconate]$_{tot}$ ≥ 10$^{-2.5}$ M, thus preventing the incorporation of Cm(III) into the C-S-H structure. The results obtained in this framework, support that the retention decrease of Eu on C-S-H 1.4 in the presence of gluconate is due to the formation of Ca-Eu(III)-Gluconate-(OH), thus highlighting the relevant role of Ca in the formation of Ca-Ac(III)/Ln(III)-L-(OH) complexes.

EURAD (Deliverables n° 3.6, 3.7 and 3.8) - Final Report of results generated in CORI
Dissemination level: PU
Date of issue of this report: **05/07/2024**

Page 227
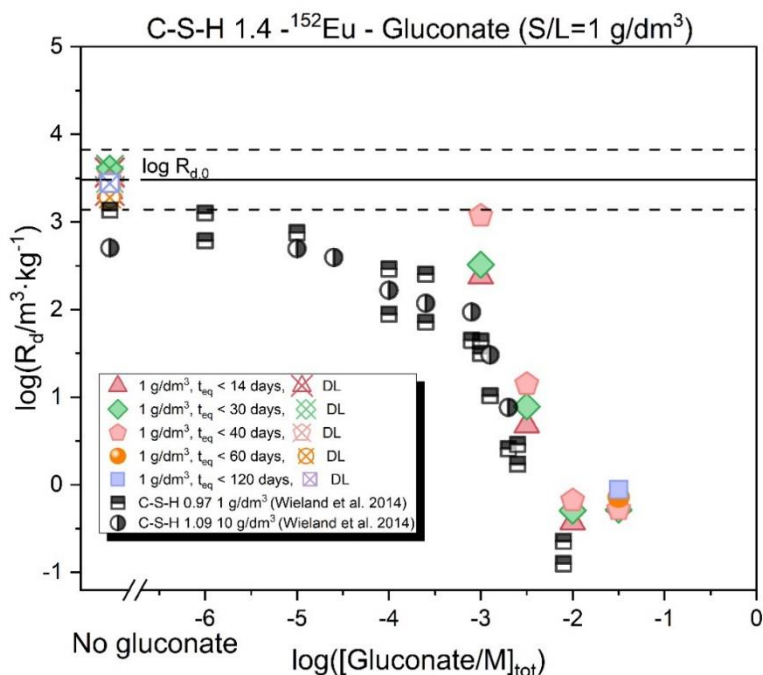
Figure 5-98: *Distribution coefficients, R_d, for the uptake of ^{152}Eu in presence of gluconate ($-3 \leq log([Gluconate]_{tot, in/M}) \leq -1.5$) on C-S-H phases with a C/S of 1.4 for a contacting time $t_{eq} < 120$ days under hyper-alkaline conditions (pH ≈ 13.3). The black solid line labelled as log R_d max indicate the maximum R_d coefficient quantifiable in the series of sorption experiments.*

[UHelsinki] determined the diffusivities of HTO, Cl-36, C-14 labelled gluconate and Cs-134 by electromigration technique in HCP samples and carried out post-mortem analysis of the samples by autoradiography. The research included the preparation of cement samples, the development of the electromigration device, and the through-diffusion experiments with different tracers (HTO, Cl-36, Cs-134 and C-14-labelled gluconate). The aim is to determine diffusion coefficients of neutral and anionic inorganic tracers, and organic molecules within the cement samples.

Table 41 summarizes all the tested samples in CORI project. The results with Cl-36 and C-14-gluconate show that both tracers can migrate through the cement samples (Samples No.6.6 and No. 3.4) under a supply voltage of 10V. A significant acceleration in the migration of both tracers was observed (*Figure 5-99*).

A comparative analysis between Sample No. 6.6 and Sample No. 3.4 revealed that the breakthrough time of both tracers was shorter in Sample No. 6.6 than in Sample No. 3.4. Thus, it was concluded that Sample No. 3.4 exhibits a greater capacity for retaining both tracers compared to Sample No. 6.6.

These results contribute also to Task 3, especially for the systems: ISA, C-14 labelled Gluconate, Cl-36 and Cs-134 diffusion in hydrated cement paste *via* electromigration (*Figure 5-99*).

EURAD (Deliverables n° 3.6, 3.7 and 3.8) - Final Report of results generated in CORI
Dissemination level: PU
Date of issue of this report: **05/07/2024**

Page 228
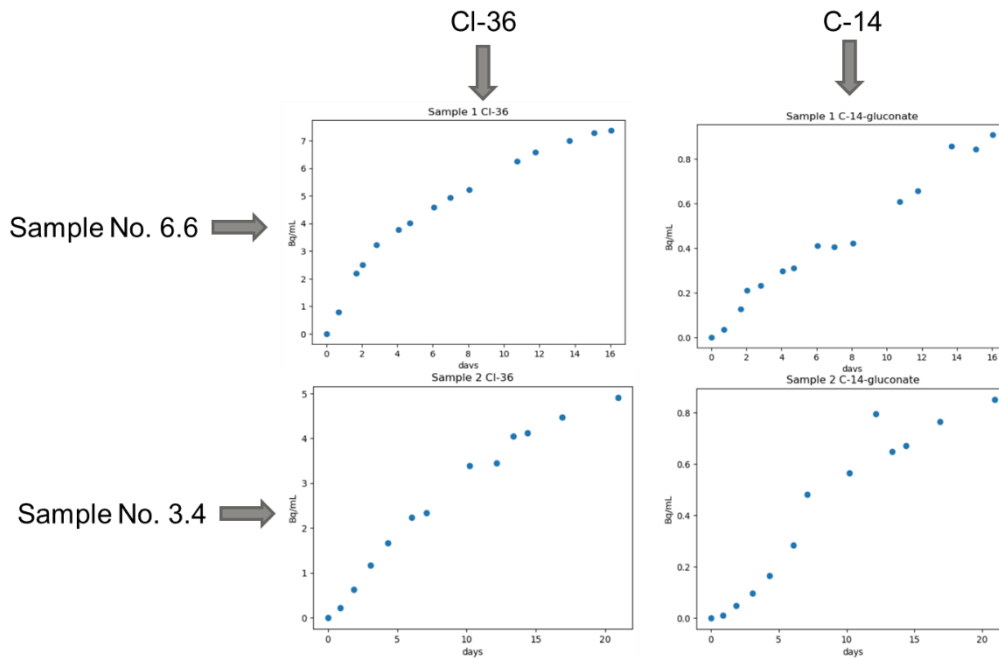
Figure 5-99: *Electromigration test results of a 1 cm cement samples with Cl-36 and C-14 Gluconate as tracers. The voltage applied to the sample was 10 V.*
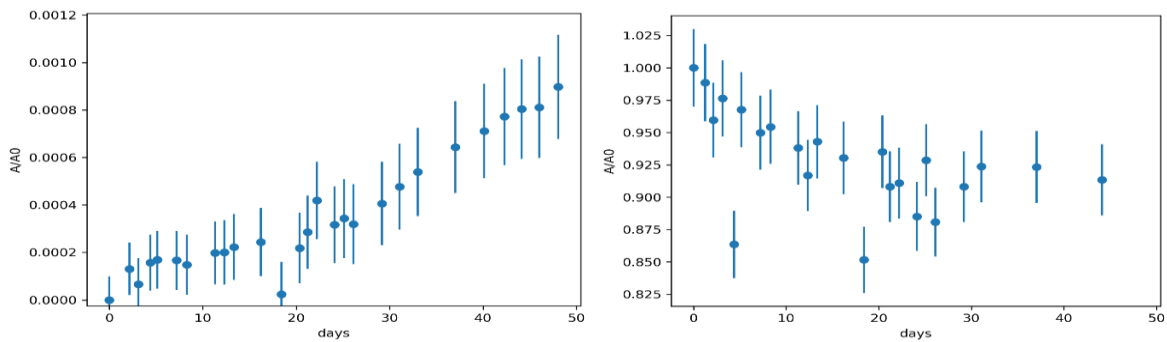
Figure 5-100: *Electromigration test result of a 1 cm cement sample 6.2 with Cl-36 as a tracer. The voltage applied to the sample was 5 V. Left: measured breakthrough curve in the Outlet chamber. Right: decrease of the tracer activity measured the Inlet chamber.*
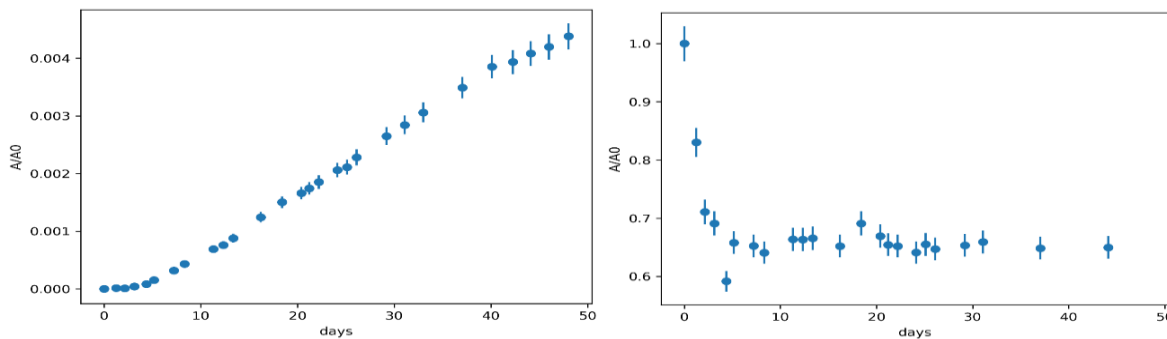
Figure 5-101: *Electromigration test result of a 1 cm cement sample 6.2 with C-14 Gluconate as a tracer. The voltage applied to the sample was 5 V. Left: measured breakthrough curve in the Outlet chamber. Right: decrease of the tracer activity measured the Inlet chamber.*

EURAD (Deliverables n° 3.6, 3.7 and 3.8) - Final Report of results generated in CORI
Dissemination level: PU
Date of issue of this report: **05/07/2024**

Page 229
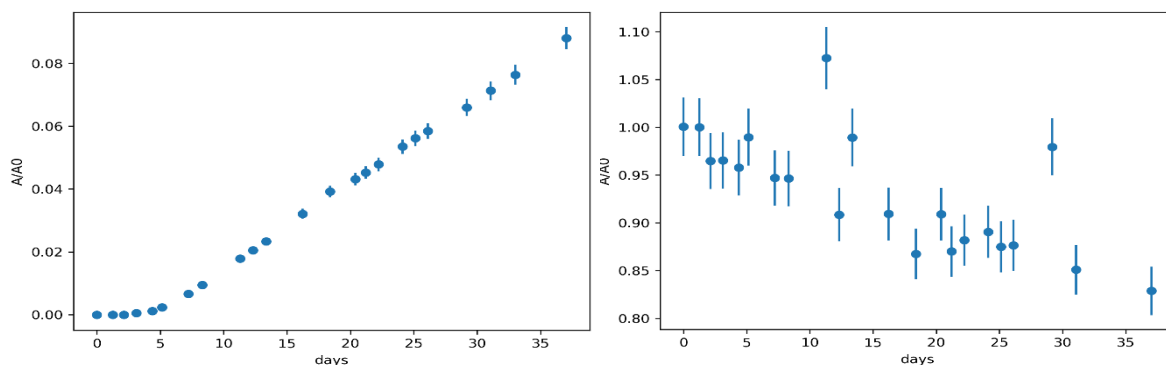
Figure 5-102. *Electromigration test result of a 1 cm cement sample 6.2 with Cs-134 as a tracer. The voltage applied to the sample was 5 V. Left: measured breakthrough curve in the Outlet chamber. Right: decrease of the tracer activity measured the Inlet chamber.*
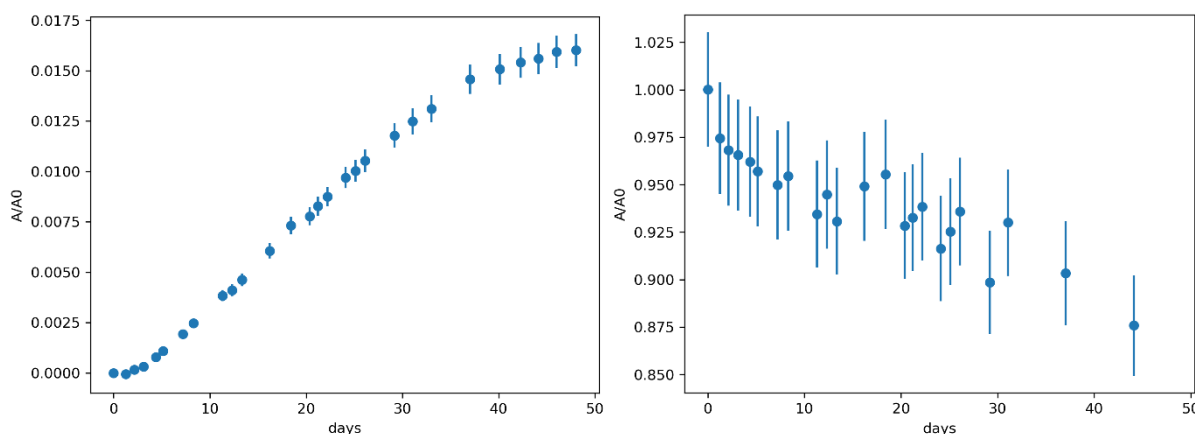
Figure 5-103. *Electromigration test result of a 1 cm cement sample 2.3 with Cl-36 as a tracer. The voltage applied to the sample was 5 V. Left: measured breakthrough curve in the Outlet chamber. Right: decrease of the tracer activity measured the Inlet chamber.*

Figure 5-100 to

Figure *5-103* shows further results obtained with ^{36}Cl, ^{14}C-GLU and ^{134}Cs. The breakthrough curves show that Cs-134 can break through sample No. 6.2 in around 4 days, the same as ^{14}C-gluconate tracer. However, the A/A$_0$ of ^{134}Cs after one month is around 6% which is much larger the A/A$_0$ value measured for ^{14}C-gluconate.

Postmortem analyses of samples after electromigration experiments were done using autoradiography technique. All used radionuclides, ^{36}Cl, ^{14}C and ^{134}Cs, are easily detectable by autoradiography. With this technique the diffusion profiles of ^{36}Cl, ^{134}Cs and ^{14}C labelled gluconate were detected qualitatively. The profiles of elemental spatial distribution within the studied samples were determined, as shown in *Figure 5-104*. The postmortem analysis helped to improve understanding of the diffusion pathways and diffusion processes within the samples.

EURAD (Deliverables n° 3.6, 3.7 and 3.8) - Final Report of results generated in CORI
Dissemination level: PU
Date of issue of this report: **05/07/2024**

Page 230
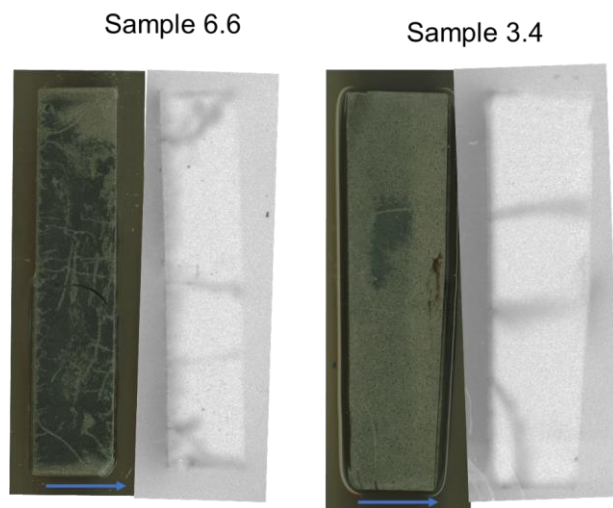
Sample 6.6 Sample 3.4

Figure 5-104. *Left: Photo image of the sawn cement paste sample 6.6 after through-diffusion test and the corresponding autoradiograph showing spatially $^{36}Cl+^{14}C$ tracer activities in the sample. Right: Photo image of the sawn cement sample 3.4 after through diffusion test and the corresponding autoradiograph showing spatially $^{36}Cl+^{14}C$ tracer activities in the sample. Blue arrow shows the direction of elements' diffusion through a 1 cm sample. The voltage applied to the sample was 5 V. In both samples there are found micro fractures along which the diffusion took place.*

5.5 Superplasticizers and real leachate of PCE

The effects of superplasticizers on radionuclide retention/migration have been studied by **[CIEMAT]** and **[UJV]**. Both organizations considered different commercial additives. In addition, the effect of degradation products of polycarboxylates (PCE), obtained by **[BGRM]** in Task 2 have been analyzed by **[CIEMAT]**.

Two superplasticizers selected by **[CIEMAT]** are described in Section 3.1.9. **[CIEMAT]** carried out batch sorption experiments in C-S-H phases at different Ca/Si ratios and in fresh cement in the presence of the superplasticizers MG or SIKA (5 wt.%). The solid to liquid ratio was 10 g/L. The results obtained for Ni in the C-S-H phases (Ca/Si=0.8, 1 and 1.2) in the presence of the SPs are shown in Figure 5-105. Sorption data of Ni in the C-S-H at different Ca/Si are published in Missana *et al.* 2022 and a summary is shown in *Figure 5-9*.
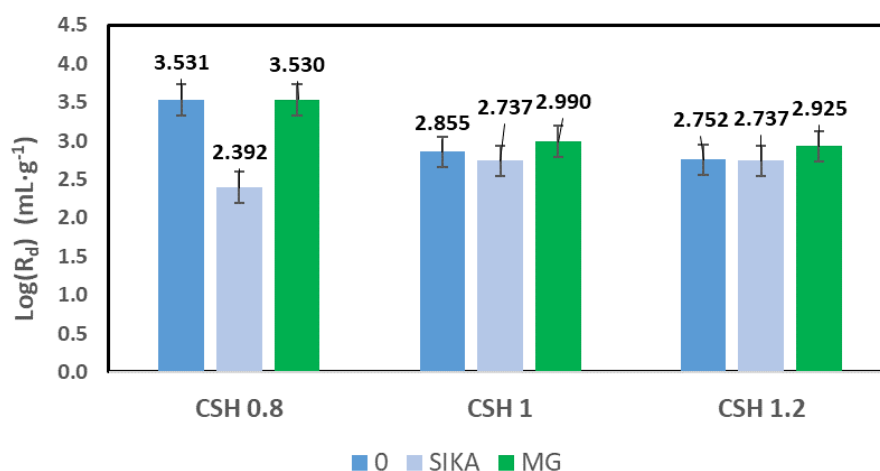
Figure 5-105: *Nickel adsorption tests in C-S-H at different Ca/Si ratio and effects of the presence of the superplasticizers SIKA and MG. [Ni] = 4.6·10^{-10} M.*

EURAD (Deliverables n° 3.6, 3.7 and 3.8) - Final Report of results generated in CORI
Dissemination level: PU
Date of issue of this report: **05/07/2024**

Page 231

In general, only small changes in the $Log(R_d)$ values for Ni in the different C-S-H, in the presence of the SP are observed, compatible with the experimental uncertainty, except for SIKA in C-S-H 0.8, where the decrease in the R_d is one order of magnitude, results which is not clear.

Sorption experiments to analyse the effects of the superplasticizers MG or SIKA (5%) were also done with different fresh HCP (CEM I, CEM IV and CEM V). In these tests, the pH was 12.7 $\pm$0.1, which is lower than the expected for the fresh material; the solid to liquid ratio was 10 g$\cdot$L^{-1}. Results are shown in Figure 5-106.

MG affects slightly Ni adsorption in CEM I and CEM IV decreasing the $Log(R_d)$ values less than 5%, which we can assume within the experimental uncertainty, whereas in CEM V the reduction is around 9%. The presence of SIKA affects more Ni adsorption in both CEM I and CEM V with $Log(R_d)$ reduction of around a 20%. However, in CEM IV the presence of SIKA increases Ni adsorption. This cannot be explained so far, but it must be outlined that the same result has been observed also in the tests with $[Ni] = 4.96 \cdot 10^{-7}$ mol/L.

[CIEMAT] analyzed the adsorption of uranium in the C-S-H phases and the effects of the presence of the superplasticizers MG and SIKA (5%) on retention, being the solid to liquid ratio 10 g/L. The results of the sorption isotherms of U ([U] from 10^{-8} M to 10^{-5} M) in the C-S-H at different Ca/Si ratio, are shown in Figure 5-107. Adsorption of uranium is quite high, above all for the C-S-H phases with Ca/Si <1.6. The mean $Log(R_d)$ values are: 5.1, 5.15, 4.85 and 4 for C-S-H 0.8, 1, 1.2 and 1.6, respectively, indicating that adsorption decreases with the Ca/Si ratio, as already seen for Ni, even if in this case, the difference between the phases with Ca/Si 0.2-1.2 is not very evident. Clear precipitation at low U concentrations (10^{-6} M) has been observed only in the case of the C-S-H 0.8. Modelling work has been started, to explain adsorption mechanisms.

EURAD (Deliverables n° 3.6, 3.7 and 3.8) - Final Report of results generated in CORI
Dissemination level: PU
Date of issue of this report: **05/07/2024**

Page 232
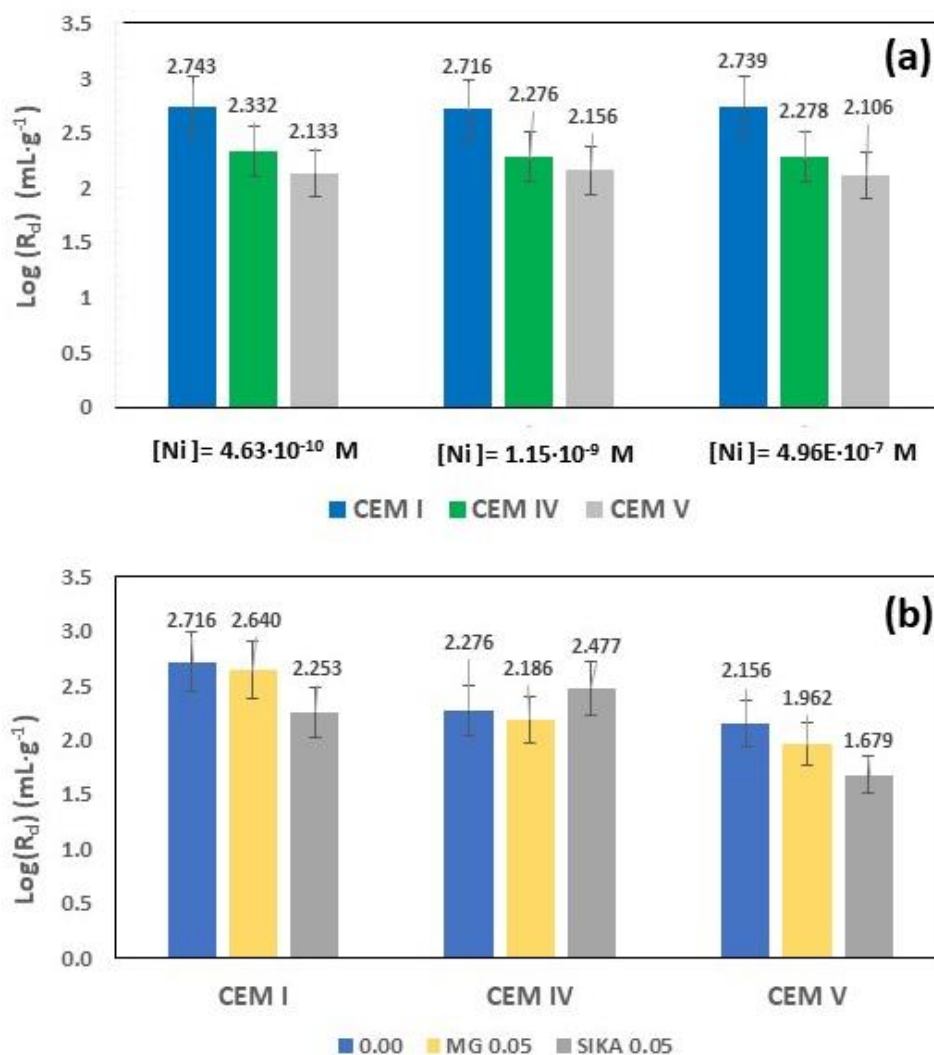
Figure 5-106: *Nickel adsorption tests in fresh cement. (a) Ni adsorption in three different cements at three different [Ni]; (b) Ni adsorption in the presence of SP in the three different cements. [Ni]=1.15·10^{-9} M.*

Figure 5-107 shows the adsorption of uranium in presence of MG or SIKA (5 wt.%) in the different C-S-H phases. In all the cases, the effect is negligible considering that U adsorption is almost quantitative in the C-S-H with Ca/Si 0.8, 1 and 1.2. The same experiment was also carried out using higher U concentration $[U] = 7.1·10^{-7}$ M, and the results were very similar. It can be concluded that the superplasticizers for a concentration below 5 wt.% do not affect U retention in the C-S-H phases.

EURAD (Deliverables n° 3.6, 3.7 and 3.8) - Final Report of results generated in CORI
Dissemination level: PU
Date of issue of this report: **05/07/2024**

Page 233
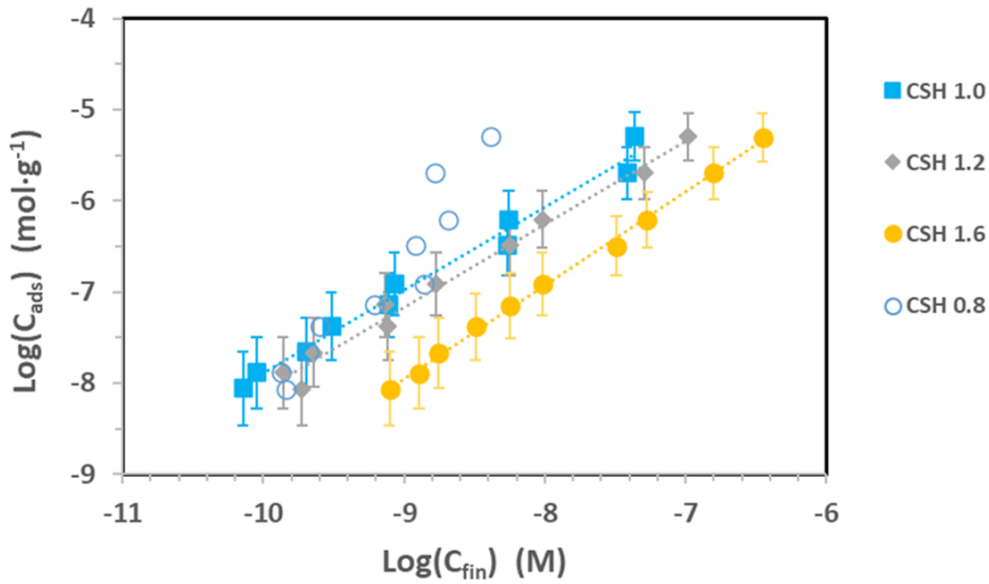
Figure 5-107: Uranium adsorption isotherms in C-S-H at different Ca/Si ratio, at a solid to liquid ratio of 10 g/L and in presence of MG or SIKA (5 wt.%).
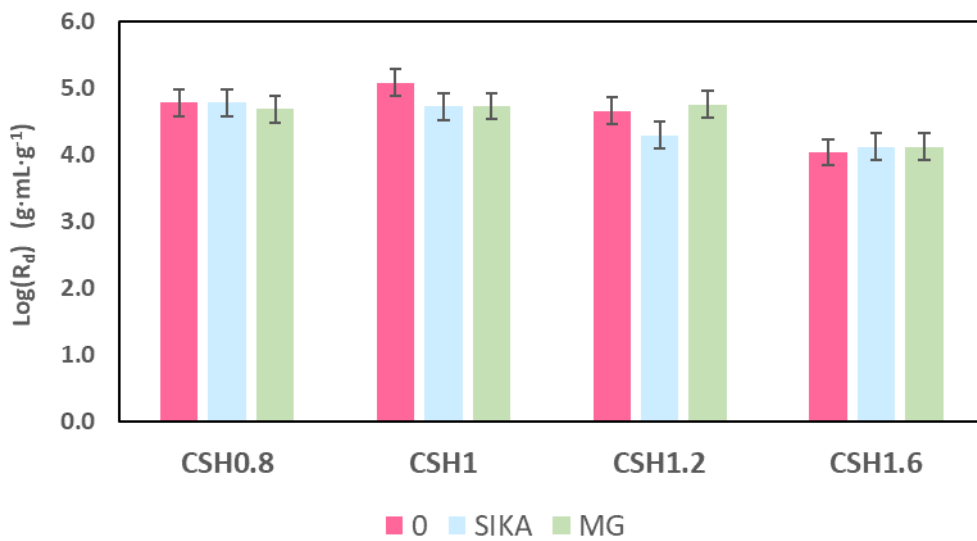
Figure 5-108: Uranium adsorption tests in C-S-H at different Ca/Si ratio and effects of the presence of the superplasticizers SIKA or MG and for [U] = 8.7·10⁻⁸ M.

Batch sorption tests were carried out with uranium with and without the superplasticizers in three different fresh HCP (CEM I, CEM IV and CEM V) and the results are shown in Figure 5-108.

In these tests the pH was 12. 85±0.05 and the solid to liquid ratio was 10 $g \cdot L^{-1}$. Adsorption tests without the additives, were carried out at three different ^{233}U concentrations ($8.7 \cdot 10^{-8}$ M, $2.17 \cdot 10^{-7}$ M and $7.11 \cdot 10^{-7}$ M) and the results are shown in Figure 5-109a. Figure 5-109b shows the results of the sorption tests in the presence of MG or SIKA (5 wt.%) at one U concentration ($2.17 \cdot 10^{-7}$ M).

EURAD (Deliverables n° 3.6, 3.7 and 3.8) - Final Report of results generated in CORI
Dissemination level: PU
Date of issue of this report: **05/07/2024**

Page 234
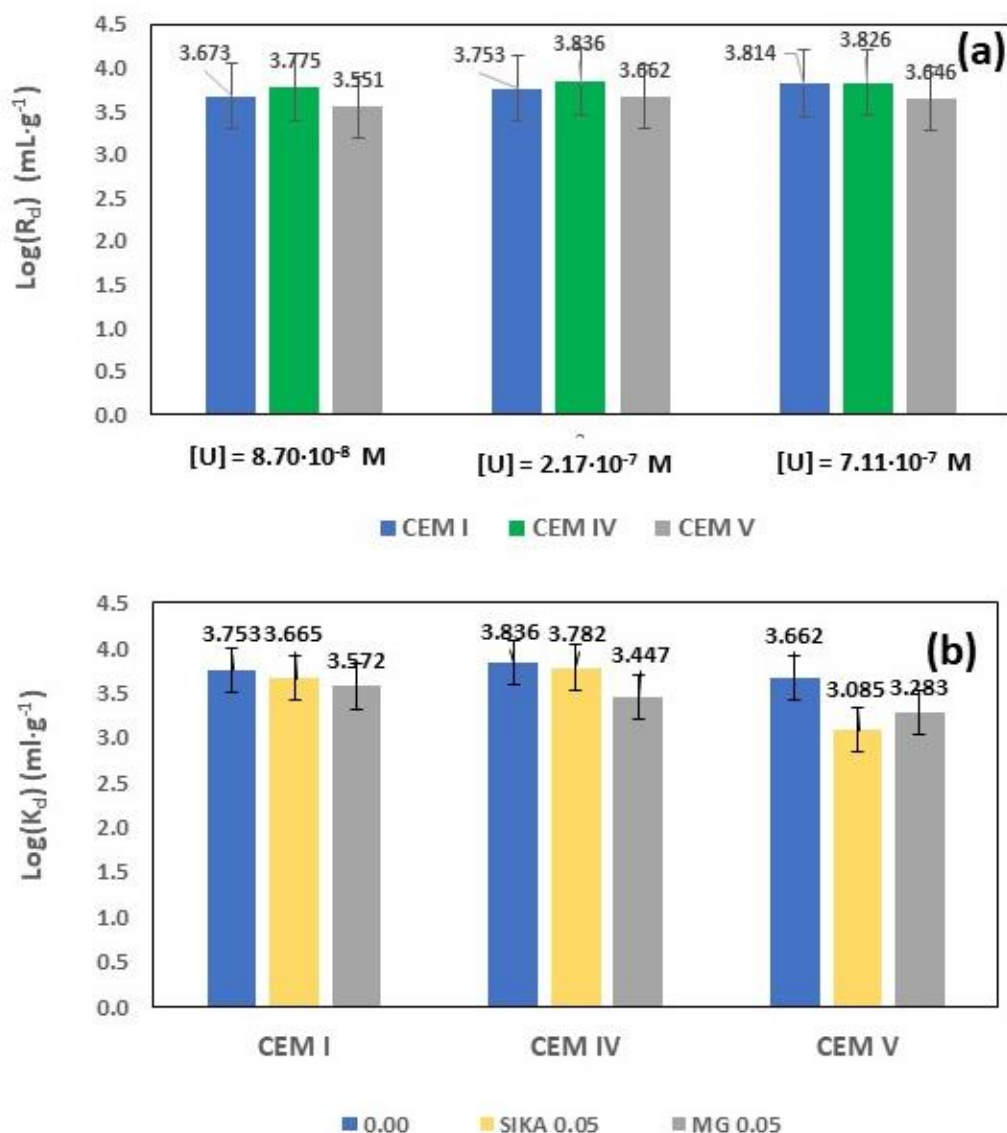
Figure 5-109:   *Uranium adsorption tests in fresh cement. (a) U adsorption in three different cements at three different [U]; (b) U adsorption in the presence of superplasticizers in the three different cements. [U]=2.17·10^{-7} M.*

The tests with U and the SP were carried out also at the other U concentrations, and the results were similar. As shown in *Figure 5-109*a, under the range of concentration used U adsorption is linear and the main Log(R_d) values are: 3.75 ± 0.07, 3.81 ± 0.03 and 3.62 ± 0.06 for CEM I, CEM IV and CEM V, respectively. The capability of the three cements for uranium under the present experimental conditions is very similar. The presence of SIKA affects slightly U sorption in all the cements, producing a decrease of Log(R_d) <6% (the maximum reduction occurs in CEM V, whereas in the others is almost negligible), which can be assumed within the uncertainty of R_d measurements. A similar quantitative effect is produced by MG in CEM I, whereas a more effective decrease is produced in the Log(R_d) values for uranium in CEM IV (-20 %) and CEM V (-10%).

EURAD (Deliverables n° 3.6, 3.7 and 3.8) - Final Report of results generated in CORI
Dissemination level: PU
Date of issue of this report: **05/07/2024**

Page 235
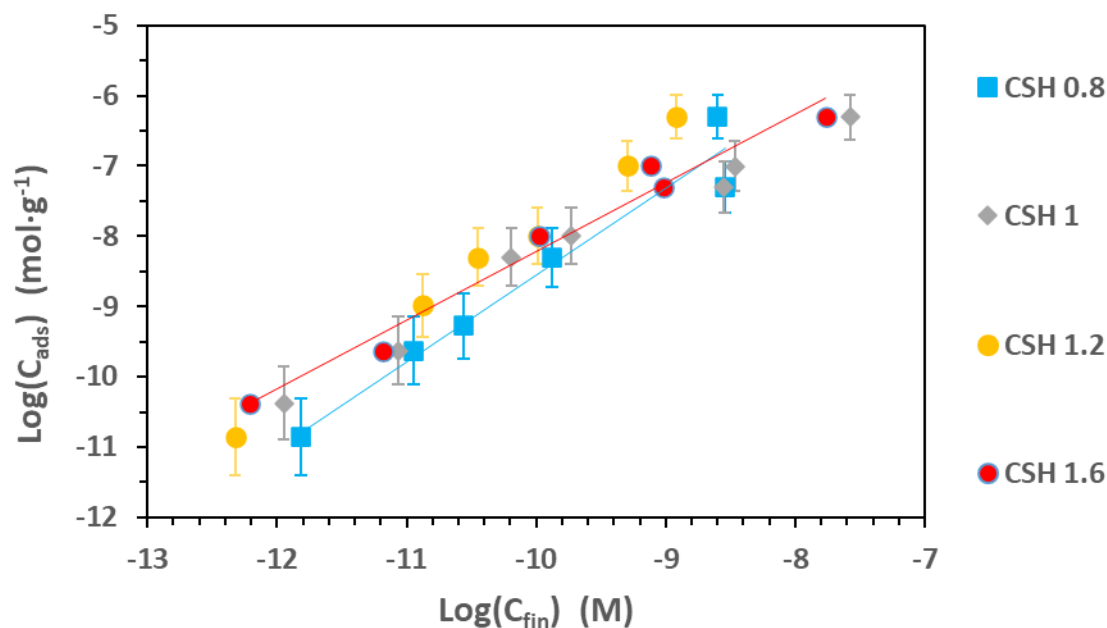
Figure 5-110:   Europium adsorption isotherms in C-S-H at different Ca/Si ratio and at a solid to liquid ratio of 10 g/L.

Figure 5-110 shows the sorption isotherms obtained for europium ([Eu] from 10^{-10} M to 10^{-5} M). Adsorption of europium is very high for all the C-S-H phases, the experimental values are highly scattered, and it is not possible to establish whether a trend with the Ca/Si ratio exist. The slopes of all the C-S-H are higher than 1, indicating that Eu (surface)precipitation may exist even at low Eu concentrations. In almost all the tests performed in the presence of the superplasticizers, the adsorption was even higher, with a final Eu concentration below the detection limit. Even these tests should be repeated with less solid to liquid ratio, results indicated negligible effects of the superplasticizers in Eu adsorption in the C-S-H phases, most probably due to the precipitation or coprecipitation of Eu.

The results of batch sorption tests with europium with and without the superplasticizers in three different fresh cements (CEM I, CEM IV and CEM V) are shown in Figure 5-111. In these tests, the pH was 12. 85±0.05; the solid to liquid ratio was 10 g·L^{-1}. Adsorption tests without the additives, were carried out with three different ^{152}Eu concentrations (1.38·10^{-10} M, 3.45·10^{-10} M and 5.29·10^{-9} M) and the results are shown in Figure 5-111a. In CEM I values tend to increase with the concentration, possibly related to some Eu precipitation in the system, whereas in the case of CEM IV and CEM V a clear trend is not evidenced (Figure 5-111a). The mean Log(R_d) values are : 4.35±0.56, 4.27±0.24 and 4.37±0.23 for CEM I, CEM IV and CEM V, respectively. These values are one order of magnitude less than those measured in the RCM. Possible variations in the equilibrium water due to the different solid to liquid ratio used may have affected the sorption results. *Figure 5-111*b shows the results of the sorption tests in the presence of MG or SIKA (5 wt.%) at one Eu concentration (3.45·10^{-10} M). The tests with Eu and the SP were carried out also at [Eu] = 5.29·10^{-9} M, and the results were similar.

The presence of SIKA clearly affects Eu sorption in CEM I (-13%) and CEM V (-33 %), but much less in adsorption in CEM IV. MG has a larger effect in all the cements with a reduction observed in the Log (R_d) values for Eu decreased by 51%; 58% and 67 % for CEM I, CEM IV and CEM V, respectively.

These results are different from the behavior observed in the C-S-H phases; therefore, the study of the effects of the superplasticizers on Eu diffusion in cements should be analyzed more in depth.

EURAD (Deliverables n° 3.6, 3.7 and 3.8) - Final Report of results generated in CORI
Dissemination level: PU
Date of issue of this report: **05/07/2024**

Page 236

Figure 5-111:   Europium adsorption tests in fresh cement (with a solid to liquid ratio of 10 g/L). (a) Eu adsorption in three different cements at three different [Eu]; (b) Eu adsorption in the presence of superplasticizers in the three different cements. [Eu] = 3.45·10^{-10} M.

Figure 5-112 shows the sorption isotherms obtained for plutonium ([Pu] from 6.7·10^{-11} M to 1.6·10^{-8} M). Adsorption of plutonium is quite high, also in this case is difficult to determine if a relation with the Ca/Si ratio exist. The slope of the isotherm is higher than one, indicating the possible precipitation/co precipitation of the actinide at very low concentrations. The last point of the isotherm, that with the highest Pu concentration, where sorption seems to decrease, generally shows less pH than the rest of the points.

Figure 5-113 shows the adsorption of plutonium in the presence of MG or SIKA (5 wt.%) in the different C-S-H phases. Considering the scattering of the data, and the high adsorption of Pu, the effect of the superplasticizers on Pu adsorption on the C-S-H phase can be considered negligible. The same experiment was also carried out using higher Pu concentration [Pu] = 6.5·10^{-10} M, and the results were similar.

EURAD (Deliverables n° 3.6, 3.7 and 3.8) - Final Report of results generated in CORI
Dissemination level: PU
Date of issue of this report: **05/07/2024**

Page 237
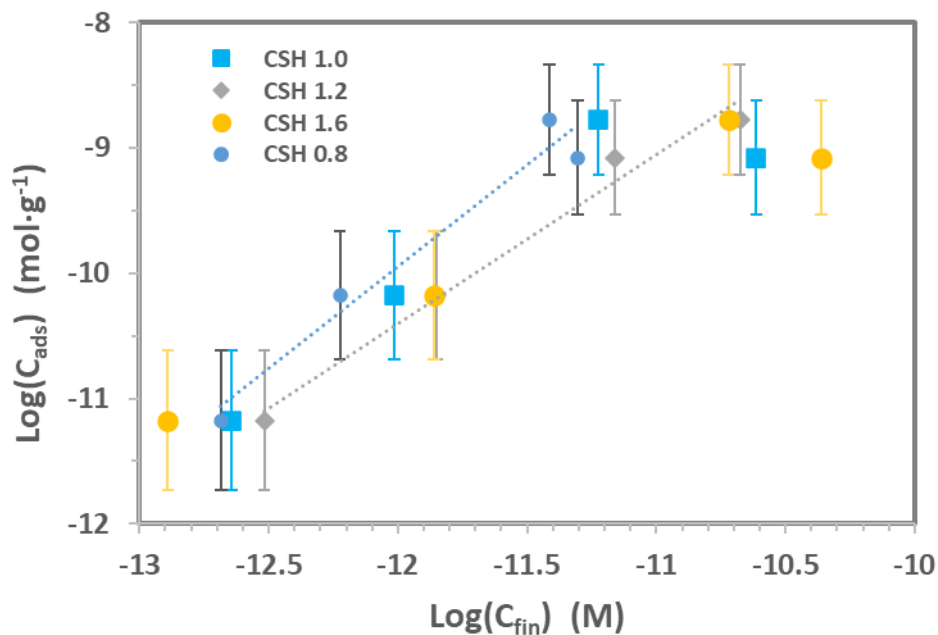
Figure 5-112:   Adsorption isotherms of plutonium in the C-S-H phases at different Ca/Si ratio.
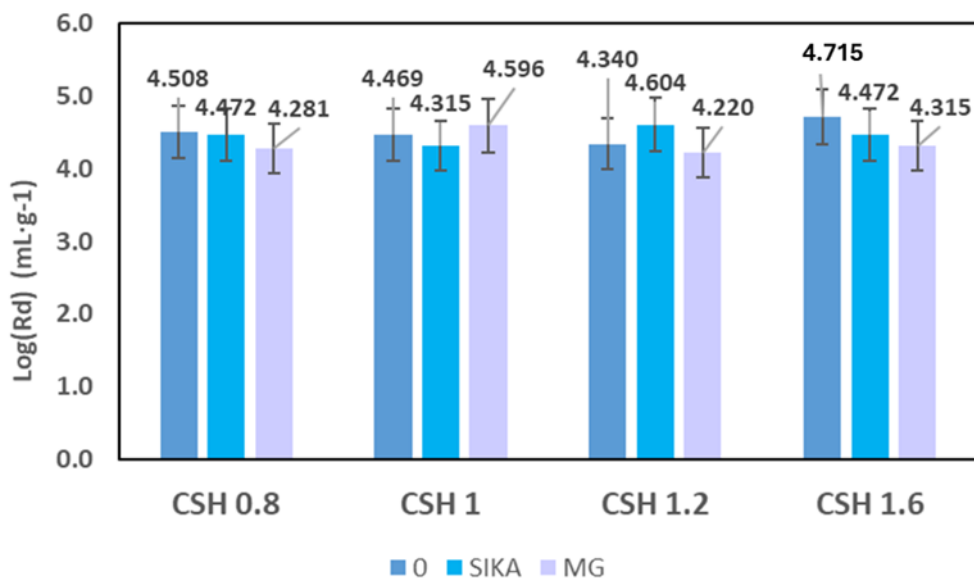
Figure 5-113:   Plutonium adsorption tests in C-S-H at different Ca/Si ratio and effects of the presence of the superplasticizers SIKA and MG. [Pu] = 6.64·10⁻¹¹ M.

EURAD (Deliverables n° 3.6, 3.7 and 3.8) - Final Report of results generated in CORI
Dissemination level: PU
Date of issue of this report: **05/07/2024**

Page 238
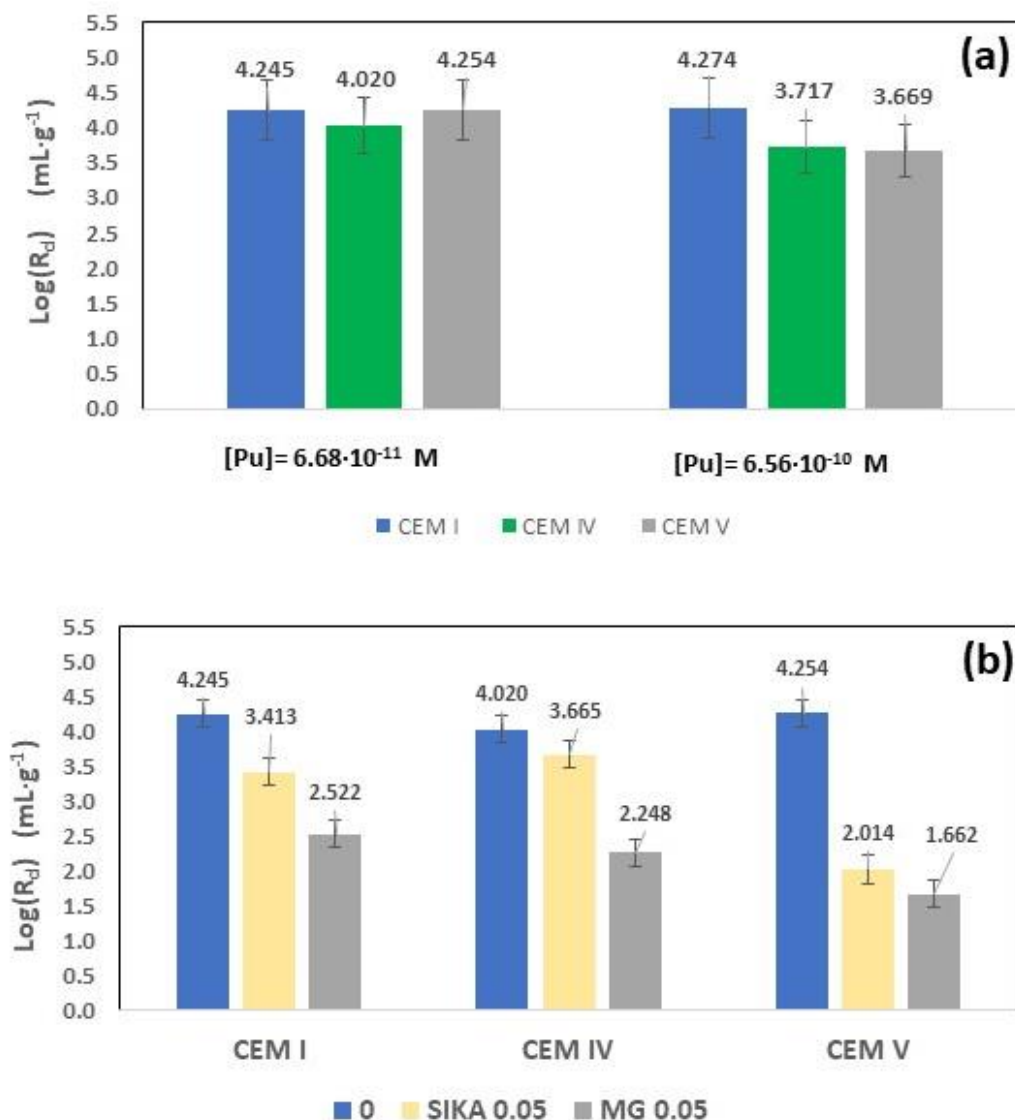
Figure 5-114:   *Plutonium adsorption tests in fresh cement. (a) Pu adsorption in three different cements at three different [Pu]; (b) Pu adsorption in the presence of superplasticizers in the three different cements. [Pu] = 6.68·10⁻¹¹ M.*

The results of batch sorption tests with plutonium with and without the superplasticizers in three different fresh HCP (CEM I, CEM IV and CEM V) are shown in Figure 5-114. The solid to liquid ratio was 10 $g \cdot L^{-1}$. Adsorption tests without the additives, were carried out at two different ^{238}Pu concentrations (6.68·10⁻¹¹ M and 6.3·10⁻¹⁰ M) and the results are shown in Figure 5-114a. In these tests the pH of the tests at the lower Pu concentration was 12.8±0.1, but for the higher concentrations decreased to pH 12±0.2, therefore data at the two concentrations are not totally comparable.

Figure 5-114b shows the results of the sorption tests in the presence of MG or SIKA (5 wt.%) at one Pu concentration (6.68·10⁻¹¹ M). The presence of SIKA significantly decreases Pu sorption in CEM V (47%), but the effect is also non negligible for CEM I (20%) and CEM IV (9 %). MG is much more effective decreasing the $Log(R_d)$ of 41%, 44 % and 61 % for CEM I, CEM IV and CEM V, respectively.

The tests with Pu and SP were carried out also at the highest Pu concentration. In this case no large effect was seen and this can be due to the more extensive precipitation of Pu. Discussing only the results obtained at low Pu concentration also for Pu, sorption in CEM V is the most affected, as observed also

EURAD (Deliverables n° 3.6, 3.7 and 3.8) - Final Report of results generated in CORI
Dissemination level: PU
Date of issue of this report: **05/07/2024**

Page 239

for other elements. Also in this case, these results are different from the behavior observed in the C-S-H phases, therefore the study of the effects of the superplasticizers on Pu diffusion in cements must be carried out.
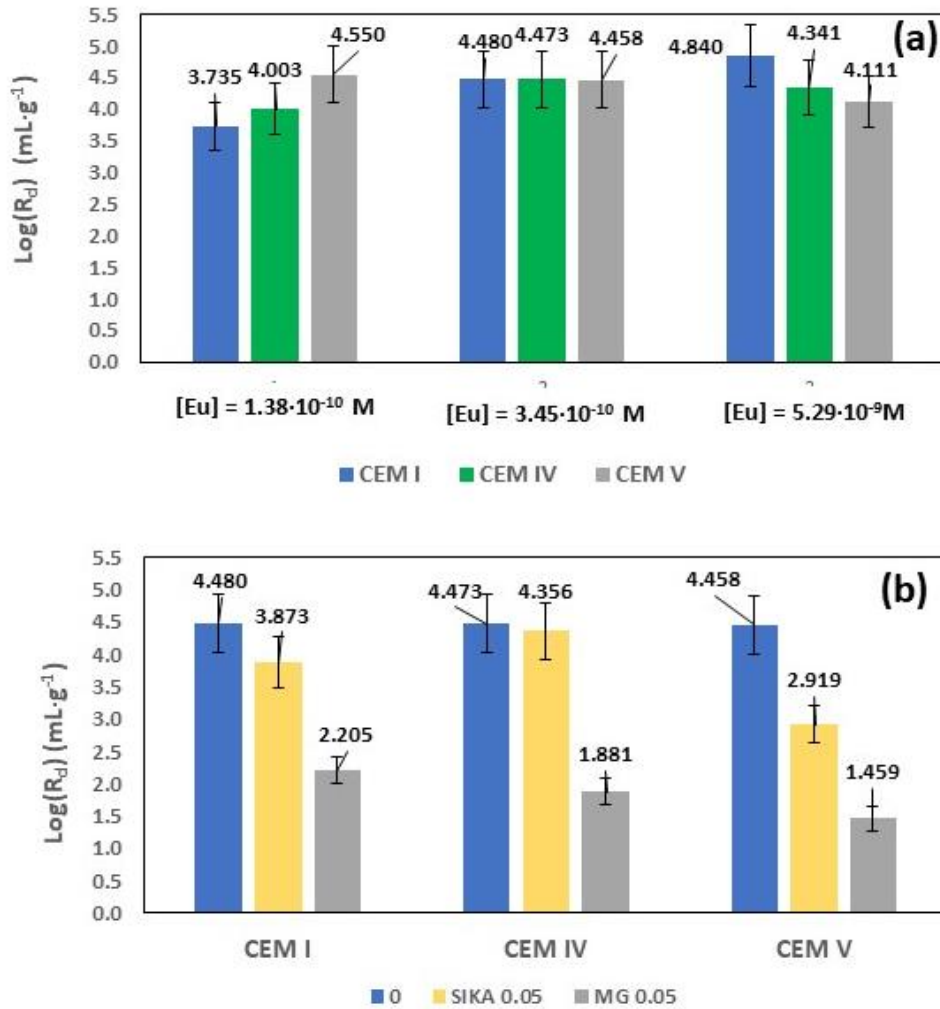
[CIEMAT] carried out in-diffusion tests in degraded HCP in absence and presence of the superplasticizers with nickel. The superplasticizers were added in the cement during the casting (not added in the solution with Ni). The D_a obtained varied approximately from 1 to $8 \cdot 10^{-15}$ m²/s for CEM I and 2 to $6 \cdot 10^{-15}$ m²/s for CEM V. Within the experimental errors, no variations could be seen between the D_a determined without the SPs and with MG or SIKA. This is expected considering the adsorption data; however, it is of interest to perform diffusion studies in HCP with Eu and Pu, where significant differences in R_d values were observed in batch sorption experiments with and without SPs.

Finally, **[CIEMAT]** carried out adsorption tests Ni, U, Pu and Eu in the presence of the "real" degradation product of PCE provided by BGRM, have been carried out with in the RCM both fresh and in degraded Stage II. The behavior of most of the investigated RN is similar at fresh and at degraded stage of RCM. Only for U, there is a more pronounced effect, with an increase of the R_d values with degradation of the RCM. Nevertheless, the increase of the concentration of the degraded PCE has a neglitable effect on the adsorption of all investigated RNs (Figure 5-115). However, according to the information received, the quantity of TOC in this sample is not very high.
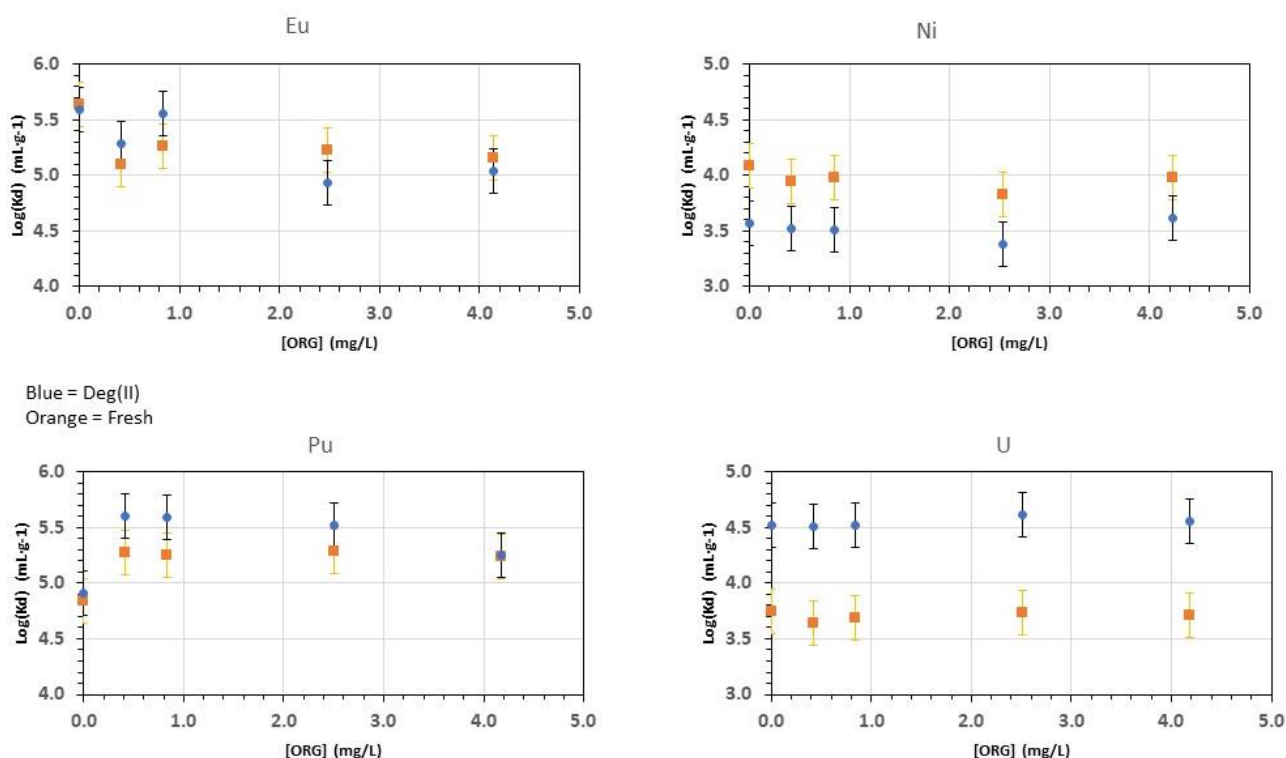
*Figure 5-115:   Sorption tests of Eu, Ni, Pu and U by various degraded RCM (blue series at Stage II and orange serie at Stage I) in presence of the degraded PCE provided by [**BGRM**].*

[UJV] analyzed the effects of the superplasticizer ISOLA on nickel retention in HCP by means of leaching experiments. The release of ^{63}Ni included in the HCP (pure CEM I paste and CEM I paste + ISOLA superplasticizer) was analyzed using as leaching solution distilled water, portlandite water and synthetic granitic water. The results can be seen in Figure 5-116.

EURAD (Deliverables n° 3.6, 3.7 and 3.8) - Final Report of results generated in CORI
Dissemination level: PU
Date of issue of this report: **05/07/2024**

Page 240
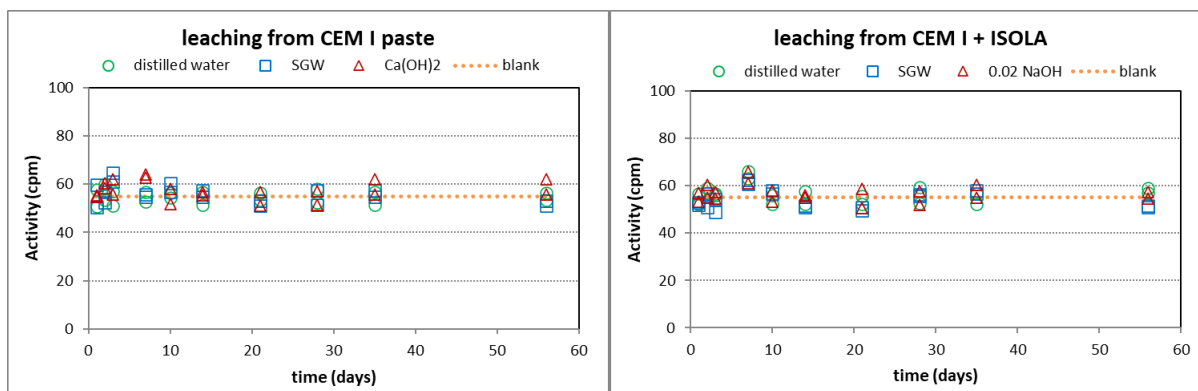
Figure 5-116: ^{63}Ni activity in the leachates from specimens with incorporated tracer; comparison of the absence and presence of organics: CEM I (left) and CEM I + ISOLA (right. No effects of SPs in leachability of Ni from CEM I).

No differences in the release of ^{63}Ni tracer incorporated in the pure cement paste CEM I and in the mixture of CEM I with addition of ISOLA superplasticizer. All measurements actually indicated Ni concentration below the detection limit.

[CTU] analysed the adsorption of lead at different solid to liquid ratios on fresh HCP (CEM I) as received, with included the superplasticizer (CX ISOPLAST 531), irradiated, or degraded to Stage II. In general, the highest adsorption is observed for the degraded HCP, whereas the presence of the SP, did not significantly affect the R_d values. The smallest R_d were observed in the irradiated material (7 MGy).
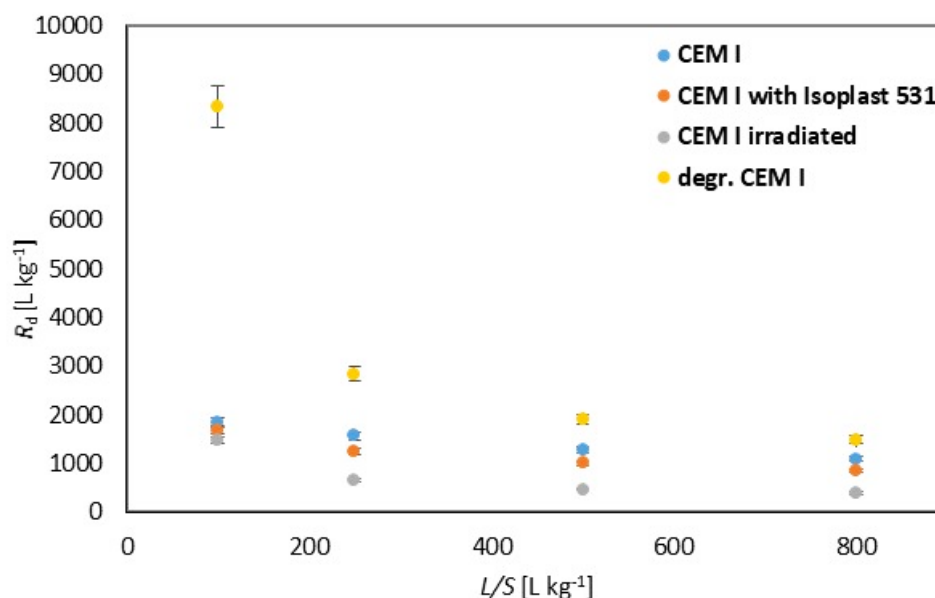
Figure 5-117: Dependence of R_d (L·kg^{-1}) on the phase ratio L/S at a lead concentration of $5 \cdot 10^{-4}$ mol/L in presence of various HCP CEM I.

EURAD (Deliverables n° 3.6, 3.7 and 3.8) - Final Report of results generated in CORI
Dissemination level: PU
Date of issue of this report: **05/07/2024**

Page 241

5.6 Degraded products of Ion Exchange Resins (IER) (GTA, HIBA, HBA proxy ligands and tri-methyl-amine (TMA)) and real leachates

[KIT] in collaboration of **[SKB]** and **[JUELICH]** investigated the effect of presence of degraded products of IER onto RN migration.

[KIT] investigated in collaboration with **[SKB]** the effects of different proxy ligand, L, ((α-hydroxyisobutyric acid (HIBA); 3-hydroxybutyric acid (HBA) and glutaric acid (GTA)) and the UP2W resins degradation leachate generated in Task 2 on the solubility of Ca(II), Ni(II), Nd(III) and Pu(IV) in cement pore water solutions with $[L]_{tot} \leq 0.1$ M. The results indicated that these investigated proxy ligands showed no significant impact on the solubility with $[L]_{tot} \leq 0.1$ M.

A slight increase in the solubility of Ni(II) is observed for the three ligands at $[L]_{tot} > 10^{-2}$ M, as can be seen in *Figure 5-118* (example for the Ni(II)-HIBA system), although this increase overlaps with the uncertainty of the solubility calculated for the equilibrium in the absence of any organic ligand, *i.e.* β-$Ni(OH)_{2(cr)} \rightleftharpoons Ni(OH)_{2(aq)}$ with $\log K°_{s},(1,2) = -(7.6 \pm 0.4)$.
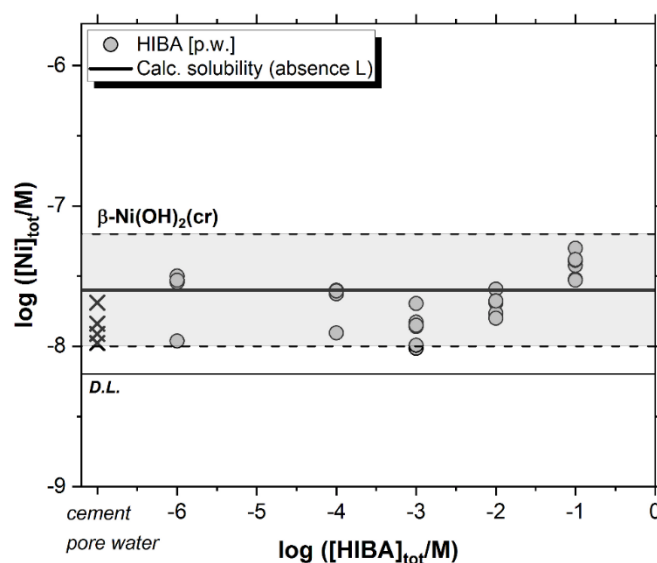
Figure 5-118: *Solubility of β-$Ni(OH)_{2(cr)}$ in cement pore water representing the Stage II and containing 10^{-6} M $\leq [HIBA]_{tot} \leq 0.1$ M. Cross symbols correspond to the Ni(II) concentration determined in the cement pore water. Black solid and dashed lines in the figure represent the calculated solubility of β-$Ni(OH)_{2(cr)}$ and corresponding uncertainty at pH = 12.5 in ligand-free systems, as calculated using the chemical and thermodynamic models reported by Gonzalez-Siso et al.(2018). D.L and p.w. stand for detection limit and present work, respectively.*

These observations suggest the possible formation of stable ternary complexes Ni-OH-L in the hyperalkaline conditions investigated in this work, although further solubility experiments at higher ligand concentrations are required to validate this hypothesis.

[KIT] also performed sorption experiments with and without proxy ligands and real leachates from the UP2W resins with Ni, Eu and Pu. Tests conducted in the absence of proxy ligands are consistent with literature data. Isotopic exchange with the inventory of [nat]Ni present in pristine HCP (including Ni in solid phases and associated with surfaces, *e.g.* of C-S-H phases) is considered as main retention mechanism of [63]Ni(II) in cement systems in Stage II. The retention of [63]Ni(II) and [242]Pu(III/IV) is slightly decreased in the presence of proxy ligands at $[L]_{tot} > 10^{-2}$ M (see *Figure 5-119* for the Pu case). The effect is less evident for Pu due to the dispersion of the data and to the increased detection limits with increasing ligand concentration. On the contrary, the uptake of [152]Eu(III) is not affected by the presence of proxy

EURAD (Deliverables n° 3.6, 3.7 and 3.8) - Final Report of results generated in CORI
Dissemination level: PU
Date of issue of this report: **05/07/2024**

Page 242

ligands up to concentrations of $[L]_{tot}$ = 0.1 M. These results are consistent with solubility studies. Moreover, these observations support that mono- and dicarboxylic acids can hardly outcompete the hydrolysis and sorption of Ni(II), Eu(III) and Pu(III/IV) in cement systems at Stage II, except if several alcohol groups are also present in the organic ligand.

A moderate decrease in the uptake of [63]Ni(II), [152]Eu(III) and [242]Pu(IV) by HCP is observed in the presence of the UP2W degradation leachate (DL) generated in Task 2 (see *Figure 5-119* for the Pu case). However, a significant retention remains for all investigated radionuclides, with log R_d([63]Ni(II)) ≈ 0.3, log R_d([152]Eu(III)) ≈ 2 and log R_d([242]Pu(IV)) ≈ 1.5 (all R_d in $m^3 \cdot kg^{-1}$). These observations reflect that the multiple functionalities expected in the macromolecules present in the UP2W degradation leachate can offer additional binding / chelating capabilities compared to the small molecular weight organic ligands considered as proxy ligands with at most bidentate bonding. These results emphasize the importance of performing sorption experiments with degradation leachates, in addition to the use of proxy ligands for complex systems such as UP2W or other organic materials disposed in repositories for nuclear waste.
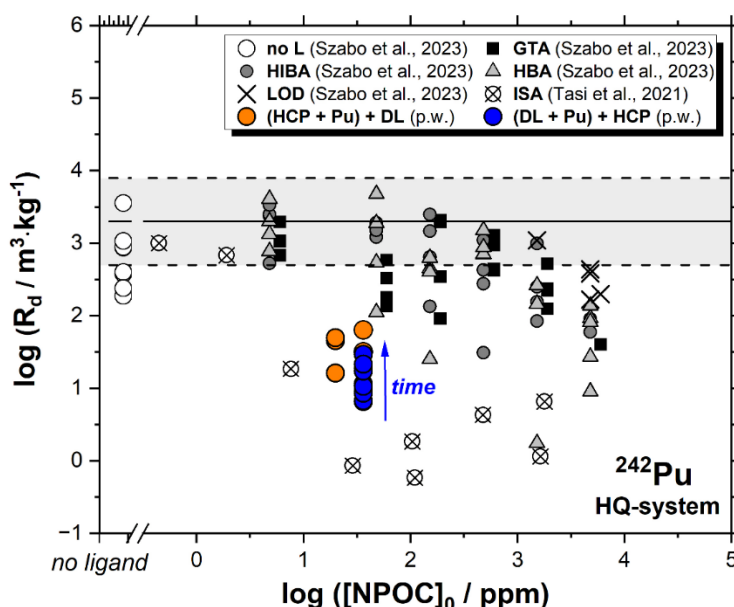
Figure 5-119: Uptake of [242]Pu(IV) by HCP in the presence of proxy ligands and the UP2W degradation leachate at S:L = 1 g·dm^{−3}. Red and green symbols correspond to experiments conducted following the order of addition "(HCP + Pu) + DL" and "(Pu + DL) + HCP", respectively. Grey and black symbols correspond to the uptake of [242]Pu(IV) by HCP in the presence of HIBA, HBA, GTA. All data correspond to Stage II, with pH = (12.4 ± 0.1). Solid line and grey-shaded area indicate the average R_d values and corresponding uncertainty reported in Tasi et al. (2021) for the uptake of Pu(IV) by HCP under analogous experimental conditions in the absence of organic ligands. Crossed circles shown sorption data from the same experimental study but in the presence of ISA.

Three publications have been published based on the results of Task 4: Szabo et al (2022); Szabo *et al.* (2023a) and Szabo et al (2023b).

[JUELICH] analyzed tri-methyl-amine (TMA) a degradation product of basic anion exchange resins, in relation to the retention behavior of [241]Am and [152]Eu at tracer concentration on hardened cement pastes (HCP) prepared from a CEM V/A 42.5N, by batch sorption experiments. Before sorption tests, solubility tests were carried out in a glove box under a controlled Ar atmosphere (O_2 and CO_2 concentrations < 5 ppm) following the experimental procedure of Tits and Wieland (2018). The batch solubility tests were carried out in 40 mL polypropylene centrifuge tubes, which were thoroughly washed and left overnight

EURAD (Deliverables n° 3.6, 3.7 and 3.8) - Final Report of results generated in CORI
Dissemination level: PU
Date of issue of this report: **05/07/2024**

Page 243

in a solution of 0.1 M HCl, then rinsed with Milli-Q water. For the solubility tests three different concentrations of ^{241}Am and ^{152}Eu (between ~10^{-8} M and ~10^{-10} M; stock solutions of the radionuclides were obtained from Eckert & Ziegler Nuclitec GmbH) were employed in CEM V/A water in the presence and absence of the organics. Tri-methyl-amine (Alfa Aesar) of 0.1 M were be prepared and diluted to obtain the required initial concentrations in the experiments. The concentration of the organics in the solubility tests ranged between 10^{-3} and 10^{-5} M. After selected times, aliquots were withdrawn from the solutions before and after centrifugation (6000 rpm ,1 hour) and analyzed for ^{241}Am and ^{152}Eu with liquid scintillation counting (TriCarb 3100 TR, Perkin Elmer, Freiburg, Germany) using Ultima Gold (Perkin Elmer) as scintillation cocktail.

Investigations of the effect of TMA on the solubility and sorption behavior of Am and Eu are currently ongoing. Ammonia and amines as "hard" bases (according to the HSAB principle of Pearson, 1963) form strong complexes with "soft" (in the sense of Pearson's acids) cations such as Ni, Pd, Ag, or Cu. On the other hand, their affinity to "hard" cations such as actinides and lanthanides or alkaline earth metals like Ca and Mg is rather weak. As a general rule, the stability constants show the relation ammonia = methylamine > dimethylamine > trimethylamine (*cf.* Van Loon und Hummel, 1995). Stability constants for metal complexes with methylamines are rather scarce and practically absent for TMA (cf. Smith *et al.*, 2004). Thus, in a scoping approach based on the aforementioned relation of the stability constants, the potential effects of TMA on the solubility and sorption of Am and Eu were assessed by thermodynamic calculations of the importance of their complex formation with ammonia. The stability constants for the reaction $Am^{3+} + NH_3 = AmNH_3^{3+}$ (log k = 2.4) was taken from Hancock and Bartolotti (2013). The stability constant of the reaction $Eu^{3+} + NH_3 = EuNH_3^{3+}$ (log k = 0.4) was interpolated from the data for La^{3+}, Gd^{3+}, and Lu^{3+} provided by Martell and Hancock (1996). Figure 6 shows the concentrations of Am and Eu species in a solution containing $5 \cdot 10^{-3}$ mol kg^{-1} Ca and $1 \cdot 10^{-3}$ mol kg^{-1} NH$_3$ as function of pH. This illustrates that complexation of trivalent actinides and lanthanides with ammonia (and thus also with TMA) is negligible in cementitious conditions.

Investigations of the effect of TMA on the sorption behavior of Am and Eu are currently ongoing. Due to the low affinity of TMA to form complexes with trivalent lanthanides and actinides, the effect of TMA on the sorption behavior of the investigated radionuclides is presumed to be very low. An effect of TMA itself on the degradation of Ca-bearing cement hydration phases is also unlikely since the Ca-TMA complexes are very weak, as indicated by the negligible formation of Ca-NH$_3$ complexes under alkaline conditions. In *Table 57* the calculated proportions of Ca and N(III) species in a young artificial cement water (ACW, pH 13.3) and a saturated portlandite solution (PSAT) are shown. This suggests that the contribution of Ca-NH$_3$ complexes – and thus even more pronounced for Ca-TMA complexes – to the total Ca concentration (~$1.5 \cdot 10^{-3}$ mol·kg^{-1} in ACW and ~$1.9 \cdot 10^{-3}$ mol·kg^{-1} in PSAT) is insignificant in cementitious systems. However, regarding the (radiolytic) degradation of anion exchange resins with quaternary amines as functional groups it has to be considered that in the course of this process also ammonia is formed (cf. Van Loon and Hummel, 1999), which in sufficient concentration is deleterious to cementitious materials (*e.g.*, Taylor, 1997).

Table 57: Relative proportions of Ca and N(III) species in young artificial cement porewater (ACW, pH 13.3) and saturated portlandite solution (PSAT, pH 12.5) containing 10^{-3} mol·kg^{-1} NH$_3$.

	pH	Ca^{2+}	$CaOH^+$	$CaNH_3^{2+}$	$Ca(NH_3)_2^{2+}$	NH_3	$CaNH_3^{2+}$	NH_4^+
ACW	13.3	46.47%	53.50%	0.04%	<0.01%	99.93%	0.06%	0.01%
PSAT	12.5	77.58%	22.37%	0.06%	<0.01%	98.78%	1.16%	0.07%

EURAD (Deliverables n° 3.6, 3.7 and 3.8) - Final Report of results generated in CORI
Dissemination level: PU
Date of issue of this report: **05/07/2024**

Page 244

5.7 Summary for Task 4

The work performed in Task 4 of CORI features experimental migration studies on binary systems (radionuclides + cement (or cement phases)) and ternary systems (radionuclides + organics + cement (or cement phases)). Studies in the binary system are required in order to assess the specific effect of organic compounds in the higher complexity ternary systems. The new studies in CORI have extended knowledge beyond the already published data in the literature. In the chapter 5, main results generated in WP3 CORI are described in details.

Considering the high complexity of the ternary systems studied in CORI Task 4 and the several variations regarding the investigated radionuclide, organic ligand and cement (or cement phase) types (see Table 43), it is challenging to provide results in a short summary. In the subsequent rather detailed sub-chapters focusing on specific groups of organic species, the new data and improved process understanding generated in CORI Task 4 are described.

Isosaccharinic acid and cellulose degradation products

In the U/C-A-S-H/α-ISA systems with C-A-S-H with Ca/Si and Al/Si ratios: 1.2-0.05 (pH= 11.3 ± 0.2) and 1.2-0.02 (pH= 10.2 ± 0.1), no large effect of the organic could be observed (**[KIT** (**Amphos21**)]). ISA significantly adsorbed on low aluminum C-A-S-H, whereas limited or no binding was observed with high aluminum C-A-S-H. Uranium showed an extremely strong binding affinity to all forms of C-A-S-H, resulting in solution concentrations mainly below the limits of instrumental detection.

In the Eu/RCM/RDP system, **[CEA]** analyzed the effects on Eu diffusion produced by cellulose RDP and they were different, using the products provided by **[PSI]** and **[SCK CEN]**. Even if some effects can be due to the composition of the different products, obtained by different methods, there is clearly an effect of the TOC concentration, which is much higher in the material provided by **[SCK CEN]**. The diffusivity of Eu is then higher with a factor of 250 in presence of high TOC content, obtained after radiolysis and hydrolysis of cellulose.

[CIEMAT] analyzed the effects of cellulose RDP provided by **[SCK CEN]**, on U, Eu, Ni and Pu adsorption on fresh and Stage II of RCM. In the case of Ni and U the adsorption in the RCM degraded at Stage II was higher than in fresh cement. In the case of Pu and Eu, no large difference between the two Stages could be observed. The RDP have a no-negligible effect on the adsorption of all the studied RN, with the unique exception of U in fresh RCM. Whereas significant decrease in K_d values was also previously observed for Eu and Pu in the presence of α-ISA, synthesized in the laboratory, this effect was not been observed for Ni, of which the sorption was not affected at all by ISA. This can be an indication that some of the still not identified cellulose degradation products obtained by hydrolysis and radiolysis by **[SCK CEN]** may have stronger effect than α-ISA on Ni retention. The adsorption behavior of Ni was analyzed also in the C-S-H phases at different Ca/Si ratio, indicating that adsorption increases as the Ca/Si decreases. The effect of the organic in the Ni/C-S-H/α-ISA system is quite limited. Diffusion experiments of Ni in the presence/absence of α-ISA in HCP Stage II did not show variation in the diffusion coefficients within the experimental error. In diffusion in HCP (CEM I, Stage II) of Pu in the presence of ISA, give measured D_a between $(9.2\pm0.8)\cdot10^{-14}$ m^2/s to $(1.5\pm0.8)\cdot10^{-13}$ m^2/s.

[JGU] analyzed the An(IV)/HCP/ISA system. They showed that Th(IV) and Pu(IV) strongly sorb on fresh cement under reducing and hyperalkaline conditions in the absence of organic ligands. ISA clearly affected the uptake of Th(IV) and Pu(IV) as can be shown in adsorption experiments (2 orders of magnitude less). Diffusion experiments also showed deeper Pu(IV) in-diffusion in the presence of ISA within 118 days.

[SCK CEN] analyzed the Ni/HCP/ISA system. They observed that Ni sorption in HCP was higher on cement at an advanced degradation stage than on fresh cement, additionally they observed that RDP (of **[SCK CEN]**) had a much stronger impact than pure α-ISA on Ni retention. This result would show

EURAD (Deliverables n° 3.6, 3.7 and 3.8) - Final Report of results generated in CORI
Dissemination level: PU
Date of issue of this report: **05/07/2024**

Page 245

that not only α-ISA has a sorption reduction power but that other products coming from the degradation of cellulose should be considered too.

[CNRS-SUBATECH] analyzed the U/HCP/ISA system. They observed ISA adsorption on HCP in Stage II higher than in Stage III. For the binary U(VI)/HCP system at Stage II, high R_d values (300 to 70 $m^3 \cdot kg^{-1}$), consistent with literature data, have been obtained. For the Stage III R_d values from 150 to 50 $m^3 \cdot kg^{-1}$) have been obtained. Desorption experiments show that uranium uptake mechanism is reversible. The results are consistent with the dissolution/recrystallization process that occurs at the surface of C-S-H particles. For the ternary U(VI)/ISA/HCP system, the main result is the existence of a threshold value for ISA concentration in solution ($[ISA]_{eq} = 2 \cdot 10^{-4}$ mol·L^{-1}) above which uranium uptake strongly diminishes. For the binary U(VI)/HCP (duration 505 days), uranium diffusion profiles have been quantified by Laser ablation HR-ICP-MS for two different locations in HCP sample. Results show that uranium profiles are characterized by a distribution gradient along the thickness of the sample. Thus, uranium concentration in solid decreases from 3000 mg·kg^{-1} (at the surface) to 5.5 mg·kg^{-1} (HCP background concentration). A penetration depth of around 40 μm has been determined. These results are consistent with a migration behavior dominates by strong sorption and/or very slow diffusion processes.

EDTA & NTA

[CEA] analyzed the HCP/U/EDTA and HCP/Ni/EDTA systems with HCP CEM V/A (or RCM) degraded at Stage II and IV analysing the kinetic of the process. At Stage II the U(VI) retention in the presence of EDTA is still significant ($R_d \sim 10^5$ L/kg) independently of the introduced EDTA concentration and contact time. The presence of EDTA tends to decrease only slightly the R_d value. For HCP CEM V/A at Stage III/IV the U(VI) sorption is still significant ($R_d \sim 10^5$ L/kg) and increases with the contact time. For an initial EDTA concentration up to 10^{-3} M, the R_d value tends to decrease, suggesting a saturation of sorption site. Similar trends are observed for [63]Ni. At Stage III/IV and for higher PHT concentration, the evolution of R_d values with the organic concentration suggests a competition effect and/or a saturation of the sorption site for EDTA concentration higher than 10^{-4} M.

[JGU] analyzed the HCP/An(IV)/EDTA system with fresh HCP. They observed a quantitative uptake of Th(IV) and Pu(IV) on HCP, and almost no difference with the order of RN ligand addition, indicating negligible influence of EDTA on Th and Pu on HCP retention after 72 hours of contact time.

[SURAO] did not observe effects of EDTA on Eu adsorption kinetic in CEM (III).

[UCYPRUS] analyzed the C-S-H/U/EDTA system under different atmosphere (N_2, ambient and 1% CO_2). Under N_2 atmosphere, the presence of EDTA in solution caused (slightly) lower Kd values due to stabilization of U(VI) in solution in the form of EDTA complexes. However, higher K_d values are observed when EDTA solutions are contacted with the C-S-H/U phase, because of the formation of ternary C-S-H/U(VI)/EDTA surfaces complexes, which stabilize U(VI) onto the C-S-H phase. On the other hand, under ambient atmosphere the U(VI) carbonate complexes govern the U(VI) chemistry in solution, resulting generally in lower K_d values. Similarly, under 1% CO_2 U(VI)-carbonate complexes govern the U(VI) chemistry in solution and result in the formation of ternary carbonate solid phases. EDTA ligand forms stable complexes with U(VI) in aqueous C-S-H suspensions. However, under environmental and subsurface conditions (CO_2 presence) the carbonate complexation will dominate the U(VI) geochemical behavior.

[HZDR] did observe and characterize for the first time the Eu(III)-NTA 2:2 complexe and formation constants of Eu(III)-NTA and Cm(III)-NTA complexes were determined, in a pH range from 1 to 9.

EURAD (Deliverables n° 3.6, 3.7 and 3.8) - Final Report of results generated in CORI
Dissemination level: PU
Date of issue of this report: **05/07/2024**

Page 246

Citrate

[KIT(EMPA)] analyzed the effect of citrate on the Cm, Pu and Eu adsorption on C-S-H phases, AFm phases and ettringite, Citrate had a negligible impact on the Pu and Eu retention by C-S-H phases, and it was observed to reduce Pu retention by AFm phases and ettringite only at $[CIT]_{tot} > 10^{-2}$ M.

Formate

[RATEN] performed solubility studies of Ni in cement porewater in the presence of formate. In water representing the fresh cement (pH 13.3) solubility is about $2 \cdot 10^{-7}$ M. When formic acid is added in the system, nickel total and in solution concentrations are not significantly influenced. The ^{63}Ni uptake was evaluated on non-degraded and degraded cement pastes based on CEM I and CEM V. The presence of formic acid, at a concentration of 10^{-3} M was found to have an impact on ^{63}Ni uptake on non-degraded CEM I HCP and to a lower extent on degraded cement, *i.e.* moderately lower R_d values were obtained for nickel sorption in the ternary systems. On CEM V HCP, the presence of formic acid, at a concentration of 10^{-3} M was found to have an inverse impact on ^{63}Ni uptake: higher Rd values were obtained for nickel sorption in the ternary system.

[KIT(EMPA)] analyzed the effect of formate on ^{242}Pu and ^{152}Eu uptake by C-S-H phases (Ca:Si = 0.8, 1.4), which was negligible. The effect of formate on ^{242}Pu adsorption on AFm phases and ettringite was also negligible.

Adipate

[CPST] showed similar effects on the presence of adipate and dioctyl adipate in Pu and Am sorption on HCP CEM I at Stage II. An increase of R_d value with the adipic acid addition in the system was observed. In contrary, a decrease of the retention is measured for Pu and Am.

Acetate and Oxalate

[CPST] showed negligible effects on the presence of adipates or oxalate in Pu and Am adsorption on HCP CEM I at Stage II.

Phthalate

No significant effects were observed by **[CEA]** due the presence of PHT on the retention of Ni and U in HCP at Stage II or Stage III/IV.

[CPST] performed sorption experiments with Pu (III/IV)] and Am(III) using Diisooctyl phthalate (DIOP). No significant effects were observed.

[JUELICH] studied the the uptake/retention and migration behavior of ^{241}Am and ^{152}Eu in the presence of phthalate on C-A-S-H phases and HCP (CEM V). At phthalate concentrations above $1 \cdot 10^{-3}$ mol·kg^{-1} a distinct decrease of the R_d values was observed. This reduction of the ^{241}Am and ^{152}Eu uptake in the presence of phthalate is suggested to be a consequence of the destabilisation/dissolution of C-S-H/C-A-S-H due to increasing Ca-complexation by phthalate in solution.

In contrast, in sorption experiments with pure synthesised C-(A)-S-H (Ca/Si ratio 1.6), only a minor effect of the phthalate addition on the retention behavior of Am and Eu was observed. In the absence of organics and at phthalate concentrations up to 10 mM, the R_d values of Am and Eu were in the order of 10^5 to 10^7 L·kg^{-1}. Only at very high phthalate additions (10^{-1} mol·kg^{-1}), a slight decrease in the radionuclide uptake was found.

EURAD (Deliverables n° 3.6, 3.7 and 3.8) - Final Report of results generated in CORI
Dissemination level: PU
Date of issue of this report: **05/07/2024**

Page 247

Gluconate & PBTC

[HZDR] studied the influence of GLU and PBTC on U(VI) retention by C-S-H with a C/S ratio of 0.8. They found that $1 \cdot 10^{-2}$ M GLU, decreases the R_d of uranium from 5.1 in absence of GLU to 4.8 ± 0.1. Regarding the U(VI) uptake, no clear trend can be seen in the tests with different addition sequences of U(VI) and GLU, thus indicating that GLU has only a very small influence on the U(VI) retention by C-S-H under these conditions. In general, it has been shown that GLU has little to no effect on the overall sorption of Eu(III), Am(III), Th(IV), Pu(IV), and U(VI) by C-S-H (C/S = 0.8). Concerning PBTC, the U(VI) retention by C(A)SH can decrease when PBTC species are present at relatively high concentrations.

[JGU] analyzed the HCP/Pu(IV)/GLU system and observed much lower R_d values of Pu(IV) obtained in the ternary system than the binary HCP/Pu(IV) system. Furthermore when Pu(IV) was added first, the uptake is higher than with GLU present, but lower compared to the binary system. This may be an indication that Pu(IV) desorbs after GLU addition. The order of addition affects Pu(IV) uptake on HCP, suggesting GLU occupies sorption sites. In the case of HCP/Th/GLU in the absence of GLU, the uptake of ^{232}Th(IV) on HCP is very high, in the samples of HCP + (GLU + Th(IV)) and HCP + GLU + Th(IV), relatively high Th concentration is detected indicating a leaching effect of Th from HCP. Additional analysis of the HCP + GLU sample (S/L = 5 g·L^{-1}) in the binary system confirmed this leaching effect. The order of additions of An(IV) and GLU have significantly influence of the uptake of An(IV) on HCP (pH > 13) during short contact times (72 h).

[KIT] in collaboration with **[EMPA]** analyzed the Pu(IV)/C-S-H/GLU; Pu(IV)/AFm-ettringite/GLU: Eu/C-S-H/GLU and EU systems. They observed that at [GLU] > 10^{-4} M the Pu uptake is decreased in both C-S-H phases with high (1.4) and low (0.8) Ca:Si ratio and redox buffer (*i.e.* HQ and Sn(II)). In the case of Pu/AFm-ettringite/GLU system, the uptake by AFm phases and ettringite has been observed, with log R_d of (5.6 ± 1.0) and (5.7 ± 1.1) (with R_d values reported in L/kg), respectively. GLU decreases the uptake of Pu by AFm phases and ettringite at GLU concentrations higher than 10^{-4} M. The impact of GLU on the retention of Pu by AFm phases and ettringite was stronger than that observed for C-S-H phases.

In the case of the ^{152}Eu/C-S-H/GLU system, high uptake of Eu(III) has been observed on C-S-H phases in the absence of organic ligands and hyper-alkaline conditions. Gluconate has a negligible effect on ^{152}Eu retention on C-S-H 0.8 at [GLU]$_{tot}$ < 10^{-2} M, whereas a moderate decrease in the retention is observed for gluconate concentrations [GLU]$_{tot}$ = $10^{-1.5}$ M and for longer equilibration times. For C-S-H 1.4, a strong decrease of Eu retention has been observed for [Gluconate]$_{tot}$ > 10^{-3} M. In the ^{248}Cm/C-S-H/GLU system, TRLFS analysis showed that Cm(III) is mostly incorporated in the C-S-H phase structure both in the presence and in absence of GLU. Conversely, for C-S-H 1.4, the formation Ca-Cm(III)-gluconate-(OH) aqueous complexes is observed at [GLU]$_{tot}$ ≥ $10^{-2.5}$ M, thus preventing the incorporation of Cm(III) into the C-S-H structure. The results obtained in this framework, support that the retention decrease of Eu on C-S-H 1.4 in the presence of gluconate is due to the formation of Ca-Eu(III)-Gluconate-(OH), thus highlighting the relevant role of Ca in the formation of Ca-Ac(III)/Ln(III)-L-(OH) complexes.

[UHelsinki] investigated the migration of RN by electromigration experiments in presence and absence of gluconate. This technique appears to be relevant to help to decrease the transient time-lag. The feasibility to measure radiotracer has been demonstrated and as each novel method, it would require further developments especially, in terms of experimental data interpretation.

Superplasticizers and PCE RDP

Studies performed in CORI Task 4 were limited to a small number of systems. Results clearly shows a very limited effect of the presence of SP in the case of nickel, where nor sorption, leaching or diffusion processes were affected by the presence of superplasticizers. For Ni, no difference of leaching behavior was observed by **[CIEMAT]** and **[UJV]**. Nevertheless, batch sorption tests performed by **[CIEMAT]** showed that the adsorption of Ni, U, Pu and Eu in C-S-H is not affected by the presence of superplasticizers (5% wt), but not negligible decrease of sorption is observed in fresh HCP for Eu and

EURAD (Deliverables n° 3.6, 3.7 and 3.8) - Final Report of results generated in CORI
Dissemination level: PU
Date of issue of this report: **05/07/2024**

Page 248

Pu in the presence of the same quantity of superplasticizers. Thus, is of interest to continue to investigate the role of SPs in diffusion tests with Eu and Pu, with the superplasticizer added during casting.

Degraded products of IER (proxy ligands GTA, HIBA, HBA and TMA) and real leachates or UP2W resins

[JUELICH] analyzed tri-methyl-amine (TMA) a degradation product of basic anion exchange resins, in relation to the retention behavior of ^{241}Am and ^{152}Eu at tracer concentration on hardened cement pastes (HCP) prepared from a CEM V/A 42.5N, by batch sorption experiments. Based on thermodynamic calculations performed by **[JUELICH]**, the affinity of tri-methyl-amine (TMA) to form complexes with An(III)/Ln(III) is very low. A small effect of TMA on the mobility of these RNs is presumed and unlikely effects of TMA on Ca-bearing cement hydration phases are expected.

[KIT] in collaboration with **[SKB]** studied the solubility of Ca(II), Ni(II), Nd(III) and Pu(IV), in cement porewater solutions containing HIBA, HBA and GTA, which are selected proxy ligand. None of these proxy ligands showed any remarkable impact on the solubility of Ca(II), Nd(III) or Pu(IV) in cement porewater solutions. GTA, HIBA and HBA induce a slight increase in the solubility of Ni(II) at $[L]_{tot}$ = 0.1 M, thus hinting the formation of stable Ni(II)-GTA, -HIBA and -HBA complexes in hyperalkaline conditions. The comparison of these results with solubility data in the presence of ISA confirms the stronger complexation properties of the latter ligand. Even though HIBA and HBA are carboxylic acids containing one alcohol group, this comparison shows that additional alcohol groups are required to efficiently chelate the metal ion and outcompete hydrolysis. The uptake of ^{63}Ni(II), ^{152}Eu(III) and ^{242}Pu(III/IV) by HCP at Stage II was investigated in the absence and presence of proxy ligands (HIBA, HBA, GTA) and the UP2W degradation leachate generated in Task 2. The presence of proxy ligands has a negligible effect on the uptake of ^{152}Eu(III) up to $[L]_{tot}$ = 0.1 M. A slight decrease in the distribution ratios for ^{63}Ni(II) and ^{242}Pu(III/IV) is observed at $[L]_{tot}$ > 10^{-2} M, although the effect is less evident in the case of plutonium due to the dispersion of the data and the increase of the detection limits with increasing ligand concentrations. Compared to strongly complexing ligands like isosaccharinic acid or gluconate, the investigated proxy ligands show a minor capacity for radionuclide mobilization in cementitious systems, even at high concentrations. The presence of the degradation leachate induces a moderate decrease in the uptake of ^{63}Ni(II), ^{152}Eu(III) and ^{242}Pu(IV) by HCP, as compared to the sorption in the presence of the proxy ligands. These observations possibly reflect that the multiple functionalities (-COOH, -OH, amide groups) expected in the macromolecules (10–15 kDa) present in the degradation leachate, can offer further binding / chelating capabilities compared to the small organic proxy ligands with at most bidentate binding.

Regarding radionuclide migration in the ternary system RN-organic-cement derived from the work in CORI, some general observations can be highlighted as follows:

• In many investigated cases **the effect of organic species on the solubility or sorption of RNs was zero or minor**. This is especially true if considering "realistic" organics concentrations in solution as expected for many repository settings. The threshold concentration of organic where an effect on solubility/sorption can be observed is higher than $1 \cdot 10^{-3}$ M.

• For RN with strong affinity for cement(phase), the results obtained in CORI task 4 are consistent with a **migration behavior dominated by strong sorption and/or very slow diffusion processes**.

• **New quantitative data** on radionuclide retention on cement-based materials under presence of organics were derived. The strong variations used in CORI regarding cement, degradation stages, organics and radionuclides open perspectives to systematize findings into material/radionuclide groups having expected „weak", „moderate", „strong" impact on retention. (See also the subsequent paragraphs).

EURAD (Deliverables n° 3.6, 3.7 and 3.8) - Final Report of results generated in CORI
Dissemination level: PU
Date of issue of this report: **05/07/2024**

Page 249

• **A strong effect of dissolved [Ca**] on the chemical speciation, reaction mechanisms and quantification was observed. This improved chemical understanding is important new input for realistic descriptions. It should be emphasized, that a comprehensive understanding of speciation (and thermodynamics) is essential for in-depths data interpretation.

• **Differences between the real leachates from Task 2 and the proxy ligands were observed** regarding impact on radionuclide retention. The real leachates tend to cause a stronger decrease in radionuclide sorption, which is also related to the organics concentrations.

EURAD (Deliverables n° 3.6, 3.7 and 3.8) - Final Report of results generated in CORI
Dissemination level: PU
Date of issue of this report: **05/07/2024**

Page 250

References

Abrahamsen-Mills, L., Small, J.S., 2021. Organic-containing nuclear wastes and national inventories across Europe, in: The Microbiology of Nuclear Waste Disposal. Elsevier, pp. 1–20. https://doi.org/10.1016/B978-0-12-818695-4.00001-0

Allen, A., O., 1961. Radiation Chemistry of Water and Aqueous Solutions, Van Nostrand Reinhold Inc. ed. Princeton, USA.

Altmaier, M., Neck, V., Fanghänel, T., 2008. Solubility of Zr(IV), Th(IV) and Pu(IV) hydrous oxides in $CaCl_2$ solutions and the formation of ternary Ca-M(IV)-OH complexes. Radiochimica Acta 96, 541–550. https://doi.org/10.1524/ract.2008.1535

Ait-Mouheb, N., 2021. Radionuclide migration in low-pH cement / clay interfaces: Derivation of reactive transport parameters (PhD thesis). Friedrich-Schiller-Universität Jena, Jena, Germany.

Androniuk, I., 2017. Effects of cement organic additives on the adsorption of uranyl ions on calcium silicate hydrate phases: experimental determination and computational molecular modelling (PhD thesis). Université de Nantes, Nantes, France.

Androniuk, I., Kalinichev, A.G., 2020. Molecular dynamics simulation of the interaction of uranium (VI) with the C–S–H phase of cement in the presence of gluconate. Applied Geochemistry 113, 104496. https://doi.org/10.1016/j.apgeochem.2019.104496

Androniuk, I., Landesman, C., Henocq, P., Kalinichev, A.G., 2017. Adsorption of gluconate and uranyl on C-S-H phases: Combination of wet chemistry experiments and molecular dynamics simulations for the binary systems. Physics and Chemistry of the Earth, Parts A/B/C 99, 194–203. https://doi.org/10.1016/j.pce.2017.05.005

ANSI/ANS, 2003. Measurement Of The Leachability Of Solidified Low-Level Radioactive Wastes By A Short-Term Test Procedure. ANSI/ANS-16.1-2003 (R2017)

Barwick, V., Prichard, E., 2011. Eurachem Guide: Terminology in Analytical Measurement—Introduction to VIM 3, Available at: www.eurachem.org. Accessed February 9, 2024.

Baston, G., Cowper, M., Davies, P., Dawson, J., Farahani, B., Health, T., Schofield, J., Smith, V., Watson, S., Wilson, J., 2017. The Impacts of PVC Additives and Their Degradation Products on Radionuclide Behaviour (No. AmecFW/0006604/4/Issue 3). Didcot, UK.

Bechtold, T., Burtscher, E., Turcanu, A., 2002. Ca^{2+}–Fe^{3+}–D-gluconate-complexes in alkaline solution. Complex stabilities and electrochemical properties. J. Chem. Soc., Dalton Trans. 2683–2688. https://doi.org/10.1039/b202086f

Bell, J.L.S., Palmer, D.A., 1994. Experimental Studies of Organic Acid Decomposition, in: Pittman, E.D., Lewan, M.D. (Eds.), Organic Acids in Geological Processes. Springer Berlin Heidelberg, Berlin, Heidelberg, pp. 226–269. https://doi.org/10.1007/978-3-642-78356-2_9

Bell, J.L.S., Palmer, D.A., Barnes, H.L., Drummond, S.E., 1994. Thermal decomposition of acetate: III. Catalysis by mineral surfaces. Geochimica et Cosmochimica Acta 58, 4155–4177. https://doi.org/10.1016/0016-7037(94)90271-2

Bejaoui, S., Bary, B., 2007. Modeling of the link between microstructure and effective diffusivity of cement pastes using a simplified composite model. Cement and Concrete Research 37, 469–480. https://doi.org/10.1016/j.cemconres.2006.06.004

Bharat, T.V., 2014. Analytical model for 1-D contaminant diffusion through clay barriers. Environmental Geotechnics 1, 210–221. https://doi.org/10.1680/envgeo.13.00035

Bildstein, O., Claret, F., 2015. Stability of Clay Barriers Under Chemical Perturbations, in: Developments in Clay Science. Elsevier, pp. 155–188. https://doi.org/10.1016/B978-0-08-100027-4.00005-X

EURAD (Deliverables n° 3.6, 3.7 and 3.8) - Final Report of results generated in CORI
Dissemination level: PU
Date of issue of this report: **05/07/2024**

Page 251

Bleyen, N., Van Gompel, V., Smets, S., Eyley, S., Verwimp, W., Thielemans, W., Valcke, E., 2023. Radiolytic degradation of cellulosic materials in nuclear waste: Effect of oxygen and absorbed dose. Radiation Physics and Chemistry 212, 111177. https://doi.org/10.1016/j.radphyschem.2023.111177

Bott, J., 2022. Diffusion von Actiniden in Zementstein (PhD thesis). Johannes Gutenberg-Universität Mainz, Mainz, Germany.

Böszörményi, É., Lado, J., Dudás, C., Kutus, B., Szabados, M., Varga, G., Pálinkó, I., Sipos, P., 2020. The structure and composition of solid complexes comprising of Nd(III), Ca(II) and D-gluconate isolated from solutions relevant to radioactive waste disposal. Pure and Applied Chemistry 92, 1709–1715. https://doi.org/10.1515/pac-2019-1010

Bruno, J., Gonzalez-Siso, M.R., Duro, L., Gaona, X., Altmaier, M., 2018. Key master variables affecting the mobility of Ni, Pu Tc and U in the near field of the SFR repository (SKB Technical Report No. TR-18-01). SKB.

Burešová, M., Kittnerová, J., Drtinová, B., 2023. Comparative study of Eu and U sorption on cementitious materials in the presence of organic substances. J Radioanal Nucl Chem 332, 1499–1504. https://doi.org/10.1007/s10967-022-08705-3

Castellote, M., Andrade, C., & Alonso, C. (2001). Measurement of the steady and non-steady-state chloride diffusion coefficients in a migration test by means of monitoring the conductivity in the anolyte chamber. Comparison with natural diffusion tests. Cement and concrete research, 31(10), 1411-1420. https://doi.org/10.1016/S0008-8846(01)00562-2

Çevirim-Papaioannou, N., Jo, Y., Franke, K., Fuss, M., De Blochouse, B., Altmaier, M., Gaona, X., 2022. Uptake of niobium by cement systems relevant for nuclear waste disposal: Impact of ISA and chloride. Cement and Concrete Research 153, 106690. https://doi.org/10.1016/j.cemconres.2021.106690

Chantreux, M., Ricard, D., Asia, L., Rossignol, S., Wong-Wah-Chung, P., 2021. Additives as a major source of radiolytic organic byproducts of polyvinyl chloride (PVC). Radiation Physics and Chemistry 188, 109671. https://doi.org/10.1016/j.radphyschem.2021.109671

Claret, F., Grangeon, S., Loschetter, A., Tournassat, C., De Nolf, W., Harker, N., Boulahya, F., Gaboreau, S., Linard, Y., Bourbon, X., Fernandez-Martinez, A., Wright, J., 2018. Deciphering mineralogical changes and carbonation development during hydration and ageing of a consolidated ternary blended cement paste. IUCrJ 5, 150–157. https://doi.org/10.1107/S205225251701836X

Colàs Anguita, E., 2014. Complexation of Th(IV) and U(VI) by polyhydroxy and polyamino carboxylic acids (PhD thesis). Universitat Politècnica de Catalunya, Barcelona, Spain.

Colombani, J., 2006. Etude de la radiolyse gamma du poly(chlorure de vinyle) : application à l'étude de la dégradation par irradiation et par lixiviation du PVC industriel (PhD thesis). Université Paul Cezanne, Marseille, France.

COMSOL Multiphysics® v. 5.4, 2018. www.comsol.com. COMSOL AB, Stockholm, Sweden.

Costagliola, A., Vandenborre, J., Blain, G., Baty, V., Haddad, F., Fattahi, M., 2017. Radiolytic Dissolution of Calcite under Gamma and Helium Ion Irradiation. J. Phys. Chem. C 121, 24548–24556. https://doi.org/10.1021/acs.jpcc.7b07299

Crank, J., 1975. The mathematics of diffusion, 2d ed. ed. Clarendon Press, Oxford, [Eng].

Crumière, F., Vandenborre, J., Essehli, R., Blain, G., Barbet, J., Fattahi, M., 2013. LET effects on the hydrogen production induced by the radiolysis of pure water. Radiation Physics and Chemistry 82, 74–79. https://doi.org/10.1016/j.radphyschem.2012.07.010

Cvetković, B.Z., Rothardt, J., Büttler, A., Kunz, D., Schlotterbeck, G., Wieland, E., 2018. Formation of Low-Molecular-Weight Organic Compounds During Anoxic Corrosion of Zero-Valent Iron. Environmental Engineering Science 35, 447–461. https://doi.org/10.1089/ees.2017.0216

EURAD (Deliverables n° 3.6, 3.7 and 3.8) - Final Report of results generated in CORI
Dissemination level: PU
Date of issue of this report: **05/07/2024**

Page 252

Dettmann, S., Huittinen, N.M., Jahn, N., Kretzschmar, J., Kumke, M.U., Kutyma, T., Lohmann, J., Reich, T., Schmeide, K., Shams Aldin Azzam, S., Spittler, L., Stietz, J., 2023. Influence of gluconate on the retention of Eu(III), Am(III), Th(IV), Pu(IV), and U(VI) by C-S-H (C/S = 0.8). Front. Nucl. Eng. 2, 1124856. https://doi.org/10.3389/fnuen.2023.1124856

Diomidis, N., 2014. Scientific basis for the production of gas due to corrosion in a deep geological repository (Nagra Arbeitsbericht No. NAB 14-21,). Nagra, Wettingen, Switzerland.

Fanghänel, T., Neck, V., 2002. Aquatic chemistry and solubility phenomena of actinide oxides/hydroxides. Pure and Applied Chemistry 74, 1895–1907. https://doi.org/10.1351/pac200274101895

Fernandez, A.F., Ooms, H., Brichard, B., Coeck, M., Berghmans, F., 2002. Test facilities at SCK•CEN for radiation tolerance assessment: from space applications to fusion environments, in: Proceedings of the RADECS 2002 Workshop. Presented at the European Workshop on Radiation and Its Effects on Components and Systems (RADECS 2002), Padua, Italy.

Flury, M., Gimmi, T., 2002. 6.2 Solute Diffusion, in: Methods of Soil Analysis: Part 4 Physical Methods, Soil Science Society of America. pp. 1323–1351.

Drtinová, B., Kittnerová, J., Bergelová, K., Burešová, M., Baborová, L., 2023. Sorption of lead on cementitious materials in presence of organics. Front. Nucl. Eng. 1, 1095233. https://doi.org/10.3389/fnuen.2022.1095233

Friedrich, S., Sieber, C., Drobot, B., Tsushima, S., Barkleit, A., Schmeide, K., Stumpf, T., Kretzschmar, J., 2023. Eu(III) and Cm(III) Complexation by the Aminocarboxylates NTA, EDTA, and EGTA Studied with NMR, TRLFS, and ITC—An Improved Approach to More Robust Thermodynamics. Molecules 28, 4881. https://doi.org/10.3390/molecules28124881

Gaona, X., Montoya, V., Colàs, E., Grivé, M., Duro, L., 2008. Review of the complexation of tetravalent actinides by ISA and gluconate under alkaline to hyperalkaline conditions. Journal of Contaminant Hydrology 102, 217–227. https://doi.org/10.1016/j.jconhyd.2008.09.017

García, D., Henocq, P., Riba, O., López-García, M., Madé, B., Robinet, J.-C., 2020. Adsorption behaviour of isosaccharinic acid onto cementitious materials. Applied Geochemistry 118, 104625. https://doi.org/10.1016/j.apgeochem.2020.104625

Garcia, E., Johnston, D., Whitaker, J.R., Shoemaker, S.P., 1993. Assessment of endo-1,4-beta-D-glucanase activity by a rapid colorimetric assay using disodium 2,2'-bicinchoninate. J Food Biochemistry 17, 135–145. https://doi.org/10.1111/j.1745-4514.1993.tb00463.x

Giffaut, E., Grivé, M., Blanc, Ph., Vieillard, Ph., Colàs, E., Gailhanou, H., Gaboreau, S., Marty, N., Madé, B., Duro, L., 2014. Andra thermodynamic database for performance assessment: ThermoChimie. Applied Geochemistry 49, 225–236. https://doi.org/10.1016/j.apgeochem.2014.05.007

Glaus, M., Van Loon, L.R., 2009. Chemical reactivity of α-isosaccharinic acid in heterogeneous alkaline Systems (PSI report No. 08–01). PSI, Villigen, Switzerland.

Glaus, M., Van Loon, L.R., 2004. Cellulose Degradation at Alkaline Conditions: Long-Term Experiments at Elevated Temperatures (Nagra Technical Report No. 03–08). Nagra, Wettingen, Switzerland.

Glaus, M., Van Loon, L.R., Achatz, S., Chodura, A., Fischer, K., 1998. Degradation of cellulosic materials under the alkaline conditions of a cementitious repository for low and intermediate level radioactive waste. Part I: Identification of degradation products. Analytica Chimica Acta 398, 111–122.

Glaus, M.A., Van Loon, L.R., 2008. Degradation of Cellulose under Alkaline Conditions: New Insights from a 12 Years Degradation Study. Environ. Sci. Technol. 42, 2906–2911. https://doi.org/10.1021/es7025517

Goudarzi, R., 2023. Prototype Repository – Sensor data report; Period 2001-09-17 to 2022-01-01 (SKB Technical Report No. SKB P-22-24).

EURAD (Deliverables n° 3.6, 3.7 and 3.8) - Final Report of results generated in CORI
Dissemination level: PU
Date of issue of this report: **05/07/2024**

Page 253

Helten, O., Ostertag-Henning, C., Bach, W., Hinrichs, K.-U., 2022. Generation and decomposition of low-molecular-weight organic acids in hydrous pyrolysis experiments with Opalinus Clay rock. Organic Geochemistry 172, 104481. https://doi.org/10.1016/j.orggeochem.2022.104481

ISO, 2009. Paper, board, pulps and cellulose nanomaterials - Determination of residue (ash content) on ignition at 525°C. ISO Standard. ISO 1762

Jelinek, J., Neufeld, P., 1982. Kinetics of Hydrogen Formation from Mild Steel in Water under Anaerobic Conditions. CORROSION 38, 98–104. https://doi.org/10.5006/1.3577332

Jo, Y., Androniuk, I., Çevirim-Papaioannou, N., De Blochouse, B., Altmaier, M., Gaona, X., 2022. Uptake of chloride and iso-saccharinic acid by cement: Sorption and molecular dynamics studies on HCP (CEM I) and C-S-H phases. Cement and Concrete Research 157, 106831. https://doi.org/10.1016/j.cemconres.2022.106831

Keith, L.H., Crummett, Warren., Deegan, John., Libby, R.A., Taylor, J.K., Wentler, George., 1983. Principles of environmental analysis. Anal. Chem. 55, 2210–2218. https://doi.org/10.1021/ac00264a003

Kittnerová, J., Drtinová, B., Štamberg, K., Deissmann, G., Lange, S., Evans, N., 2023. Study of Radium Behavior in Contact With Calcium-Silicate-Hydrates. Journal of Nuclear Engineering and Radiation Science 9, 011901. https://doi.org/10.1115/1.4055160

Kretzschmar, J., Tsushima, S., Drobot, B., Steudtner, R., Schmeide, K., Stumpf, T., 2020. Trimeric uranyl(vi)–citrate forms Na $^+$, Ca $^{2+}$, and La $^{3+}$ sandwich complexes in aqueous solution. Chem. Commun. 56, 13133–13136. https://doi.org/10.1039/D0CC05460G

Kretzschmar, J., Tsushima, S., Lucks, C., Jäckel, E., Meyer, R., Steudtner, R., Müller, K., Rossberg, A., Schmeide, K., Brendler, V., 2021. Dimeric and Trimeric Uranyl(VI)–Citrate Complexes in Aqueous Solution. Inorg. Chem. 60, 7998–8010. https://doi.org/10.1021/acs.inorgchem.1c00522

Lahallh, S.M., Absl-Halabi, M., Ali, A.M., 1988. Effect of polymerization conditions of sulfonated-melamine formaldehyde superplasticizers on concrete. Cement and Concrete Research 18, 513–531. https://doi.org/10.1016/0008-8846(88)90044-0

Lamouroux, C., Cochin, F., 2012. Study of Long Term Behavior of Intermediate Level Long Lived Waste Packages: An Overview of the R&D Approach and Results. Procedia Chemistry 7, 559–566. https://doi.org/10.1016/j.proche.2012.10.085

Landesman, C., Macé, N., Radwan, J., Ribet, S., Bessaguet, N., David, K., Page, J., Henocq, P., 2018. Effect of high saline alkaline conditions onto radionuclide transport in a CEM V/A hardened cement paste. Presented at the NUWCEM-2018 (cement based materials for nuclear wastes), Avignon, France.

Legand, S., 2023. Effets de la radiolyse sur le transfert et la spéciation de radionucléides en milieu cimentaire adjuvanté (PhD thesis). Université Paris-Saclay, Saclay, France.

Linnenbom, V.J., 1958. The Reaction between Iron and Water in the Absence of Oxygen. J. Electrochem. Soc. 105, 322. https://doi.org/10.1149/1.2428838

Linstrom, P., 1997. NIST Chemistry WebBook, NIST Standard Reference Database 69. https://doi.org/10.18434/T4D303

Macé, N., Fichet, P., Savoye, S., Radwan, J., Lim, C., Lefèvre, S., Page, J., Henocq, P., 2019. Use of quantitative digital autoradiography technique to investigate the chlorine-36-labelled radiotracer transport in concrete. Applied Geochemistry 100, 326–334. https://doi.org/10.1016/j.apgeochem.2018.12.014

Macé, N., Wieland, E., Dähn, R., Tits, J., Scheinost, A.C., 2013. EXAFS investigation on U(VI) immobilization in hardened cement paste: influence of experimental conditions on speciation. Radiochimica Acta 101, 379–389. https://doi.org/10.1524/ract.2013.2024

EURAD (Deliverables n° 3.6, 3.7 and 3.8) - Final Report of results generated in CORI
Dissemination level: PU
Date of issue of this report: **05/07/2024**

Page 254

Maddalena, R., Li, K., Chater, P.A., Michalik, S., Hamilton, A., 2019. Direct synthesis of a solid calcium-silicate-hydrate (C-S-H). Construction and Building Materials 223, 554–565. https://doi.org/10.1016/j.conbuildmat.2019.06.024

Maragkou, E., Pashalidis, I., 2021. Investigations on the Interaction of EDTA with Calcium Silicate Hydrate and Its Impact on the U(VI) Sorption. Coatings 11, 1037. https://doi.org/10.3390/coatings11091037

Marx-Figini, M., 1978. Significance of the intrinsic viscosity ratio of unsubstituted and nitrated cellulose in different solvents. Angew. Makromol. Chem. 72, 161–171. https://doi.org/10.1002/apmc.1978.050720114

McCollom, T.M., Seewald, J.S., 2003a. Experimental study of the hydrothermal reactivity of organic acids and acid anions: II. Acetic acid, acetate, and valeric acid. Geochimica et Cosmochimica Acta 67, 3645–3664. https://doi.org/10.1016/S0016-7037(03)00135-2

McCollom, T.M., Seewald, J.S., 2003b. Experimental constraints on the hydrothermal reactivity of organic acids and acid anions: I. Formic acid and formate. Geochimica et Cosmochimica Acta 67, 3625–3644. https://doi.org/10.1016/S0016-7037(03)00136-4

McCollom, T.M., Seewald, J.S., 2007. Abiotic Synthesis of Organic Compounds in Deep-Sea Hydrothermal Environments. Chem. Rev. 107, 382–401. https://doi.org/10.1021/cr0503660

Missana, T., García-Gutiérrez, M., Mingarro, M., Alonso, U., 2017. Analysis of barium retention mechanisms on calcium silicate hydrate phases. Cement and Concrete Research 93, 8–16. https://doi.org/10.1016/j.cemconres.2016.12.004

Missana, T., García-Gutiérrez, M., Alonso, U., Almendros-Ginestá, O., 2022a. Nickel retention by calcium silicate hydrate phases: Evaluation of the role of the Ca/Si ratio on adsorption and precipitation processes. Applied Geochemistry 137, 105197. https://doi.org/10.1016/j.apgeochem.2022.105197

Missana, T., García-Gutiérrez, M., Alonso, U., Fernández, A.M., 2022b. Effects of the presence of isosaccharinate on nickel adsorption by calcium silicate hydrate (C-S-H) gels: Experimental analysis and surface complexation modelling. Journal of Environmental Chemical Engineering 10, 108500. https://doi.org/10.1016/j.jece.2022.108500

Mollah, M.Y.A., Adams, W.J., Schennach, R., Cocke, D.L., 2000. A review of cement–superplasticizer interactions and their models. Advances in Cement Research 12, 153–161. https://doi.org/10.1680/adcr.2000.12.4.153

Mozdyniewicz, D.J., Nieminen, K., Sixta, H., 2013. Alkaline steeping of dissolving pulp. Part I: cellulose degradation kinetics. Cellulose 20, 1437–1451. https://doi.org/10.1007/s10570-013-9926-2

Murata, K., Hirano, Y., Sakata, Y., Uddin, Md.A., 2002. Basic study on a continuous flow reactor for thermal degradation of polymers. Journal of Analytical and Applied Pyrolysis 65, 71–90. https://doi.org/10.1016/S0165-2370(01)00181-4

Nagra, 2008. Effects of post disposal gas generation in a repository for low- and intermediate-level waste sited in the Opalinus Clay of Northern Switzerland (No. NTB 08-07). Nagra, Wettingen, Switzerland.

Nalet, C., Nonat, A., 2016. Ionic complexation and adsorption of small organic molecules on calcium silicate hydrate: Relation with their retarding effect on the hydration of C3S. Cement and Concrete Research 89, 97–108. https://doi.org/10.1016/j.cemconres.2016.08.012

Nardi, A., de Vries, L., 2017. GibbsStudio, https://gibbsstudio.io/

Nieminen, K., Testova, L., Paananen, M., Sixta, H., 2015. Novel insight in carbohydrate degradation during alkaline treatment. Holzforschung 69, 667–675. https://doi.org/10.1515/hf-2014-0306

EURAD (Deliverables n° 3.6, 3.7 and 3.8) - Final Report of results generated in CORI
Dissemination level: PU
Date of issue of this report: **05/07/2024**

Page 255

Nushi, E., Bleyen, N., Hendrix, K., Mastroleo, F., 2023. Cellulose degradation and nuclear waste management: Characterization of cellulose degradation products by ESI-ToF MS (Master of Science). IMT Atlantique - Campus de Nantes UPM, Universidad Politécnica de Madrid.

Ochs, M., Mallants, D., Wang, L., 2016. Radionuclide and metal sorption on cement and concrete. Topics in safety, Risk, reliability and Quality, Springer. ed. Springer International Publishing, Switzerland.

Ochs, M., Vriens, B., Tachi, Y., 2018. Retention of uranium in cement systems: effects of cement degradation and complexing ligands. Progress in Nuclear Science and Technology 5, 208–212. https://doi.org/10.15669/pnst.5.208

Olmeda, J., Missana, T., Grandia, F., Grivé, M., García-Gutiérrez, M., Mingarro, M., Alonso, U., Colàs, E., Henocq, P., Munier, I., Robinet, J.C., 2019. Radium retention by blended cement pastes and pure phases (C-S-H and C-A-S-H gels): Experimental assessment and modelling exercises. Applied Geochemistry 105, 45–54. https://doi.org/10.1016/j.apgeochem.2019.04.004

Palmer, D.A., Drummond, S.E., 1986. Thermal decarboxylation of acetate. Part I. The kinetics and mechanism of reaction in aqueous solution. Geochimica et Cosmochimica Acta 50, 813–823. https://doi.org/10.1016/0016-7037(86)90357-1

Pashalidis, I., Czerwinski, K.R., Fanghänel, Th., Kim, J.I., 1997. Solid-Liquid Phase Equilibria of Pu(VI) and U(VI) in Aqueous Carbonate Systems. Determination of Stability Constants. Radiochimica Acta 76, 55–62. https://doi.org/10.1524/ract.1997.76.12.55

Pavasars, I., Hagberg, J., Borén, H., Allard, B., 2003. Alkaline degradation of cellulose: Mechanism and kinetics. Journal of Polymers and the Environment 11, 39–47. https://doi.org/10.1023/A:1024267704794

Pilkington, N.J., Stone, N.S., 1990. The solubility and sorption of nickel and niobium under high pH conditions (No. NSS/R--186). United Kingdom.

Pitkänen, L., Sixta, H., 2020. Size-exclusion chromatography of cellulose: observations on the low-molar-mass fraction. Cellulose 27, 9217–9225. https://doi.org/10.1007/s10570-020-03419-9

Plank, J., Pöllmann, K., Zouaoui, N., Andres, P.R., Schaefer, C., 2008. Synthesis and performance of methacrylic ester based polycarboxylate superplasticizers possessing hydroxy terminated poly(ethylene glycol) side chains. Cement and Concrete Research 38, 1210–1216. https://doi.org/10.1016/j.cemconres.2008.01.007

Pointeau, I., Coreau, N., Reiller, P.E., 2008. Uptake of anionic radionuclides onto degraded cement pastes and competing effect of organic ligands. Radiochimica Acta 96. https://doi.org/10.1524/ract.2008.1503

Pointeau, I., Landesman, C., Giffaut, E., Reiller, P., 2004. Reproducibility of the uptake of U(VI) onto degraded cement pastes and calcium silicate hydrate phases. Radiochimica Acta 92. https://doi.org/10.1524/ract.92.9.645.55008

Pointeau, I., Piriou, B., Fedoroff, M., Barthes, M.-G., Marmier, N., Fromage, F., 2001. Sorption Mechanisms of Eu3+ on C-S-H Phases of Hydrated Cements. Journal of Colloid and Interface Science 236, 252–259. https://doi.org/10.1006/jcis.2000.7411

Potthast, A., Radosta, S., Saake, B., Lebioda, S., Heinze, T., Henniges, U., Isogai, A., Koschella, A., Kosma, P., Rosenau, T., Schiehser, S., Sixta, H., Strlič, M., Strobin, G., Vorwerg, W., Wetzel, H., 2015. Comparison testing of methods for gel permeation chromatography of cellulose: coming closer to a standard protocol. Cellulose 22, 1591–1613. https://doi.org/10.1007/s10570-015-0586-2

Putrawan, I.D.G.A., Indarto, A., Octavia, Y., 2022. Thermal stabilization of polyvinyl chloride by calcium and zinc carboxylates derived from byproduct of palm oil refining. Heliyon 8, e10079. https://doi.org/10.1016/j.heliyon.2022.e10079

EURAD (Deliverables n° 3.6, 3.7 and 3.8) - Final Report of results generated in CORI
Dissemination level: PU
Date of issue of this report: **05/07/2024**

Page 256

Ramachandran, V.S., Malhotra, V.M., Jolicoeur, C., Spiratos, N., 1998. Superplasticizers: properties and applications in concrete, Natural Resources Canada. Canada Centre for Mineral & Energy Technology (CANMET), Ottawa, Canada.

Reardon, E.J., 2005. Zerovalent Irons: Styles of Corrosion and Inorganic Control on Hydrogen Pressure Buildup. Environ. Sci. Technol. 39, 7311–7317. https://doi.org/10.1021/es050507f

Rojo, H., Gaona, X., Rabung, T., Polly, R., García-Gutiérrez, M., Missana, T., Altmaier, M., 2021. Complexation of Nd(III)/Cm(III) with gluconate in alkaline NaCl and CaCl2 solutions: Solubility, TRLFS and DFT studies. Applied Geochemistry 126, 104864. https://doi.org/10.1016/j.apgeochem.2020.104864

Seewald, J.S., 2001. Aqueous geochemistry of low molecular weight hydrocarbons at elevated temperatures and pressures: constraints from mineral buffered laboratory experiments. Geochimica et Cosmochimica Acta 65, 1641–1664. https://doi.org/10.1016/S0016-7037(01)00544-0

Senior, N., Newman, R., Wang, S., Diomidis, N., 2017. Understanding and quantifying the anoxic corrosion of carbon steel in a Swiss L/ILW repository environment. Corrosion Engineering, Science and Technology 52, 78–83. https://doi.org/10.1080/1478422X.2017.1303102

Sihtola, H., Kyrklund, B., Laamanen, L., Palenius, I., 1963. Comparison and conversion of viscosity and DP-values determined by different methods. Papper och Trä Spec. No. 4a, 225-232.

Simon, P., Oremusova, J., Valko, L., Kovarik, P., 1991. Influence of metal stearates on thermal-stability of poly(vinyl chloride). 2. Magnesium stearate. Chemical Papers 127–134.

Small, J., Nykyri, M., Helin, M., Hovi, U., Sarlin, T., Itävaara, M., 2008. Experimental and modelling investigations of the biogeochemistry of gas production from low and intermediate level radioactive waste. Applied Geochemistry 23, 1383–1418. https://doi.org/10.1016/j.apgeochem.2007.11.020

Small, J.S., 2021. Final Synthesis report for WP1. MIND project deliverable D1.9. Horizon 2020 Project. Euratom, European Union.

Smart, N.R., Rance, A.P., Nixon, D.J., Fennell, P.A.H., Reddy, B., Kursten, B., 2017. Summary of studies on the anaerobic corrosion of carbon steel in alkaline media in support of the Belgian supercontainer concept. Corrosion Engineering, Science and Technology 52, 217–226. https://doi.org/10.1080/1478422X.2017.1356981

Smith, V., Magalhaes., S., Schneider, S., 2013. The role of PVC additives in the potential formation of NAPLs (Report AMEC No. AMEC/PPE/2834/001). Didcot, UK.

Spinks, J.W.T., Woods, R.J., 1990. An introduction to radiation chemistry, 3rd ed. ed. John Wiley and Sons Inc., New York, NY 10150 (USA).

St. John, P.C., Guan, Y., Kim, Y., Kim, S., Paton, R.S., 2020. Prediction of organic homolytic bond dissociation enthalpies at near chemical accuracy with sub-second computational cost. Nat Commun 11, 2328. https://doi.org/10.1038/s41467-020-16201-z

Stietz, J., Amayri, S., Häußler, V., Scholze, R., Reich, T., 2023a. The Uptake of Actinides by Hardened Cement Paste in High-Salinity Pore Water. Minerals 13, 1380. https://doi.org/10.3390/min13111380

Stietz J., Amayri S., Häußler V., Prieur D. and Reich, T. 2023b. Uptake of Pu(IV) by hardened cement paste in the presence gluconate at high and low ionic strengths. Front. Nucl. Eng. 2:1268767. https://doi.org/10.3389/fnuen.2023.1268767

Sun, Z.-X., Su, F.-W., Forsling, W., Samskog, P.-O., 1998. Surface Characteristics of Magnetite in Aqueous Suspension. Journal of Colloid and Interface Science 197, 151–159. https://doi.org/10.1006/jcis.1997.5239

EURAD (Deliverables n° 3.6, 3.7 and 3.8) - Final Report of results generated in CORI
Dissemination level: PU
Date of issue of this report: **05/07/2024**

Page 257

Sutton, M., Warwick, P., Hall, A., 2003. Uranium(vi) interactions with OPC/PFA groutThis work was performed as part of a PhD Doctoral Thesis at Loughborough University, UK. J. Environ. Monitor. 5, 922. https://doi.org/10.1039/b308554f

Szabo, P.G., Tasi, A.G., Gaona, X., Maier, A.C., Hedström, S., Altmaier, M., Geckeis, H., 2023a. Impact of the degradation leachate of the polyacrylonitrile-based material UP2W on the retention of Ni(ii), Eu(iii) and Pu(iv) by cement. Dalton Trans. 52, 13324–13331. https://doi.org/10.1039/D3DT02122J

Szabo, P.G., Tasi, A.G., Gaona, X., Maier, A.C., Hedström, S., Altmaier, M., Geckeis, H., 2023b. Uptake of Ni(II), Eu(III) and Pu(III/IV) by Hardened Cement Paste in the Presence of Proxy Ligands for the Degradation of Polyacrylonitrile. Front. Nucl. Eng. 2, 1117413. https://doi.org/10.3389/fnuen.2023.1117413

Szabo, P.G., Tasi, A.G., Gaona, X., Polly, R., Maier, A.C., Hedström, S., Altmaier, M., Geckeis, H., 2022. Solubility of Ca(ii), Ni(ii), Nd(iii) and Pu(iv) in the presence of proxy ligands for the degradation of polyacrylonitrile in cementitious systems. Dalton Trans. 51, 9432–9444. https://doi.org/10.1039/D2DT01409B

Szabo, P. G., Tasi, A. G., Gaona, X., Maier, A. C., Hedström, S., Altmaier, M., & Geckeis, H. (2022). Uptake of selected organic ligands by hardened cement paste: Studies on proxy ligands for the degradation of polyacrylonitrile and general considerations on the role of different functionalities in the uptake process. Frontiers in Nuclear Engineering, 1, 997398. https://doi.org/10.3389/fnuen.2022.997398

Takeda, M., Nakajima, H., Zhang, M., Hiratsuka, T., 2008. Laboratory longitudinal diffusion tests: 1. Dimensionless formulations and validity of simplified solutions. Journal of Contaminant Hydrology 97, 117–134. https://doi.org/10.1016/j.jconhyd.2008.01.004

TAPPI, 2021. Acid-insoluble lignin in wood and pulp. TAPPI standard T 222 om-21.

TAPPI, 2009. Alpha-, Beta- and Gamma-Cellulose in Pulp. TAPPI standard T 203 cm-09.

Tasi, A., Gaona, X., Fellhauer, D., Böttle, M., Rothe, J., Dardenne, K., Polly, R., Grivé, M., Colàs, E., Bruno, J., Källstrom, K., Altmaier, M., Geckeis, H., 2018. Thermodynamic description of the plutonium – α–d–isosaccharinic acid system ii: Formation of quaternary Ca(II)–Pu(IV)–OH–ISA complexes. Applied Geochemistry 98, 351–366. https://doi.org/10.1016/j.apgeochem.2018.06.014

Tasi, A., Gaona, X., Rabung, Th., Fellhauer, D., Rothe, J., Dardenne, K., Lützenkirchen, J., Grivé, M., Colàs, E., Bruno, J., Källstrom, K., Altmaier, M., Geckeis, H., 2021. Plutonium retention in the isosaccharinate – cement system. Applied Geochemistry 126, 104862. https://doi.org/10.1016/j.apgeochem.2020.104862

Taylor, H.F.W., 1997. Cement chemistry, 2nd ed. ed. T. Telford, London.

Tits, J., Fujita, T., Harfouche, M., Dähn, R., Tsukamoto, M., Wieland, E., 2014. Radionuclide uptake by calcium silicate hydrates: case studies with Th(IV) and U(VI) (No. PSI Bericht, Report No.: 14-03). Paul Scherrer Institute, Villigen, Switzerland.

Tits, J, Jakob, A., Wieland, E., Spieler, P., 2003a. Diffusion of tritiated water and 22Na+ through non-degraded hardened cement pastes. Journal of Contaminant Hydrology 61, 45–62. https://doi.org/10.1016/S0169-7722(02)00112-2

Tits, Jan, Stumpf, T., Rabung, T., Wieland, E., Fanghänel, T., 2003b. Uptake of Cm(III) and Eu(III) by Calcium Silicate Hydrates: A Solution Chemistry and Time-Resolved Laser Fluorescence Spectroscopy Study. Environ. Sci. Technol. 37, 3568–3573. https://doi.org/10.1021/es030020b

Tits, J., Walther, C., Stumpf, T., Macé, N., Wieland, E., 2015. A luminescence line-narrowing spectroscopic study of the uranium(VI) interaction with cementitious materials and titanium dioxide. Dalton Transactions 44, 966–976. https://doi.org/10.1039/c4dt02172j

EURAD (Deliverables n° 3.6, 3.7 and 3.8) - Final Report of results generated in CORI
Dissemination level: PU
Date of issue of this report: **05/07/2024**

Page 258

Tits, J., Wieland, E., 2018. Actinide sorption by cementitious materials (No. PSI Report 18–02). Paul Scherrer Institute, Villigen, Switzerland.

Tits, J., Wieland, E., Bradbury, M.H., 2005. The effect of isosaccharinic acid and gluconic acid on the retention of Eu(III), Am(III) and Th(IV) by calcite. Applied Geochemistry 20, 2082–2096. https://doi.org/10.1016/j.apgeochem.2005.07.004

Tits, J., Wieland, E., Bradbury, M.H., Eckert, P., Schaible, A., 2002. The uptake of Eu(III) and Th(IV) by calcite under hyperalkaline conditions. Paul Scherrer Institute, Villigen, Switzerland.

Van Loon, L.R., Eikenberg, J., 2005. A high-resolution abrasive method for determining diffusion profiles of sorbing radionuclides in dense argillaceous rocks. Applied Radiation and Isotopes 63, 11–21. https://doi.org/10.1016/j.apradiso.2005.02.001

Van Loon, L.R., Hummel, W., 1995. The radiolytic and chemical degradation of organic ion exchange resins under alkaline conditions: Effect on radionuclide speciation (Nagra technical Report No. 95–08). Nagra, Wettingen, Switzerland.

Van Loon, L.R., Glaus, M.A., Laube, A., Stallone, S., 1999a. Degradation of Cellulosic Materials under the Alkaline Conditions of a Cementitious Repository for Low- and Intermediate Level Radioactive Waste. Part III: Effect of Degradation Products on the Sorption of Radionuclides on Feldspar. Radiochimica Acta 86, 183–190. https://doi.org/10.1524/ract.1999.86.34.183

Van Loon, L.R., Glaus, M., 1999b. Experimental and theoretical studies on alkaline degradation of cellulose and its impact on the sorption of radionuclides (PSI Bericht No. 98–07). PSI, Villigen, Switzerland.

Van Loon, L.R., Hummel, W., 1999. The Degradation of Strong Basic Anion Exchange Resins and Mixed-Bed Ion-Exchange Resins: Effect of Degradation Products on Radionuclide Speciation. Nuclear Technology 128, 388–401. https://doi.org/10.13182/NT99-A3039

Van Loon, L.R., Glaus, M.A., Stallone, S., Laube, A., 1997. Sorption of Isosaccharinic Acid, a Cellulose Degradation Product, on Cement. Environ. Sci. Technol. 31, 1243–1245. https://doi.org/10.1021/es960505i

Vercammen, K., 2000. Complexation of Calcium, Thorium and Europium by a-Isosaccharinic Acid under Alkaline Conditions (PhD thesis). Swiss Federal Institute of Technology Zurich, Zurich, Switzerland.

Vercammen, K., Glaus, M.A., Van Loon, L.R., 2001. Complexation of Th(IV) and Eu(III) by α-isosaccharinic acid under alkaline conditions. Radiochimica Acta 89, 393–402. https://doi.org/10.1524/ract.2001.89.6.393

Verlinden, B., Zsabka, P., Van Hecke, K., Verguts, K., Mihailescu, L.-C., Modolo, G., Verwerft, M., Binnemans, K., Cardinaels, T., 2021. Dosimetry and methodology of gamma irradiation for degradation studies on solvent extraction systems. Radiochimica Acta 109, 61–72. https://doi.org/10.1515/ract-2020-0040

Wiborgh, M., Höglunf, L., Pers, K., 1986. Gas formation in a L/ILW repository and gas transport in the host rock (Nagra Technical Report No. NTB 85-17). Nagra, Wettingen, Switzerland.

Whistler, R.L., BeMiller, J.N., 1963. alpha-D-Isosaccharino-1,4-lactone, Action of Lime Water on Lactose, in: Methods in Carbohydrate Chemistry, Vol. 2: Reactions of Carbohydrates. Academic Press, New York, USA, pp. 477–479.

Wieland, E., Hummel, W., 2015. Formation and stability of 14 C-containing organic compounds in alkaline iron-water systems: preliminary assessment based on a literature survey and thermodynamic modelling. Mineral. mag. 79, 1275–1286. https://doi.org/10.1180/minmag.2015.079.6.03

Wieland, E., 2014. Sorption database for the cementitious near-field of L/ILW and ILW repositories for provisional safety analyses for SGT-E2 (No. NAGRA Technical Report 14-08). Paul Scherrer Institute.

EURAD (Deliverables n° 3.6, 3.7 and 3.8) - Final Report of results generated in CORI
Dissemination level: PU
Date of issue of this report: **05/07/2024**

Page 259

Wieland, E., Macé, N., Dähn, R., Kunz, D., Tits, J., 2010. Macro- and micro-scale studies on U(VI) immobilization in hardened cement paste. Journal of Radioanalytical and Nuclear Chemistry 286, 793–800. https://doi.org/10.1007/s10967-010-0742-y

Wieland, E., Tits, J., Ulrich, A., Bradbury, M.H., 2006. Experimental evidence for solubility limitation of the aqueous Ni(II) concentration and isotopic exchange of 63 Ni in cementitious systems. Radiochimica Acta 94, 29–36. https://doi.org/10.1524/ract.2006.94.1.29

Wieland, E., Tits, J., Dobler, J.P., Spieler, P., 2002. The effect of α-isosaccharinic acid on the stability of and Th(IV) uptake by hardened cement paste. Radiochimica Acta 90, 683–688. https://doi.org/10.1524/ract.2002.90.9-11_2002.683

EURAD (Deliverables n° 3.6, 3.7 and 3.8) - Final Report of results generated in CORI
Dissemination level: PU
Date of issue of this report: **05/07/2024**

Page 260

Acknowledgements

EURAD (Deliverables n° 3.6, 3.7 and 3.8) - Final Report of results generated in CORI
Dissemination level: PU
Date of issue of this report: **05/07/2024**

Page 261

Contributors to CORI Task 4:

David Garcia (Amphos21), Marta Lopez (Amphos21), Nathalie Macé (CEA), Virginie Blin (CEA), Yaana Bruneel (CEA), Pascal E. Reiller (CEA), Pascal Fichet (CEA), Jacques Page (CEA), Elise Fayette (CEA), Almendros-Ginestà Oscar (CIEMAT), Ursula Alonso (CIEMAT), Miguel García-Gutiérrez (CIEMAT), Manuel Mingarro (CIEMAT), Tiziana Missana (CIEMAT), Rūta Druteikienė (CPST), Barbora Drtinová (CTU), Jana Kittnerová (CTU), Marta Burešová (CTU), Vit Rosnecky (CV REZ), Zbynek Hlavac (CV REZ), Lukas Prochazka (CV REZ), Ivana Ruzickova (CV REZ), Naila Ait-Mouheb (FZJ), Larissa Klass (FZJ), Murat Güngör (FZJ), Giuseppe Modolo (FZJ), Guido Deissmann (FZJ), Dirk Bosbach (FZJ), Katja Schmeide (HZDR), Jerome Kretzschmar (HZDR), Peter G. Szabo (KIT), Rosa E. Guidone (KIT), Agost G. Tasi (KIT), Xavier Gaona (KIT), Marcus Altmaier (KIT), Crina Bucur (RATEN), Camelia Ichim (RATEN), Delphine Durce (SCK CEN), Nele Bleyen (SCK CEN), Lander Frederickx (SCK CEN), Norbert Maes (SCK CEN), Tom Maes (SCK CEN), Peter Thomas (SCK CEN), Marc Van Gompel (SCK CEN), Anneleen Vanleeuw (SCK CEN), Dorien Verhaegen (SCK CEN), Prisca Verheyen (SCK CEN), Göran Verpoucke (SCK CEN), Greet Verstrepen (SCK CEN), Lian Wang (SCK CEN), Katinka Wouters (SCK CEN), Catherine Landesman (SUBATECH), Nicolas Bessaguet (SUBATECH), Karine David (SUBATECH), Solange Ribet (SUBATECH), Jihan Ben Attig (SUBATECH), Zdena Lahodová (SURAO), Ioannis Paschalidis (UCyprus), Elena Maragkou (UCyprus), Petr Večerník (UJV), Hana Kořenková (UJV), Radek Pošvař (UJV), Vlastimil Miler (UJV), Monika Kiselová (UJV), Karol Kočan (UJV), Diana Tkachenok (UJV), Václav Znamínko (UJV), Marta Hybášková (UJV), Simona Králová (UJV), Lukáš Brázda (UJV), Samer Amayri (UMainz), Alexander Bösch (UMainz), Sebastian Kissel (UMainz), Gerrit Kraus (UMainz), Tamara Kutyma (UMainz), Janik Lohmann (UMainz), Tobias Reich (UMainz), Fabian Schröder (UMainz), Leon Spittler (UMainz), Janina Stietz (UMainz), Jonas Stricker (UMainz), Toni Haubitz (UPotsdam), Sophie Zenkter/Dettmann (UPotsdam), Michael U. Kumke (UPotsdam)

EURAD (Deliverables n° 3.6, 3.7 and 3.8) - Final Report of results generated in CORI
Dissemination level: PU
Date of issue of this report: **05/07/2024**

Page 262